JOINT INSTITUTE FOR NUCLEAR RESEARCH

E4-94-370

PROCEEDINGS OF THE IV INTERNATIONAL CONFERENCE ON SELECTED TOPICS IN NUCLEAR STRUCTURE

Dubna, July 5—9, 1994

Editor V.G.Soloviev

Supported by Russian Fund for Fundamental Research

Dubna 1994

ADVISORY COMMITTEE

S.Åberg, Sweden
P.F.Bortignon, Italy
Ch.Briançon-Mikhailova, France
D.G.Burke, Canada
M.Di Toro, Italy
Chen Yongshow, China
B.S.Dzhelepov, Russia
R.A.Eramzhyan, Russia
A.Faessler, FRG
T.Fenyes, Hungary
I.Hamamoto, Sweden
M.N.Harakeh, The Netherlands
R.Hoff, USA
B.Imanishi, Japan
J.Kern, Switzerland
R.Mach, Czechia
E.R.Marshalek, USA
P.Prokofjevs, Latvia
S.Raman, USA
P.Ring, FRG
Ch.Stoyanov, Bulgaria
I.N.Vishnevsky, Ukraina
P. von Brentano, FRG

THE ORGANIZING COMMITTEE

V.G.Soloviev — Chairman
K.Ya.Gromov — Vice-Chairman
L.A.Malov — Vice-Chairman
V.M.Shilov — Scientific Secretary

S.I.Bastrukov, N.M.Dokalenko, Yu.P.Gangrsky, R.V.Jolos, I.N.Mikhailov, V.Yu.Ponomarev, Yu.P.Popov, A.I.Romanov, V.V.Voronov, Ts.Vylov — Members of the Organizing Committee

© Объединенный институт ядерных исследований. Дубна, 1994

CONTENTS

PREFACE

The Fourth International Conference on Selected Topics in Nuclear Structure was held at Dubna, Russia on July 5-9, 1994. The Conference was organized by Bogoliubov Laboratory of Theoretical Physics, Laboratory of Nuclear Problems, Flerov Laboratory of Nuclear Reactions and Frank Laboratory of Neutron Physics of the Joint Institute for Nuclear Research under the financial support of the Russian Fund for Fundamental Research. This Conference is part of a series of meetings which were held in Dubna in 1968, 1976 and 1989.

The five-day Conference was attended by 157 participants from 22 countries. The program was maintained in the proceeding conference, with emphasis on recent experimental and theoretical developments in nuclear structure. Topics discussed during the Conference were the following: nuclear structure at low-energy excitations (collective and quasiparticle phenomena, proton-neutron interactions), microscopic and phenomenological theory of nuclear structure, nuclear structure studies with charged particles, heavy-ions, neutrons and photons, nuclei at high angular momenta and superdeformation, structure and decay properties of giant resonances, charge-exchange resonances and β-decay, semiclassical approach of large amplitude collective motion and structure of hot nuclei.

The Conference began with the welcoming address of Prof. V.G. Kadyshevsky, Director of the Joint Institute for Nuclear Research. The general scope of the Conference program was developed in consultation with the Advisory Committee. The program was comprised of 54 invited papers. The invited talks were presented in 22 sessions during mornings and afternoons and were organized according to topics. The contributed papers were presented as posters. The session chairmen who presided during the oral presentations were Bortignon P.F., Covello A., Di Toro M., Eramzhyan R.A., Filippov G.F., Gangrsky Yu.P., Gromov K.Ja., Harakeh M.N., Imanishi B., Ishkhanov B.S., Kern J., Lizurej H., Malov L.A., Mikhailov I.N, Ponomarev V.Yu., Quentin Ph., Raman S.R., Shilov V.M., Soloviev V.G., Stoyanov Ch., Szpikowski S. and Voronov V.V.. We have disregarded to have a summary talk at the end of the Conference. In fact, several speakers have given review talks pointing to the interesting developments in specific domains. Brief concluding remarks were made by P.F. Bortignon, R.W. Hoff and S.R. Raman.

The proceedings contain the papers of the Conference which were received in the form of camera-ready copy; the contents of these original papers have not been edited. The papers in this volume have been arranged in the order in which they were presented at the Conference. Several speakers did not give the manuscripts of their talks and therefore were not included in the Proceedings.

In addition to the scientific program, the organizers offered social and cultural events. A reception took place on Tuesday, July 5. Thursday afternoon was a boat trip on the Volga river. The banquet took place on Friday evening in the International Conference Hall.

Many people contributed to the organization of the Conference. First I want to thank the Director of JINR and the Directors of Laboratories for their support and the Russian Fund for Fundamental Research for financial help. I am very thankful to the chairmen who prevented the schedule from getting chaotic. Thanks are due to all speakers and to all participants who have participated in the lively discussions. I want to thank members of the Organizing Committee and especially L.A. Malov and V.M. Shilov for their hard work and attention to detail that was so essential to success of the Conference. Finally, I acknowledge the help of many collaborators and administrative staff of the International department and of the Bogoliubov Laboratory of Theoretical Physics.

V.G. Soloviev
July 1994

Looking inside giant resonance fine structure

V.V. Voronov and V.Yu. Ponomarev

Bogoliubov Laboratory of Theoretical Physics, Joint Institute for Nuclear Research, 141980 Dubna, Moscow Region, Russia

Microscopic calculations of the fine structure of giant resonances for spherical nuclei are presented. Excited states are described by wave functions which take into account the coupling of simple one-phonon configurations with two-phonon states. Few examples are presented: the γ-decay of resonances to the ground and low-lying excited states and the relativistic Coulomb excitation of the double giant dipole resonance states.

1. INTRODUCTION

A lot of information on the giant resonances have been gotten from experiments using different kinds of probes like electrons, hadrons, heavy ions and others ones [1,2]. A main part of this information is related to the integral characteristics like an excitation energy and a width. An essential development of the experimental setup enables one to perform the coincidence experiments to study the decay channels of the giant resonances. By different measurements one may separate information on different states contributing to giant resonances in non-coincidence experiments and thus look inside the resonance structure. Another source of information on the fine structure of giant resonances is inelastic scattering experiments with a high resolution. We can mention here (e,e') experiments [3] or recent (p,p') measurements below the particle threshold which distinguish fragmentation of a resonance in a group of many discrete states [4]. These exclusive data require rather complete theoretical models to be explained [5-7]. One of them will be presented and used in this work.

2. FORMALISM AND DETAILS OF CALCULATIONS

Microscopic analysis of states forming giant resonances as well as low-lying states has been performed within the Quasiparticle Phonon Model (QPM) [6-7]. The model Hamiltonian $\mathcal{H}$ includes an average field $V_{p(n)}$ for protons and neutrons, a monopole pairing interaction and isoscalar and isovector residual interaction of a separable type with a form factor proportional to $dV_{p(n)}/dr$. Excited states of even-even nuclei are treated in terms of phonon excitations built upon the ground state that is considered as a phonon vacuum $|0>_{ph}$. Phonon creation operator $Q^{+}_{\lambda\mu i}$ for multipolarity $\lambda\mu$ is introduced as a linear combination of two quasiparticle creation α^{+}_{jm} and annihilation α_{jm} operators with the shell quantum numbers jm of the average field V as follows:

$$Q^{+}_{\lambda\mu i} = \frac{1}{2}\sum_{jj'}^{p,n}\left\{\psi^{\lambda i}_{jj'}[\alpha^{+}_{jm}\alpha^{+}_{j'm'}]_{\lambda\mu} + (-1)^{\lambda-\mu}\phi^{\lambda i}_{jj'}[\alpha_{jm}\alpha_{j'm'}]_{\lambda-\mu}\right\} \quad , \tag{1}$$

where

$$[\alpha^{+}_{jm}\alpha^{+}_{j'm'}]_{\lambda\mu} = \sum_{mm'} < jmj'm'|\lambda\mu > \alpha^{+}_{jm}\alpha^{+}_{j'm'} \quad .$$

The forward $\psi^{\lambda i}_{jj'}$ and backward $\phi^{\lambda i}_{jj'}$ amplitudes are obtained by solving RPA equations that yield a set of one-phonon configurations with excitation energies $\omega_{\lambda i}$ and RPA root number i. Among phonons we obtain both collective and practically pure two-quasiparticle excitations.

We assume that mixing of one-phonon configurations, through which giant resonances are excited in inelastic scattering, with more complex configurations is sufficiently strong in the resonance region. Thus, we write the wave function of resonance states as a sum of configurations of different complexity by the number of phonons. If we limit this sum to one- and two-phonon configurations only, the wave function for the λ^{π}_{ν}–state has the form:

$$\Psi_{\nu}(\lambda\mu) = \{\sum_{i} R_{i}(\lambda\nu)Q^{+}_{\lambda\mu i} + \sum_{\lambda_1 i_1 \lambda_2 i_2} P^{\lambda_2 i_2}_{\lambda_1 i_1}(\lambda\nu)\left[Q^{+}_{\lambda_1\mu_1 i_1}Q^{+}_{\lambda_2\mu_2 i_2}\right]_{\lambda\mu}\}|0>_{ph} \quad . \tag{2}$$

In actual calculations we do not include two-phonon configurations made of both non-collective phonons for the second term of the wave function (2). By this truncation of the two-phonon basis, we remove complex configurations that are weakly coupled to one-phonon states and, on the other hand, may strongly violate the Pauli principle.

For the amplitudes $R_i(\lambda\nu)$ and $P^{\lambda_2 i_2}_{\lambda_1 i_1}(\lambda\nu)$, eq. (2), we diagonalize the model Hamiltonian on the basis of wave functions (2). Eigenvalues E_ν of states (2) are got as the roots of the following determinant:

$$F(E_\nu) = det|(\omega_{\lambda i} - E_\nu)\delta_{ii'} - \frac{1}{2}\sum_{\lambda_1 i_1, \lambda_2 i_2}\frac{U^{\lambda_2 i_2}_{\lambda_1 i_1}(\lambda i)U^{\lambda_2 i_2}_{\lambda_1 i_1}(\lambda i')}{\omega_{\lambda_1 i_1} + \omega_{\lambda_2 i_2} - E_\nu}| = 0 \quad , \tag{3}$$

where

$$U^{\lambda_2 i_2}_{\lambda_1 i_1}(\lambda i) = < Q_{\lambda i} || \mathcal{H} || \left[Q^+_{\lambda_1 i_1} Q^+_{\lambda_2 i_2} \right]_\lambda >$$

is the matrix element of interaction between one- and two-phonon configurations which is a function [6] of the amplitudes $\psi^{\lambda i}_{jj'}$ and $\phi^{\lambda i}_{jj'}$ eq. (1) and thus, calculated microscopically as soon as a phonon basis is fixed. The rank of the determinant (3) is determined by the number of one-phonon configurations included in the first term of the wave function (2).

Numerical calculations have been performed with the Woods-Saxon potential for an average field with the parameters from ref. [8]. Parameters of the residual interactions were adjusted to the properties of the low-lying collective levels. Natural parity phonons with $\lambda^\pi = 1^- - 8^+$ have been included in the two-phonon term of the wave function (2).

3. SOME RESULTS

With a complete information on the fine structure of giant resonances obtained in this way, we may consider different physical processes in which different states from the resonance region are excited by different probes, and in coincidence technique of measuring decay properties of these states, fingerprints of some specific states from the resonance region can be observed. This allows one to consider giant resonances not as broad featureless structures but as a set of a great number of states with their own properties and also serves as a good test for existing nuclear models.

3.1. Fine structure of the GDR

First, let us demonstrate the fragmentation of the B(Eλ) strength due to the coupling of one-phonon configurations to two-phonon ones in the resonance region. We take as an example the giant dipole resonance (GDR) in ^{136}Xe. The top part of Figure 1 presents the B(E1) strength distribution over one-phonon configurations. The major part of the B(E1) strength is carried by these configurations, the direct excitation of two-phonon 1^- states from the ground state is about three orders of magnitude weaker. The coupling of simple (one-phonon) configurations to more complex (two-phonon) ones results in a strong fragmentation of one-phonon states over the states with the wave function (2) the bottom part of Figure 1. This example clearly shows how the width of a giant resonance appears. Calculations on the set of wave functions, eq. (2), somewhat underestimate within a few hundred of keV the experimentally measured widths of giant resonances. This is not surprising since configurations more complex than two-phonon ones are not included. To achieve better

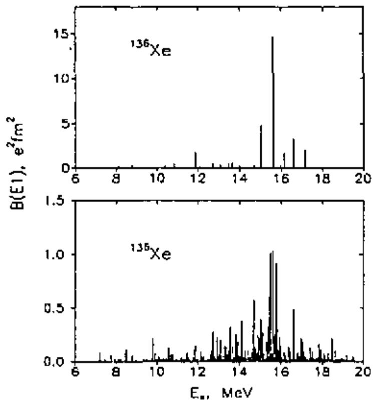

Figure 1. GDR in ^{136}Xe. Top: E1-strength distribution over one-phonon configurations. Bottom: Coupling to complex configurations, wave function, eq. (2), is allowed for.

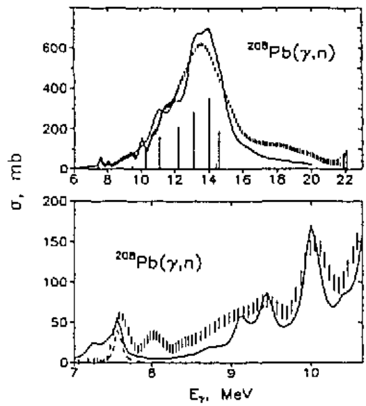

Figure 2. Experimental and theoretical $(\gamma,n)^{208}$Pb cross section. Calculations are performed with $\Delta = 1$ MeV (top) and 0.2 MeV (bottom).

agreement with an experiment in the B(Eλ) strength distribution, an additional artificial damping width, which effectively simulates truncated complex configurations, is included by using the well known strength function method.

3.2. Substructures of the (γ,n)Pb cross section

Some substructures of the GDR have been observed in the (γ,n) cross sections at low excitation energies [9]. The experimental $(\gamma,n)^{208}$Pb cross section is presented in the top part of Figure 2. It is compared to the calculated energy averaged cross section of the dipole photon adsorption

$$\sigma_{\gamma t}(E_\gamma) = 4,025\, E_\gamma\, b(E1,E_\gamma) \quad , \tag{4}$$

where

$$b(E1,E) = \sum_\nu |< \nu||M(E1)||0 >|^2 \frac{1}{2\pi} \frac{\Delta}{(E-E_\nu)^2+\Delta^2/4} \tag{5}$$

is the strength function of the dipole strength distribution calculated with the artificial damping parameter $\Delta = 1$ MeV. One can see from Figure 2 a rather good agreement of experimental data with the theoretical calculations for the photoneutron cross section. Some overestimation of a cross section near a maximum and underestimation of a high energy part in our calculation are caused by the truncation of a large number of two phonon configurations which are weakly coupled with one-phonon states. An integral contribution of these components may be essentially taken into account by increasing the energy averaging parameter Δ. The results of the RPA calculation for the dipole strength distribution are shown in the same figure by vertical lines. As can be seen from Figure 2, there are substructures in the low energy part of the cross section. They are located near the RPA collective states. The coupling of the last with the two-phonon states results in a redistribution of the dipole strength. For the low energy part where a level density is not so high substructures are pronounced. The increasing of the excitation energy leads to increasing of the level density, and as a result, substructures disappear. One cannot observe any substructures in nuclei with open shells because of the high level densities and strong coupling between configurations [10].

To shed more light on the problem of the substructure existence, the low energy part of the cross section with smaller $\Delta = 0.2$ MeV has been calculated. The results of calculations are given in the bottom part of Figure 2. Our calculations reproduce the main structures observed by the experiment at the excitation energies 7.6, 8.6, 9.1, 9.5, 10.0 and 11.3 MeV. The substructure at the energy 7.6 MeV is formed by E1- and M1(dashed line)-transitions. As can be seen from the bottom part of Figure 2, the isovector M1-resonance contributes essentially to the cross section in this energy region. This result is in good agreement with the experimental M1 strength distribution which has been measured with highly polarized tagged photons [11]. We fail to reproduce the substructure at the energy 8 MeV, nevertheless, there is a two-bump structure in the calculated absorption cross section at lower energies. Some disagreement between calculations and experimental data may be caused apparently by inaccuracies of our single particle energies but we did not try to get an ideal description of experimental data. It is worth mentioning that E2-transitions do not give any noticeable contribution to the cross section.

3.3. γ decay of the HEOR

The experimental [12] and the theoretical [13,14] investigations of the gamma-decay of the giant resonances into the low-lying states in ^{208}Pb enable one to understand particularities of the decay in *different channels* and they are in a good agreement with each other. The idea that giant resonance states can be excited via one-phonon configurations and then decay by means of two-phonon configurations of their wave functions can be applied to

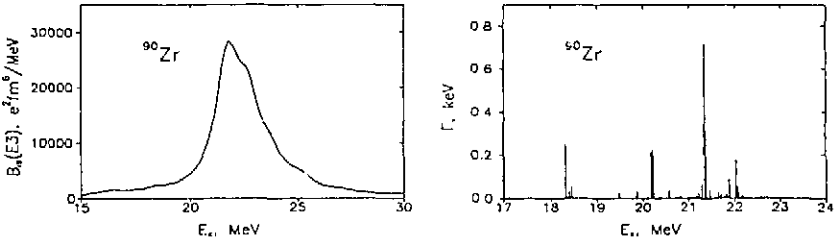

Figure 3. Calculated strength function of the isoscalar E3 strength distribution in the HEOR region (left) and γ decay widths of the HEOR to low-lying 2^+ and 4^+ states (right) in ^{90}Zr.

investigation of giant resonances of high multipolarity for which γ-decay to the ground state is strongly suppressed. As an example, we consider γ-decay properties of the High Energy Octupole Resonance (HEOR) in ^{90}Zr. It may be excited by some isoscalar probe and the corresponding, calculated within the QPM, strength function is presented in the left part of Figure 3. In this calculation, the HEOR has the energy centroid $E_x = 22.4$ MeV and the total width $\Gamma = 4.4$ MeV.

Because of the high density of two-phonon configurations in the HEOR region we have succeeded in calculating the HEOR γ-decay into the low-lying collective $2^+_{1,4}$ and $4^+_{1,2}$ states only on the truncated two-phonon basis. The partial γ-decay widths for these transitions calculated under the assumption of isoscalar nature of the HEOR excitation are shown in the right part of Figure 3. The total $\Gamma_{HEOR \to 2^+_{1,4}, 4^+_{1,2}}$ is equal to 3 keV or about 10% of the GDR γ-decay width into the ground state. It opens a new possibility to investigate the HEOR in spherical nuclei.

4. EXCITATION OF DOUBLE GDR RESONANCES

The excitation of ^{136}Xe on ^{208}Pb target at $E_{lab} = 690$ MeV/n has recently been measured [15]. A prominent structure centered around twice the energy of the GDR was observed and interpreted as a multi-step excitation of the double GDR. Making use of the results of nuclear structure calculations within the QPM and of the theory of relativistic Coulomb excitation [16], the cross sections associated with the one-phonon giant resonances as well as two-step excitation of double resonances have been calculated [17]. A similar calculation within a phenomenalogical approach for the giant resonance characteristics has been done recently too [18]. These cross sections can be written in terms of the first- and second-order amplitudes $a^{(1)}$ and $a^{(2)}$ respectively as

$$\sigma^{(k)} = 2\pi \int_{R_{min}}^{\infty} bdb \int_{0}^{\infty} d\omega |\sum_{M_f} a^{(k)}_{I_f,M_f;I_o,M_o}(\omega,b)|^2 \ , k=1,2, \tag{6}$$

For $k=1$, the final states have angular momentum $I_f=1$ for the GDR and $I_f=2$ for the GQR, while for $k=2$, both $I_f=0$ and 2 are possible. The amplitudes depend on the impact parameter b and on the excitation energy $\hbar\omega$. The first-order amplitude is equal to [16]

$$a^{(1)}_{I_f,M_f;I_o,M_o}(\omega) = \frac{4\pi Z_t e}{i\hbar(2\lambda+1)}(-1)^{I_o-M_o} \begin{pmatrix} I_o & \lambda & I_f \\ -M_o & M_o-M_f & M_f \end{pmatrix} < I_o||M(E\lambda)||I_f >$$
$$\times\ S_{\lambda,M_o-M_f}(\omega)\ , \tag{7}$$

where Z_t is the charge of the target. The radial integral S, carried out on a straight-line trajectory in keeping with the relativistic character of the reaction, is given by

$$S_{\lambda\mu} = \frac{1}{4\pi v\gamma}(2\lambda+1)^{3/2} G_{E\lambda,\mu}\left(\frac{c}{v}\right) K_\mu(\xi(b)) \left(\frac{\omega}{c}\right)^{\lambda}\ . \tag{8}$$

Here $\xi(b) = \omega b/v\gamma$ is the adiabaticity parameter. The functions K_μ are modified Bessel functions, while the polynomials $G_{E\lambda,\mu}$ are related to the Legendre polynomials. The lower limit of integration over impact parameter is to be taken in such a way as to exclude nuclear reactions.

For the GDR we have used the B(E1) strength distribution calculated as described above in Sect. 3.1. The isoscalar and the isovector GQR have also been calculated within the same approach. The centroid, width and percentage of the EWSR associated with the isoscalar mode are 12.5 MeV, 3.2 MeV and 75% respectively. The corresponding quantities associated with the isovector GQR are 23.1 MeV, 3.6 MeV and 80%.

The second order amplitude needed in the calculation of the double phonon excitation can be written as

$$a^{(2)}_{I_f,M_f;I_o,M_o}(\omega_{fo}) = \frac{1}{2}\sum_{I_i,M_i} a^{(1)}_{I_f,M_f;I_i,M_i}(\omega_{fi}) a^{(1)}_{I_i,M_i;I_o,M_o}(\omega_{io})$$
$$+ \frac{i}{2\pi}\sum_{I_i,M_i} \mathcal{P}\int_{-\infty}^{\infty}\frac{dq}{q} a^{(1)}_{I_f,M_f;I_i,M_i}(\omega_{fi}-q) a^{(1)}_{I_i,M_i;I_o,M_o}(\omega_{io}+q)\ , \tag{9}$$

where $I_i M_i$ denotes the angular momentum and projection of the intermediate state. A central aspect of the above expression is the interference between the different E1-amplitudes, and thus between the different components of the dipole response (cf. eq.(2)). The principal integral in eq.(9) has been neglected in the calculations reported here. It vanishes for the excitation of a sharp dipole state, and is expected to give a small contribution even when the state has a finite width.

The evaluation of $a^{(2)}$ requires the knowledge of the matrix element $< I_f||M(E1)||I_i >$ $= < \nu_1\nu_2||M(E1)||\nu_1 >$. Because of the phonon character of the operators $Q_{\lambda\mu}$, it can be shown that

$$< \nu_1\nu_2||M(E1)||\nu_1 >= \sqrt{1+\delta_{\nu_1\nu_2}}\sum_i R_i(\nu_2) < 0||Q_{1i}M(E1)||0 >$$

$$= \sqrt{1+\delta_{\nu_1\nu_2}} < \nu_2||M(E1)||0 > \ . \tag{10}$$

This result emerges from the interference of 10^3 states, and shows that the strength function for the excitation of the double giant dipole resonance can be derived from the one–phonon strength function, considering the multiple excitation of all the $|\nu >$ states, with the appropriate boson factor and phase which account for the double excitation of the same state.

The resulting differential Coulomb-excitation cross sections associated with the two-phonon dipole excitation displays a centroid at 30.6 MeV, about twice that of the one-phonon 1^--states, while the width is $\Gamma \approx 6$ MeV, the ratio to that of the one-phonon excitation being 1.5.

The associated integrated values are displayed in Table 1, in comparison with the experimental findings. The value of the integrated cross section reported in ref. [16] is 1.85 ± 0.1 b. The nuclear contribution has been estimated to be about 100 mb, while about 3% (50 mb) of the cross section is found at higher energy. Subtracting these two contributions and the 2-phonon cross section leads to the value 1480 mb shown in the last row of Table 1.

As can be seen from Eq. (6), the calculated cross sections depend on the choice of the value of $R_{min} = r_o(A_p^{1/3} + A_t^{1/3})$. In keeping with the standard "safe distance", that is, the distance beyond which nuclear excitation can be safely neglected, we have used $r_o = 1.5$ fm. It is satisfactory that the measured cross section is rather close to this value. Also shown in Table 1 are the predictions associated with the sequential excitation of the double giant dipole resonance. The calculated value of 50 mb is a factor of 4 smaller than experimentally observed. Reducing r_o to 1.2 fm increases the cross section to 130 mb, a value which is still 50% smaller than the reported experimental value. The fact that the one-phonon cross

Table 1. Calculated for two values of r_o and experimental cross section (in mb) for the excitation of giant resonances in ^{136}Xe.

	GDR	$GQR_{T=0}$	$GQR_{T=1}$	GDR + GQR	$[GDR \otimes GDR]_{0^+,2^+}$
$r_o = 1.5$ fm	1480	110	60	1650	50
Experiment	–	–	–	1480	215 ± 50

section becomes a factor 1.7 larger than reported indicates that this way to proceed is likely not to be correct, and seems to be in contradiction with basic predictions of the harmonic picture of the GDR which is at the basis of the RPA description of these modes. It is worth to mentioning that an essential discrepancy between the experimental cross sections and calculated ones takes place for other calculations and other experiments too [18,19].

5. CONCLUSIONS

The Quasiparticle Phonon Model has been applied to calculations of the fine structure of giant resonances. The model Hamiltonian has been diagonalized on the basis of the wave functions of excited states which include one- and two-phonon configurations. The wave functions produced for each state contributing to a giant resonance allow one to consider different properties of single and double resonances on a microscopic basis. To understand a puzzle of a large experimental value for the Coulomb excitation cross section of the double giant resonances in comparison with the calculated one it is necessary to continue such investigations.

We acknowledge financial support from the Russian foundation for fundamental research under the grant 94-02-05137 and from the International Science Foundation under the grant № N6N000.

REFERENCES

1. K. Goeke and J. Speth , Ann. Rev. Nucl. Part. Sci. **32** (1982) 65.

2. A. van der Woude, Electric and Magnetic Giant Resonances in Nuclei, ed. J. Speth, World Scientific Publishing Company (1991) 99.

3. G. Kilgus et al., Z.Phys. **A326** (1987) 41.

4. Y. Fujita et al., Phys. Rev. **C40** (1989) 1595.

5. G.F. Bertsch, P.F. Bortignon and R.A. Broglia, Rev. Mod. Phys. **55** (1983) 287; J. Wambach, Rep. Prog. Phys. **51** (1988) 989.

6. A.I. Vdovin and V.G. Soloviev, Particles and Nuclei **14** (1983) 237.

7. V.V. Voronov and V.G. Soloviev, Particles and Nuclei **14** (1983) 1380.

8. V.Yu. Ponomarev et al., Nucl. Phys. **A323** (1979) 446.

9. S.N. Belyaev et al., Sov. Journ. of Nucl. Phys. **55** (1992) 157.

10. V.G. Soloviev et al., Nucl. Phys. **A304** (1978) 503.

11. R.M. Laszewski et al., Phys. Rev. Lett. **61** (1988) 1710.

12. J.R. Beene et al., Phys. Rev. **C41** (1990) 920.

13 P.F. Bortignon et al., Phys. Let.**148B** (1984) 20.

14. V. Voronov and V. Ponomarev, Nucl. Phys.**A520** (1990) 619c.

15. R. Schmidt et al., Phys. Rev. Lett. **70** (1993) 1767.

16. K. Alder and A. Winther, Nucl. Phys. **A319**(1979) 518.

17. V. Yu. Ponomarev et al., Phys. Rev. Lett. **72** (1994) 1168.

18. C.A. Bertulani and V.G. Zelevinsky, Phys. Rev. Lett. **71** (1993) 967.

19. J.R. Beene Nucl. Phys., **A569** (1994) 163c.

Microscopic Structure of Spin-isospin Modes in ^{208}Bi

M.N. Harakeh[a], H. Akimune[b], I. Daito[c], Y. Fujita[d], M. Fujiwara[c], M.B. Greenfield[e], T. Inomata[c], J. Jänecke[f], K. Katori[g], S. Nakayama[h], H. Sakai[i], Y. Sakemi[c], M. Tanaka[j] and M. Yosoi[b]

[a]KVI, Zernikelaan 25, 9747 AA Groningen, The Netherlands

[b]Department of Physics, Kyoto University, Kyoto 606, Japan

[c]RCNP, Osaka University, Suita, Osaka 567, Japan

[d]College of General Education, Osaka University, Osaka 560, Japan

[e]Natural Science Division, ICU, Mitaka, Tokyo 181, Japan

[f]Department of Physics, University of Michigan, Ann Arbor, MI 48109-1120, U.S.A.

[g]Department of Physics, Osaka University, Osaka 560, Japan

[h]Department of Physics, Tokushima University, Tokushima, Japan

[i]Department of Physics, University of Tokyo, Tokyo 113, Japan

[j]Kobe Tokiwa Jr. College, Nagata 653, Japan

1. Introduction

A systematic study of the charge-exchange spin-flip collective excitations began in the early eighties making use of the (p,n) charge-exchange reaction at intermediate bombarding energies (100 MeV $< E_p <$ 500 MeV) [1-3]. At these energies, the (p,n) reaction preferentially excites spin-flip states [4-8], such as the Gamow-Teller resonance (GTR) and the spin-flip $\Delta L=1$ resonances that were already predicted earlier [9-11].

The microscopic structure of $\Delta T_Z = -1$ charge-exchange modes, which can be described as a coherent superposition of one-proton particle one-neutron hole configurations, can be investigated by studying their proton decay. The (^{3}He,t$\bar{p}$) reaction has already been used at bombarding energies of $\simeq$ 30 MeV/u to study the structure of the non-spin-flip isobaric analog resonance (IAR) in heavy nuclei [12-14] and the charge-exchange $\Delta L=1$ modes in light nuclei [15,16]. At intermediate energies ($\geq$ 100 MeV/u), the preferential excitation of spin-isospin-flip modes in the (^{3}He,t) reaction [17,18] allows, in conjunction with proton decay, the study of the microscopic structure of these modes.

2. Experimental procedure and data analysis

The experiments were performed at the Research Center for Nuclear Physics (RCNP) in Osaka. A 450 MeV $^3He^{++}$ beam extracted from the ring cyclotron was achromatically transported without any momentum defining slits onto a ^{208}Pb target of 5.2 mg/cm^2 thickness and of 99.86% isotopic enrichment. The ejectile tritons were detected in the spectrometer Grand Raiden [19], which has a K-value of 1400 MeV. The spectrometer was set at $-0.3°$ with vertical and horizontal opening angles of 40 mrad each. The $^3He^{++}$ beam, having lower magnetic rigidity than the tritons, was fully intercepted by a specially designed Faraday cup in the first dipole magnet of the spectrometer. The $^3He^+$ particles, which are formed in the target and have about the same rigidity as the ejectile tritons, served as a calibration for the energy as well as for the scattering angle since they define the 0° spectrometer angle.

The ejectile tritons were detected with the focal-plane detection system which has two 2-dimensional position-sensitive multi-wire drift chambers (MWDC) backed by two ΔE-scintillation counters for particle identification. The horizontal and vertical scattering angles at the target were determined by ray-tracing techniques from the horizontal and vertical positions determined in the two position-sensitive detectors with uncertainties of less than 2 mrad and 10 mrad, respectively. Because of the characteristic angular distributions of the IAR, GTR and spin-flip $\Delta L=1$ resonances at angles near 0°, software cuts on the deduced scattering angles can be used in later off-line analyses to enhance the relative contributions of these resonances in the spectra.

Recently, the results for the GTR and IAR determined from our experiment have been published [20]. In this paper, use was made of the characteristic angular distribution of $\Delta L=0$ transitions, which is sharply peaked at 0°, to enhance their contributions in spectra relative to those of transitions of higher multipolarity and/or continuum background due to the quasi-free, charge-exchange process. Transitions of higher multipolarity have minima in their angular distributions at 0°, and the continuum due to the quasi-free charge-exchange process has a rather flat angular distribution near 0°.

Figure 1 shows two singles spectra where the triton scattering angles have been selected by ray-tracing to be centered at 0° (fig. 1a) and at 1° (fig. 1b). The software gates define horizontal and vertical opening angles of 14 mrad and 20 mrad, respectively. In the spectrum centered at 0°, the $^3He^+$ peak is prominent and also the structure due to the IAR and GTR. These resonances are superimposed on a non-resonant continuum background, which results from quasi-free charge exchange. Figure 1a displays the decomposition into the GTR, IAR and the non-resonant background. The continuum background (dash-dotted curve) has been calculated according to the prescription given in ref. [21]. The total width of the GTR was determined from fitting the GTR in this 0° spectrum [20] to be $\Gamma = 3.75 \pm 0.25$ MeV, and its excitation energy to be 15.63 ± 0.07 MeV. In the spectrum centered at 1°, the $^3He^+$ peak is absent and, moreover, the contributions of the IAR and GTR are reduced in agreement with expectations based on their angular distributions [20]. However, the relative contributions from the $\Delta L=1$ spin-flip excitations (denoted by SDR) are enhanced.

Protons from the decay of the IAR, GTR and SDR were measured in coincidence with tritons in eight solid-state detectors (SSD) arranged in two rings containing 4 SSD's each.

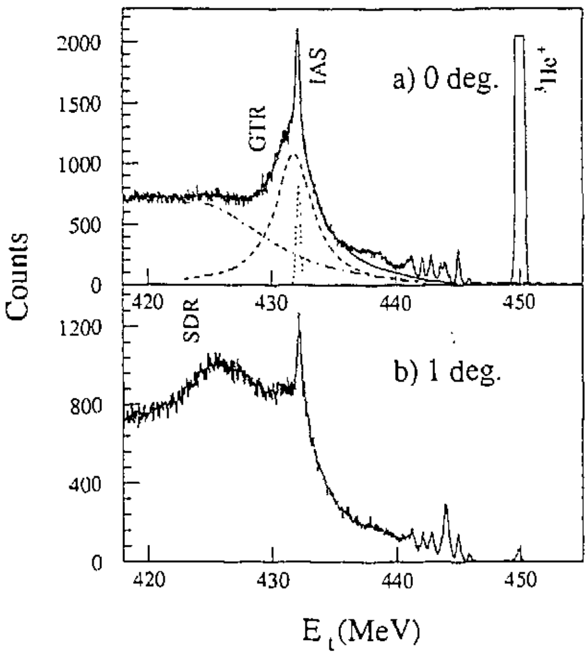

Figure 1. Triton energy spectra from $^{208}Pb(^3He,t)^{208}Bi$ obtained at $E(^3He) = 450$ MeV and at $\theta = 0°$. a) Spectrum gated on the smallest scattering angles near $\theta = 0°$ from -7 to $+7$ mrad horizontally and from -10 to $+10$ mrad vertically. Here, IAS, GTR and $^3He^+$ peak are prominent. The dashed, dotted, and dash-dotted lines represent fits obtained for GTR, IAS, and non-resonant background, respectively. b) Spectrum gated on scattering angles near $\theta = 1°$ with horizontal and vertical opening angles identical to those of fig. 1a. Spin-flip $\Delta L=1$ resonances (denoted by SDR) are enhanced, whereas IAS and GTR are strongly suppressed, and the $^3He^+$ peak is absent.

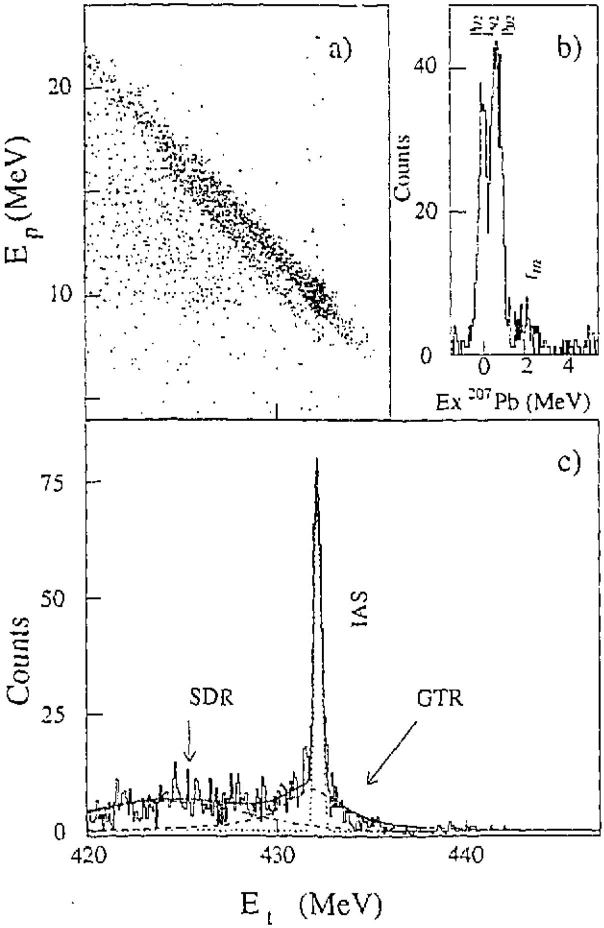

Figure 2. a) Two-dimensional scatter plot of proton energy versus triton energy (or excitation energy in ^{208}Bi) gated on scattering angles centered at 0° (see fig. 1a). The loci indicate decay of states in ^{208}Bi by protons to final neutron-hole states in ^{207}Pb. b) The final-state spectrum of neutron-hole states populated in ^{207}Pb as obtained from projecting loci of fig. 2a onto the ^{207}Pb excitation-energy axis. c) Triton energy spectrum gated on proton decay to neutron-hole states in ^{207}Pb after subtraction of random coincidences. The dashed, dotted, and dash-dotted lines represent the fits obtained for GTR, IAS, and SDR, respectively.

The detectors in the outer ring were at $\theta = 132°$, whereas those in the inner ring were at 157°. The SSD's in both rings were positioned at $\phi = 45°$, 135°, 225° and 315°. The detectors in the outer and inner rings were collimated to subtend solid angles of $\Delta\Omega =$ 57.8 and 47.0 msr, respectively.

Time-of-flight spectra were generated for each SSD by starting and stopping a time-to-digital convertor with timing signals from the focal-plane scintillator and the SSD, respectively. The time spectra (not shown here) had a ratio of prompt to random events of about 10. Two-dimensional scatter plots of proton energy measured in SSD versus excitation energy in ^{208}Bi were generated for prompt and random events by gating on prompt and random peaks in the time spectra. These 2-dimensional spectra were generated with gates on solid angles centered at 0° and 1°. In figure 2, a prompt 2-dimensional spectrum obtained for a gate on the solid angle centered at 0° is shown (fig. 2a). The loci for decay of the IAR, GTR and higher-lying resonances to the ground state (g.s.) and the low-lying neutron-hole states in ^{207}Pb (i.e. $3p_{1/2}$, $2f_{5/2}$, $3p_{3/2}$, $1i_{13/2}$, $2f_{7/2}$) can be observed. The total resolution of the proton and triton sum energy was about 400 keV. This was not sufficient to completely resolve the decay to the 1st and 2nd excited states of ^{207}Pb. This can also be seen in the final-state spectrum obtained by projecting the loci on the excitation-energy axis of ^{207}Pb. This is shown in fig. 2b, which is obtained by gating on the combined region of the GTR and IAR. The various peaks corresponding to decay to neutron-hole states in ^{207}Pb can be clearly observed.

A triton energy spectrum is shown in fig. 2c. This was obtained by gating on decays to neutron-hole states in ^{207}Pb and subtracting random coincidences. It is worth noting that in this spectrum the yield of the IAS relative to that of the GTR is much bigger compared to the singles spectrum because the IAS has a much larger branching ratio for proton decay to ^{207}Pb. At excitation energies higher than that of the GTR, it is observed that the spin-flip ΔL=1 resonances, which are excited even near 0° (after the cut on the core solid angle), also decay by proton emission to the neutron-hole states in ^{207}Pb. This is observed more clearly in spectra generated for scattering angles centered at 1° as discussed below. The continuum due to quai-free charge exchange, leading to emission of protons at very forward angles, is strongly suppressed (and therefore can be neglected) because coincidence is required with protons emitted at very backward angles. Thus the spectrum only contains the three contributions (IAR, GTR, and SDR) mentioned above. The branching ratios and partial proton escape widths can be determined from these spectra as discussed in ref. [20] and below.

In figure 3 the spectrum for triton angles centered at 1° is shown including the decomposition into the GTR, IAR, SDR and the non-resonant background. The continuum background (dash-dotted curve) has been calculated as described above. The total width of the SDR was determined from fitting the IAR, GTR and SDR in this 1° spectrum to be $\Gamma = 8.9 \pm 1.4$ MeV, and its excitation energy to be 21.01 ± 0.05 MeV. The parameters for the IAR, GTR and quasi-free continuum determined from this spectrum were in agreement with those determined from the 0° spectrum.

A final-state spectrum obtained by gating on the solid angle centered at 1° and on the region of the SDR in the singles spectrum (not shown here) shows that the decay pattern for the SDR is different than that for the GTR. A relatively weaker population of the $3p_{1/2}$ and stronger populations of the $1i_{13/2}$ and $2f_{7/2}$ neutron-hole states are observed for

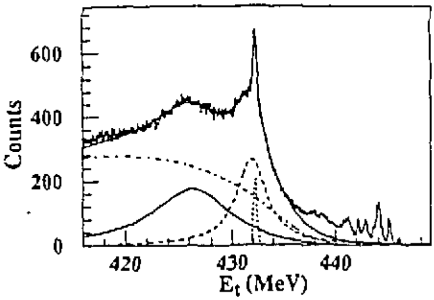

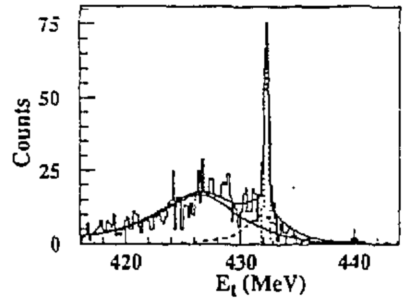

Figure 3. Triton energy spectrum from $^{208}Pb(^3He,t)^{208}Bi$ obtained at $E(^3He) = 450$ MeV and at $\theta = 1°$. The dashed, dotted, solid and dash-dotted lines represent fits obtained for GTR, IAR, spin-flip $\Delta L=1$ resonances (denoted by SDR) and non-resonant background, respectively.

Figure 4. Triton energy spectrum at $\theta = 1°$ gated on proton decay to neutron-hole states in ^{207}Pb after subtraction of random coincidences. The dashed, dotted, and solid lines represent the fits obtained for GTR, IAR, and SDR, respectively (see also fig. 3).

the SDR.

A triton energy spectrum is shown in figure 4. It was obtained by gating on decays to the neutron-hole states in ^{207}Pb and subtracting random coincidences. The yield of the SDR in this spectrum relative to that of the GTR is larger than in the singles spectrum. Furthermore, the continuum due to quasi-free charge exchange is again strongly suppressed because of the coincidence required with protons emitted at very backward angles. Thus this coincidence spectrum again contains only the contributions of the IAR, GTR and SDR.

3. Results and discussion

The total width of the IAR, GTR or SDR can be written as $\Gamma = \Gamma^{\uparrow} + \Gamma^{\downarrow}$, where $\Gamma^{\downarrow}$ is the spreading width. In heavy nuclei, this leads to neutron decay. Statistical decay in the GTR region in ^{208}Bi favours neutron to proton decay by about three orders of magnitude as a consequence of the high Coulomb barrier. $\Gamma^{\uparrow}$ is the escape width connected with the microscopic, one-proton particle, one-neutron hole structure of the GTR. This leads to direct proton decay to the neutron-hole states of ^{207}Pb in the reaction studied here. The escape width can thus be written as

$$\Gamma^{\uparrow} \simeq \Gamma_p^{\uparrow} = \sum_i \Gamma_{p_i}^{\uparrow} \quad , \tag{1}$$

where $\Gamma_{p_i}^{\uparrow}$ is the partial proton escape width associated with decay to the ith neutron-hole state of ^{207}Pb. The ratio of $\Gamma^{\uparrow}$ to the total width Γ can be obtained from the ratios of the coincidence double-differential cross sections to the singles cross section as

$$\frac{\Gamma_{p_i}^{\uparrow}}{\Gamma} = \frac{\int \frac{d^2\sigma_{p_i}}{d\Omega_t d\Omega_p} d\Omega_p}{\frac{d\sigma}{d\Omega_t}} = \frac{4\pi \frac{d^2\sigma_{p_i}}{d\Omega_t d\Omega_p}}{\frac{d\sigma}{d\Omega_t}} \quad . \tag{2}$$

Here, it is implicitly assumed that the double-differential and singles cross sections have been integrated over the excitation energy of the resonance. Since the decay of the GTR and IAR is expected to be isotropic, integrating the double-differential cross section yields a factor of 4π (right hand side of Eq. 2). In the case of the SDR one has to integrate over the observed angular correlation pattern.

The partial proton escape widths of the IAR and the GTR in ^{208}Bi to the $3p_{1/2}$, $2f_{5/2}$, $3p_{3/2}$, and $2f_{7/2}$ neutron-hole states in ^{207}Pb were determined from the measured branching ratios. The latter were determined from the peak areas of the IAR and GTR in the spectrum shown in fig. 2c which is obtained by gating on the various final hole states in ^{207}Pb as described above. For the GTR the proton escape widths are given in column 7 of table 1. Since the resolution was not sufficient to separate the decay to the $2f_{5/2}$ and $3p_{3/2}$ neutron-hole states in ^{207}Pb, the sum of the partial decay widths is given. This was also the case in the earlier experiment [12]. The present results for the IAR: 51.4 ± 5.6 keV ($\Gamma^{\uparrow}_{p_{1/2}}$), 79.4 ± 9.4 keV ($\Gamma^{\uparrow}_{f_{5/2}} + \Gamma^{\uparrow}_{p_{3/2}}$) and 3.5 ± 1.6 keV ($\Gamma^{\uparrow}_{f_{7/2}}$) are in very good agreement with the earlier experimental values [14] of 51.9 ± 1.6 keV, $(26.4 \pm 2.0 + 64.7 \pm 3.4)$ keV and 4.2 ± 0.6 keV, respectively. This nice agreement for the values determined for the IAR lends credence to the extracted values for the GTR which are in complete disagreement with the earlier experimental results listed in column 6. This confirms [22] that the earlier measurement [12] was not able to reliably measure the decay of the GTR due to the weak excitation of the GTR (no GTR bump could be observed) and to proton emission from competing reaction processes.

Table 1
Theoretical and experimental partial and total (escape) proton widths, $\Gamma^{\uparrow}_{p_i}$ and $\Sigma_i \Gamma^{\uparrow}_{p_i}$, in keV for the decay of the GTR in ^{208}Bi into neutron-hole states in ^{207}Pb.

neutron-hole states in ^{207}Pb	E_x [keV]	theor[a]	theor[b]	theor[c]	exp[d]	exp[e]
$3p^{-1}_{1/2}$	0	123.7	114.1	33	570 ±70	58.4 ±11.2
$2f^{-1}_{5/2}$	570	192.8	108.7	18	incl. in $p_{3/2}$	incl. in $p_{3/2}$
$3p^{-1}_{3/2}$	898	239.5	185.1	21	1130 ±300	101.5 ±15.6
$1i^{-1}_{13/2}$	1633	7.1	6.3	0.04	1780 ±500	8.3 ±9.2
$2f^{-1}_{7/2}$	2340	16.6	4.8	0.26	850 ±300	15.6 ±7.4
$1h^{-1}_{9/2}$	3413	7.9	2.9	0.02		
total		587.6	421.9	72.3	~ 4330	184 ±49

[a] ref. [22] obtained with SGII interaction.
[b] ref. [22] obtained with SIII interaction.
[c] ref. [23,24].
[d] ref. [12]; see also ref. [22].
[e] Present experimental results.

Table 2
Recent theoretical partial and total (escape) proton widths, $\Gamma^{\uparrow}_{p_i}$ and $\Sigma_i\Gamma^{\uparrow}_{p_i}$, in keV for the decay of the GTR in ^{208}Bi into neutron-hole states in ^{207}Pb.

neutron-hole states in ^{207}Pb	E_x [keV]	theor[a)]	theor[b)]	theor[c)]	theor[d)]	theor[e)]
$3p^{-1}_{1/2}$	0	111	66	33	43.4	54.5
$2f^{-1}_{5/2}$	570	153	90	18	29.2	47.7
$3p^{-1}_{3/2}$	898	165	99	21	37.7	45.2
$1i^{-1}_{13/2}$	1633	3	3	0.04	0.21	0.20
$2f^{-1}_{7/2}$	2340	27	15	0.26	3.3	3.4
$1h^{-1}_{9/2}$	3413	3	3	0.02	0.07	0.14
total		462	276	72.3	113.9	151.1

a) ref. [26] obtained in TD with SIII interaction.
b) same as a) but proton escape energies and neutron spectroscopic factors taken from experiment.
c) ref. [23,24] obtained in RPA with $g' = 1.2$.
d) ref. [27] same as c) but proton escape energies taken from experiment.
e) same as d) but $g' = 1.4$.

Columns 3-5 display theoretical predictions. Columns 3 and 4 list the partial proton escape widths calculated by Van Giai et al. [22] in the Tamm-Dancoff approximation (TDA) with explicit coupling to the continuum. These calculations were performed within the framework of a self-consistent microscopic theory where the single-particle states and the residual particle-hole interaction are derived from the same Skyrme force. Two different forces were considered, but only that used for the calculations of column 4 yielded an escape width for the IAR compatible with the experimental value. All theoretical results for the GTR, including those obtained by Muraviev and Urin [23,24] in RPA with coupling to the continuum (column 5) do not reproduce the data. Only the theoretically predicted dominance of the decays into the three lowest single-neutron hole states is confirmed by the new data.

It is worth noting that recent calculations by Udagawa et al. [25], Coló et al. [26] and Muraviev and Urin [27] showed good to reasonable agreement with the experimental results. The recent results of Coló et al. and Muraviev and Urin are given in table 2. Coló et al. calculated the various characteristics of the GTR in TDA with explicit coupling to the continuum. The results obtained with the SIII Skyrme force are given in column 3. These are similar to the earlier results given in column 4 of table 1. However, when the experimental proton escape energies and spectroscopic factors for neutron pickup from ^{208}Pb were used better agreement with the experimental results was obtained (column 4). The older results of Muraviev and Urin obtained in RPA with coupling to the continuum and with the strength of the Landau-Migdal force given by $g' = 1.2$ are reproduced in column 5. Better agreement with the experimental results is obtained when the experimental proton escape energies are used (column 6) and the agreement becomes almost perfect when the strength parameter of the Landau-Migdal force is chosen $g' = 1.4$. The implications of this are not clear, however.

For the decay of the SDR in ^{208}Bi, the partial proton escape widths to the various neutron-hole states in ^{207}Pb have not been determined nor have the various spin components (2^-, 1^- and 0^-) of the SDR been disentangled using their angular correlation patterns. However, one can infer from the final-state spectra (not shown here) that the population pattern of the various neutron-hole states is different for the SDR than that for the GTR, in that the $1i_{13/2}$ and $2f_{7/2}$ are more strongly and the $3p_{1/2}$ more weakly populated. Furthermore, the total proton decay branching ratio has been determined from the coincidence spectra to be $14.6 \pm 1.3\%$. If assumed to be due to decay of one single resonance with a width of 8.9 MeV, this would lead to a total proton escape width of 1.30 ± 0.23 MeV. However, the SDR bump consists of three spin components, i.e. 2^-, 1^- and 0^-. Even if one considers that the total proton escape width determined above should be divided among these three components, the resulting proton escape width per component is still considerably larger than for the GTR. This has to do with the increase of the proton energy available above the Coulomb barrier and also the average decrease of the angular-momentum barrier for the decay protons as compared to the GTR. Indications also appear for proton decay to the $1h_{9/2}$ broad neutron deep-hole state in ^{207}Pb.

REFERENCES

1. D.E. Bainum et al., Phys. Rev. Lett. 44 (1980) 1751.
2. C.D. Goodman et al., Phys. Rev. Lett. 44 (1980) 1755.
3. D.J. Horen et al., Phys. Lett. B95 (1980) 27.
4. F. Petrovich and W.G. Love, Nucl. Phys. A354 (1981) 499c.
5. N.S.P. King et al., Phys. Lett. B175 (1986) 279.
6. W.P. Alford et al., Phys. Lett. B179 (1986) 20.
7. T.N. Taddeucci et al., Nucl. Phys. A469 (1987) 125.
8. B.S. Flanders et al., Phys. Rev. C 40 (1989) 1985.
9. K. Ikeda, S. Fujii and J.I. Fujita, Phys. Lett. 3 (1963) 271.
10. J.I. Fujita and K. Ikeda, Nucl. Phys. 67 (1965) 145.
11. H. Ejiri, K. Ikeda and J.I. Fujita, Phys. Rev. 176 (1968) 1277.
12. C. Gaarde et al., Phys. Rev. Lett. 46 (1981) 902.
13. H.J. Hofmann et al., Nucl. Phys. A433 (1985) 181, and references therein.
14. S.Y. van der Werf, M.N. Harakeh and E.N.M. Quint, Phys. Lett. B216 (1989) 15, and references therein.
15. W.A. Sterrenburg et al., Nucl. Phys. A405 (1983) 109.
16. W.A. Sterrenburg et al., Nucl. Phys. A420 (1984) 257.
17. C. Ellegaard et al., Phys. Rev. Lett. 50 (1983) 1745.
18. I. Bergqvist et al., Nucl. Phys. A469 (1987) 669.
19. M. Fujiwara et al., Nucl. Instr. Meth. Phys. Res. A, (to be published).
20. H. Akimune et al., Phys. Lett. B323 (1994) 107.
21. J. Jänecke et al., Phys. Rev. C 48 (1993) 2828, and references therein.
22. N. Van Giai et al., Phys. Lett. B233 (1989) 1.
23. S.E. Muraviev and M.G. Urin, Nucl. Phys. A569 (1994)267c.

24. S.E. Muraviev and M.G. Urin, Nucl. Phys. A572 (1994)267.
25. T. Udagawa et al., Nucl. Phys. A (in print).
26. G. Coló et al., elsewhere in these proceedings, and to be published.
27. S.E. Muraviev and M.G. Urin, elsewhere in these proceedings.

FRAGMENTATION AND SPLITTING OF GAMOW-TELLER RESONANCES IN Sn(^{3}He,t)Sb CHARGE-EXCHANGE REACTIONS, A=112 to 124

J. Jänecke,[a] H. Akimune,[b] G. P. A. Berg,[c] S. Chang,[c] B. Davis,[d] M. Fujiwara,[e] M. N. Harakeh,[f] J. Liu,[c] K. Pham,[a] D. A. Roberts,[a] E. J. Stephenson[c]

[a] Department of Physics, Ann Arbor, Michigan 48109, U.S.A.
[b] Kyoto University, Kyoto 606, Japan
[c] Indiana University Cyclotron Facility, Bloomington, Indiana 47408, U.S.A.
[d] University of Notre Dame, Notre Dame, Indiana 46556, U.S.A.
[e] Research Center for Nuclear Physics, Osaka University, Osaka 567, Japan
[f] Kernfysisch Versneller Instituut, 9747AA Groningen, The Netherlands

The (^{3}He,t) charge-exchange reaction has been investigated with a magnetic spectrometer at E(^{3}He) = 200 MeV and angles near $\Theta = 0°$ on essentially all stable Sn targets with an energy resolution of 80−100 keV. Fragmentation of the Gamow-Teller resonance into three to four major components of the particle-hole type has been observed over the entire range of Sb isotopes. These components are often refered to as direct, core-polarization, and back-spin-flip. The excitation energies of the most collective main Gamow-Teller resonances of 1 to 3 MeV above the respective isobaric analog states decrease with neutron excess. They seem to display the influence of the filling of the $1h_{11/2}$ neutron orbit in the target nuclei. The widths are $\Gamma \approx 5-6$ MeV. The "pygmy" resonances are located below the isobaric analog states, and they show a systematic energy dependence as well. They display further substructures and are split into typically eight strong fragments which presumably represent doorway states. Low-lying 1^+ states (the ground states in ^{118,120}Sb) and corresponding $1/2^+$ states in ^{117,119}Sb are strongly excited and display a systematic pattern.

1. Introduction

The existence of collective 1^+ states with structures related to isobaric analog states (IAS) has been predicted many years ago [1]. This was followed by extensive experimental studies using the (p,n) charge-exchange reaction in the eighties [2,3,4]. Properties of Gamow-Teller resonances (GTR) have been investigated in subsequent years in great detail supplemented more recently by investigations using the (^{3}He,t) charge-exchange reaction with its increased detection efficiency and energy resolution.

Fragmentation and splitting of the Gamow-Teller strength in the Sb isotopes into three (or more) fragments has also been predicted early using a quasi-classical treatment [5]. High-lying 1^+ states with maximum collectivity are mainly associated with excitations of neutrons into the proton orbits of the spin-orbit-partner, $j = \ell + \frac{1}{2} \rightarrow j = \ell - \frac{1}{2}$. The energy differences E_x(GTR) − E_x(IAS) for these GTR in medium-heavy nuclei are expected to be on the order of a few MeV but should decrease with increasing neutron excess and mass. So-called "pygmy" resonances sometimes described in the literature as $j \rightarrow j$ core-polarization and (only in neutron-rich nuclei) $j = \ell - \frac{1}{2} \rightarrow j = \ell + \frac{1}{2}$ back-spin-flip components are expected at lower excitation energies. This fragmentation into three or more components has been observed recently [6] in the (^{3}He,t) charge-exchange reaction on targets of ^{117}Sn and ^{120}Sn.

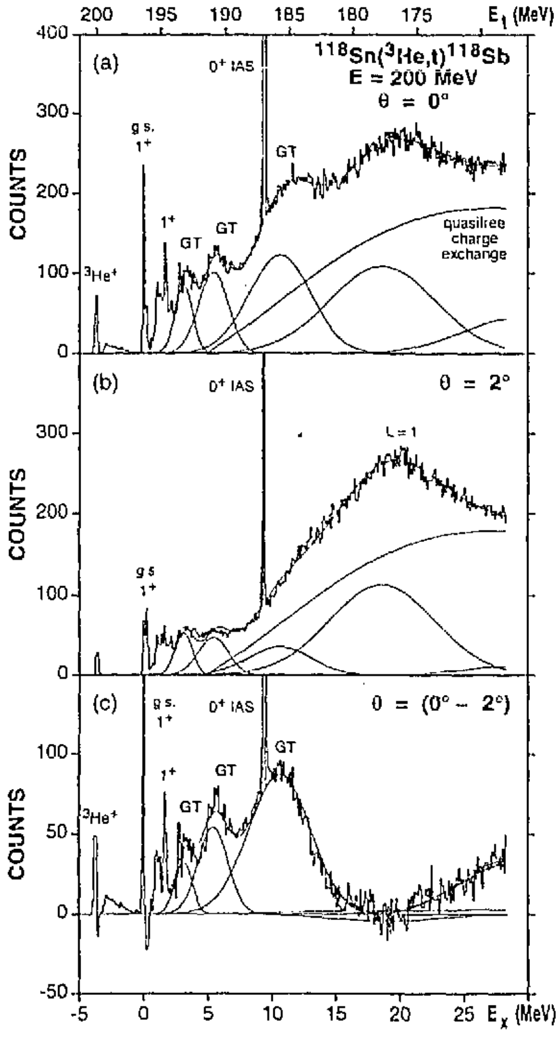

Fig. 1. Triton energy spectra for $^{118}Sn(^3He,t)^{118}Sb$ at $E(^3He)$ = 200 MeV and (a) $\Theta \approx 0°$, and (b) $\Theta \approx 2°$. Spectrum (c) is the difference spectrum ($\Theta \approx 0° - 2°$).

A splitting of the most collective main GTR for Ge and Sn targets into two components has also been predicted theoretically [7]. For the Sb isotopes this splitting should be most pronounced near ^{118}Sb at the onset of the filling of the $1h_{11/2}$ neutron orbit in the ground states of the Sn targets. This splitting could not be observed experimentally for the targets of ^{117}Sn and ^{120}Sn [6] possibly due to the fact that the total widths $\Gamma \approx 5-6$ MeV exceeds the predicted splitting.

It was the purpose of the present investigation to study the various effects systematically with the (^{3}He,t) charge-exchange reaction at E(^{3}He) = 200 MeV near $\Theta = 0^\circ$ with good energy resolution over the entire range of stable Sn targets from A = 112 to A = 124.

2. Experimental procedures and results

The experiment was carried out at the Indiana University Cyclotron Facility (IUCF) with the K600 high-resolution magnetic spectrometer at E(^{3}He) = 200 MeV near $\Theta = 0^\circ$. Isotopically enriched targets were used. The ray-tracing capabilities permit the simultaneous measurement of triton spectra centered near 0° and 2°. The sharp decrease in cross section for $\Theta > 0^\circ$ provides a powerful signature for L=0 transitions since non-resonant background and other resonances change much more weakly with angle. Difference spectra for 0° minus 2° are therefore very sensitive to L=0 contributions. This conclusion becomes immediately apparent from Fig. 1 which displays as an example triton energy spectra measured for ^{118}Sn(^{3}He,t)^{118}Sb at $\Theta = 0^\circ$ and 2° and their difference. The main GTR, two or three lower components including discrete low-lying 1^+ states (including the ground state) are seen in addition to the 0^+ IAS. The spectra also show a higher-excited L=1 resonance and non-resonant background which cancel to a large extent in the difference spectrum. Also included in the figure is the decomposition of the observed spectra into non-resonant background from quasi-free charge exchange and from the various resonances. Spectra measured for the other targets display very similar characteristics. Only the spectra for the ^{114}Sn target which had lowest isotopic abundance of 71 % showed pronounced contributions from heavier Sn isotopes which have more positive Q-values. However, clean ^{114}Sn(^{3}He,t) spectra could be obtained by subtracting properly normalized contributions from the ^{116,118,120}Sn contaminants.

Fig. 2 displays the same three spectra for the ^{118}Sn target but with expanded energy scales for the region of low excitation energies. The energy binning has also been reduced to permit the observation of fine structures. Numerous L=0 transitions, presumably 1^+ states, are seen. Interestingly, the five lowest states observed in ^{116}Sb (not shown) can be identified with known 1^+ states. The transition to the 1^+ ground state in ^{118}Sb seen in the figure is particularly strong; there are states clustered in the range from 1 to 2 MeV; there are states clustered in the regions of the pygmy resonances near 3 MeV and 5.5 MeV (labeled GT3 and GT2, respectively). Only one state close to the ground state is clearly identified with L≠0. No such fine structure is present for the main GTR. The systematics of these structures will be discussed below. Very similar characteristics have been observed for all even-A targets and with minor differences also for the two odd-A targets.

3. Discussion

Fig. 3 displays as function of A the excitation energies and total widths (indicated by the error bars) of the three Gamow-Teller resonances including the main resonance and the two lower components. The energies are given relative to the excitation energies of the respective isobaric analog states (IAS). Also shown in the figure are the strong 1^+ ground states (in ^{118,120}Sb) or low-excited states (in ^{112,114,116,122,124}Sb) in the even-A Sb isotopes and the

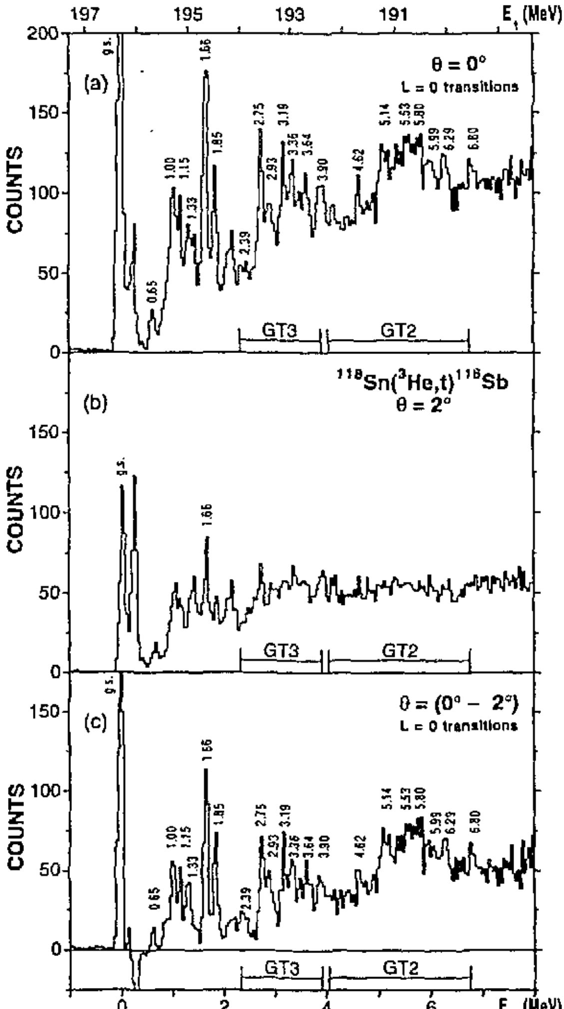

Fig. 2. Triton energy spectrum similar to Fig. 1 but with expanded scales for low excitation energies and reduced binning of channels.

corresponding $1/2^+$ (or $3/2^+$) states in the two odd-A isotopes (in ^{117,119}Sb). There is no indication for a doublet for odd A, and the strong state seen in ^{117}Sb is a known $1/2^+$ state. The heavy dashed line represents the energies of the ground states which display odd-even staggering due to pairing. The lighter dashed lines represent the limits below which neutron or proton emission are energetically not possible. The (upper) neutron line confirms the known fact that isospin-forbidden neutron decay from IAS is energetically not possible [8] for $A \leq 115$. Essentially all pygmy resonances are stable with respect to (allowed) neutron as well as proton emission.

The excitation energies for all three Gamow-Teller components relative to the energies of the IAS display a systematic dependence on neutron excess. This includes the odd-A isotopes. The energies decrease with increasing neutron excess as expected, and they follow crudely the trend already suggested in Ref. [5]. For ^{117}Sb and ^{120}Sb the energies are also in reasonable agreement with those calculated by Urin *et al.* (see Ref.[6]). The main GTR have total widths of $\Gamma \approx 5-6$ MeV, whereas the widths of the pygmy resonances are significantly smaller. The splitting of the pygmy resonances into individual states as shown in Fig. 2 is present for all targets, and it also displays a general trend. It is more pronounced for the light Sb isotopes where the threshold for neutron emission is higher than for the heavy isotopes. This splitting into typically about 8 components is believed to depend on the coupling to 2-particle/2-hole doorway states. The splitting is most pronounced at low excitation energies which may reflect upon the dependence on the density of doorway states. The substructures are also much less pronounced for the odd-A resonances, and no splitting is observed for the main GTR.

The systematic dependence of the excitation energies of the low-lying 1^+ states ($1/2^+$ states in the odd-A isotopes) on neutron excess is striking. The energies for the even-A and odd-A isotopes follow an almost straight line, except that the energies for the odd-A isotopes are displaced downward by about 200 keV. Clearly, all these states must be related and have a similar nuclear structure, possibly excitations from the essentially full $2d_{5/2}$ or $1g_{7/2}$ neutron orbits leading to particle-hole configurations of the type $(1g_{7/2})(2d_{5/2})^{-1}$ or $(2d_{5/2})(1g_{7/2})^{-1}$. Interestingly, only one state is observed in the odd-A cases, apparently a $1/2^+$ state, and not a $(1/2^+, 3/2^+)$ spin doublet as one might expect.

Special attention is given to the excitation energies of the main GTR. The measured excitation energies are displayed on an expanded scale in Fig. 4 as filled circles. Related more limited data for ^{112,116,124}Sn(p,n) at E(p)=200 MeV [4] have been reported earlier with similar results, and data for ^{114,116,118,120,122,124}Sn(^{3}He,t) at E(^{3}He)=450 MeV have become available very recently [9]. The experimental excitation energies decrease with increasing neutron excess. The initial fast decrease for the light isotopes is followed by a much slower decrease.

Also included in Fig. 4 are calculated energies. Two essentailly straight lines are obtained by connecting the calulated values (small open circles) from the work of Guba, Nikolaev, and Urin [7]. The lower line represents the calculated GTR based on the excitation of all possible particle-hole configurations excluding the $1h_{11/2} \rightarrow 1h_{9/2}$ excitation. The neutron occupation probabilities for the $1h_{11/2}$ neutron BCS wave functions in the ground states of the Sn isotopes are very small for the light isotopes, and this curve should therefore represent the energy dependence of the GTR in this region.

The upper line for the heavy isotopes represents the calculated GTR based on all particle-hole configurations including $1h_{11/2} \rightarrow 1h_{9/2}$. A transition from the lower to the upper curve is expected due to the gradual filling of the $1h_{11/2}$ neutron orbit in the target nuclei. Furthermore, in the transition region near the onset of the filling of this orbit centered at ^{118}Sn, a configuration splitting of the GTR is predicted [7] due to constructive and destructive interference with the $(1h_{9/2})(1h_{11/2})^{-1}$ component. A gradual transition in strength from the lower to the upper component should take place. However, no such splitting was observed earlier in

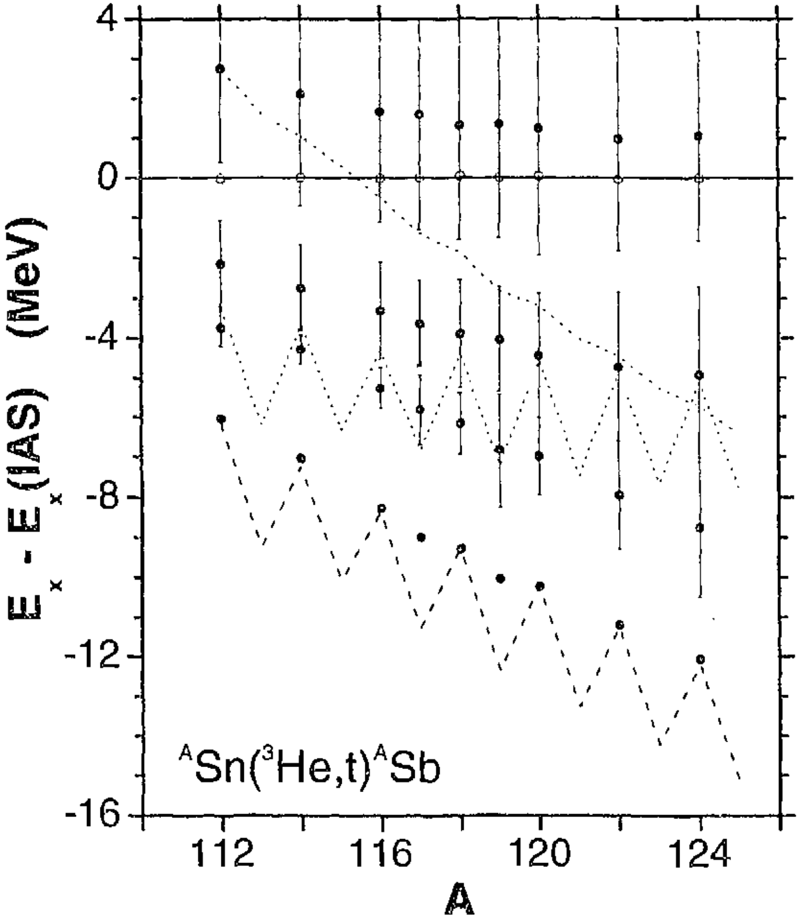

Fig. 3. Experimental excitation energies relative to the isobaric analog states for the three components of the GTR as function of nucleon number. The "error bars" in this figure (only) represent the measured total widths Γ of the resonances. The low-lying 1^+ states in the even-A isotopes and $1/2^+$ states in the odd-A isotopes are also shown. The heavy and light dashed lines represent the energies of the ground states and the neutron and proton separation energies, respectively.

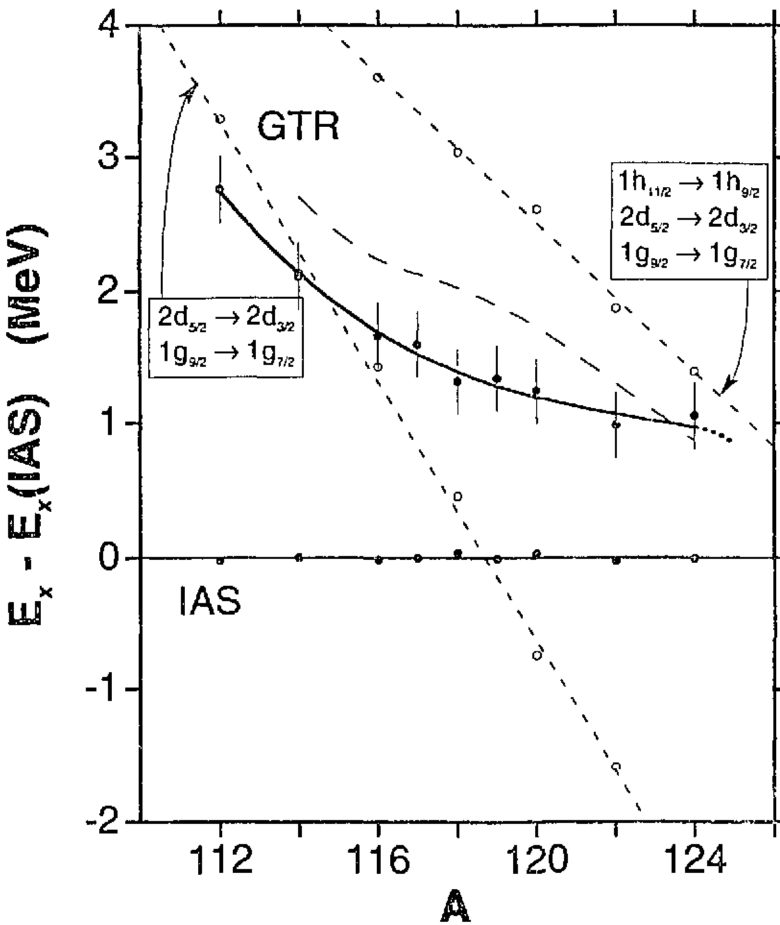

Fig. 4. Experimental excitation energies relative to the isobaric analog states for the main component of the GTR as function of nucleon number. The heavy solid line is to guide the eye. The dashed straigth lines represent the theoretical predictions [7] for this component without (lower line) and with (upper line) the inclusion of mixing with *the the* $1h_{11/2} \rightarrow 1h_{9/2}$ particle-hole configuration. The curved dashed line is the calculated centroid energy.

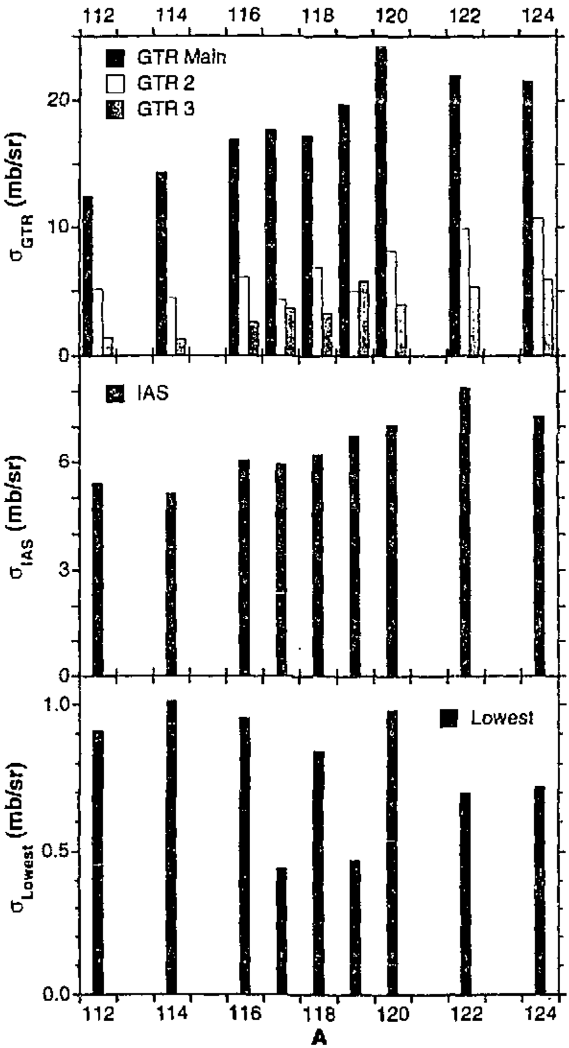

Fig. 5. Cross sections for the transitions to the three components of the GTR (top), the isobaric analog states (middle), and low-lying 1^+ and $1/2^+$ states (bottom) as function of the nucleon number.

the investigation [6] of the ^{117,120}Sn(^{3}He,t) reactions, and no such splitting was observed in the present experiment involving all Sn targets. This result may be due to the fact that the total widths of $\Gamma \approx 5-6$ MeV of the GTR exceed the predicted splitting.

However, the observed excitation energies (centroid energies) of the GTR seem to display the influence of the filling of the $1h_{11/2}$ neutron orbit in the target nuclei. Based on the energies of the two calculated components and their relative strengths [7], the curved dashed line was obtained. It represents the calculated centroid energies. The measured centroid excitation energies display the transition from the lower to the upper curve similar to the predicted behavior. Furthermore, a weak increase observed for the total widths Γ in the region A = 116−120 is compatible with widths expected from two components separated by 2−3 MeV.

The observed centroid energies and total width of the L=1 resonances (not shown) follow a similar systematic trend for both even-A and odd-A nuclei with the excitation energies decreasing from 11 to 8 MeV and $\Gamma \approx 10$ MeV. The increased excitation energies reflect upon the shell crossing associated with L=1. Interestingly, the excitation energies appear to be similar for the giant electric dipole resonances and the spin-dipole resonances suggesting a near degeneracy as observed earlier for the 1^- component in ^{12}N.

Bar diagrams for some of the observed 0° cross sections are displayed in Fig. 5. The top diagram gives the values for the three components of the GTR. Clearly, the cross section for the main component dominates, and all three cross sections display a weak increase with neutron excess. This is also the case for the cross sections leading to the IAS (middle). If the reaction mechanisms for the transitions to the main component of the GTR with maximum collectivity and the IAS are assumed to result from pure charge-exchange spinflip and non-spinflip interactions with interaction energies $V_{\sigma\tau}$ and V_τ, respectively, then the Gamow-Teller and Fermi strengths, B(GT) and B(F), become proportional to the differential cross sections at $\Theta = 0°$ [10]. Assuming B(F) = N−Z for the IAS, it becomes possible to estimate the Gamow-Teller strengths. For the main component of the GTR, B(GT) was found consistently to be $\sim 65\%$ of the sumrule of 3(N−Z) in approximate agreement with calculated values of $\sim 80\%$ [7]. However, if the expected quenching (e.g. Ref. [11]) of the GT strength is considered, both the experimental and the calculated values may represent overestimates.

Using the observed 0° cross sections for the other two GT components and for the energetically low-lying 1^+ states, it became apparent that the above procedure leads to significant overestimates of B(GT). This is particularly apparent for the transitions to the 1^+ ground states of ^{118}Sb and ^{120}Sb where reliable B(GT) values can be deduced from the β^+ decays of these ground states into the respective 0^+ ground states in Sn. The enhanced cross section probably result from the fact that at our bombarding energy of E(^{3}He) = 200 MeV, or 65 MeV/u, there are still significant contributions from the tensor charge-exchange interaction $V_{T\tau}$. These contributions appear to lead to constructive interference which enhances the transitions to the pygmy resonances and the low-lying 1^+ states, particularly if the wave functions contain components as decribed above. This interference effect seems to make the observation of these lower components and states possible. However, the extraction of Gamow-Teller strength B(GT) is more involved and has to wait for the analysis of our ^{12,13,14}C(^{3}He,t)^{12,13,14}N data and the determination of the interaction energies V_τ, $V_{\sigma\tau}$, and $V_{T\tau}$,

The lowest bar diagram in Fig. 5 displays the cross sections for the low-lying 1^+ and $1/2^+$ states. It is interesting to note that the cross sections for the odd-A cases display a behavior reminiscent of Pauli blocking seen in (p,t) and (d,α) reactions.

Cross sections were also determined for the non-resonant background. This background is based on the quasi-free charge-exchange reaction on bound neutrons. The cross sections can be compared to the charge-exchange reaction on the free neutron. Following the procedures outlined in Ref. [6], it was found that typically 14 to 22 neutrons or about 85 % of the excess neutrons participate in the quasi-free process at this bombarding energy. Given the uncertainties for these cross sections, the agreement with the occupation probabilities observed in electron-induced proton knockout from valence shells of $\sim 70\%$ is quite satisfactory [12].

Non-resonant background from the breakup/pickup reaction [6] occurs only at higher effective excitation energies and was not observed in the present experiment.

4. Summary

A comprehensive study of the (^{3}He,t) reaction on essentially all stable Sn isotopes has been performed at E(^{3}He)=200 MeV near $\Theta = 0°$. Difference spectra for the angles $\Theta = 0°$ and 2° are very sensitive to the presence of transitions with angular momentum transfer L=0. Interference between the transition strengths from spin-flip charge exchange and the non-central tensor charge exchange leads to enhanced cross sections for low-lying particle-hole components. The Gamow-Teller resonance is strongly excited as well as several fragments at lower excitation energies (pygmy resonances). The energy dependence of the main GTR on neutron excess reflects upon the filling of the $1h_{11/2}$ neutron orbit in the Sn target nuclei. Configuration splitting near the onset of the filling of this orbital has been predicted theoretically but was not observed probably due to the fact that the total widths exceed the predicted splitting. Essentially all pygmy resonances were found to display substructures and to be strongly fragmented into typically eight components. These components are interpreted as doorway states, and the observed characteristics seem to reflect upon the variation of the density of these states. Neutron and proton emission from the pygmy resonances is strongly hindered or forbidden on account of energy systematics. A systematic energy and cross section dependence was observed for strong 1^+ ground or very low-excited states in all even-A Sb isotopes together with corresponding $1/2^+$ states in the odd-A Sb isotopes.

Acknowledgements

The authors acknowledge the support by the technical staff of the IUCF and in particular by C. C. Foster and W. R. Lozowski as well as helpful discussions with M. H. Urin, K. T. Hecht and F. D. Becchetti. This research was supported in part by the National Science Foundation Grant Nos. PHY-8911831 and PHY-9208468. The travel grant No. 90-0219 provided by the Scientific Affairs Division, North Atlantic Treaty Organization, is gratefully acknowledged.

[1] K. Ikeda, S. Fujii, and J. I. Fujita, Phys. Lett. **3B**, 271 (1963).
[2] D. E. Bainum *et al.*, Phys. Rev. Lett. **44**, 1751 (1980)
[3] C. D. Goodman *et al.*, Phys. Rev. Lett. **44**, 1755 (1980).
[4] D. J. Horen *et al.*, Phys. Lett. **95B**, 27 (1980).
[5] Yu. V. Gaponov and Yu. S. Lyutostanskii, Yad. Fiz. **19**, 62 (1974); Yad. Elem. Chastits Yadra **12**, 1324 (1981).
[6] J. Jänecke *et al.*, Phys. Rev. C **48**, 2828 (1993); Nucl. Phys. **A526**, 1 (1991).
[7] V. G. Guba, M. A. Nikolaev, and M. H. Urin, Phys. Lett. **218**, 283 (1989); M. H. Urin, private communication.
[8] J. Jänecke, J. A. Bordewijk, S. Y. van der Werf, and M. N. Harakeh, Nucl. Phys. **A552**, 323 (1993).
[9] M. Fujiwara, private communication.
[10] T. N. Taddeucci *et al.*, Phys. Rev. C **25**, 1094 (1981).
[11] F. Osterfeld, Rev. Mod. Phys. **64**, 491 (1992) and references therein.
[12] L. Lapikas, Nucl. Phys. **A553**, 297c (1993).

Electromagnetic excitation of the two-phonon giant dipole resonances

R. Kulessa
Institute of Physics, Jagellonian University, Kraków , Poland

1. Introduction

The existence of giant resonances dates back to the 1940-ies, when they were first predicted theoretically by Migdal in 1944 [1] and proved experimentally as a resonant photo-absorption by Baldwin and Klaiber in 1947/48 [2]. In the last almost 50 years the giant resonances appeared to be a general property of all nuclei throughout of the periodic table. The best known giant resonance is the giant dipole resonance (GDR). In the hydrodynamic collective model the nucleus is described as a classical liquid drop with a fixed surface consisting of two incompressible fluids. The GDR is described as the vibration of the neutron fluid against the proton fluid. It is now experimentally proven that giant dipole resonances are built not only on the ground state, but also on excited nuclear states and exist in fast rotating nuclei [3]. They may be also built on top of each other forming multiphonon excitations. In this short presentation I will not refer to many other high energy collective excitations as e.g isoscalar and isovector electric quadrupole resonance or the giant monopole resonance. Many detailed review articles may be found in the literature [3,4,5]. The status of very recent investigations on giant resonances was presented in the 1993 Gull Lake Nuclear Physics Conference on Giant Resonances [6]. The natural way of excitation of GDR is the photoabsorption process. The energy dependence of the photoabsorption cross section in spherical nuclei can be parametrized using a lorentzian form;

$$\sigma_{phot}(E) = \frac{2 \cdot \sigma_{tot}}{\pi\Gamma(1 + (E^2 - E_r^2)^2/E^2\Gamma^2}.$$

E_r is the energy of the maximal absorption cross-section. The total photoabsorption cross-section is usually compared to the TRK (Thomas-Reiche-Kuhn) [7] sum rule:

$$\int \sigma_{phot}(E)dE = \frac{2\pi^2 e^2}{mc}\frac{NZ}{A} = 60\frac{NZ}{A}[MeV \cdot mb],$$

where m is the mass of the nuclei.
The dependence of other integral parameters describing the GDR as e.g the resonance shape center energy on the mass number is in general very well known. The dependence of the width on the mass number is not so evident. In deformed nuclei a splitting of the GDR is observed, which is dependent on the nuclear deformation.

Very recently an extensive review of experimental evidence on the two-phonon excitation of the GDR was given by H. Emling [8]. In this review the theoretical background for the excitation of double giant dipole resonance (DGDR) can be found.

In the last years intermediate and high energy heavy ion beams have provided improved conditions for excitation of giant resonances. Large cross-sections observed in excitation of GDR using heavy ions make highly probable the excitation of higher phonon states. If one assume, that GDR obeys the condition of harmonic vibration, it may happen, that an excitation occurs when the nucleus vibrates in the GDR region, leading to a double or even higher-order phonon excitation. According to the harmonic approximation, the excitation energy should then be proportional to the number of excited phonons, giving an equidistant excitation spectrum. For a lorentzian description of the shape of the GDR, the width of the multi-phonon states (Γ_{nGDR}) will be a simple multiplication of GDR width (Γ_{GDR}) with the number of phonons n, $\Gamma_{nGDR} = n \cdot \Gamma_{GDR}$, provided an assumption of independent phonons is valid. Under this assumption the electromagnetic decay rate is obtained by summing the decay rate of individual phonons, as it was shown by Bohr and Mottelson [9]

$$\sum_{\xi_{n-1}, I_{n-1}} B(E\lambda; n, \xi_n, I_n \rightarrow n-1, \xi_{n-1}, I_{n-1}) = n \cdot B(E\lambda; n=1 \rightarrow n=0).$$

where I_n denote the phonon spin and ξ_n additional quantum numbers.

The largest amount of experimental data concerning the excitation of DGDR states was obtained by (π^+, π^-) and (π^-, π^+) pion double charge exchange reaction on several targets ^{40}Ti [10], ^{93}Nb [10], ^{115}In [11], ^{138}Ba [10] and ^{197}Au [11]. The measured cross section was usually of an order of a few microbarns. Much higher cross-sections up to several hundreds of milibarns may be obtained by electromagnetic excitation with relativistic heavy ions. This excitation process can be understood as absorption of intense virtual photons [12] created according to the Weizsäcker Williams approach (see e.g [13]) by the rapidly changing electromagnetic field as a heavy ion passes the target with relativistic energies. It was shown [12], that this approach is equivalent to the semiclassical perturbation approach used since many years in Coulomb excitation description [14]. At high bombarding energies ($\geq 1A{\cdot}GeV$) high-lying collective nuclear states can be excited, due to high-frequency Fourrier components of the virtual photon field. The maximum energy transferred to the nucleus can be calculated from the cut-off energy

$$E_m = \frac{\hbar\beta\gamma}{b_{min}} \approx 200\frac{\beta\gamma}{R_1 + R_2},$$

where the minimum internuclear distance $b_{min} \approx R_1 + R_2$ was introduced, and $\beta = v/c, \gamma = 1/\sqrt{1-\beta^2}$. This cut-off energy is strictly related to the mean interaction time Δt, that means to the width of the transversal electric field component acting on the target nucleus. This interaction time should be short compared to the relaxation time of the excited nuclear state. If one derive the relaxation time from the width of the giant resonances, which are of the order of a few MeV, at a bombarding energy of $1\ A \cdot GeV$ the interaction time is one order of magnitude shorter than the relaxation time.

Results of calculations of cross-sections for excitation of multiphonon giant resonances based on the semi-classical perturbation theory, can be found in ref. [8].

Meanwhile a number of experiments was carried out using heavy ion beams in order to search for multiphonon giant resonance excitations [6].

In the following I will present the results obtained for the electromagnetic excitation of the double giant dipole resonance in ^{136}Xe and ^{208}Pb obtained by the Large Area Neutron Detector [LAND] collaboration [15].

2. Excitation of multiphonon states

2.1. The experiment

The experimental method was developed to measure the projectile excitation rather than of the targets, making use of the kinematically focusing of the excited projectile nuclei into a narrow forward cone. This allows to construct a detection system covering a substantial part of the solid angle and having an efficiency close to unity. It allows exclusive measurements of the electromagnetic excitation process and the subsequent decay. In our case the main attention was devoted to the neutron decay channel. A schematic view of the experimental setup is shown in Fig. 1. The setup allows the

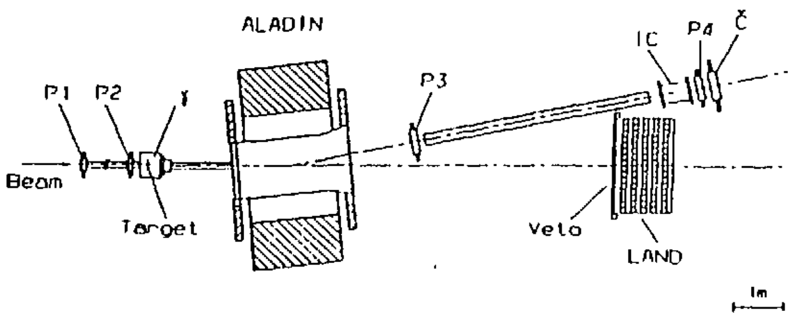

Figure 1: Schematic view of the experimental setup [16]. Shown are the beam and fragment detectors (P1-P4) including an ionization chamber (IC) and a Cherenkov detector (Č), the dipole magnet (ALADIN), the γ-detector array (γ), and the neutron detector (LAND, Veto).

tracking of the projectile and of the heavy fragments emerging from the target by a set of position-sensitive multi-wire gas counters and plastic detectors. This detectors are also delivering an accurate time-of-flight information. An ionisation chamber and Cherenkov detector is used to determine the charge of the heavy fragment. The charged fragments are deflected in a large dipole magnet allowing an unperturbed measurement of the neutron around 0°. Also neutrons emitted from the excited fragments can reach the neutron detector. The LAND having dimensions 2x2 m is placed 10 m after the target. The detector has a modular structure allowing accurate position and time-of-flight measurements of the registered neutrons. In front of LAND a charged particle veto detector is placed. In addition to the particle detectors an array of BaF_2 scintillation counters surrounding the target allows the total γ-ray energy determination.

This information together with the momenta of fragments and neutrons are used to determine the differential cross section with respect to the excitation energy of the projectile by reconstructing the final state invariant mass,

$$M^2 = (m_{proj} + E^*)^2 = (\sum_j P_j)^2.$$

P_j denotes the 4-momenta of fragment and neutrons, m_{proj} and E^* denote the ground state mass and excitation energy, respectively. For the used experimental technique all requirements concerning the invariant mass reconstruction were fulfilled allowing for an overall resolution of σ_{E^*} of ≈ 2 MeV. More details of the experimental method and of the data analysis are described in Ref. [16].

2.2. Excitation of double giant dipole resonance

Two experiments of this type were performed by the LAND collaboration; for the semi-magic nucleus $^{136}_{54}Xe$ (published in Ref. [16]) at 700 $A \cdot MeV$ bombarding energy using Pb and C targets, and for the doubly magic $^{208}_{82}Pb$ nucleus at 650 $A \cdot MeV$ with C, Sn, Gd, Pb and U targets, respectively. Preliminary results of the ^{208}Pb experiment with the Pb target was published in Ref. [18]

2.2.1. Excitation spectrum for ^{136}Xe

For the ^{136}Xe projectile the invariant mass reconstruction was performed for the 1n- to 3n removal channels [16]. The resulting excitation energy spectra obtained with Pb and C targets are shown in Fig. 2.

The total energy integrated cross section was determined as 1.85(10) barn. The comparison of the Pb and C spectra proofs, that the nuclear interaction contribution to the total cross section may be disregarded. Consequently the spectrum obtained for the Pb target was analyzed in terms of electromagnetic excitations. For the Pb target a dominant structure centered around the mean excitation energy of the isovector giant dipole resonance at $E^* \approx 15$ MeV is observed. Below 25 MeV excitation energy also an indication for isovector and isoscalar giant quadrupole resonance (GQR) was found. The solid line represents the result of an quantitative analysis for the excitation spectrum obtained with the Pb target, performed on the basis of semiclassical description of the electromagnetic process [14] performed in Ref. [16]. The total cross section comprised in the GDR and GQR's amounts to 1460(80) mb. After subtracting the result of this calculation from the measured spectrum a prominent structure of a mean energy of 28.3(7) MeV with a width of 6.3(1.6) MeV and integrated cross section of 215(50) mb remains. (see lower left part in Fig.2). This structure can hardly be explained with a single step excitation, and according to Ref. [16] it was assigned to a two-step excitation of the double isovector giant dipole resonance in ^{136}Xe.

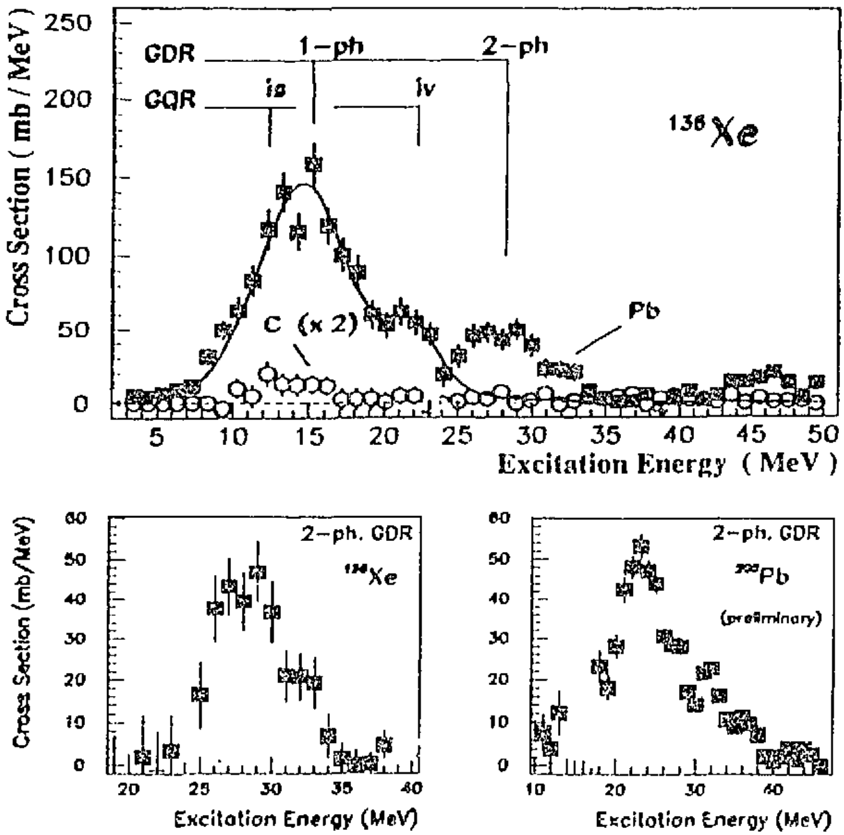

Figure 2: (upper part) Spectrum of ^{136}Xe (projectile) excitation on a Pb target (squares) and on a C target (open circles). The resonance energies for the one- and two-phonon giant dipole resonance (GDR-1ph,2ph) and for the isoscalar (is) and isovector (iv) quadrupole resonance (GQR) are indicated. The solid curve reflects the the result of a first-order semiclassical calculation for the Pb target [16].
(lower left part) Spectrum for ^{136}Xe obtained after subtracting the calculating spectrum from the experimental one displayed in the energy range relevant for the DGDR. (lower right part) Same as left part, however, for the excitation of ^{208}Pb ($650\ A \cdot MeV$) on a Pb target [18]. The same procedure of subtracting single step excitations was applied as in the case of ^{136}Xe. In addition, contributions from nuclear interactions determined by means of a measurement with C target are subtracted.

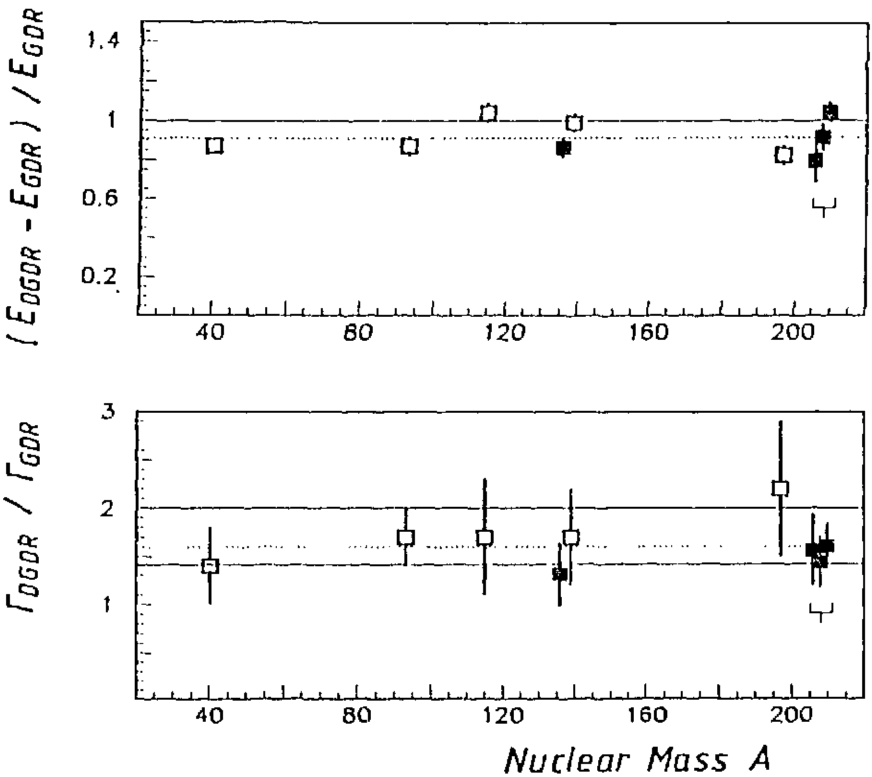

Figure 3: (upper part) Energy of the second phonon of the DGDR, relative to the energy of the single-phonon GDR. Open symbols denote data from (π^+, π^-) reactions, full symbols denote data from heavy ion induced electromagnetic excitation. The dashed line represents the mean value of all data, the solid line indicates the harmonic value.

(lower part) Same as above, however, for the DGDR width relative to the GDR width. The solid line indicate the theoretical limits $\Gamma(DGDR)/\Gamma(GDR) = 2$ and $\Gamma(DGDR)/\Gamma(GDR) = \sqrt{2}$.

2.2.2. Search for DGDR in ^{208}Pb

A similar analysis was performed for the excitation spectrum obtained for ^{208}Pb projectile of 650 $A \cdot MeV$ energy impinging on a Pb target. The preliminary analysis published in Ref. [18] results in a structure presented in the lower right part of Fig. 2. The same arguments as for ^{136}Xe leads to the assignment of this structure to the excitation of the DGDR in ^{208}Pb. The preliminary values for this DGDR in ^{208}Pb are a mean energy of 24.1(1.5) MeV, a width (FWHM) of 6.3(1) MeV and a cross section of 350(60) mb. These values seems to be consistent with a recent measurement of the DGDR in ^{208}Pb performed looking at the γ- decay channel by the TAPS collaboration [19,21].

3. Discussion and summary

The parameters describing the DGDR obtained by the LAND collaboration for ^{136}Xe and ^{208}Pb, as well as other reported DGDR excitations with heavy ions and (π^+, π^-) reactions are presented in Table 1. A simple discussion of the behavior of the E(DGDR)

Table 1: Parameters of the DGDR obtained from heavy ion electromagnetic excitation and from (π^+, π^-) reactions. E(DGDR), Γ(DGDR) and σ(DGDR) denote the energy of maximum cross section, the width (FWHM) and total cross section respectively.

Nucleus	Reaction	E(DGDR) [MeV]	Γ(DGDR) [MeV]	σ(DGDR) [mb]
^{136}Xe [16]	$Pb(^{136}Xe,^{136-xn}Xe + xn)$ 700 A·MeV	28.3(7)	6.3(1.6)	215(50)
^{197}Au [17]	$^{197}Au(^{197}Au,^{197-xn}Au)$ 1000 A·MeV			450(110)
^{208}Pb [18]	$Pb(^{208}Pb,^{208-xn}Pb + xn)$ 650 A·MeV	24.(1.5)	6.3(1.5)	360(50)
^{208}Pb [19]	$^{208}Pb(^{209}Bi, X + 2\gamma)$ 1000 A·MeV	25.6(9)	5.8(1.1)	0.20(6)
^{208}Pb [20]	$^{208}Pb(^{86}Kr,^{86}Kr + \gamma)$ 80 A·MeV	27.4(9)	6.5(1.0)	
^{208}Pb [20]	$^{208}Pb(^{36}Ar,^{36}Ar + \gamma)$ 95 A·MeV			
^{40}Ti [10]	$^{40}Ca(\pi^+, \pi^-)$ 295 MeV	37.2(5)	9.0(1.4)	0.013
^{93}Tc [10]	$^{93}Nb(\pi^+, \pi^-)$ 295 MeV	31.1(8)	8.8(2.6)	0.018
^{115}Sb [11]	$^{115}In(\pi^+, \pi^-)$ 295 MeV	31.8(8)	8.5(9.0)	0.066
^{139}Ce [10]	$^{138}Ba(\pi^+, \pi^-)$ 295 MeV	30.4(8)	8.5(2.6)	0.024
^{197}Tl [11]	$^{197}Au(\pi^+, \pi^-)$ 295 MeV	25.2(8)	9.0(3.0)	0.041

and Γ(DGDR) can be done, assuming the model of independent harmonic oscilator quanta. In this case one should expect the following relation between the parameters describing the GDR and DGDR ; $(E(DGDR) - E(DGR))/E(GDR) = 1$ and $\Gamma(DGDR)/\Gamma(DGR) = 2$. In Fig. 3 (taken from Ref. [8]) this simple relations for the data of Table 1 are presented. In Ref. [8], also a detailed discussion on the strength distribution of DGDR can be found.

The average values for the relative energy of the second phonon and the relative width of the DGDR is 0.91 ± 0.02 and 1.60 ± 0.11, respectively. In Fig. 3 these values are marked by the dotted line. The value of the relative energy of the second phonon is close to the predictions of the harmonic model. Only a small amount of anharmonicity $\sim 10\%$ may be attributed to the reported value. The width of the DGDR is closer to the value $\sqrt{2} \cdot \Gamma(GDR)$ then to $\Gamma(GDR)$. One would obtain the $\sqrt{2}$ multiplication factor assuming a gaussian and not lorentzian strength distribution. More general discussions on the width of the DGDR can be found in Refs. [22,23,24]. For ^{136}Xe calculations within the quasi-particle phonon model were performed by Ponomarev et al. [25]. I refer also to the presentation of V.V. Voronov at this conference.

Several theoretical calculations were performed to describe the unexpectedly large cross section for the electromagnetic DGDR excitation, found not only for ^{136}Xe [16], and ^{208}Pb [18,20]. The same feature of enhanced cross section for DGDR population was reported from activation measurements [17]. An enhancement of the DGDR excitation cross section was also reported in (π^+, π^-) reactions [10,11]. A larger cross section then expected was also reported in the nuclear excitation of the isoscalar double giant quadrupole resonance [28]. Cross sections for a two-step excitation of DGDR under the assumption of independent photons were calculated by using of the folding model [26], and by the semiclassical second order perturbation approach [22,23,25]. All this calculations are very sensitive to the choice of the lower cut-off impact parameter b_{min}. The experimental and calculated cross sections can be brought into agreement choosing the minimum impact parameter $b_{min} \approx 1.2 \cdot (A_1^{1/3} + A_2^{1/3})$.

The measured DGDR excitations delivered very important information on the high energy nuclear collective excitation. The electromagnetic excitation was proved to be a very promising method in the study of multiple giant resonances. The parameters E(DGDR) and Γ(DGDR) are not far away from theoretical expectations. The enhancement of the DGDR cross section seems to be independent on the excitation mechanism, indicating, that structural effects are responsible for it. Dependence of the multi-phonon excitation with regard to other parameters as e.g. the impact parameter should be studied with high quality cooled beams. On the theoretical side exact coupled channel calculations should be performed to study the interplay of single and multi-step excitations and also the Coulomb-nuclear interferences.

The experiments on ^{136}Xe and ^{208}Pb discussed in this report have been done in the framework of the LAND collaboration including Th. Blaich, Th.W. Elze, H. Emling, H. Freiesleben, K. Grimm, W. Henning, R. Holzmann, J.G. Keller, H. Klingler, R. Kulessa, J.V. Kratz, D. Lambrecht, J.S. Lange, Y. Leifels, E. Lubkiewicz, E.F. Moore, E. Wajda, W. Prokopowicz, Ch. Schütter. H. Spies, K. Stelzer, J. Stroth, W. Waluś, H.J. Wollersheim, M. Zinser and E. Zude.

References

1. A.B. Migdal, J. Phys. USSR, 8:331(1944).
2. G.C. Baldwin and G.S. Klaiber, Phys.Rev. **71** (1947)3; Phys. Rev. **73** (1949)1156.
3. A.K. Snower, Ann.Rev.Nucl.Part.Sci. **36**,1(1986).
4. A. van der Woude, Prog.Part.Nucl.Phys. **18**, 217(1987).
5. J. Speth, ed. International Review of Nuclear Physics, Vol. **7**, World Scientific(1991).
6. Proceedings of the Gull Lake Nuclear Physics Conference on Giant Resonances, Gull Lake, Michigan, August 17-21, 1993, Nucl.Phys. **A569** (1994) Vol.1,2
7. J.S. Levinger, Nuclear Photo-Desintegration, Oxford University Press, Oxford (1960).
8. H. Emling, Preprint GSI-94-16, Accepted for publication in Prog.Part.Nucl.Phys., Vol. 3, (1994).
9. A. Bohr and B.R. Mottelson, Nuclear Structure Vol. II W.A. Benjamin, Inc. (1975).
10. S. Mordechai, et al., Phys.Rev. **C41**, 202(1990)
11. D.A. Smith, et al., Phys.Rev. **C47**, 1053(1993).
12. C.A. Bertulani and G. Baur, Phys.Rep. **163**, 299(1988).
13. J.D. Jackson, Classical Electrodynamics, Wiley, New York (1975).
14. K. Alder and A. Winther, Electromagnetic Excitation, Nort Holland, Amsterdam (1975).
15. Th. Blaich, et.al (LAND Collaboration), Nucl.Instr. and Meth. **A314**, 136(1992).
16. R. Schmidt, et al., (LAND Collaboration), Phys.Rev.Lett. **70**, 1767(1993).
17. T. Aumann, et al., Phys. Rev. **C47**,1728(1993) and Nucl. Phys. **A569**, 157c(1994).
18. E. Wajda, et al., (LAND Collaboration), Nucl.Phys **A569**, 141c(1994).
19. J.L. Ritman, et al., Phys.Rev.Lett. **70**, 533(1993) and erratum Phys.Rev.Lett. **70**, 2659(1993).
20. J.R. Beene, Nucl.Phys. **A569**, 163c(1994).
21. W. Kühn et al. Nucl.Phys. **A569**, 175c(1994).
22. C.A. Bertulani and V.G. Zelevinsky, Phys.Rev.Lett. **71**, 967(1993).
23. C.H. Lewenkopf and V.G. Zelevinsky, Nucl.Phys. **A569**, 183c (1994)
24. P.F. Bortignon et al., Nucl.Phys. **A569**, 237c(1994).
25. V.Yu. Ponomarev et al., Nucl.Phys. **A569**, 333c(1994).
26. W. Llope and P. Braun-Munziger, Phys.Rev. **C45**, 799(1994).
27. H.T. Fortune, Nucl.Phys. **A522**, 241c(1991).
28. N. Frascaria, Nucl.Phys. **A522**, 111c(1991).

Angular distribution and width of the GDR in hot rotating nuclei in the *mass region* $A = 170$

A. Bracco, M. Mattiuzzi, F. Camera, B. Million, and M. Pignanelli

Dipartimento di Fisica, Universitá di Milano and INFN sez. Milano, via Celoria,16 20133 Milano (Italy).

J.J. Gaardhøje, A. Maj *, T. Ramsøy, T. Tveter and Z. Zelazny

The Niels Bohr Institute, Copenhagen

Abstract

A study of the spectral function and of the angular distribution of the high energy gamma-rays emitted by the giant dipole resonance state in hot ^{176}W is presented. The two GDR observables are for the first time studied in this mass region at the fixed temperature of 1.5 MeV for different values of spin in the interval 35 to 55 $\hbar$. Nuclei in this mass region and at these temperatures are of particular interest because are expected to have smaller and different type of deformations than at zero temperature due to the vanishing of shell effects. The data are well reproduced by calculations of thermal shape and orientation fluctuations with the zero temperature value of the intrinsic width for all the angular momenta presently measured.

Introduction

One of the very interesting topics currently investigated is the nuclear shape change due to temperature and rotational frequency effects. The experiments made in the last decade studying the decay of the giant dipole resonance state (GDR) in hot rotating nuclei have demonstrated the important role of the coupling of the GDR vibration to the quadrupole deformation and that nuclear properties far away from the "yrast" line can be investigated through this decay. In addition, thermal and quantal fluctuations have been shown to he important to describe the properties of hot nuclei and of the damping mechanisms of the collective states [1,2].

Most of the data so far obtained are relative to rather inclusive experiments in which the experimental sensitivity to the changing of nuclear properties is rather reduced. Furthermore, only in few cases the angular distribution was measured, quantity that is important to understand the evolution with spin and excitation energy of the different damping mechanisms of the GDR. Two are the important damping mechanisms of the

GDR state at finite temperature : 1) the collisional damping due to the coupling of the simple one particle-one hole states describing microscopically the giant resonance state to the more complicated n particle- n hole states and 2) the breaking of the dipole strength due to the coupling to the ensamble of shapes describing a hot rotating nucleus. The collisional damping width will be here referred as *intrinsic width.* Recently, exclusive measurements of the angular distribution and of the spectral function as a function of spin at a temperature of $\approx$ 2 MeV were made [3] from which it has been found that both the width and particulary the angular anisotropy increase with spin. Only with the analysis of both observables it is possible to infer that the collisional damping width is not changing while the deformation of the nucleus increases.

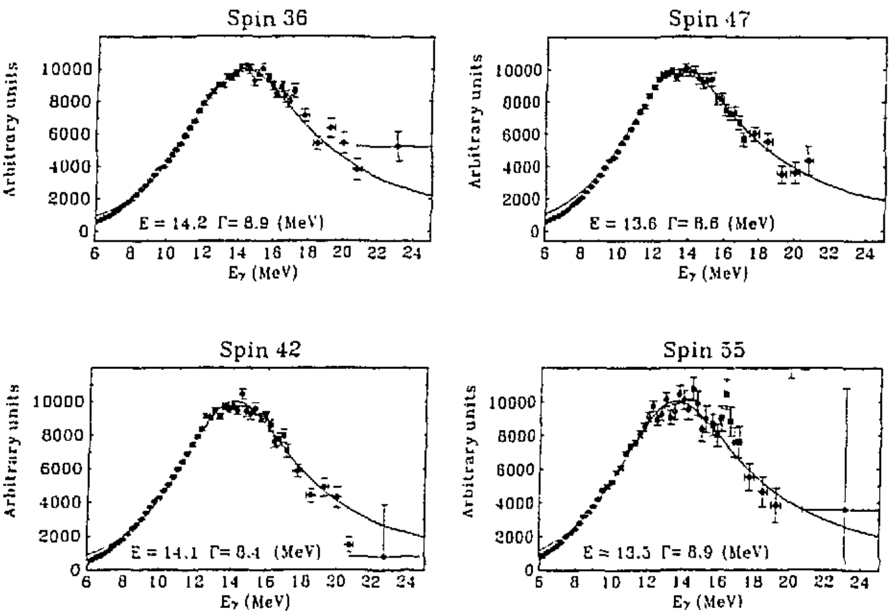

Fig. 1-*Strength Function at the temperature of $T = 1.42$ MeV for the ^{176}W nucleus at four different spin windows centered around the average value reported above each panel. The full drawn lines display the Lorentzian obtained from the best fitting statistical model calculations. The GDR energies E and widths Γ are given in the bottom part of each panel.*

Detailed studies of this type were so far made only for $^{110,109}Sn$, nuclei characterized by spherical shapes at T = 0 and ω = 0. However, in order to stress the role of deformation in the GDR response it is very important to study with the same detail a nucleus with the opposite behaviour, as in the case of ^{176}W which is characterized by well prolate shapes (β = 0.3) at T = 0 and ω = 0 and that at T $\approx$ 1.5 MeV is expected to have almost oblate deformations that are in general smaller than the ones of Sn at the same temperatures and at the same values of the angular momentum.

In the following we present and discuss a new exclusive measurement of the strength function and of the angular distribution of the high energy γ-ray emitted by the GDR in the ^{176}W nucleus formed by compound nucleus reaction. It will be shown that at this temperature the width does not change with spin in the region 35-55 $\hbar$. The angular anisotropy has a similar behaviour with the exception of the highest angular momentum case. While the result on the width is a consequence of the thermal averaging of the GDR over the shape distributions that are in the present case similar and characterized by rather small equilibrium deformations (β < 0.15), for the angular distribution results beside shape fluctuations the effects of orientation fluctuations are shown to be important and larger at the lowest rotational frequencies. In addition, the collisional damping width is found independent of angular momentum and equal to the zero temperature value.

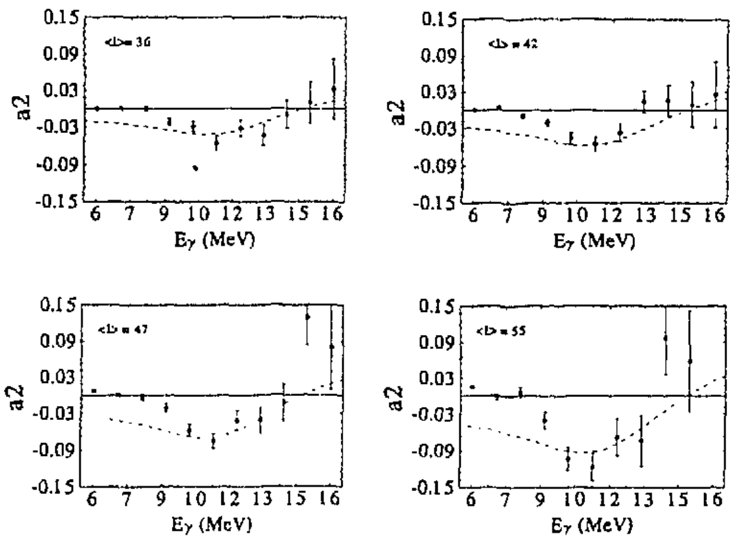

Fig. 2. *The $a_2(E_\gamma)$ coefficient as a function of the transition energy of the γ rays emitted by ^{176}W at an excitation energy of 94 MeV. The four plots are associated to different spin windows centered at the average value shown in the top left part of each panel. The dotted curves are the result of calculations of shape and orientation fluctuations in the adiabatic regime.*

1. The experiment

The ^{176}W was formed with the reaction ^{28}Si+ ^{148}Nd at the incident energy of 147 MeV leading to an average angular momentum 38 $\hbar$. The experiment was performed at the tandem laboratory of the Niels Bohr Institute using the Tandem + Booster accelerator system. The detection system used was HECTOR [4,5] in its upgraded configuration. This detector array consists of 8 large volume BaF_2 scintillators (placed at different angles with respect to the beam direction) for measuring high energy photons and of a multiplicity filter of 38 smaller BaF_2 detectors measuring the coincidence fold (i.e. the number of detected low energy γ rays). Only the high energy γ-rays associated to coincidence fold larger that 10 were considered in the analysis since the ones associated to lower coincidence folds seem to be contaminated to large extent from reactions different than fusion. The quadrupole coefficient a_2 was extracted as a function of the γ energy E_γ by fitting the measured spectra of the high energy γ rays with the function $N(E_\gamma,\theta) = N_0(E_\gamma)[1 + a_2(E_\gamma)P_2(cos\theta)]$, where $P_2(cos\theta)$ is the Legendre Polynomial in the polar angle θ between the direction of emission of the γ rays and the beam.

In figure 1 some spectral data are shown in a linearized form, namely the quantity $f(E_\gamma) * Y_\gamma^{exp}(E_\gamma)/Y_\gamma^{cal}(E_\gamma)$ is plotted to emphasize the details of the high energy γ-ray spectrum in the GDR region. The quantity $Y_\gamma^{exp}(E_\gamma)$ is the measured spectrum while $Y_\gamma^{cal}(E_\gamma)$ is the spectrum calculated with the statistical model and f(E_γ) is the lorentzian function giving the best fit to the data. In the statistical model analysis the energy and the width of the GDR were free to vary until the χ^2 was minimized. The calculated and measured spectra were normalized in the region E_γ= 9-19 MeV assuming 100% of the EWSR strength and that the GDR parameters do not change in the different steps of the decay cascades of the compound nucleus. The statistical model calculations were folded with the detector response function calculated using GEANT3 [6] libraries. For the statistical model calculations the measured spin distribution of the fusion cross section associated to the selected coincidence fold intervals was used. For the level density parameter the value used was a=A/8. An attempt to fit the data with 2 lorentzian functions was also made but gave results that were rather ambiguous and unstable. The width and the angular anisotropy of the high energy γ-rays (see figure 2) were found to be rather constant with spin with the exception of the point at $< I >$ = 55 for which the $a_2(E_\gamma)$ is larger than the other cases.

The interpretation of the present results requires a study of the shape distributions based on calculations of the nuclear free energy. This discussion is presented in the next section.

2. Comparison with model predictions

A rather constant behaviour with angular momentum is seen not only for the measured width but also in the distribution of shapes of ^{170}W at T = 1.42 MeV at the rotational frequencies associated to the measured points. In figure 3 a three dimensional representation of the Boltzman factor $exp(-F(\beta,\gamma)/T)$ calculated at the temperature and rotational frequencies of the present experimental data is displayed. The Boltzman

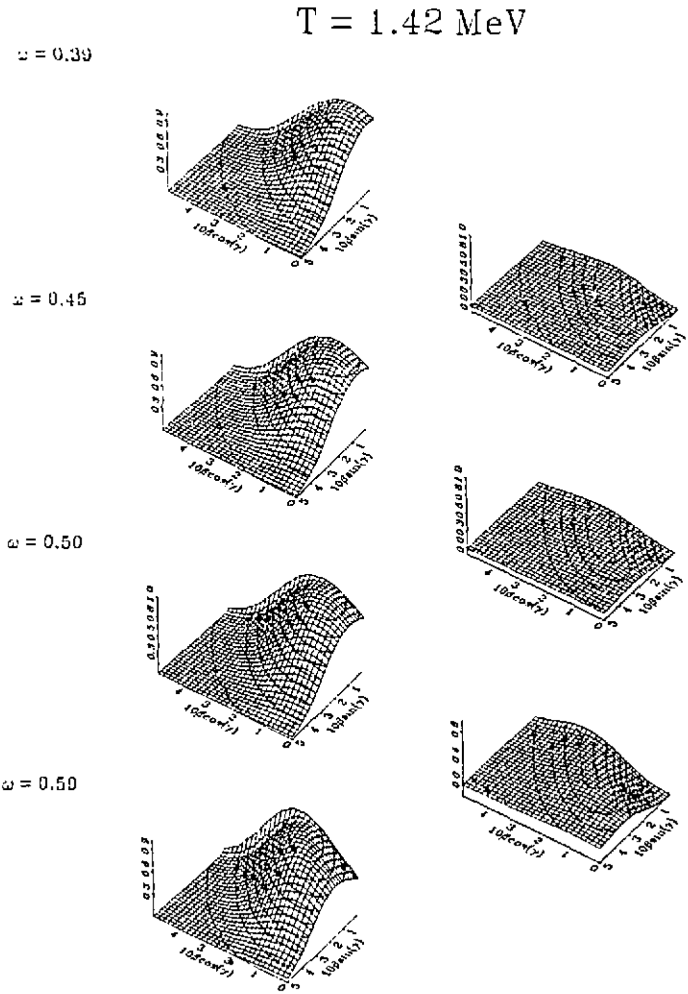

Fig. 3. *Three dimensional representation of the shape probability given by the Boltzman factor* $\exp(-F(T,\omega,\beta,\gamma)/T)$ *(in the z axis), where F is the free energy. The calculations are shown in the left part as a function of the quadrupole deformation parameters* β *and* γ *at a constant temperature T and at four rotational frequencies* ω. *In the right part of the figure the difference between two consecutive plots of the right hand side is displayed to see better how the shape probability distribution changes by going from one rotational frequency to the next one.*

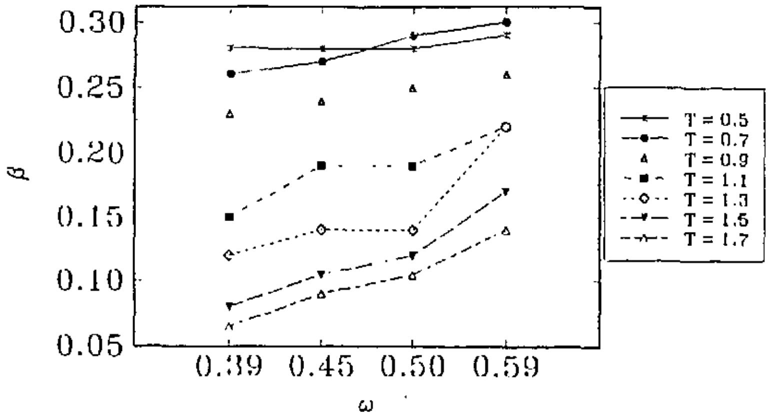

Fig. 4. *Deformation parameter β at the minimum of the free energy (equilibrium value) for the hot ^{176}W nucleus as a function of its rotational frequency. The different curves are associated to different temperature values used in the calculations.*

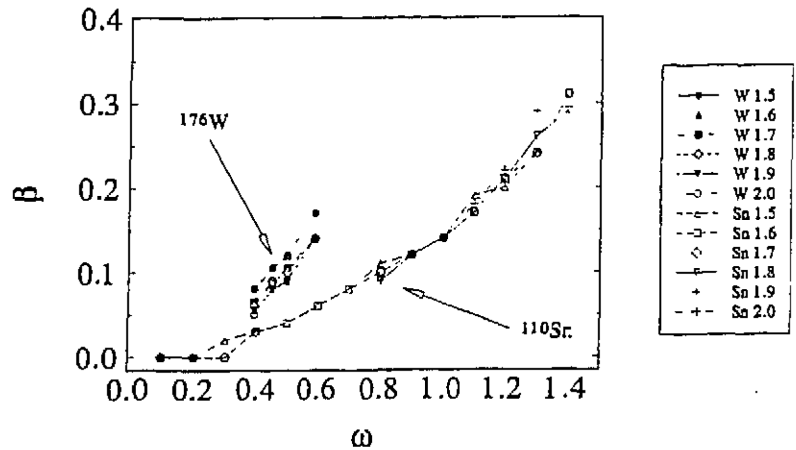

Fig. 5. *Deformation parameter β at the minimum of the free energy for the two nuclei ^{176}W and ^{110}Sn as a function of the rotational frequency. Each curve of the two sets corresponds, for the specific nucleus, to a temperature value reported in the legend on the right panel.*

factor gives the probability of finding the nucleus at a particular deformation. The free energies $F(\beta,\gamma)$ (β and γ being the quadrupole deformation parameters) were calculated at constant temperature T and rotational frequency ω making use of the liquid drop model and of the shell corrections with the Nilsson-Strutinsky method. Examining this figure one can notice that the shape distributions are almost identical. To make this point more clear the difference among two consecutive distributions is also plotted in figure 3. The values of the deformation parameter β that maximises the Boltzman factor (equilibrium shape) are plotted in figure 4 and in figure 5 in comparison with calculations for ^{110}Sn. Contrary to the present case, in ^{109,110}Sn the width and particularly the angular anisotropy were found to increase with spin [3]. This different behaviour is in agreement with the fact at the rotational frequencies studied (from 0.8 to 1.4 MeV) the deformation involved in the shape distributions were much larger. While ^{110}Sn is a nucleus spherical at T= 0 and ω = 0 and that at the temperature T in the interval from 1 to 2 MeV is oblate with rather large deformations driven by angular momentum, ^{176}W is prolate with rather large deformations at T = 0 and ω = 0 (see figure 5) and after shell effects have vanished (at approximately 1.0 MeV) it acquires shape distributions characterized by rather small oblate equilibrium deformations. In fact, at the angular momenta involved smaller rotational frequencies (0.4 - 0.6 MeV) than in the Sn case are associated.

A very simple analysis of the $a_2(E_\gamma)$ can be made by assuming that the angular distribution reflects an apparent nuclear deformation that can be obtained determining the β value that better reproduces the $a_2(E_\gamma)$ data [7]. The values of beta that reproduce the measured $a_2(E_\gamma)$ are plotted in figure 6 in comparison with the equilibrium beta deformations. The trend of the data and of the calculations are the same but not

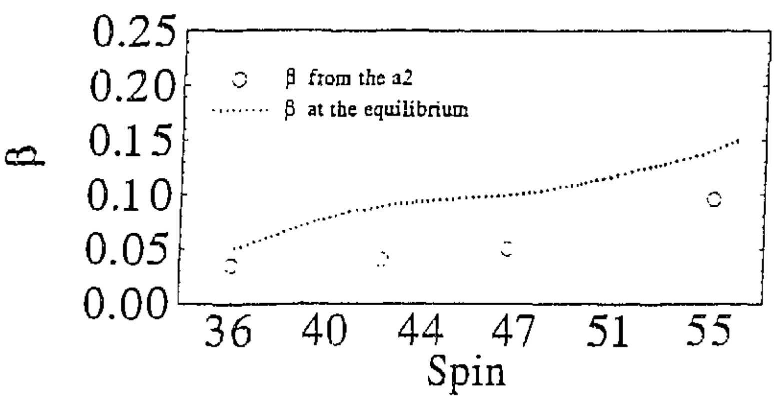

Fig. 6. *Deformation parameter β as a function of spin of the rotating hot nucleus. The filled circles are the experimental values deduced from the $a_2(E_\gamma)$ data whereas the dotted curve gives the value of β at the minimum of the free energy (equilibrium deformation)*

the absolute values. It is then clear that neither from the analysis of the strength function, that cannot be reproduced by two Lorentrian function, nor from the simple analysis of the $a_2(E_\gamma)$ it is possible to extract the equilibrium deformations. A more proper analysis is necessary to describe consistently the two GDR observables.

Calculations of the two observables were made with the model of thermal fluctuations in the adiabatic limit [1]. The predictions for the minimum value of the $a_2(E_\gamma)$ (in the γ-transition energy region 10-12 MeV) and for the values of the GDR width are compared with the present experimental results in figure 7. In the top part of the figure the data are compared with calculations of thermal fluctuations of the nuclear shape. In this case only the measured width is well reproduced and not the a_2. For these calculation the intrinsic width was taken equal to the zero temperature value. If one tries to reproduce the a_2 by making the intrinsic width smaller (see calculation in the first panel of the second row) one finds that it is not possible to reproduce at the same time the measured width. Instead, hy adding to the shape fluctations also orientation fluctuations a consistent description of the two ohservables is obtained (see third row of figure 7). In fact, orientation fluctuations do not change the strength function and are able to to account for the measured anisotropy.

The present study based on the first exclusive measurements of both the strength function and the angular distribution in the $A = 170$ region demonstrat the important role of thermal fluctuations, particularly of orientation fluctuations and also that the intrinsic width does not seem to depend on rotational frequency. It will be very interesting to perform such studies at higher excitation energy and higher angular momentum, where very large deformations ($\beta = 0.5$-0.6) were deduced by the analysis of the GDR strength function [8], to investigate consistently the effects of very large shapes and of their fluctuations in both GDR observables.

Conclusion

The angular distribution and the strength function of the γ rays emitted hy the giant dipole resonance in ^{176}W at T = 1.42 MeV and at 4 nuclear angular momentum values between 35 and 55 $\hbar$ were studied.

A rather constant value of the two observables with spin was found that is well reproduced by calculations of thermal shape and orientation fluctuations in the adiabatic limit. Orientation fluctuations are very important to describe the measured $a_2(E_\gamma)$ and do not affect the GDR strength function.

The present study also indicate that the intrinsic width has not appreciably changed from the T= 0 value and that does not depend on angular momentum. While the temperature dependence of the intrinsic width has been theoretically studied and recent calculations are in general agreement with the present finding [9], predictions of the intrinsic width as a function of rotational frequency were never made. Therefore, these results should motivate theoretical efforts towards the understanding of the intrinsic width as a function of rotational frequency at finite temperature.

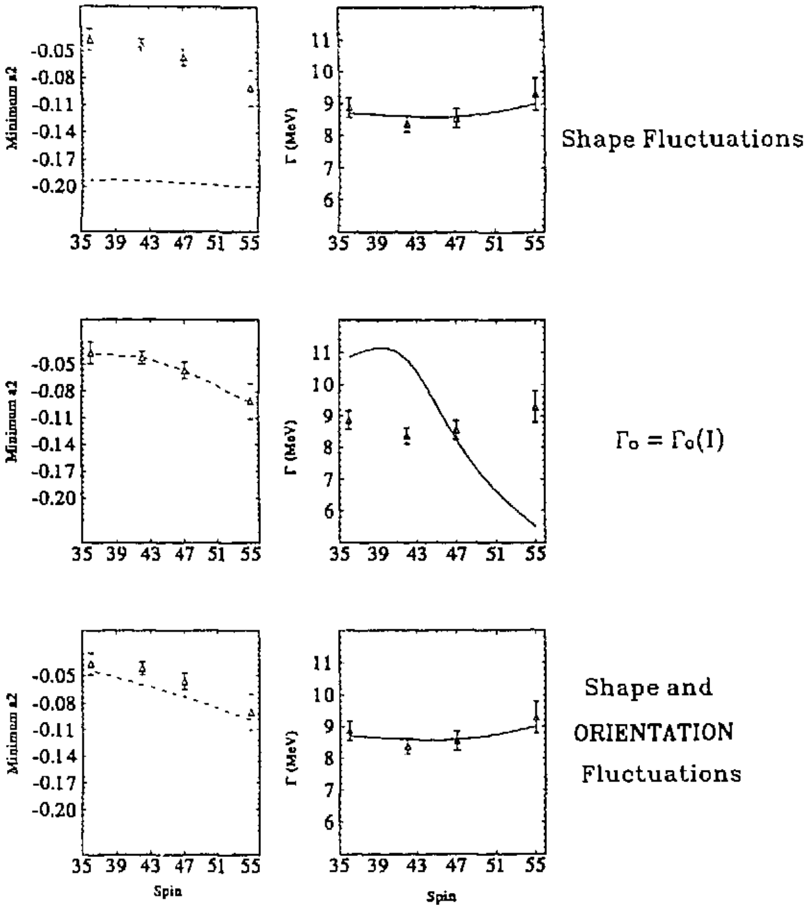

Fig. 7. *The measured a_2 (left column) and Γ_{GDR} (right column) as a function of spin of the compound nucleus ${}^{176}W$ are compared with three different calculations. In the first row, adiabatical model calculations of shape fluctuations with the intrinsic width equal to the zero temperature value are shown. In the second row, in addition to shape fluctuations, the values of the intrinsic width Γ_o were varied to reproduce the measured a_2. In the third row shape and orientation fluctuations are considered and the intrinsic width is taken equal to the zero temperature value.*

References

* Permanent address: *Niewodniczanski Institute of Nuclear Physics*, Krakow, Poland

[1] E. W. Ormand, F. Camera, A. Bracco, A. Maj, B. Million, P. F. Bortignon , R. A. Broglia Phys. Rev. Lett. **69**(1992) 2905 and references therein.
[2] Y. Alhassid, B. Bush, Phys. Rev. Lett. **65**(1990)2527 and references therein.
[3] A. Bracco, F. Camera, M. Mattiuzzi, B. Million, M. Pignanelli, C. Volpe,J.J. Gaardhøje, A.Maj Z. Zelazny, and T. Tveter Nucl. Phys. **A569**(1994)51c.
[4] F. Camera, Ph. D. Thesis, University of Milano 1992
[5] A. Maj, J.J. Gaardhøje, A. Atac, S. Mitarai, J. Nyberg, A. Virtanen, A. Bracco, F. Camera, B. Million, and Pignanelli M. Nucl. Phys. **A 571**(1994)185
[6] Geant User Manual CERN
[7] F. Camera, A. Bracco, B. Million, Pignanelli, J.J. Gaardhøje, Z. Zelazny, T. Ramsøy, and A. Maj, Nucl. Phys. **A572**(1994)401.
[8] M. Thoennessen, J.R. Beene, F.E. Bertrand, C. Baktash, M. L. Halbert, D.J. Horen, D.C. Hensley, D. G. Sarantites, W. Spang, D.W. Stracener and R.L. Varner. Phys. Lett. B **282**(1992)288.
[9] F. V. De Blasio, W. Cassing, M. Tohyama, P.F. Bortignon and R. A. Broglia, Phys. Rev. Lett. **68**, 1663 (1992).

Decay properties
of charge-exchange resonances

G. Colò, N. Van Giai
Division de Physique Théorique, Insitut de Physique Nucléaire,
91406 Orsay Cedex, France

P.F. Bortignon
Dipartimento di Fisica, Università degli Studi,
and INFN, Sezione di Milano, Via Celoria 16, 20133 Milano, Italy

R.A. Broglia
Dipartimento di Fisica, Università degli Studi,
and INFN, Sezione di Milano, Via Celoria 16, 20133 Milano, Italy,
and Niels Bohr Institute, University of Copenhagen, 2100 Copenhagen, Denmark

Abstract

Recent exclusive measurements have provided new results on the particle decay of nuclear giant resonances, which is probably the only way to get detailed information about the wave function of these collective modes. Correspondingly, in the present work the decay properties of the Gamow-Teller resonance in ^{208}Bi are studied within a self-consistent framework. Preliminary results about the charge-exchange isovector monopole resonance in ^{208}Tl are also presented.

PACS numbers: 21.60.Jz, 24.30.Cz, 25.55.Kr.

1. Introduction

Improvements in the experimental techniques have made possible exclusive measurements of the decay of high-lying states in nuclei, both of single-particle and collective character [1, 2]. Giant resonances are coherent superpositions of particle-hole (p-h) excitations and the analysis of their particle decays to hole states of the (A-1)-system have provided so far the only experimental information about the p-h amplitudes, that is, about the wave function of the giant mode. This information is especially valuable to test different nuclear models which can give similar predictions for the global properties of giant resonances (mean energy, width and fraction of the appropriate sum rule) but different results for their wave functions.
In the case of the Gamow-Teller resonance (GTR) in ^{208}Bi, the results of an (^{3}He,tp) experiment on ^{208}Pb have been available for more than ten years [3]. But these results for the proton decay seemed to imply a vanishing spreading width for the GTR, in strong

contrast with two theoretical expectations [4, 5] of ~ 4 MeV. Probably, the low energy of the projectile (27 MeV/A) did not allow a strong and selective excitation of the GTR as this resonance is optimally excited when the projectile energy reaches a few hundreds MeV/A [6]. The availability of adequate beams have led to a new investigation of the proton decay of the GTR, by means of two experiments performed at Osaka [2] and MSU [7]. The results of the first experiment disagree with previous theoretical calculations [8, 9]. Some indications about the second experiment seem to lead to a somewhat different result than the first experiment. This situation has motivated us to study the decay properties of the GTR from the theoretical point of view.

Much larger uncertainities prevent a detailed knowledge of the properties of the charge-exchange isovector monopole resonance (IVGMR). A first claim about its identification came from a (π^-,π^0) reaction on ^{208}Pb [10]. But the resonance appeared (cf. Fig. 5 of [10]) as a very weak bump on a large background and its excitation energy with respect to the target ground state (12 MeV) must be compared with a nearly equal width (11.6 MeV). More recently, it has been pointed out that the $(^{13}C,^{13}N)$ reaction at incident energy of about 50 MeV/A should populate strongly the electric isovector modes of the target [11]. The reason is that Fermi transitions in the projectile dominate over Gamow-Teller transitions as can be inferred by β-decay data [12]. This reaction has therefore been performed on a set of nuclear targets at GANIL [13]. In almost all cases a wide resonance has been identified at more or less the same energy quoted as the IVGMR excitation energy in [10]. But just in the case of ^{208}Tl the discrepancy between the two experiments is quite large, as the excitation energy measured in the $(^{13}C,^{13}N)$ reaction is 21.5 MeV (as before, with respect to the target ground state). The width is 3.1 MeV, therefore the bump is better resolved than in the other measurement but still some problems exist in the angular distrubutions which prevent the unambigous determination of the resonance multipolarity (see the Ref. [13] for a detailed discussion). The conclusion might be that a reliable experimental study of the IVGMR is still needed. Some work along this line is in progress as results of a new measurement with the $(^{13}C,^{13}N)$ reaction are under analysis [14]. We have performed a preliminary calculation of the IVGMR strength distribution which will be shown in this paper.

2. The theoretical model

We have applied to the GTR and to the IVGMR a theoretical model which has as the only phenomenological input an effective nucleon-nucleon interaction of the Skyrme type and which includes both a mean-field description of the giant resonance excitation and a consistent treatment of the couplings responsible for its subsequent damping. One version of this model has been used in the past to study the properties of the isoscalar giant monopole resonance in ^{208}Pb [15]. We have then extended the model to the case of charge-exchange excitations and reported this in detail in Ref. [16], where we discuss the results for the GTR as well as for the isobaric analog resonance (IAR) in ^{208}Bi. The latter resonance has been considered as a test case for the extension of the theoretical model to charge-exchange resonances as its properties are very well known. The reader is referred to [16] for more details.

The starting point of our procedure is the Hartree-Fock (HF) set of equations which are solved for a given nucleus (A,Z). The two Skyrme interactions SIII [17] and SGII [18] have been employed in the present calculation. The self-consistent single-particle mean field is diagonalized on a basis made up with harmonic oscillator wave functions in order to obtain a set of levels labeled by $|i\rangle$ which includes the quasi-bound levels and extend up to positive energies.
We then apply the projection operators method, whose general formulation can be found in Ref. [19]. Definite subspaces of the whole nuclear configuration space are selected and projectors on these subspaces will be denoted with the same symbols as the subspaces they span. The space Q_1 is made up with the HF ground state and all the possible one particle-one hole (1p-1h) excitations built within the set $|i\rangle$. The nuclear Hamiltonian restricted to this space will be written as

$$Q_1 H Q_1 = H_0 + V_{ph}, \tag{1}$$

where H_0 is the HF Hamiltonian and V_{ph} is the p-h interaction determined as the functional derivative of the self-consistent mean field with respect to the density. The usual Tamm-Dancoff approximation (TDA) or Random Phase Approximation (RPA) are suitable ways to obtain a diagonal representation of the Hamiltonian (1).
Nuclear giant resonances are also known to have a damping width, and we can distinguish two main mechanisms which give rise to it. The energy of the collective motion can be transferred out of the system by an escaping nucleon but it can be also distributed among internal degrees of freedom, coupled to the initial one through residual interaction terms, leading to many particle-many hole configurations (possibly correlated) up to the limiting situation of a compound nucleus state. The contributions to the damping width coming from these two kinds of processes are usually denoted respectively by $\Gamma^{\uparrow}$ ("escape width") and $\Gamma^{\downarrow}$ ("spreading width"). These effects lie beyond the discrete TDA (or RPA) description, which includes only as a source of strength broadening the so-called Landau spreading, which manifests itself as a fragmentation of the strength over more than one main discrete peak emerging from the solution of (1).
Our description of the widths $\Gamma^{\uparrow}$ and $\Gamma^{\downarrow}$ requires the definition of two further nuclear subspaces P and Q_2. The space P is build up with particle-hole configurations where the particle is in an unbound state, made orthogonal by construction to all states $|i\rangle$. To determine these unbound states we solve, for each partial wave $c \equiv (l,j)$ and at a positive energy ϵ, the radial scattering equation for H_0 projected on the orthogonal complement of set $|i\rangle$.
The space Q_2 is built with a set of "doorway states" which are the first step in the coupling of the ordered resonance motion with the more complicated configurations mentioned above. These "doorway states" are indicated by $|N\rangle$. We have built the configurations of subspace Q_2 by coupling a p-h pair with a collective vibration of the ^{208}Pb core. These collective vibrations have been calculated in self-consistent RPA with the same SIII or SGII interaction used throughout the whole work. Isoscalar vibrations with $\Delta L \leq 4$ were taken into account in order to build the doorway states.
Having defined the working subspaces, the nuclear Green's function G can be decomposed as a sum of terms like $Q_1 G Q_1 + Q_1 G P + \cdots$. It can be shown [19] that the Green's function

Q_1GQ_1 obeys an equation of motion governed by an effective Hamiltonian,

$$\begin{aligned}\mathcal{H}(\omega) &\equiv Q_1HQ_1 + W^{\uparrow}(\omega) + W^{\downarrow}(\omega)\\ &= Q_1HQ_1 + Q_1HP\frac{1}{\omega - PHP + i\epsilon}PHQ_1 + Q_1HQ_2\frac{1}{\omega - Q_2HQ_2 + i\epsilon}Q_2HQ_1,\end{aligned} \tag{2}$$

where ω is the excitation energy. The use of this energy-dependent, complex Hamiltonian allows to work *inside* the space Q_1 and therefore, with matrices of not too large dimensions. The escape term $W^{\uparrow}(\omega)$ can be more easily evaluated if one replaces the complete Hamiltonian H by the one-body part H_0. The neglect of matrix elements of $Q_1V_{ph}P$ should be, in the present case, rather safe since discrete and continuum wave functions are essentially restricted to different radial intervals while the V_{ph} interaction has zero range. A discussion of this point, as well as a detailed description of the evaluation of the matrix elements of $W^{\uparrow}(\omega)$ on the basis of the TDA or RPA eigenstates of Q_1HQ_1 (this part of the nuclear Hamiltonian is actually previously diagonalized) is given in Ref. [16].
The matrix elements on the same basis can be also determined in a straightforward way for the spreading term $W^{\downarrow}(\omega)$. We make the ansatz that the configurations $|N\rangle$ of Q_2 are not mutually interacting. The interaction between the basis states and the configurations $|N\rangle$ can be calculated provided a particle-vibration coupling is defined. This is done by introducing a one-body field which can be written in the form

$$V = \sum_{\alpha\beta}\sum_{LnM}\langle\alpha|\varrho_n^{(L)}(r)v(r)Y_{LM}(\hat{r})|\beta\rangle\, a_\alpha^\dagger a_\beta, \tag{3}$$

where the radial transition density $\varrho_n^{(L)}(r)$ of the $|n\rangle$ state of the spectrum of phonons with angular momentum L is introduced, as well as the form factor $v(r)$ which is related to the p-h residual interaction of (1) by $V_{ph}(\vec{r}_1,\vec{r}_2) = v(r_1)\delta(\vec{r}_1 - \vec{r}_2)$. By using (3), the analytic expressions for the matrix elements of the last term of (2) come out as described in Ref. [16].
The eigenvalue equation for the effective Hamiltonian (2) can then be written in matrix form on the TDA or RPA basis for different values of the energy ω. At each energy a set of states labeled by $|\nu\rangle$ whose eigenfrequencies are $(\Omega_\nu - i\frac{\Gamma_\nu}{2})$ is obtained. The corresponding eigenvectors form a matrix which will be written as F. Rather than the eigenvalue distribution, a more useful quantity to be shown and compared with experiment is the strength function corresponding to the excitation operator $\hat{O}$ of the resonance under consideration,

$$S(\omega) \equiv -\frac{1}{\pi}Im\langle 0|\hat{O}^\dagger\frac{1}{\omega - \mathcal{H}(\omega) + i\epsilon}\hat{O}|0\rangle. \tag{4}$$

In terms of the calculated solutions of (2) the strength function is

$$S(\omega) = -\frac{1}{\pi}Im\sum_\nu\langle 0|\hat{O}|\nu\rangle^2\frac{1}{\omega - \Omega_\nu + i\frac{\Gamma_\nu}{2}}\ , \tag{5}$$

where the squared matrix element of $\hat{O}$ appears instead of the squared modulus due to the properties of the eigenvectors $|\nu\rangle$ which form a biorthogonal basis.

Another quantity which can be extracted from the model and which is actually measured in the particle decay experiments is the branching ratio B_c corresponding to a particular decay channel. An escaping nucleon with energy ε leaves the residual (A-1) system in a hole state such that (by energy conservation) $\varepsilon_h = \varepsilon - \omega$ where ω is the initial excitation energy. The cross section σ_c for this decay, as well as the excitation cross section σ_{exc}, can be calculated by assuming a plane wave Born approximation (PWBA) to describe the reaction mechanism and in the limit of small momentum transfer. This procedure is carried out in Appendix B of Ref. [16], and the branching ratio comes out as

$$B_c(\omega) \equiv \frac{\sigma_c(\omega)}{\sigma_{exc}(\omega)} = \frac{\sum_{\nu,\nu'} S_{\nu'\nu}\gamma_{\nu'\nu,c}(\omega - \Omega_\nu - i\frac{\Gamma_\nu}{2})^{-1}(\omega - \Omega_{\nu'} + i\frac{\Gamma_{\nu'}}{2})^{-1}}{-2Im\sum_{\nu,\nu'} S_{\nu'\nu}(F^*F^T)_{\nu\nu'}(\omega - \Omega_{\nu'} - i\frac{\Gamma_{\nu'}}{2})^{-1}} \tag{6}$$

where $S_{\nu\nu'}$ is given by

$$S_{\nu\nu'} \equiv \langle\nu|\hat{O}|0\rangle\langle\nu'|\hat{O}|0\rangle^*, \tag{7}$$

and

$$\gamma_{\nu\nu',c} = \int d\Omega_k \gamma_{\nu,c}(\vec{k})\gamma^*_{\nu',c}(\vec{k}). \tag{8}$$

In the last equation,

$$\gamma_{\nu,c}(\vec{k}) = \langle\varphi_c\, u^{(-)}_{c,\varepsilon}(\vec{k})|H_0|\nu\rangle, \tag{9}$$

and φ_c is the wave function describing the residual (A-1) nucleus in channel c, while $u^{(-)}_{c,\varepsilon}(\vec{k})$ is the escaping particle wave function belonging to P space. The strength functions and the branching ratios are the main quantities we are going to show as results of the present model as they can be compared with experimental findings.

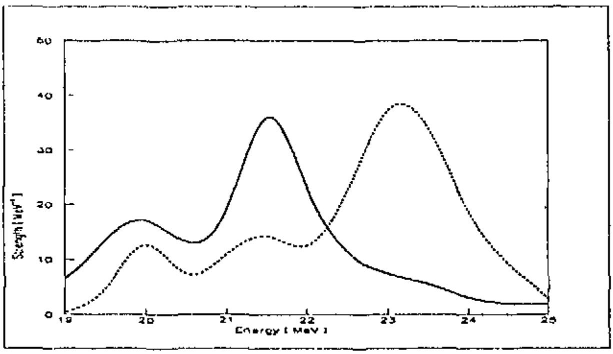

Figure 1: Strength function of the GTR calculated by using SIII interaction (full line) or SGII (dashed line).

3 · Results

The operator $\hat{O}$ which is responsible for the excitation of the GTR is

$$\beta_- = \frac{1}{2} \sum_{\mu=0,\pm1} \sum_{i=1}^{A} \sigma_\mu(i)\tau_-(i), \tag{10}$$

which means that this resonance is made up of proton particle-neutron hole excitations. The calculation for the GTR in ^{208}Bi has therefore been performed within the formalism seen above in its TDA version because results must not be seriously affected by the neglecting of neutron particle-proton hole ground-state correlations in a nucleus with large neutron excess. On the other hand, careful respect of isospin conservation rules must be ensured. The coupling (3) is manifestly a scalar in the total fermion-boson isospin space. But the intermediate states $|N\rangle$ do not have pure isospin as they contain a proton particle and a neutron hole while only isoscalar phonons have been considered. This leads to a coupling of the GTR, which has isospin quantum numbers $|T, T_z\rangle = |T_0 - 1, T_0 - 1\rangle$ where $T_0 = \frac{N-Z}{2}$, with states which in general have a mixture of different T components. The nuclear part of the Hamiltonian actually forbids this coupling, and we impose that it is strictly forbidden (this amounts to neglecting Coulomb effects in the residual interaction). This can be done by projecting out the $T_0 - 1$ component of the intermediate state $|N\rangle$.

Table 1: Averaged quantities obtained from the strength distributions of GTR and IMR. The excitation energies are always referred to the ground state of ^{208}Pb.

Gamow-Teller resonance in ^{208}Bi

	Theory		Experiment [2]
	SIII	SGII	
Mean Energy	21.11 MeV	22.43 MeV	19.2 MeV
Width	3 MeV	3.1 MeV	3.7 MeV
Percentage of strength	61%	68%	~ 60-70% [20]

Isovector monopole resonance in ^{208}Tl

	Theory (SIII)		Experiment	
	peak I	peak II	(π^-, π^0)[10]	$(^{13}C, ^{13}N)$[13]
Mean Energy	8.33 MeV	16.63 MeV	12.0± 2.8 MeV	21.5± 0.6 MeV
Width	1.7 MeV	4 MeV	11.6± 7.1 MeV	3.1± 0.5 MeV
Percentage of EWSR	12%	55%		

The strength distribution for the GTR has been calculated with both interaction SIII and SGII and the results are shown in Fig. 1. Secondary bumps contribute to the line shape of the resonance and the large density of states which can couple to this mode (~ 500-1000 per MeV) is probably responsible for its fragmentation. The main results concerning these strength distributions are summarized in Table 1. The mean excitation energy $< \omega >$ is overestimated with respect to the experimental value. The width Γ is ~ 75% of the experimental value and this can be considered reasonable as only a class of "doorway states" is included in the calculation and not their full hierarchy. The calculated energies and widths of Table 1 are obtained from the moments m_k of the strength distribution as

$$
\begin{aligned}
<\omega> &\equiv \frac{m_1}{m_0} \\
\sigma^2 &\equiv \frac{m_2 - m_1^2}{m_0} \\
\Gamma &\cong 2.4\sigma.
\end{aligned}
\qquad (11)
$$

The experimental result concerning the percentage of strength in the region around the main hump (which is far from 100% in contrast with many other giant resonances) is well reproduced by the calculation. The remaining strength is found in our calculation outside the interval 19-25 MeV and is rather fragmented.

Table 2: Branching ratios for the decay of GTR in ^{208}Bi, obtained by using SGII force.

Decay channel	Theory			Experiment
	only $W^{\uparrow}$	$W^{\uparrow} + W^{\downarrow}$		
		(a)	(b)	[2]
$p_{\frac{1}{2}}$	0.223	0.033	0.018	0.013±0.002
$p_{\frac{3}{2}}$	0.418	0.035	0.019	0.023±0.003
$i_{\frac{13}{2}}$	0.014	0.003	0.001	0.002±0.002
$f_{\frac{5}{2}}$	0.319	0.013	0.007	includ. in $p_{\frac{3}{2}}$
$f_{\frac{7}{2}}$	0.016	0.010	0.003	0.003±0.002
$h_{\frac{9}{2}}$	0.010	0.001	$< 10^{-3}$	-
$\sum_c B_c$	1.0	0.095	0.048	0.041±0.009

In order to evaluate branching ratios for proton decay we have made an average over the whole energy interval in which the strength is appreciably different from zero of the numerator and of the denominator of (6) and we have thus defined

$$
B_c(\mathrm{GTR}) \equiv \frac{\langle\sigma_c\rangle}{\langle\sigma_{exc}\rangle}. \qquad (12)
$$

These branching ratios calculated with SGII interaction are shown in Table 2. Here, column "only $W^{\uparrow}$" refers to a calculation in which only the coupling with the continuum configurations is taken into account. The sum of branching ratios is 1 as no further decay channels are allowed. The other columns under "Theory" include the results of the complete calculation. Column (a) shows results of the plain self-consistent model. In column (b) the final state energy ε_h has been corrected in order to give the escaping proton the same energy ε it has in the experiment ($\varepsilon = \varepsilon_h + \omega$) which differs from our estimate due to the discrepancy in the excitation energy ω. Also empirical spectroscopic factors [21] are included to renormalize the final state. The results in column (b) are in good agreement with the experimental data. On the other hand, indications from the MSU experiment [7] leave open the possibility that experimental branching ratios might be larger than found in [2]. Branching ratios calculated with SIII interaction are some 50% larger [16] as these quantities seem to be rather sensitive to the choice of the inputs of the calculation (mean field properties and p-h residual interaction).

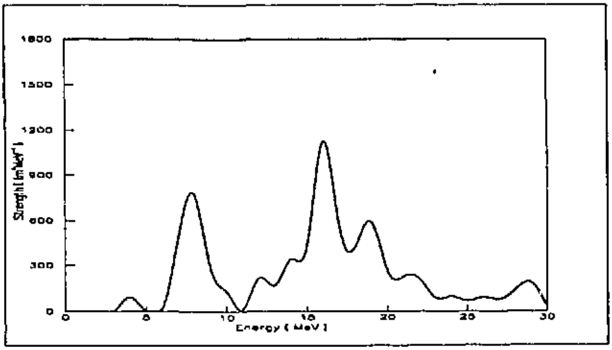

Figure 2: Strength function of the IVGMR calculated by using SIII interaction.

As pointed out in the introduction, the properties of the IVGMR are not yet well known despite their important relations with quantities like the symmetry energy of nuclear matter and Coulomb mixing in nuclei. The IVGMR is excited by

$$M_k = \frac{1}{2}\sum_{i=1}^{A} r^2(i)\tau_k(i), \; k = 0, \pm. \tag{13}$$

We have considered the case M_+ which corresponds to the experiments of Refs. [10, 13]. We deal with a neutron particle-proton hole states superposition which defines an excited state of good isospin and we do not need to project out spurious isospin couplings as it was mentioned above for the GTR. On the other hand, there is no argument here to justify the neglection of ground state correlations and we have performed for the IVGMR a complete charge-exchange RPA calculation. The force SIII has been used in the present case. After coupling with the continuum configurations the results are very similar to the ones already obtained in [22]. The coupling with "doorway states" pushes downward the main peak which results at $\sim$ 16 MeV and also fragments out a sizable fraction of strength in a smaller peak at lower energy ($\sim$ 8 MeV). This can be seen in Fig. 2 where the strength distribution is depicted. With the same procedure already adopted in the case of GTR the mean excitation energies and widths are extracted for the two peaks separately and reported in Table 1. The energies of the two peaks do not coincide with experimental findings but calculations employing other forces are in progress in order to test the sensitivity of the results. The energy difference between the peaks is of the same order as the discrepancy between the two experiments. A calculation of the transition densities of the states in the two energy regions is in progress in order to understand if they correspond to different kinds of excitations which would respond differently to various probes. Preliminary estimates seem to indicate a non negligible neutron decay branch from the higher bump region. The experimental observation of this decay and of its isotropic angular distribution could be a signature of the $\Delta L = 0$ character of the resonance.

4. Conclusions

A model which self-consistently includes the mean-field description of nuclear giant resonances plus their coupling to continuum states and to "doorway states" composed of 1p-1h configurations and collective, mainly surface, vibrations has been applied to the study of two charge-exchange states, namely the GTR in ^{208}Bi and the IVGMR in ^{208}Tl which have been objects of controversial experimental and theoretical studies. The model contains no free parameters but depends on the choice of the effective nucleon-nucleon interaction. The quantities calculated are the strength distributions and the decay cross sections in plane wave Born approximation. From these quantities centroids, total widths and particle-decay branching ratios can be obtained. Theory provides for the first time an overall account of the experimental findings in the case of GTR. In the case of IVGMR still some questions are open.

5. Acknowledgements

One of us (G.C.) would like to gratefully acknowledge the support of ECT* in Trento, where a part of this work was carried out, as well as the European Community fellowship (contract CHRXCT92-0075) which allowed his stay in Orsay.

References

[1] See: D. Beaumel, S. Fortier, S. Galès, J. Guillot, H. Langevin-Joliot, H. Laurent, J.M. Maison, J. Vernotte, J.A. Bordewijk, S. Brandenburg, A. Krasznahorkay, C.M. Crawley, C.P. Massolo and M. Renterìa, Phys. Rev. C49, 2444 (1994), and the contribution by S. Fortier in these proceedings.

[2] H. Akimune, M. Yosoi, I. Daito, M. Fujiwara, T. Inomata, Y. Sakemi, Y. Fujita, M.B. Greenfield, M.N. Harakeh, J. Jänecke, K. Katori, S. Nakayama, H. Sakai and M. Tanaka, Phys. Lett. B323, 107 (1994). See also the contribution by M.N. Harakeh in these proceedings.

[3] C. Gaarde, J.S. Larsen, A.G. Drentje, M.N. Harakeh and S.Y. van der Werf, Phys. Rev. Lett. 46, 902 (1981).

[4] H.R. Fiebig and J. Wambach, Nucl. Phys. A386, 381 (1982).

[5] P.F. Bortignon, F. Zardi and R.A. Broglia, in: *Proceedings of the Int. Conference on Spin Excitations in Nuclei, Telluride, 1982*, edited by F. Petrovich *et al.* (Plenum Press, New York, 1984), p. 425.

[6] See e.g.: T.N. Taddeucci, C.A. Goulding, T.A. Cary, R.C. Byrd, C.D. Goodman, C. Gaarde, J. Larsen, D. Horen, J. Rapaport and E. Sugarbaker, Nucl. Phys. **A469**, 125 (1987).

[7] S. Galès, private communication.

[8] N. Van Giai, P.F. Bortignon, A. Bracco and R.A. Broglia, Phys. Lett. **B233**, 1 (1989).

[9] S.E. Muraviev and M.H. Urin, Nucl. Phys. **A569**, 267c (1994) and **A572**, 267 (1994).

[10] A. Erell, J. Alster, J. Lichtenstadt, M.A. Moinester, J.D. Bowman, M.D. Cooper, F. Irom, H.S. Matis, E. Piasetzky and U. Sennhauser, Phys. Rev. **C34**, 1822 (1986).

[11] C. Bérat, M. Buénerd, J. Chauvin, J.Y. Hostachy, D. Lebrun, P. Martin, J. Barrette, B. Berthier, B. Fernandez, A. Miczaïka, W. Mittig, E. Stiliaris, W. von Oertzen, H. Lenske and H.H. Wolter, Phys. Lett. **B218**, 299 (1989).

[12] S. Raman, C.A. Houser and T.A. Wielkiewicz, At. Data Nucl. Data Tables **21**, 567 (1978).

[13] C. Bérat, M. Buénerd, J.Y. Hostachy, P. Martin, J. Barrette, B. Berthier, B. Fernandez, A. Miczaïka, A. Villari, H.G. Bohlen, S. Kubono, E. Stiliaris and W. von Oertzen, Nucl. Phys. **A555**, 455 (1993).

[14] I. Lhenry, private communication.

[15] G. Colò, P.F. Bortignon, N. Van Giai, A. Bracco and R.A. Broglia, Phys. Lett. **B276**, 279 (1992).

[16] G. Colò, P.F. Bortignon, N. Van Giai, and R.A. Broglia, to appear in Phys. Rev. C (1994).

[17] D. Vautherin and D.M. Brink, Phys. Rev. **C5**, 626 (1972); M. Beiner, H. Flocard, N. Van Giai and P. Quentin, Nucl. Phys. **A238**, 29 (1975).

[18] N. Van Giai and H. Sagawa, Phys.Lett. **B106**, 379 (1981).

[19] S. Yoshida, Suppl. Progr. Theor. Phys. **74& 75**, 142 (1983).

[20] C. Gaarde, in: *Proceedings of the Niels Bohr Centennial Conference on Nuclear Structure*, edited by R.A. Broglia *et al.* (North-Holland, Amsterdam, 1985), p. 449c.

[21] C. Mahaux and R. Sartor, Adv. Nucl. Phys. **20**, 1 (1991).

[22] N. Auerbach and A. Klein, Nucl. Phys. **A395**, 77 (1983).

Evidence for the Isoscalar Giant Dipole Resonance in ^{208}Pb using Inelastic α Scattering at and near 0°

B. F. Davis[1], H. Akimune[2], A. Bacher[3], G. P. A. Berg[3], C. C. Foster[3], M. Fujiwara[2], U. Garg[1], M. N. Harakeh[4], J. Jänecke[5], J. Lissanti[6], K. Pham[5], W. Reviol[1,*], D. Roberts[5], E. J. Stephenson[3], Y. Wang[3].

[1]*Physics Department, University of Notre Dame, Notre Dame, IN 46556, U.S.A.*
[2]*RCNP, Ibaraki, Mikogaoka 10-1, 567 Osaka, Japan.*
[3]*IUCF, 2401 Milo B. Sampson Lane, Bloomington, IN 47405, U.S.A.*
[4]*KVI, 9747 AA Groningen, The Netherlands.*
[5]*Department of Physics, University of Michigan, Ann Arbor, MI 48109, U.S.A.*
[6]*Department of Physics, Centenary College, Shreveport, LA 71134, U.S.A.*

ABSTRACT

The isoscalar giant dipole resonance (ISGDR) in ^{208}Pb has been investigated using inelastic scattering of 200 MeV α particles at and near 0° where the angular distribution of the ISGDR can be clearly differentiated from other modes. The "difference of spectra" technique was employed to separate the contribution from the high-energy octupole resonance (HEOR). Preliminary angular distribution data provide clear evidence for the ISGDR adjacent to the HEOR.

The term "giant dipole resonance" almost universally brings to mind the *isovector* giant dipole resonance (IVGDR), a collective mode that has been a subject of intensive experimental and theoretical investigation since its discovery almost fifty years ago. This paper, instead, reports our investigation of the *isoscalar* giant dipole resonance (ISGDR), an "exotic" mode of collective vibration, best described as a "hydrodynamical density oscillation" in which the volume of the nucleus remains constant and the state can be visualized in the form of a compression wave—analogous to a sound wave—oscillating back and forth through the nucleus; this phenomenon also has been referred to as the "squeezing mode" [1]. This is a second-order effect; in the first order, of course, the isoscalar dipole mode corresponds merely to spurious center-of-mass motion. In addition to being of substantial intrinsic interest as an exotic and fundamental mode of collective

*Present address: University of Tennessee, Department of Physics, Knoxville, TN 37966, U.S.A.

oscillation, the ISGDR also has its importance in that it provides, like the giant monopole resonance (or "breathing mode"), a direct measurement of the nuclear incompressibility.

The excitation energy of the ISGDR is given by the scaling model [2] as:

$$E_x = \sqrt{\frac{7}{3} \cdot \frac{K_A + \frac{27}{25}\varepsilon_F}{m <r^2>}}$$

where K_A is the incompressibility of the nucleus and ε_F is the Fermi energy. The most common and well-known experimental determination of the nuclear incompressibility so far has been achieved via measurement of the excitation energies of the giant monopole resonance (GMR), the systematics of which are already quite well established [3]. There have been concerns, however, about the suitability of the available GMR data alone in the extraction of the nuclear incompressibility of infinite nuclear matter [4–6] and a detailed and systematic investigation of the ISGDR could provide additional information, leading, it is hoped, to a more precise determination of the incompressibility of nuclear matter.

The evidence for the ISGDR has been rather sparse so far. Indications for this resonance have been reported in inelastic scattering experiments at forward angles on ^{208}Pb and ^{144}Sm [7–9]. However, since it lies very close in energy to the high-energy octupole resonance (HEOR), an unambiguous identification of the ISGDR, based on the angular distributions, is possible only at angles near 0°—DWBA calculations indicate that any appreciable differences in the angular distributions of the two resonances appear only in the near-0° angular region. The situation, thus, is quite similar to that of the GMR more than a decade ago: unambiguous evidence for GMR could be established only by measurements at the smallest angles where the GMR angular distribution differs substantially from that of the giant quadrupole resonance (GQR) which lies at an excitation energy very close to that of the GMR.

Fig. 1 shows the expected inelastic α scattering angular distributions for the ISGDR and HEOR in ^{208}Pb over the angular range 0°–14° as calculated by the program CHUCK3 [10]. The optical model parameters used in this calculation were: V = 155, r = 1.282, a = 0.677, W = 23.26, r_W = 1.478, a_W = 0.733 and r_C = 1.3 and were adopted from Ref. [11]. For the HEOR, the standard collective form factor [12] was used; for the ISGDR, the form factor was taken from Ref. [1]. Inelastic scattering of alpha particles near 0° has the advantage that, because of the isoscalar nature of this reaction, only these two giant resonances are expected to be predominantly excited at the excitation energies of interest. In addition, as indicated by the calculations presented in Fig. 1, the cross sections for these resonances are at or near their maximum values at these angles.

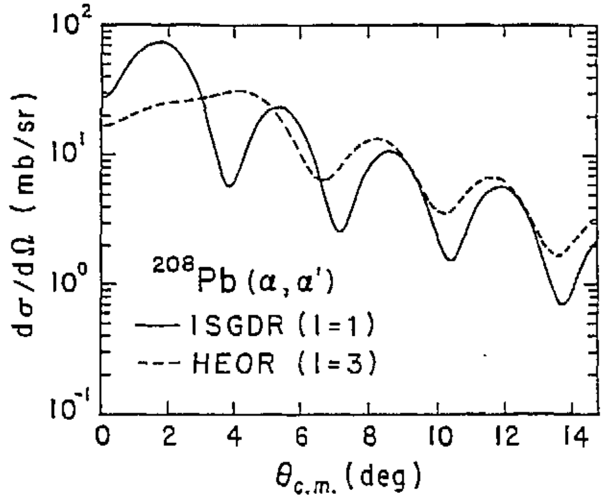

Figure 1. Angular distributions for the ISGDR (solid line) and the HEOR (dashed line) as obtained in a DWBA calculation using the program CHUCK3. For details of the calculation and the parameters used, see text.

We have undertaken a detailed investigation of the ISGDR in ^{208}Pb to obtain conclusive evidence for its existence via measurements at very small angles. The expected angular distributions make imperative the use of the "difference-of-spectra technique"; this procedure has been used very effectively in detailed investigations of the GMR [13] and is briefly described here. The inelastic spectrum near 0° (0°→2° in our case--the angular acceptance of the IUCF K600 spectrometer) may be divided into two parts (0°→1° and 1°→2°, respectively). Since the ISGDR cross section is rising rapidly in this region whereas the HEOR cross section remains nearly constant, if one subtracts the spectrum for the 0°→1° angular cut from that for the 1°→2° angular cut, the difference of these two spectra would show only a very small contribution from the HEOR or from the background. In principle, this would yield a spectrum that is a lucid representation of primarily the ISGDR strength.

(α, α') measurements were performed at very small angles (including 0°) using a 200 MeV alpha-particle beam in conjunction with the K600 spectrometer at the Indiana University Cyclotron Facility. The K600 is a versatile, high resolution dipole spectrometer with an elaborate detector array in the focal plane [14]. In our experiment, the detector system consisted of two clusters of horizontal and vertical drift chambers--one vertical drift chamber to measure horizontal position x, and two horizontal drift chambers with staggered sense-wire positions to measure the vertical position y. The two clusters were spaced approximately 20 cm apart so that slope information for the particle track could be obtained in both the x and y directions. This information was essential in performing the ray-tracing required for angle reconstruction. Particle identification was obtained using the ΔE signals provided by two plastic scintillators placed behind the drift-chamber clusters.

Data was obtained at $(0\pm2)^\circ$ (the maximum angular opening possible at 0° in the K600), as well as at 4°, 5°, 6°, 7°, 8° and 10°, with an energy resolution of approximately 130 keV. Although the resolution achievable for this system is significantly better, no serious attempts were made to optimize the resolution for this work since this resolution was more than adequate for measuring the ISGDR and greater statistics through increased data production time was judged more desirable than an improved resolution. The non-zero angle measurements were taken during an experimental run using a newly-commissioned septum magnet which allowed measurements below 7° for the first time at the K600; however, this report concerns the 0° measurements only. A 3.0 mg/cm^2 thick ^{208}Pb target was employed; data were also obtained on ^{24}Mg for purposes of calibration.

The measurements at small angles, as is well known, require a very careful tuning of the beam to minimize the contributions from the background due to beam halo and slit-scattering, etc. After considerable effort, it was possible to obtain a rather "clean" beam; further "cleaning" of the spectra was achieved in part by employing a gate on the TOF signal from the scintillators.

Fig. 2(a) shows the $0^\circ\rightarrow2^\circ$ spectrum for ^{208}Pb. A broad "bump", most likely comprised of the ISGDR and the HEOR, is clearly visible above background. The data has been fitted with a polynomial background and two Gaussian peaks and the results of the fit are shown superimposed; using a single, wider peak always resulted in a significantly worse fit. The centroids of the two peaks (19.7 ± 0.5 MeV and 22.4 ± 0.5 MeV) are in agreement with the energies previously suggested [4–6] for the HEOR and ISGDR, respectively; the widths of the two peaks in these fits (<3 MeV) are, however, somewhat smaller than those previously reported. The "difference" spectrum, obtained by subtracting the $0^\circ\rightarrow1^\circ$ cut from the $1^\circ\rightarrow2^\circ$ cut, as described previously, is shown in Fig. 2(b) along with a two-peak fit employing peak parameters identical to those used in the peak fits shown in Fig. 2(a). In this case, a "free" fit always preferred a single, slightly broader, peak; the fit as shown was obtained by requiring two-peaks in order to show the reduction in the strength of one of the components. As can be seen, the "HEOR component" of the bump is almost completely eliminated in this spectrum, leaving only the "ISGDR component", as expected. A similar conclusion can be drawn from a comparison of the centroids of the "bumps" in the two spectra: the centroid of the "difference" spectrum (22.5 MeV) is located at almost 1 MeV higher in excitation energy than that in the full spectrum

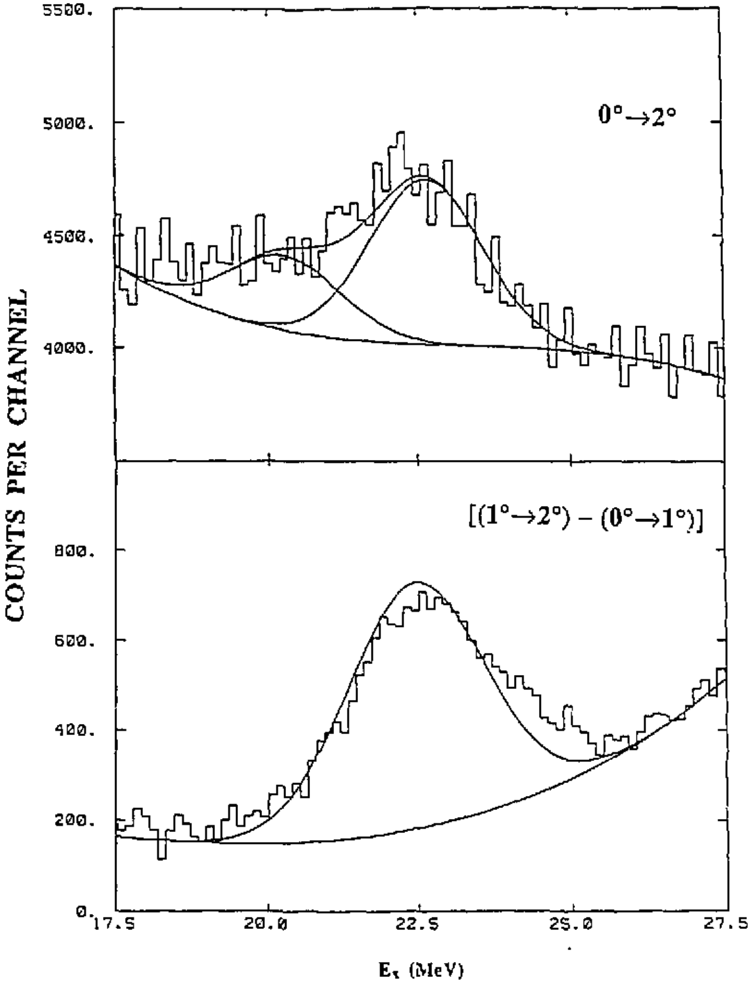

Figure 2. (a) Inelastic α scattering specra for ^{208}Pb for (0±2)°. A two-peak+polynomial background fit to the data is shown superimposed with the peaks corresponding to the HEOR and the ISGDR indicated.
(b) The "difference" spectrum, obtained as described in the text. Also shown is a fit using peak-parameters identical to those in (a); note that the fit corresponds to no HEOR strength.

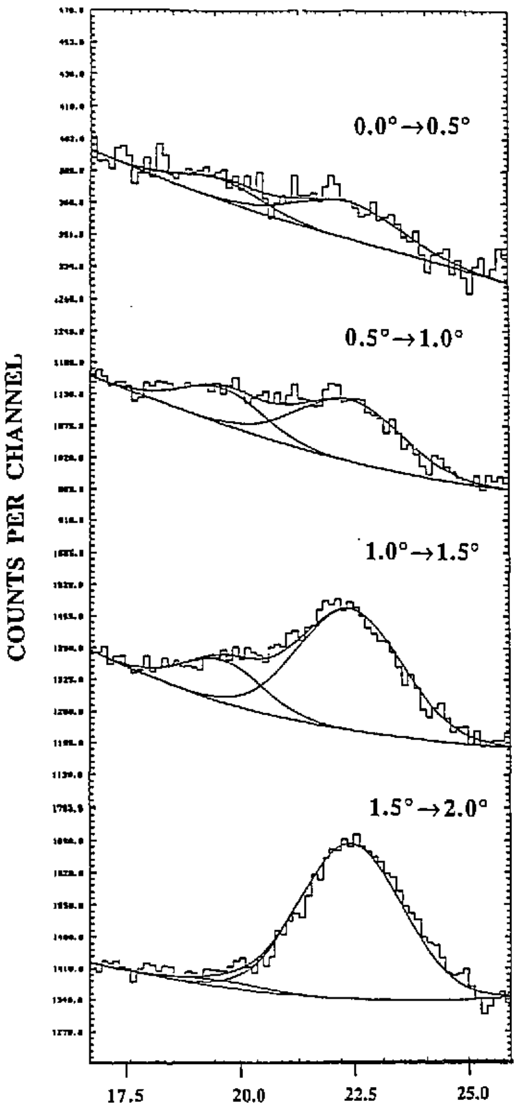

Figure 3. Inelastic α scattering spectra for ^{208}Pb for four angular bins between 0→2°. Two-peak + polynomial background fits to the data, as described in the text, are shown superimposed.

(21.3 MeV), again consistent with a reduction in the HEOR strength as expected from the predicted angular distributions for the HEOR and the ISGDR. The "bump" in Fig. 2(b), thus, represents primarily the ISGDR strength and can be subjected to detailed investigation to extract the properties of this resonance. We also note that the position and width extracted for the ISGDR from our data are in very good agreement with the theoretical predictions for this resonance by [15].

Further extension of data analysis has been possible by dividing the data into 0.5° wide angular bins corresponding to 0°→0.5°, 0.5°→1°, 1°→1.5°, and 1.5°→2°, thus providing a rough angular distribution for the two components of the GR bump identified as the HEOR and the ISGDR. Fig. 3 shows these four spectra along with the two-peak fits as described above; again, the same position and width parameters have been employed in fits to all spectra. It is clear from these spectra themselves, that the two components are displaying an "angular distributions" quite different from each other, confirming further that the GR bump is comprised of two distinctly different resonances. Fig. 4 shows these

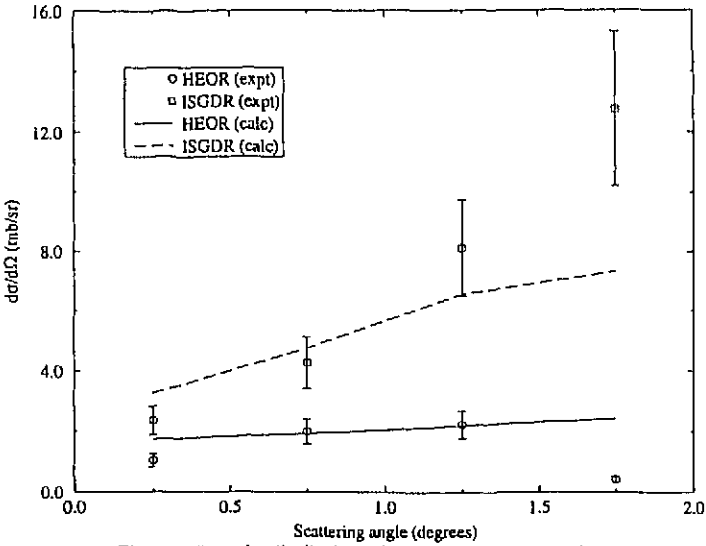

Figure 4. "Angular distributions" for the two components of the GR bump and their comparison with the angular distributions for ISGDR (solid line) and the HEOR (dashed line) expected from DWBA calculations.

"angular distributions" for the two components and compares them with the angular distributions for the HEOR and ISGDR expected from DWBA calculations; the experimental data appear to follow the qualitative behavior of the expected angular distributions quite well. Considering the rather poor statistics in spectra associated with the individual angle bins and the uncertainties in the angular cuts, this apparent agreement is indeed quite remarkable.

To summarize, we have measured inelastic α-scattering spectra at and near 0° with a view to obtaining conclusive evidence for the ISGDR. Our data provide good evidence for the ISGDR, located adjacent to the HEOR in ^{208}Pb. The excitation energies of the two resonances, as extracted from our data, are in agreement with those previously suggested for ISGDR and HEOR in ^{208}Pb; the widths are somewhat smaller, however. The rough angular distributions of the two resonances appear to follow those expected from DWBA calculations. Further, the efficacy of the "difference of spectra" technique in identifying the ISGDR has been affirmed and future experiments using this technique will be carried out on a numer of nuclei over the periodic table to study the systematics of the ISGDR.

It is with pleasure that we acknowledge the cooperation of the operations crew of the Indiana University Cyclotron Facility in providing the high quality α beams required for this work. This work has been supported in part by the National Science Foundation and the NATO Division of Scientific Affairs.

REFERENCES

[1] M. N. Harakeh, Phys. Lett. **B90** (1980) 13; M. N. Harakeh and A. E. L. Dieperink, Phys. Rev. **C 23** (1981) 2329.

[2] S. Strignari, Phys. Lett. **B108** (1982) 232.

[3] See, for example, A. van der Woude in *Electric and Magnetic Giant Resonances in Nuclei*, J. Speth, Ed. (World Scientific, 1991) pp 100.

[4] J. M. Pearson, Phys. Lett. **B271** (1991) 12.

[5] M. M. Sharma in *Slide Report for the Notre Dame Workshop on Giant Resonances and related Phenomena, Notre Dame*, 1991, U. Garg, Ed. (unpublished).

[6] S. Shlomo and D. H. Youngblood, Phys. Rev. **C 47** (1993) 529.

[7] H. P. Morsch *et al.*, Phys. Rev. Lett. **45** (1980) 337; and, Phys. Rev. **C 28** (1983) 1947.

[8] C. Djalali *et al.*, Nucl. Phys. **A380** (1982) 42.

[9] G. S. Adams *et al.*, Phys. Rev. **C 33** (1986) 2054.

[10] P. D. Kunz, University of Colorado, 1983 (unpublished).

[11] H. P. Morsch *et al.*, Phys. Rev. C **20** (1979) 1600.

[12] G. R. Satchler, Particles and Nuclei **5** (1973) 105.

[13] S. Brandenburg *et al.*, Nucl. Phys. **A446** (1987) 29.

[14] G. P. A. Berg in *Slide Report for the Notre Dame Workshop on Giant Resonances and related Phenomena, Notre Dame*, 1991, U. Garg, Ed. (unpublished).

[16] S. E. Murav'ev and M. G. Urin, Bull. Acad. Sci. USSR (Phys. Ser.) **52** (1988) 123.

Excitation and Decay of Giant Resonances in the ^{40}Ca(e,e'x) and ^{40}Ca(p,p'x) Reactions*

P. von Neumann-Cosel

Institut für Kernphysik, Technische Hochschule Darmstadt, Schlossgartenstr. 9, D-64289 Darmstadt, Germany

Abstract

Results of (e,e'x) and (p,p'x) coincidence studies (with x = p,α) of the giant resonance excitation region in ^{40}Ca are discussed. A multipole decompostion of the (e,e'x) cross sections demonstrates excellent agreement of the E1 strength with photonuclear data. The E2 (plus E0) strength is strongly fragmented with maxima at about 12, 14 and 17 MeV and exhausts 80(16) % of the energy-weighted sum rule (EWSR). A multipole analysis of the (e,e'α_0) angular correlation functions reveals an E0 cross section contribution of about 50 % while little E0 strength is found in the p_0 decay from a comparison of electron and proton scattering results. The unfolded E2 and E0 strength distributions in the α_0 channel are in good agreement with hadron induced coincidence experiments.

1. Introduction

The doubly magic nucleus ^{40}Ca has always been a favoured subject of both experimental and theoretical work. Giant resonances in ^{40}Ca have been extensively studied with electromagnetic and hadronic probes and a rather compact giant dipole resonance (GDR) with a maximum at 19.5 MeV and a strongly fragmented isoscalar giant quadrupole resonance (GQR) at about 18 MeV have been observed [1]. However, the multipole strength is strongly mingled in the 10 - 25 MeV excitation energy region and a number of open problems remain. Different results have been reported for the total strength and fine structure of the GQR. A ^{40}Ca(α,α'x) experiment [2] found a roughly equal splitting of the energy weighted sum rule (EWSR) strength with a second maximum at about 14 MeV in contrast to all previous investigations. Also isoscalar giant monopole resonance (GMR) strength was detected in inelastic α scattering at very forward angles not seen in earlier experiments [3].

The present work reports an investigation of ^{40}Ca with the (e,e'x; x=p,α) reaction in the excitation region $E_x = 8 - 26$ MeV. Electron scattering coincidence experiments are especially attractive for giant resonance studies since they allow an efficient suppression of the huge

*Supported by the German BMFT under contract 06 DA 641 I and by the South African FRD.

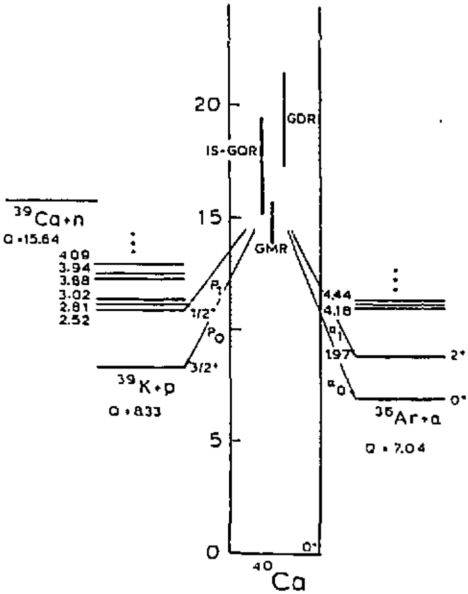

Fig. 1. Relevant excitation region in ^{40}Ca and possible decay channels.

radiative tails which usually limit the extraction of broad structures in inclusive measurements. Additionally, first results of a ^{40}Ca(p,p′x) study are reported which aims at a detailed study of the GQR fine structure. Furthermore, these data together with the previous (α,α′x) experiment [2] represent a unique set of coincidence experiments on a single nucleus to study the properties of giant multipole strength decay. Because of the space limitations the discussion is limited here to the extraction of multipole strength distributions and the fine structure observed in the decay into ground states of the daughter nuclei. Additional results on the (e,e′p) angular correlation functions and the relative importance of statistical and direct decay can be found in Refs. [4, 5].

The relevant excitation and decay features in ^{40}Ca are displayed schematically in Fig. 1. Proton and α decay into low-lying states of ^{39}K (p_0 - p_3) and ^{36}Ar (α_0, α_1), respectively, could be resolved. Neutron emission, which was not measured in the present experiments, competes above the threshold energy E_n = 15.67 MeV. However, photon induced reactions [6] indicate a neutron contribution of only about 20 % at the GDR maximum excitation energy.

2. Experiments

2.1. The $^{40}Ca(e,e'x)$ reaction

The (e,e'x) experiments were performed at the accelerators MAMI A in Mainz and at the S-DALINAC in Darmstadt. In Mainz, 183.5 MeV electrons were used and the scattered electrons were detected with a magnetic spectrometer at angles (momentum transfers) Θ_e = 22.0° ($q = 0.35$ fm^{-1}), 31.4° (0.49 fm^{-1}) and 43.0° (0.66 fm^{-1}). In Darmstadt data were taken with a large solid-angle QCLAM spectrometer at E_0 = 78 MeV and Θ_e = 40.0° (0.26 fm^{-1}). The small momentum transfers lead to a preferential excitation of low multipole ($\lambda \leq 2$) transitions. The decay products were detected relative to the q axis with up to 10 charged particle detector telescopes consisting of 75 - 100 μm ΔE and two 1000 μm E Si counters. The telescopes were placed on a goniometer out of plane under an azimuthal angle Φ_x = 135° (using the convention of Ref. [7]) in order to cancel the transverse-transverse interference contribution to the reaction cross section.

Angular correlation functions (ACF) were extracted for resolved decay channels in typical excitation energy bins of about 1 MeV which were defined as a compromise between visible fine structure and the need of statistics. Branching ratios of the decay into the final channels were derived from a 4π integration of the measured coincidence cross sections assuming purely longitudinal excitation. Details of the data analysis and a summary of the experimental results can be found in Ref. [8].

2.2. The $^{40}Ca(p,p'x)$ reaction

The experiment was performed at the National Accelerator Centre cyclotron at Faure (South Africa) with 100 MeV protons using a recently built K = 600 magnetic spectrometer. Scattered protons were measured at angles Θ_p = 17°, 23° and 27°. Charged particle decay was detected with three semiconductor detector telescopes placed on a rotatable table in the reaction plane. A typical energy resolution of $\Delta E \simeq 35$ keV FWHM was achieved in the ^{40}Ca excitation spectra. The data analysis is still in progress and the discussion is restricted to results for the decay into the ^{36}Ar and ^{39}K ground states.

3. Results

3.1. Multipole decomposition from the variation of the momentum transfer

A multipole strength analysis based on the variation of the momentum transfer was per-

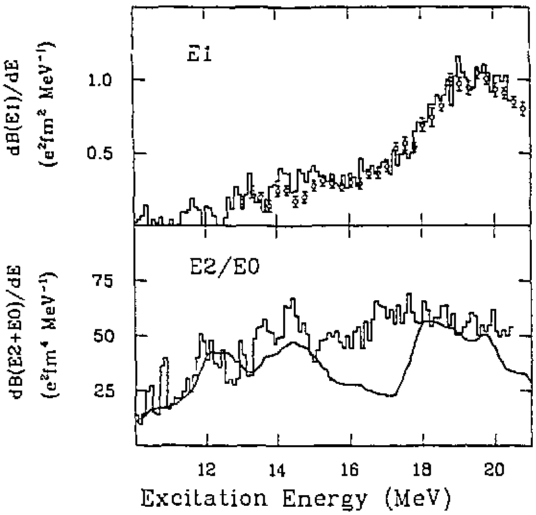

Fig. 2. E1 and E2 (plus E0) strength distributions resulting from the multipole analysis of (e,e'x) cross sections following Ref. [9]. The open circles are the difference of total photoabsoorption [10] and (γ,n) [11] data. The solid line is a RPA calculation of E2 strength in ^{40}Ca [13].

formed following the method described in Ref. [9]. It is based on the assumption that the form factors are excitation energy independent and that the contributing multipoles are limited to $\lambda \leq 2$. One should note that possible E0 contributions cannot be unfolded from E2 strength with this method because of the similarity of the form factors. Since it was found that the solutions of the linear equations system according to Ref. [9] are not unique an additional constraint was introduced. It combines the minimization of the number of negative strength coefficients and the minimization of the deviations from theoretical form factors.

The resulting GDR and GQR (plus GMR) strength functions are displayed in Fig. 2. The GDR results are compared to photonuclear cross sections derived from the difference of total photoabsorption [10] and (γ,n) [11] data (open circles). The shapes and absolute values of the two curves agree very well. The E2 (plus E0) strength distribution is strongly fragmented and shows maxima around 12, 14 and 17 MeV. The latter corresponds to E2 strength observed in numerous previous experiments. The strength around 12 MeV corresponds to a number of discrete E2 transitions which could be resolved in high resolution (e,e') experiments [12].

The solid line presents the result of a state-of-the-art RPA calculation of isoscalar E2 strength including 1p1h$\otimes$phonon configurations and proper continuum coupling [13]. For a description of the approach see Ref. [14]. The quality of reproduction of the experimental results is remarkable and, for the first time, a realistic theoretical approach of the strongly frag-

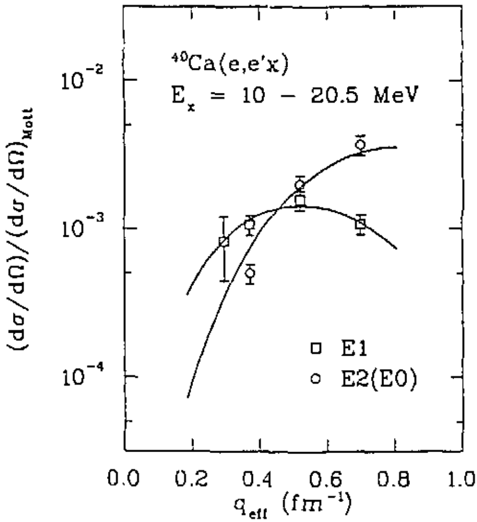

Fig. 3. Form factors resulting from the multipole analysis. The theoretical E1 form factor is a MSI-RPA calculation [15] and the theoretical E2 form factor was generated from the transition densities of the RPA calculation described in Ref. [13].

mented E2 strength with significant parts below $E_x = 15$ MeV is achieved. A detailed analysis reveals that the low-lying strength can be traced back to 2p2h ground state correlations which are treated beyond the usual RPA level in the present model.

The E1 form factor resulting from the analysis is displayed in Fig. 3 and compared to a RPA calculation [15] using the model of separable interactions (MSI). Good correspondence is obtained. Different to the multipole analysis decribed in Ref. [4], where the same model was used for the E2 form factor, in this case the E2 form factors were generated from transitions densities given in Ref. [13]. The integrated strengths for charged particle decay in the energy interval 10 - 20.5 MeV exhaust 58(15) % of the GDR, respectively 80(16) % of the isoscalar GQR energy weighted sum rule. The above value constitutes an upper limit for the GQR charged particle decay strength because of the possible monopole contributions.

3.2. Multipole analysis of the (e,e'α_0) angular correlation function

In general, a model independent multipole analysis of (e,e'x) ACF is not possible. One exception is the (e,e'α_0) channel for an even-even target nucleus, where one has a particularly simple spin sequence $0 \rightarrow \lambda \rightarrow 0$. The ACF can be written in the static limit of resonance approximation [7] as

$$W(\Theta) = |\sum_{\lambda=0}^{2} \sqrt{2\lambda+1}\, C_\lambda\, e^{i\delta_\lambda}\, P_\lambda(cos\Theta)|^2 \equiv \sum_{n=0}^{2\lambda} b_n\, cos^n\Theta \ , \tag{1}$$

where C_λ denotes the product of the longitudinal matrix element with the overlap of resonance and decay channel, δ_λ are the relative phases and the P_λ are Legendre polynomials. If the experimental ACF are analyzed by a $cos^n\Theta$ power series, the resulting coefficients b_n permit an analytical determination of the C_λ and δ_λ values [16].

Such an analysis for the ^{40}Ca(e,e$'\alpha_0$) data was performed with 100 keV binsize. The total cross section and the E0, E1, E2 decomposition are displayed in Fig. 4 for $q = 0.49$ fm^{-1} as an example. Results for other momentum transfers are similar. The E1 contribution is very small since GDR decay is isospin forbidden. The structures around $E_x = 14$ MeV (labeled 1 - 4) which have been subject of some discussion [19] can be assigned unique multipolarity.

The resulting spectrum of E2 cross sections is compared in the l.h.s. of Fig. 5 to results of the (p,p'x) study for the α_0 decay channel. The latter are shown for a scattering angle where $\lambda = 2$ is strongly enhanced with respect to other multipolarities. Indeed, almost identical structures are seen in both cases with somewhat more fine structure (because of the better energy resolution) in the proton data. The comparison also shows that similar to the findings in the (α,α'x) experiment [2] there is no sign of a continuum background below $E_x \simeq 16$ MeV. In the electron scattering experiment 9(2)% of the isoscalar E2 EWSR are found while 17(8)% are obtained in (p,p') using a derivative collective form factor and the optical model paramters of Schwandt *et al.* [20]. On the other hand, 16(1)% are obtained in the (α,α'x) measurement [2].

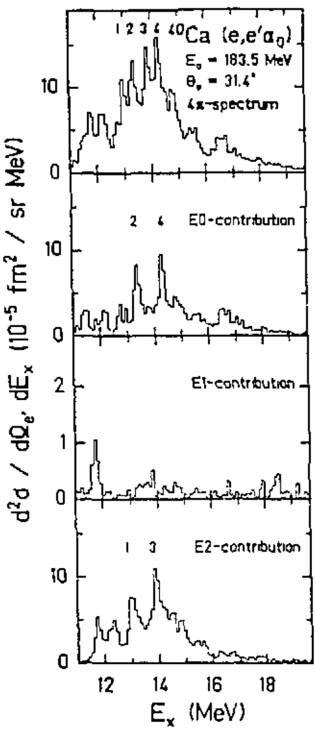

Fig. 4. The 4π integrated spectrum of the ^{40}Ca(e,e$'\alpha_0$) reaction at $q = 0.49$ fm^{-1} and E0, E1, E2 cross sections resulting from the multipole analysis of the ACF.

The r.h.s. of Fig. 5 compares the E0 part of the multipole analysis to the E0 strength extracted in Ref [3]. Again, good qualitative agreement of the main structures observed in the two

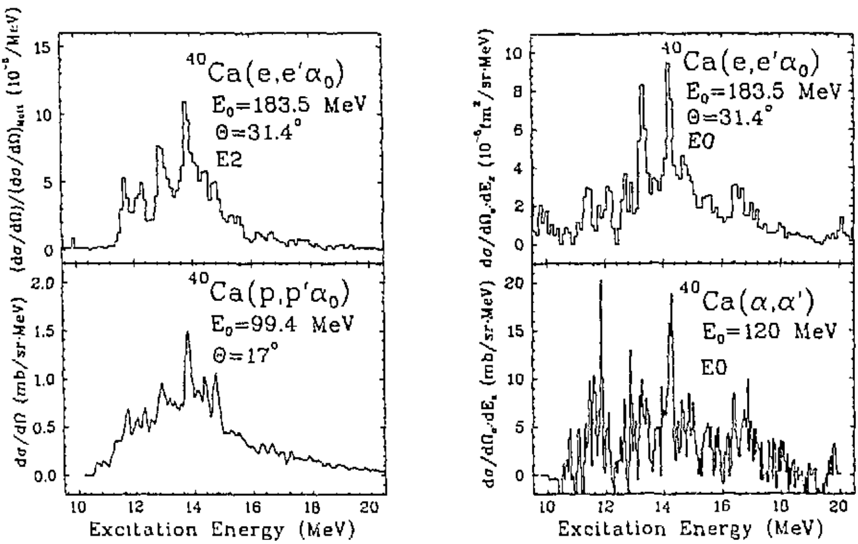

Fig. 5. E2 spectrum from the multipole analysis of the (e,e'α_0) ACF compared to a 4π integrated spectrum of the ^{40}Ca(p,p'α_0) reaction at an angle where E2 is strongly enhanced (l.h.s.). E0 spectrum compared compared to E0 strength extracted in (α,α') scattering [3] (r.h.s.).

experiments can be stated. 13(3) % of the EWSR for the GMR are exhausted in the electron scattering experiment, while 23(7) % are found in Ref. [3].

3.3. *Fine structure of the GQR in the p_0 decay channel*

The multipole analysis described in Sect. 3.1 can also be used for the experimentally resolved (e,e'p) channels. The upper part of Fig. 6 shows the resulting E2 (plus E0) cross sections for population of p_0 and the lower part the (p,p'p_0) spectrum at Θ_p = 17°, where quadrupole excitation dominates. Neglecting the data below $E_x \simeq 11$ MeV, where the (p,p') data are plagued by an efficiency cut-off in the detector, very good correpondence is obtained even on a level-by-level-basis. The close similarity supports the conclusion of the previous section on the absence of significant background in the (p,p') data up to $E_x \simeq 16$ MeV.

The EWSR fraction is 18(4) % in the (e,e'p_0) experiment and 36(8) % in the (p,p'p_0) experiment. Since equal E0 and E2 transition strength would lead to four times smaller E0 cross sections for the (p,p'), but roughly equal cross sections for (e,e') scattering one can conclude that little monopole strength is present in the p_0 decay channel. This is supported by the consistency of E0 contributions obtained in inclusive (α,α') and exclusive (α,$\alpha'\alpha_0$) scattering [3] which should differ by that amount.

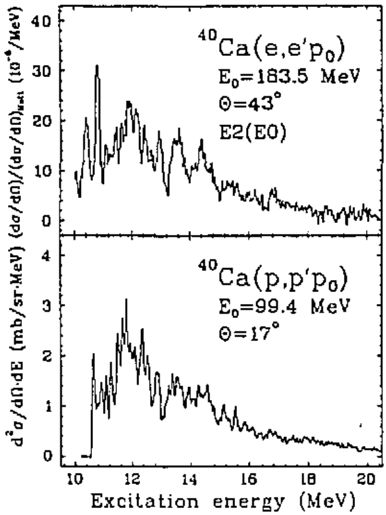

Fig. 6. E2 (plus E0) part of the cross section in the ^{40}Ca(e,e'p_0) channel obtained from the multipole analysis decribed in Sect. 3.1 compared to a ^{40}Ca(p,p'p_0) spectrum at $E_0 = 100$ MeV and $\Theta_p = 17°$, where E2 is strongly enhanced.

4. Conclusions

A multipole analysis of the strongly interweaved E0, E1 and E2 strength contributions in ^{40}Ca is presented on the basis of an (e,e'x) experiment. The decomposition of the total charged particle decay strength utilizing the variation of the momentum transfer demonstrtates excellent agreement with photonuclear data for the E1 part. The E2 strength distribution is strongly fragmented over the investigated energy range $E_x = 10 - 20.5$ MeV. The RPA approach described in Ref. [14] is able to account remarkably well for the obtained structures and indicates that the low-lying ($E_x < 15$ MeV) part is induced by 2p2h ground state correlations.

A multipole decomposition of the ACF measured in the (e,e'α_0) channel is presented. It is found that about 50 % of the total cross section is due to E0 contributions. Good agreement with the (p,p'x) and (α,α'x) experiments is obtained for the resulting E0 and E2 spectra such that multipole assignments become feasible for the more prominent levels. Excellent agreement between electron and proton scattering results is also found for E2 strength in the p_0 channel. The consistency of the extracted EWSR results in the different experiments is discussed.

Acknowledgements

The work described above would not have been possible without the contributions of many people. For the (e,e′x) experiments these are H. Diesener, U. Helm, J. Horn, C. Rangacharyulu, A. Richter, G. Schrieder, A. Stascheck, A. Stiller and S. Strauch. The (p,p′x) experiments were performed together with J. Carter, A.A. Cowley, R.W. Fearick, S. Förtsch, J.J. Lawrie, S.J. Mills, R.T. Newman, J.V. Pilcher, R.D. Smit, D.M. Steyn, Z.Z. Vilakazi and D.M. Whittal. I am particularly indebted to A. Richter for his generous support and invaluable discussions, and to J. Carter for a continuous collaboration on the subject. The help of M.N. Harakeh and J. Ryckebusch with model calculations and discussions with S. Kamerdzhiev are gratefully acknowledged.

References

[1] *Electric and Magnetic Giant Resonances in Nuclei*, ed. J. Speth (World Scientific, Singapore, 1991).

[2] F. Zwarts, A.G. Drentje, M.N. Harakeh and A. van der Woude, Phys. Lett. **B125** (1983) 123; Nucl. Phys. **A439** (1985) 117.

[3] S. Brandenburg, R. de Leo, A.G. Drentje, M.N. Harakeh, H. Sakai and A. van der Woude, Phys. Lett. **B130** (1983) 9.

[4] H. Diesener, U. Helm, G. Herbert, V. Huck, P. von Neumann-Cosel, C. Rangacharyulu, A. Richter, G. Schrieder, A. Stascheck, A. Stiller, J. Ryckebusch and J. Carter, Phys. Rev. Lett. **72** (1994) 1994.

[5] P. von Neumann-Cosel, H. Diesener, U. Helm, G. Herbert, V. Huck, A. Richter, G. Schrieder, A. Stascheck, A. Stiller, J. Carter, A.A. Cowley, R.W. Fearick, J.J. Lawrie, S.J. Mills, R.T. Newman, J.V. Pilcher, F.D. Smit, Z.Z. Vilakazi and D.M. Whittal, Nucl. Phys. **A569** (1994) 373c.

[6] D. Brajnik, D. Jamnik, G. Kernel, U. Miklavzic and A. Stanovnik, Phys. Rev. C **9** (1974) 1901.

[7] W.E. Kleppinger and J.D. Walecka, Ann. Phys. (N.Y.) **146** (1983) 349.

[8] U. Helm, Ph.D. thesis, Technische Hochschule Darmstadt (1990), unpublished.

[9] Th. Kihm, K.T. Knöpfle, H. Riedesel, P. Voruganti, H.J. Emrich, G. Fricke, R. Neuhausen and R.K.M. Schneider, Phys. Rev. Lett. **56** (1986) 2789.

[10] J. Ahrens, H. Borchert, K.H. Czock, H.B. Eppler, H. Gimm, H. Gundrum, M. Kröning, P. Riehm, G. Sita Ram, A. Zieger and B. Ziegler, Nucl. Phys. **A251** (1975) 479.

[11] A. Veysièrre, H. Beil, R. Bergère, P. Carlos, A. Lepêtre and A. de Miniac, Nucl. Phys. **A227** (1974) 513.

[12] R. Benz, Diploma thesis, Technische Hochschule Darmstadt (1984), unpublished.

[13] S. Kamerdzhiev, J. Speth and G. Tertychny, KFA Jülich Annual Report 1993, p. 157; and to be published.

[14] S. Kamerdzhiev, G. Tertychny and J. Speth, Nucl. Phys. **A569** (1994) 313c.

[15] W. Knüpfer, private communication.

[16] M. Spahn, T. Kihm and K.T. Knöpfle, Z. Phys. **A330** (1988) 345.

[17] T. Yamagata, S. Kishimoto, K. Iwamoto, B. Saeki, K. Yuasa, K. Ogino, S. Matsuki, T. Fukuda, M. Inoue, K. Hosono, A. Shimizu, N. Matsuoka, I. Miura, Y. Ikku and H. Ogata, Phys. Rev. **C36** (1987) 573.

[18] P. Schwandt, H.O. Mayer, W.W. Jacobs, A.D. Bacher, S.E. Vigdor, M.D. Kaitchuk and T. R. Donoghue, Phys. Rev. **C26** (1982) 55.

Excitation of the isovector GDR by inelastic α-scattering and the neutron skin of nuclei

A. Krasznahorkay,[a,b] M.N. Harakeh,[a] A. van der Woude, [a]
M. Csatlós, [b] Zs. Dombrádi, [b] A.T. Kruppa, [b] Z. Máté, [b] and D. Sohler [b]

[a] Kernfysisch Versneller Instituut, Zernikelaan 25, 9747AA, Groningen, The Netherlands
[b] Institute of Nuclear Research (ATOMKI), Debrecen, P.O. Box 51, H-4001, Hungary

Abstract: The cross section of the isovector giant dipole resonance (GDR) has been measured in the ^{116,124}Sn$(\alpha,\alpha'\gamma_0)$, ^{150}Nd$(\alpha,\alpha'\gamma_0)$ and ^{208}Pb$(\alpha,\alpha'\gamma_0)$ reactions at $E_\alpha = 120$ MeV and $0° \leq \Theta_{\alpha'} \leq 3°$. The results are compared with DWBA calculations performed with nuclear GDR form factors that depend on the relative difference between the radii of proton and neutron distributions $(\Delta R_{PN}/R_0)$. The ΔR_{PN} values for ^{116}Sn, ^{124}Sn and ^{208}Pb were deduced by comparing measured and calculated cross sections to be 0.02 ± 0.12 fm, 0.21 ± 0.11 fm, and 0.19 ± 0.09 fm, respectively. For the deformed ^{150}Nd, the neutron-skin thickness along and perpendicular to the symmetry axis was found to be 0.22 ± 0.16 and 0.50 ± 0.15 fm, respectively, yielding $\beta_2^n/\beta_2^p = 0.92 \pm 0.08$. The nuclear quadrupole deformation parameter was also investigated by analyzing the cross sections of the 0^+ and 2^+ members of the ground state band excited with low energy α-particle beams. The measured cross sections as a function of the bombarding energy (14-20 MeV) and the scattering angle (60°-140°) were analyzed in the framework of the implicit folding model. The resulting deformation parameter is $\beta_2^m = 0.271 \pm 0.008$. The deduced ratio to the Coulomb deformation parameter $\beta_2^m/\beta_2^c = 0.93 \pm 0.03$ is very close to that derived from GDR excitation. The ratio of the charge and neutron quadrupole deformation parameters was also calculated in Hartree-Fock approximation using the Skyrme SIII interaction. The calculated value $\beta_2^n/\beta_2^p = 0.94$ agrees well with the present experimental data.

1. Introduction

In our macroscopic world it is a natural desire to order and characterise things by their sizes and shapes. It is a primary gross property of nuclei that they have a uniform central density and a reasonably sharp nuclear surface. The size and shape determination of the nuclear matter density distribution has received continued interest throughout the history of nuclear physics [1, 2]. Experiments with electrons and muons have provided reliable data for the charge density of stable nuclei. Unambiguous determination of neutron density distributions is much harder as this necessarily involves a hadron-nucleus interaction, and a model-independent description of this interaction and reaction mechanism is still missing. According to Batty et al. [2] the analysis of $E_p \approx 800$ MeV polarized proton scattering data has the promise of being able to yield absolute results on the neutron density distribution. Recent analyses [3, 4] of such data, using a non-relativistic impulse approximation (NRIA) with various corrections included or a relativistic impulse approximation (RIA), give a good description of the spin observables. However, with respect to the determination of nuclear densities there are still some problems [4, 5].

The radii of neutron and proton distributions were calculated by Angeli et al.

[6] in the Hartree-Fock-BCS method for about 700 spherical even-even nuclei, by Dechargé and Gogny [7] using a Density-Dependent Hartree-Fock-Bogoliubov approximation and by Negele and Vautherin [8] using a simpler density matrix expansion method (DME). Recently, Sharma and Ring [9] calculated the neutron rms radii of nuclei in the relativistic and the Skyrme mean-field approaches. They showed that the relativistic mean-field theory overestimates the neutron-skin thickness compared to that obtained with the Skyrme interactions and also to the empirical data. This behaviour of the relativistic mean-field theory is not yet clear and further work is in progress [9].

Another long-standing question in nuclear physics is also whether the collective model properly describes the relative isoscalar and isovector ground state deformations of the rare-earth nuclei [10]. Recently it was suggested [11] that the pion charge-exchange reaction on polarized ^{165}Ho target could be a good probe for measuring the differences between the ground-state deformations of the neutron and proton distributions. In such an experiment Knudson et al. [12] found significantly different proton (β_2^p) and neutron (β_2^n) deformation parameters: $\beta_2^n = (0.84 \pm 0.08)\beta_2^p$ contrary to the earlier results obtained with elastic π^+ and π^- scattering on unpolarized ^{165}Ho target [13]. This poses new challenges to models of nuclear structure and reaction mechanisms.

In this work we used a novel approach based on the fact that the GDR excitation cross section in inelastic α-scattering at small angles including 0° depends strongly on $\Delta R_{PN}/R_0$ [14, 15] to determine this fundamental quantity for a few spherical nuclei. Here we report on the measurement and analysis of data for the spherical nuclei ^{116,124}Sn, and ^{208}Pb, and also for the deformed nucleus ^{150}Nd.

2. Experimental methods

In order to separate effectively the GDR from the GMR, GQR and the nuclear continuum excited in inelastic α-scattering coincidence measurements were performed between the scattered α-particle and the emitted γ-ray. Since this photon decay occurs mainly by E1 transitions, a strong enhancement of the GDR ground-state γ_0-decay is expected, compared to the γ_0-decay of other multipolarities [16].

For the measurements, a momentum-analyzed 120 MeV α-particle beam provided by the KVI cyclotron was used to bombard the enriched (90 - 99 %), rolled, self-supporting targets. The thicknesses of the targets varied between 20 and 30 mg/cm^2. The layout of the experimental set-up is shown in Fig. 1. The QMG/2 magnetic spectrograph [17] was set at 0° with respect to the beam direction. The inelastically scattered α-particles, with scattering angles between -3° and +3° in the horizontal and vertical directions, were detected in a 47.5 cm version of the multi-wire detection system placed in the focal plane of the spectrograph. This system provides position, angle and energy information for the detected particles [18]. The beam was also stopped in the focal plane of the spectrograph.

The coincident γ-rays were detected in a large 10" x 14" NaI(Tl) crystal with a plastic anticoincidence shield [19], placed at 125° with respect to the beam direction.

The background due to capture of slow neutrons was reduced by placing a 12 cm thick ^{6}LiH absorber directly in front of the NaI(Tl) crystal. The remaining neutrons

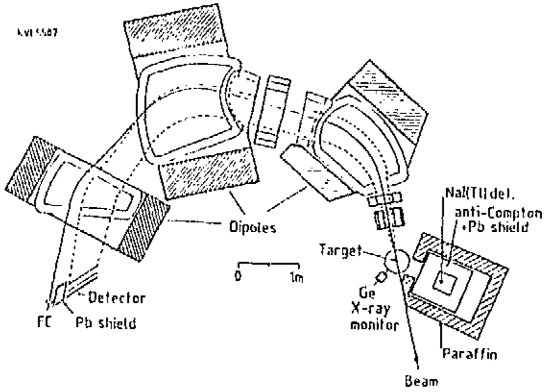

Figure 1: Layout of the experimental set-up showing the QMG/2 magnetic spectrograph and the NaI(Tl) spectrometer with the anti-coincidence, lead and paraffin shields.

were effectively separated from the γ-rays by time-of-flight discrimination. The resolution of the NaI(Tl) detector was typically 3.5% at 6.13 MeV and improving to 2% at 20 MeV. The efficiency of the NaI(Tl) detector was calculated with the Monte Carlo code EGS [20] for a number of γ-ray energies and has been checked experimentally at E_γ=6.13, 7.12 and 22.6 MeV. From the comparison between the data and calculations a 10% systematic error was associated with the calculated values. The solid angle of the detector was 70 msr.

In order to check the charge collection efficiency of the Faraday-cup placed at the focal plane of the spectrograph, the K X-ray yield from the target was also measured with a 2 cm^2 x 10 mm Ge detector placed at -125° with respect to the beam direction.

3 Experimental results

Final-state spectra of the residual nuclei after γ-decay were constructed by combining for each event the energy of the inelastically-scattered α-particle with the energy of the coincident γ-radiation. Random coincidences, caused mainly by γ-rays produced in compound nuclear reactions, were subtracted. Final-state spectra for the spherical nuclei are shown in Fig. 2.

In order to separate the ground-state transition from transitions to other low-lying states, the real-coincidence spectra, shown in Fig. 2 c), were fitted with a "gaussian + exponential-tail" line shape. For ^{150}Nd, the energy of the ground-state transition was very close to the energies of transitions to other low-lying states: e.g. the 2_1^+ state ($E_{2_1^+}$ = 130 keV) and the β-bandhead at $E_{0_2^+}$ = 676 keV. Therefore, it was not possible to separate the ground-state transition. In this case we assumed that the complete strength in the final-state spectrum came only from the decay of the GDR. The contribution of the above-mentioned transitions to this strength were

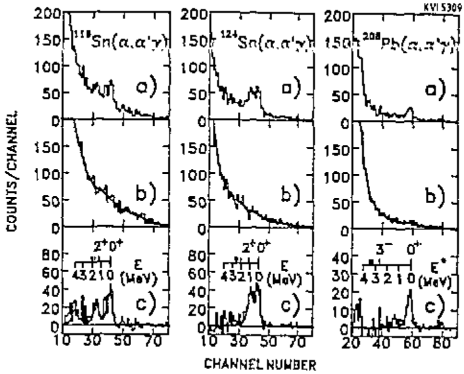

Figure 2: Final-state spectra of ^{116}Sn, ^{124}Sn and ^{208}Pb after γ-decay constructed for the excitation energy regions $12\ MeV \leq E_r \leq 17\ MeV$ for ^{116,124}Sn and $11 MeV \leq E_x \leq 14 MeV$ for ^{208}Pb populated in the (α, α') reaction with E_α = 120 MeV and $\Theta_{\alpha'} = (0 \pm 3)°$. a) spectra without subtraction of random events, b) random-coincidence spectra; the smoothed curves are used for random subtraction and c) the real-coincidence spectra, obtained by subtracting the random spectrum b) from spectrum a), along with the results of the peak fitting.

Table 1
Summary of the measured $\alpha' - \gamma_0$ coincidence cross sections integrated over the excitation energy region ΔE

Isotope	ΔE [MeV]	$d\sigma/d\Omega$ [μb/sr]	Stat. err. [%]	Syst. err. [%]
^{116}Sn	12 - 17	23.6	15	17
^{124}Sn	12 - 17	35.6	15	17
^{208}Pb	11 - 14	34.3	13	16

taken into account in the calculation of the cross section.

The coincidence cross sections for the ground-state transitions are summarized in Table 1.

These cross sections are obtained for the full opening angle of the spectrograph, i.e. an α'-particle angle of $(0 \pm 3)°$ and for the full (i.e. 4π) γ-ray solid angle. The errors are calculated from statistical uncertainties, and from the systematical errors coming from X-ray normalization and the uncertainties in the detection efficiencies of the NaI(Tl) detector and the focal-plane detection system.

The cross sections have also been corrected for a small contribution from the γ_0-decay of the isoscalar GQR which can be estimated by taking into account the cross section of the GQR [21, 22] and the ratio $\Gamma(E2)/\Gamma(E1) = 0.01$ [16]. These contributions of $\leq 1.4\ \mu b/sr$ and $\leq 2.3\ \mu b/sr$ for $^{116,124}Sn$ and ^{208}Pb, respectively, were subtracted from the cross sections.

4. Calculation of the GDR excitation cross section

To calculate the excitation cross section of the GDR by inelastic α scattering we used the usual approach [23] which connects the oscillations of the proton and neutron density distribution with the oscillations of the associated optical potential.

DWBA cross sections for the excitation of the GDR in inelastic α-scattering were calculated using the code ECIS [24] with the optical model parameters determined by Brissaud et al. for ^{116}Sn and ^{124}Sn [25], by Nolte et al. for ^{150}Nd [26] and by Goldberg et al. for ^{208}Pb [27]. In the derivation of the coupling potentials, which are the most crucial quantities in the calculations, the prescription of Satchler [23] was followed.

For the density oscillations we adopted both the Goldhaber-Teller (GT) and the Jensen-Steinwedel (JS) macroscopic models and in the final analysis we used a combination of the two.

In the GT model, rigid but interpenetrating proton and neutron spheres oscillate against each other keeping the center of mass fixed. Following Satchler [23] we assumed similar proton and neutron distributions with slightly different radii,

$$c_{n,p} = c(1 \pm \frac{1}{3}\gamma x), \tag{1}$$

where the upper sign is for neutrons and the lower sign for protons, $x = (N-Z)/A$, and γ can vary between 0 and 1. ($\gamma = 0$ gives $\rho_n/\rho_p = N/Z$, while $\gamma = 1$ results in $\rho_n = \rho_p$ at small r.)

The parameter γ is closely related to the relative difference in the radii of the neutron and proton density distributions:

$$\frac{\Delta R_{PN}}{R_0} = \frac{R_n - R_p}{(R_n + R_p)/2} = \gamma\frac{2(N-Z)}{3A} \ . \tag{2}$$

The transition potential is then:

$$\Delta U_{tr} = \alpha_1\gamma(\frac{N-Z}{A})\left[\frac{dU_0}{dr} + \frac{1}{3}R_0\frac{d^2U_0}{dr^2}\right] \ , \tag{3}$$

which is thus obtained from the real (V) and imaginary (W) parts of the optical potential (U_0) and

$$\alpha_1^2 = \frac{\pi\hbar^2}{2mE_x}\frac{A}{NZ}.$$

Within the SJ model, it is assumed that the GDR results from out-of-phase density oscillations of the neutron and proton fluids within a fixed nuclear surface, keeping the total density ρ_0 constant.

Using the same procedure as in the GT case the transition potential is [15]:

$$\Delta U_{tr} = -\beta_1\gamma(\frac{N-Z}{A})r\left[U_0 + \frac{1}{3}R\frac{dU_0}{dr}\right] \ , \tag{4}$$

Table 2
Ratio of the CN to total ground-state γ_0-decay width for the different targets

Isotope	^{116}Sn	^{124}Sn	^{150}Nd	^{208}Pb
CN/(CN + Direct) [a]	0.06	0.01	0.00	0.24

[a] This ratio depends sensitively on the excitation energy region considered (see ΔE in Table 1 and ΔE=12-17 MeV for ^{150}Nd).

with

$$\beta_1^2 = \frac{9\pi\hbar^2}{2mE_x}\frac{A}{NZ}\frac{1}{\langle r^2\rangle^2}.$$

4.1. Cross-section calculations

Coulomb excitation is included in the calculations by adding the usual [23] Coulomb transition potential. The cross sections $\sigma_{\alpha\alpha'}^{100\%}(E)$ were calculated (assuming 100 % EWSR) as a function of excitation energy, then the results were folded with the photonuclear strength distribution ($\sigma_\gamma(E)$) [28] as follows:

$$\sigma_{\alpha\alpha'}(E) = \sigma_{\alpha\alpha'}^{100\%}(E)\frac{A}{0.06NZ}\sigma_\gamma(E) \ , \tag{5}$$

with $\sigma_\gamma(E)$ in barns. This folding was found to be very important due to the strong energy dependence of the Coulomb-excitation cross section [16].

The $\sigma_{\alpha,\alpha'\gamma_0}(E)$ coincidence cross sections were deduced following the procedure described in ref. [16] :

$$\sigma_{\alpha,\alpha'\gamma_0}(E) = \sigma_{\alpha,\alpha'}(E)[\frac{\Gamma_{\gamma_0}(E)}{\Gamma} + \frac{\Gamma^\downarrow}{\Gamma}B_{CN}(E)] \ , \tag{6}$$

where $\Gamma_{\gamma_0}(E)$ is the ground-state photon-decay width of the doorway state, Γ is the width of the resonance, $\Gamma^\downarrow$ is the spreading width and $B_{CN}(E)$ is the γ_0-decay branching ratio of the compound nucleus (CN). We assumed that $\Gamma^\downarrow/\Gamma \approx 1$ [16]. The dominant direct-decay part of the expression was calculated from the experimentally known photoneutron cross sections

$$\frac{\Gamma_{\gamma_0}(E)}{\Gamma} = \frac{1}{3\pi^2\hbar^2c^2}\frac{E^2}{\Gamma}\int_{Resonance}\sigma_\gamma(E_x)dE_x \ . \tag{7}$$

The $B_{CN}(E)$ γ_0-decay branching ratios for ^{116,124}Sn and for ^{150}Nd were obtained from statistical-model calculations using a modified version of the program CASCADE [29] with level density parameters of Dilg et al. [30]. In the case of ^{208}Pb, the experimental $B_{CN}(E)$ values [16] were averaged over our excitation energy region ($11MeV \leq E_x \leq 14MeV$). The relative contribution of CN γ_0-decay for the nuclei studied is summarized in Table 2.

4.2 Generalization of the method to deformed nuclei

The method described above, which was already checked for spherical nuclei [14], can also be generalized to prolate-deformed nuclei by assuming completely independent K=0 and K=1 vibrational modes along the long and the short axis, respectively. From the neutron skin along the different axes, we can then determine the ratio of the neutron to proton quadrupole deformation parameters, β_2^n/β_2^p. In this generalization two sets of transition potentials were calculated for the two vibrational modes in a similar way as we did for spherical nuclei but with different radii according to the deformation parameter.

For the calculation of $\sigma_{\alpha\alpha'\gamma_0}$ in case of ^{150}Nd we used the elastic photon-scattering data of reference [31]. Neglecting the CN contribution in eq. 6, which was negligible in the case of ^{150}Nd, and using the connection between the photoabsorption cross section and the cross sections for elastic photon scattering derived by Starr et al. [32] one gets the following simple expression for the $\alpha'-\gamma$ coincidence cross section which can be used for deformed nuclei:

$$\sigma_{\alpha\alpha'\gamma_0}(E) = \sigma_{\alpha\alpha'}^{100\%}(E)\frac{A}{0.06NZ}\sigma_{\gamma\gamma_0}^{EXP}(E) , \tag{8}$$

where $\sigma_{\gamma\gamma_0}^{EXP}(E)$ is now the experimental cross section for elastic photon scattering from which the contribution of Thompson scattering, which does contribute to the (γ,γ_0) reaction but not to the $(\alpha,\alpha'\gamma_0)$ process, has been subtracted according to the relations given in ref. [32]. The Thompson-scattering correction was calculated from the photoabsorption data [28] using the formula given in reference [32].

The $(\alpha,\alpha'\gamma_0)$ cross sections can then be calculated according to eq. 8 as a sum of the K=0 and K=1 components:

$$\sigma_{\alpha\alpha'\gamma_0}(E) = \frac{A}{0.06NZ}[\sigma_{\alpha\alpha'}^{100\%}(K=0)\sigma_{\gamma\gamma_0}(K=0) + \sigma_{\alpha\alpha'}^{100\%}(K=1)\sigma_{\gamma\gamma_0}(K=1)] , \tag{9}$$

where $\sigma_{\gamma\gamma_0}(K=0)$ and $\sigma_{\gamma\gamma_1}(K=1)$ are, respectively, the K=0 and K=1 components of the measured cross sections for elastic photon scattering corrected for the contribution of Thompson scattering.

The actual situation is somewhat more complicated since in both the $(\alpha,\alpha'\gamma)$ and the (γ,γ') [31] experiments on ^{150}Nd the γ-decay to the low-lying 2^+ state at 130.1 keV and the K=0 β-band head at 676 keV contributes. (In both measurements NaI(Tl) detectors were used with about the same energy resolution.) However, since in both measurements their relative contributions are the same, eqs. 8 and 9 can still be applied, if one replaces the cross sections $\sigma_{\alpha\alpha'\gamma_0}(E)$ and $\sigma_{\gamma\gamma_0}^{EXP}(E)$ by the experimentally measured cross sections $\sigma_{\alpha\alpha'\gamma}(E)$ and $\sigma_{\gamma\gamma}^{EXP}(E)$.

In order to deconvolute the measured cross sections, $\sigma_{\gamma\gamma}^{EXP}(E)$, into the cross sections $\sigma_{\gamma\gamma}(K=0)$ and $\sigma_{\gamma\gamma}(K=1)$, the experimental cross section $\sigma_{\gamma\gamma}^{EXP}(E)$ [32] (see eq. 8 and eq. 9) was fitted by two Lorentzian distributions the positions and widths of which were very close ($E_1 = 12.3MeV, \Gamma_1 = 3.0MeV, E_2 = 15.6MeV, \Gamma_2 = 5.0MeV$) to the ones determined from the analysis of the photonuclear cross sections ($E_1 = 12.3MeV, \Gamma_1 = 3.3MeV, E_2 = 16.0MeV, \Gamma_2 = 5.2MeV$). The actual $\sigma_{\gamma\gamma}(K=0)$ and $\sigma_{\gamma\gamma}(K=1)$ cross sections were then obtained by multiplying the fitted Lorentzian distributions by E_γ^2.

Table 3
Neutron-skin thicknesses determined in the present work compared to previously measured and calculated values

Isotope	Present work $\Delta R_{PN}/R_0$ (%)	Present work ΔR_{PN} (fm)	Batty et al. [2] ΔR_{PN} (fm)	Angeli et al.[6] ΔR_{PN} (fm)	Dechargé et al. [7] ΔR_{PN} (fm)
^{116}Sn	0.5±2.7	0.02±0.12	0.15±0.05	0.13	0.08
^{124}Sn	4.4±2.4	0.21±0.11	0.25±0.05	0.22	0.14
^{208}Pb	$3.5^{+1.5}_{-1.6}$	0.19±0.09	0.14±0.04	0.22	0.13

5. Results

Although the transition potentials obtained from the GT and SJ models are quite different inside the nucleus, the resulting $(\alpha,\alpha'\gamma_0)$ cross sections are found to be very similar. This can be explained by the strong absorption of the α-particles inside the nucleus. The ratio of the cross sections using the two models was found to be unity within 15%. In the final analysis we calculated the cross sections for a linear combination of GT and SJ transition potentials using the ratio of the two modes given by Myers et al. [33], which is 0.58, 0.60, 0.65 and 0.73 for ^{116}Sn, ^{124}Sn, ^{150}Nd and ^{208}Pb, respectively.

5.1. Results for spherical nuclei

The $\sigma_{\alpha,\alpha'\gamma_0}$ cross sections averaged over the solid angle of the spectrograph and integrated over the energy range of the GDR as a function of the relative difference in the radii of the neutron and proton density distributions were calculated for ^{116}Sn, ^{124}Sn and ^{208}Pb, respectively. Using the completely different optical-model parameter set of Rozsa et al. [34] for ^{116}Sn, the calculated cross section was 6 to 11 % less than the previous one. This difference gives an indication of the accuracy of the calculations due to the choice of optical-model parameters. By comparing the experimentally determined cross sections to the theoretical cross sections calculated as a function of $\Delta R/R_0$, the $\Delta R/R_0$ values and their errors can be deduced. The resulting neutron-skin thicknesses are summarized and compared to the previously measured and calculated values in Table 3.

Our results for the ΔR_{PN} values are, within the uncertainties, in agreement with the theoretical predictions [6, 7], and also the agreement with an analysis of 800 MeV proton scattering data, as summarized in ref. [2], is satisfactory.

5.2. Results for the deformed nucleus ^{150}Nd

The $\alpha-\gamma$ coincidence requirement reduced the contribution of the GQR very much but its contribution was still not negligible. The fact that the shape of the GQR in the case of ^{150}Nd [35] was found to be very similar to the shape of the GDR calculated in this work made the correction very easy. The GQR contribution was estimated to be about 4% of our measured values at each energy point.

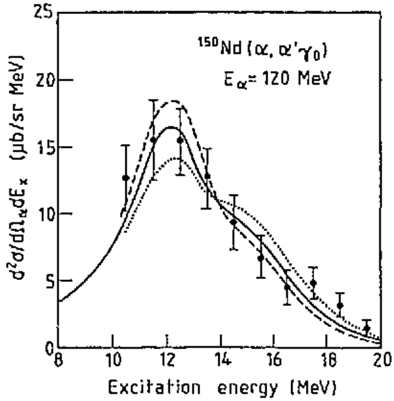

Figure 3: The measured differential cross sections (full circles) of the GDR in ^{150}Nd in inelastic α-scattering as a function of excitation energy in comparison with the calculated ones (solid lines) for neutron skin thicknesses of 0.22 ± 0.16)fm and (0.50 ± 0.15)fm along and perpendicular to the major symmetry axis, respectively. The dashed and dotted lines represent the boundaries of the 1σ (68 % confidence) fits corresponding to the given errors of the neutron-skin thicknesses.

The comparison of the measured and calculated cross sections for ^{150}Nd can be seen in Fig. 3. The experimental values are averages of the results of two independent measurements. In these experiments the same coincidence set-up was used. A systematic error of $\approx 17\%$ due to uncertainties in the calibration of the coincidence set-up was not included in the errors in Fig. 3.

Taking into account only quadrupole deformations and using a simple geometrical picture of the nucleus, one can determine the ratio of the quadrupole deformation parameters for the neutron and proton distributions from the above neutron-skin thicknesses. As a result of the transformation we get $\beta_2^n/\beta_2^p = 0.92 \pm 0.08$, which includes the systematic errors.

6. Nuclear deformations from inelastic α-scattering on ^{150}Nd at energies near the Coulomb barrier

It was suggested that the most sensitive way to study the connection between nuclear and charge deformation is the measurement of the Coulomb-nuclear interference effect [36]. Many inelastic scattering measurements have been made for the rotational states of deformed nuclei. The data are analysed by means of a coupled-channels calculation in which the excitation is described by a deformed optical model potential. The deformation parameters, which fit the data, were taken to be the nuclear deformation parameters. Many authors criticised the above method, which delivered significantly smaller nuclear deformation parameters than the charge deformation parameters. Clearly a more fundamental approach is required. Attempts have been made to relate the deformed field to the deformed nuclear densities by means of folding models. It was shown that for a normal folding model (where a density-independent projectile-nucleon folding interaction was used) the multipole moments of the resulting optical potential are equal to those of the nucleus [37].

In this work we wanted to check if we could get consistent data for the β_2^n/β_2^p ratio of ^{150}Nd using inelastic α-particle scattering and the above implicit folding model. Prior to this work there was no such data available for ^{150}Nd.

6.1. Experimental procedure

The α-beams were accelerated by the Debrecen 103 cm isochronous cyclotron. The bombarding energy varied between 14 and 20 MeV in 1 MeV steps. This region covers energies below and above the Coulomb barrier where the Coulomb-nuclear interference is expected to appear.

Isotopically enriched (91.8 %) Nd_2O_3 was evaporated onto 20 μg/cm^2 carbon foils and had a thickness of around 50 μg/cm^2. The scattered α-particles were observed in a split-pole magnetic spectrograph with about 20 keV energy resolution. The angle of the spectrograph was varied between 60° and 140° in 10° increments. The intensity of the peaks were extracted by means of a peak-fitting program using an experimental line shape determined from the elastic scattering peak. The uncertainties are of the order of 1-3 %. Some excitation functions and differential cross sections normalized to the cross sections of the pure Coulomb-excitation probability are shown in Fig. 4.

6.2. Analysis and results

The analysis of the data was performed in the framework of the deformed optical model using the coupled-channels code ECIS [24]. Our treatment of the problem followed the standard lines which are discussed in the literature [38, 36]. The Coulomb equations were integrated to rather large distances (matching radius=150 fm) and many partial waves (200) were included. The charge matrix elements and density distribution parameters were taken from the literature and they were not varied [39]. The optical potential was expanded in powers of the deformation parameters up to the fourth order.

Most of the calculations were done by limiting the number of levels to 3. In some test cases the 6^+ level was also included, but only a negligible effect was observed. The hexadecapol deformation of the optical potential was assumed to be the same as that of the charge distribution determined by Sandor et al. [40] from (e,e') scattering. This has very little effect on the excitation of the 2_1^+ state.

Different optical model parameters were tried in fitting the data. The geometry used in ref. [36] was not found satisfactory. A much better fit could be obtained using smaller radius (r) or diffuseness (a) values. By varying the r or the a values as well as V and β_2 ranging from 1.25 fm to 1.37 fm, 0.6 fm to 0.7 fm 110 MeV to 260 MeV and 0.20 to 0.25, respectively, we could get a few equally good fits to the data. When a good fit is obtained the quadrupole moment of the mass distribution was calculated from the optical potential used assuming implicit folding model [41]. The results showed only a small scatterering (± 2 %) around a mean value for the various optical

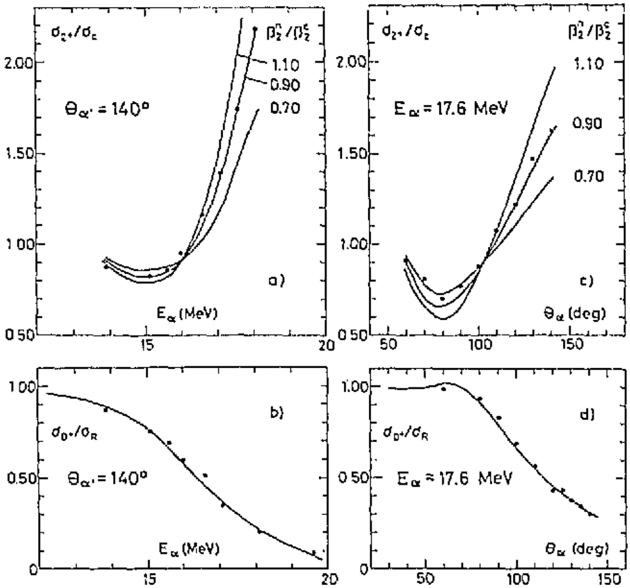

Figure 4: Measured (full dots) and calculated (solid lines) inelastic a),c) and elastic b),d) scattering cross sections of ^{150}Nd(α,α'). The inelastic and elastic scattering cross sections were normalized to the pure Coulomb-excitation and the Rutherford scattering cross sections, respectively. The coupled-channels calculations were performed for different ratios of nuclear/Coulomb quadrupole deformation parameters to show the sensitivity of the method.

model potentials used. The charge deformation parameter β_2^c was obtained from the E2 transition rates [42] assuming a uniform charge distribution with $r_c = 1.2 fm$. For reasons of comparison, we have calculated the mass deformation parameter β_2^m from the mass quadrupole moment also assuming a uniform mass distribution with $r_m = 1.2 fm$.

The result for the β_2^m/β_2^c ratio was found to be 0.93±0.03. This ratio agrees reasonably with the GDR results and stimulates further investigations.

7. Mean field analysis of the p–n asymmetry

In order to get a deeper insight into the difference of the proton and neutron distributions of ^{150}Nd we have calculated its ground state properties in Hartree-Fock approximation using the Skyrme SIII interaction [43]. This effective interaction was

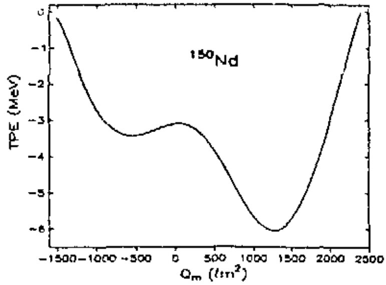

Figure 5: The total potential energy (TPE) of ^{150}Nd as a function of the mass quadrupole moment (Q_m).

applied already to describe the difference in proton–neutron density distributions in the rare earth region [44]. Since the Skyrme forces are known not to have good pairing properties, we treated the pairing separately as proposed in ref. [45, 46].

In the HF+BCS calculations a quadratic constraint was applied to the mass quadrupole moment and the calculations were performed in a wide range of this moment, Q_m. The minimum of the potential energy surface was found at Q_m=1255 fm^2. The slice of the potential energy surface along the β axis is shown in Fig. 5. The calculated charge radius and quadrupole moment were found in a reasonably good agreement with the experimental and recently calculated values [39, 40]. The deviations were less than twice of the experimental uncertainties.

The quadrupole deformation parameters were obtained from the calculated quadrupole moments by assuming homogenous proton and neutron distributions with sharp surfaces. The resulting parameters are: $\beta_2^n = 0.266$ and $\beta_2^p = 0.281$, respectively. Their ratio, $\beta_2^n/\beta_2^p = 0.94$, is found in good agreement with the present experimental results.

From the HF+BCS calculations we have got not only the quadrupole moments, but also the *complete density distributions for both protons and neutrons*. These distributions are shown in parts *a*) and *b*) of Fig. 6. To see the origin of the difference in quadrupole deformations, we subtracted the density distributions. Since we are interested in difference of deformations, the density distributions were first normalized to have the same volume integrals. The difference of the resulting neutron and proton density distributions is shown in part *c*) of Fig. 6 in 3-dimensional view, and in part *d*) in topographic representation. It is seen that the proton excess (white in Fig. 6 d) is concentrated along the prolate direction, while the neutron excess has its maximum (black in Fig. 6 d) at the middle of the nucleus, and dominates normal to the prolate direction.

^{150}Nd

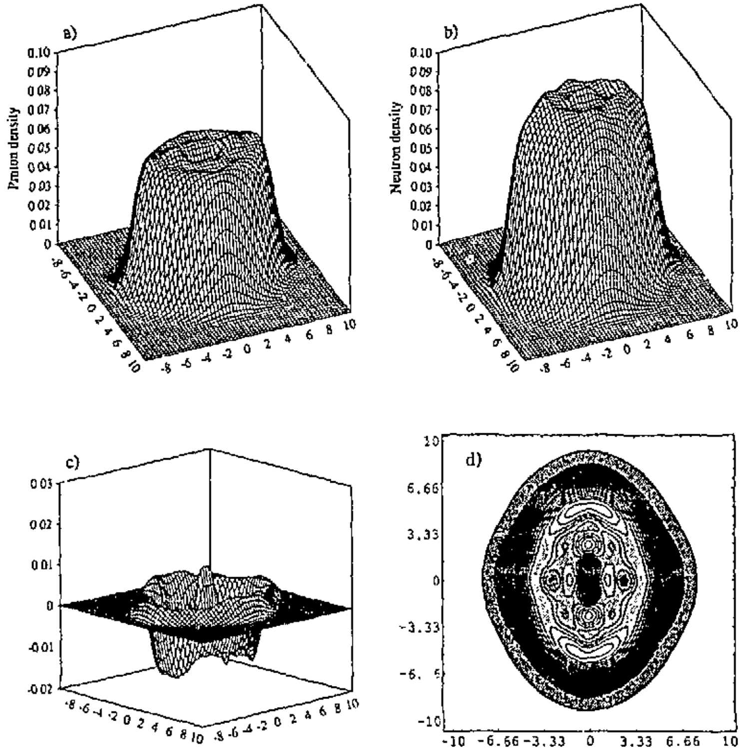

Figure 6: Density distributions in ^{150}Nd given in $1/\mathrm{fm}^3$. a) Neutron density distribution, b) proton density distribution, c) the difference of the normalized neutron and proton distributions, d) the same as c) but in topographic representation. The values on the x and y axes are the distances from the centre of mass measured in fm.

Acknowledgements

We would like to thank our colleagues A. Balanda, S. Brandenburg, N. Kalantar-Nayestanaki, B.M. Nyakó and J. Timár for their cooperation and help. This work was performed as part of the research program of the Stichting voor Fundamenteel Onderzoek der Materie (FOM) with financial support from the Nederlandse Organisatie voor Wetenschappelijk Onderzoek (NWO) and partly by the Hungarian National Scientific Research Foundation (OTKA No: 7486).

References

[1] R.C. Barrett and D.F. Jackson, Nuclear Sizes and Structure, Clarendon Press, Oxford (1977)

[2] C.J. Batty, E. Friedman, H.J. Gils, H. Rebel, Adv. Nucl. Phys. **19** (1989) 1

[3] W. Rory Coker and L. Ray, Phys. Rev. **C42** (1990) 659

[4] L. Ray, Phys. Rev. **C41** (1990) 2816

[5] L. Ray and G.W. Hoffmann, Phys. Rev. **C31** (1985) 538

[6] I. Angeli, et al., J. Phys **G6** (1980) 303

[7] J. Dechargé and D. Gogny, Phys. Rev. **C21** (1980) 1568

[8] J.W. Negele and D. Vautherin, Phys. Rev. **C5** (1972) 1472

[9] M.M. Sharma and P. Ring, Phys. Rev. **C45** (1992) 2514

[10] D.L. Hendrie, Phys. Rev. Lett. **31** (1973) 478

[11] H.C. Chiang and M.B. Johnson, Phys. Rev. Lett. **53** (1984) 1996

[12] J.M. Knudson et al., Phys. Rev. Lett **66** (1991) 1026

[13] J. Bartel and M.B. Johnson, Ann. Phys. **195** (1989) 89

[14] A. Krasznahorkay et al., Phys. Rev. Lett. **66** (1991) 128

[15] A. Krasznahorkay et al., Nucl. Phys. **A567** (1994) 521

[16] J.R. Beene et al., Phys. Rev. **C41** (1990) 920; Phys. Rev. **C41** (1990) R1332

[17] A.G. Drentje, H.A. Enge and S.B. Kowalski, Nucl. Instr. Meth. **122** (1974) 485

[18] J.M. Schippers, W.T.A. Borghols and S.Y. van der Werf, Nucl. Instr. Meth. **A247** (1986) 467

[19] H.J. Hofmann et al., KVI Annual report (1985) 110

[20] R.L. Ford and W.R. Nelson, SLAC Report No. 210, (1979), unpublished

[21] S. Brandenburg et al., Nucl. Phys. **A466** (1987) 29

[22] M.M. Sharma et al., Phys. Rev. **C38** (1988) 2562

[23] G.R. Satchler, Nucl. Phys. **A472** (1987) 215

[24] J. Raynal, coupled-channel computer code ECIS, private communication.

[25] I. Brissaud et al., Phys. Rev. **C6** (1972) 585

[26] M. Nolte, H. Machner and J. Bojowald, Phys. Rev. **C36** (1987) 1312

[27] P.A. Goldberg et al., Phys. Rev. **C7** (1973) 1938

[28] S.S. Dietrich and B.L. Berman, At. Data Nucl. Data Tables **38** (1988) 199, and references therein.

[29] F. Pühlhofer, Nucl. Phys. **A280** (1977) 267; M.N. Harakeh, computer code CASCADE, extended version.

[30] W. Dilg et al., Nucl. Phys. **A217** (1973) 269

[31] S.D. Hoblit and A.M. Nathan, Phys. Rev. **C44** (1991) 2372

[32] R.D. Starr, P. Axel and L.S. Cardman, Phys. Rev. **C25** (1982) 780

[33] W.D. Myers et al., Phys. Rev. **C15** (1977) 2032

[34] C.M. Rozsa et al., Phys. Rev. **C21** (1980) 1252

[35] A. van der Woude, Prog. Part. Nucl. Phys. **18** (1987), 217

[36] W. Brückner et al., Phys. Rev. Lett. **30** (1973) 57

[37] *R.S. Mackintosh, Nucl. Phys.* ***A266*** *(1976) 379*

[38] A.A. Aponick et al., Nucl. Phys. **A159** (1970) 367

[39] At. Data and Nucl. Data Tabl. **14** (1974) 509

[40] R.K.J. Sandor et al., Nucl. Phys. **A551** (1993) 349

[41] M.N. Harakeh, "BEL" KVI internal report **77i** (1981) unpublished

[42] S. Raman et al., At. Data and Nucl. Data Tables **36** (1987) 24

[43] T.H.R. Skyrme, Phyl. Mag. **1** (1956) 1043

[44] J. Bartel and M. Johnson, Ann. Phys. **105** (1989) 89

[45] M. Beiner et al., Nucl. Phys. **A238** (1975) 29

[46] P. Bonche et al., Nucl. Phys. **A443** (1985) 39

PAIRING AND CORIOLIS ATTENUATION IN DEFORMED NUCLEI

A. COVELLO, A. GARGANO, and N. ITACO
Dipartimento di Scienze Fisiche, Università di Napoli Federico II
and Istituto Nazionale di Fisica Nucleare
Mostra d'Oltremare, Pad. 20, 80125 Napoli, Italy

ABSTRACT

In this paper, we present some results of a study of strongly deformed nuclei carried out within the framework of the many-particle plus rotor model. In particular, we consider the two nuclei ^{163}Er and ^{165}Er. We treat the pairing interaction between the valence nucleons in the intrinsic deformed field by a new method, the chain-calculation method, which yields extremely accurate results. We focus attention on the role of the recoil term as a mechanism that produces attenuation of the Coriolis coupling. It turns out that the low-energy spectra of the decoupled bands are very well reproduced. A very good agreement with experiment is also obtained for the band-head energies.

1. Introduction

The study of the interplay between single-particle and collective degrees of freedom in strongly deformed nuclei has long been a topical problem in nuclear structure theory. A particularly appropriate framework for tackling this problem is provided by the many-particles plus rotor model.[1-3]. The most serious difficulty with this model is the treatment of the pairing correlation of the valence nucleons in the intrinsic deformed field. On the one hand the model space dimensionalities generally preclude a standard diagonalization procedure, on the other hand the use of the BCS approximation may well result in a poor description of the intrinsic structure.[3,4]

We have succeeded in overcoming this difficulty by developing a new method,[5] the chain-calculation method (CCM), which provides a highly effective way for cutting down the size of the energy matrices while yielding extremely accurate results. This has opened up the possibility of assessing the real scope of the MPR model.

In this paper, we present some representative results of an extensive study which we are carrying out in the rare-earth region. In particular, we consider here the two nuclei ^{163}Er and ^{165}Er, focusing attention on the lowest-lying decoupled bands. The study of these bands provides in fact the opportunity to understand the role of the various terms of the model Hamiltonian. In this context, of particular interest is the mechanism that leads to the attenuation of the Coriolis interaction.

In Sec. 2 we give an outline of the MPR model and describe our method of solution. In Sec. 3 we present and compare with experiment the results of our calculations. Sec. 4 presents some concluding remarks.

2. Many-particles plus rotor model and method of solution

In the strong coupling representation the model Hamiltonian describing a system of N valence particles coupled to an axially-symmetric rotor is written

$$H_{MPR} = H_I + H_{intr} + H_c\,, \tag{1}$$

where

$$H_I = A(\mathbf{I}^2 - I_3^2)\,, \tag{2}$$

$$H_{intr} = H_0 + H_{pair} + H_{rec}\,, \tag{3}$$

$$H_{rec} = A(\mathbf{J}^2 - J_3^2)\,, \tag{4}$$

$$H_c = -A(I_+J_- + I_-J_+)\,, \tag{5}$$

with standard notation. The recoil term H_{rec} is of particular relevance in the MPR model,[2,6] as it contains both one-body and two-body terms. In fact, the angular momentum $\mathbf{J}$ due to the valence particles has the form

$$\mathbf{J} = \sum_{i=1}^{N} \mathbf{j}(i)\,, \tag{6}$$

which implies that H_{rec} becomes

$$H_{rec} = A\left[\sum_{i=1}^{N}\mathbf{j}^2(i) - \left(\sum_{i=1}^{N} j_3(i)\right)^2 + 2\sum_{i<k}\mathbf{j}(i)\cdot\mathbf{j}(k)\right]\,. \tag{7}$$

The eigenstates of $H_I + H_{intr}$ can be written in the form

$$\Psi^I_{M\Omega\tau} = \sqrt{\frac{2I+1}{16\pi^2}}\left[D^I_{M\Omega}(\omega)\chi_{\Omega\tau} + (-)^{I+\Omega}D^I_{M-\Omega}(\omega)\chi_{\overline{\Omega}\tau}\right]\,, \tag{8}$$

where the intrinsic wave functions $\chi_{\Omega\tau}$ are solutions to the eigenvalue equation

$$(H_0 + H_{pair} + H_{rec})\chi_{\Omega\tau} = \mathcal{E}_{\Omega\tau}\chi_{\Omega\tau}. \tag{9}$$

Once Eq. (9) is solved the Coriolis term can be diagonalized in this representation. In the following part of this section we shall discuss in some detail our treatment of the intrinsic Hamiltonian and of the Coriolis coupling.

Let us first consider the Hamiltonian $H = H_0 + H_{pair}$ which is written as

$$H = \sum_{\nu}\epsilon_\nu \hat{N}_\nu - \sum_{\nu\nu'} G_{\nu\nu'} A^\dagger_\nu A_{\nu'}\,, \tag{10}$$

where

$$H_0 = \sum_{i=1}^{N} H_{sp}(i)\,, \tag{11}$$

$$\hat{N}_\nu = a_\nu^\dagger a_\nu + a_{\overline{\nu}}^\dagger a_{\overline{\nu}}\,, \tag{12}$$

$$A_\nu^\dagger = a_\nu^\dagger a_{\overline{\nu}}^\dagger\,. \tag{13}$$

The index ν stands for all quantum numbers specifying the single-particle states while $\overline{\nu}$ denotes the time reversal partner. In cases where Ω is essential, ν will represent only the asymptotic quantum numbers $[Nn_3\Lambda]$.

We describe the intrinsic deformed field H_0 by a nonspheroidal axial and reflection symmetric Woods-Saxon potential.[7] Thus we write

$$H_{sp} = -\frac{\hbar^2}{2m}\,\Delta + V(\mathbf{r}) + V_{so}(\mathbf{r};\mathrm{spin})\,, \tag{14}$$

$$V(\mathbf{r}) = \frac{-V_0}{1+\exp\left[\left(r - R(\theta)\right)/a\right]}\,, \tag{15}$$

$$R(\theta) = R_0\left\{1 + \beta_0 + \beta_2 Y_{20}(\theta) + \beta_4 Y_{40}(\theta)\right\}\,, \tag{16}$$

$$V_{so}(\mathbf{r};\mathrm{spin}) = -\kappa\,\boldsymbol{\sigma}\cdot\left[\mathrm{grad}\;\mathrm{V}(\mathbf{r}) \times \mathbf{p}/\hbar\right]. \tag{17}$$

As already mentioned in the Introduction, we treat the pairing correlations between the valence particles by the CCM. A detailed description of this approach as well as a test case evidencing its degree of accuracy are to be found in Refs. 3 and 5. We only emphasize here that our solutions of the pairing Hamiltonian are practically exact.

We now turn our attention to the recoil term (7), which in second quantization reads

$$H_{rec} = A\Big[\sum_{\nu\nu'} F_{\nu\nu'} a_\nu^\dagger a_{\nu'} + \sum_{\nu_1\nu_2\nu_3\nu_4} R_{\nu_1\nu_3} R_{\nu_4\nu_2} a_{\nu_1}^\dagger a_{\nu_2}^\dagger a_{\nu_4} a_{\nu_3}\Big], \tag{18}$$

where

$$F_{\nu\nu'} = \langle\nu|\mathbf{j}^2 - j_3^2|\nu'\rangle, \tag{19}$$

$$R_{\nu'\nu'} = \begin{cases} \langle\nu|j_-|\nu'\rangle & \text{if } \Omega_\nu < \Omega_{\nu'}, \\ \langle\nu'|j_-|\nu\rangle & \text{if } \Omega_\nu > \Omega_{\nu'}, \\ \langle\overline{\nu}|j_-|\nu'\rangle & \text{if } \Omega_\nu = \Omega_{\nu'} = \frac{1}{2}. \end{cases} \tag{20}$$

Here we are interested in the treatment of odd-A nuclei. In this case we diagonalize H_{rec} within the set of $v = 1$ states obtained by treating the Hamiltonian (10) by the CCM. The intrinsic wave function has therefore the form

$$\chi_{\Omega\tau} = \sum_{\beta\mu} f^{\Omega}_{\beta\tau\mu}|\beta,\mu\Omega\rangle. \tag{21}$$

The states $|\beta, \mu\Omega\rangle$ are $v = 1$ eigenstates of the pairing Hamiltonian, the label μ referring (here and in the following) to the quantum numbers of the blocked level and the index β standing for all the other quantum numbers necessary to completely specify the states.

The matrix elements of H_{rec} between $v = 1$ states are given by

$$\langle\beta, \mu\Omega|H_{rec}|\beta', \mu'\Omega\rangle = A\Bigg\{\delta_{\mu\mu'}\Big[2\sum_{\nu>0} F_{\nu\nu}T^{\mu\mu'}_{\beta\beta'\nu} - \sum_{\nu,\nu'>0} R^2_{\nu\nu'}T^{\mu\mu'}_{\beta\beta'\nu\nu'}\Big]+$$

$$[1-(1-\delta_{\beta\beta'})\delta_{\mu\mu'}]F_{\mu\mu'}S^{\mu\mu'}_{\beta\beta'} - \sum_{\nu>0} R_{\nu\mu'}R_{\nu\mu}S^{\mu\mu'}_{\beta\beta'\nu}\Bigg\}, \tag{22}$$

where the quantities S and T, whose explicit expressions may be found in Ref. 8, are expressed in terms of the coefficients of the $v = 1$ pairing eigenstates in the occupation number representation. These coefficients are defined in Eq. (19) of Ref 3.

Let us now discuss briefly the effects produced by the recoil term. We first consider the diagonal matrix elements. The first two sums in Eq. (22) represent the so-called core contribution.[6,9] In fact, they are just the expectation value of the recoil term with respect to the even-mass nucleus, whose $N - 1$ valence particles are distributed over all the available levels except the blocked one. This contribution, being almost independent of the level blocked by the unpaired particle, does not significantly affect the spectrum of the odd nucleus. The remaining two terms in Eq. (22) are the contribution of the unpaired particle. The third one reduces to the single-particle matrix element $F_{\mu\mu}$ ($S^{\mu\mu}_{\beta\beta} = 1$) while the quantity $\sum_{\nu>0} R^2_{\nu\mu}S^{\mu\mu}_{\beta\beta\nu}$ represents the correction arising from the other valence nucleons. The latter is strongly dependent both on the nature of the level μ and on the pairing correlations.

As regards the off-diagonal matrix elements, they may have $\beta \neq \beta'$ and/or $\mu \neq \mu'$. We have found, in agreement with the results of other authors,[4] that the matrix elements with $\mu \neq \mu'$ are very small. Through the matrix elements with $\beta \neq \beta'$ different eigenstates of the pairing Hamiltonian may be brought into the intrinsic wave function. In this way the recoil term affects the pair distribution of particles.[10] This effect may be particularly important when the involved levels originate from the so-called intruder states (in the case considered in this paper this is the spherical $i_{13/2}$ state).

As a final step we take into account the Coriolis interaction (5). Its matrix elements are given by

$$\langle\Psi^I_{M\Omega\tau}|H_c|\Psi^I_{M\Omega'\tau'}\rangle = -A\Bigg\{\sum_{\mu\mu'}\Big[(I+\Omega')(I-\Omega'+1)\Big]^{\frac{1}{2}}R_{\mu\mu'}\delta_{\Omega'\Omega+1}$$

$$+\Big[(I-\Omega')(I+\Omega'+1)\Big]^{\frac{1}{2}}R_{\mu'\mu}\delta_{\Omega'\Omega-1} + (-)^{I+\frac{1}{2}}(I+\frac{1}{2})R_{\mu\mu'}\delta_{\Omega\frac{1}{2}}\delta_{\Omega'\frac{1}{2}}\Bigg\}P^{\Omega\Omega'}_{\tau\mu\tau'\mu'}, \tag{23}$$

where

$$P^{\Omega\Omega'}_{\tau\mu\tau'\mu'} = \sum_{\beta\beta'} f^{\Omega}_{\beta\tau\mu}f^{\Omega'}_{\beta'\tau'\mu'}S^{\mu\mu'}_{\beta\beta'}. \tag{24}$$

We see that the matrix elements (23) are written as the product of two factors. The first one corresponds to the contribution of the odd particle while the second takes into account the many-particle correlations induced from both the pairing and the recoil interaction. Since the quantities $F^{\Omega\Omega'}_{r\mu r'\mu'}$ are all ≤ 1, they produce an attenuation of the Coriolis coupling.

3. Results

We now come to discuss the results of our calculations for ^{163}Er and ^{165}Er. In both these nuclei there are five low-lying bands, four with negative parity (essentially rotational in character) built on the $\frac{1}{2}^-[521]$, $\frac{3}{2}^-[521]$, $\frac{5}{2}^-[523]$ and $\frac{11}{2}^-[505]$ single-particle states, and one with positive parity originating from the $i_{13/2}$ shell-model state.

It is this experimental situation that we have tried to reproduce within the framework of the MPR model as described in the previous section, concentrating our attention on the decoupled $i_{13/2}$ band for which the recoil term is of particular relevance.

For both ^{163}Er and ^{165}Er we have considered nineteen valence neutrons distributed over eighteen levels chosen in such a way that on both sides of the Fermi surface lies the same number of single-particle states. As already mentioned in Sec. 2, the intrinsic deformed field is represented by a nonspheroidal axial and reflection symmetric Woods-Saxon potential. We adopt a unique value of the potential depth V_0 and of the radius parameter r_0, namely $V_0 = 43$ MeV and $r_0 = 1.29$ fm. These values are in agreement with those reported in Ref. 11, taking into account that we use a single value of r_0 for the central and spin-orbit terms. The deformation parameter β_2 is taken from the experimental $B(E2; 2 \to 0)$ values [12,13] in the neighbouring doubly even nuclei, which leads to the common value of 0.335. The values of the spin-orbit strength κ, the diffuseness a and the deformation parameter β_4 are: $\kappa = 0.425$ fm^2, $a = 0.68$ fm, $\beta_4 = 0.052$ for ^{163}Er and $\kappa = 0.387$ fm^2, $a = 0.65$ fm, $\beta_4 = 0.062$ for ^{165}Er. These values of κ and a are within the range of those reported in the literature,[11,14] while the values of β_4 come quite close to those obtained from the equilibrium shape calculations of Ref. 15 for this region.

It should be noted that in the model spaces used for ^{163}Er and ^{165}Er we include the five lowest-lying states originating from the $i_{13/2}$ level, leaving out the two states $\frac{11}{2}^+[615]$ and $\frac{13}{2}^+[606]$. These latter, lying very high in energy, are not expected to contribute significantly to the wave functions of the lowest positive-parity bands. The only two other positive-parity states, $\frac{1}{2}^+[400]$ and $\frac{3}{2}^+[402]$, that might contribute to this band are also included.

As for the pairing strength G, we use a value of 0.190 MeV for ^{163}Er and 0.189 MeV for ^{165}Er, which give an odd-even mass difference for neutrons in agreement with the experimental values of 0.975 and 0.905 MeV, respectively.

For the rotational parameter A, we take the value 14 keV for ^{163}Er and 13 keV for ^{165}Er. These values are intermediate between the values obtained from the $E_{2^+} - E_{0^+}$ energy difference in the neighbouring even-even isotopes and those derived from the spectra of the four low-lying negative-parity bands in both ^{163}Er and ^{165}Er.

We now present the results of our calculations for ^{163}Er. In Fig. 1 we show the spectrum of the lowest positive-parity band. We see that the right level ordering and an overall satisfactory agreement with experiment is obtained up to $J = \frac{21}{2}$. It should be stressed that this is not the case when the pairing correlations are treated by the usual BCS method. In fact, the use of this approximation makes it necessary to introduce an ad-hoc attenuation factor.[3,4] The comparison between case (a) and (b) shows the relevance of the recoil term. Concerning the higher-spin states, which lie above 1 MeV excitation energy, our calculation fails to reproduce the observed pattern. This is not surprising, however, as it may be taken as an indication that states of seniority higher than one ($v = 3$) should be taken into account.

As regards the spectra of the negative-parity bands $\frac{1}{2}^-[521]$, $\frac{3}{2}^-[521]$, $\frac{5}{2}^-[523]$ and $\frac{11}{2}^-[505]$, which are practically purely rotational, a very good agreement with experiment is obtained up to about 1.5 MeV excitation energy (relative to each bandhead), the largest discrepancy being about 60 keV. It should be stressed that for these bands the calculations with and without recoil yield practically the same results. The origin of the difference in the spectra of the positive parity band is to be found in the strong Coriolis coupling and in the attenuation of such a coupling produced by the recoil term. In Table 1 we report the values of the intrinsic

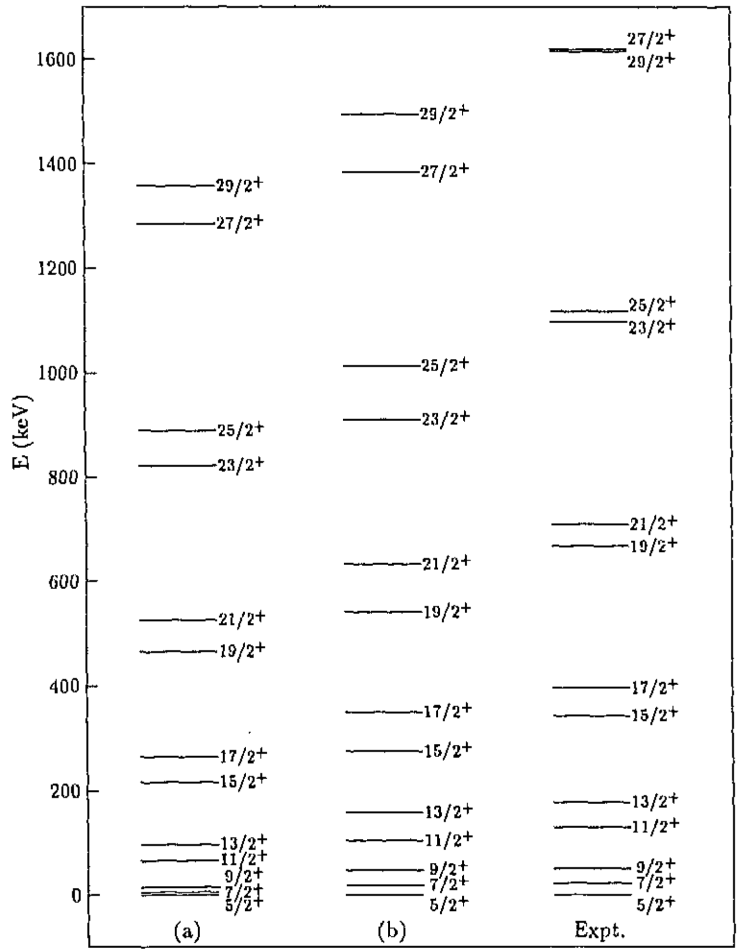

Fig. 1. Experimental and calculated [(a) without recoil; (b) with recoil] positive-parity spectrum of ^{163}Er.

energies for the positive-parity states originating from the $i_{13/2}$ level (they are characterized by $[Nn_3\Lambda]$, since, as already mentioned in Sec. 2, there is no appreciable mixing of states corresponding to different blocked levels). From this table we see that the recoil term produces an increase in the intrinsic level spacings. In Table 2 we give the attenuation

Table 1. Values of the intrinsic energies $\mathcal{E}_{\mu\Omega} - \mathcal{E}_{[642]5/2^+}$ (keV) for ^{163}Er calculated : (a) without recoil; (b) with recoil.

$\mu\Omega$	(a)	(b)
$[660]\frac{1}{2}^+$	1245	1504
$[651]\frac{3}{2}^+$	761	955
$[642]\frac{5}{2}^+$	0	0
$[633]\frac{7}{2}^+$	1032	1054
$[624]\frac{9}{2}^+$	2634	2650

factors $P_{\mu\mu'}^{\Omega\Omega'}$ (see Eq. 24), which show the effect of the recoil term on the off-diagonal Coriolis matrix elements. Therefore, we see that both effects produce a reduction of the Coriolis coupling. As regards the wave functions of the states of the decoupled band, they result in a rather complex mixture of the of the $\frac{1}{2}^+[660]$, $\frac{3}{2}^+[651]$, $\frac{5}{2}^+[642]$ and $\frac{7}{2}^+[633]$ states. This mixture, however, is significantly reduced by the recoil term. Finally, in Table 3 we compare

Table 2. Values of the quantities $P_{\mu\mu'}^{\Omega\Omega'}$, as given by Eq. (24), calculated for ^{163}Er : (a) without recoil; (b) with recoil.

$\mu\Omega$	$\mu'\Omega'$	(a)	(b)
$[660]\frac{1}{2}^+$	$[651]\frac{3}{2}^+$	0.99	0.96
$[651]\frac{3}{2}^+$	$[642]\frac{5}{2}^+$	0.95	0.86
$[642]\frac{5}{2}^+$	$[633]\frac{7}{2}^+$	0.91	0.84
$[633]\frac{7}{2}^+$	$[624]\frac{9}{2}^+$	0.99	0.99

Table 3. Experimental and calculated band-head energies (keV) for ^{163}Er.

Bandhead	Expt.	Calc.
$\frac{5}{2}^-$	0	0
$\frac{5}{2}^+$	69	85
$\frac{3}{2}^-$	104	96
$\frac{1}{2}^-$	347	367
$\frac{11}{2}^-$	444	434

with experiment the band-head energies. We see that the agreement is at most within 20 keV.

Fig. 2 and Tables 4, 5 and 6 present the results obtained for ^{165}Er. We see that the situation is quite similar to that which emerged for ^{163}Er, the overall agreement with experiment being of comparable quality. It may be noted, however, that the spectrum of the decoupled band is even better reproduced while the theoretical band-head energy of the $\frac{1}{2}^-$[521] band lies 170 keV below the experimental value. There are, however, some indications that this state may have a small γ-vibration admixture.[18] As in the case of ^{163}Er, the spectra of the negative-parity bands are also very well reproduced by the theory.

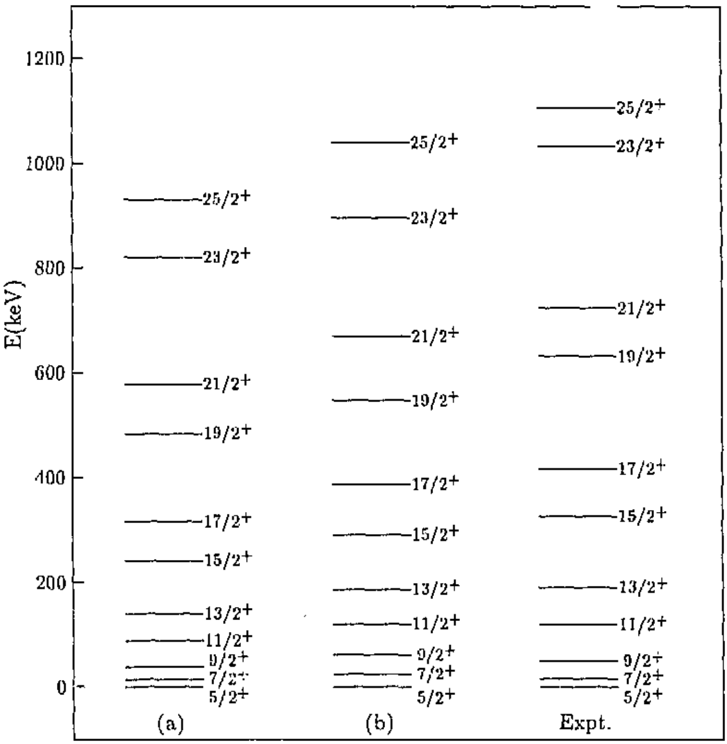

Fig. 2. Experimental and calculated [(a) without recoil; (b) with recoil] positive-parity spectrum of ^{165}Er.

Table 4. Values of the intrinsic energies $\mathcal{E}_{\mu\Omega} - \mathcal{E}_{[642]5/2^+}$ (keV) for ^{165}Er.

$\mu\Omega$	(a)	(b)
$[660]\frac{1}{2}^+$	1502	1798
$[651]\frac{3}{2}^+$	970	1241
$[642]\frac{5}{2}^+$	0	0
$[633]\frac{7}{2}^+$	946	911
$[624]\frac{9}{2}^+$	2593	2604

Table 5. Values of the quantities $P^{\Omega\Omega'}_{\mu\mu'}$, as given by Eq. (24), for ^{165}Er.

$\mu\Omega$	$\mu'\Omega'$	(a)	(b)
$[660]\frac{1}{2}^+$	$[651]\frac{3}{2}^+$	1.00	0.98
$[651]\frac{3}{2}^+$	$[642]\frac{5}{2}^+$	0.99	0.94
$[642]\frac{5}{2}^+$	$[633]\frac{7}{2}^+$	0.82	0.75
$[633]\frac{7}{2}^+$	$[624]\frac{9}{2}^+$	0.99	0.99

Table 6. Experimental and calculated band-head energies (keV) for ^{165}Er.

Bandhead	Expt.	Calc.
$\frac{5}{2}^-$	0	0
$\frac{5}{2}^+$	47	51
$\frac{3}{2}^-$	243	242
$\frac{1}{2}^-$	297	127
$\frac{11}{2}^-$	551	530

4. Concluding remarks

In this paper, we have applied the MPR model to the study of the low-energy bands in the strongly deformed nuclei ^{163}Er and ^{165}Er. A salient feature of our calculations is the very accurate treatment of the intrinsic structure. As a result, the role played by the recoil term has been clearly evidenced.

The results of our calculations for both nuclei have turned out to be in good agreement with experiment. Of particular interest is the fact that the $i_{13/2}$ decoupled band is well reproduced up to rather high values of the angular momentum. In fact, this is not possible with the BCS approximation unless an ad-hoc attenuation factor of the Coriolis term is introduced. This speaks in favour of the MPR model as a valuable theoretical basis for the description of deformed nuclei.

In the present calculations we have only included $v = 1$ eigenstates of the pairing Hamiltonian. As a next step we intend to take into account the $v = 3$ states. We expect that this will greatly enlarge the scope of the MPR model.

Acknowledgments

This work was supported in part by the Italian Ministero dell'Università e della Ricerca Scientifica e Tecnologica (MURST).

References

1. P. Ring and P. Schuck, *The Nuclear Many-Body Problem* (Springer-Verlag, New York, 1980), Chap. 3, and references therein.

2. T. Engeland, in *International Review of Nuclear Physics*, Vol. 2, edited by T. Engeland, J. Rekstad, and J. S. Vaagen (World Scientific, Singapore, 1984), p. 155, and references therein.
3. A. Covello, A. Gargano, and N. Itaco, in *Proceedings of the Predeal International Summer School, Predeal, Romania, 1993*, edited by W. Scheid and A. Sandulescu (Plenum Press, 1994).
4. T. Engeland, *Physica Scripta* **25** (1982) 467.
5. A. Covello, F. Andreozzi, A. Gargano, and A. Porrino, in *Proceedings of the Fourth International Spring Seminar on Nuclear Physics, Amalfi, 1992*, edited by A. Covello (World Scientific, Singapore, 1993), p. 301.
6. E. Osnes, J. Rekstad, and O. Gjøtterud, *Nucl. Phys.* **A253** (1975) 45.
7. F. A. Gareev, S. P. Ivanova, V. G. Soloviev, and S. I. Fedotov, *Sov. J. Particles Nucl.* **4** (1973) 148.
8. F. Andreozzi, A. Covello, A. Gargano, N. Itaco, and A. Porrino, to be published.
9. G. Ehrling, and S. Wahlborn, *Physica Scripta* **6** (1972) 94.
10. T. Engeland, and J. Rekstad, *Phys. Lett.* **89B** (1979) 8; J. Rekstad and T. Engeland, *Phys. Lett.* **89B** (1980) 316.
11. J. Dudek and T. Werner, *J. Phys.* **G4** (1978) 1543.
12. R. G. Helmer, *Nucl. Data Sheets* **64** (1991) 79.
13. E. N. Shurshikov and N. V. Tomofeeva, *Nucl. Data Sheets* **65** (1992) 365.
14. W. Ogle, S. Wahlborn, R. Piepenbring, S. Frederiksson, *Rev. Mod. Phys.* **43** (1971) 424.
15. R. Bengtsson, J. Dudek, W. Nazarewicz, and P. Olanders, *Physica Scripta* **39** (1989) 196.
16. T. Burrows, *Nucl. Data Sheets* **56** (1989) 313.
17. L. K. Peker, *Nucl. Data Sheets* **65** (1992) 439.
18. A. K. Jain, R. K. Sheline, P. C. Sood, and Kiran Jain, *Rev. Mod. Phys.* **62** (1990) 393.

Quadruple pairing correlations at superdeformation

Y.S. Chen
China Institute of Atomic Energy ,Beijing 102413
China

Abstract

The Harmonic Oscillator Quadruple Pairing Cranking HFB theory was established and applied to the superdeformed rotational states. The collapse of the pairing fields, including Y_{20}, Y_{21} and Y_{22} fields at superdeformation and high spins are studied through the pairing selfconsistent calculations for the SD bands of Hg nuclei. It was found that the correct rotational frequency ω-dependence of the pairing fields is crucial for the theory to reproduce the smooth rising bevavior of dynamic moment of inertia $J^{(2)}$. The calculated $J^{(2)}$ of ^{192}Hg is in a good agreement with data up to $\hbar\omega$ =0.32 MeV beyond which it has a too sharp rising caused by a rather early and sudden collapse of the pairing fields.

1. Introduction

The pairing correlations and its collapse in a highly rotating nuclear system have been one of major topics in high spin physics starting with a classical work by Mottelson and Valatin [1]. The resent discoveries of superdeformed rotational bands in the rare earth nuclei around ^{152}Dy [2] and in the A=190 nuclei around ^{192}Hg [3,4] opens a new possibility to study a competition between rotation, deformation and pairing in very extreme conditions. It is still impossible to identify spins of these SD bands as no discrete γ-rays linking the SD band and any lower known bands has been measured. Only quantity that can be unambiguously determined from data is the dynamic moment of inertia $J^{(2)}(\approx 4\Delta E_\gamma)$, extracted from transition energies E_γ and thus independent of the spin assignment. The dynamic moment of inertia is defined as the second derivative of the total energy E with respect to spin I, $J^{(2)} = d^2E/dI^2$, and thus is very sensitive to small changes in the intrinsic structure of a nucleus, such as changes in the nuclear shapes and pairing fields. A most surprising feature observed for the SD bands in A=190 region is that the dynamic moment of inertia was found to increase steadily with rotational frequency ω. In contrast, the dynamic moment of inertia of SD bands in the A=150 region was found to decrease with the rotational frequency except a SD band in nucleus ^{151}Dy which has also a rising $J^{(2)}$ feature. It was observed that $J^{(2)}$ increases by 30 – 40% over rotational frequency range $\hbar\omega$=0.1 - 0.4 MeV for SD bands in the A=190 region.

The inclusion of pairing is crucial for the mean field theory to reproduce the smooth increase of $J^{(2)}$ with frequency. Calculations without pairing result in essentially no frequency dependence of $J^{(2)}$. The CSM calculations with pairing have been successful in explaining some of general feature related to superdeformation in the A=190 region. The shell structure in the vicinity of the Fermi surface seems to be well understood as the measured excitations in the second well potential can be essentially reproduced by means of the rotating quasiparticle spectra. For example, the observed differences in the behavior of $J^{(2)}$ with ω in ^{193}Tl and ^{191,192}Hg can be accounted for satisfactorily when blocking arguments are invoked [5-7]. There are many indications that pairing correlations play a significant role in the SD band in the mass region. On the other hand, there exist also reasons that pairing correlations are very weak at superdeformation. For example, moments of inertia in this mass region are very similar and blocking effects are very weak [8], and in fact, calculations even with a strongly reduced pairing field give a too strong quasipareticle alignment and predict a too early downturn in the $J^{(2)}$ with ω. The weakness of the pairing field in SD bands is basically associated with the fact that the low density of single particle states in the SD configuration leads to seriously quenching of the pairing correlations already at a low frequency.

The mean field theory is under a great challenge as the system to be described by the theory is at extreme conditions of very large shape - elongation, highly rotating and 'fragile' pairing correlations which are very weak but play an important role. The recent cranked HFB calculation with monopole pairing gives a dynamic moment of inertia $J^{(2)}$ for ^{192}Hg which agrees with experimental data up to $\hbar\omega$=0.2 MeV and then grows too faster than that derived from data [9]. The cranking shell model (CSM) calculations with a constant monopole pairing again leads to too fast rise of the $J^{(2)}$ with ω (see e.g. ref.[10]).

It was known that the band crossing shifts to higher frequencies when the quadrupole pairing Y_{20} is included in calculations for normal deformed nuclei (see e.g. ref. [11]). It is known that the presence of the $K^{\pi} = 1^{+}$ (e.g. Y_{21}) pairing interaction leads to an effective attenuation of Coriolis matrix elements [12]. Recently, the effect of the Y_{21} pairing on the nuclear moment of inertia of SD rotational bands has been studied within the single-j shell model and it is found that the frequency dependence of the moments of inertia can be appreciably modified [13].

In the present paper, we study to what extent the inclusion of quadrupole pairing, Y_{20}, Y_{21} and Y_{22} can influence the moments of inertia of the SD bands in A=190 region and investigate the collapse of the pairing fields in a rotating superdeformed nucleus by means of the Harmonic Oscillator Quadrupole Pairing HFB approach (HOQHFB) developed recently with Hamamoto and Nazarewicz [14].

2. The theoretical model

2.1 The hamiltonian

The hamiltonian which consists of an anisotropic harmonic oscillator $H_{h.o.}$, monopole and quadrupole pairing interactions and the Coriolis and centrifugal forces $-\omega L_1$ may be written as,

$$H = H_{h.o.} - \omega L_1 - \frac{1}{4} G_0 P_{00}^+ P_{00} - \frac{1}{4} G_2 \sum_m P_{2m}^+ P_{2m},$$

$$H_{h.o.} = \frac{P_i^2}{2m} + \frac{1}{2} m \sum_i \omega_i^2 x_i^2, \; (i = 1, 2, 3). \tag{1}$$

The oscillator frequencies for an axil symmetric shape are determined with the elongation parameter ε as,

$$\omega_1 = \omega_2 = \omega_0(1 + \varepsilon/3), \; \omega_3 = \omega_0(1 - 2\varepsilon/3), \tag{2}$$

where ω_0 is obtained from the volume conservation condition:

$$\omega_1\omega_2\omega_3 = \tilde{\omega_0}^3, \; \tilde{\omega_0} = 41/A^{1/3} \; (MeV). \tag{3}$$

The *cranking harmonic oscillator hamiltonian*

$$H_{h.o.}^{\omega} = H_{h.o.} - \omega L_1 \tag{4}$$

may be diagonalized first and the result is three uncoupled harmonic oscillators (see e.g. ref.[15] and ref.s here in)

$$H_{h.o.}^{\omega} \mid n_1 n_\alpha n_\beta >= [\hbar\omega_1(n_1 + \frac{1}{2}) + \hbar\Omega_\alpha(n_\alpha + \frac{1}{2}) + \hbar\Omega_\beta(n_\beta + \frac{1}{2})] \mid n_1 n_\alpha n_\beta >, \tag{5}$$

with the new normal frequencies

$$\omega_1, \; \Omega_{\alpha(\beta)} = \sqrt{\frac{1}{2}(\omega_2^2 + \omega_3^2) + \omega^2 \mp \frac{1}{2} S}, \tag{6}$$

where

$$S = sign(\omega_3 - \omega_2)\sqrt{(\omega_3^2 - \omega_2^2)^2 + 8\omega^2(\omega_2^2 + \omega_3^2)}. \tag{7}$$

2.2 The overlap matrix

The overlap between rotating and nonrotating single particle states $| K,\omega >$ and $| \mu >$,

$$D_\mu^K(\omega) = < K,\omega \mid \mu > \tag{8}$$

can be calculated analytically with an explicit expression [15,16],

$$D_{n_1' n_2 n_3}^{n_1' n_\alpha n_\beta} = \delta_{n_1' n_1} \sqrt{\frac{n_2! n_3!}{n_\alpha! n_\beta!}} \sum_{k=0}^{n_\alpha} \binom{n_\alpha}{k} \sum_{l=0}^{n_\beta} \binom{n_\beta}{l}$$

$$N(k,l,n_2,X_\alpha^\pm,Y_\beta^\pm) N(n_\alpha - k, n_\beta - l, n_3, Y_\alpha^\mp, X_\beta^\mp). \tag{9}$$

Where

$$N(k,l,n_2,X_\alpha^\pm,Y_\beta^\pm) = \frac{1}{2^{(k+l-m)/2}} (X_\alpha^+)^k (Y_\beta^-)^l$$

$$\left(\frac{Y_\beta^+}{Y_\beta^-}\right)^{(k+l-m)/2} \sum_{n=0}^{[\frac{k}{2}]} \frac{(-k)_{2n}}{n!} \left(\frac{X_\alpha^- Y_\beta^-}{X_\alpha^+ Y_\beta^+}\right)^n$$

$$\sum_{j=j_{min}}^{j_{max}} \frac{2^j (2n-k)_j (-l)_{k+l-m-2n-j}}{j!((k+l-m)/2-n-j)!}, \tag{10}$$

with

$$j_{max} = min\{l, k-2n, (k+l-m)/2 - n\},$$

$$j_{min} = max\{0, k-m-2n\}, \tag{11}$$

$$(k)_0 = 1, (k)_n = k(k+1)(k+2)...(k+n-1). \tag{12}$$

The $X^\pm$ and $Y^\pm$ are the coefficients of general Bogolyubov transformation between the boson operators in rotating and nonrotating systems [17,18] :

$$a_\alpha = X_\alpha^+ a_2 + X_\alpha^- a_2^+ + Y_\alpha^+ a_3^+ + Y_\alpha^- a_3,$$

$$a_\beta = X_\beta^+ a_3 + X_\beta^- a_3^+ + Y_\beta^+ a_2^+ + Y_\beta^- a_2. \tag{13}$$

The coefficients of transformation (13) are given by

$$X_\alpha^\pm = \frac{1}{2}\sqrt{\frac{m\omega_2}{| m_\alpha | \Omega_\alpha}} \left(\frac{A \mid m_\alpha \mid \Omega_\alpha}{m\omega_2} \pm 1\right), \tag{14a}$$

$$X_\beta^\pm = \frac{1}{2}\sqrt{\frac{m\omega_3}{| m_\beta | \Omega_\beta}} \left(1 \pm \frac{A \mid m_\beta \mid \Omega_\beta}{m\omega_3}\right), \tag{14b}$$

$$Y_\alpha^\pm = \frac{1}{2}\sqrt{\frac{m\omega_3}{| m_\alpha | \Omega_\alpha}} \left(B \mid m_\alpha \mid \Omega_\alpha \pm \frac{C}{m\omega_3}\right), \tag{14c}$$

$$Y_\beta^{\pm} = \frac{1}{2}\sqrt{\frac{m\omega_2}{\mid m_\beta \mid \Omega_\beta}}(\frac{C}{m\omega_2} \pm B \mid m_\beta \mid \Omega_\beta), \qquad (14d)$$

where the frequency dependent masses are calculated by the expression,

$$m_{\alpha(\beta)} = m\frac{\Omega^2_{\alpha(\beta)} - \Omega^2_{\beta(\alpha)}}{\Omega^2_{\alpha(\beta)} - \omega^2_{3(2)} + \omega^2}, \qquad (15)$$

and the auxiliary coefficients can be calculated by the expressions,

$$A = \frac{1}{2}(1 + (\omega_3^2 - \omega_2^2)/S), \qquad (16)$$

$$B = \frac{2\omega}{mS}, \qquad (17)$$

$$C = \frac{m}{4\omega}(\omega_3^2 - \omega_2^2 - S). \qquad (18)$$

In the present paper we have chosen the phase convenience

$$R_2(\pi)\hat{T} = 1, \qquad (19)$$

where the $R_2(\pi)$ and $\hat{T}$ is operator describing a rotation around the axis-2 by an angle of π and the time reversion respectively. With this phase convenience the coefficients of transformation (13) and thus the overlap matrix (8) become to real numbers instead of the complex numbers given in ref.s [15,17,18]. This advantage can be taken particularly in the presence of quadrupole pairing interaction as the Y_{2m} is invariant under the action of $R_2(\pi)\hat{T}$.

2.3 The pairing matrix

For simplicity the oscillator quantum numbers $n_1n_2n_3$ and $n'_1n_\alpha n_\beta$ are abbreviated to μ and K respectively. We can then introduce the tree dimensional oscillator creation operators a^+_μ and a^+_K as,

$$\mid \mu >= a^+_\mu \mid n_1, n_2, n_3 = 0 >, \qquad (20)$$

$$\mid K >= a^+_K \mid n'_1, n_\alpha, n_\beta = 0 >, \qquad (21)$$

and one has

$$\hat{T} \mid \mu > \equiv \mid \bar{\mu} >= (-1)^{n_1+n_3} \mid \mu >, \qquad (22)$$

$$R_1(\pi) \mid K > \equiv \mid \check{K} >= (-1)^{n_\alpha+n_\beta} \mid K > . \qquad (23)$$

The transformation of the pair creation operator P^+ to the rotating harmonic oscillator representation can be performed by means of the overlap matrix (8) as follows.

$$P^+_{00} = \sum_{KL} P^{00}_{KL} a^+_K a^+_L, \qquad (24)$$

$$P^{+}_{2m} = \sum_{K\bar{L}} P^{2m}_{K\bar{L}} a^{+}_{K} a^{+}_{\bar{L}}, \tag{25}$$

where

$$P^{00}_{K\bar{L}} = \sum_{\mu>0} D^{K}_{\mu} D^{\bar{L}}_{\bar{\mu}}, \tag{26}$$

$$P^{2m}_{K\bar{L}} = \sum_{\mu,\nu>0} < \mu \mid Q_{2m} \mid \nu > D^{K}_{\mu} D^{\bar{L}}_{\bar{\nu}}. \tag{27}$$

The quadrupole pairing operators may been written as

$$Q_{2m} = \sqrt{\frac{28\pi}{3}} r^{2} Y_{2m} / R^{2}, \tag{28}$$

where the R is the average radius of nucleus and the Q_{2m} has been normalized to a sphere with a radius R.

2.4 The HFB equations

The harmonic oscillator HFB equations with quadrupole pairing interactions may be written in the form of matrix array,

$$\begin{pmatrix} (e-\lambda) & -\Delta \\ -\Delta & -(e-\lambda) \end{pmatrix} \begin{pmatrix} A \\ B \end{pmatrix} = E \begin{pmatrix} A \\ B \end{pmatrix}. \tag{29}$$

The pairing matrix elements may be calculated by the expression

$$\Delta_{K\bar{L}} = \Delta^{00} P^{00}_{K\bar{L}} + \Delta^{20} P^{20}_{K\bar{L}} + \Delta^{21}(P^{21}_{K\bar{L}} + P^{2-1}_{K\bar{L}}) + \Delta^{22}(P^{22}_{K\bar{L}} + P^{2-2}_{K\bar{L}}), \tag{30}$$

where

$$\Delta^{00} = G_0 \sum_{K,L>0} P^{00}_{K\bar{L}} \chi_{K\bar{L}}, \tag{31a}$$

$$\Delta^{2m} = G_2 \sum_{K,L>0} P^{2m}_{K\bar{L}} \chi_{K\bar{L}}. \tag{31b}$$

The pair density matrix χ may be calculated with the wave function of the quasiparticle vacuum, the solution of eq. (29),

$$\chi_{K\bar{L}} = < a_K a_{\bar{L}} > . \tag{32}$$

The Fermi level λ should be determined by the particle number constraint

$$< \hat{N} > = N. \tag{33}$$

It is straightforward to include the spin degrees of freedom by adding the term $-\omega S_1$ to the rotating s.p. energies e in the eq.(29).

3. Results of calculations and discussion

The HOQHFB equations are solved selfconsistently with respect to the Fermi level λ (particle number conservation) and the pairing gaps Δ^{00}, Δ^{20}, Δ^{21} and Δ^{22}. The pairing strength parameters taken in the present self-consistent calculations are $(G_0, G_2/G_0)$ = (0.038, 0.7) and (0.055, 0.85) for neutrons and protons respectively. The used deformation parameter ϵ =0.42 was taken from ref.[19] as a reasonable value. The basis of the s.p. states in which the hamiltonian is diagonalized spans a space of equal numer of rotating s.p. states below an above the Fermi surface within the oscillator shells $N = 4 - 9$ of neutrons and $N = 3 - 8$ of protons. With the strength parameters and the space of the basis the present calculation yields an equilibrium monopole pairing gap Δ^{00} of only few hundreds KeV at $\hbar\omega \approx 0$, which is a reasonable value for the strongly weakened pairing field in the SD nuclei.

The dynamic moment of inertia $J^{(2)}$ for ^{192}Hg was calculated as a function of ω and plotted and compared with the experimental data in Fig.1. It is seen that the calculated $J^{(2)}$ is in a good agreement with the data up to $\hbar\omega$ = 0.32 MeV. This result is one of best nowadays that one can achieve within microscopic selfconsistent calculations. For a comparison a recent result of the $J^{(2)}$ for ^{192}Hg calculated with cranked HFB theory with HF mean field and monopole pairing was extracted from Fig.5 of ref.[9] and plotted in Fig.1, see the dash curve, which consists with data up to $\hbar\omega$ =0.2 MeV and presents a too fast rising with ω. The problem of the too fast rising of $J^{(2)}$ with ω remains also in the calculations of the CSM type with a constant monopole pairing (see e.g. ref.[10]).

It was found that the rising behavior of the $J^{(2)}$ sensitively depends on the ω-dependence of the pairing fields. The nice agreement between the theory and the experimental data obtained in the present calculations indicates that a generally correct ω-dependence of the pairing fields has been achieved in the present model. It was found that inclusion of the quadrupole pairing is important to reproduce the smooth rising behavior of the $J^{(2)}$. The alignment of quasiparticles at the Fermi surface can be retarded, namely sets in at a higher value of ω, when the Y_{20} pairing is included. The calculated Y_{21} pairing field shows a linear increase with ω at low frequencies and increases before the critical frequency ω_c ~0.33 MeV where the pairing fields starts to collapse down. The contribution of the Y_{21} pairing is known as the Migdal term which increases the moment of inertia. The linear increasing behavior of the Y_{21} pairing field has played an important role in reproducing the smooth rising behavior of the observed $J^{(2)}$.

However, first of all, the present calculations still predict a rather too early alignment of the lowest neutron quasiparticles and thus a rather too early upturn of the $J^{(2)}$ with ω. Second, the calculation yield a too weak band interaction between the SD ground and the excited two neutron quasiparticle SD bands and therefore gives rise to a too sharp upturn of the $J^{(2)}$ at $\hbar\omega$ =0.33 MeV. The experimental data shows an upturn of $J^{(2)}$ starting at $\hbar\omega$ =0.38 MeV and rising to 140 $\hbar^2$MeV^{-1} at $\hbar\omega$ =0.42 MeV, and we still do not know whether the observed $J^{(2)}$ will continue to increase. Nevertheless, a rather sharp upbend, in comparing with other SD bands, has been indicated in the data and this consists with the result of the present calculation. It was found that the rather too early sharp growth in the calculated $J^{(2)}$ is due to the rather too early and too sudden collapse of the neutron pairing fields as one can see in Fig.2 where sudden drops to zero of both the monopole and the quadrupole pairing gaps occur at around $\hbar\omega$ =0.34 MeV.

It is known that the low density of the single particle levels at the superdeformation leads to a strong quenching of the pairing correlations already at a low frequency. The further reduction of the pairing fields is caused by the Coriolis antipairing effect and the alignment of the high-N quasiparticle orbits. One of striking feature for the pairing field in a superdeformed nucleus is that the pairing gaps could reduce to zero once a pair of nucleons is broken. In contrast to the case of normal deformation, the pairing gap only reduces about 20-30% just beyond the first band crossing frequency where a pair of nucleons are aligned. It seems that the pairing field at superdeformation is much more 'fragile' than that at normal deformation. It is generally believed that the pairing fields, including the quadrupole pairing, must be gone away beyond the ω_c according to the present calculation. Then any nowaday model based on the mean field theory and the picture of quasiparticle fails to work at this phase transition region. It is a great challenge for the mean field theory to reproduce the detail of the upturning behavior of the observed $J^{(2)}$ at high frequencies and superdeformation. It is interesting to carry out calculations of the dynamic pairing fields based on the present model, the work along this line is in progress.

4. Conclusion

The inclusion of the pairing is crucial for the mean field theory to reproduce the smooth rising behavior of observed $J^{(2)}$ for the SD bands in the A=190 region. The present pairing selfconsistent calculations by means of the HOQHFB theory yield a correct smooth rising behavior of $J^{(2)}$ for ^{192}Hg and have achieved a good agreement between theory and experiment up to $\hbar\omega$ =0.32 MeV. An important role played by the quadrupole pairing fields, particularly the Y_{20} and Y_{21} pairing, was found in reproducing the smooth rising behavior of $J^{(2)}$ with ω. In general, a correct ω-dependence of the pairing fields may be achieved within the present microscopic approach and therefore a good agreement between theoretical and experimental $J^{(2)}$ can be

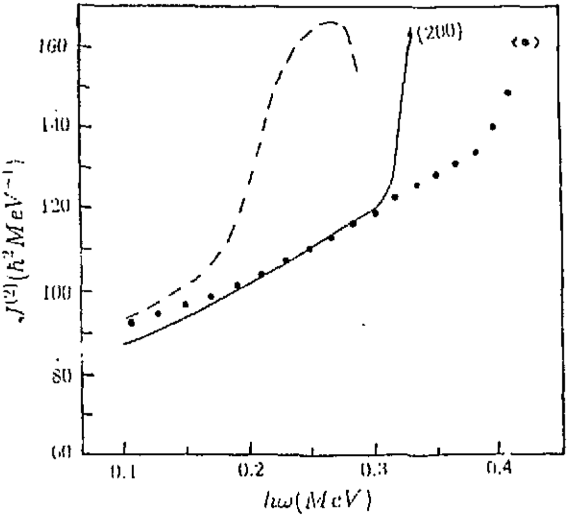

Fig.1 The dynamic moment of inertia $J^{(2)}$ for ^{192}Hg versus frequency ω. The present result (solid curve) is compared with the experimental data taken from ref.[3] (solid circle) and the CHFB result (dash curve) extracted from Fig.5 of ref.[9], not accurate but for guiding our eyes.

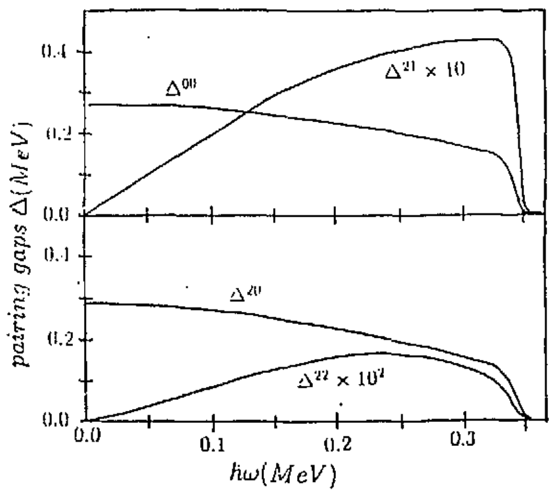

Fig.2 The neutron pairing gaps calculated as functions of frequency ω. The pairing fields collapse around 0.34 MeV.

obtained. However, the model fail to reproduce the critical frequency ω_c and predict a too sharp upturn of $J^{(2)}$, namely the calculation yields rather too small ω_c and too small band interaction. The reason for that was found due to the rather too early and too sudden collapse of the pairing fields, including quadrupole pairing, which come out from the present pairing selfconsistent calculations. It is a hope that with appropriate improvements the mean field theory should be able to face the challenge set by the detailed spectroscopy at superdeformation.

ACKNOWLEDGMENTS

the author gratefully thanks I. Hamamoto and W. Nazarewicz for most valuable discussions and cooperation that starts the present approach at the Joint Institute for Heavy Ion Research, ORNL. The work is supported by the National Science Foundation of China and the Nuclear Industry Science Foundation of Chena.

References

[1] B.R. Mottelson and J.G. Valatin, Phys. Rev. Lett. 5 (1960) 511
[2] P.J. Twin, et al., Phys. Rev. Lett. 57 (1986) 811
[3] T. Lauritsen, et al., Phys. Lett. B279 (1992) 239
[4] J.A. Becker et al., Phys. Rev. C41(1990) R9
[5] R.V.F. Janssens and T.L. Khoo, Ann. Rev. Nucl. Part. Sci. 41(1991)321
[6] M.P. Carpenter, et al., Phys. Lett. B240 (1990)44
[7] P.B. Fernandez, et al., Nucl. Phys. A517 (1990) 386
[8] P. Fallon, et al., Phys. Lett. B276 (1992) 427
[9] H. Flocard, et al., Nulc. Phys. A557 (1993) 559c
[10] M.A. Riley, et al., Nucl.Phys. A512 (1990) 178
[11] M. Diebel, Nucl. Phys. A419 (1984) 221
[12] I. Hamamoto, Nucl. Phys. A232 (1974) 445
[13] I. Hamamoto and W. Nazarewicz, private communication
[14] Y.S. Chen, I. Hamamoto and W. Nazarewicz, to be published
[15] W. Satula, Z. Szymanski and W. Nazarewicz,
Physica Scripta 42 (1990) 515
[16] D. Bes, et al., Ann. Phys. (NY) 182 (1988) 237
[17] V.G. Zelevinskey, Sov. J. Nucl. Phys. 22 (1975) 565
[18] D. Glas, U. Mosel and P.G. Zint, Z. Phys. A285 (1978) 83
[19] W. Satula, et al., Nucl. Phys. A529 (1991) 289

Classical Equations of Breathing Mode Dynamics in Magic Nuclei

G.F.Filippov
Bogoliubov Institute for Theoretical Physics
252143, Kiev 143, Ukraine*

The generalized coherent states (GCS) [1] have become one of frequently used tools of studying the character of motion in many-body system. No exception are the GCS introduced as the generating invariants of symplectic groups for the constructing the dynamical equations describing collective degrees of freedom of nuclear systems [2].

The GCS may also be interpreted as a kernel of an integral transform mapping the wave function of a system from the usual configurational (coordinate and spin-isospin) space to the Fock–Bargmann space where the GCS parameters become the independent variables. Also, employing the GCS we can construct in the Fock–Bargmann space the operators of various physical quantities [3].

Each of the GCS is a wave packet, therefore, the GCS is a convenient starting point in the derivation of the classical equations of motion describing the evolution of the wave packet parameters [4]. The way of constructing the equations is shown by the Ehrenfest theorem and the Poisson quantum brackets [5].

The problem of classical equation of motion for the symplectic group wave packets has already been discussed in Refs. 6, 7, 8, 9. However, our approach differs in two aspects. Firstly, our parametrization of the GCS leads to the natural for the Fock–Bargmann space independent variables and simple expressions for the kinetic and potential energy operators in the Fock–Bargmann representation. Therefore, secondly, the Ehrenfest theorem immediately yields the dynamical equations not only for the breathing mode (already obtained in Refs. 6, 7) but also for the monopole-quadrupole oscillations of nuclear systems studied with the $Sp(6,\Re)$ model.

Since now we are discussing only the principal points of deriving the classical dynamical equations of the collective degrees of freedom, and our conclusions differ from those of Refs. 6 and 7, we shall be paying our attention only to the simplest example of the of the breathing mode leaving for the following contribution the analysis of solution of dynamical equations and the generalization for the case of other degrees of freedom.

We consider first the monopole oscillations of magic nuclei (^{4}He, ^{16}O, ^{40}Ca) when the wave packet is constructed as the GCS of the $Sp(2,\Re)$ group and define the quantum Poisson brackets in the Fock–Bargmann space which significantly simplifies the derivation.

The structure of the $Sp(2,\Re)$ group wave packet is completely determined by the value of one complex parameter ε. The GCS has the following form

$$\begin{aligned}\Phi &= (1-\varepsilon)^{-J}\exp\left\{-\frac{1}{2}\frac{1+\varepsilon}{1-\varepsilon}\rho^2\right\}\chi_J \\ &= \sum_{n=0}^{\infty}\varepsilon^n\, e^{-\rho^2/2}\, L_n^{J-1}(\rho^2)\,\chi_J \qquad (1)\end{aligned}$$

*E-mail address: `gfilippov@gluk.apc.org`

where ρ is the global radius (ρ^2 is the sum of squares of Jacobi vectors), χ_J is the hyperspherical function,

$$J = 3f + \frac{3}{2}(A-1) = K + \frac{3}{2}(A-1)$$

is the $Sp(2,\Re)$ irrep index, A is number of nucleons, $f = 0, 4, 20$ for ^{4}He, ^{16}O, ^{40}Ca, respectively. We assume that the oscillator length r_0 equals unity.

Note that the set of functions

$$\sqrt{\frac{\Gamma(J+n)}{\Gamma(J)\Gamma(n+1)}}\,\varepsilon^n, \qquad n = 1, 2, \ldots$$

define the basis of harmonic oscillator states orthogonal with the Bargmann measure, intended for the description of the breathing mode.

First we calculate the overlap integral of the generating invariants Φ and Φ^* in order to obtain their normalization.

$$\langle \Phi^* \mid \Phi \rangle \;=\; (1-\varepsilon)^{-J} = \sum_{n=0}^{\infty} \frac{\Gamma(n+J)}{\Gamma(J)n!}(\varepsilon\varepsilon^*)^n \tag{2}$$

Two other overlap integrals

$$\langle \Phi^* \mid \mathsf{T} \mid \Phi \rangle \;=\; \frac{\hbar^2}{2m} J \frac{(1+\varepsilon)(1+\varepsilon^*)}{1-\varepsilon\varepsilon^*} \langle \Phi^* \mid \Phi \rangle \tag{3}$$

$$\langle \Phi^* \mid \rho^2 \mid \Phi \rangle \;=\; J \frac{(1+\varepsilon)(1+\varepsilon^*)}{1-\varepsilon\varepsilon^*} \langle \Phi^* \mid \Phi \rangle \tag{4}$$

are necessary to construct the image of the kinetic energy operator T and the square of global radius in the Fock-Bargmann space. The image T_ε of the kinetic energy operator and that of ρ^2 (Q) will be found using the following relations

$$\mathsf{T}_\varepsilon \langle \Phi^* \mid \Phi \rangle \;=\; \langle \Phi^* \mid \mathsf{T} \mid \Phi \rangle, \tag{5}$$

$$\mathsf{Q} \langle \Phi^* \mid \Phi \rangle \;=\; \langle \Phi^* \mid \rho^2 \mid \Phi \rangle. \tag{6}$$

The right-hand sides of (5) and (6) and the overlap integral (2) are known, so one immediately gets

$$\mathsf{T}_\varepsilon \;=\; \frac{\hbar^2}{2m}\left[(1+\varepsilon)^2 \frac{\partial}{\partial\varepsilon} + J(1+\varepsilon)\right], \tag{7}$$

$$\mathsf{Q} \;=\; -(1-\varepsilon)^2 \frac{\partial}{\partial\varepsilon} + J(1-\varepsilon). \tag{8}$$

The average value of T_ε and Q in the state described by the wave packet Φ can be calculated by using (3) and (4)

$$T_\varepsilon \;=\; \frac{\langle \Phi^* \mid \mathsf{T} \mid \Phi \rangle}{\langle \Phi^* \mid \Phi \rangle} = \frac{\hbar^2}{2m} J \frac{(1+\varepsilon)(1+\varepsilon^*)}{1-\varepsilon\varepsilon^*}, \tag{9}$$

$$Q \;=\; \frac{\langle \Phi^* \mid \rho^2 \mid \Phi \rangle}{\langle \Phi^* \mid \Phi \rangle} = J \frac{(1-\varepsilon)(1-\varepsilon^*)}{1-\varepsilon\varepsilon^*} \quad . \tag{10}$$

The average value of the potential energy of nucleon-nucleon interaction, taken as the Gaussian potential U_{ij} with the depth V_0 and the radius b_0, for ^{4}He can be expressed in terms of Q

$$\langle \Phi^* \mid \mathrm{U} \mid \Phi \rangle = 6V_0 \left[1 + \frac{2}{b_0^2} \frac{(1-\varepsilon)(1-\varepsilon^*)}{1-\varepsilon\varepsilon^*} \right]^{-3/2} \langle \Phi^* \mid \Phi \rangle. \tag{11}$$

Let Q be a generalized coordinate describing the size of a wave packet Φ. In order to find the corresponding generalized velocity $\dot{Q}$ and to express the total energy of the system in terms of Q and $\dot{Q}$ we define an operator of generalized velocity $\dot{\mathrm{Q}}$. It is given by the Poisson quantum brackets, i.e., the commutator of the square of global radius operator and the kinetic energy. We shall write the Poisson brackets in the Fock–Bargmann space where the operators $\dot{\mathrm{Q}}$ and T_ε are already known.

$$i\hbar\dot{\mathrm{Q}} = \mathrm{Q}\mathrm{T}_\varepsilon - \mathrm{T}_\varepsilon\mathrm{Q} = 2\frac{\hbar^2}{m}[-(1-\varepsilon^2)\frac{\partial}{\partial\varepsilon} + J\varepsilon]. \tag{12}$$

It then follows that

$$\dot{\mathrm{Q}} = -i2\frac{\hbar}{m}[-(1-\varepsilon^2)\frac{\partial}{\partial\varepsilon} + J\varepsilon]. \tag{13}$$

Now it is not difficult to obtain the generalized velocity

$$\dot{Q} = -2\frac{\hbar}{m}J\frac{\varepsilon-\varepsilon^*}{1-\varepsilon\varepsilon^*}. \tag{14}$$

It remains to express T_ε in terms of $\dot{Q}$ and Q. It can be done by expressing ε and ε^* in terms of $\dot{Q}$ and Q and then eliminating ε and ε^* from the right-hand side of (9):

$$T_\varepsilon = \frac{m}{8}\frac{\dot{Q}^2}{Q} + \frac{\hbar^2 J^2}{2mQ}. \tag{15}$$

The first term in the right-hand side of (15) differs from the kinetic energy obtained in [9] only by notation, but Eq. 15 contains also the second term absent in [9]. It has a simple physical meaning of the centrifugal potential due to the high dimensionality of the space where the hyperharmonics χ_J are defined and by the effects of the hypermomentum $K = 3J$.

The dynamical equation for the generalized velocity $\dot{Q}$ immediately follows from the energy conservation law. For example, for ^{4}He ($J = 9/2$) this law has the form

$$\frac{m}{8}\frac{\dot{Q}^2}{Q} + \frac{81}{8}\frac{\hbar^2}{mQ} + 6V_0\left[1 + \frac{4}{9}\frac{Q}{b_0^2}\right]^{-3/2} = E. \tag{16}$$

The potential energy of ^{16}O is the sum of three terms corresponding to direct and exchange nuclear interaction and the Coulomb interaction, respectively.

$$\begin{aligned} U(^{16}\mathrm{O}) \;&=\; 8V_0\{\frac{31}{4}\Delta^{-3/2} + \frac{9}{2}\Delta^{-5/2} + \frac{15}{4}\Delta^{-7/2}\} - \\ &\quad - 2V_0\{\frac{31}{4}\Delta^{-3/2} - \frac{15}{2}\Delta^{-5/2} + \frac{15}{4}\Delta^{-7/2}\} + \frac{83}{4}\sqrt{\frac{69}{\pi Q}}e^2, \end{aligned} \tag{17}$$

$$\Delta = 1 + \frac{4}{69b_0^2}Q.$$

Note that the potential energy decreases slowly, as $Q^{-3/2}$, with increasing Q (this fact has already been interpreted with the hyperspherical functions method). Adding the centrifugal potential to $U(^{16}O)$, we obtain the effective potential energy. The Bohr–Sommerfeld conditions can provide an estimate for the energies of quantum levels in the effective field and the information on some remarcable properties of these levels.

The period of breathing-mode oscillations increases with the energy counted off the ground state (it does not decrease inversely proportional to E as in the harmonic oscillator case). While for the first excited state ($E^* \approx 12$ Mev) it is $\sim 10^{-21}$ sec (see the Table), for the ninth excited state it becomes almost five times greater. Finally, for the resonance $E \approx 2.94$ Mev it is $15.7 \cdot 10^{-21}$ sec.

N	E, MeV	T, 10^{-24} sec	$T_<$, 10^{-24}sec	R_l, Fm	R_r, Fm	width, keV	R_e, Fm
1	-115.1	167	64.5	1.93	2.57	4762	0
2	-91.9	190	57.6	1.79	2.96	3289	0
3	-71.6	219	54.1	1.71	3.32	2337	0
4	-54.0	255	51.8	1.66	3.68	1654	0
5	-39.0	302	50.2	1.62	4.08	1144	0
6	-26.5	363	49.1	1.60	4.51	769	0
7	-16.2	449	48.2	1.58	5.02	495	0
8	-8.0	574	47.6	1.56	5.61	299	0
9	-1.7	772	47.1	1.55	6.35	164	0
10	2.8	1138	46.8	1.54	7.33	75	26.41
11	5.6	2141	46.6	1.53	8.90	21	13.88

In the process of its motion, the nucleon system changes its root-mean-square (rms) radius from the minimum ~ 1.5–1.9 Fm to the maximum of ~ 7.5 Fm. Unill the system radius is less than its doubled radius in the ground state, the probability of collisions of nucleons is great so that the breathing-mode energy can be transferred to the other nuclear degrees of freedom. With the increase of the rms radius the collision probability decreases as also the probability of the breathing mode dissipation.

To estimate the widths of collective excitations we introduce two half-periods $T_<$ and $T_>$. The are defined as the fractions of time when the rms radius is less or greater than the doubled ground-state radius, respectively. With such definitions the ratio $T_</T_>$ would be the rough estimate for the probability of dissipation of collective energy and, therefore, of the nucleus decay for the period T, while the value

$$\Gamma = 2\pi \frac{T_<}{T_>} \frac{h}{T}$$

can be assumed as the estimate for the level width. For the first excited state $\Gamma \approx 5$ Mev, while for higher excited states Γ decreases to ~ 100 kev and to 20 kev for the 5.6 Mev resonance.

Thus, as the energy of monopole collective excitations increases, significantly increase also the amplitude and the period of monopole oscillation. The nucleon system passes to the state in which the coupling of the monopole degree of freedom with the other degrees of freedom responsible for the nucleus decay is weak. Theoretical estimates of life-time in these states support the conclusions made in [10] and give reasons to a conclusion on the possibility of existence of narrow collective resonances with high excitation energy.

The author thanks I. Yu. Rybkin for useful discussions and V. V. Mikhailovsky who carried out numerical calculations.

References

[1] A.M.Perelomov, *Generalized Coherent States and their Applications* (Springer, Berlin, 1987).

[2] G.F. Filippov, V.S. Vasilevsky, L.L. Chopovsky, Sov. J. Part. Nucl. **15** 1338 (1984), *Ibid* **16**, 349 (1985).

[3] V.S.Vasilevsky, G.F.Filippov, in *Group Theoretical Methods in Physics*, Proceedings of the third seminar, Jurmala, May 22–24, 1985 (Nauka, Moscow, 1986, in Russian), p.572.

[4] R.G.Glauber, Phys.Rev. **130**, 2529 (1963).

[5] A.Messiah, *Quantum Mechanics* (North-Holland, Amsterdam, 1962)

[6] J.Broeckhove, M.Buysse and P.Van Leuven, Phys.Lett. **134B**, 379 (1984)

[7] F.Arickx, J.Broeckhove and P.Van Leuven, Journal de Physique **C6 45**, 311 (1984)

[8] F.Arickx, J.Broeckhove and P.Van Leuven, Nuovo Cim. **104B**, 629 (1989).

[9] F.Arickx, J.Broeckhove and P.Van Leuven, Phys.Rev. **A 43**, 1211 (1991).

[10] G.F.Filippov, Riv.Nuovo Cim. No. **9**, 1 (1989).

VIBRATIONAL BANDS IN DEFORMED NUCLEI; AN sdg BOSON MODEL PERSPECTIVE

SERDAR KUYUCAK
Department of Theoretical Physics, Research School of Physical Sciences
Australian National University, Canberra, ACT 0200, Australia

ABSTRACT

We present a study of vibrational bands in deformed nuclei in the framework of the sdg boson model. We point out the importance of the hexadecapole degree of freedom in studies of K=4^+ bands, and caution that not all such bands are necessarily $\gamma\gamma$ vibrational bands.

1. Introduction

Low-lying quadrupole excitation modes in deformed nuclei (called β and γ bands) have been known since the early fifties.[1] Higher lying excitations built on these elementary modes, however, escaped detection until recently. New developments in detector technology allowed observation of such double-phonon bands, with a number of candidates having been proposed during the past few years.[2,3,21,5,6] The quadrupole double-phonon bands occur at about the same energy as the hexadecapole single-phonon bands, and one has to be very careful in the assignment of these bands. In order to provide theoretical guidance, one needs a model which treats the quadrupole and hexadecapole degrees of freedom on an equal footing. The interacting boson model (IBM)[7] presumably offers one of the simplest frameworks for this extension.

At a phenomenological level, the IBM corresponds to the second quantization of the geometrical model (GM),[1] and hence describes basically the same physics. Admittedly, there are some differences between the two models (mainly due to finite number of bosons in the IBM), but these are in details and do not detract from their basic equivalence. The real difference lies in their mathematical representations, the GM is based on differential equations and the IBM is on algebra. This is precisely where the IBM description offers the gratest advantage, namely algebraic formalism is much easier to handle than solving differential equations. This becomes even more apparent when the extensions of the models beyond the quadrupole collectivity are considered. Extension of the geometrical model to include the hexadecapole degree of freedom would involve solving a 14-dimensional differential equation which is a highly non-trivial problem. In contrast, such an extension in the IBM involves adding g bosons with $L = 4$ to the sd boson system in a rather straightforward manner, and it has already been applied to nuclear structure problems in dozens of papers (see Refs.[7,8] for reviews).

In this talk, we address the issues raised above within the sdg IBM, through a systematic study of band energies and electromagnetic transition rates in deformed nuclei. Our ultimate aim in these studies is to explain the experimental systematics, and to offer clear signatures for the experimentalists to identify the double-phonon bands. In this regard, we focus on the following questions;

i) The energy ratio of the double- to single-phonon bands: From simple arguments, this ratio is expected to be around 2. However, most of the proposed bands have a ratio in the range 1.5 to 2.5. Whether realistic models can accommodate so much anharmonicity

has not been well investigated. The alternative explanation, of course, is that some of these are in fact either hexadecapole bands or heavily mixed with them.
ii) Electromagnetic transition rates and branching ratios: Again simple arguments predict that the E2 transitions between the double- and single-phonon bands should be similar to that of the ground and single-phonon bands. Such an argument is valid only if the band structures are relatively pure. As stressed above, due to proximity of the hexadecapole bands, strong mixing between the quadrupole and hexadecapole bands is possible, and detailed calculations are necessary before one can make predictions. Similarly, branching ratios could be very sensitive to mixing effects, and the use of Alaga rules, which ignore mixing, are too simplistic for identification purposes.

2. Inadequacy of the sd Boson Model

The sdg IBM is considerably more complicated than the sd IBM, therefore, one should justify its necessity before introducing g bosons. Here we point out some of the shortcomings of the sd model when it is applied beyond the low-lying levels of ground, β and γ bands. The most direct evidence for g bosons come from the extra bands in spectra and the lack of boson cut-off in yrast $B(E2)$ values. These are kinematical in origin and simply follow from the expansion of the model space. For example, in going from the sd to the sdg model, the number of single-phonon bands is increased from 2 (β,γ) to 7 ($\beta,\beta',\gamma,\gamma',K = 1^+,3^+,4^+$), and the boson cut-off is pushed from spin $L = 2N$ to $L = 4N$. There are many hexadecapole vibrational bands in nuclear spectra, especially with $K = 3^+,4^+$. (In the case of the $K = 4^+$ band, one has to make sure that it is not a double-γ excitation. In this regard, strong $E4$ excitation of 4^+ states provides a clean signature for hexadecapole bands. This point is further discussed in the next section.) $B(E2)$ measurements are relatively harder to find as evidence for g bosons because, due to band crossing, it is usually not possible to follow the ground band to very high spins in coulomb-excitation experiments. Nevertheless, a spectacular example was recently provided in ^{232}Th where the ground band $B(E2)$ values were measured up to spin $L = 28$ and showed no sign of boson cut-off.[9] (^{232}Th has $N = 12$ bosons, hence the ground band terminates at $L = 24$ in the sd model.)

Another question of interest is whether the sd IBM can describe the double-phonon (β, γ) bands which are within its model space. As this question is mostly ignored in the literature, a brief discussion of the sd IBM predictions is in order. This will also provide a useful reference point for the sdg IBM calculations in the next section. A popular choice for study of deformed nuclei in the sd IBM is the consistent-Q formalism (CQF) introduced by Casten and Warner.[8] In CQF, the Hamiltonian has the simple form

$$H = \kappa_1 L \cdot L + \kappa_2 Q \cdot Q, \tag{1}$$

where L is the angular momentum and Q is the quadrupole operator given by

$$Q = [s^\dagger \tilde{d} + d^\dagger \tilde{s}]^{(2)} + \chi [d^\dagger \tilde{d}]^{(2)}. \tag{2}$$

The additional constraint is that the same quadrupole operator is used in the calculation of $E2$ transitions, i.e. $T(E2) = e_2 Q$ where e_2 is an effective charge. In Table 1, we present CQF calculations along the SU(3)-O(6) leg of the Casten's triangle[8] as the χ parameter is varied from $-\sqrt{7}/2$ to 0. The first row shows the energy ratio of the double- to single-γ bands, and the rest various interband (reduced) $E2$ matrix elements among the ground, γ and $\gamma\gamma$ bands. Leaving aside the the dynamical symmetry limits,

Table 1: Band energy and $E2$ transition systematics of γ and $\gamma\gamma$ bands for a quadrupole Hamiltonian in the sd IBM. The parameters are $N = 12$, $\kappa_1 = 0$, $\kappa_2 = -20$ keV, and χ is varied. The $E2$ m.e. should be multiplied by e_2 for comparison with experiment.

$\chi/\chi_{SU(3)}$	1.00	.75	.50	.25	.00
$E_{\gamma\gamma}/E_\gamma$	1.87	1.88	1.89	1.91	2.80
$E2(2_g^+ \to 0_g^+)$	18.00	16.61	15.31	14.09	13.85
$E2(2_\gamma^+ \to 0_g^+)$	0.00	0.99	1.97	3.04	0.00
$E2(2_\gamma^+ \to 2_g^+)$	0.00	1.28	2.69	4.82	16.30
$E2(4_{\gamma\gamma}^+ \to 2_g^+)$	0.00	0.00	0.01	0.25	0.00
$E2(4_{\gamma\gamma}^+ \to 2_\gamma^+)$	0.00	2.21	4.34	5.98	0.00

all the ratios remain remarkably constant. In particular one has $E_{\gamma\gamma}/E_\gamma \sim 1.9$ and $E2(4_{\gamma\gamma}^+ \to 2_\gamma^+)/E2(2_\gamma^+ \to 0_g^+) \sim 2.2$. These are very close to the geometrical model values given by 2 and 2.25, respectively. (In fact, in the limit of large N, the agreement would be exact.) Thus the double-phonon bands in the sd IBM are very close to the harmonic limit of the geometrical model, even after allowing for variations in the χ parameter. In other words, the sd model is not flexible enough to describe either the anharmonicities in band energies or the variations in interband $E2$ transitions.

3. sdg Boson Models for Deformed Nuclei

Extension of the IBM to g bosons is straightforward and there are computer codes that can diagonalize a given sdg IBM Hamiltonian efficiently.[10] There are, however, two problems that need to be addressed before realistic applications of the sdg IBM can be carried out in deformed nuclei. First is the large basis space which puts the exact diagonalization beyond the reach of even super computers for $N > 12$. Thus one needs approximation methods that either truncate the basis space to manageable sizes or allow analytic calculations. Here we briefly mention and comment on some of these schemes used in the literature (see Ref.[7,8] for reviews). The first three are based on analytic approaches and the last three on numerical diagonalization.

i) SU(3) limit[11]: Unlike the sd model, the SU(3) symmetry is badly broken in the sdg model because of the large single-boson energy ϵ_g. It provides only a qualitative picture for the band structures in deformed nuclei and needs to be improved for realistic comparisons.

ii) Hartree-Bose and Tamm-Dancoff approximations[12]: This approach gives leading order expressions (in N) for the ground and single-phonon band energies, providing guidelines for the breaking of the SU(3) symmetry. It is limited in scope and accuracy, however, and not likely to be useful in the actual analysis of data.

iii) $1/N$ expansion[13]: This method is based on angular momentum projected mean field theory, and in principle, allows accurate calculation of band energies and transition rates among low-lying levels. It has been very useful in systematic studies of the sdg model.[14] The main limitation of the method is that beyond the single-phonon bands, band-mixing effects become too complicated to incorporate.

iv) Truncated SU(3) basis[15]: In this scheme, a Hamiltonian consisting of various SU(3) tensor operators is diagonalized in a basis of low-lying SU(3) representations. It has been applied to ^{168}Er with success, however at the expense of relatively large number of parameters (14), and loss of the usual physical picture associated with the quadrupole Hamiltonians via CQF.

v) Truncation to one g boson ($n_g \leq 1$)[16]: The Hamiltonian is diagonalized in the basis space restricted to the $\{(sd)^N, (sd)^{N-1}g\}$ configurations. This is a rather severe approximation and could only work in cases where g boson is weakly coupled to sd bosons, for example in vibrational nuclei.

vi) Truncation to a maximum of n_{gmax} g bosons ($n_g \leq n_{gmax}$)[17]: Here the configuration space is extended to include up to n_{gmax} g bosons which provides more accurate results for deformed nuclei. In practice, n_{gmax} is determined from a study of convergence properties of some key physical quantites, that is diagonalization is carried out for $n_g = 1, 2, 3, ...$ until the desired level of accuracy is obtained. Our results indicate that for $n_{gmax} \sim N/3$, level energies and transition rates converge to better than 1% which is sufficient for purposes of spectroscopy. The resulting basis space is large but still manageable on a super computer. Some results from these calculations will be reported later in the paper.

The second problem is that the number of free parameters in the sdg model (32 in total) are too many for a meaningful analysis of experimental data. Application of the model, therefore, hinges on identification of a simple set of parameters that captures the essential physics. In the sd model, the concept of dynamical symmetries played an important role in this process. For example, the U(5), O(6) and SU(3) dynamical symmetries of the parent group U(6) are associated with the vibrational, γ-unstable and rotational spectra, respectively. In the Casten's triangle, these limiting symmetries form the corners, and any other collective spectra can be described as a point in this triangle. Unfortunately, most of the dynamical symmetries in the sdg model do not have such a simple physical picture. We have already mentioned above that the SU(3) limit is badly broken. In additon, the SU(5), SU(6) and O(15) limits of the parent group U(15) lead to spectra which have the spin sequence (0, 4, 8, ...) in the ground band, and hence have no use in nuclear spectroscopy. Clearly, one needs an alternative guiding principle in finding a simple enough Hamiltonian. For this purpose, we propose study of shapes associated with the sdg model Hamiltonians. The energy surface of an IBM Hamiltonian is intimately linked to the geometrical shape and to the type of spectrum a nucleus has. Thus by studying shapes, one can eliminate terms in the Hamiltonian which are superflous, and more importantly, identify interactions which have effects not contained in the sd model. To this end, a recent study of shapes in the sdg boson model[18] has shown that (i) one-body terms control the spherical to deformed shape transition but have no effect on the γ-degree of freedom, (ii) odd multipole interactions do not play any role on shapes, (iii) quadrupole interaction always leads to an axial shape except when the diagonal terms vanish (q_{ll}=0) which results in a γ-unstable shape, (iv) for certain choices of hexadecapole interaction, one can obtain stable triaxial shapes which are γ-soft. If we take the sd model as a starting point, then the above points suggest that a minimal extension of Eq. (1) should contain the single g boson energy because they are relatively weakly coupled to the sd bosons, and the hexadecapole interaction because it can induce triaxial shapes, a feature which is missing in the standard sd model. Thus, we propose a Hamiltonian of the form

$$H = \epsilon_g n_g + \kappa_1 L \cdot L + \kappa_2 Q \cdot Q + \kappa_4 T_4 \cdot T_4, \tag{3}$$

for the description of deformed nuclei. The various multipole operators are given by

$$n_g = \sum_\mu g_\mu^\dagger g_\mu,$$

$$L_\mu = \sqrt{10}[d^\dagger \tilde{d}]^{(1)}_\mu + \sqrt{60}[g^\dagger \tilde{g}]^{(1)}_\mu,$$

$$Q_\mu = [s^\dagger \tilde{d} + d^\dagger \tilde{s}]^{(2)}_\mu + q_{22}[d^\dagger \tilde{d}]^{(2)}_\mu + q_{24}[d^\dagger \tilde{g} + g^\dagger \tilde{d}]^{(2)}_\mu + q_{44}[g^\dagger \tilde{g}]^{(2)}_\mu,$$

$$T_{4\mu} = [s^\dagger \tilde{g} + g^\dagger \tilde{s}]^{(4)}_\mu + h_{22}[d^\dagger \tilde{d}]^{(4)}_\mu + h_{24}[d^\dagger \tilde{g} + g^\dagger \tilde{d}]^{(4)}_\mu + h_{44}[g^\dagger \tilde{g}]^{(4)}_\mu. \tag{4}$$

This Hamiltonian contains 10 parameters namely, ϵ_g, the single g-boson energy, κ_1, κ_2 and κ_4 which are the strength parameters for the dipole, quadrupole and hexadecapole interactions, and the quadrupole and hexadecapole parameters q_{jl} and h_{jl}. Although it has a substantially lower number of free parameters, a further reduction would be desirable. Phenomenological determination of the hexadecapole parameters h_{jl}, however, poses a problem as the $E4$ data are rather scarce. In order to avoid proliferation of parameters, in the past, we have determined h_{jl} from q_{jl} through a commutation condition which ensures that the quadrupole and the hexadecapole mean fields are coherent.[14] That is, we impose $[\bar{h}, \bar{q}] = 0$ which yields

$$\bar{h}_{22} = \bar{q}_{24}, \;\; \bar{h}_{24} = \bar{q}_{44}, \;\; \bar{h}_{44} = \bar{q}_{24} + (\bar{q}_{44}^2 - \bar{q}_{22}\bar{q}_{44} - 1)/\bar{q}_{24}\,, \tag{5}$$

where $\bar{q}_{jl} = < j0l0|20 > q_{jl}$ and $\bar{h}_{jl} = < j0l0|40 > h_{jl}$.

In the following, we consider the Hamiltonian (3) with a general quadrupole operator but with the hexadecapole parameters still determined from the condition (5). In addition, we will keep using the consistent $E2$ and $E4$ operators

$$T(E2) = e_2 Q, \quad T(E4) = e_4 T_4. \tag{6}$$

in the calculation of electromagnetic transitions, so that, apart from the effective charges e_2 and e_4, no new parameters are introduced.

4. Application to Os and Pt isotopes

The initial applications of the Hamiltonian (3) with the consistent transition operators (6) were concentrated on nuclei with relatively low number of bosons ($N < 12$) so that an exact diagonalization was still possible.

Here we consider the application to the Os-Pt isotopes[19] which, although transitional, may have important lessons for deformed nuclei. The philosophy of the calculations was not to fit each individual nucleus in detail but rather stress the overall trend. In this

Table 2: Parameters used in the sdg model calculations of the Os and Pt isotopes. κ and ϵ are in keV.

Nucleus	N	κ_1	κ_2	κ_4	ϵ_g	q_{22}	q_{24}	q_{44}
^{192}Os	8	15.0	-30.0	-12.0	500	-0.24	0.90	0.50
^{190}Os	9	12.5	-34.0	-13.0	540	-0.26	0.90	0.50
^{188}Os	10	5.5	-40.0	-15.0	630	-0.28	0.90	0.50
^{198}Pt	5	21.0	-50.0	-18.0	1000	0.21	0.80	-1.00
^{196}Pt	6	18.0	-49.0	-18.0	1000	0.20	0.80	-1.00
^{194}Pt	7	16.0	-48.5	-18.0	1000	0.18	0.80	-1.00
^{192}Pt	8	15.0	-47.5	-18.0	1000	0.17	0.80	-1.00

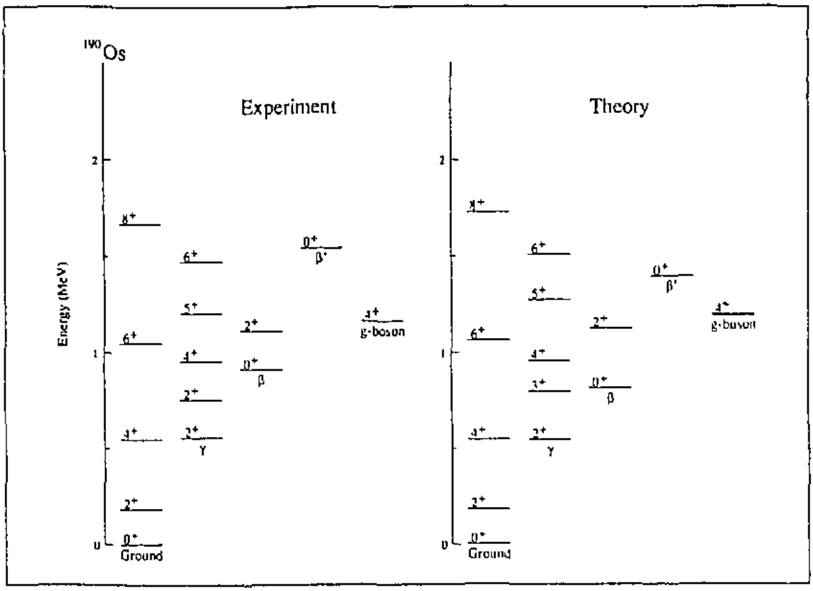

Figure 1: Energy levels of ^{190}Os compared with the sdg model calculations. The model parameters are given in Table 2.

way, a smooth variation of the parameters was possible and their number is kept to a minimum (see Table 2).

As a representative of the sort of agreement obtained for energy spectra, we show in Fig. 1 a comparison of the experimental energy levels in ^{190}Os with the sdg model calculations. Apart from small discrepancies in the β and γ bands (which are due to not having enough triaxiality), the energies are rather well described. Note that we have identified the 4_3^+ state as a g boson state despite the fact that its energy is about twice as large as that of the 2_2^+ state as would be expected from a double-phonon band. As will be discussed below, there are very strong evidence from the $E4$ transitions that this state is in fact mainly hexadecapole vibrational.

In Table 3, we compare the reduced $E2$ matrix elements obtained in the present calculations with the experimental data in the Os isotopes. As can be seen from the table, there is an extensive set of $E2$ data available for the Os isotopes, and the overall agreement is quite good. The low boson number together with accurate $E2$ measurements along the yrast band already allow a test of the boson cut-off at these relatively low spins. The present data show no indication of drop in the $B(E2)$ values predicted in the sd IBM, and one needs the g bosons to describe the yrast E2 transitions. From the perspective of double-γ bands, the most interesting $E2$ transitions are those emanating from the 4_3^+ state. Note that these are fairly well described despite the fact that this state is hexadecapole vibrational in these calculations, and hence has a rather different

Table 3: Comparison of reduced $E2$ matrix elements $|\langle J_f \| T(E2) \| J_i \rangle|$ for the Os isotopes. The effective charges are $e_2 = 0.144$, 0.137, 0.128 eb for ^{192,190,188}Os, respectively. The data are from Refs. [20–23].

	^{192}Os		^{190}Os		^{188}Os	
$J_i \rightarrow J_f$	Calc.	Exp.	Calc.	Exp.	Calc.	Exp.
$2_1^+ \rightarrow 0_1^+$	1.457	1.457 ± 0.018	1.539	1.539 ± 0.013	1.584	1.584 ± 0.022
$4_1^+ \rightarrow 2_1^+$	2.330	$2.115\ (^{+0.038}_{-0.044})$	2.476	2.366 ± 0.042	2.556	2.646 ± 0.057
$6_1^+ \rightarrow 4_1^+$	2.960	$2.93\ (^{+0.10}_{-0.08})$	3.152	2.970 ± 0.515	3.257	3.314 ± 0.109
$8_1^+ \rightarrow 6_1^+$	3.445	$3.58\ (^{+0.17}_{-0.15})$	3.688	3.712 ± 0.105	3.823	3.950 ± 0.329
$0_2^+ \rightarrow 2_1^+$	0.152	$0.066\ (^{+0.012}_{-0.013})$	0.156	0.118 ± 0.011	0.149	0.077 ± 0.029
$0_2^+ \rightarrow 2_2^+$	0.689	$0.449\ (^{+0.014}_{-0.056})$	0.695	0.387 ± 0.032		
$2_2^+ \rightarrow 0_1^+$	0.289	$0.425\ (^{+0.008}_{-0.014})$	0.344	0.456 ± 0.012	0.374	0.483 ± 0.010
$2_2^+ \rightarrow 2_1^+$	1.231	$1.224\ (^{+0.030}_{-0.016})$	1.123	1.095 ± 0.030	0.991	0.866 ± 0.023
$4_2^+ \rightarrow 2_1^+$	0.098	$0.125\ (^{+0.018}_{-0.010})$	0.056	0.202 ± 0.007	0.004	0.283 ± 0.018
$4_2^+ \rightarrow 2_2^+$	1.562	1.637 ± 0.050	1.623	1.871 ± 0.040	1.623	1.775 ± 0.113
$4_2^+ \rightarrow 4_1^+$	1.327	$1.35\ (^{+0.10}_{-0.08})$	1.291	1.439 ± 0.031	1.208	1.098 ± 0.090
$6_2^+ \rightarrow 4_1^+$	0.262	0.067 ± 0.076	0.259	0.194 ± 0.090	0.227	0.127 ± 0.025
$6_2^+ \rightarrow 4_2^+$	2.270	$2.09\ (^{+0.13}_{-0.17})$	2.425	2.598 ± 0.156	2.505	2.456 ± 0.274
$6_2^+ \rightarrow 6_1^+$	1.324	$1.49\ (^{+0.30}_{-0.20})$	1.331	1.766 ± 0.184	1.278	1.442 ± 0.406
$4_3^+ \rightarrow 2_1^+$	0.153	$0.113\ (^{+0.064}_{-0.046})$	0.125	0.052 ± 0.006		
$4_3^+ \rightarrow 2_2^+$	0.694	$0.79\ (^{+0.12}_{-0.14})$	0.781	0.775 ± 0.065	0.853	0.837 ± 0.149
$4_3^+ \rightarrow 3_1^+$	0.836	$1.63\ (^{+0.20}_{-0.36})$	0.906	$1.543\ (^{+0.091}_{-0.340})$		
$4_3^+ \rightarrow 4_2^+$	0.583	1.19 ± 0.22	0.695	1.587 ± 0.113	0.607	1.643 ± 0.246
$2_1^+ \rightarrow 2_1^+$	1.25	1.21 ± 0.18	1.50	1.56 ± 0.04	1.66	1.72 ± 0.19
$2_2^+ \rightarrow 2_2^+$	1.18	0.98 ± 0.10	1.41	1.19 ± 0.53	1.57	1.32 ± 0.33

structure. This is due to the strong coupling of the g bosons to the sd states. If the g bosons were weakly coupled, these transitions would be small and such a successful description would not have been possible. The $E2$ ratio $E2(4_3^+ \rightarrow 2_2^+)/E2(2_2^+ \rightarrow 0_1^+)$ is around 1.7-1.8 which is somewhat smaller than expected from the harmonic limit of 2.25 discussed in section 2. but nevertheless, it is close enough. In addition, the $B(E2)$ branching ratio for $(4_3^+ \rightarrow 2_1^+)/(4_3^+ \rightarrow 2_2^+)$ is small consistent with 4_3^+ being a double-γ state. Thus all the energy $E2$ data appear to suggest that the 4_3^+ state is a double-γ excitation. At this point, it will be useful to discuss the $E4$ data and explain why such an assignment is untenable.

In Table 4, we show all the available $E4$ data for the Os and Pt isotopes together with the sdg model predictions. It is worthwhile to point out from the outset that the (α, α') experiments are sensitive to the details of the reaction mechanism and are therefore less reliable than the (e, e') or (p, p') experiments. Considering that the $E4$ operator is derived from that of $E2$, the overall agreement between the calculations and various measurements is very good. For reference we note that in the sd model, one obtains an order of magnitude smaller value for the $E4(0_1^+ \rightarrow 4_2^+)$ m.e., and the $E4(0_1^+ \rightarrow 4_3^+)$ m.e., which corresponds to the $E4$ excitation of the $\gamma\gamma$ band, is practically zero. Thus there is

Table 4: Comparison of $E4$ matrix elements in the Os and Pt isotopes. The effective $E4$ charges are e_4=0.046 eb^2 for Pt isotopes and e_4=0.034 eb^2 for Os isotopes. 4_h^+ denotes the hexadecapole vibrational (g boson) state which could be the third or fourth 4^+ state depending on the nucleus.

	$E4(0_1^+ \rightarrow 4_1^+)$		$E4(0_1^+ \rightarrow 4_2^+)$		$E4(0_1^+ \rightarrow 4_h^+)$	
Nucleus	Calc.	Exp.	Calc.	Exp.	Calc.	Exp.
^{198}Pt	0.150	0.217(7)[a]	0.129	0.188(7)[a]	0.223	0.138(14)[a]
		0.144(3)[c]		0.124(6)[c]		0.094(7)[c]
		0.176[d]		0.207[d]		-
^{196}Pt	0.175	0.175(7)[b]	0.135	0.157(9)[b]	0.243	0.200(5)[b]
		0.155(16)[e]		0.141(14)[e]		0.210(31)[e]
		0.202[d]		0.141[d]		-
		0.131(7)[f]		-		-
^{194}Pt	0.203	0.195(7)[a]	0.140	0.115(7)[a]	0.260	0.229(7)[a]
		0.191(9)[b]		0.131(6)[b]		0.280(10)[b]
		0.132(3)[c]		0.066(11)[c]		0.159(4)[c]
		0.155[d]		0.118[d]		-
		0.175(16)[f]		0.039(3)[f]		-
^{192}Pt	0.230	0.202[g]	0.146	0.20/0.34[g]	0.262	-
^{192}Os	0.196	0.196(11)[h]	0.144	0.116(29)[h]	0.170	0.108(27)[h]
		0.220(10)[f]		-		0.071/0.058[i]
^{190}Os	0.206	0.212(12)[f]	0.163	-	0.163	0.078/0.067[i]
^{188}Os	0.215	0.217(11)[f]	0.181	-	0.159	0.109/0.094[i]

[a] (p,p') experiment[32], [b] (p,p') experiment[31], [c] (p,p') experiment[30],
[d] (p,p') experiment[26], [e] (e,e') experiment[27], [f] (e,e') experiment[28],
[g] (α,α') experiment[25], [h] (p,p') experiment[29], [i] (α,α') experiment[24].

no chance of explaining the $E4$ data in the Os-Pt isotopes unless g bosons are included, and the 4_3^+ state cannot be a $\gamma\gamma$ excitation. As stressed at the beginning of this section, we have not fitted each nucleus in detail, and therefore there are discrepancies which could be improved by fine tuning the parameters. For example, the $E2(4_3^+ \rightarrow 4_2^+)$ and $E2(4_3^+ \rightarrow 3_1^+)$ transitions are underpredicted whereas $E4(0_1^+ \rightarrow 4_3^+)$ are a bit too strong. This points out to a stronger mixing between the 4_3^+ and $4_{\gamma\gamma}^+$ states than envisaged in the calculations, and can be easily accomplished by adjusting the κ_4 strength.

5. Application to Deformed Nuclei

We have recently implemented the SDGBOSON code on the Fujitsu supercomputer and started applying the sdg model to deformed nuclei. In this section, we present some preliminary results that were obtained using the Hamiltonian and transition operators described in section 3. In particular, we are interested in the effect of the hexadecapole interaction on the spectra, and whether it can lead to variations from the harmonic limit for vibrational states. In Table 5, we show various energy ratios and $E2$ transitions for both the $\gamma\gamma$ and the hexadecapole vibrational 4^+ states. The quadrupole parameters (q_{22}, q_{24}, q_{44}) are scaled from their SU(3) values with the factors (1/2, 1, 1/2), and the hexadecapole parameters are determined from the coherence condition (5). The other parameters are the same as in Table 1. The 4_h^+ state is seen to be sensitive to variations in κ_4 as would be expected. The γ and $\gamma\gamma$ bands, on the other hand, show almost no dependence on κ_4. In fact, the energy and $E2$ ratios are almost identical to the sd model results discussed in section 2. This implies that the coherent choice for the hexadecapole parameters reinforces the underlying harmonicity of bands and is not useful for generating anharmonic effects at all. Clearly, one needs a very different hexadecapole operator in order to describe anharmonicities. A clue is offered by the recent geometrical model calculations which have suggested a link between anharmonicity and triaxiality. We are currently exploring this possibility by employing hexadecapole interactions which generate triaxiality.[18] This program will hopefully lead to a better understanding of anharmonic effects in vibrational excitations of deformed nuclei.

Table 5: Effect of the hexadecapole interaction on γ, $\gamma\gamma$ and $K = 4_h^+$ band properties in the sdg IBM. Parameters are explained in the text.

κ_4/κ_2	-0.4	-0.2	0.0	0.2	0.4
$E_{\gamma\gamma}/E_\gamma$	1.88	1.89	1.90	1.91	1.92
E_{4_h}/E_γ	2.32	2.26	2.19	2.10	1.98
$E2(2_\gamma^+ \to 0_g^+)$	2.24	2.24	2.24	2.24	2.25
$E2(2_\gamma^+ \to 2_g^+)$	2.89	2.92	2.94	2.98	3.02
$E2(4_{\gamma\gamma}^+ \to 2_g^+)$	0.01	0.01	0.01	0.02	0.08
$E2(4_{\gamma\gamma}^+ \to 2_\gamma^+)$	5.14	5.11	5.07	5.04	4.98
$E2(4_h^+ \to 2_g^+)$	2.14	2.51	2.41	1.96	1.26
$E2(4_h^+ \to 2_\gamma^+)$	0.68	0.32	0.45	0.66	0.89

6. Conclusions

We have discussed in this paper some features of the sdg boson model which are relevant for the description of deformed nuclei. On the technical side, we have shown that the $1/N$ expansion method coupled with numerical diagonalization in a truncated basis offer the most promising alternatives for the sdg model calculations. Application of the sdg model to the Os-Pt isotopes have generated some cautionary messages for other nuclei where double-phonon bands are currently being pursued. Namely, hexadecapole vibrational $K = 4^+$ bands could conspire to be a $\gamma\gamma$ band by mocking up all the signatures attributed to $\gamma\gamma$ bands! The only sure way to avoid confusion is to look at the $E4$ transitions. We therefore emphasize the importance of $E4$ measurements in pinning down the hexadecapole features, and strongly suggest further (e, e') and/or (p, p') experiments in the rare-earth region.

Our preliminary results in search of anharmonic effects in vibrational bands suggest that the coherent choice for the hexadecapole operator, which led to a successful description of the $E2$ and $E4$ properties in the Os-Pt region, is not useful for this purpose. Following the hints from geometrical model, we are currently experimenting with forms which generate stable triaxial shapes, and hope to report on these calculations in the next conference.

7. Acknowledgements

This research is supported by the Australian Research Council and by a grant from the supercomputer facility at the Australian National University. I thank Vi-Sieu Lac and Siu-Cheung Li for performing some of the numerical calculations presented in the paper.

8. References

1. A. Bohr and B.M. Mottelson, *Nuclear Structure*, Vol. 2 (Benjamin, Reading, 1975).
2. H.G. Borner *et al.*, *Phys. Rev. Lett.* 66 (1991) 691.
3. M. Oshima *et al.*, *Nucl. Phys.* **A557** (1993) 635.
4. X. Wu *et al.*, *Phys. Lett.* **B316** (1993) 235; *Phys. Rev.* C49 (1994) 1837.
5. W. Korten *et al.*, *Phys. Lett.* **B317** (1993) 19.
6. G. Siems *et al.*, *Phys. Lett.* B320 (1994) 1.
7. F. Iachello and A. Arima, *The Interacting Boson Model* (Cambridge University Press, Cambridge, 1987).
8. R.F. Casten and D.D. Warner, *Rev. Mod. Phys.* 60 (1988) 389.
9. M.R. Schmorak, *NDS* **63** (1991) 139.
10. I. Morrison, *Computer code SDGBOSON* (University of Melbourne, 1986); S-C. Li, *SDGBOSON for the supercomputer* (Australian National University, 1993).
11. H.C. Wu and X.Q. Zhou, *Nucl. Phys.* A417 (1984) 67.
12. S. Pittel *et al.*, *Phys. Lett.* B144 (1984) 145.
13. S. Kuyucak and I. Morrison, *Ann. Phys.* (N.Y.) **181** (1988) 79; **195** (1989) 126.
14. S. Kuyucak, I. Morrison, and T. Sebe, *Phys. Rev.* C43 (1991) 1187.
15. N. Yoshinaga, Y. Akiyama, and A. Arima, *Phys. Rev.* **C38** (1988) 419.
16. P. Van Isacker *et al.*, *Nucl. Phys.* **A380** (1982) 383.
17. S. Kuyucak and S-C. Li, to be published.
18. S. Kuyucak and I. Morrison, *Phys. Lett.* **B255** (1991) 305.
19. V-S. Lac and S. Kuyucak, *Nucl. Phys.* **A539** (1992) 418.
20. P. Raghavan, *Atomic Data and Nuclear Data Tables* 42 (1989) 189.
21. C.Y. Wu, Ph. D. thesis, (University of Rochester, 1983).
22. B. Singh, *Nuclear Data Sheets* 61 (1990) 243.
23. B. Singh, *Nuclear Data Sheets* 59 (1990) 133.
24. D.G. Burke, M.A.M. Shahabudin and R.N. Boyd, *Phys. Lett.* B78 (1978) 48.
25. F. Todd Baker, et al., *Phys. Rev.* **C17** (1978) 1559.
26. P.T. Deason, et al., *Phys. Rev.* C23 (1981) 1414.
27. W.T.A. Borghols, et al., *Phys. Lett.* **B152** (1985) 330.
28. W. Boeglin, et al., *Nucl. Phys.* **A477** (1988) 399.
29. F. Todd Baker, et al., *Nucl. Phys.* **A501** (1989) 546.
30. A. Sethi, et al., *Nucl. Phys.* **A518** (1990) 536.
31. A. Sethi, et al., *Phys. Rev.* C44 (1991) 700.
32. A. Sethi, *Private communication* (1991).

Vibrational states in doubly even well-deformed nuclei

V.G. Soloviev, A.V. Sushkov and N.Yu. Shirikova

Bogolubov Laboratory of Theoretical Physics,
Joint Institute for Nuclear Research
141980 Dubna, Russia

Abstract

The energies and wave functions of non-rotational states below 2.3 MeV in doubly even well-deformed nuclei of the rare earth region have been calculated within the Quasiparticle-Phonon Nuclear Model. General properties of vibrational states are formulated. The wave function of excited states below 2.3 MeV is dominated by the one-phonon term. The contributions of the two-phonon configurations to the wave functions of the $K^{\pi} \neq 0^{+}$ and 4^{+} states are smaller than 10%. The $K^{\pi} = 4_{1}^{+}$ state in ^{168}Er contains the double gamma vibrational term equal to 30%. The existence of the double gamma vibrational state with $K^{\pi} = 4^{+}$ at (2.0-2.2) MeV in ^{166}Er is predicted. The $K_{\nu}^{\pi} = 4_{1}^{+}$ and 4_{2}^{+} states in ^{156,158,160}Gd and ^{162}Dy are hexadecapole ones. High intensities of the one-nucleon transfer reactions are explained by the relevant large two-quasiparticle components of the one-phonon terms of the wave functions. The calculated B(E1;$0^{+}0_{g.s.} \rightarrow 1^{-}K_{\nu}$)values for the $K^{\pi} = 0^{-}$ and 1^{-} states are 3-5 times larger than the experimental ones. The fragmentation of the one-phonon $K^{\pi} = 0^{-}$ and 1^{-} states in the energy range 2.3-4.0 MeV is not so strong. The concentration of the E1 strength in $K^{\pi} = 0^{-}$ states at energies 2.6-3.5 MeV in ^{168}Er and 3.6-3.9 MeV in ^{164}Dy and in $K^{\pi} = 1^{-}$ states at energies 3.2-3.4 MeV in ^{160}Gd is predicted.

1. Introduction

The low-lying non-rotational states in doubly even deformed nuclei have been studied experimentally and theoretically. The experimental data on the excited states above the lowest two-quasiparticle and first quadrupole and octupole vibrational states are still fragmentary. These states have a more complex structure and many branches of decay to low-lying states. Their experimental and theoretical investigation is very important for understanding nuclear structure. The vibrational states and gamma-ray transition rates in well-deformed doubly even nuclei have been calculated within the Quasiparticle-Phonon Nuclear Model (QPNM) [1-7]. The QPNM is used for a microscopic description of the low-spin, small-amplitude vibrational states in spherical nuclei not far from closed shells and well-deformed nuclei. The QPNM calculations were performed in nuclei with small ground state correlations. The ground state correlations increase with the collectivity of the first one-phonon states. A particle-particle interaction reduces the ground state correlation. Therefore, the energies and wave functions of many well-deformed nuclei have been calculated in the QPNM.

The energies and wave functions of non-rotational states in ^{150}Nd [8], ^{156,158,160}Gd [10,12], ^{162,164}Dy [6,9,13], ^{166,168}Er [6,7,11] and other nuclei have been calculated within the QPNM. The results of calculation were compared with the relevant experimental data. In this paper, we sum up our investigation of the doubly even well-deformed nuclei in the rare earth region.

2. Description of non-rotational states in the QPNM

The QPNM Hamiltonian contains the average field of a neutron and a proton systems in a form of the axial-symmetric Woods-Saxon potential, monopole pairing, isoscalar and isovector particle-hole (ph) and particle-particle (pp) multipole interaction between quasiparticles. The procedure of calculation is the following. A canonical Bogolubov transformation is used in order to replace the particle operators by the quasiparticle ones. Then, the phonon operators $Q_{\lambda\mu i\sigma}$ are introduced and the RPA equations are solved. The phonon space is used as a QPNM basis. The RPA phonons for the $K^\pi = 0^-$ and 1^- states have been calculated in [5] with ph and pp isoscalar and isovector octupole and ph isovector dipole interactions. The RPA equation for the $K^\pi = 0^+$ states is given in [3] and for $K^\pi \neq 0^+$, 0^- and 1^- states in ref. [2,4].

The QPNM wave functions consist of one- and two- phonon terms, namely,

$$\Psi_\nu(K_0^{\pi_0}\sigma_0) = \Big\{\sum_{i_0} R^\nu_{i_0} Q^+_{\lambda_0\mu_0 i_0\sigma_0} + \sum_{\substack{\lambda_1\mu_1 i_1\sigma_1\\ \lambda_2\mu_2 i_2\sigma_2}} \frac{(1+\delta_{\lambda_1\mu_1 i_1,\lambda_2\mu_2 i_2})^{1/2}\delta_{\sigma_1\mu_1+\sigma_2\mu_2,\sigma_0 K_0}}{2[1+\delta_{K_0,0}(1-\delta_{\mu_1,0})]^{1/2}} \times P^\nu_{\lambda_1\mu_1 i_1,\lambda_2\mu_2 i_2} Q^+_{\lambda_1\mu_1 i_1\sigma_1} Q^+_{\lambda_2\mu_2 i_2\sigma_2}\Big\}\Psi_0, \tag{1}$$

where $\mu_0 = K_0$, $\sigma = \pm 1$. The secular equation for energies E_ν has the form

$$det \parallel (\omega_{\lambda_0\mu_0 i_0} - E_\nu)\delta_{i_0,i'_0} - \sum_{(\lambda_1\mu_1 i_1)\geq(\lambda_2\mu_2 i_2)} \frac{1+\mathcal{K}^{K_0}(\lambda_1\mu_1 i_1, \lambda_2\mu_2 i_2)}{(1+\delta_{\lambda_1\mu_1 i_1,\lambda_2\mu_2 i_2})(1+\delta_{K_0,0}(1-\delta_{\mu_1,0}))} \times \frac{U^{\lambda_0\mu_0 i_0}_{\lambda_1\mu_1 i_1\lambda_2\mu_2 i_2} U^{\lambda_0\mu_0 i'_0}_{\lambda_1\mu_1 i_1\lambda_2\mu_2 i_2}}{\omega_{\lambda_1\mu_1 i_1} + \omega_{\lambda_2\mu_2 i_2} + \Delta\omega(\lambda_1\mu_1 i_1\lambda_2\mu_2 i_2) + \Delta(\lambda_1\mu_1 i_1\lambda_2\mu_2 i_2) - E_\nu} \parallel = 0. \tag{2}$$

Here $\omega_{\lambda\mu i}$ is the RPA energy, the function $\mathcal{K}^{K_0}(\lambda_1\mu_1 i_1, \lambda_2, \mu_2 i_2)$ is responsible for the effect of the Pauli principle in two-phonon terms in (1), the function $U^{\lambda_0\mu_0 i_0}_{\lambda_1\mu_1 i_1,\lambda_2\mu_2 i_2}$ describes the coupling of one- and two-phonon terms in (1); $\Delta\omega(\lambda_1\mu_1 i_1,\ \lambda_2\mu_2 i_2)$ is the shift of the two-phonon pole due to the Pauli principle, $\Delta(\lambda_1\mu_1 i_1, \lambda_2\mu_2 i_2)$ represents the effect of three-phonon terms added to the wave function (1) and approximately equals $-0.2\Delta\omega(\lambda_1\mu_1 i_1, \lambda_2\mu_2 i_2)$.

The doubly even deformed nuclei were calculated with the parameters of the Woods-Saxon potential fixed earlier. The isoscalar constants $\kappa_0^{\lambda\mu}$ of ph interactions are fixed so as to reproduce experimental energies of the first $K^\pi_{\nu=1}$ nonrotational states described by (1). The calculations were performed with the isovector constant $\kappa_1^{\lambda\mu} = -1.5\kappa_0^{\lambda\mu}$ for ph interactions and the constant $G^{\lambda\mu} = \kappa_0^{\lambda\mu}$ for pp interactions. The monopole pairing constants were fixed by pairing energies at $G^{20} = \kappa_0^{20}$. The radial dependence of the multipole interactions has the form $dV(r)/dr$, where V(r) is the central part of the Woods-Saxon potential. The phonon basis consists of ten (i_0 = 1,2,....10) phonons of each multipolarity: quadrupole $\lambda\mu = 20, 21, 22$, octupole $\lambda\mu = 30, 31, 32, 33$, hexadecapole $\lambda\mu = 43, 44$ and $\lambda\mu = 54, 55$.

3. Low-lying one-phonon states. Mixing and fragmentation of one-phonon states

The first three-five states having the same K^π below 2 MeV are almost one-phonon states. The contribution of the two-phonon components to the normalization of the wave functions is less than 10%. The four 0^+ one-phonon states in ^{158}Gd and ^{166,168}Er have been observed. The five $K^\pi = 2^+$ states have been studied in the one-nucleon transfer reaction [14] in ^{168}Er. The four collective one-phonon $K^\pi = 3^-$ states in ^{168}Er have been excited by using of inelastic scattering [15]. The three $K^\pi = 2^-$ states have been observed in ^{162}Dy and so on. The wave functions of these states have different two-quasiparticle components and were well described in the QPNM.

The quasiparticle-phonon interaction is responsible for the fragmentation of one-phonon states and for their mixing. Two closely-spaced one-phonon states having the same K^π state are mixed. For example, the wave function of the second $K^\pi_\nu = 1^+_2$ state with excitation energy of 1.93 MeV in ^{158}Gd has 85% of the second, 212, and 13% of the third 213 one-phonon components. Two large one-phonon components of the wave function of the excited states can be observed experimentally in two relevant one-nucleon transfer reactions and in the gamma-ray decay to low-lying states.

An onset of the fragmentation of the one-phonon states takes place at an energy above 2.5 MeV. In the energy range from 2.5 to 4.0 MeV the fragmentation of one-phonon states is not so strong. The fragmentation of strongly collective one-phonon states is larger than the fragmentation of weakly collective states. The one-phonon states with large K quantum number are weakly fragmented compared with ones with small K. There are levels below 4 MeV the wave function of which has a large one-phonon component. Therefore, there are states with large E1 or E2 or E3 or E4 strength and states with large M1 or M2 or M3 strength. These states can be excited in the inelastic scattering, in (γ, γ'), one-nucleon transfer and other reactions. For example, the E2, E3 and E4 strength distribution in ^{150}Nd up to excitation energies of 3–4 MeV have been investigated in proton- and deuteron-scattering experiments [8]. The experimental strength distribution has been compared with the predictions of the IBM and of the QPNM. The experimental strength distributions are reasonably well described in both the models. The quasiparticle-phonon interaction leads to a strong fragmentation of most of the one-phonon states in well-deformed nuclei with energy larger than 4 MeV.

4. E1 transition rates

The $K^\pi = 0^-$ and 1^- states in deformed nuclei are usually treated as collective octupole states. The calculated B(E1) values for the excitation of $I^\pi K_\nu = 1^-0_1$ and 1^-1_1 states are much larger than the experimental values. The E1 transition rates from the ground state to the $I^\pi K = 1^-0$ and 1^-1 states in ^{172}Yb have been calculated [16] within the QPNM. It has been shown that the inclusion of the isovector particle-hole (ph) electric dipole interaction (together with the isoscalar and isovector ph octupole interaction) decreases the E1 strength by more than an order of magnitude, thus bringing it close to experimental data. The description of the octupole states and B(E1) values without particle-particle (pp) interaction is not good enough. Therefore, in [5] the mathematical apparatus has been formulated in which the ph and pp octupole and ph dipole interactions are simultaneously taken into account in the RPA.

The origin of E1 strength in the low-energy region in deformed nuclei has been investigated in [5]. It is known that there are no one-phonon 1^- states below the particle threshold in spherical nuclei. Quadrupole deformation is responsible for the splitting of the subshells of a spherical basis into twice-degenerate single-particle states. Due to this splitting, part of the E1 strength is shifted to low-lying states. An octupole isoscalar interaction between quasiparticles leads to the formation of collective octupole states. Due to the octupole interaction, the summed E1 strength for the transition to $K^\pi = 0^-$ and 1^- states in the (0–4) MeV energy region increases by two orders of magnitude. An isovector dipole ph interaction shifts the largest part of E1 strength from the low-lying states to the region of the isovector GDR.

Table 1. The experimental and calculated energies and B(E1) for transition from the ground states to the $I^\pi K = 1^- K$ states with $K = 0$ and 1.

		Experiment		Calculation in the QPNM				
						Effective charge		
					$e^1_{eff}(p)$ $\frac{N}{A}$	$e^1_{eff}(n)$ $-\frac{Z}{A}$	$e^1_{eff}(p)$ $0.3\frac{N}{A}$	$e^1_{eff}(n)$ $-0.3\frac{Z}{A}$
Nuclei	K^π	E_ν	B(E1)↑	E_ν	B(E1)↑	$\frac{B(E1)_{calc}}{B(E1)_{exp}}$	B(E1)↑	$\frac{B(E1)_{calc}}{B(E1)_{exp}}$
		MeV	$e^2fm^2 10^{-3}$	MeV	$e^2fm^2 10^{-3}$		$e^2fm^2 10^{-3}$	
^{168}Er	0^-_1	1.786	27.2 ± 1.6	1.8	97	3.6	29	1.07
	1^-_1	1.358	8	1.3	28	3.5	8.4	1.05
	1^-_2	1.936	0.7	1.9	3	4.3	0.9	1.29
^{166}Er	0^-_1	1.662	26 ± 1.6	1.8	90	3.5	27	1.04
	0^-	2.2	8	2.2	20	2.5	6	0.75
	0^-	2.7	2	2.6	36	18	11	5.5
	0^-	2.8	12	2.9	24	2	7	0.6
	1^-_1	1.830	3	1.8	20	7	6	2
^{164}Dy	0^-_1	1.675	22.0 ± 3.0	1.7	72	3.3	22	1.0
	0^-_2	2.330	5.9 ± 0.9	2.2	20	3.4	6	1.02
	0^-_3	2.670	4.1 ± 0.7	2.6	41	10	12	2.93
^{162}Dy	0^-_1	1.276	14.7 ± 2.5	1.3	73	5.0	22	1.5
	0^-_2	1.986	11.2 ± 1.4	2.0	56	5.0	17	1.5
	0^-_3	2.520	5.0 ± 0.4	2.4	30	6.0	9	1.8
^{160}Dy	0^-_1	1.489	21.7 ± 2.2	1.5	156	7.2	47	2.16
	0^-	2.876	2.5					
^{160}Gd	0^-_1	1.224	19.1 ± 5.3	1.3	75	3.9	22	1.17
	0^-_2	1.967	3.7 ± 0.5	1.9	33	8.9	10	2.67
	$\left.\begin{matrix}0^-\\1^-\end{matrix}\right\}$	2.471	3.1 ± 0.5	2.55	16	5.2	4.8	1.55
		$R_{exp} = 1.56 \pm 0.21$		$R_{calc} = 1.58$				
	1^-	3.415	3.9 ± 0.5	3.23	17	4.4	5	1.30
	1^-	3.460	3.4 ± 0.5	3.33	6	1.8	1.8	0.5
^{158}Gd	0^-_1	1.263	19.9 ± 4.7	1.3	60	3.0	18	0.9
	1^-_1	0.977	2.2 ± 0.6	1.0	45	20	14	6.1
^{156}Gd	0^-_1	1.366	16.0 ± 5.9	1.4	150	9.4	45	2.8
	1^-_1	1.242	10.0 ± 4.0	1.1	90	9.0	27	2.7

The calculations of the energies, wave function and B(E1) values within the QPNM have been performed in [12] with effective charge $e^1_{eff}(p) = \frac{N}{A}$, $e^1_{eff}(n) = -\frac{Z}{A}$ and $e^1_{eff}(p) = 0.3\frac{N}{A}$, $e^1_{eff}(n) = -0.3\frac{Z}{A}$. The operators of phonons with $K^\pi = 0^-$ and 1^- are calculated in the RPA taken the ph and pp isoscalar and isovector octupole and ph isovector dipole interaction into account simultaneously. These phonons are used in the QPNM calculations with the wave function (1). The results of calculations of the energies and B(E1) values for the excitation of 1^-K states with $K = 0$ and 1 and experimental data [17–19] are given in Table 1.

On the basis of the investigation of the E1 transition rates in [5,12], it is possible to make the following statements:

1) The B(E1) values for transition from the ground state to the $I^\pi = 1^-$ states with $K = 0$ and 1 are mainly determined by the ph isoscalar octupole and isovector dipole interactions between quasiparticles. These B(E1) values more strongly depend on the radial function of the interactions between quasiparticles compared with energies of the levels and B(E3) values.

2) The energies and wave functions of the $K^\pi = 0^-$ and 1^- states and E1 transition rates from the ground state to the excited states 1^-K_ν with $K = 0$ and 1 have been calculated with the constant of the isovector dipole interaction $\kappa_1^{1K} = -1.5\kappa_0^{3K}$; the GDR was correctly described with this constant.

3) The calculated B(E1) values for the excitation of the first $K^\pi_\nu = 0^-_1$ states with the effective charge $e^1_{eff}(p) = \frac{N}{A}$, $e^1_{eff}(n) = -\frac{Z}{A}$ are 3–5 times as large as experimental ones. The B(E1) values calculated with the renormalized charge are in better agreement with the experimental data. But this improvement is very artificial.

4) The total E1 strength for the excitation of the $K^\pi = 0^-$ states is 3–4 times as large as for excitation of the $K^\pi = 1^-$ states in the energy region below 3 MeV.

5) A strong correlation takes place between B(E1) and B(E3) values for transitions to the same band with energy below 4 MeV. No correlation was observed between B(E1) and B(M2) values.

6) One phonon states below 2.5 MeV are slightly fragmented due to quasiparticle-phonon interactions. The wave function of those states has a dominant one-phonon component. The B(E1) values for the excitation of several 1^- states are relatively large and they can be observed experimentally.

7) The influence of the two-phonon terms of the wave functions of the initial states with $K^\pi = 1^-$ on the E1 transition rates to the ground state is very small.

8) The fragmentation of the one-phonon states with $K^\pi = 0^-$ and 1^- in the energy range 2.5–4.0 MeV is not so strong. Therefore, there are states with a relatively large E1 strength. We predict the concentration of the E1 strength in $K^\pi = 0^-$ states at energies 2.6–3.5 MeV in ^{168}Er, 3.6–3.9 MeV in ^{164}Dy and in $K^\pi = 1^-$ states at energies 3.2–3.4 MeV in ^{160}Gd.

5. Contribution of the two-phonon configurations to the wave function of low-lying states

A state is determined to be a two-phonon state if the contribution of two-phonon configuration to the wave function normalization exceeds 50%. Energy centroids of two-phonon collective states in deformed nuclei are calculated in [20]. It has been shown that due to a shift of two-phonon poles, the density of levels in the energy region of the first two-phonon poles is large. Therefore, the two-phonon states should be strongly fragmented. Based on the QPNM calculation of the energy centroids of two-phonon states, it has been concluded in ref. [20] that two-phonon states consisting of two collective phonons can't exist in well-deformed nuclei. This prediction is true in the most cases. In our previous calculations [20,21], the shift $\Delta\omega(\lambda_1\mu_1 i_1, \lambda_2\mu_2 i_2)$ at $\lambda_1 = \lambda_2$, $\mu_1 = \mu_2$ and $i_1 = i_2$ for the $K^\pi = 4^+$ states was twice as large as it should have been. Therefore, the contribution of the two-phonon {221,221} components to the normalization of the wave functions of $K^\pi = 4^+$ was very small. The contribution of the hexadecapole 441 and 442 phonons and double-gamma vibrational {221,221} components to the normalization of the wave function of the 4^+ states and B(E2;$4^+4_\nu \to 2^+2_1$) values are given in Table 2.

Table 2. Energies and structure of the $K^\pi = 4^+$ states and $B(E2; 4^+4_\nu \to 2^+2_1)$ values.

Nuclei	K^π_ν	exp E_ν MeV	E_ν MeV	Calculation in QPNM Structure	$B(E2;4^+4_\nu \to 2^+2_1)$ e^2fm^4 exp[ref.]	calc.
^{168}Er	4^+_1	2.055	2.0	441 60% {221,221} 30%	280 ± 140 [22]	175
					315 [24]	
					389 ± 89 [23]	
^{166}Er	4^+_1	1.978	1.96	441 76% {221,221} 21%	-	115
	4^+_2	-	2.05	442 23% {221,221} 73%	-	500
^{162}Dy	4^+_1	1.536	1.5	441 97% {221,221} 2,3%	17	23
^{160}Gd	4^+_1	1.070	1.2	441 98% {221,221} 1%	-	14
	4^+_2	(1.531)	1.5	442 99%	-	5
^{158}Gd	4^+_1	1.380	1.4	441 96% {221,221} 2%	-	50
	4^+_2	1.920	1.9	442 95% {221,221} 2%	-	20
^{156}Gd	4^+_1	1.511	1.5	441 94% {221,221} 5%	-	64
	4^+_2	1.861	1.9	442 90% {221,221} 4%	-	24

The nuclei ^{166,168}Er and ^{164}Dy are the most favourable for the observation of the $K^\pi = 4^+$ double-gamma vibrational states in the energy range (2.0–2.3) MeV. Much attention has been paid to ^{168}Er. Experimental investigations [22–24] have established a large double gamma vibrational component in the first $K^\pi_\nu = 4^+_1$ state in ^{168}Er. According to the multiphonon method [25] and *sdg* IBM [26], the first $K^\pi_\nu = 4^+_1$ state in ^{168}Er should be a two-phonon state. According to the QPNM calculation [7], the contribution of hexadecapole, {441}, one-phonon and double-gamma vibrational {221,221} components to the normalization of the wave function of the 4^+_1 state in ^{168}Er equals 60% and 30%, respectively. The calculated energies of the $K^\pi_\nu = 2^+_1, 4^+_1$ and 4^-_1 states and the B(E2;$2^+_1 \to 0^+_{g.s.}$), B(E4;$4^+_1 \to 0^+_{g.s.}$) and B(E1;$4^+_1 \to 4^-_1$) values closely agree with experimental data analyses in [27].

According to the calculation in [11], the double-gamma vibrational strength with $K^\pi_\nu = 4^+$ in ^{166}Er is concentrated on one or two levels at the energy 2.0–2.2 MeV. When the energy and B(E2;$0^+0_{g.s.} \to 2^+2_1$) value of the $K^\pi_\nu = 2^+_1$ state are correctly described, the second $K^\pi_\nu = 4^+_2$ state at energy 2.05 MeV should be the double-gamma vibrational state. The existence of the $K^\pi = 4^+$ double-gamma vibrational state in ^{166}Er is due to a very small density of the

$K^\pi = 4^+$ states near the $\{221,221\}$ pole and a very small value for the function $U^{441}_{221,221}$, which is responsible for a coupling between one- and two-phonon terms in the wave function (1).

A situation with the $K^\pi = 4^+$ double gamma vibrational state in ^{164}Dy is not yet clear. According to the calculation in the QPNM, the largest part of the $4^+\{221,221\}$ strength is concentrated on one or two levels in the energy range (2.15–2.30) MeV. The results of calculations depend on the constants κ_0^{22} and κ_0^{44}. According to the calculation in ref. [10,12], the $K^\pi_\nu = 4^+_1$ and 4^+_2 states in ^{156,158,160}Gd are hexadecapole ones. The admixture of the double-gamma vibrational components in their wave functions is less than 5%. The energy of the largest part of the $4^+\{221,221\}$ strength is higher than 2.4 MeV.

Difficulty of identification of two-phonon octupole states in spherical nuclei is that deexcitation of the two-phonon states through unspecific low-multipolarity radiation can dominate so that specific E3 transition can't be observed. There is an enhanced E1 transition in deformed nuclei from the two-phonon $\{301,301\}$ or $\{311,311\}$ state to the relevant one-phonon state. The enhanced E1 transition takes place between excited states if the wave function of the initial state has a large two-phonon term consisting of the octupole phonon with $K = 0$ or 1 and another phonon corresponding to the one-phonon final states. The E1 and E3 transition rates from several 1^-_ν states with $I = 1$ and 3 to gamma-vibrational state in ^{160}Gd are demonstrated in Table 3.

Table 3. E1 and E3 transition rates from the $K^\pi = 1^-$ states to the gamma-vibrational state with energy of 0.988 MeV in ^{160}Gd

Initial state $I^\pi K_\nu$	E_ν MeV	Eλ	B(Eλ) $\downarrow$, e^2fm$^{2\lambda}$	Branching ratio $\frac{W(E1;1^-1_\nu \to 2^+2_1)}{W(E3;3^-1_\nu \to 2^+2_1)}$	Structure			
1^-1_1	1.524	E1	$2.0 \cdot 10^{-5}$	$3 \cdot 10^{10}$	311	99%		
3^-1_1	1.590	E3	16					
1^-1_2	1.997	E1	$2.7 \cdot 10^{-5}$	$7 \cdot 10^{7}$	312	98%		
3^-1_2	2.067	E3	0.65					
1^-1_5	2.567	E1	$4.8 \cdot 10^{-6}$	$6 \cdot 10^{6}$	315	95%	$\{441,551\}$	4%
3^-1_5	2.637	E3	0.27					
1^-1_6	2.900	E1	$6.8 \cdot 10^{-6}$	$4 \cdot 10^{5}$	315	3%	$\{441,551\}$	90%
3^-1_6	2.970	E3	3.1		316	3%	$\{221,311\}$	2%
1^-1_7	2.950	E1	$9.1 \cdot 10^{-4}$	$5 \cdot 10^{5}$	316	33%	$\{221,311\}$	30%
3^-1_7	3.020	E3	240		317	20%	$\{441,551\}$	5%
1^-1_{11}	3.415	E1	$4.8 \cdot 10^{-4}$	$2 \cdot 10^{6}$	317	27%	$\{221,311\}$	22%
3^-1_{11}	3.485	E3	52		318	21%	$\{221,301\}$	8%
1^-1_{14}	3.460	E1	$1.5 \cdot 10^{-3}$	$7 \cdot 10^{3}$	318	22%	$\{221,312\}$	20%
3^-1_{14}	3.530	E3	$1.3 \cdot 10^{3}$		3111	10%	$\{221,313\}$	8%
							$\{221,311\}$	4%

The intensities of the E1 transitions are 10^3–10^{10} times larger than the intensities of the E3 transitions. It means that these states can be indentified through the fast E1 transitions. The B(E1) values for transitions between one-phonon configurations of the wave functions of the initial and final states are small. The B(E1) values for transitions from the $K^\pi_\nu = 1^-_7$, 1^-_{11} and 1^-_{14} states to the 2^+_1 state are larger than those from other states due to a large contribution of the $\{221,311\}$ configuration to their wave functions.

The two-phonon states consisting of two collective phonons are, as a rule, fragmented strongly. The two phonon states consisting of the one collective phonon and another weakly collective phonon are not fragmented so strongly. The wave functions of many states in well-deformed nuclei in the energy range (2–4) MeV have rather large two-phonon components.

Information on the large and small components of the wave function of the excited states above 2 MeV in doubly even well-deformed nuclei is very important for the investigation of the nuclear structure. It is reasonable to expect that the experimental study of the nuclear structure will be continued in the (n,γ) reaction as well as at new generation of accelerators and detectors.

References

1. V.G. Soloviev, Sov. J.Part.Nucl.,**9** (1978) 343.
2. V.G. Soloviev, Theory of Atomic Nuclei: Quasiparticles and Phonons (Institute of Physics, Bristol and Philadelphia, 1992).
3. V.G. Soloviev, Z.Phys., **A334** (1989) 143.
4. V.G. Soloviev, A.V. Sushkov and N.Yu. Shirikova, Part.Nucl., **25** (1994) 377.
5. V.G. Soloviev and A.V. Sushkov, Yad.Fiz., **57** (1994) N 8.
6. V.G. Soloviev and N.Yu. Shirikova, Nucl.Phys., **A542** (1992) 410.
7. V.G. Soloviev, A.V. Sushkov and N.Yu. Shirikova, J.Phys. G **20** (1994) 113.
8. M. Pignanelli et al., Nucl.Phys., **A559** (1993) 1.
9. V.G. Soloviev and A.V. Sushkov, Z.Phys., **A345** (1993)155.
10. V.G. Soloviev, A.V. Sushkov and N.Yu. Shirikova, Nucl.Phys., **A568** (1994) 244.
11. V.G. Soloviev, A.V. Sushkov and N.Yu. Shirikova, (to be published).
12. V.G. Soloviev, A.V. Sushkov and N.Yu. Shirikova, (to be published).
13. J.Berzins et al., Nucl.Phys. A (to be published).
14. D.G. Burke et al., Nucl.Phys., **A445** (1985) 70.
15. I.M. Govil et al., Phys.Rev., **C33** (1986) 793.
16. V.G. Soloviev and A.V. Sushkov, Phys.Lett., **B262** (1991) 189.
17. A.Zilges et al., Z.Phys., **A340** (1991) 155.
18. H. Friedrichs et al., Phys.Rev., **C45** (1992) R 892.
19. H. Friedrichs et al., Nucl.Phys., **A567** (1994) 266.
20. V.G. Soloviev and N.Yu. Shirikova, Z.Phys. **A301** (1981) 263.
21. V.G. Soloviev and N.Yu. Shirikova, Z.Phys. **A334** (1989) 149.
22. H.G. Börner, J. Jolie, S.J. Robinson et al., Phys.Rev.Lett. **66** (1991) 691.
23. M. Oshima et al., Nucl.Phys., **A557** (1993) 635c.
24. R. Neu and F. Hoyler, Phys.Rev., **C46** (1992) 208.
25. R. Piepenbring and M.K. Jammari, Nucl.Phys., **A481** (1989) 81.
26. N. Yoshinaga, Y. Akiyama and A. Arima, Phys.Rev., **C38** (1988) 419.
27. A. Aprahamian, Phys.Rev., **C46** (1992) 2093.

Hexadecapole vibrations in deformed rare earth nuclei

D.G. Burke
Department of Physics and Astronomy, McMaster University, Hamilton, Ont., L8S 4M1, Canada

Abstract

Recent interpretations of $K^\pi = 4^+$ bands as double-γ-phonons in even-even nuclei of the deformed rare earth region are shown to be in serious conflict with single-nucleon-transfer results and other data. The main argument for the double-γ-phonon interpretation was the existence of large B(E2) values connecting the $K^\pi = 4^+$ bands with gamma bands, and an alternate explanation for these B(E2) values exists in terms of g-bosons. All available data, including E4 strengths, single-nucleon-transfer results, allowed β-decays, etc., are best explained if the 4^+ bands are predominantly hexadecapole vibrations (or g-boson structures), which contain large two-quasiparticle components in their microscopic compositions.

One of the principal objectives in the study of low energy nuclear structure is to understand the fundamental types of excitations, such as the single-particle and collective modes of motion. Among the lowest energy excitations are oscillations in the nuclear shape, described in terms of vibrations or phonons, and the single-phonon states of quadrupole (λ=2) and octupole (λ=3) types have been observed across most regions of nuclear mass. In spherical even-even nuclei there is abundant evidence for multi-phonon excitations, but the existence of such states in deformed nuclei has been controversial. In many deformed nuclei the lowest energy phonon is the $K^\pi = 2^+$ quadrupole one, called the gamma-vibration. Two phonons of this type would be expected to form double-γ-vibrational bands with K^π values of 0^+ and 4^+. In a number of early studies, bands were found that could be considered as candidates for such configurations.

Later, a considerable amount of evidence was presented[1, 2, 3, 4] for a predominant hexadecapole (λ=4) character for a number of $K^\pi = 3^+$ and $K^\pi = 4^+$ bands in the deformed rare earth region, including many of the $K^\pi = 4^+$ bands which had earlier been suggested as double-γ-phonons. Soloviev and co-workers[4, 5, 6], showed that the detailed microscopic structures of these bands are well-described in terms of hexadecapole phonons in the QPNM (Quasiparticle Phonon Nuclear Model). Devi and Kota have given[7] a corresponding description for many of these structures in terms of the Interacting Boson Model (IBM), in a survey paper which demonstrates overwhelmingly the need for including g bosons. The $K^\pi = 4^+$ bands introduced by including g bosons have "hexadecapole" character, whereas those present in the sd IBM are analogous to multiphonon configurations. Soloviev and Shirikova[8] have also pointed out that, as a consequence of the Pauli principle, the double-γ-phonon and other multiphonon states should be shifted upwards in energy and should become severely fragmented through mixing with other states. However, the search for such configurations has continued.

It is often found that the $K^\pi = 4^+$ bands considered as possible double-γ-phonons decay preferentially to the $K^\pi = 2^+$ γ-bands, rather than to members of the ground state band. In a number of early papers it was argued that this mode of decay was evidence for the double-γ-phonon nature of the $K^\pi = 4^+$ bands, as it would be expected that the decay to the ground state band would require a two-step process, destroying one phonon in each step. However, this argument is questionable because there may be other explanations for the hindrance of the E2 transitions to the ground band. For example, in a deformed nucleus in which K is a good quantum number, E2 transitions from the $K^\pi = 4^+$ band to the γ-band are allowed, whereas those to the ground band have two degrees of K-forbiddeness. Thus, more recently attempts have been made to measure the absolute B(E2) values, to determine whether transitions between the $K^\pi = 4^+$ and the γ-bands are enhanced, as would be expected for the double-γ-phonon description. An innovative lifetime-measuring technique was used to determine the B(E2) value connecting the lowest $K^\pi = 4^+$ band with the γ-band in ^{168}Er, and the result was used to argue for a double-γ-phonon interpretation for the $K^\pi = 4^+$ state[9]. Following this, several attempts have been made to extend this description to other nuclei. For example, Oshima et al[10] have measured B(E2) values in ^{192}Os, and the results have been analysed in terms of multiple phonons[11]. Also, Aprahamian and co-workers[12, 13] have suggested the double-γ-phonon interpretation of $K^\pi = 4^+$ states in ^{154,156}Gd and a number of other nuclei.

In this report, it is pointed out that these recent papers have argued for the double-γ-phonon description primarily on the basis of one type of information, the B(E2) values coupling the $K^\pi = 4^+$ bands with the γ-bands, and have not discussed several other types of data which conflict with this interpretation. These include results from single-nucleon-transfer reactions, β-decay studies, and inelastic scattering experiments. Furthermore, it will be pointed out that the double-γ-phonon description is not a *unique* explanation of these B(E2)'s because such values are also predicted for hexadecapole vibrations in the SU(3) limit of the sdg IBM.

As an example of the single-nucleon-transfer data, results for population of the $K^\pi = 4^+$ band at 1646 keV in ^{154}Gd by the (^{3}He,d) reaction are shown in Figure 1. These are part of a larger study[14] which included results from ^{153}Eu(^{3}He,d)^{154}Gd and ^{153}Eu(α,t)^{154}Gd single-proton-stripping reactions. Full details of these experiments will be published elsewhere[15], with discussions of all the populated bands. Beams of 24 MeV ^{3}He from the McMaster University Tandem Accelerator bombarded targets of metallic europium, enriched to 98.76% ^{153}Eu, made by vacuum-evaporation on carbon backings. Reaction products were analyzed by an Enge split-pole magnetic spectrograph and detected with nuclear emulsions. The overall resolution was $\sim$ 15 keV. It can be noticed immediately that the largest peaks observed in the (^{3}He,d) spectrum of Fig. 1 are for the well-known $I^\pi = 4^+$ and $I^\pi = 5^+$ levels at 1646 and 1770 keV, which are members of the $K^\pi = 4^+$ band in question. Although a quantitative analysis is presented below, it can be recognized at once that this band must have a large two-quasiparticle admixture. To first order, the (^{3}He,d) reaction transfers one nucleon to the target nucleus without altering the single-particle orbits of other nucleons. In the present case the target nucleus ^{153}Eu has an odd proton in the $\frac{5}{2}^+[413]$ Nilsson orbital, and the reaction adds another proton to form two-quasiproton states in ^{154}Gd.

One very important feature of single-nucleon-transfer reactions in deformed nuclei is that the relative cross sections for members of a rotational band form a distinctive pattern, or fingerprint, which depends primarily on the wavefunction of the transferred nucleon. This has proven to be a very powerful technique for identifying the configurations populated in many nuclides[16]. Theoretical cross sections for pure two-quasiparticle configurations were calculated, using Nilsson model wavefunctions and the distorted wave Born approximation with the formalism of ref. [16]. Standard optical model parameters were used[17]. Experience with many similar studies in this mass region has shown that for the strongest transitions in a spectrum, a reasonable estimate of the uncertainty for the predicted absolute cross sections is $\sim 30\%$, arising mainly from ambiguities in optical model parameters and in the normalisation.

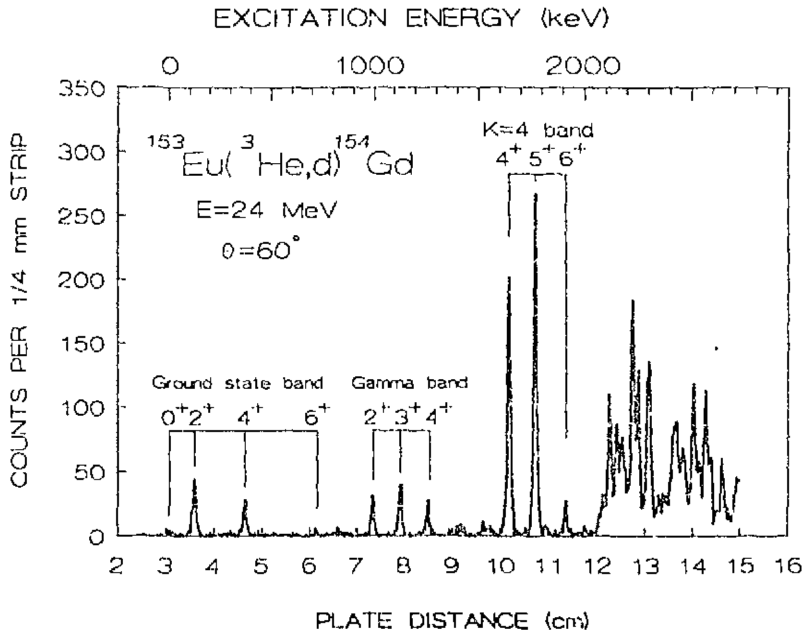

Figure 1. Deuteron spectrum from the ^{153}Eu(^{3}He,d)^{154}Gd reaction at $\theta = 60°$. A quantitative analysis of the large cross sections for the $K^{\pi}=4^{+}$ band at 1646 keV indicates that this band has a dominant $\frac{5}{2}^{+}[413]_{\pi} + \frac{3}{2}^{+}[411]_{\nu}$ component.

The calculated cross sections at $\theta = 30°$ for the I^π=4$^+$, 5$^+$, and 6$^+$ members of a pure K^π=4$^+$, $\frac{5}{2}^+$[413] + $\frac{3}{2}^+$[411] two-quasiproton band at 1646 keV are 42, 43, and 1 μb/sr, respectively. A value of 0.8 was used for the pairing factor U^2 for the $\frac{3}{2}^+$[411] orbital in the ^{153}Eu target. These are the largest predicted cross sections for any of the bands expected below 2 MeV excitation, and are in reasonable agreement with the experimental values of 30, 40, and ~1 μb/sr, respectively. This indicates that the $\frac{5}{2}^+$[413] + $\frac{3}{2}^+$[411] two-quasiproton configuration forms the dominant component of the K^π=4$^+$ band at 1646 keV in ^{154}Gd.

Single-phonon states can be populated in single-nucleon-transfer reactions as they consist of a superposition of two-quasiparticle states, one or more of which may satisfy the selection rules for being populated. The microscopic compositions of gamma vibrational states in terms of their two-quasiparticle components have been calculated by Soloviev and coworkers[18]. Kern et al[19] compared the observed (d,p) cross sections for a series of gamma vibrations in deformed rare earth even-even nuclei with predictions based on these structures, and showed that the agreement was reasonable. The microscopic compositions of octupole and higher order phonons have also been calculated[18, 20]. Many two-quasiparticle components of the various single-phonon states have now been observed, and in general there is good qualitative agreement with the admixtures predicted. Although one usually thinks of a collective vibration as a superposition of many two-quasiparticle components, each with a small amplitude, it is often found that one or two components will dominate, and all the others will make up only a few percent of the wavefunction. However, the correlated effects of these many small components can still produce a significant B(Eλ) for the state.

If one now considers double-phonon states, in which each phonon is a superposition of two-quasiparticle components, the structures involve four quasiparticles. Such states should not be populated in first order with single-nucleon-transfer reactions, which can produce at most two unpaired nucleons in an even-even nucleus. One higher-order process through which double-phonon configurations might be populated in such reactions would be through the existence of single-phonon admixtures in the odd-mass target ground state. However, these are expected to be relatively weak. The strongest such case known to the author is in a spherical nucleus, ^{114}Cd, where the 1283 keV 4$^+$ level interpreted as a two-phonon state has a (d,^{3}He) spectroscopic strength of ~0.28, which is only about 10% of the largest strength in the spectrum[21]. In deformed nuclei such effects would be expected to be smaller because the calculated admixtures of single-phonon configurations in the ground states of odd-mass nuclides are smaller. The largest such admixtures are calculated[22] to be typically of the order of 2 to 5%. Such an admixture could give rise to weak populations of double-phonon states, but the strengths would be only a few percent of the largest ones in the spectrum. Thus, since the K^π=4$^+$ band at 1646 keV in ^{154}Gd has the strongest population in the (^{3}He,d) spectrum, and this strength is consistent with an almost pure $\frac{5}{2}^+$[413] + $\frac{3}{2}^+$[411] two-quasiproton configuration, it must be predominantly a two-quasiparticle state and not a double-phonon.

Examination of the literature shows that many of the other K^π=4$^+$ bands suggested as *double-γ-phonons*[10, 11, 12, 13] also have dominant two-quasiparticle components. These are summarized in Table 1, where the specific two-quasiparticle configurations, and the experiments in which they were established, are listed in columns 3 and 4. It can be seen from the comments in column 5 that transfer reaction data such as those described above have been used to establish the character of the K^π=4$^+$ bands in ^{158}Gd, ^{162}Dy, ^{172}Yb, ^{176,178}Hf, and ^{190,192}Os. In most cases, the transitions discussed correspond to some of the largest peaks in the spectra.

Table 1. Evidence for dominant two-quasiparticle components in K^π=4$^+$ bands which had previously been suggested as double-γ-phonons.

Nuclide	K^π=4$^+$ bandhead energy (keV)	Dominant two-quasiparticle component	Experiment	Comments	Ref.
^{154}Gd	1646	$\frac{5}{2}^+[413]_\pi + \frac{3}{2}^+[411]_\pi$	(^{3}He,d)	Largest peak in spectrum	[15]
^{156}Gd	1510	$\frac{5}{2}^+[413]_\pi + \frac{3}{2}^+[411]_\pi$	$g_K - g_R$		[24]
^{158}Gd	1920	$\frac{5}{2}^-[523]_\nu + \frac{3}{2}^-[521]_\nu$	(d,p)		[29]
^{158}Dy	1895	$\frac{5}{2}^-[523]_\nu + \frac{3}{2}^-[521]_\nu$	β^+-decay	log ft=4.9 from ^{158}Ho (5$^+$)	[30]
^{160}Dy	1694	$\frac{5}{2}^-[523]_\nu + \frac{3}{2}^-[521]_\nu$	β^+-decay	log ft=4.9 from ^{160}Ho (5$^+$)	[23]
^{162}Dy	1536	$\frac{5}{2}^-[523]_\nu + \frac{3}{2}^-[521]_\nu$	(d,t), (^{3}He,α)	Largest peak in (d,t) spectrum	[31, 32]
^{162}Er	1712	$\frac{5}{2}^-[523]_\nu + \frac{3}{2}^-[521]_\nu$	β^+-decay	log ft=4.6 from ^{162}Tm (5$^+$)	[23]
^{168}Yb	2204	$\frac{7}{2}^-[523]_\pi + \frac{1}{2}^-[541]_\pi$	β^+-decay	log ft=5.0 from ^{168}Lu (3$^+$)	[23]
^{172}Yb	2073	$\frac{7}{2}^+[404]_\pi + \frac{1}{2}^+[411]_\pi$	(p,α)	Largest peak in spectrum	[33]
^{176}Hf	1888	$\frac{7}{2}^-[514]_\nu + \frac{1}{2}^-[521]_\nu$	(d,t)	Largest peak in spectrum	[34]
^{178}Hf	1513	$\frac{7}{2}^-[514]_\nu + \frac{1}{2}^-[510]_\nu$	(d,p)	Very large peak in spectrum	[35, 36]
^{190}Os	1162	$\frac{5}{2}^+[402]_\pi + \frac{3}{2}^+[402]_\pi$	(t,α)	Largest peak in spectrum $\leq$2 MeV	[2]
^{192}Os	1070	$\frac{5}{2}^+[402]_\pi + \frac{3}{2}^+[402]_\pi$	(t,α)	Largest peak in spectrum $\leq$2 MeV	[2]

Also listed in Table 1 are cases in which the two-quasiparticle characters have been assigned on the basis of β-decay with log ft values of ≤ 5.0, which are strong indicators of allowed unhindered transitions of the spin-flip type. In this mass region, these have been shown to be due to transitions such as $\frac{7}{2}^-[523]_\pi \Leftrightarrow \frac{5}{2}^-[523]_\nu$ or $\frac{9}{2}^-[514]_\pi \Leftrightarrow \frac{7}{2}^-[514]_\nu$. An examination of 122 cases showed[23] that, without exception, all decays with log $ft \leq 5.2$ could be assigned to this type of transition. The observation of such a small log ft value indicates the presence of one of the above nucleons in the configuration, making possible the assignment of the dominant two-quasiparticle configuration. In this way the K^π=4$^+$ bands suggested as double-γ-phonons in ^{158,160}Dy, ^{162}Er and ^{168}Yb had previously been assigned as being predominantly two-quasiparticle in character. The K^π=4$^+$ band at 1510 keV in ^{156}Gd is also included in Table 1. It has been found to have a large $\frac{5}{2}^+[413]+\frac{3}{2}^+[411]$ two-quasiproton component on the basis of $g_K - g_R$ values determined from in-band E2/M1 mixing ratios[24].

All of these results are difficult to reconcile with the double-γ-phonon interpretations. A more satisfactory description of these bands is suggested by evidence pointing to a hexadecapole-phonon description for several of these cases. Direct E4 strengths have been reported in inelastic scattering experiments for the K^π=4$^+$ bands in ^{156}Gd[25] and in ^{190,192}Os[3]. The populations of the K^π=4$^+$ bandheads are more than an order of magnitude larger than expected for double-γ-phonons.

With this in mind, one can examine how a hexadecapole description succeeds in explaining the main piece of evidence which has been used to argue for the double-phonon interpretation, namely the B(E2) values connecting the K^π=4$^+$ bands with the γ-bands. Numerical calculations with g bosons included in the IBM have been performed for ^{156}Gd by van Isacker *et al.*[26]. They refer to the new structures that appear in addition to the usual bands in the sd IBM as Γ, or hexadecapole, bands. The large B(E2) values connecting the K^π=4$^+$ band at 1511 keV with the gamma band can be well reproduced, with the K^π=4$^+$ band interpreted as hexadecapole in character, arising from the introduction of the g-boson. This can be seen from Figure 2, where the experimental and calculated B(E2) values are compared. The trend for E2 decays to populate preferentially the gamma band, rather than the beta or ground state bands, is clearly reproduced, and the absolute values are also in agreement. Later, Devi and Kota[27] derived analytical expressions for the B(E2) values in the various symmetry limits of the IBM, and in the SU(3) limit found that such B(E2) values can occur systematically between the Γ-bands and the γ-bands, and are not restricted to isolated cases.

Thus, the "large" B(E2) values can be explained by both the double-γ-phonon and the hexadecapole-phonon descriptions, and their observation does not, by itself, indicate the presence of double-γ-phonons. That is, the B(E2) values do not appear to provide a sensitive means of distinguishing between the two interpretations.

It should be noted that hexadecapole-phonon interpretations have been previously proposed for most of the K^π=4$^+$ bands discussed here, and that this description provides a good explanation of the observed two-quasiparticle components. Soloviev and co-workers have calculated the microscopic compositions of many of these states, and for all cases the observed large two-quasiparticle states are correctly predicted to dominate the wavefunction. For example, the K^π=4$^+$ bands at 1510 keV in ^{156}Gd and 1380 keV in ^{158}Gd are predicted[6] to be the lowest K^π=4$^+$ hexadecapole bands, and to have dominant components (83% in ^{156}Gd and 80% in ^{158}Gd) which are the $\frac{5}{2}^+[413] + \frac{3}{2}^+[411]$ two-quasiproton configuration. Levels in ^{156}Gd are not accessible by single-proton-transfer reactions on any stable target but, as indicated in Table 1, the $g_K - g_R$ value has been used to suggest a $\frac{5}{2}^+[413] + \frac{3}{2}^+[411]$ character for the 1510 keV band. For ^{158}Gd, (t,α) results using polarised triton beams have shown[28] that the K^π=4$^+$ band at 1380 keV has the same configuration. The (3He,d) data show this band to be at 1646 keV in ^{154}Gd, and its systematic occurrence at low energy would be expected since the two proton orbitals involved are the ones immediately above and below the Fermi surface in all of these gadolinium nuclei. The K$^\pi$=4$^+$ band which has been suggested[12, 13] as a double-γ-phonon in ^{158}Gd is the second K$^\pi$=4$^+$ one, which is predicted[6] to contain a large $\frac{5}{2}^-[523]_\nu + \frac{3}{2}^-[521]_\nu$ component, consistent with (d,p) data[29].

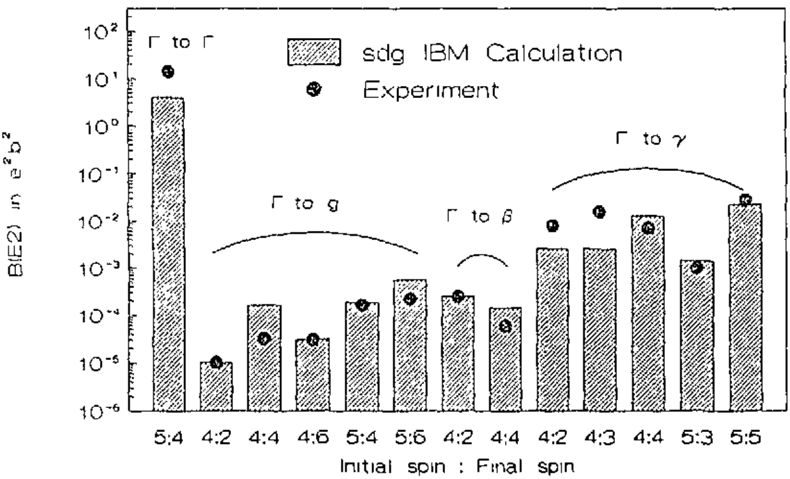

Figure 2. Comparison of experimental and calculated B(E2) strengths for decays from the K^π=4$^+$ band at 1511 keV in ^{156}Gd. This figure is adapted from Fig. 2 of van Isacker *et al.*[26], who interpreted the K^π=4$^+$ band as a Γ, or hexadecapole, band. The good agreement, especially for the $\Gamma \rightarrow \gamma$ strengths, shows that a double-γ-phonon description does not provide the only successful explanation of these results, but that a hexadecapole-phonon interpretation does also.

Calculations in the QPNM show[6] that the lowest $K^\pi=4^+$ bands in ^{156,158}Gd have small (2 to 5%) admixtures of the double-γ-phonon, which result in B(E2) values to the gamma bands which are typically a fraction of a Weisskopf unit. This is about an order of magnitude smaller than the observed values, some of which are ~3 Weisskopf units in ^{154}Gd and ^{156}Gd. However, the hexadecapole bands in the QPNM are most likely analogous to the Γ bands in the sdg IBM, in which the observed strengths could be reproduced. It is worth considering, for example, that since in the QPNM calculation the predicted B(E2) value results from a small (2% to 5%) admixture of the double-γ-phonon, some fine-tuning of the model may increase this admixture somewhat, resulting in B(E2) values comparable to those observed, while still retaining the predominant hexadecapole character which successfully explains the single-nucleon-transfer data. Overall, it is seen that a description in terms of hexadecapole phonons provides a more reasonable explanation for *all* the data than does the double-γ-phonon interpretation. Unfortunately, the IBM description does not provide predictions for the microscopic structures of these states, so a direct comparison with the available data cannot be made at present.

The lowest $K^\pi=4^+$ bands in osmium isotopes were assigned as hexadecapole phonons when the ones in ^{190,192}Os were found to be strongly populated in the (t,α) reaction[2], and evidence for direct E4 excitation in the (α,α') process was observed[3] for ^{188,190,192}Os. It was noted, however, that the decay pattern for this band did not resemble that predicted by the Alaga selection rules for a $K^\pi=4^+$ band in a well-deformed nucleus. Baker et al[37] performed numerical calculations for ^{192}Os in the sdg IBM between the SU(3) and O(6) limits. They concluded the best description was obtained by including a g-boson in the IBM, and were able to reproduce the observed E2 branching ratios and the E4 matrix elements with a g-boson, or hexadecapole, admixture of ~ 77 % in the $K^\pi=4^+$ bandhead. In this case, a large admixture of the $\frac{5}{2}^+[402] + \frac{3}{2}^+[402]$ two-quasiproton state would be expected, and thus the (t,α) results would also be explained. Lac and Kuyucak[38] have performed numerical calculations in the sdg IBM for ^{188,190,192}Os, and reproduced very well the observed electromagnetic matrix elements, including those for transitions from the $K^\pi=4^+$ to the γ bands. More recently, however, it has been claimed[10, 11] that the $K^\pi=4^+$ band in ^{192}Os has a double-γ-phonon structure, because the observed B(E2) results could be explained in the sd IBM. This work did not consider the single-nucleon-transfer data or the E4 strengths that conflict with this description and, in view of the demonstrated need for g-bosons[7, 38], it would seem that truncation to the sd IBM is not justified for these states. Although Devi and Kota have shown[27] that E2 transitions from the $K^\pi=4^+$ Γ band to the γ-band are forbidden in the O(6) limit of the sdg IBM, it is quite likely that the osmium nuclei are between the SU(3) and O(6) limits, and the SU(3) part could contribute the large observed B(E2) values. In fact, the ratios R(Q) shown in Fig. 2 of ref. [11] suggest that these nuclei are nearer the SU(3) limit.

In summary, this study has shown that there appears to be no strong evidence for claims[10, 11, 12, 13] that the $K^\pi = 4^+$ bands discussed above are double-γ-phonons. The B(E2) values used to make this claim appear to be explained equally well if the bands are hexadecapole phonon, or g-boson, in nature. Furthermore, the hexadecapole description appears to give a good explanation of other data, such as the single-nucleon-transfer results and E4 strengths, which conflict with the double-γ-phonon interpretation. Thus, these bands are better described as hexadecapole vibrations.

It is, of course, quite likely that a minor component for each of these $K^\pi = 4^+$states is of double-γ-phonon character. It would be expected that such a component could be responsible for a significant fraction of the gamma decay strength, and may possibly even dominate the gamma decay mode of the $K^\pi = 4^+$ band. Thus, by considering only the gamma decay data one may be seeing the effects of a minor component of the level structure. It is noted that *none* of the above discussion affects the proposed double-γ-phonon K^π=4^+ band in ^{168}Er, which was not populated significantly in any of the single-nucleon-transfer reactions.

Financial support from the Natural Sciences and Engineering Research Council of Canada is gratefully acknowledged.

References

[1] P.M. Walker, J.L.S. Carvalho and F.M. Bernthal, Phys. Lett. **108B**, 393 (1982).

[2] R.D. Bagnell *et al.*, Phys. Lett. **66B**, 129 (1977); Phys. Rev. **C20**, 42 (1979).

[3] D.G. Burke, M.A.M. Shahabuddin and R.N. Boyd, Phys. Lett. **78B**, 48 (1978).

[4] V.O. Nesterenko *et al.*, Sov. J. Nucl. Phys. **44**, 938 (1986).

[5] V.G. Soloviev and N.Yu. Shirikova Z. Phys. **A334**, 149 (1989).

[6] V.G. Soloviev, A.V. Sushkov and N.Yu. Shirikova, Nucl. Phys. **A568**, 244 (1994).

[7] Y.D. Devi and V.K.B. Kota Pramana - J. Phys. **39**, 413 (1992).

[8] V.G. Soloviev and N.Y. Shirikova, Z. Phys. **A301**, 263 (1981).

[9] H.G. Börner *et al.*, Phys. Rev. Lett. **C66**, 691 (1991).

[10] M. Oshima *et al.*, Nucl. Phys. **A557**, 635c (1993).

[11] M. Sugita and T. Otsuka, Nucl. Phys. **A557**, 643c (1993).

[12] A. Aprahamian *et al.*, Proc. 8th Int. Symp. Capt. Gamma-ray Spect., Fribourg, 1993, ed. by J. Kern *(World Scientific, Singapore, 1994)*, p. 57.

[13] X. Wu *et al.*, Phys. Rev. **C49**, 1837 (1994).

[14] O.P. Jolly, Ph.D. Dissertation, McMaster University (1976).

[15] D.G. Burke, J.C. Waddington, and O.P. Jolly, to be published.

[16] B. Elbek and P.O. Tjøm, Adv. in Nucl. Phys. **3**, 259 (1969).

[17] O. Straume, G. Løvhøiden and D.G. Burke, Nucl. Phys. **A266**, 390 (1976).

[18] K.M.Zheleznova *et al.*, Dubna preprint D-2157, (1965).

[19] J. Kern *et al.*, Nucl. Phys. **A104**, 642 (1967).

[20] V.G. Soloviev and A.V. Sushkov, J. Phys. G., **16**, L57 (1990).

[21] D.C.J.M. Hagemann *et al.*, Nucl. Phys. **A200**, 1 (1977).

[22] N.A. Bonch-Osmolovskaya and V.O. Nesterenko, Bull. Russ. Acad. Sc. (Phys.) **56**, 1694 (1992).

[23] P.C. Sood and R.K. Sheline, At. Data and Nucl. Data Tables, **43**, 259 (1989).

[24] J. Konijin *et al.*, Nucl. Phys. **A352**, 191 (1981).

[25] P.B. Goldhoorn *et al.*, Phys. Lett. **103B**, 291 (1981).

[26] P. van Isacker, K. Heyde, M. Waroquier and G. Wenes, Phys. Lett. **104B**, 5 (1981); Nucl. Phys. **A380**, 383 (1982).

[27] Y.D. Devi and V.K.B. Kota J. Phys. G **17**, 465 (1991).

[28] D.G. Burke *et al.*, Nucl. Phys. **A366**, 202 (1981).

[29] R.C. Greenwood *et al.*, Nucl. Phys. **A304**, 327 (1978).

[30] D.L. Anderson, D. Brenner and R.A. Meyer, Phys. Rev. **C18**, 383 (1978).

[31] A. Bäcklin *et al.*, Phys. Rev. **160**, 1011 (1967).

[32] E. Andersen *et al.*, Nucl. Phys. **A550**, 235 (1992).

[33] D.G. Burke and J.W. Blezius, Can. J. Phys, **60**, 1751 (1982).

[34] J.I. Zaitz and R.K. Sheline, Phys. Rev. **C6**, 506 (1972).

[35] R.K. Sheline *et al.*, Pramana – J. Phys. **41**, 151 (1993).

[36] R.K. Sheline *et al.*, Phys. rev. **C48**, 911 (1993).

[37] F.T. Baker, *et al.* Phys. Rev. **C32**, 2212 (1985).

[38] V.-S. Lac and S. Kuyucak, Nucl. Phys. **A539**, 418 (1993).

Two-phonon γ-vibrational state in ^{166}Er and ^{164}Dy

M. Oshima, T. Morikawa, Y. Hatsukawa, H. Iimura, S. Hamada, and T. Ishii
Japan Atomic Energy Research Institute, Tokai, Ibaraki 319-11, Japan

H. Kusakari, N. Kobayashi, and M. Taki
Faculty of Education, Chiba University, Inage, Chiba 263, Japan

M. Sugawara
Chiba Institute of Technology, Shibazono, Narashino 274, Japan

E. Ideguchi and Y. Gono
Department of Physics, Kyushu University, Hakozaki, Fukuoka 812, Japan

ABSTRACT

Two-phonon γ-vibrational state in ^{166}Er and ^{164}Dy has been studied through multiple Coulomb excitation. Absolute E2 transition probabilities between two- and one-phonon states are derived. Experimental results for the well deformed nuclei are reviewed.

1. Introduction

Surface vibration is a fundamental collective motion of atomic nucleus. Such vibrational mode is well established as one-phonon β- and γ-vibrational states at low excitation energy. On the other hand, multi-phonon vibrational excitations are not well known especially in deformed or transitional region. Their existence and collectivity is one of the central problem for elucidating the collective excitation of nuclei. Currently new results[1-4] on two-phonon states with couplings of quadrupole and octupole phonons are emerging. For the identification of two-phonon state, it is very important to determine the B(E2) values which are the direct measure of collectivity. There are a number of theoretical investigations for the description of the two-phonon states such as the Quasiparticle-Phonon Nuclear Model (QPNM),[5] the Multi-Phonon Method (MPM),[6] the Dynamic Deformation Model (DDM),[7] the extended Interacting Boson Model with s, d and g bosons (sdg-IBM),[8] and the Selfconsistent Collective Coordinate Method (SCCM).[9] However, only a few experimental data have been reported as to the absolute transition rates. Because of this we made a multiple-Coulomb-excitation experiment for ^{168,166}Er, ^{164}Dy and ^{192}Os nuclei. Here the new results for ^{166}Er and ^{164}Dy are presented.

2. Experiment and analysis

Collective states which are connected to the ground state with strong E2 cascading transitions can be well excited through multiple Coulomb excitation. The Coulomb-excitation cross section is a direct function of E2 matrix element so that, once the transition is observed, the yield can be converted to the B(E2) values in a model independent manner.

The ^{166}Er and ^{164}Dy nuclei were multiply Coulomb-excited with beams of 295-MeV ^{74}Ge and 235-MeV ^{58}Ni, respectively, which were obtained from the JAERI tandem accelerator. The target was a self-supporting metallic foil of 1.4 mg/cm^2 for ^{166}Er and 1.2 mg/cm^2 for ^{164}Dy. The bombarding energies have been chosen so as to achieve the "safe energy"(4 - 4.5 fm of closest distance). Coulomb scattered particles by target nucleus are detected by two parallel plate avalanche counters which subtended the backward angles. γ-rays in coincidence with the scattered particles are detected by four Ge-BGO anti Compton spectrometers surrounding the target chamber. The observed γ-ray spectra were corrected for Doppler shifts kinematically by using the position signals of the scattered particles.

In order to derive Eλ matrix element we have made analysis based on Coulomb excitation code GOSIA,[10] which takes into account energies and Eλ matrix elements of all the states and transitions concerned. Here the general behavior of Coulomb-excitation cross section is shortly reviewed. Figure 1 shows a γ-ray yield of $4_{\gamma\gamma} \rightarrow 2_\gamma$ transition as a function of excitation energy of $4_{\gamma\gamma}$ state. The yield logarithmically deceases and it becomes difficult to observe the two-phonon state at higher excitation energy. Figure 2 shows the yield versus E2 matrix element between the $4_{\gamma\gamma}$ and 2_γ states. In this calculation the E2 matrix element between the one- and zero-phonon states are fixed. This indicates that the yield is proportional to the square of E2 matrix element or B(E2), which is expected in one-step Coulomb excitation from the one-phonon states.

3. Experimental results and discussion

Figure 3 shows a partial level scheme of ^{166}Er. Three transitions deexciting a known level at 2101.6 keV were observed in our experiment. The spectroscopic information for such highly excited states is not sufficient and the spins and parities have not been assigned yet. But from the branching ratio and the relatively large transition intensity, we tentatively assigned these transitions as E2 and the state as 4^+ with K=4.

The ^{164}Dy is known to have the lowest-lying one-phonon γ band in the rare earth region. As

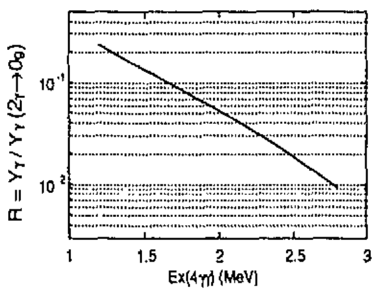

Fig. 1. Yield of $4_{\gamma\gamma} \rightarrow 2_\gamma$ transition as a function of excitation energy.

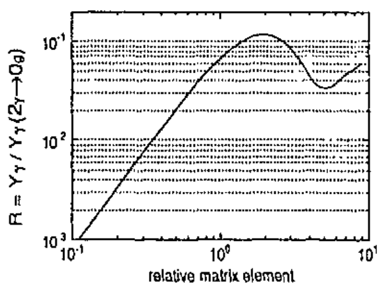

Fig. 2. Yield of $4_{\gamma\gamma} \rightarrow 2_\gamma$ transition as a function of E2 matrix element.

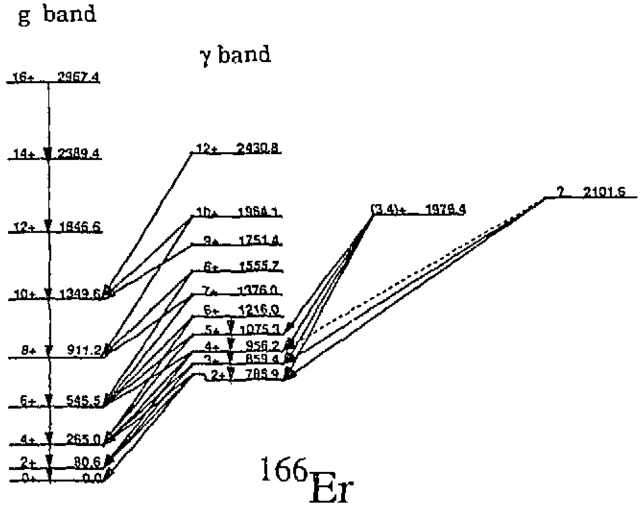

Fig. 3. A partial level scheme of ^{166}Er.

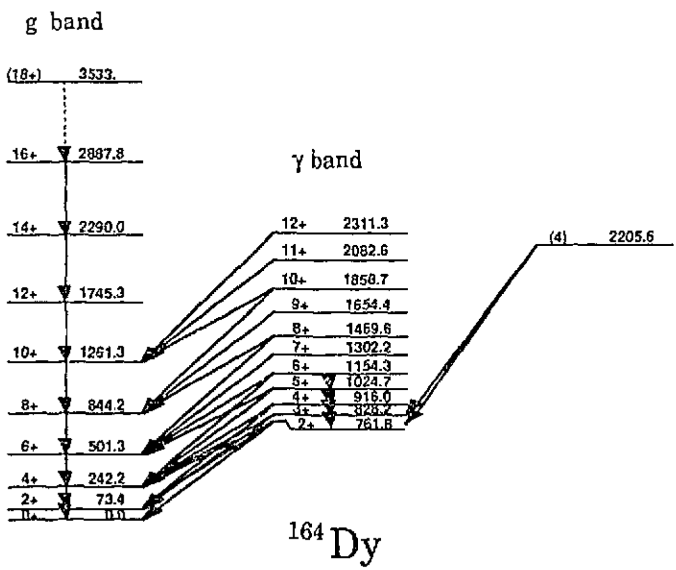

Fig. 4. A partial level scheme of ^{164}Dy.

Table I Summary of two-phonon states in deformed nuclei.

	exp		cal		
nucleus	$\frac{E(4_{\gamma\gamma}^+)}{E(2_\gamma^+)}$	$\frac{B(E2;2_\gamma \to 4_{\gamma\gamma})}{B(E2;0_g \to 2_\gamma)}$	$\frac{E(4_{\gamma\gamma}^+)}{E(2_\gamma^+)}$	$\frac{B(E2;2_\gamma \to 4_{\gamma\gamma})}{B(E2;0_g \to 2_\gamma)}$	reference
Harmonic vibration			2.00	1.00	
^{164}Dy	2.894	0.9 ± 0.5			present
			2.83 - 2.93	-	QPNM [5]
			2.64	0.66	SCCM [9]
^{166}Er	2.517	0.16 ± 0.12			present
	2.673	0.47 ± 0.35			present
			2.67 - 3.02	-	QPNM [5]
			2.57	0.68	SCCM [9]
^{168}Er	2.503	0.53 ± 0.12			present
	"	0.38 ± 0.20			Börner et al. [1]
			-	0.16	QPNM [5]
			2.5	0.40	MPM [6]
			2.5	1.44	DDM [7]
			2.5	0.50	sdgIBM [8]
			2.54	0.68	SCCM [9]
^{232}Th	1.801	1.1 ± 0.4			Korten et al. [4]

shown in Fig. 1, the Coulomb-excitation cross section increases drastically as the excitation energy decreases so that the low excitation energy is advantageous in assigning the two phonon state. In spite of this speculation, we could not observe any strong peak at the energy lower than 1.34 MeV. Thus we have reported previously[11] that ^{164}Dy has no well concentrated two-phonon state below 2.1 MeV.

Table I summarizes the energy ratio and B(E2) ratios of the two-phonon state in well deformed nuclei. The energy and B(E2) are obtained in absolute basis but the ratios of $E(4^+)$ / $E(2^+)$ and $B(E2; 2_\gamma \to 4_{\gamma\gamma})/B(E2; 0_g \to 2_\gamma)$ are convenient for the comparison with theoretical calculations. ^{168}Er is the first case where two-phonon state is reported[1] and the data for ^{232}Th is recently reported. The anharmonicity of the two-phonon state in ^{164}Dy and ^{166}Er is larger than these nuclei. The QPNM calculation[5] seems to be consistent with the present result.

Table II shows the decay of the observed two phonon states. The B(E2) values between the two phonon and one phonon states show a collectivity of 6 to 10 Weisskopf estimates. Since, in the harmonic limit, ratio of $B(E2; J_{\gamma\gamma} \to 2_g)/B(E2; J_{\gamma\gamma} \to 2_\gamma)$ becomes zero, it gives a measure of goodness of the two phonon picture. The B(E2) ratios are sufficiently small for the experimental data currently available, and supports the interpretation of two-phonon picture for these states. As to ^{154}Gd, B(E2) ratios were derived from the γ-ray branching-ratios even though the absolute B(E2) values were not determined.

In a recent sdg IBM calculation,[14] it was suggested that g-boson contribution is large in $K=4_1$ bands in transitional Sm-Gd and Os-Pt nuclei. The g-boson corresponds to the hexadecapole contribution and the observed enhancement of B(E4) in Os-Pt region[15] is well explained through

Table II Properties of two-phonon γ-vibrational states

nucleus	J	$B(E2;2_\gamma \to J_{\gamma\gamma})$ (W.u.)	$\frac{B(E2;J_{\gamma\gamma}\to 2g)}{B(E2;J_{\gamma\gamma}\to 2_\gamma)}$	ref.
Harmonic limit	4,0		0.0	
^{154}Gd	4	-	0.0001	Wu et al.[12]
^{164}Dy	4	11 (6)	0.014(7)	present
^{168}Er	4	5.9 (13)	<0.005	present
^{190}Os	4	11 (2)	0.0045 (6)	NDS[13]
	0_2	13 (2)	0.093 (12)	NDS[13]
^{192}Os	4	9.2 (9)	0.0030 (8)	present
	0_2	6.9 (7)	0.0182 (7)	present
	(0_3		>0.25)	present
^{232}Th	4	10 (3)	0.006(3)[a)]	Korten et al.[4]

a) present

this model. In order to understand the apparent low-excitation energy of the $K=4_1$ band head, it will be necessary to take into account the hexadecapole contribution.

4. Summary

Two-phonon γ-vibrational states in well deformed nuclei, ^{168}Er and ^{164}Dy, and a transitional nucleus, ^{192}Os, have been studied through multiple Coulomb excitation. Our result and recently reported results for ^{188,190}Os and ^{232}Th reveal the following features of the two phonon states.

The energy ratio, $E(4_{\gamma\gamma}^+)/E(2_\gamma^+)$, for the two-phonon states are fluctuated between 1.8 to 2.8. It is interesting to see that, although the phonon states are collective and expected to be observed systematically in the same energy range, the experimentally observed energy changes much even in a narrow region of ^{166,168}Er and ^{164}Dy. This suggests the necessity of further investigations with microscopic basis. The QPNM approach may be expected to explain such structure of two-phonon states. A gross feature of the energy ratio and $B(E2; 4_{\gamma\gamma}\to 2_\gamma)$ indicates that as the neutron number increases the harmonicity becomes large; in ^{232}Th a near harmonic vibration has been achieved. This feature has not been fully understood.

Acknowledgements

The authors are indebted to the accelerator crew of the JAERI tandem accelerator for providing beams. We are thankful for valuable discussions by Drs. Matsuyanagi, Sugita, and Otsuka.

References

1 H.G.Börner et al., *Phys. Rev. Lett.* **66** (1991) 691.
2 M.Oshima et al., *Nucl. Phys.* **A557** (1993) 635c.
3 U. Kneissl et al., *Phys. Rev. Lett.* **71** (1993) 2180.
4 W.Korten et al., *Phys. Lett.* B **317** (1993) 19.
5 V.G.Soloviev and N.Yu.Shirihova, Z. *Phys.* A301, 263 (1981); and private communication.
6 M.K.Jammari and R.Piepenbring, *Nucl. Phys.* **A487**, 77 (1988).
7 K. Kumar, in *Nuclear Models and the Search for Unity in Nuclear Physics* (Universitetforlaget, Bergen, Norway, 1984).
8 N.Yoshinaga, Y.Akiyama, and A.Arima, *Phys. Rev. Lett.* **56** (1986) 1116.
9 M.Matsuo and K.Matsuyanagi, *Prog. Theor. Phys.* **76** (1986) 93; *ibid* **78** (1987) 591.
10 D.Cline, *Ann. Rev. Nucl. Part. Sci.* **36** (1986) 681; and references therein.
11 M.Oshima et al., *Nucl. Phys.* **A557** (1993) 635c.
12 X. Wu et al., *Phys. Rev.* **C49** (1994) 1837.
13 *Nucl. Data Sheets* **61** (1990) 243.
14 V.-S. Lac and S.Kuyucak, *Nucl. Phys.* A539 (1992) 418.
15 F. T. Baker et al., *Nucl. Phys.* **A501** (1989) 546.

A test of QPM model by inelastic excitations and the (p,t) reaction

N. Blasi,[a] R. De Leo,[b] S. Micheletti,[a] M. Pignanelli,[a] V. Yu. Ponomarev[c]
[a] *Dipartimento di Fisica dell'Universita' and Sezione INFN, Milan, Italy*
[b] *Dipartimento di Fisica dell'Universita' and Sezione INFN, Bari, Italy*
[c] *Joint Institute for Nuclear Research, Dubna, Russian Federation*

Abstract. Experimental data from proton and deuteron scattering and the (p,t) reaction on the even Nd isotopes are compared with Quasi-Particle Phonon Model evaluations. The B(Eλ) values are satisfactory reproduced in spherical nuclei (^{142,144,146}Nd). The same model accounts for ^{148,146}Nd(p,t) reactions. In particular the present study is aimed to obtain information on the residual quadrupole particle-hole and pairing interactions.

1. Introduction

Particle-hole (*p-h*) and particle-particle (*p-p*) correlations play a fundamental role in the structure of nuclei. The first type of correlations gives rise to the well established rotational and vibrational modes, which are strongly excited in inelastic processes. The *p-p* correlations affect particles moving around the Fermi surface and produce vibrations which change the number of particles by two (pair vibrations). They can be excited by two-nucleon transfer reactions. To obtain information on these correlations, excited states in even Nd isotopes, up to excitation energies of about 4 MeV, has been investigated by proton- and deuteron-scattering and by the (p,t) reaction.

The reduced transition probabilities, for natural-parity states with J^π from 0^+ up to 6^+, have been extracted from inelastic scattering experiments. The experimental strength distributions were compared[1]) with the predictions of the interacting boson model (IBM)[2]) and the quasi-particle-phonon model (QPM)[3]). The latter is a microscopic model in which the basis states, called "phonons", are the collective and non-collective solutions of the BCS quasi-particle RPA equations. In a second step of the QPM evaluations, two- and three-phonon states are constructed and simultaneously coupled and mixed. The fact that QPM is taking into account not only the strong collective configurations, but also states with a weaker collectivity down to quasi-particle states is of some interest in comparing with experimental results including also weak transitions. The interplay between the different multi-phonon configurations has an essential role in determining the gross structure of the different strength distributions. This is especially evident in the case of the even-parity transitions (E2, E4 and E6), in which several one- and two-phonon configurations are of some importance. The model describes reasonably well[1]) the isoscalar and isovector strength distributions for the different multipolarities from $\lambda = 2$ to $\lambda = 6$.

The collective states have been studied by inelastic scattering processes and gave information on *p-h* correlations in terms of a residual interaction. To implement this information with that on *p-p* correlations, the ^{142,144,146,148}Nd(p,t) reactions have been studied. In a superfluid description *p-h* and *p-p* correlations should affect the same states. In this case it is necessary to analyze simultaneously inelastic scattering and two-neutron transfer reactions. The data from these experiments have been compared with QPM predictions. The data and, in particular, the B(E2) value and the (p,t) cross section for the excitation of the first 2^+ state are used to obtain information on the quadrupole pairing force.

2. The experiment

Differential inelastic cross sections have been measured for proton and deuteron scattering on ^{142,144,146,148,150}Nd using momentum-analyzed beams from KVI cyclotron. The incident energies were about 30.5 and 50.8 MeV, respectively, for protons and deuterons. The scattered particles were detected in the focal plane of the QMG/2 spectrograph with an energy resolution of 12-15 keV in (p,p') and of 15-22 keV in (d,d') experiments. The ^{142,144,146}Nd(p,t) reactions have been studied at an incident energy of 35.6 MeV and with an energy resolution of 20-25 keV. The ^{148}Nd reaction has been studied using a 25 MeV proton beam from the Munich MP tandem accelerator, with an energy resolution of 7-9 kev. The weakest transitions detected have differential (p,p') cross sections reaching, at the maximum in the angular distribution, a value of the order of 10 μb/sr. The weakest (p,t) cross sections have, at the maximum, a value of 2-3 μb/sr in (p,t) experiments perfomed at KVI and about 1 μb/sr in the Munich experiment. In spite of the fact that also the weak transitions are detected in these experiments, only a part of the states results to be excited both in inelastic scattering and in the (p,t) reaction. For instance 37 2^+ states have been detected in ^{146}Nd below 3.8 MeV. Between them 12 are excited both in (p,p') and (p,t) reactions, 4 are excited only in (p,p') and 21 only in (p,t). This is an evidence of the fact that collective configurations are mixed with *2p-2h* configurations, but only in a part of the states. Also for the other multipolarities in ^{144}Nd as well as in ^{146}Nd the fraction of states excited in both reactions is at least 1/3. In ^{142}Nd this fraction becomes 1/4. The summed cross section, at the maximum of the angular distributions, for the excitation of 2^+ states in ^{142,144,146}Nd by the (p,t) reaction results of the order of 1 mb/sr. The cross section of the states excited both in inelastic and (p,t) reactions is about the 43 % of the total in ^{144,146}Nd and only the 22 % in ^{142}Nd. Also for 4^+ states the lowest percentage is found in ^{142}Nd. These findings could due to a larger decoupling of collective from *2p-2h* states in the magic nucleus ^{142}Nd.

About 360 (p,t) transitions to final states of the above four nuclei have been studied. Several states, not reported in literature, have been detected and the spin-parity has been assigned. This result is of some interest in connection to the fact that a large body of data is required to test nuclear structure models. Reactions that provide "complete spectroscopy" are therefore very important. It has been shown[4]) that resonance neutron capture and charged-particle fusion reactions have completeness properties. The number of states in ^{144}Nd, lying at an excitation energy below 4 MeV and for which the spin-parity has been assigned is: 50 for states detected by (p,t) experiments, 40 by inelastic scattering and 34 by other reactions, as reported in Nuclear Data Tables. "Other reactions" include: (n,γ), (n,n'γ), (light,xn), (HI,xn γ), one-nucleon transfer, beta decay, etc. Similarly in ^{146}Nd we have 92 states found in (p,t), 64 from (p,p') and 56 from other

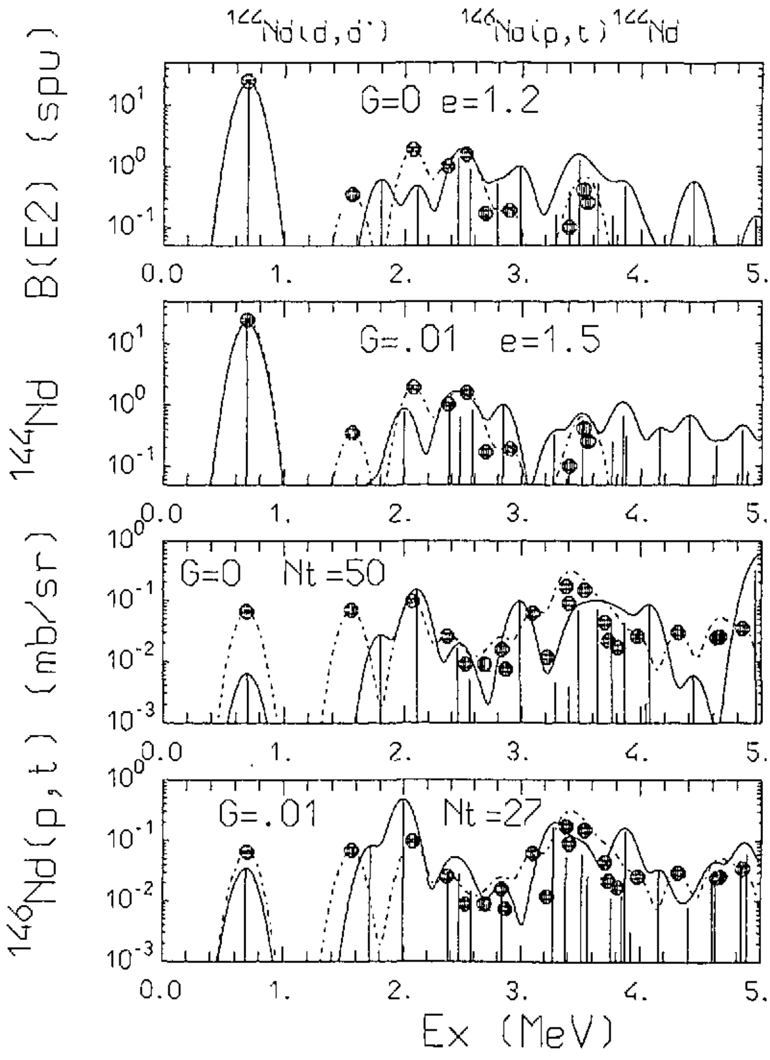

Fig. 1 - Experimental transition probabilities, B(E2), and (p,t) cross sections (full points) compared with QPM predictions (vertical lines). The pairing interaction, the effective charge and the (p,t) cross section normalization factor (G, e, Nt) are given in the figures. To better appreciate the gross structure of the spectra, the data and QPM evaluations are also represented as overlapping distributions after smearing with a 200 keV wide gaussian function (dashed and full curves).

reactions. The largest number of states has been, therefore, detectd in (p,t) experiments. We like to stress here that with the (p,t) reaction, especially if studied with a high resolving power as in the ^{148}Nd(p,t)^{146}Nd case, complete sets of levels in certain spin and excitation energy ragions can be populated.

3. QPM analysis

QPM evaluations have been compared with inelastic scattering experiments on Nd isotopes: ^{142}Nd(e,e')[5], ^{144}Nd(e,e')[6], ^{146}Nd(e,e')[7], (p,p') and (d,d') on ^{142,144,146,150}Nd[1]. Some assumptions used in these studies have been considered also in the present calculations. The single-particle hamiltonian includes Saxon-Woods potentials with radial parameters taken as in the above references. All bound and narrow quasi-bound states were included in the calculation. The derivative of the SW-well is assumed for the radial dependence of the *p-h* interaction. In principle, for each multipolarity the parameters $k_{0,1}^{J^\pi}$ of the effective residual force can be chosen to reproduce the experimental excitation energy of the lowest state. To restrict the number of free parameters involved in the calculation the isovector constants are fixed to the isoscalar ones by the following relation: $k_1^{J^\pi} = -1.2k_0^{J^\pi}$ for all J^π. A further constrainth has been introduced since for the higher multipolarities (J$\geq$ 5), the adjustement of the *p-h* force on the excitation energies of the lowest states leads to unrealistic values. For 5^- states $k_0^{5^-}$ was taken equal to the value of that of the octupole states, i.e. $k_0^{3^-}$, and for 6^+ states the same value for the quadrupole states, $k_0^{2^+}$, was used.

The monopole pairing constant was fixed by the pairing energy In the analysis of ref. 1 no other multipoles of the pairing interaction were used. The experimental and calcultated B(E2) and (p,t) cross sections for the excitation of the 2^+ states in ^{144}Nd are given in fig. 1. The (p,t) cross section for the excitation of the 2_1^+ state is strongly underestimated. To explore the effect on the (p,t) cross sections, the quadrupole pairing interaction, $G^{(2)}$, has been varied between 0 and 0.012. In these calculations $G^{(2)}$ was taken with equal values for protons and neutrons. This interaction produces a change in the calculated excitation energies. The agreement with the experiment can be restored adjusting slightly the multipole force in the *p-h* channel. For instance in ^{144}Nd a variation in $G^{(2)}$ from 0 to 0.010 leads

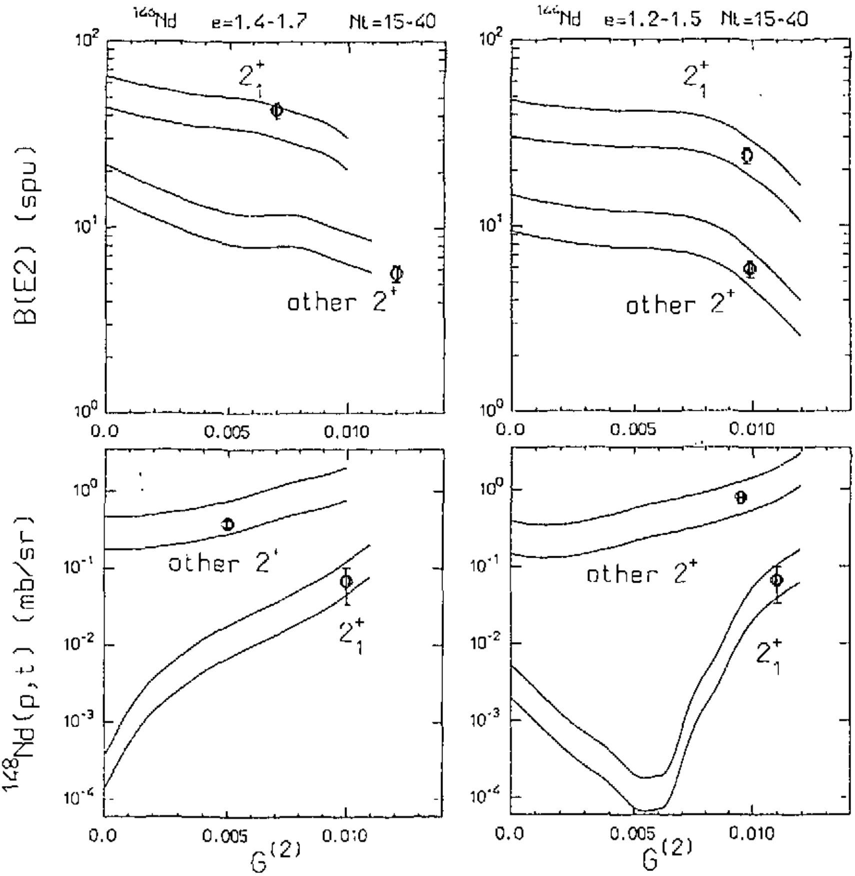

Fig. 2 - The experimental B(E2) and the (p,t) cross section for the excitation of the 2_1^+ state in ^{144,146}Nd are given as full points. The same observables summed over the other 2^+ states lying below 3.8 MeV are also given. The $G^{(2)}$ dependeces predicted by QPM using different effective charges e and normalization factors Nt are given as full curves.

to the following changes in the values of $k_0^{2^+}$, $k_0^{3^-}$, $k_0^{4^+}$: *0.0139→0.0125*, 0.0126→0.0110, 0.0129→0.129 fm^2 MeV^{-1} respectively. Similarly in ^{146}Nd the change is 0.0137→0.0120, 0.0123→0.0119, 0.0127→0.0124. The dependence from the quadrupole pairing interaction of the B(E2) values and of the (p,t) cross sections for ^{144}Nd and ^{146}Nd is given in fig. 2. The B(E2) of the 2_1^+ state decreases by a factor of about 3 in the explored $G^{(2)}$ range. The dependence of the summed B(E2)'s value for the other 2^+ states, lying at low excitation energies ($\leq$ 3.8 MeV), is very similar. A more complex and mostly increasing trend is instead found for the (p,t) cross sections. The effect is particularly evident, as exspected, in the cross section for the excitation of the 2_1^+ state. The role of B(E2) and σ(p,t) would be interchanged as compared with fig. 2 increasing the k_0^2 value at a fixed $G^{(2)}$ value.

In searching for the best $G^{(2)}$ value one must take into account the uncertainties in the different quantities considered in the comparison between the calculation and the experiment. The uncertanties are rather limited in the experimental data ($\leq$ 10%), except the case of the cross section for the excitation of the 2_1^+ state in the (p,t) reaction, at the cause of large two steps contributions. Larger uncertainties are found, however, in the calculated B(E2) values and (p,t) cross sections. The former are due to the method used to obtain the B(Eλ) values from the QPM transition matrix elements. The latter are due to the method (DWBA or CCBA) used to calculate the (p,t) cross sections from the QPM spectroscopic amplitudes. The first type of uncertainty is connected to the need of effective charges. Their use compensates for the truncation of the basis states of the average field, namely in our case the neglect of unbound states. For quite heavy nuclei, like Nd isotopes, and low-lying states we expect the role of the continuum to be not very strong and thus, the continuum can be substituted by a limited number of quasi-bound states. This is the motivation in refs. 5 and 6 for not using effective charges in the analysis of the transition densities in ^{142,144}Nd. In the calculations of the strength distributions in ^{142,144,146}Nd we have found instead necessary[1]) to use effective charges of the order of 1.2-1.3. When quadrupole pairing interaction is considered one finds, as shown in fig. 2, an enhancement of (p,t) cross sections, while the

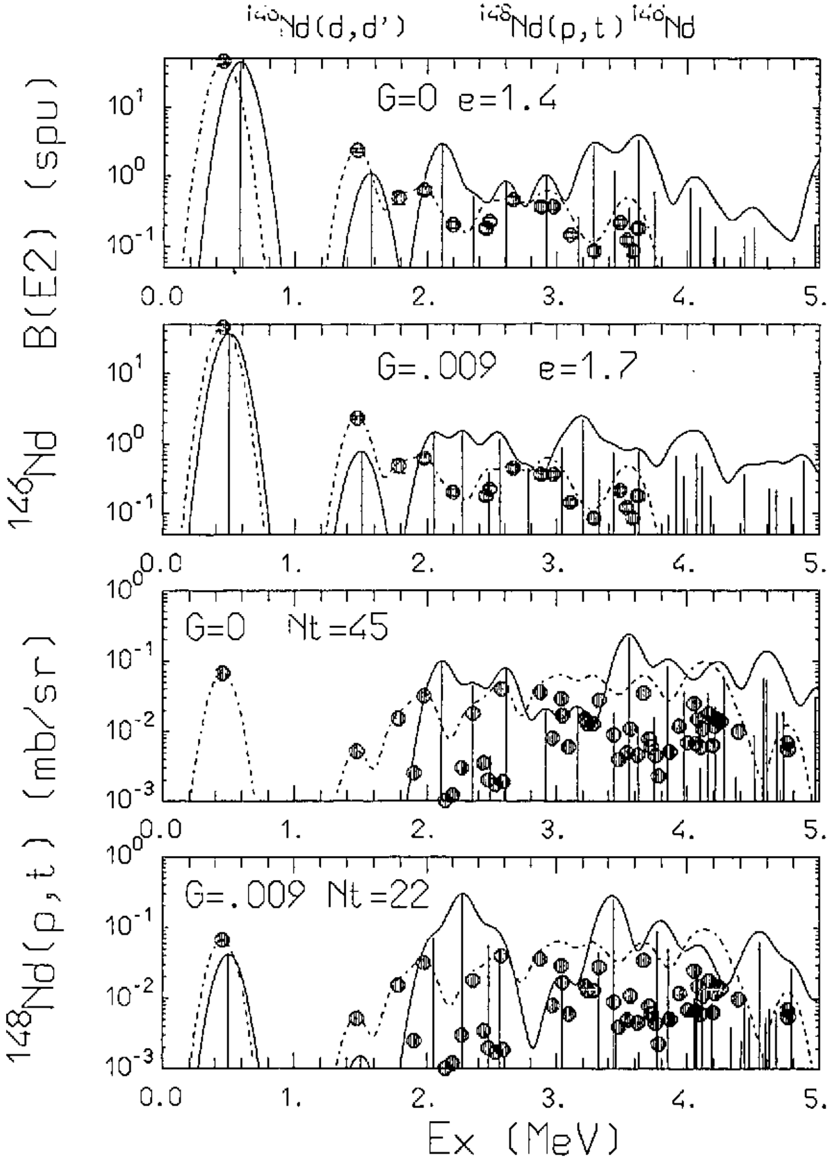

Fig. 3 - As in fig. 1 for the residual nucleus ^{146}Nd.

B(E2) transition probabilities are strongly reduced. To compensate this effect one could use larger effective charges.

The zero-range DWBA method reproduces the angular distributions and the relative magnitude of cross sections. However, the method fails to reproduce the absolute values. The empirical value of the normalization constant, $D_0^2 N_t$, of zero-range DWBA calculations, is larger by at least an order of magnitude if the constant D_0 is obtained by simple theoretical considerations. Finite-range calculations improve the calcultated absolute cross sections, but this is not sufficient to cover the difference between theory and experiment. We have used DWUCK and CHUCK codes and the zero-range approximation. In this case the maximum expected range for the empirical normalization factor N_t should be 17-35.[7]) Considering these uncertainties the comparison between calculated and experimental (p,p') or (d,d') cross sections (or B(E2) values deduced from the inelastic cross sections) and the (p,t) cross sections cannot be limited to the 2_1^+ state. For this reason also the sum of B(E2)'s and (p,t) cross sections for the other 2^+ states lying below 3.8 MeV have been considered. Assuming $G^{(2)} = 0$ as in ref. 1, the 2_1^+ B(E2) value in ^{144}Nd, as well as the rest of the B(E2) distribution, is rather well reproduced assuming an effective charge $e = 1.2$. In this case however the (p,t) cross section to the 2_1^+ state is strongly underestimated, while the rest of the (p,t) distribution is accounted for assuming N_t=50. A value larger than those usually found. Assuming a value of $G^{(2)}$ of 0.009-0.010 we have $e = 1.5$ and $N_t = 27$ (fig. 1).

In ^{146}Nd, without the quadrupole pairing interaction, acceptable fits to B(E2) and (p,t) data are obtained with e=1.4 and $N_t = 45$, but the B(E2) of the 2_1^+ state is underestimated and the (p,t) transitions to the 3 lowest states are completely missing (fig. 3). The overall best agreement is found with $G^{(2)} = 0.009$, e=1.7 and $N_t = 22$. The less satisfactory agreement found in ^{146}Nd in respect to that in ^{144}Nd is probably due, as already evidenced in ref. 1, to the fact that QPM calculations, with the model space used in the present study, underestimate the collectivity of ^{146}Nd.

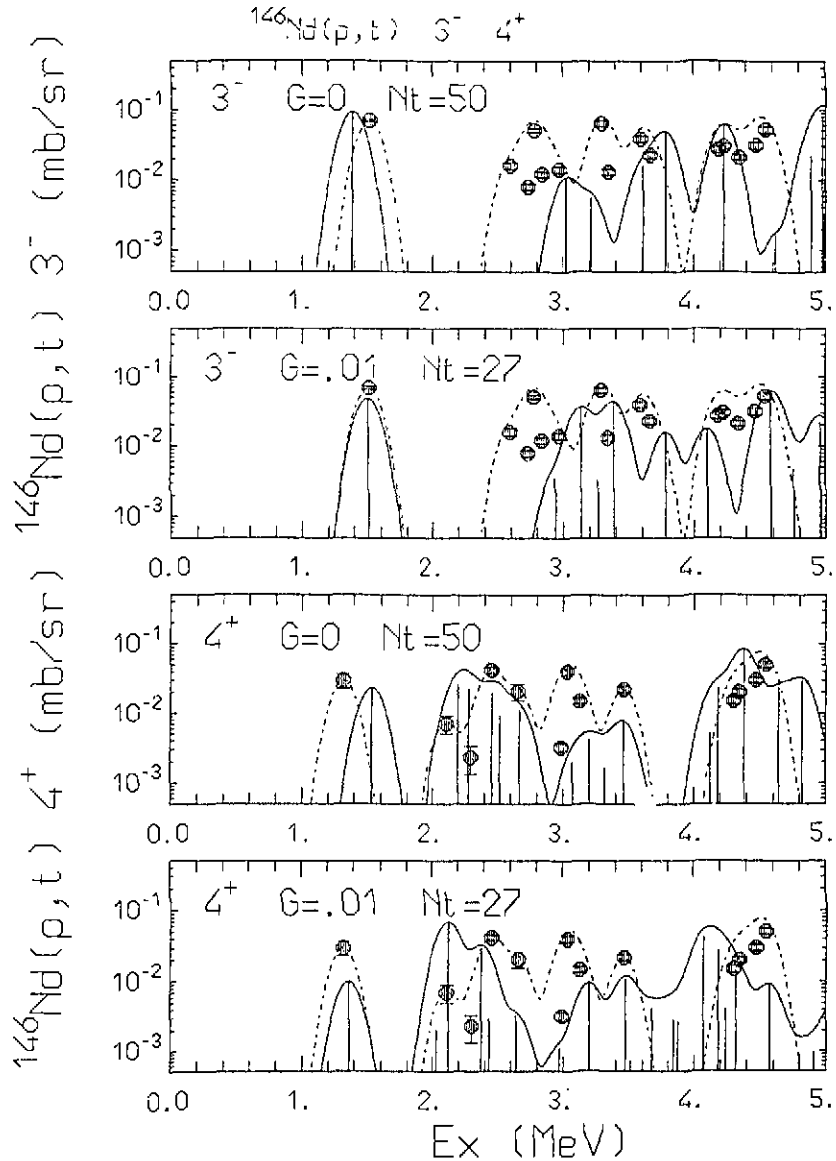

Fig. 4 - The (p,t) cross sections for the excitation of the 3^- and the 4^+ states in ^{144}Nd, compared with QPM evaluations as in fig. 1.

The effect of the quadrupole pairing interaction is smaller in the transitions with a multipolarity different from 2, but still important. Two examples are given in fig. 4. In the (p,t) cross sections to 3^- states in ^{144}Nd one finds, using $G^{(2)}=0.010$, a better agreent with the experiment, at excitation energies between 3 and 4 MeV. An equivalent agreement is instead found for the 4^+ states. In this connection it should be of some interest to take into account also the higher multipoles of the pairing force.

Finally we must mention two unsuccessful results of the present QPM calculations. The ^{142}Nd(p,p') transitions are completely decoupled from those calculated for the reaction ^{144}Nd(p,t). It is to say the two reactions are exciting two completely different sets of states. Experimentally, as sayd above, we have found an indication of a partial, but not complete decoupling. The second failure of the present calculations concerns the fact that the calculated cross sections in the ^{142}Nd(p,t) reaction results to be much larger than in the other Nd targets. Unfortunately QPM in the present form seems to overestimate the contribution of levels near the Fermi surface to the lowest phonons. This is not seen in B(λ), which are determined by coherent contributions from many weak configurations. This is also not seen in ^{144,146}Nd, because the cancellation between different terms present in the spectroscopic amplitude in particle-filling nuclei. The resulting effect is instead evident in nuclei filling hole levels as ^{140}Nd. This effect can be partially reduced if the g.s. correlations are evaluated beyond the RPA.[9]) Further calculations are in progress.

4. Discussion

The two quadrupole forces (p-h and pairing) are very important in determining the energy spectra and the strength distributions. The energy of the 2^+ state decreases from the 2-qp energy to the experimental value for an increasing value of k_0^2. At the same time the B(E2) value increases, while σ(p,t) shows the opposite behaviour. These effects are due to ground state correlations generated by the p-h interaction. These correlations can be viewed microscopically as scattering of quasi-particles across the Fermi surface. The pairing interaction produces another type of correlations, that correspond to $2p$-$2h$ type excitations which enhance the two neutron

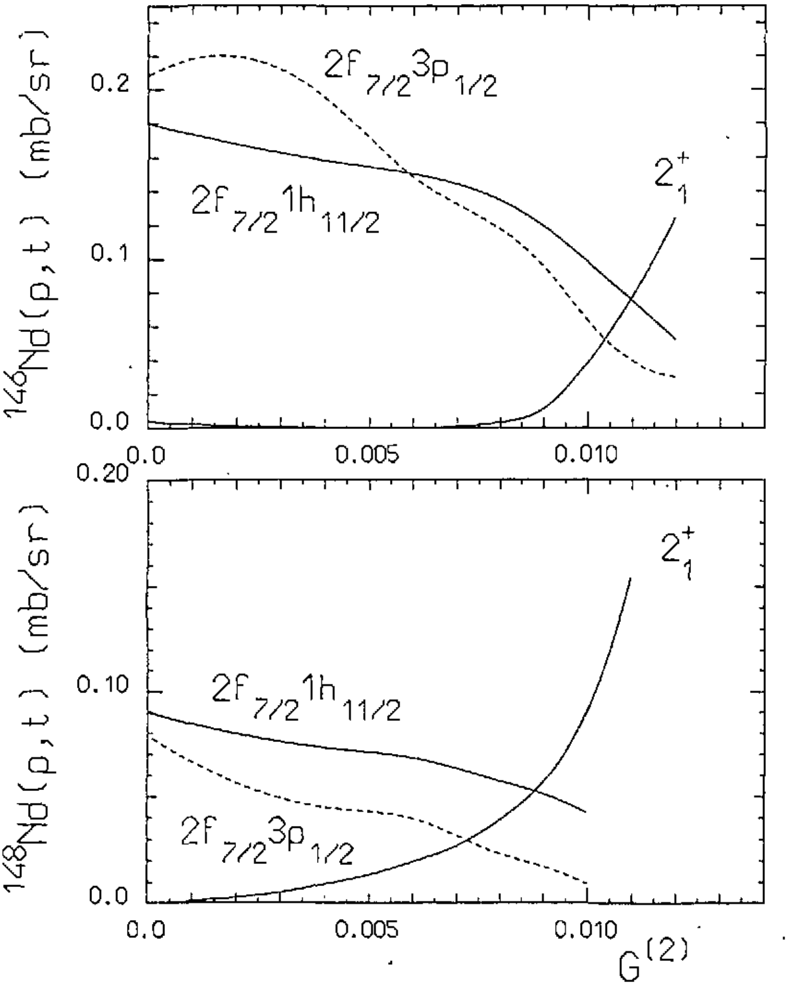

Fig. 5 - The curve 2_1^+ in the upper part displays the $G^{(2)}$ dependence of the (p,t) cross section for the excitation of the first 2^+ state in ^{144}Nd, calculated as a coherent sum of several two-neutron configurations. The same in the lower part for ^{146}Nd. The other curves display the dependence of the contribution coming from pure configurations.

transfer cross sections, while producing destructive coherence in the B(E2) transition probabilities, as shown in the present study. The physical basis for this behaviour is found in the fact that the existence of *p-h* correlations blocks single-particle states which cannot be used by the *2p-2h* type of excitations and viceversa. The total amount of ground states correlations is then a result of this competition. It can be remarked that the increasing trend of the (p,t) cross sections with $G^{(2)}$ is not due to the enhancement of the spectroscopic amplitude of specific configurations (that are instead decreasing, as shown in fig. 5) but to a more constructive interference between the contributions from different configurations.

The enhancement of (p,t) cross sections is therefore originated by a cooperative effect due to g.s. correlations and results to be analogous to that produced by *p-h* correlations in B(E2) values. The best $G^{(2)}$ values (0.009-0.010) obtained in the present study are in a rather good agreement with the value estimated by Soloviev and Sushkov[10]) in the case of deformed nuclei: $G_0^{20} = 0.9k_0^{20} \simeq 0.011$.

We would like to acknowledge the colleagues who have collaborated to the present study: J.A. Bordewijk, M.N. Harakeh, M.A. Hofstee, S.Y. van der Werf, G. Graw, D.Hofer and prof. R. Broglia for fruitful discussions.

5. References

1) M. Pignanelli et al., Nucl. Phys. A559(1993)1
2) A. Arima and F. Iachello, Ann. of Phys. 111(1978)201
3) V.G. Soloviev, Z. Phys. A334(1989)143
4) J. Kern, Phys. Lett. B320(1994)7
5) R.K.J. Sandor et al., Nucl. Phys. A535(1991)669
6) R. Perrino et al., Nucl. Phys. A561(1993)343
7) R.K.J. Sandor et al., Nucl. Phys. A551(1993)378
8) R. Broglia et al., Adv. in Nucl. Phys. 6(1973)287
9) D. Karadjov et al., Phys. Lett. B 306(1993)197
10) V.G. Soloviev and A.V. Sushkov, Z. Phys. A345(1993)155

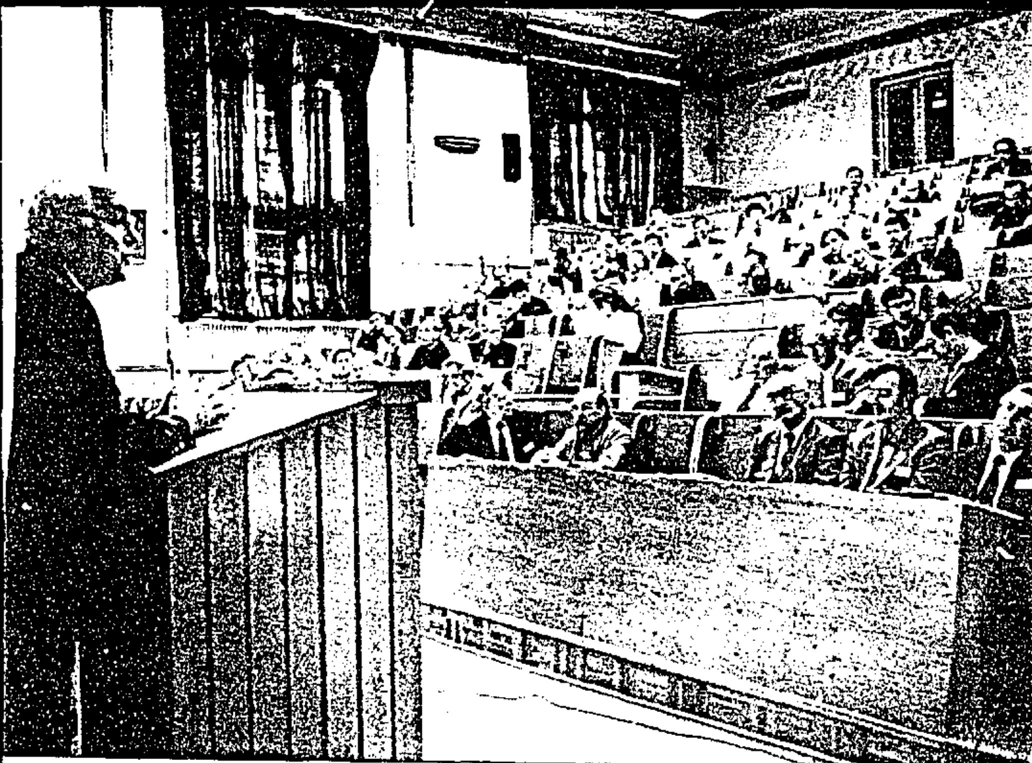

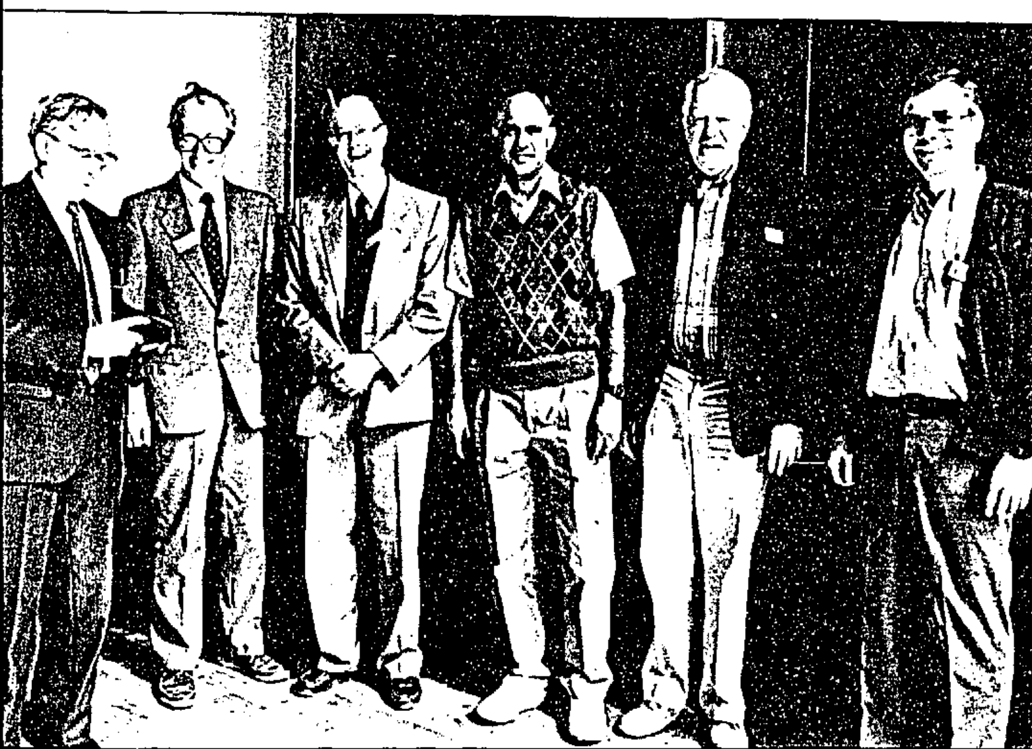

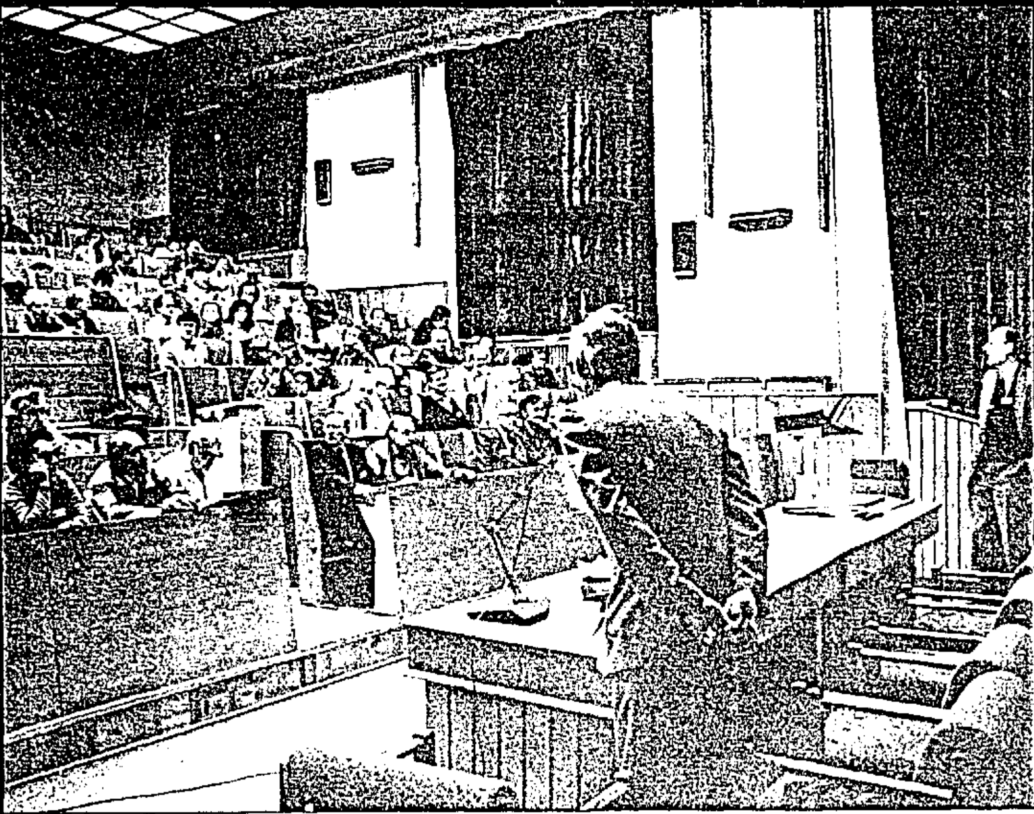

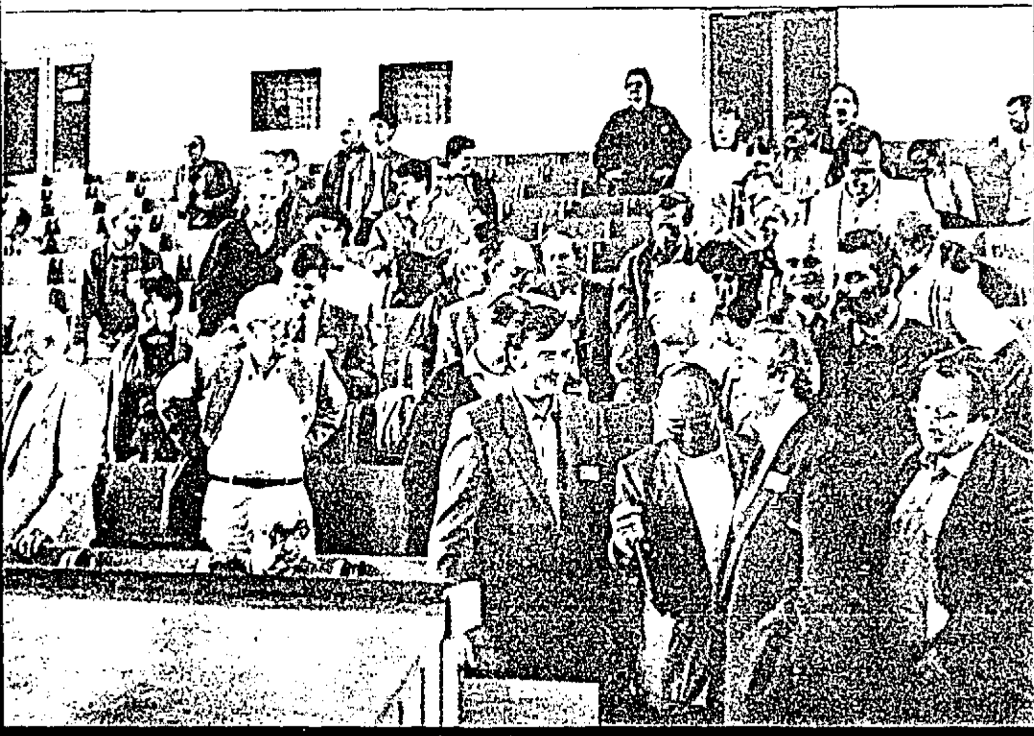

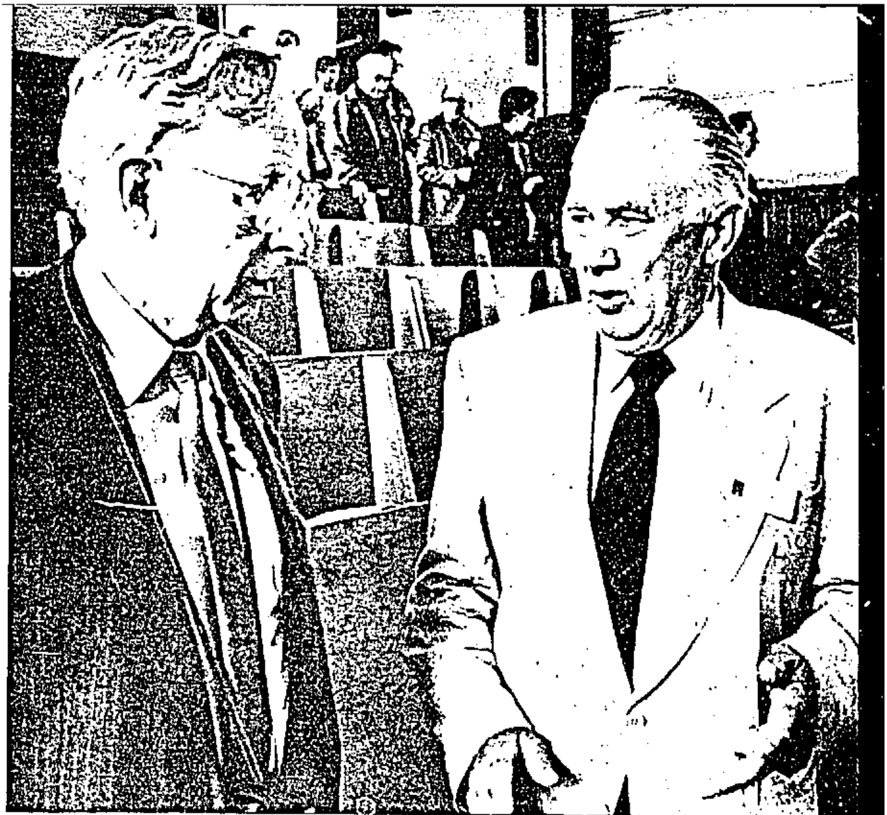

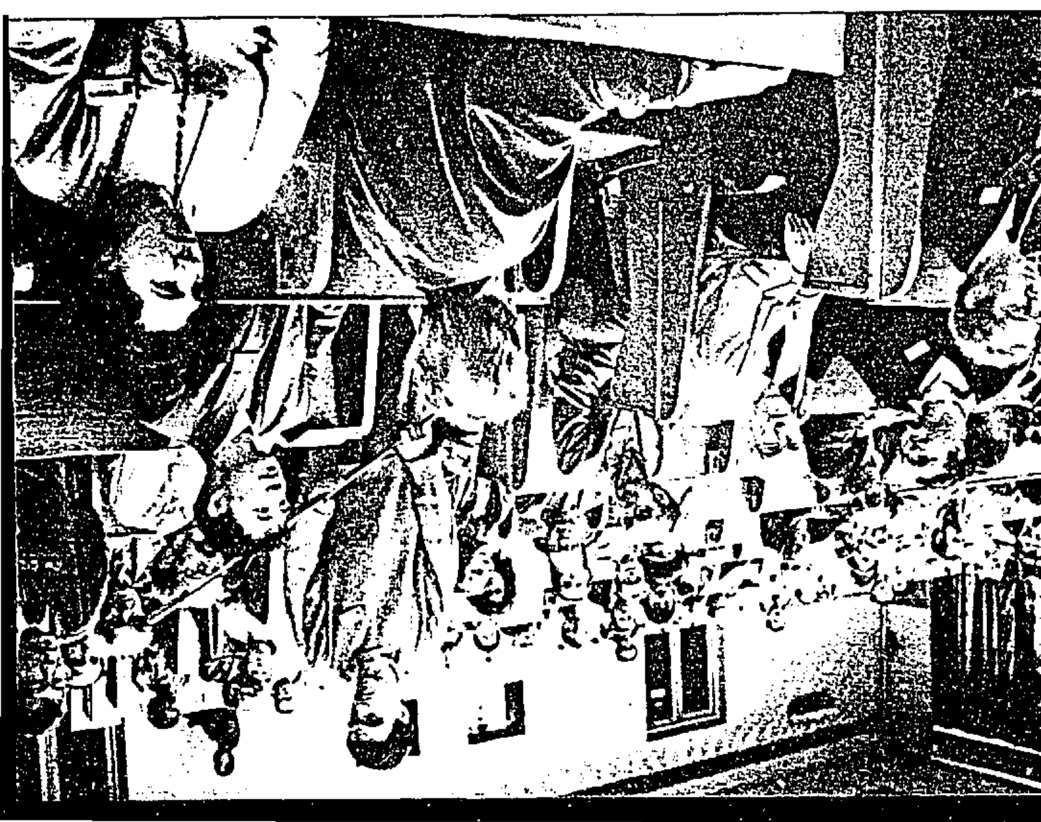

THE n-p INTERACTION IN ODD-ODD DEFORMED NUCLEI*

Richard W. Hoff
Lawrence Livermore National Laboratory
Livermore, California 94550, USA

ABSTRACT

After many years of study and with the inclusion of many forms for the nucleon-nucleon force, the n-p interaction, as manifested in the nuclear structure of odd-odd nuclei, still has not been characterized with sufficient precision to allow satisfactory predictions of unmeasured matrix elements. We have critically surveyed the experimental data and configuration assignments for quasiparticle excitations in odd-odd nuclei of the rare earth region and have derived a set of most reliable values for Gallagher-Moszkowski matrix elements. We find that the empirical matrix elements, when compared with simple zero-range central force calculations, show potentially useful correlations with Δl, the difference in orbital angular momenta of the underlying proton and neutron spherical states. A systematics for predicting GM matrix elements is outlined.

1. Introduction

The n-p interaction in odd-odd deformed nuclei (i.e., those that exhibit quadrupole deformation) has been discussed in a series of papers, beginning with that of Pyatov[1] in 1963. Two of the more comprehensive treatments of this phenomenon are those of Boisson, Piepenbring, and Ogle[2] (hereafter referred to as BPO) and Nosek et al.[3] These authors evaluated experimental data on level properties, i.e. energies and other data that lead to assignment of spins and parities, to the grouping into rotational bands, and to configuration assignments for these bands. From the data, they extracted matrix elements for Gallagher-Moszkowski (GM) splittings and Newby shifts. These matrix elements were then compared with calculations made with various assumptions as to the nature of the interaction between the unpaired nucleons. We will follow the same general procedure in this paper, beginning with a critical evaluation of experimental data. We have tried to identify the most comprehensive and most reliable experimental data on which to base GM splittings in the rare earth region. In a previous paper[4], we performed a similar survey of experimental data for K=0 bands from which Newby shifts are deduced for both the rare-earth and actinide regions of quadrupole deformation. In the latter stage of our present discussion, we present a comparison with calculations made assuming a simple zero-range central force in order to see what patterns emerge in the empirical data.

2. Critical Survey of Experimental Data

The odd-odd nucleus, with its two unpaired nucleons, has the potential for a great variety of quasiparticle excitations, even at low energies. Thus, the level densities observed in these nuclei are higher than for other species. Therefore, it is essential that odd-odd nuclei be probed using spectroscopic techniques that can provide the highest resolution and the highest sensitivity. Neutron-capture gamma-ray spectroscopy, as performed at modern high-flux research reactors at the Institut Laue-Langevin (ILL) and the Brookhaven National Laboratory (BNL), has become the single most important experimental probe for examining the nuclear structure of odd-odd deformed nuclei at low angular momentum. The high precision of the crystal-diffraction gamma-ray spectrometers (GAMS) and the electron spectrometer (BILL; no longer in operation) at the ILL is an essential feature of making the best studies of these nuclei. The averaged resonance capture technique (ARC), where filtered neutron beams are employed (at BNL and in Kiev, currently), is one of the few experimental probes that can promise complete detection of excited levels within a certain range of angular momentum and parity. Thus, it has become a powerful technique that is complementary to thermal-neutron spectroscopy. Another important experimental probe, one that is essential to any comprehensive study of low-energy nuclear structure, is the use of single-nucleon transfer reactions with a modern high-resolution charged-particle spectrometer as exemplified by measurements performed at the Technical University of Munich's (TUM) tandem accelerator. In classifying experimental evidence for rotational bands in the rare earth-region odd-odd nuclei, we find those nuclei studied using all of the experimental probes mentioned here exhibit the greatest reliability.

The results of our survey are shown in Table 1. The data are listed according to the orbitals occupied by each of the unpaired nucleons. In columns (cols.) 7-14 of the table, data for each pair of rotational bands are summarized, including the criteria upon which we have ranked the reliability of the data. Due to limitations on space in this paper, references to the relevant experimental papers for the data summarized in the table are not given. In each case, these data were taken from the most recent survey published in Nuclear Data Sheets, which for the nuclei of Table 1 range in publication date from 1987 to 1994. A summary of all rotational band levels determined experimentally in odd-odd deformed nuclei[5] will be published in 1995. The rank for each matrix element is given in col. 6, with that of the lower spin band listed first. For our purposes, the most reliable data are defined as those matrix elements with rank BB or better.

3. Extraction of Experimental GM Matrix Elements

Once the energies of both bands of a GM pair have been determined, one can extract a value for the GM matrix element, i.e. that part of the band-separation energy that can be ascribed to the residual interaction between the unpaired nucleons, by correcting for other factors that contribute to the observed energy separation. Corrections for the intrinsic rotational energy of bandhead levels are made using the following expression:

$$E_{rot} = \hbar^2/2J\,[I(I+1) - K^2] \tag{1}$$

The matrix elements listed in Table 1 have all been corrected for this energy; thus, this correction does not figure in any of the following discussion. Another common correction is that of allowing for energy shifts due to Coriolis mixing with rotational bands where $\Delta K=1$. Particle-particle couplings can also perturb rotational band energies.[2] Another correction can arise from

THE n-p INTERACTION IN ODD-ODD DEFORMED NUCLEI*

Richard W. Hoff
Lawrence Livermore National Laboratory
Livermore, California 94550, USA

ABSTRACT

After many years of study and with the inclusion of many forms for the nucleon-nucleon force, the n-p interaction, as manifested in the nuclear structure of odd-odd nuclei, still has not been characterized with sufficient precision to allow satisfactory predictions of unmeasured matrix elements. We have critically surveyed the experimental data and configuration assignments for quasiparticle excitations in odd-odd nuclei of the rare earth region and have derived a set of most reliable values for Gallagher-Moszkowski matrix elements. We find that the empirical matrix elements, when compared with simple zero-range central force calculations, show potentially useful correlations with Δl, the difference in orbital angular momenta of the underlying proton and neutron spherical states. A systematics for predicting GM matrix elements is outlined.

1. Introduction

The n-p interaction in odd-odd deformed nuclei (i.e., those that exhibit quadrupole deformation) has been discussed in a series of papers, beginning with that of Pyatov[1] in 1963. Two of the more comprehensive treatments of this phenomenon are those of Boisson, Piepenbring, and Ogle[2] (hereafter referred to as BPO) and Nosek et al.[3] These authors evaluated experimental data on level properties, i.e. energies and other data that lead to assignment of spins and parities, to the grouping into rotational bands, and to configuration assignments for these bands. From the data, they extracted matrix elements for Gallagher-Moszkowski (GM) splittings and Newby shifts. These matrix elements were then compared with calculations made with various assumptions as to the nature of the interaction between the unpaired nucleons. We will follow the same general procedure in this paper, beginning with a critical evaluation of experimental data. We have tried to identify the most comprehensive and most reliable experimental data on which to base GM splittings in the rare earth region. In a previous paper[4], we performed a similar survey of experimental data for K=0 bands from which Newby shifts are deduced for both the rare-earth and actinide regions of quadrupole deformation. In the latter stage of our present discussion, we present a comparison with calculations made assuming a simple zero-range central force in order to see what patterns emerge in the empirical data.

2. Critical Survey of Experimental Data

The odd-odd nucleus, with its two unpaired nucleons, has the potential for a great variety of quasiparticle excitations, even at low energies. Thus, the level densities observed in these nuclei are higher than for other species. Therefore, it is essential that odd-odd nuclei be probed using spectroscopic techniques that can provide the highest resolution and the highest sensitivity. Neutron-capture gamma-ray spectroscopy, as performed at modern high-flux research reactors at the Institut Laue-Langevin (ILL) and the Brookhaven National Laboratory (BNL), has become the single most important experimental probe for examining the nuclear structure of odd-odd deformed nuclei at low angular momentum. The high precision of the crystal-diffraction gamma-ray spectrometers (GAMS) and the electron spectrometer (BILL; no longer in operation) at the ILL is an essential feature of making the best studies of these nuclei. The averaged resonance capture technique (ARC), where filtered neutron beams are employed (at BNL and in Kiev, currently), is one of the few experimental probes that can promise complete detection of excited levels within a certain range of angular momentum and parity. Thus, it has become a powerful technique that is complementary to thermal-neutron spectroscopy. Another important experimental probe, one that is essential to any comprehensive study of low-energy nuclear structure, is the use of single-nucleon transfer reactions with a modern high-resolution charged-particle spectrometer as exemplified by measurements performed at the Technical University of Munich's (TUM) tandem accelerator. In classifying experimental evidence for rotational bands in the rare earth-region odd-odd nuclei, we find those nuclei studied using all of the experimental probes mentioned here exhibit the greatest reliability.

The results of our survey are shown in Table 1. The data are listed according to the orbitals occupied by each of the unpaired nucleons. In columns (cols.) 7-14 of the table, data for each pair of rotational bands are summarized, including the criteria upon which we have ranked the reliability of the data. Due to limitations on space in this paper, references to the relevant experimental papers for the data summarized in the table are not given. In each case, these data were taken from the most recent survey published in Nuclear Data Sheets, which for the nuclei of Table 1 range in publication date from 1987 to 1994. A summary of all rotational band levels determined experimentally in odd-odd deformed nuclei[5] will be published in 1995. The rank for each matrix element is given in col. 6, with that of the lower spin band listed first. For our purposes, the most reliable data are defined as those matrix elements with rank BB or better.

3. Extraction of Experimental GM Matrix Elements

Once the energies of both bands of a GM pair have been determined, one can extract a value for the GM matrix element, i.e. that part of the band-separation energy that can be ascribed to the residual interaction between the unpaired nucleons, by correcting for other factors that contribute to the observed energy separation. Corrections for the intrinsic rotational energy of bandhead levels are made using the following expression:

$$E_{rot} = \hbar^2/2J\ [I(I+1) - K^2] \qquad (1)$$

The matrix elements listed in Table 1 have all been corrected for this energy; thus, this correction does not figure in any of the following discussion. Another common correction is that of allowing for energy shifts due to Coriolis mixing with rotational bands where $\Delta K=1$. Particle-particle couplings can also perturb rotational band energies.[2] Another correction can arise from

Table 1. Gallagher-Moszkowski Matrix Elements

	Proton	Neutron	Orbitals[1]	Nucl	E(GM)exp (keV)	Rank[2]	LOWER SPIN BAND K^π	Energy[3] (keV)	#lvl	Criteria[4]	HIGHER SPIN BAND K^π	Energy[3] (keV)	#lvl	Criteria[4]	E(GM)calc[5]	Exp/Calc
1	3/2+411↑	3/2-521↑	d5f7	158Tb	133.0	CA	0-	110	5	b	3-	0	3	bd	196	0.68
2		3/2-521↑	d5f7	160Tb	124.0	AA	0-	79	5	bdf	3-	0	3	bdf	196	0.63
3		5/2-523↓	d5h9	160Tb	-164.8	AB	1-	64	5	cf	4-	258	2	(f)	-130	1.27
4		5/2+642↑	d5i13	160Tb	92.6	AB	1+	139	4	cf	4+	64	2	cdf	97	0.95
5		7/2+633↑	d5i13	166Ho	191.2	AB	2+	430	4	bcf	5+	264	3	b	147	1.30
6	7/2-523↑	1/2+400↑	h11s1	164Ho	101.0	DD	3-	925	2		4-	833	1		107	0.94
7		3/2+402↓	h11d3	164Ho	-88.0	DD	2-	620	2		5-	733	1		-126	0.70
8		3/2-521↑	h11d3	164Ho	175.0	CC	2+	486	4		5+	343	3	b		
9		5/2-523↓	h11h9	164Ho	-148.0	AC	1+	0	5	df	6+	191	2		-322	0.46
10		7/2+633↑	h11i13	166Ho	80.4	AA	0-	0	8	bd	7-	6	3	bdf	236	0.34
11		1/2-521↓	h11f5	166Ho	-172.1	AA	3+	191	5	abcdf	4+	372	3	abcdf	-169	1.02
12		5/2-512↑	h11f7	166Ho	178.0	AB	1+	426	5	cf	6+	295	2	b	103	1.73
13	1/2+411↓	7/2+633↑	d3i13	168Tm	-143.7	BB	3+	0	4	bf	4+	148	4	f	-148	0.97
14		7/2+633↑	d3i13	170Tm	-163.8	AB	3+	183	4	abcdf	4+	355	3	abcf	-151	1.08
15		5/2-512↑	d3f7	170Tm	-230.7	AA	2-	204	4	bcdf	3-	447	3	bcf	-330	0.70
16		1/2-521↓	d3f5	168Tm	194.4	CC	0-	167	4	d	1-	3	4	df	198	0.98
17		1/2-521↓	d3f5	170Tm	191.7	AA	0-	150	6	abcdf	1-	0	7	abdf	198	0.97
18		3/2-521↑	d3f7	170Tm	-194.6	BB	1-	649	3	acf	2-	854	2	acf	-214	0.91
19		7/2-514↓	d3h9	176Lu	120.0	AB	3-	843	3	abf	4-	723	3	abf	286	0.42
20	1/2-541↓	5/2-512↑	h9f7	174Lu	-180.0	BD	2+	227	13	a	3+	414	1	a		
21	7/2+404↓	1/2-521↓	g7f5	174Lu	80.0	AA	3-	433	5	abf	4-	365	5	abcdf	80	1.00
22		5/2-512↑	g7f7	174Lu	-117.8	AA	1-	0	11	bf	6-	171	7	bcdf	-127	0.93
23		5/2-512↑	g7f7	176Lu	-75.9	AB	1-	638	5	bcf	6-	766	2	bf	-146	0.52
24		7/2+633↑	g7i13	174Lu	-111.0	AA	0+	281	9	b(c)f	7+	431	7	b(c)f	-152	0.73
25		9/2+624↑	g7i13	176Lu	-12.0	AA	1+	339	7	f	8+	425	4	f	-192	0.06
26		7/2-514↓	g7h9	176Lu	246.4	AA	0-	237	8	bcdf	7-	0	4	bcf	257	0.96
27		1/2-510↑	g7p3	176Lu	-117.3	AB	3-	658	4	abf	4-	788	2	ab	-119	0.99

29	7/2+404↓	3/2-512↓	g7f5	182Ta	96.8	AA	2-	270	5	b(c)f	5-	173	2		197	0.49
30		7/2-503↑	g7f7	182Ta	-126.3	AD	0-	583	6	b(c)f	7-	776	1	b	-293	0.43
31	9/2-514↑	5/2-512↑	h11f7	174Lu	168.0	BC	2+	635	5	bf	7+	531	3	b	218	0.77
32		7/2-514↓	h11h9	176Lu	-244.0	AB	1+	194	7	df	8+	488	3	bf	-413	0.59
33		1/2-510↑	h11p3	182Ta	147.7	AA	4+	150	4	a(c)f	5+	16	3	acdf	194	0.76
34	5/2+402↑	5/2-512↑	d5f7	174Lu	115.3	DC	0-	554	2		5-	457	4	f	235	0.49
35		7/2-514↓	d5h9	176Lu	-117.8	AB	1-	387	6	bcf	6-	564	3	bf	-153	0.77
36		1/2-510↑	d5p3	186Re	120.0	AA	2-	211	4	acf	3-	99	4	adf	115	1.04
37		1/2-510↑	d5p3	188Re	100.0	BB	2-	257	3	bc	3-	169	3	cf	115	0.87
38		1/2-510↑	d5p3	182Ta	114.9	BA	2-	648	4	a(c)f	3-	547	3	a(c)f	115	1.00
39		3/2-512↓	d5f5	186Re	-163.0	AB	1-	0	5	df	4-	174	3	cf	-200	0.82
40		3/2-512↓	d5f5	188Re	-149.0	AC	1-	0	5	bdf	4-	183	2	f	-200	0.75
41		7/2-503↑	d5f7	186Re	208.0	AC	1-	317	5	cf	6-	186	1		484	0.43
42		7/2-503↑	d5f7	188Re	209.0	BB	1-	291	3	c	6-	172	1		484	0.43

Footnotes, Table 1:

1) An orbital designation, e.g. d5f7, that denotes a $d_{5/2}$ proton and an $f_{7/2}$ neutron.

2) A letter rank is given to each band with the rank of the lower spin band listed first, according to the following scheme:
A - The data are complete enough to allow the configuration assignment to be made with a high level of confidence; B - The data are reasonably complete and the configuration assignment seems logical and rather certain; C - The data lack certain items that would allow greater confidence in the configuration assignment; D - The data are seriously lacking; configuration assignments must be considered extremely tentative.

3) Energy of the I = K level in the band.

4) Criteria for classifying experimental data on rotational bands as to reliability: a) For this band pair, ΔK = 1(or 2); strong linking transitions between the bands are observed; b) The configuration includes orbitals receiving major single-nucleon transfer-reaction strength; in the case of (d,p) and (d,t) reactions, such strength has been observed empirically in odd-mass nuclei; c) Levels in the rotational band are well-defined by depopulating gamma rays of measured multipolarity; the pattern of gamma-ray depopulation is strongly indicative of the assigned configuration; e) The rotational band occurs at such low excitation energy that assignment of these levels to some other configuration is extremely unlikely; f) Rotational spacings are similar in the two bands of the GM pair and show agreement with modeled rotational parameters.

5) Calculated Gallagher-Moszkowski matrix elements assuming a zero-range central force.

the coupling of the unpaired nucleons with the vibrations of the even-even core via the quasiparticle-phonon interaction. This interaction was taken into account explicitly in recent calculations of the microscopic structure of intrinsic states in five odd-odd holmium isotopes.[6] As might be expected, the main strength of the gamma vibrations is concentrated in intrinsic states with energies greater than 1 MeV. An exception to this observation occurs in ^{166}Ho, the Ho isotope best understood experimentally, where a GM pair of rotational bands with appreciable vibrational components (as much as 26%) are predicted to occur at 260 and 525 keV. Experimental evidence for the higher energy band of this pair has been reported. It is evident that the best understanding of level structure in these nuclei will come by comparing empirical data with fully microscopic calculations such as those made by Kvasil et al.[6] Until the results of such calculations are available for a wider range of nuclei, much information regarding the n-p interaction matrix elements can be obtained by making simple corrections to band energies for the effects already discussed, particularly if the corrections lead to relatively minor revisions in these energies.

One form of evidence for Coriolis interactions between bands is the perturbation of the band's rotational parameters that is observed empirically in several nuclei. Rotational parameters of bands in these rare earth nuclei show a general increase with mass number, perhaps due to the lessening of deformation as one reaches the limits of the region. Beyond this general trend, certain bands exhibit perturbed parameters that are somewhat smaller or greater than average. For example, rotational parameters of most of those configurations that include an $i_{13/2}$ neutron have lower values than the others. In certain instances two interacting bands can lie very close to each other and, because the major part of the observed perturbations arise from this single interaction, their energies can be corrected rather easily. An example of this instance occurs in ^{182}Ta for the bands that make up the π7/2[404]ν1/2[510] and π7/2[404]ν3/2[512] GM pairs. The authors of an experimental paper[7] on ^{182}Ta have calculated the extent of this Coriolis interaction. The matrix elements listed in Table 1 for ^{182}Ta (numbers 28 and 29) have been corrected for this specific instance of band mixing with reductions of 15% and 32%, respectively.

In a 1989 paper, Jain et al.[8] published the results of calculations of the Coriolis mixing among a broad range of bands in ^{182}Ta, ^{168}Tm, and ^{176}Lu, i.e. all experimentally known bands and many others with estimated energies were included. These calculations provide band energies corrected for shifts due to Coriolis mixing. On this basis, the remaining ^{182}Ta matrix elements in Table 1, numbers 30, 33, and 38, were corrected by +5%, -7%, and +2%, respectively. In ^{168}Tm, the calculated corrections due to Coriolis mixing resulted in small increases in the matrix elements in Table 1, namely +3% and +1% for numbers 13 and 16, respectively. In ^{176}Lu, Jain et al. calculated small corrections for three of the GM band pairs listed in Table 1 (2% or less for entries 19, 26, and 35). Since that time, two more comprehensive experimental papers[9,10] have been published on the level scheme of ^{176}Lu that exchange configuration assignments of two low-lying 1^+ bands. To a first approximation, the mixing calculations of Jain et al. still apply. On this basis, the magnitude of matrix element number 32 shows an increase of 11% after correction for this mixing. In Table 1, we list Coriolis-corrected values for all of these ^{176}Lu matrix elements. A special case in ^{176}Lu is the matrix element for the π7/2 [404]ν9/2[624] GM pair. The uncorrected empirical value of this matrix element is -12 kev, which represents a very major deviation from theoretical calculations. This problem is especially magnified by the aforementioned change in configuration assignments made by Klay et al.[9] for the low-lying 1^+ bands. It is our estimate that Coriolis effects alone cannot explain the deviation between experiment and theory for this matrix element. None of the remaining matrix elements in Table 1 have been corrected for Coriolis mixing due, in part, to the lack of other calculations. It should be kept in mind that some of the deviations from theory that will be discussed later may very well arise from this omission.

4. Calculation of Theoretical GM Matrix Elements

The n-p interaction between unpaired nucleons in odd-odd deformed nuclei becomes manifest in two kinds of observables: 1) the Gallagher-Moszowski energy splitting of rotational bands with identical Nilsson quantum numbers, but with opposite relative orientation of the projections of odd-nucleon angular momentum, and 2) the Newby shift, which is exhibited by K=0 bands wherein the levels with odd angular momenta are systemically shifted in energy from those with even angular momenta. The matrix elements for these energy splittings and energy shifts can be expressed, as follows:

$$E(GM) = \langle \chi_p^k \chi_n^{-k} \; |V_{np}| \; \chi_p^k \chi_n^{-k} \rangle - \langle \chi_p^k \chi_n^k \; |V_{np}| \; \chi_p^k \chi_n^k \rangle \tag{2}$$

and
$$E(N) = \langle \chi_p^k \chi_n^{-k} \; |V_{np}| \; \chi_p^{-k} \chi_n^k \rangle \tag{3}$$

Here, the χ^k's are the intrinsic single-particle wave functions (not explicit in this notation is that k may take different values for the proton and the neutron) and V_{np} denotes an effective n-p interaction.

In the earliest theoretical treatments of the n-p interaction, a central force with zero range (ZRCF) was assumed.[1,11] The calculated GM matrix elements showed some correlation with empirical data, but not with very great precision. In subsequent studies, more elaborate forms for the n-p interaction were introduced. Several authors have studied this problem since the original work. We have discussed the evolving description of this n-p force in some detail in previous papers.[4,12,13] In brief form, we summarize certain aspects of this evolution, as follows: 1) The ZRCF (with its one adjustable parameter) and the finite range central force (FRCF; with three adjustable parameters) produce rather similar results when comparing calculations with experiment. 2) Those authors who attempted to fit experimental data for both the GM and Newby matrix elements with a single description of the n-p force have found it necessary to combine a tensor force with the FRCF. Otherwise, these two types of data can only be fit separately by FRCF's that have widely differing parameters. 3) In more recent studies,[2,3] other possible features of an n-p force have been employed in attempting to improve the fit to empirical data, e.g. polarizing the intrinsic spin operators to allow for core polarization, extending the description of the force by employing both short- and long-range, as well as tensor, components, while also necessarily increasing the number of adjustable parameters. Whereas one of the more complex forms, i.e. that described by Boisson et al.[2] in 1975 as their "CPTL" force (with 7 adjustable parameters), produced a significantly lower root-mean-squared deviation for their data set, we have found, in most cases, that this force did not adequately predict values for most of the experimental GM matrix elements reported since 1975.[13]

In a very recent paper, Nosek et al.,[3] have analyzed the problem of characterizing the n-p force in much the same style as that of BPO,[2] beginning with a ZRCF and progressing to more complex forms, but making use of a much larger data base of GM and Newby matrix elements than were available earlier. They examined 162 empirical E(GM) values from both the rare earth and actinide regions. They included the same variations of the n-p force as before, except a long range component. Values for the force parameters were determined by minimizing the sum of the squared differences between calculation and experiment (SSD). Even when allowing 7 adjustable parameters, they were able to reduce the SSD by only 20-25%, as compared with the ZRCF calculation where a single free parameter is used to scale the calculations. In this study, several of the force parameters proved to be insensitive to the SSD and, thus, were determined only imprecisely by the fitting exercise.

In the present work, we have employed a simple ZRCF formulation and have used basic harmonic oscillator (h.o.) or Nilsson wave functions to calculate GM matrix elements.[14] Parameters (κ and μ) that describe the h.o. force were taken from the formulation of Bengtsson and Ragnarsson.[15] The calculated deformation for each nucleus in its ground state was used in determining the matrix element. Due to the (x-y) algebraic nature of the GM matrix element, we have found that rather small values (<80 keV) cannot be calculated with good precision, i.e. the results tend to be strongly dependent on the specific choice of values for κ and μ and/or the assumed nuclear deformation. For example, this problem occurred when calculating the $\pi 1/2[541]\nu 5/2[512]$ matrix element. The larger calculated matrix elements (the majority of the cases in this paper) showed good stability with minor changes of the h.o. or deformation parameters. Surprisingly, this limitation on calculating small matrix elements has not been mentioned in previous studies.

5. GM Matrix Elements: Comparison of Experiment with Theory

The comparison of our selected data set with calculations, in the form of ratios, experimental to calculated, is listed in the last column of Table I and is shown in Fig. 1. The calculations were scaled by making the best fit to the majority of the ratios shown in the figure rather than by minimizing the SSD. We have employed a value for the scaling factor (αW) of 1.2 MeV, which is about 50% higher than those determined previously.[2,3] The data in Fig. 1 are plotted against $\Delta\ell$, i.e. the difference in ℓ values for the spherical states from which the proton and neutron orbitals arise. For matrix elements with $\Delta\ell \geq 2$, one sees that most of the ratios lie between limits of 0.7 and 1.3. The calculated matrix elements for this group all lie in the range of 100-200 keV. A few of the members of this set lie outside the ±30% limits. The very low value, a $g_{7/2}i_{13/2}$ GM pair, occurs in ^{176}Lu. We suspect that configuration mixing has not yet been adequately taken into account here. There are two GM pairs of 1^+ and 8^+ bands that lie close to each other in ^{176}Lu. The very high ratio, an $h_{11/2}f_{7/2}$ GM pair that exists in ^{166}Ho and includes the ground-state band, is harder to understand since one doesn't expect strong band mixing.

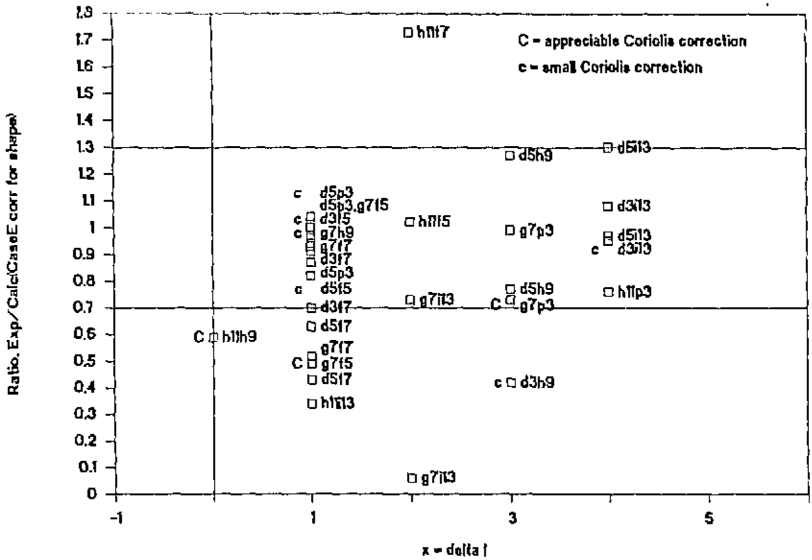

Figure 1. Systematic behavior of experimental to calculated ratios for Gallagher-Moszkowski matrix elements from odd-odd nuclei in the rare earth region. The ratios are plotted against $\Delta\ell$, the difference in ℓ value of the spherical states from which the proton and neutron orbitals arise (see data labels; each number equals 2j).

It can be seen in Fig. 1 that the data points for the $\Delta\ell$ = 1(or 0) matrix elements show somewhat greater spreading than the others (if one neglects the highest and lowest ratios that occur for $\Delta\ell$ = 2). This behavior is more difficult to interpret. The $\Delta\ell$ = 1(or 0) ratios are shown plotted against absolute values of calculated E(GM) in Fig. 2. There is an obvious trend of decreasing ratios with increasing calculational value; the data points that show the best agreement with calculation occur when the calculated E(GM)'s are in the range 100-250 keV, although several others in this range deviate markedly in the direction of lower ratios. The observed ratios fall off rapidly when the calculated E(GM)'s are greater than 300 keV. The empirical matrix elements appear to exhibit considerable damping for orbitals with the greatest overlap.

In spite of the imperfect agreement with theory for many of the data points shown in the two figures, we have arrived at a crude systematics for the behavior of empirical E(GM) matrix elements in the rare earth region. This is based on the following observations: a) If $\Delta\ell \geq 2$, the experimental matrix element is likely to agree with calculation (within the range, exp/calc = 0.7 to 1.3); b) If $\Delta\ell$ = 1(or 0), agreement with calculation is less likely (all of the data in this set that

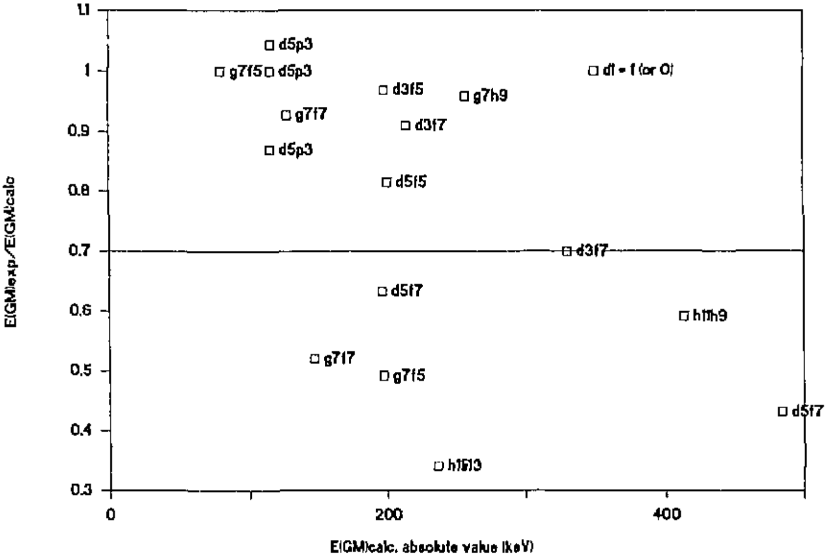

Figure 2. Gallagher-Moszkowski data ratios for $\Delta \ell = 1$(or 0) configurations plotted against calculated values of the GM matrix element.

deviate have ratios less than 0.7); c) When the calculated E(GM) $\geq$ 200 keV and $\Delta \ell = 1$(or 0), it is quite likely that the observed ratio will be considerably less than 1.0. These observation provide the first systematic scheme with which to predict unmeasured matrix elements. Combining this tool with the previously recognized ability to model two-quasiparticle excitations in odd-odd deformed nuclei (before turning on the n-p residual interaction) allows one to calculate predicted level schemes with greater precision than before. Preliminary checks have shown similar behavior for the matrix elements in the actinide region. Returning to the entries in Table I that were ranked as less reliable and do not appear in Figs. 1 or 2, we find these data follow the systematics listed above. The ratios for $\Delta \ell \geq 2$ matrix elements lie within the 0.7 to 1.3 range and all but one of the $\Delta \ell = 1$(or 0) ratios fall below 0.7.

6. Acknowledgments

It is a pleasure to thank the following persons for helpful discussions: at Banaras Hindu University, India, P.C. Sood; at Florida State University, R.K. Sheline; at Charles University, Prague, J. Kvasil; at the University of Roorkee, India, A.K. Jain.

7. References

* Work performed under the auspices of the U.S. Department of Energy by the Lawrence Livermore National Laboratory under contract W-7405-ENG-48.

1. N.I. Pyatov, Bull. Acad. Sci. USSR, Phys. Ser. **27**, 1409 (1963); N.I.Pyatov and A.S. Chernyshev, Bull. Acad. Sci. USSR, Phys. Ser. **28**, 1073 (1964).

2. J.P.Boisson, R. Piepenbring, and W. Ogle, Phys. Rpts. **26**, 99 (1976).

3. D. Nosek, J. Kvasil, R.K. Sheline, P.C. Sood, and J. Noskova, accepted for publication in Intl. J. Mod. Phys. E (1994).

4. R.W. Hoff, Proc. Intl. Conf. on Selected Topics in Nuclear Structure, Dubna, June 1989 (JINR report, 1989), p. 66.

5. R.K. Sheline et al., to be published in At. Data and Nucl. Data Tables (1995).

6. J. Kvasil, R.K. Sheline, V.O. Nesterenko, I. Hrivncova, D. Nosek, Z. Phys. **A343**, 145(1992).

7. C.W. Reich, R.G. Helmer, and R.C. Greenwood, Nucl. Phys. **A168**, 487(1971).

8. A.K. Jain, J. Kvasil, R.K. Sheline, and R.W. Hoff, Phys. Rev. **C40**, 432 (1989).

9. N. Klay et al., Phys. Rev. **C44**, 2801 (1991).

10. K.T. Lesko, E.B. Norman, R-M. Larimer, B. Sur, and C.B. Beausang, Phys. Rev. **C44**, 2850 (1991).

11. N.D. Newby, Phys. Rev. **125**, 2063 (1962).

12. R.W. Hoff, A.K. Jain, J. Kvasil, P.C. Sood, and R.K. Sheline, *Exotic Nuclear Spectroscopy*, ed. W.C. McHarris (Plenum Press, New York, 1990), p. 413.

13. R.W.Hoff, Proc. 8th Intl. Symp. on Capture Gamma-Ray Spectroscopy and Related Topics, ed. J. Kern (World Scientific, Singapore, 1994), p. 132.

14. G.L. Struble, J. Kern, and R.K. Sheline, Phys. Rev. **137**, B772 (1965); H.T. Motz et al., Phys. Rev. **155**, 1265 (1967).

15. T. Bengtsson and I. Ragnarsson, Nucl. Phys. **A436**, 14 (1985).

OCTUPOLE SHAPES IN HEAVY NUCLEI

Irshad Ahmad
*Physics Division, Argonne National Laboratory, 9700 South Cass Avenue
Argonne, Illinois 60439, USA*

ABSTRACT

Theoretical calculations and measurements show the presence of strong octupole correlations in the ground states and low-lying states of odd-mass and odd-odd nuclei in the Ra-Pa region. Evidence for octupole correlations is provided by the observation of parity doublets and reductions in M1 matrix elements, decoupling parameters, and Coriolis matrix elements involving high-j states. Enhancement of E1 transition rates has also been observed for some of the octupole deformed nuclei. The most convincing argument for octupole deformation is provided by the similarities of the reduced alpha decay rates to the two members of parity doublets.

1. Introduction

Soon after the collective model [1,2] of the nucleus was established, low-lying K = 0 rotational bands with spin-parity sequence 1^-, 3^-, 5^- .... were identified [3,4] in even-even Ra and Th nuclei in high-resolution alpha spectroscopic measurements. Since the energies (~300 keV) of these bands were much lower than the energies of the two-quasi-particle states (~1.0 MeV), these bands were interpreted as octupole vibrations about a spheroidal equilibrium shape. Ever since the discovery of the octupole vibrations, suggestions have been made [5,6] concerning the possibility of permanent octupole deformation in nuclei.

The octupole vibration or octupole deformation in nuclei is produced by the long-range octupole-octupole interaction between nucleons. The octupole correlations depend on the matrix elements of Y_3^0 between single-particle states with $\Delta j = \Delta \ell = 3$ near the Fermi surface and the spacings between them. Calculations of shell model states show that for nuclei with Z~88, the Fermi surface lies between the $f_{7/2}$ and $i_{13/2}$ orbitals and for N~134 nuclei, the Fermi surface lies between the $g_{9/2}$ and $j_{15/2}$ states. Since nuclei with these nucleon numbers are deformed, the maximum octupole deformation will be spread over several nucleon numbers. Figure 1 shows the dependence of octupole collectivity on neutron number. The excitation energy of the K,I^π = 0,1^- state is decreasing with the decrease in the neutron number and becomes the lowest at N=136, suggesting maximum octupole correlations in ^{226}Th. The hindrance factors for the alpha decays to Th nuclei are also shown in the figure and these correlate nicely with the octupole collectivity.

Calculations [7] show that the gain in the binding energy due to octupole deformation is much smaller (~1.0 MeV) than the gain in the binding energy (~10 MeV) when a spherical nucleus becomes quadrupole deformed. The amount of octupole correlations in nuclei can be estimated from the spacings of positive and negative parity levels. The shapes and the potential energy diagrams [8-10]

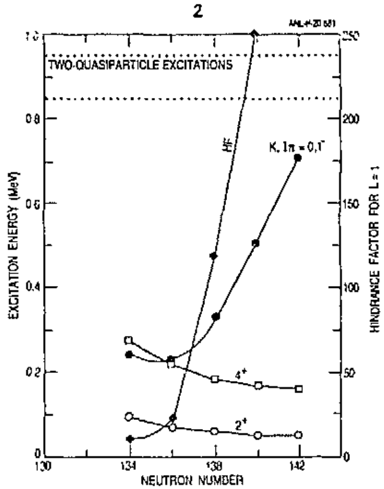

Fig. 1. Excitation energies of low-lying states in even-even Th isotopes. Also shown are α-decay hindrance factors to the $K,I^{\pi} = 0,1^{-}$ states in Th.

associated with them are shown in Fig. 2. The situation in Fig. 2a, which applies to heavy actinides, occurs when the nucleus has a spheroidal equilibrium shape in the ground state and has a $K^{\pi} = 0^{-}$ vibrational band at ~1.0 MeV. The other limit (Fig. 2c) is achieved when the nucleus has β_3 deformation in its ground state and there is an infinite barrier between the reflection asymmetric

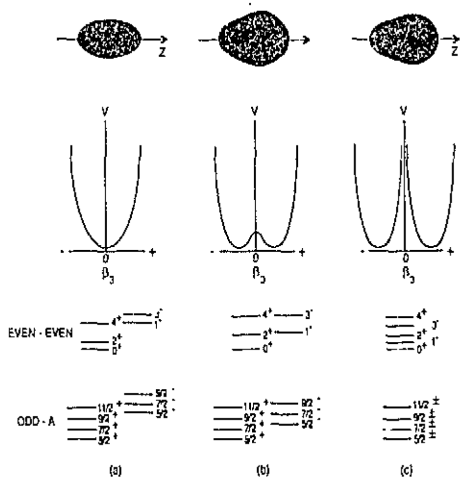

Fig. 2. Plots of potential energy against β_3 deformation and level spectra for three axially symmetric shapes. The left panel represents a rigid reflection symmetric spheroidal nucleus. The right panel shows a rigid pear-shaped nucleus, which is reflection asymmetric. The middle panel shows a soft pear-shaped nucleus with β_2 ~0.15 and β_3 ~0.09.

shape and its mirror image. Such a nucleus has permanent octupole deformation and is completely stable against a tunneling transition to its mirror image. The rotational levels of these nuclei are expected to be quite similar to those of well studied levels of asymmetric molecules. The third possible shape, displayed in Fig. 2b, is intermediate between these two limits, where a finite barrier exists between the reflection asymmetric shape and its mirror image and tunneling motion is possible between these two shapes. The rotational level sequences for these three shapes are included in Fig. 2.

Unlike quadrupole deformation, which can be deduced from measured quadrupole moments, octupole deformation is difficult to determine from direct measurements. In general, level sequences of rotational bands provide evidence for octupole deformation. The signature of octupole deformation in even-even nuclei is the presence of a rotational band of interleaved positive and negative parity levels. In odd-mass and odd-odd nuclei, the signature of octupole deformation is a parity doublet. A parity doublet is defined as a pair of states with the same spin, opposite parities, and a large B(E3) value between them. Experimentally, properties characteristic of large octupole-octupole correlations were discovered soon after their prediction in both odd-mass nuclei at low spins [11,12] and in even-even nuclei at high spins [13,14]. These include appropriate energy level sequences, enhanced E1 transition rates, and enhancement in alpha decay rates to opposite parity bands in the daughter nuclei. In the present article we will discuss experimental data which provide evidence for large octupole correlations in the ground and low-lying states of odd-mass and odd-odd nuclei in the Ra-Pa region.

2. Theoretical Development

The earliest calculations on the single particle states for actinide nuclei with octupole deformation were carried out by Chasman [15] and Leander and Sheline [16]. The presence of large octupole correlations was indicated by earlier calculations which provided a better explanation [17] of the excited 0^+ state in ^{234}U and improved [18] the agreement between measured and calculated atomic masses for nuclei in A~222 region. The calculation in ref. 15 used microscopic many-body approach where the Hamiltonian included quadrupole-quadrupole and octupole-octupole interaction. These calculations predicted parity doublets in several odd-proton and odd-neutron nuclei which have larger B(E3) values than the values encountered in the neighboring even-even nuclei. The single-particle spectra of odd-proton nuclei calculated in ref. 15 are displayed in Fig. 3.

The method of ref. 16 was a Nilsson-Strutinsky type calculation where the potential included β_3 deformation. It was found that the inclusion of $\beta_3 = 0.09$ in the potential reproduced most of the observed properties of octupole deformed nuclei. In this model all doublets should have the same β_3 deformation and the two members of the doublets should have equal matrix elements with appropriate signs. On the other hand, in the microscopic model different doublets can have different β_3 values, as shown in Fig. 3, and also there is no constraint on the matrix elements. Recently, shell correction type calculations with a Woods-Saxon average potential [19] have been carried out but these do not provide any better agreement with experimental data.

Some of the properties of the octupole deformed nuclei have also been explained by a multiphonon octupole model [20] which uses axially symmetric equilibrium shape.

ANL-P-20,880

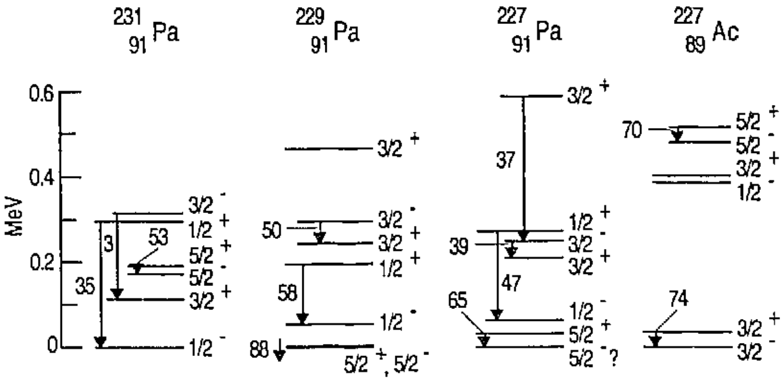

Fig. 3. Low-lying proton single-particle states calculated with a microscopic many-body approach [15]. States are denoted by K^π quantum numbers. The numbers beside the arrows represent intrinsic B(E3) values.

3. Experimental Evidence

As pointed out in the previous section, the signature of octupole deformation in even-even nuclei is the presence of the ground rotational band with level sequence 0^+, 1^-, 2^+, 3^-, ... No nucleus in the periodic table has been observed with this level sequence indicating that no even-even nucleus is octupole deformed in its ground state. However, the energy of the $K,I^\pi = 0,1^-$ state in some Ra and Th nuclei becomes very low (~0.25 MeV) suggesting large octupole-octupole correlations. Experimental data and calculations show that the octupole correlation may increase when an odd particle is added to these even-even nuclei or the even-even nucleus undergoes rotation. In the following sections we present experimental evidence for large octupole octupole correlations in odd-mass and odd-odd Ra, Ac and Pa nuclei. Additional details on octupole deformation can be found in ref. 21.

3.1. Energy Levels

In the fifties and sixties, large amount of information was gathered on energy levels of odd-mass Ra, Ac, Th and Pa nuclei but the observed levels could not be understood in terms of the Nilsson model of the axially symmetric nucleus which was extremely successful in explaining the structure of heavier actinide nuclei. Inclusion of octupole deformation in the potential changed the ordering of Nilsson single particle states and provided a natural explanation of the observed ground state spins [22]. The level structures of ^{223}Ra [23], ^{225}Ra [24-27], ^{223}Ac [28,29], ^{225}Ac [30,31], ^{227}Ac [12,32], ^{229}Pa [11,33] and ^{224}Ac [34,35] are found to be in better agreement with the results of calculations using octupole deformation in the potential than the results of a reflection symmetric model.

3.2. Decoupling parameter

The K = 1/2 bands arising from $i_{13/2}$ and $j_{15/2}$ orbitals have very large decoupling parameters, *a*. The 1/2 proton orbital in ^{227}Ac is expected to be predominantly $1/2^+$[660] configuration with a = ~6.0 and the $1/2^-$ neutron state in Ra isotopes are expected to have predominantly $1/2^-$[770] single-particle component with a = ~7.0. Experimental level energies give much smaller values of *a*. This can be understood in terms of the mixing of these states with opposite parity low-*j* states through the octupole term. As the data in table 1 show, the experimental values are in much better agreement with the calculations using a reflection asymmetric shape (with β_3 ~0.1) than the values calculated with a reflection symmetric model.

Table 1. Decoupling parameter

Nucleus	State	Decoupling parameter Experimental	Theory (β_3=0)	Theory (β_3=0.1)	Theory (Microscopic)
^{227}Ac	$1/2^-$	-2.01	-1.8	-3.0	-1.75
	$1/2^+$	+4.56	+5.9	+3.0	+4.95
^{225}Ra	$1/2^+$	+1.54	-0.68 (for $1/2^+$[631])	+2.5	---
			-4.5 (FOR $1/2^+$[640])		
		-2.59	-7.79 (FOR $1/2^-$[770])	-2.5	---
^{223}Ra	$1/2^+$	+1.35			
		-2.00			

3.3. Coriolis matrix element

It is well known that single-particle states arising from the proton $i_{13/2}$ shell state and the neutron $j_{15/2}$ shell state have large Coriolis matrix elements. The matrix elements between single-particle states have been calculated for axially symmetric actinide nuclei [36]. These matrix elements are reduced because of the pair occupation probabilities. The experimental energies of levels in bands in ^{245}Am [37,38] and ^{225}Ac, which originate from the $i_{13/2}$ shell orbit are displayed in Fig. 4. Favored alpha transition proceeds from the $7/2^+$[633] ground state of ^{249}Bk to the 327-keV level in ^{245}Am with a hindrance factor of 1.4. The mixing of the $7/2^+$[633] state with the I = 7/2 member of the $5/2^+$[642] band increases the alpha decay rate to the 19.2-keV level. Similarly, Coriolis mixing enhances the alpha decay rate to the I=5/2 member of the $3/2^+$[651] band. The spacing between the interacting levels in ^{245}Am is much larger (300 keV) than the spacing of 100 keV in ^{225}Ac. The fact that the relative alpha rates are larger in ^{245}Am than in ^{225}Ac and the lower band is more compressed in ^{245}Am than in ^{225}Ac clearly shows that the Coriolis matrix element is smaller in ^{225}Ac than in ^{245}Am. As shown in table 2, the deduced Coriolis matrix elements are in better agreement with the value calculated with a reflection asymmetric model with β_3 = 0.1 than the value obtained with β_3 = 0.

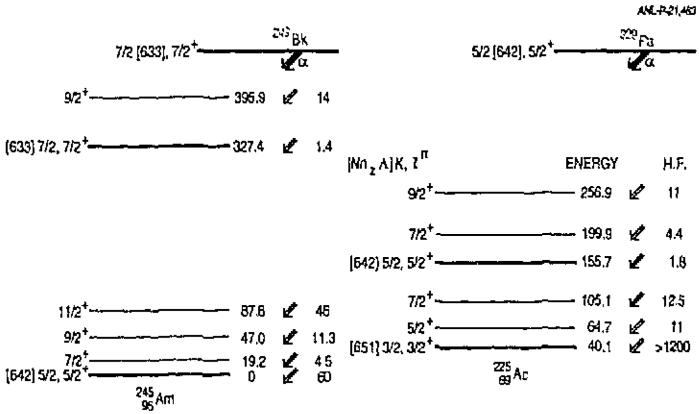

Fig. 4. Energy levels in ^{245}Am [37] and ^{225}Ac [31].

Table 2. Coriolis matrix elements

Nucleus	States	Matrix element Exp.	Theo. with β_3 = 0	Theo. with β_3 = 0.1
^{225}Ac	$3/2^+, 5/2^+$	0.9	~4.0	+0.6
	$3/2^-, 5/2^-$	0.6	~1.0	-0.6

3.4. E1 transition rates

Soon after the observation of properties characteristic of octupole deformation in odd-mass nuclei, enhancement in E1 transition rates over the typical E1 rates in midactinide nuclei was discovered [39]. The B(E1) values in odd-mass Np and Am nuclei are between 10^{-4} to 10^{-7} Weisskopf units. In nuclei which display octupole deformation, the B(E1) values are 10^{-3} to 10^{-2} W.u.. Rates for E1 transitions in odd-mass Ra and heavier nuclei are displayed in Fig. 5. The nuclei which display characteristics of octupole deformation have, in general, higher B(E1) values. E1 transition rates are difficult to calculate and so far have not been calculated for odd-mass and odd-odd nuclei.

3.5. Alpha decay rates

Alpha decay rates provide one of the best means of deducing the relationship between the wavefunctions of the parent ground state and the levels populated in the daughter nucleus. The reduced α decay rate is fastest for the transition involving the same configuration in the parent and the daughter nucleus. Such transitions occur between the ground states of even-even nuclei and in odd-mass and odd-odd nuclei when the unpaired nucleon occupies the same orbital in the parent and the daughter. These transitions are called favored transitions and have hindrance factor (HF) close to unity. The hindrance factor is defined as the ratio of the experimental partial half-life to a level to the half-life calculated with the spin-independent theory of Preston [40].

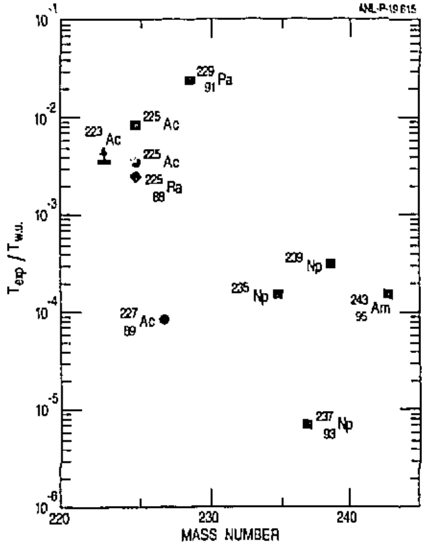

Fig. 5. Transition rates for K = 0 E1 gamma rays in actinide nuclei. T_{exp} denotes the experimental γ-ray transition probabilities and $T_{W.u.}$ refers to Weisskopf single-particle units.

In the octupole deformation limit, the two members of a parity doublet are different projections from the same intrinsic state of broken reflection symmetry. Hence the hindrance factors for alpha transitions to the two members of a parity doublet should be almost equal. Since the intensities of strong peaks can be more reliably measured, intensities of favored α transitions and α transitions to the opposite parity member of the doublet, given in table 3, can be used to assess octupole collectivity in a nucleus.

Table 3. Alpha decay hindrance factor

Parent nucleus	Parent state	State in daughter	Hindrance factor
^{227}Pa,	$5/2^+$	$5/2^+$	2.5
		$5/2^-$	7.0
^{229}Pa,	$5/2^+$	$5/2^+$	1.8
		$5/2^-$	7.5
^{227}Th	$1/2^+$	$1/2^+$	6.1
		$1/2^-$	15
^{228}Pa	(3^+)	(3^+)	12
		(3^-)	20

The hindrance factors to the opposite-parity members of the parity doublets relative to that of the favored decay in ^{223}Ac, ^{225}Ac and ^{224}Ac are 2.8, 4.2 and 2.0, respectively. From the hindrance factors to the rotational members of a band one can deduce the hindrance factors for $\ell = 0$ and $\ell = 1$ partial waves. Also, centrifugal barrier increases the hindrance factor. To obtain the α-decay matrix elements, the hindrance factors for $\ell = 1$ transitions should be reduced [41] by a factor P_ℓ/P_0 which is 0.77 in ^{225}Ac and neighboring nuclei. We find reduced hindrance factors for $\ell = 1$ partial waves for ^{223}Ac, ^{225}Ac and ^{224}Ac as 1.2, 2.2 and 1.0, respectively. These numbers are relative to the hindrance factors for $\ell = 0$ alpha transitions and clearly indicate that the alpha-decay matrix elements to the opposite parity members are almost equal to that of the favored transitions. This is exactly what is expected for an octupole deformed nucleus. In the absence of octupole deformation these numbers should be in the 10-100 range [38].

4. Conclusion

Although no direct evidence has been obtained for the existence of nuclei with permanent octupole deformation, matrix elements have been deduced from experimental data which clearly demonstrate large octupole correlations in the ground states of ^{223}Ac, ^{224}Ac ^{225}Ac and ^{229}Pa. Parity doublets with very small splitting energies have been observed in these nuclei. Very large B(E1) values have been measured between the members of the doublets in these nuclei which provide another evidence for the octupole deformation. Finally, Coriolis matrix elements and reduced alpha decay rates have been deduced which show that the wavefunctions of the two members of the parity doublet are almost identical. This is the strongest evidence for octupole deformation in these nuclei.

Acknowledgement

The author wishes to thank R. R. Chasman for many helpful discussions. This work was supported by the US Department of Energy, Nuclear Physics Division, under contract No. W-31-109-ENG-38.

References

[1] A. Bohr, Mat. Fys. Medd. Dan. Vid. Selsk, 26 No. 14 (1952)
[2] A. Bohr and B. R. Mottelson, Mat. Fys. Med. Dan. Vid. Selsk 27, No. 16 (1953)
[3] F. Asaro, F. S. Stephens and I. Perlman, Phys. Rev. 92, 1495 (1953)
[4] F. S. Stephens, F. Asaro and I. Perlman, Phys. Rev. 96, 1568 (1954)
[5] K. Alder, A. Bohr, T. Huus, B. Mottelson and A. Winther, Rev. Mod. Phys. 28, 432 (1956)
[6] K. Lee and D. R. Inglis, Phys. Rev. 108, 774 (1957)
[7] R. R. Chasman, Nuclear Structure, Reactions and Symmetries. Singapore: World Scientific (1986), p. 5-29
[8] G. A. Leander, R. K. Sheline, P. Moller, P. Olanders, I. Ragnarsson and A. J. Sierk, Nucl. Phys. A388, 452 (1982)
[9] V. M. Strutinsky, Atom. Energiya 4, 150 (1956)
[10] V. Yu. Denisov, Sov. J. Nucl. Phys. 49, 644 (1989)
[11] I. Ahmad, J. E. Gindler, R. R. Betts, R. R. Chasman and A. M. Friedman, Phys. Rev. Lett. 49, 1758 (1982)
[12] R. K. Sheline and G. A. Leander, Phys. Rev. Lett. 51, 359 (1983)
[13] J. Fernandez-Niello, H. Puchta, F. Riess and W. Trautman, Nucl. Phys. A391, 221 (1982)

[14] D. Ward, G. D. Dracoulis, J. R. Leigh, R. J. Charity, D. J. Hinde and J. O. Newton, Nucl. Phys. A406, 591 (1983)
[15] R. R. Chasman, Phys. Lett. 96B, 7 (1980)
[16] G. A. Leander and R. K. Sheline, Nucl. Phys. **A413**, 375 (1984)
[17] R. R. Chasman, Phys. Rev. Lett. **42**, 630 (1979)
[18] P. Möller and J. R. Nix, Nucl. Phys. **A361**, 117 (1981)
[19] S. Ćwiok and W. Nazarewicz, Nucl. Phys. **A529**, 95 (1991)
[20] R. Piepenbring, Z. Physik **A323**, 341 (1986)
[21] I. Ahmad and P. A. Butler, Ann. Rev. Nucl. Part. Sc. **43**, 71 (1993)
[22] S. A. Ahmad, W. Klempt, R. Neugart, E. W. Otten, K. Wendt, C. Ekstrom and the ISOLDE collaboration, Phys. Lett. **133B**, 47 (1983)
[23] R. K. Sheline, Phys. Lett. **166B**, 269 (1986)
[24] R. K. Sheline et al., Phys. Lett. **133B**, 13 (1983)
[25] K. Nybo et al., Nucl. Phys. **A408**, 127 (1983)
[26] R. G. Helmer, M. A. Lee, C. W. Reich and I. Ahmad, Nucl. Phys. **A474**, 77 (1987)
[27] E. Andersen et al., Nucl. Phys. **A491**, 290 (1989)
[28] R. K. Sheline, C. F. Liang and P. Paris, Int. J. Mod. Phy. A5, 2821 (1990)
[29] I. Ahmad, R. Holzmann, R. V. F. Janssens, P. Dendooven, M. Huyse, G. Reusen, J. Wauters and P. Van Duppen, Nucl. Phys. **A505**, 257 (1989)
[30] P. Aguer, A. Peghaire and C. F. Liang, Nucl. Phys. **A202**, 37 (1973)
[31] I. Ahmad, J. E. Gindler, A. M. Friedman, R. R. Chasman and T. Ishii, Nucl. Phys. **A472**, 285 (1987)
[32] H. E. Matz et al., Phys. Rev. **C37**, 1407 (1988)
[33] V. Grafen, B. Ackermann, H. Baltzer, T. Bihn, C. Gunther, J. de Boer, N. Gollwitzer, G. Graw, R. Hertenberger, H. Kader, A. Levon and A. Losch, Phys. Rev. **C44**, 1728 (1991)
[34] R. K. Sheline, J. Kvasil, C. F. Liang and P. Paris, Phys. Rev. **C44**, 1732 (1991); J. Phys. **G19**, 617 (1993)
[35] I. Ahmad, J. E. Gindler, M. P. Carpenter, D. J. Henderson, E. F. Moore, R. V. F. Janssens, I. G. Bearden and C. F. Foster, Nucl. Phys. A, in press
[36] R. R. Chasman, I. Ahmad, A. M. Friedman and J. R. Erskine, Rev. Mod. Phys. **49**, 833 (1977)
[37] I. Ahmad, Ph.D thesis, Lawrence Radiation Laboratory Report No. UCRL-16888 (1988), unpublished
[38] C. M. Lederer and V. M. Shirley, Table of Isotopes, 7th ed. (Wiley, New York, 1978)
[39] I. Ahmad, R. R. Chasman, J. E. Gindler and A. M. Friedman, Phys. Rev. Lett. **52**, 503 (1984)
[40] M. A. Preston, Phys. Rev. 71, 865 (1947)
[41] J. O. Rasmussen, Phys. Rev. **115**, 1675 (1959)

COMPARISON OF RADIATIVE CHARACTERISTICS OF EXCITED STATES FOR EVEN - EVEN NUCLEI WITH Z = 50 AND N = 82

Demidov A.M., Govor L.I., Kurkin V.A. and Mikhailov I.V.
Russian Research Center "Kurchatov Institute", Moscow

Abstract

Comparison of the radiative properties of 1^-_1, 1^+_1, 2^+_{1-4}, 3^-_1 and 3^+_1 levels for even-even nucleus chains with Z = 50 at neutron numbers from 66 to 74 and with N = 82 at neutron numbers from 56 to 62 has been carried out. The properties of levels with $J^\pi = 1^-_1$, 1^+_1, 2^+_1 and 3^-_1 was found to be very similar in these nuclear regions. Apparently the 3^+_1 level differences in radiative properties are caused by the difference in neutron number (at Z = 50) and in proton number (at N = 82). Much attention is given to the consideration of the constancy of mixing ratio signs for M1 and E2 radiations in $2^+_{2,3,4}$ - 2^+_1 transitions for isotope and isotone chains.

The closed proton shell at Z = 50 in tin isotopes and the closed neutron shell at N = 82 in corresponding isotones should not influented upon a structure and the radiative characteristics of low-lying excited states. An exception is the appearance of intruder states in tin isotopes near N = 66, that manifests itself in the properties of the low-lying 0^+, 2^+, 4^+ and 6^+ levels. If we neglect the influence of the intruder states in tin isotopes then comparison of radiative characteristics (lifetimes of levels, branching ratios, multipole mixing ratios) for low-lying levels in nuclei with Z = 50 and N = 82 makes it possible to compare a behaviour of neutron and proton systems in nucleus.

It follows from considerations of the present day excited state schemes of even-even nuclei that the best-investigated nuclei are the stable nuclei, and for their study a variety of methods including inelastic scattering both charged particles and neutrons are used. In particular, investigations of γ - rays from inelastic scattering of fast neutrons provide a chance to establish the complete level system up to $\geq$ 3 MeV excitation energy, without that it is impossible to juxtapose the level systems of the neighbouring nuclei and to compare them with theoretical calculations.

Unfortunately for stable nucleus chains with fixed Z = 50 and N = 82 the ranges of changing Z and N almost do not overlap. However a comparison of the systems mentioned above is possible if we limit ourselves to consideration of the first levels with fixed J^{π}. These levels in a broad range of nucleons numbers conserve their radiative characteristics constantly or their properties change smoothly. It's connected with high collectivity of these levels (collectivity gives decreasing of the level energy) and with the most simple two-quasiparticles nature since at the low energies subshells of the considered basic shell are mainly excited.

In tables 1 and 2 some radiative characteristics of 1^-_1, 1^+_1, 2^+_1, 3^-_1 and 3^+_1 levels are given for $^{116-124}Sn$ [1–7] and ^{138}Ba, ^{140}Ce [8], ^{142}Nd and ^{144}Sm [9]. Data for ^{138}Ba and ^{142}Nd we are publishing for the first time. In recent years we have been investigated the indicated nuclei (excluding ^{144}Sm) in the $(n,n'\gamma)$ reaction with the reactor's fast neutrons. In our experiments we have measured γ–spectra, angular distributions and linear polarizations of γ–rays, level lifetimes and have established the completeness of the level schemes. The tables 1 and 2 were prepared using the additional information from Nuclear Data Sheets for 2^+_1 levels and data from the (γ,γ') reaction for 1^- levels in $^{116,124}Sn$ and isotones with N = 82 [10,11].

From the data in tables 1 and 2 it follows that in nuclei with Z = 50 and with N = 82 the radiative properties are identical for 1^-_1, 1^+_1, 2^+_1 and 3^-_1 levels. These levels at neutron or proton excitations have approximately the same B(ML) values and de-excitation schemes. In particular the 1^-_1 level de-excites mainly to the ground state ($I_\gamma(1^-_1 - 0^+_1)/I_\gamma(1^-_1 - 2^+_1) > 0{,}90$ including ^{138}Ba according our data). The negative parity for the 1^-_1 level in $^{118-122}Sn$ is assumed authors. The 3^-_1 level de-excites to the 2^+_1 level. The observed exceeding of B(E1) in 2–3 times for the $1^-_1 - 0^+_1$ and $3^-_1 - 2^+_1$ transitions in nuclei with N = 82 in comparison with Z = 50 nuclei is apparently determined by the differences in the giant E1 resonance positions or, alternatively, by the excitation effects of proton or neutron systems.

The 3^+_1 level is an exception. A drastic distinction between radiative properties of this level in nuclei with Z = 50 and N = 82 is apparently determined by a difference in the level nature. In nuclei with N = 82 this level is most probably the two-quasiparticles

Some radiative characteristics of the 1_1^-, 1_1^+, 2_1^+, 3_1^- and 3_1^+ levels for Sn isotopes. (B(ML) – reduced probabilities of γ-transitions in Weisskopf units, τ – lifetimes of levels, I_γ – relative intensities of γ-transitions, δ – multipole mixing ratio in γ-transitions)

Table 1

	$^{116}Sn_{66}$	$^{118}Sn_{68}$	$^{120}Sn_{70}$	$^{122}Sn_{72}$	$^{124}Sn_{74}$
$E_i(1_1^-)$, keV	3334	3271	3279	3359	3490
$B(E1, 1_1^- - 0_1^+)$ $\cdot 10^3$, W. u.	1.42(14) [10]	$1.6^{+2.2}_{-0.7}$	$0.67^{+0.28}_{-0.17}$	$1.2^{+1.0}_{-0.4}$	1.27(13) [10]
$E_i(1_1^+)$, keV	2586	2738	2835	2880	>3000
$\frac{I_\gamma(1_1^+ - 0_1^+)}{I_\gamma(1_1^+ - 2_1^+)}$	0.30	0.34	0.32	0.16	–
τ, ps	$0.38^{+0.69}_{-0.16}$	$0.28^{+0.22}_{-0.09}$	$0.19^{+0.08}_{-0.05}$	$0.16^{+0.08}_{-0.04}$	–
$B(M1, 1_1^+ - 0_1^+)$ $\cdot 10^3$, W. u.	$1.1^{+0.8}_{-0.7}$	$1.4^{+0.7}_{-0.6}$	$1.8^{+0.6}_{-0.5}$	1.1(4)	–
$E_i(2_1^+)$, keV	1294	1230	1171	1141	1132
$B(E2, 2_1^+ - 0_1^+)$ W. u.	11.6(6)	12.6(3)	11.38(18)	10.8(6)	9.04(20)
$E_i(3_1^-)$, keV	2266	2325	2400	2493	2602
τ, ps	$0.42^{+0.23}_{-0.11}$	$0.21^{+0.04}_{-0.03}$	0.167(12)	$0.114^{+0.007}_{-0.008}$	0.098(8)
$B(E1, 3_1^- - 2_1^+)$ $\cdot 10^3$, W. u.	$1.09^{+0.27}_{-0.49}$	$1.47^{+0.22}_{-0.28}$	1.29(11)	1.41(9)	1.26(10)
$E_i(3_1^+)$, keV	2296	> 3000	3077	2945	2836
$\frac{I_\gamma(3_1^+ - 2_1^+)}{I_\gamma(3_1^+ - 4_1^+)}$	1.0/0	–	1.0/0.61	1.0/0	1.0/0.54
$\delta(3_1^+ - 2_1^+)$	+9(2)	–	+4.2(16)	+5.1(17)	+1.5(3)

Some radiative characteristics of the 1_1^-, 1_1^+, 2_1^+, 3_1^- and 3_1^+ levels in the isotones with N=82

Table 2

	$^{138}_{56}Ba$	$^{140}_{58}Ce$	$^{142}_{60}Nd$	$^{144}_{62}Sm$
$E(1_1^-)$, keV	4025	3643	3425	3225
$B(E1, 1_1^- - 0_1^+) \cdot 10^3$, W. u. [11]	3.0(3)	3.4(3)	3.1(5)	3.5(5)
$E(1_1^+)$, keV	2583	2547	2586	2644
$\frac{I_\gamma(1_1^+ - 0_1^+)}{I_\gamma(1_1^+ - 2_1^+)}$	0.17	0.18	0.21	0.20
τ, ps	$0.23^{+0.08}_{-0.05}$	$0.27^{+0.16}_{-0.07}$	$0.47^{+0.21}_{-0.13}$	$0.27^{+0.09}_{-0.06}$
$B(M1, 1_1^+ - 0_1^+) \cdot 10^3$, W. u.	1.2(3)	1.1(4)	$0.65^{+0.29}_{-0.18}$	1.1(3)
$E_i(2_1^+)$, keV	1436	1596	1576	1660
$B(E2, 2_1^+ - 0_1^+)$ W. u.	11.4(3)	14.1(4)	12.04(18)	11.5(3)
$E_i(3_1^-)$, keV	2881	2464	2084	1810
τ, ps	$0.067^{+0.007}_{-0.006}$	0.144(29)	$1.2^{+1.9}_{-0.5}$	-
$B(E1, 3^- - 2^+) \cdot 10^3$, W. u.	1.82(18)	3.9(8)	$2.3^{+1.7}_{-1.4}$	2.8(4)
$E_i(3_1^+)$, keV	2445	2412	2547	2688
$\frac{I_\gamma(3_1^+ - 2_1^+)}{I_\gamma(3_1^+ - 4_1^+)}$	1/0.36	1/0.83	1/1.0	1/1.3
$\delta(3_1^+ - 2_1^+)$	−0.14(3) or 2.90(15)	−0.056(12)	−0.07(2)	−0.22(6) or −2.1(3)

state (multipole mixing ratio for $3_1^+ - 2_1^+$ transitions is small and the 3_1^+ level is disposed lower than the expected energy of three-phonon excitation). In nuclei with Z = 50 the 3_1^+ level has the essential admixture of the three-phonon excitation. Of some interest is the difference in signs of δ in $3_1^+ - 2_1^+$ transitions under the conservation of sign in each nucleus group (Z = 50 and N = 82). The constancy of δ-sign in nucleus chains is observed as well at the consideration of $2_{2,3,4}^+ - 2_1^+$ transitions. In ref. [12] we have paid attention to a constancy of the sign of multipole mixing ratio in $2_{2,3}^+ - 2_1^+$ transitions for chains of even-even spherical nuclei with the fixed proton number. The opposite signs of δ in $2_2^+ - 2_1^+$ and $2_3^+ - 2_1^+$ transitions have been pointed out as well.

Values of δ for some $2^+ - 2_1^+$ transitions in Cd [13], Sn, Te [14] isotopes and isotones with N = 82 are given in table 3. Transitions from 2_{in}^+ intruder states in Cd, Sn and Te isotopes are shown in separate lines. Thus in $^{114-120}$Sn isotopes these levels are 2_2^+ states. But in our consideration we are not going to consider intruder states and therefore we consider in these nuclei the next 2_3^+ level as 2_2^+ level which we marked 2_2^{+*}. With increasing of neutron number in Te isotopes a sign of δ in $2_2^+ - 2_1^+$ and $2_3^+ - 2_1^+$ transitions changes simultaneously that reflects the constancy of δ-sign only in certain range of nucleon numbers.

In ref. [12] it have been supposed that the sign of δ is determined by the contributions in excited states quasipartical configurations having large orbital momentum. In particular negative sign of δ can be explained by the negative sign of magnetic momentum of neutron in the states with $j_n = l_n + 1/2$. However this assumption contradicts some data about signs of δ accumulated at the present time.

In table 4 contributions of the main two-quasipartical configurations in 2^+ levels of ^{140}Ce [15] are given in the columns 3-6. We take into account only the main configurations as the small contributions of other configurations differ essentially for neighbouring isotopes and so they cannot provide the constancy of the δ-sign in isotopic chains. As it follows from data in 3-6 columns of table 4 δ-values for $2_2^+ - 2_1^+$ and $2_3^+ - 2_1^+$ transitions in ^{140}Ce have a different sign in spite of almost the same set of two-quasipartical configurations for 2_2^+ and 2_3^+ levels.

Values of δ in the 2^+-2_1^+ transitions for Cd [13], Sn [6] and Te [14] isotopes

Table 3

2_i^+	δ-values for $2_i^+ - 2_1^+$ transitions					
	^{106}Cd	^{108}Cd	^{110}Cd	^{112}Cd	^{114}Cd	^{116}Cd
2_2^+	-1.4(3)	-1.5(3)	$-1.4^{+0.4}_{-1.0}$	$-1.7^{+0.4}_{-1.0}$	$-1.3^{+0.4}_{-1.0}$	$-1.5^{+0.3}_{-0.9}$
2_{in}^+	+0.06(15) or +2.1(7)	+0.13(2)	+0.33(8)	+0.13(2)	+0.50(25)	+1.10(20)
2_4^+	+2.5(2)	+3.8(3) or −.151(14)	+0.06(3)	+1.45(30)	$+2.4^{+0.4}_{-0.2}$	-0.54(15)
	^{114}Sn	^{116}Sn	^{118}Sn	^{120}Sn	^{122}Sn	^{124}Sn
2_2^{+*}	$+7.5^{+1.8}_{-1.3}$	2.9(4)	$+56^{+70}_{-20}$	+1.0(2)		
2_2^+					+3.8(4)	+3.4(4)
2_{in}^+	$-7.1^{+1.2}_{-1.9}$	-1.0(2)	-2.34(16)	-12(2)	-3.5(6)	-
	^{122}Te	^{124}Te	^{126}Te	^{128}Te	^{130}Te	
2_2^+	$-3.7^{+0.7}_{-1.1}$	-3.3(2)	$-7.2^{+1.0}_{-1.6}$	+4.7(2)	+0.65(15)	
2_{in}^+	+.038(26)	+0.13(4)				
2_3^+			-0.04(3)	-0.210(11)	-0.175(10)	
2_3^{+*}	+2.62(12)	-0.12(2)				

In Cd isotopes the 2_{in}^+ level is 2_3^+ levels.

In $^{122,124}Te$ isotopes the 2_{in}^+ level is 2_3^+ levels.

In $^{114-120}Sn$ isotopes the 2_{in}^+ level is 2_2^+ levels.

Values of δ in $2^+ - 2_1^+$ transitions for isotones with N=82

Table 3 (continued)

Level 2_i^+	δ-values for $2_i^+ - 2_1^+$ transitions		
	^{138}Ba	^{140}Ce	^{142}Nd
2_2^+	$+0.07(10)$ or $+2.0^{+0.6}_{-0.4}$	$+0.36(3)$	$+0.16^{+0.06}_{-0.05}$
2_3^+	$-0.5^{+0.3}_{-0.7}$	$-0.17(2)$	$-0.28(3)$
2_4^+	$-0.74(4)$ or $-4.2(5)$	$-1.5^{+0.4}_{-1.0}$	$-0.6^{+0.2}_{-0.3}$ or -6^{+3}_{-29}

At present the certain success in the explanation of the excited state structure of even–even nuclei is connected with the quasipartical–phonon model (QPM) developed by Soloviev V.G. and his colleagues [16]. In particular calculations for even–even nuclei near N = 82 carried out in the framework of this model explain satisfactorily experimental results of (e,e')-reaction research up to 4 MeV excitation energy [17,18].

In the last column of table 4 theoretical results of the 2^+ level structure for ^{140}Ce [18] are listed in QPM. In this table next notations were adopted: Q_2+ is the one-phonon 2^+ state and $[Q_2+ Q_2+]$ is the two-phonon state. At first let's pay attention to a principal difference in the phonon structure of 2_2^+ and 2_3^+ levels. The opposite signs of δ for $2_2^+ - 2_1^+$ and $2_3^+ - 2_1^+$ transitions in nuclei with N = 82 are possibly connected with this difference.

Wave functions for 2^+ levels obtained in QPM were published as well for ^{144}Nd [17]. These data for main components of wave functions are given in table 5. In the same table our δ-data for $2^+ - 2_1^+$ transitions in ^{144}Nd [19] and in ^{142}Ce [20] are given. As it follows from these data the $2_{3,4,5}^+$ levels with large contributions one-phonon component and the two-phonon level in nuclei with N = 84 have opposite signs of δ in $2^+ - 2_1^+$ transitions.

Values δ for $2^+ - 2_1^+$ transitions, main configurations in two-quasiparticle (TPM) and quasiparticle-phonon (QPM) models in ^{140}Ce

Table 4

Lev.	δ for 2_i^+-2_1^+ transition in ^{140}Ce [8]	Contribution (%) of main configurations in TQM for ^{140}Ce [15]				Contribution of main components in QPM for ^{140}Ce*) [18]
		$g_{7/2}^5 d_{5/2}^3$	$g_{7/2}^4 d_{5/2}^4$	$g_{7/2}^6 d_{5/2}^2$	$g_{7/2}^7 d_{5/2}^1$	
2_1^+		5.5	27.2	44.8	1.4	$0.95\ Q_{2_1^+}$
2_2^+	+0.36(3)	23.0	10.2	36.8	17.5	$0.68\ Q_{2_2^+} + 0.68\ Q_{2_3^+}$
2_3^+	−0.17(2)	21.3	10.2	39.5	18.2	$0.70\ Q_{2_2^+} - 0.70\ Q_{2_3^+}$
2_4^+	$-1.5^{+0.4}_{-1.0}$	12.9	32.9	29.0	-	$0.72\ Q_{2_4^+} + 0.39[Q_{2_1^+} + Q_{2_1^+}]_{2^+}$

*) Contribution is not normalized. For 2_1^+ state the normalized contribution of Q_2^+ is 91% [18].

Values of δ for $2_i^+ - 2_1^+$ transitions in ^{142}Ce and ^{144}Nd and main components for 2^+ levels of ^{144}Nd in the quasiparticle-phonon model

Table 5

Levels	δ-values for $2^+ - 2_1^+$ transitions		Contributions of main components in 2^+ levels of ^{144}Nd in QPM [17]
	^{142}Ce [20]	^{144}Nd [19]	
2_1^+			78% $Q_{2_1^+}$
2_2^+	−0.76(8)	−0.74(11)	10% $Q_{2_2^+}$; 63% $[Q_{2_1^+}\ Q_{2_1^+}]_{2^+}$
2_3^+	+0.22(4)	+0.08(4)	70% $Q_{2_2^+}$; 10% $[Q_{2_1^+}\ Q_{4_1^+}]_{2^+}$
2_4^+	$+0.36^{+0.17}_{-0.07}$	+0.08(6)	87% $Q_{2_3^+}$; 4% $[Q_{2_1^+}\ Q_{4_1^+}]_{2^+}$
2_5^+	-	$+0.23<\delta<+1.34$	77% $Q_{2_4^+}$; 6% $Q_{2_3^+}$

The first levels with a large contribution of two-phonon excitation in the isotopes with Z = 50 are the 2_2^+ (or 2_2^{+*}) levels and in the isotones with N = 82 are the 2_4^+ levels (see table 4). All γ-transitions from these levels to the 2_1^+ level have $\delta >> 0$, but the opposite signs of δ in nuclei with Z = 50 and with N = 82. In collective models (for the consideration of the second approximation) the *opposite signs* of δ in $2^+ - 2_1^+$ transitions are expected for predominant motion of neutrons or protons in the radiative process.

Conclusions

1. We have not found the considerable difference in radiative properties of the first levels with $J^\pi = 1^+, 1^-, 2^+$ and 3^- in chains of nuclei with fixed numbers Z = 50 and N = 82.

2. The difference in radiative characteristics for 3_1^+ levels, apparently, is caused by the difference in neutron and proton numbers in unclosed shell for nuclei with Z = 50 and N = 82.

3. The radiative characteristics of the 2^+ low-lying levels (and probably 4^+ levels) by apart from the intruder states existing in Sn isotopes, essentially depend on the different energy positions of these levels relative to the energy of two-phonon excitation in the nucleus chains with Z = 50 and N = 82.

4. It is of interest to investigate the behaviour of multipole mixing ratio sign in γ-transitions for isotope and isotone chains. It is desirable to consider the δ-sign behaviour under various model assumptions.

References

1. Demidov A.M., Mikhailov I.V. – Topics in Atomic Science and Technology. Series: Nuclear Constants. In Russian. Moscow. 1990. No.4, p.24.
2. Mikhailov I.V. et al. – Bull. AN USSR. Ser. Phys., 1989, 53, p.892.
3. Demidov A.M. et al. – Jour. Nucl. Phys., 1992, 55, p.865.
4. Demidov A.M. et al. – Bull. AN USSR. Ser. Phys., 1991, 55, p.2112.

5. Demidov A.M. et al. – Bull. AN USSR. Ser. Phys., 1990, 54, p.2126.
6. Govor L.I. et al. – Sov. J. Nucl. Phys., 1991, 53, p.3.
7. Govor L.I. et al. – Sov. J. Nucl. Phys., 1991, 54, p.330.
8. Govor L.I. et al. – Jour. Nucl. Phys., 1993, 56, No.12, p.15.
9. Gatenby R.A. et al. – Nucl. Phys., 1993, A560, p.633.
10. Govaert K. et al. – Institut fur Stralenphysik. Universitat Stuttgart. Annual Report. 1993. p.18.
11. Pitz H.H. et al. – Nucl. Phys., 1990, A509, p.587.
12. Demidov A.M. et al. – Sov. J. Nucl. Phys., 1988, 47, p.897.
13. Araddad S.Y. et al. – Sov. J. Nucl. Phys., 1990, 52, p.3.
14. Berendakov S.A. et al. – Sov. J. Nucl. Phys., 1990, 52, p.609.
15. Dioszegi I. et al. – J.Phys. (London), 1985, G11, p.853.
16. Soloviev V.G. – Prog. Part. Nucl. Phys., 1987. 19. p.107.
17. Perrino R. et al. – Nucl. Phys., 1993, A561, p.343.
18. Kim W. et al. – Phys. Rev., C45, p.2290.
19. Demidov A.M., Govor L.I., Baskova K.A. – Investigation of Nuclear Excited States. Alma-Ata: Nauka. 1986. p.70.
20. Alhamidi M.M. et al. – Jour. Nucl. Phys., 1992, 55, p.890.
21. Barfield A.F. et al. – Z.Phys., 1989, A332, p.29.

The Breathing Mode and Nuclear Matter Incompressibility Coefficient*

S. Shlomo[1,2] and D. H. Youngblood[1]

[1] *Cyclotron Institute, Texas A&M University, College Station, Texas 77843, USA*

[2] *ECT*, Villa Tambosi, I-38050 Villazzano (Trento), Italy*

Abstract

We consider the nuclear matter incompressibility coefficient, K_{nm}, and review the experimental and theoretical methods used to determine the value of K_{nm}. We examine, in particular, the most sensitive method which is based on experimental data on the strength function distribution of the isoscalar giant monopole resonance in nuclei. We review the present status of the entire data set, accumulated from measurements carried out in several laboratories, and the theoretical methods used to determine K_{nm}, which are based on microscopic self-consistent Hartree-Fock with random phase approximation and semi-empirical approaches, and provide some conclusions.

I. INTRODUCTION

The nuclear matter (N=Z and no Coulomb interaction) equation of state (EOS), $E = E(\rho)$, is a basic physical quantity which is very important for the study of properties of nuclei, supernova collapse, neutron stars and heavy ion collisions. Our knowledge of the EOS is very limited. The saturation (minimum) point at zero temperature is known with good accuracy. From the extrapolation of empirical mass formula we have $E(\rho_0) = -16MeV$ and from electron scattering analysis we have $\rho_0 = 0.17/fm^{-3}$. To extend our knowledge of the EOS, an accurate determination of the nuclear matter incompressibility coefficient, K_{nm}, is needed, since it is directly related to the curvature of the nuclear matter equation of state,[1] $E = E(\rho)$, at the saturation point $(E, \rho) = (-16MeV, 0.17/fm^3)$. The coefficient K_{nm} is defined by,

$$K_{nm} = k_f^2 \frac{d^2(E/A)}{dk_f^2}\Big|_{k_{f0}} = 9\rho_0^2 \frac{d^2(E/A)}{d\rho^2}\Big|_{\rho_0}, \tag{1}$$

where E/A is the binding energy per particle of the nuclear matter, and k_{f0} and ρ_0 are the Fermi momentum and the matter density at saturation.

There have been may attempts to determine K_{nm} by considering properties of nuclei which are sensitive to a certain extent to the value of K_{nm} (see a recent review by Glendenning in ref. 2). In a microscopic approach analysis of the experimental data of a physical quantity which is sensitive to K_{nm}, one considers various effective two-body interactions which differ in their value for K_{nm} but reproduce data of other physical quantities fairly well. One then determines the effective interaction which best fit the data which is sensitive to K_{nm}, leading to a constraint on the value of K_{nm}. In a macroscopic approach analysis, K_{nm} appears in the expression for the physical quantity under consideration. The value of K_{nm} is thus deduced by a direct fit to the data. We mention in particular the attempts[2] considering the physical quantities: nuclear masses, nuclear radii, supernova collapses, masses of neutron stars, matter flow in heavy ion collisions and the interaction parameters F_0 and F_1 in Landau's Fermi liquid theory. However, these attempts were not able to constraint the value of K_{nm} to better than a factor of two.

The study of the isoscalar giant monopole resonances (ISGMR) in various nuclei provides an important source of information for K_{nm} since the excitation energy of the ISGMR is sensitive to K_{nm}. The ISGMR was first discovered in ^{208}Pb at excitation energy[3] of 13.7 MeV. Random phase approximation (RPA) calculations using existing or modified effective interactions having $K_{nm} = 210 \pm 30MeV$ were in agreement with experiment.[4]

There have been several attempts in the past to determine K_{nm} by a least square (LS) fit to the ISGMR data of various sets of nuclei using a semi-empirical expansion of the nucleus incompressibility coefficient, K_A, in power of $A^{-1/3}$. The value deduced for K_{nm} varied significantly, depending on the set of data of the ISGMR used in the fit. Recently, using this approach, Sharma and collaborators reported[5-6] a value of $K_{nm} = 300 \pm 20MeV$ which is quite different from the commonly accepted value of $K_{nm} = 210 \pm 30MeV$. Recently, Pearson[7] has pointed out that K_{nm} is strongly dependent on the value assumed for the coefficient of the Coulomb term, K_{coul}, and that the relation between K_{coul} and K_{nm} is model dependent (see also ref. 8).

In the present study, we take a closer look at the self consistent Hartree-Fock (HF)-RPA and the semi-empirical analysis of the ISGMR data, in an attempt to extract a reliable value for K_{nm}. We have attempted to include the entire ISGMR data set, reconciling differences between different laboratories and taking the parameters in the $A^{-1/3}$ expansion of K_A as free parameters. In the following, we first discuss the microscopic approach based on Hartree-Fock approximation for the ground state properties of nuclei and the RPA calculation of the ISGMR. Next, we discuss the theoretical and experimental observations concerning the semi-empirical procedure and then provide some conclusions.

II. MICROSCOPIC APPROACH

In the microscopic HF-RPA approach[9-11] and its semi classical approximation[4,12] one adopts a certain form of effective two-body interaction, such as the Skyrme interaction, involving a set of few parameters. Carrying out self-consistent HF calculations with this interaction, the parameters are varied so as to reproduce experimental data of a wide range of nuclei on nuclear masses, nucleon separation energies, charge and mass density distributions, etc. The parameters of the interaction are further constrained by considering experimental data on the nuclear response function (giant resonances). The nuclear response function is evaluated within the RPA, i.e., small amplitude oscillation. The RPA particle-hole (p-h) Green's function is given by the integral equation

$$G^{RPA} = G^0 + G^{RPA} V_{ph} G^0 \tag{2}$$

where G^0 is the non-interacting (p-h) Green's function and V_{ph} is the residual p-h interaction. For self-consistency, G^0 and V_{ph} are deduced from the same two-body interaction. The excitation strength function for a given one body operator, F, is then obtained from

$$S(E) = \sum_n |\langle n | F | 0 \rangle|^2 \delta(E - E_n) = \frac{1}{\pi} Im T_r (F^+ G^{RPA} F). \tag{3}$$

We add that using Skyrme type interaction, G^0 can be evaluated from

$$G^0(\bar{r}_1, \bar{r}_2, E) = \sum_h \Psi_h^*(\bar{r}_1) \left[\frac{1}{H_0 - \epsilon_h - E - i\eta} + \frac{1}{H_0 - \epsilon_h + E - i\eta} \right] \Psi_h(\bar{r}_2) \tag{4}$$

where H_0 is the HF hamiltonian and ϵ_h and Ψ_h are the single particle energy and wave function of the occupied state, respectively. Moreover, continuum effects, such as particle escape width, can be taken into account using[9]

$$\left\langle r_1 \left| \frac{1}{H_0 - Z} \right| r_2 \right\rangle = \frac{2m}{\hbar^2} U(r_<) V(r_>) / W \tag{5}$$

where $r_<$ and $r_>$ are the lessor and greater of r_1 and r_2, respectively, U and V are the regular and irregular solution of $(H_0 - Z)\Psi = 0$, with the appropriate boundary conditions, and W is the Wronskian.

There have been quite a few calculations[1,4,10,11] of the ISGMR in various nuclei using several forms of effective two-body interactions. With the discovery of the ISGMR at 13.7 MeV in ^{208}Pb, it was found[4] that existing or modified effective interactions having $K_{nm} = 200 MeV$ reproduce the experimental results. However, it is worthwhile to note the following: (i) Only a limited class of effective interactions were explored, (ii) For a certain interaction, calculations of the strength distribution of the ISGMR were carried out only for a limited number of nuclei, (iii) Although deviations are small, there are some indications that the A dependence of the ISGMR energy is different from that calculated by the HF-RPA method with currently used interactions and (iv) Possible effects of more complicated configurations, such as $2p - 2h$ were ignored.

III. SEMI-EMPIRICAL APPROACH

With the increase in ISGMR data in various nuclei, it became worthwhile to attempt using a semi-empirical approach to deduce K_{nm}. In this approach, which is similar to the semi-empirical mass formula, one writes[4,13] the compressibility K_A of the nuclei with mass number A, as an expansion in $A^{-1/3}$.

$$K_A = K_{vol} + K_{surf} A^{-1/3} + K_{curv} A^{-2/3} + (K_{sym} + K_{ss} A^{-1/3}) \left(\frac{N-Z}{A}\right)^2 + K_{coul} \frac{Z^2}{A^{4/3}} + \dots, \tag{6}$$

where K_A is defined by

$$K_A = \frac{m}{\hbar^2} E^2_{GMR} \langle r^2 \rangle. \tag{7}$$

Here $< r^2 >$ is the mean square radius of the nucleus and E_{GMR} is taken to be the energy of the ISGMR defined using a certain ratio of the RPA sum rules,[14]

$$m_k = \sum_n (E_n - E_0)^k \mid \langle o \mid r^2 \mid n \rangle \mid^2 . \tag{8}$$

For example, in the scaling approximation[13] ($r \to \alpha r$),

$$E_{GMR} = \sqrt{m_3/m_1}. \tag{9}$$

Expressions of the form (6) can be deduced by considering the asymptotic behavior of the RPA sum rules m_k. The interpretation of the coefficients, such as K_v, depend on the particular sum rule used (m_{-1} or m_3). However, it is well known that at least for medium and heavy nuclei, the ISGMR is a collective state with the strength concentrated in a limited region and the transition density, $\delta\rho$, obtained in a microscopic HF-RPA approach agrees nicely with that deduced in the scaling approximation $r \to \alpha r$. We note that m_3 is related to the scaling of the equilibrium wave function (or the density) by

$$m_3 = \frac{1}{2} \left(\frac{2\hbar^2}{2m}\right)^2 \frac{d^2 E(\alpha)}{d\alpha^2} \Big|_{\alpha=1}, \tag{10}$$

where, in the energy density formalism,

$$E(\alpha) = \int d^3r H[\alpha^3\rho(\alpha r)]. \qquad (11)$$

Using

$$m_1 = 2A\frac{\hbar^2}{m} < r^2 >, \qquad (12)$$

and assuming a Fermi form for $\rho(r)$,

$$\rho(r) = \rho_0/[1 + exp(\frac{r-c}{a})], \qquad (13)$$

one deduces equation (6) from (10) - (12) by carrying out a leptodermos expansion of $\rho(r)$. One thus obtained[13] that $K_v = K_{nm}$ provided E_{GMR} is determined from (9).

In the following, we first summarize some theoretical and experimental observations concerning the procedure of eqs. (6) to (9) and then provide some numerical results and conclusions. We now discuss the following considerations that must be taken into account when using the eqs. (6) to (9) in a fit to the experimental data for the ISGMR.

1. In using (9) to determine E_{GMR}, the entire ISGMR energy weighted sum rule (EWSR) must be known experimentally. This appears to be the case for heavy nuclei where the ISGMR strength is fitted by a Gaussian with centroid E_0 and width Γ. In this case, one has

$$E_{GMR}^2 = E_0^2 + 3(\Gamma/2.35)^2. \qquad (14)$$

2. In deformed nuclei, a splitting of the ISGMR strength into clearly identifiable components occurs.[15–17] In this case, eq. (9) cannot be used to obtain E_{GMR}, which corresponds to the spherical configuration. Theoretical considerations indicate[17] that to a good approximation the higher component is shifted upward by an amount proportional to the deformation parameter β. We have therefore included in our analysis the ISGMR data for deformed nuclei by adopting the centroid E_0 and width Γ of the higher component and adding to eq. (6) the term βK_{def}.

3. At present, any attempt to include ISGMR data for light nuclei should be considered with extreme care due to the following reasons:

3.a. RPA calculations of the ISGMR predict that the strength is fragmented[10-11] over quite a large range (over 10 MeV). Therefore, ISGMR strength must be carefully searched for over a wide range of energy.

3.b. The particle decay width[9-10] of the ISGMR is quite large (5-16 MeV), particularly for high energy components. This makes the experimental task of determining the ISGMR strength distribution rather difficult, and

3.c. For light nuclei, the scaling approximation may not be as good an approximation as in the case of heavy nuclei, introducing[11] errors of about 5% in the determination of E_{GMR} from eq. (9). In this work, we also discuss the implication of the present data on ISGMR in light nuclei.

4. In determining K_A from eq. (7), one usually adopts a certain expression for $< r^2 >$ with a specific $A^{1/3}$ dependence. The $A^{1/3}$ dependence of $< r^2 >$ affects the $A^{1/3}$ expansion of K_A. Since different expressions for $< r^2 >$ will lead to different values for the coefficients in the expansion (6) for K_A, adopting theoretical values for some of the coefficients will be inconsistent.

5. In previous analysis of the ISGMR data, such as in refs. [5,6,13,18], the number of free parameters in (6) was reduced by adopting relations between the parameters, such as $K_{surf} = -K_{vol}$ and

$$K_{coul} = \frac{3e^2}{5r_0}\left(\frac{1215}{K_{nm}} - 12.5\right) MeV \tag{15}$$

obtained from theory.[13] It should be pointed out that these relations were derived using a limited class of effective interactions and that they are not unique.[7] Therefore, from points 4) and 5) we conclude that all parameters of eq. (6) should be determined by a least square fit to the experimental ISGMR data.

Extensive investigations of the isoscalar giant monopole resonance have occurred at three laboratories: Texas A&M, Grenoble, and Groningen. Each has taken spectra into the very small angles necessary to separate monopole from quadrupole strength, a technique pioneered at Texas A&M.[3] At Texas A&M, substantial monopole strength was identified in

17 nuclei using inelastic alpha scattering between 96 and 130 MeV.[3,19–22] At Grenoble, monopole strength was observed in 42 nuclei with 100 MeV ^{3}He scattering,[23] and in three nuclei with alpha scattering.[24]. At Groningen, 13 nuclei were investigated with 120 MeV alpha scattering.[16,25–28] The nuclei investigated and the resulting monopole parameters are summarized in Ref. 29. Of these 75 potential data points, only 27 (9 TAMU, 11 Groningen, 2 Grenoble alpha, 5 Grenoble ^{3}He) have EWSR fractions consistent with 100% of the monopole strength. These 27 data points represent 16 different nuclei with $24 \leq A \leq 232$.

If all of the available data is to be used, it is important to attempt to put the data from different laboratories on a similar footing. Both the actual value of the energy and width and their uncertainties are important. Systematic differences between different data sets will distort the fits, and data with lower stated uncertainties will dominate the fits. Thus we have explored both the parameters and the uncertainties reported by the different laboratories. We looked for energy calibration systematic differences by comparing energies obtained for both the ISGMR and the nearby giant quadrupole resonance (GQR) by the three laboratories. We chose to accept the TAMU energies and modify the other works by the average difference to correct for systematic errors. At present there is little experimental reason to pick one of the data sets as more accurate on an absolute basis. Where multiple measurements of the same parameter are available, weighted averages (done after correction for systematic errors) were taken.

Using the data of the ISGMR, we have performed fits for several data sets.[29] Using all the α scattering data for $A \geq 90$ (19 points), we obtained similar results to those obtained with the 7 data points adopted of Sharma *et al.*[5–6] It should be emphasized that we assumed uncertainties in E_{GMR} about twice those adopted by Sharma *et al.*[5–6] We then explored including additional data points where the entire sum rule is not seen and cannot be accounted for. First we added all ^{3}He data points with $A \geq 89$. This reduced the uncertainties slightly. Then we added the lighter nuclei (Zn, Ca, Si) where not all the strength was seen, to ascertain the effects on the fits. For Ca, we arbitrarily assumed $E_x \sim 18 \pm 1$ MeV as there is some evidence of monopole strength coincident with the GQR.

For ^{28}Si, we assumed $E_x \sim 20 \pm 1$ MeV because only 65% of the strength was observed with a centroid of 19 MeV. Probably the rest of the strength lies higher. In this fit, we left out the ^{24}Mg point since it is much lower than ^{28}Si. This resulted in substantially smaller uncertainties for the parameters and illustrates the importance of including lighter nuclei.

Our analysis[29] shows that it is important to include K_{coul} as a free parameter in the fit of eq. (6). Including both K_{coul} and K_{surf} in (6) as free parameters lead to errors exceeding 100% for all coefficients. This instability of the semi-empirical approach of eq. (6) can be understood by considering the following: (i) The value of K_A is practically independent of A and (ii) Most of the (reliable) data points for E_{GMR} are found in the region of $A \geq 100$ where the value of $A^{-1/3}$ changes only slightly, in the region of 0.17 to 0.25. We therefore find that the value of $K_{nm} = 300 \pm 20$ MeV reported by Sharma *et al.*[5,6] is not reliable.

IV. SUMMARY AND OUTLOOK

Within the semi-empirical approach, the present complete data set is clearly not adequate to limit the range of K_{nm} to better than about a factor of 1.7 (200 to 350 MeV). Several things need to be done to pin down K_{nm}. We need measurements on considerably more than 16 nuclei and with more variation in mass. To the extent possible, spherical nuclei should be chosen to eliminate effects of deformation. These measurements need to provide the centroid and width of the ISGMR to better than 150 keV, after taking into account possible uncertainties in the continuum. Significant systematic errors between differing measurements must be removed. The strength distribution in light nuclei must be mapped over a wide energy range.

Considering the results of microscopic HF-RPA calculations it is important to emphasize that at present, effective interactions which reproduce the ground state properties of a wide range of nuclei seem to account for the current data of ISGMR in nuclei, i.e., reproducing excitation energies of the ISGMR within 1 MeV if the corresponding $K_{nm} = 210 \pm 30$ MeV. However, a systematic microscopic calculation of the strength distribution of the ISGMR over a wide range of nuclei is required for a firm conclusion.

REFERENCES

[1] A. Bohr and B. M. Mottleson, Nuclear Structure II (Benjamin, New York, 1975).

[2] N. K. Glendenning, Phys. Rev. C **37** (1988) 2733.

[3] D. H. Youngblood, C. M. Rozsa, J. M. Moss, D. R. Brown, and J. D. Bronson, Phys. Rev. Lett. **39** (1977) 1188.

[4] J. P. Blaizot, Phys. Rep. **64** (1980) 171.

[5] M. M. Sharma, W. Stöcker, P. Gleissl and M. Brack, Nucl. Phys. **A504** (1989) 337; M. M. Sharma, in *Proceedings of the NATO Advanced Study Institute on Nuclear Equation of State*, Pensicola (Spain), 1989, edited by W. Greiner and H. Stöcker (Plenum, New York, 1990), Vol. 216A, p. 661.

[6] M. M. Sharma (unpublished); M. M. Sharma, in Slide Report of the Notre Dame Workshop on Giant Resonances and Related Phenomena, Notre Dame, IN, 1991 (unpublished).

[7] J. M. Pearson, Phys. Lett. **B271** (1991) 12.

[8] J. P. Blaizot, in *Proceedings of the NATO Advanced Study Institute on Nuclear Equation of State*, Pensicola (Spain), 1989, edited by W. Greiner and H. Stöcker (Plenum, New York, 1990), Vol. 216A, p. 667.

[9] S. Shlomo and G. Bertsch, Nucl. Phys. **A243** (1975) 507.

[10] N. Van Giai and H. Sagawa, Nucl. Phys. **A371** (1981) 1.

[11] Ph. Chomaz, T. Suomijarvi, N. Van Giai and J. Treiner, Phys. Lett. **B281** (1992) 6.

[12] O. Bohigas, A. M. Lane and J. Martorell, Phys. Rep. **51** (1979) 267.

[13] J. Treiner, H. Krivine, and O. Bohigas, Nucl. Phys. **A371** (1981) 253.

[14] E. Lipparini, G. Orlandini, and R. Leonardi, Phys. Rev. Lett. **36** (1976) 660.

[15] M. Buenerd, D. Lebrun, Ph. Martin, P. de Santignon and C. Perrin, Phys. Rev. Lett. 45 (1980) 1667; U. Garg, P. Bogucki, J. D. Bronson, Y.-W. Lui, C. M. Rozsa, and D. H. Youngblood, Phys. Rev. Lett. 45 (1980) 1670.

[16] Y. Abgrail, B. Morand, E. Caurier and B. Grammaticos, Nucl. Phys. A346 (1980) 431.

[17] S. Jang, Nucl. Phys. A401 (1983) 303.

[18] M. M. Sharma, W. T. A. Borghols, S. Brandenburg, S. Crona, A. Van der Woude, and M. H. Harakeh, Phys. Rev. C38 (1988) 2562; M. M. Sharma, in *Proceedings of the International Winter Meeting on Nuclear Physics*, Bormio, Italy, 1988, edited by I. Iori (University of Milan, Italy, 1988), Vol. 63, p. 510.

[19] Y.-W. Lui, J. D. Bronson, D. H. Youngblood, Y. Toba, and U. Garg, Phys. Rev. C31 (1985) 1642, and references therein.

[20] U. Garg, P. Bogucki, J. D. Bronson, Y.-W. Lui, and D. H. Youngblood, Phys. Rev. C29 (1984) 93.

[21] Y.-W. Lui, P. Bogucki, J. D. Bronson, D. H. Youngblood, and U. Grag, Phys. Rev. C30 (1984) 51.

[22] D. H. Youngblood and Y.-W. Lui, Phys. Rev. C44 (1991) 1878.

[23] M. Buenerd, in *Proceedings of International Symposium on Highly Excited States and Nuclear Structure*, Orsay, France, edited by N. Marty and N. Van Giai, J. Phys. (Paris) Colloq. 45 (1984) C4-115, and references therein.

[24] G. Duhamel, M. Buenerd, P. de Saintignon, J. Chauvin, D. Lebrun, Ph. Martin and G. Perrin, Phys. Rev. C38 (1988) 2509.

[25] H. J. Lu, S. Brandenburg, R. De Leo, M. N. Harakeh, T. D. Poelhekkend, and A. Van der Woude, Phys. Rev. C33 (1986) 1116.

[26] S. Brandenburg, R. De Leo, A. G. Drentje, M. N. Harakeh, H. Sakai, and A. Van der Woude, Phys. Lett. B130 (1983) 9.

[27] W. T. A. Borghols, S. Brandenburg, J. H. Meier, J. M. Schippers, M. M. Sharma, A. Van der Woude, M. N. Harakeh, A. Lindholm, L. Nilsson, S. Crona, A. Hakansson, L. P. Ekstrom, N. Olsson, and R. De Leo, Nucl. Phys. **A504** (1989) 205.

[28] S. Brandenburg, W. T. A. Borghols, A. G. Drentje, L. P. Ekstrom, M. N. Harakeh, A. Van der Woude, A. Hakanson, L. Nilsson, N. Olsson, M. Pignanelli, and R. De Leo, Nucl. Phys. **A466** (1987) 29.

[29] S. Shlomo and D. H. Youngblood, Phys. Rev. C**47** (1993) 529.

*Supported in part by the Department of Energy Grant DE-FG05-86ER40256, the National Science Foundation Grant 9107008, and the Robert A. Welch Foundation.

Study of the Giant Dipole Resonance Built on Highly-Excited States via Inelastic Alpha-Scattering

M. Thoennessen, E. Ramakrishnan, T. Baumann, A. Azhari,
R. A. Kryger, R. Pfaff, and S. Yokoyama

*National Superconducting Cyclotron Laboratory and
Department of Physics & Astronomy,
Michigan State University, East Lansing, Michigan 48824, USA*

J. R. Beene, F. E. Bertrand, M. L. Halbert,
P. E. Mueller, D. W. Stracener, and R. L. Varner

Oak Ridge National Laboratory, Oak Ridge, Tennessee 37831, USA

G. Van Buren, R. J. Charity, J. F. Dempsey, P-F. Hua,
D. G. Sarantites, and L. G. Sobotka

*Department of Chemistry, Washington University,
St. Louis, Missouri 63130, USA*

Abstract

High energy γ rays were measured in coincidence with inelastically scattered α particles at beam energies of 40 MeV/nucleon (on ^{120}Sn and ^{208}Pb targets) and 50 MeV/nucleon (on ^{120}Sn). High energy target excitations were observed and the giant dipole resonance (GDR) built on these excited states was measured by its γ-ray decay. The width of the GDR increases with excitation energy. This increase is not as strong as in the corresponding fusion-evaporation reactions.

1. INTRODUCTION

In recent years the study of the giant dipole resonance (GDR) built on highly excited states has yielded important information on the nuclear structure of hot nuclei [1, 2] and on reaction dynamical effects [3, 4]. Typically, the GDR is observed by its γ-ray decay following heavy-ion fusion reactions. The well established dependence of the parameters of the GDR strength function on nuclear size and deformation makes it possible to use the GDR to explore shape evolution as a function of excitation energy and angular momentum.

A systematic effort to explore the evolution of the GDR as a function of increasing excitation energy has recently been made, using heavy-ion fusion evaporation reactions. Two particularly interesting aspects are an increase in width of the GDR with increasing bombarding energy [5], and the apparent disappearance of GDR strength at very high energies [6]. The increase in excitation energy with increasing bombarding energy in a heavy-ion fusion reaction is accompanied by an increase in the mean angular momentum of the compound nucleus. Consequently it has not been possible to disentangle the effects of increasing angular momentum from those of the increase in excitation energy.

We used a different approach in order to separate the effects of angular momentum and excitation energy on the increase of the GDR width. Small-angle inelastic scattering of light or heavy ions can populate highly excited states without transferring large amounts of angular momenta. It should therefore be possible to study the GDR as a function of excitation energy independent of angular momentum. However, two main conditions have to be fulfilled: (i) The cross section for large energy losses of the inelastically scattered particles must be dominated by target excitation and should not be due to other processes, for example projectile pickup and sequential decay or nucleon or cluster knock-out; and (ii) If the inelastic particle spectrum is predominantly due to target excitation, these excited states have to equilibrate rapidly, so that the subsequent decay can be described within the statistical model. The GDR built on highly excited states should then be observed in the same way as in fusion-evaporation reactions.

2. EXPERIMENTS AND DATA ANALYSIS

The experiments were performed at the National Superconducting Cyclotron Laboratory at Michigan State University (MSU). Isotopically enriched 3 mg/cm^2 ^{208}Pb and 16.8 mg/cm^2 ^{120}Sn targets were bombarded with 40 MeV/A α particles. The experiment on the ^{120}Sn target was also performed at 50 MeV/A. The inelastically scattered α particles were detected in the Washington University Dwarf Wall [7] which consisted of 35 CsI(Tl) detectors, covering angles between 12° and 36°. The discrimination of the inelastically scattered α particles from other light charged particles (p,d,t,^{3}He) was achieved by pulse shape analysis. High energy γ rays were measured with the Oak Ridge National Laboratory BaF_2 array consisting of 76 detectors arranged in four arrays of 19 crystals each and a fifth array from MSU. The arrays were centered at 60°, 90° and 120° and covered total solid angle of $\sim$ 10% of 4π. The γ-ray energy deposited in seven neighboring detectors was summed to improve the response of the detectors. Separation between γ rays and neutrons was achieved by time-of-flight. In addition, light charged particles at larger angles not covered by the Dwarf Wall were detected with the Dwarf Ball [7].

2.1. *Alpha Spectra*

It is essential to show that the spectra of the scattered α particles are dominated by target excitations and to understand the contributing background processes before any detailed analysis of the γ-ray spectra can be performed.

The top row of Figure 1 shows the inelastic α spectra integrated over all measured angles at E_α = 200 MeV on ^{120}Sn (left) and E_α = 160 MeV on ^{208}Pb (right). It shows the relatively slow decrease of the cross section towards lower α energies, corresponding to higher target excitation energies. The bottom row of Figure 1 shows the same spectra in coincidence with γ rays ($E_\gamma > 4$ MeV). The clearly observed peak structure is due to the successive opening of neutron evaporation thresholds. These structures have been previously observed [8, 9] and are strong evidence for an equilibrated system up to at least $\sim$ 50 MeV. This observation is also consistent with the analysis of neutron spectra following inelastic α scattering [10].

In Figure 2 the α spectrum is extended to even lower α (higher excitation) energies for the two beam energies on the ^{120}Sn target. It shows a rapid increase of the cross section at apparent high target excitation energies. Previous measurements of inelastic α scattering at comparable incident energies did not include these high excitation energies [11, 12, 13]. The rise at these energies is too large to result from evaporated α particles following fusion. These α particles correspond to pre-equilibrium emission where the observed α is not necessarily the initially scattered α particle, but could be an α from the target. This is also supported by the comparison of the two beam energies shown in Figure 2. The shapes of the spectra scale with the α energy and not with the α energy loss. These processes have been studied in similar reactions [14, 15, 16] and can

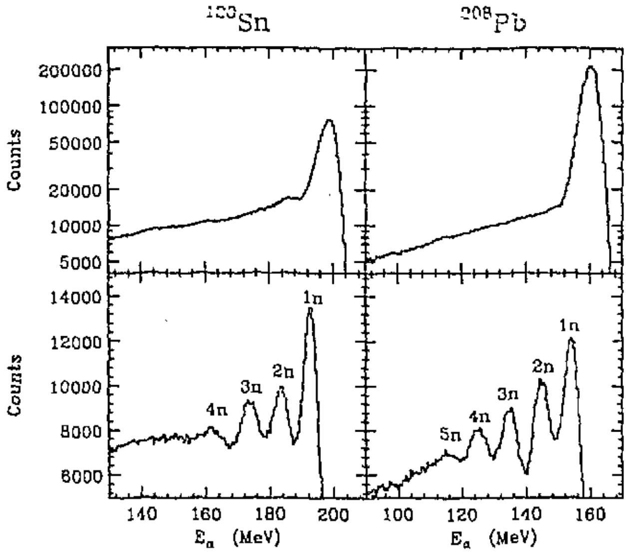

Figure 1: Inelastic α singles spectra (top) and in coincidence with γ rays (bottom) at $E_\alpha = 200$ MeV on ^{120}Sn (left) and at $E_\alpha = 160$ MeV on ^{208}Pb (right). The peaks in the coincidence data correspond to the successive opening of neutron evaporation channels as described in the text.

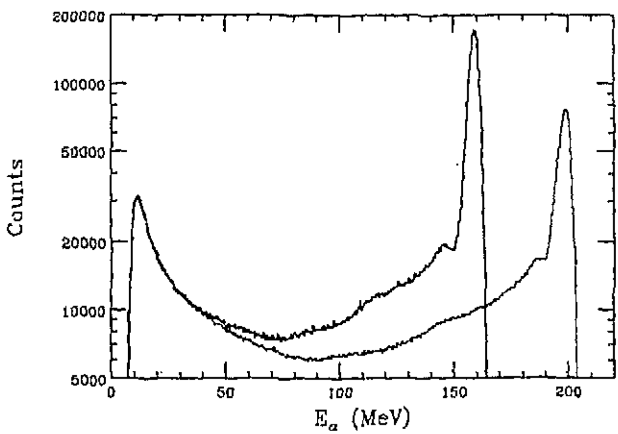

Figure 2: Inelastic α singles spectra at $E_\alpha = 200$ MeV and $E_\alpha = 160$ MeV on ^{120}Sn.

be explained within the multistep direct emission model [17, 18]. Detailed calculations of this type for the present data are under way [19].

Other processes that contribute to the α energy spectra are neutron [20] and proton [21] pickup by the projectile and subsequent decay. Due to the large solid angle coverage of the Dwarf-Ball/Wall for charged particles it is possible to extract the proton pickup-decay contribution and estimate the neutron pickup-decay contribution to the total spectrum. The contribution of these processes to the high energy γ-ray spectra is negligible, since they result in relatively low residual target excitation energies.

2.2 Gamma-Ray Spectra

Another confirmation of high target excitation energy is provided by the γ-ray spectra presented in Figure 3. The γ-ray spectra shown in the left panel were obtained by gating on the same α energy for the two incident beam energies on the ^{120}Sn target. The two spectra are clearly different with a more prominent contribution in the region of the GDR at the higher bombarding energy indicating a higher excitation energy. However, when the γ-ray spectra are gated on the same apparent excitation energy of 40-50 MeV, corresponding to α energies of 110-120 MeV and 150-160 MeV for the incident energies of 160 MeV and 200 MeV respectively (Figure 3, right), they are essentially identical within the statistical uncertainties.

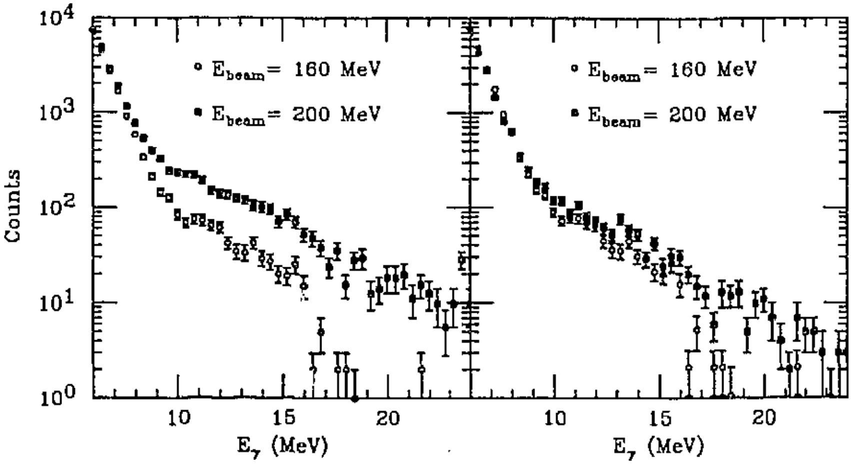

Figure 3: Comparison of the γ-ray spectra at E_{beam} = 200 MeV (■) and E_{beam} = 160 MeV (o) on ^{120}Sn gated on the same scattered α energy range (110-120 MeV, left) and the same α energy-loss (target excitation energy) range (40-50 MeV, right).

Figure 4 presents further evidence that the γ-ray spectra reflect the GDR built on highly excited states of the target nucleus. The spectra for the ^{208}Pb and the ^{120}Sn targets at excitation energies of 120-130 MeV were divided by the identical statistical model (CASCADE) calculation which did not include a GDR strength function. With this method the spectra can be compared on a linear scale. It is evident that the ^{208}Pb spectrum exhibits a peak at lower energies compared to the ^{120}Sn spectra. This is consistent with the measured mean ground state GDR energies which are 13.5 MeV and 15.4 MeV for ^{208}Pb and ^{120}Sn, respectively [22].

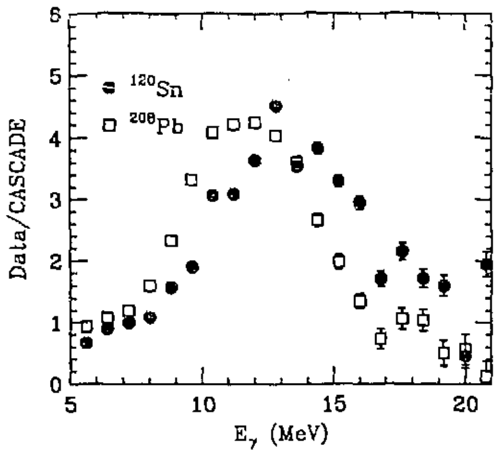

Figure 4: Experimental γ-ray spectra for the ^{208}Pb (□) and the ^{120}Sn (•) targets divided by a statistical model (CASCADE) calculation assuming a constant γ-ray strength function.

3. RESULTS

The γ-ray spectra in coincidence with the inelastically scattered α particles exhibited no statistically significant differences for either different angles of the γ-ray detectors or for different α scattering angles. Thus the γ-ray spectra of all five arrays were summed together. γ-ray spectra for 10 MeV wide excitation energy bins were created. Statistical model calculations using CASCADE [23] were performed and the calculated γ-ray spectra were folded with the response function for the detectors before they were compared with the data. The excitation energy spread in the α spectra for each bin of 10 MeV was used as the initial population distribution for CASCADE. This distribution was spread over an assumed angular momentum transfer of 0-5$\hbar$.

Figure 5 shows fits for the energy bins of 60-70 MeV (left) and 90-100 MeV (right) for the ^{120}Sn target. The extracted width increases from Γ_{GDR} = 7.7 MeV to Γ_{GDR} = 8.7 MeV over this excitation energy range. The resonance energy for these preliminary calculations was kept constant at the ground state value of E_{GDR} = 15.4 MeV.

The preliminary results for the extracted widths are shown in Figure 6. The left side of the figure compares the present results from the inelastic scattering data on ^{120}Sn with fusion-evaporation data on ^{110}Sn [24]. The excitation energies plotted for the fusion data were corrected for the average rotational energy, determined from the calculated mean angular momentum populated in the reactions. The dashed line corresponds to an almost quadratic increase of the width with excitation energy as was shown in Ref. [24]. However, the width increase in the present inelastic scattering data is approximately linear as indicated by the solid line. This difference indicates that the width increase is partially due to the increase in excitation energy and partially due to the increase of angular momentum. Detailed free energy surface calculations need to be performed so that an analysis similar to Ref. [25] can be carried out in order to quantify our conclusions.

In order to compare the width of the ^{120}Sn with the ^{208}Pb data, the extracted widths are plotted as a function of temperature, calculated as $T = \sqrt{E^*/a}$ with the level density parameter $a = A/9$. The width increase in ^{208}Pb is also linear with increasing excitation

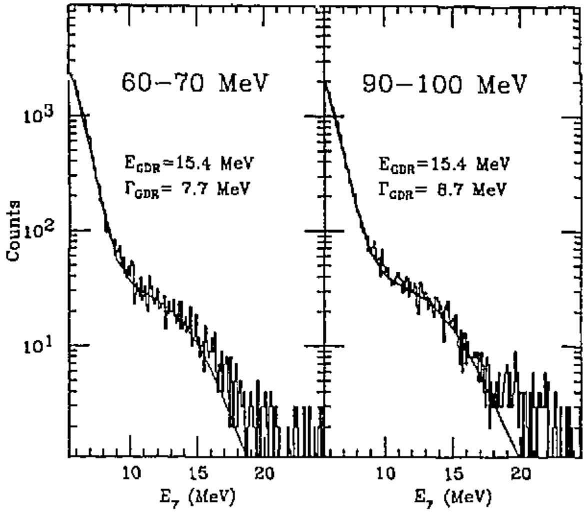

Figure 5: Sample γ-ray spectra and results of CASCADE calculations (smooth curve) for the ^{120}Sn target at excitation energies of 60-70 MeV (left) and 90-100 MeV (right).

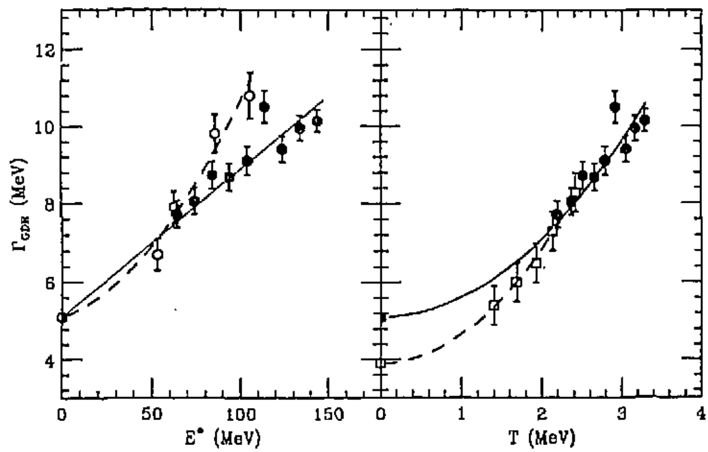

Figure 6: The width of the GDR as a function of excitation energy in ^{120}Sn (left) for fusion-evaporation measurements (from Ref. [24], ∘) and inelastic scattering (•) and as a function of temperature (right) in ^{120}Sn (•) and ^{208}Pb (□).

energy, and therefore quadratic with temperature as shown by the dashed line in Figure 6. Although the analysis is still preliminary, the figure indicates a stronger increase in ^{208}Pb compared to ^{120}Sn. This observation is consistent with potential energy calculations [26] for both systems as a function of temperature. The free energy surface calculations for ^{208}Pb show a steeper surface at low temperatures due to the doubly closed shell. However the shell structure effects wash out rather rapidly between 1 and 2 MeV. This results in a rather rapid broadening of the minimum of the free energy surface and thus could explain the larger increase of the GDR width.

4. SUMMARY AND CONCLUSIONS

Inelastic α scattering was used to populate highly excited states of the target nucleus. These states equilibrate quickly so that their decay can be treated within the statistical model. Thus it is possible to study the GDR built on these excited states by their γ-ray decay. The advantage of inelastic scattering reactions over fusion-evaporation reactions is that relatively low angular momentum states are populated, almost independent of the excitation energy. The excitation energy dependence of the GDR width can therefore be studied with little influence from increasing angular momentum. In the first application of this method we studied ^{208}Pb and ^{120}Sn. The preliminary analysis shows that in ^{120}Sn the width increase with increasing excitation energy is smaller than in fusion reactions, indicating that the increase observed in fusion reactions is only partly due to excitation energy, with a significant contribution from angular momentum increase. The comparison between the ^{120}Sn and the ^{208}Pb data seems to show a stronger increase for ^{208}Pb. This observation is in qualitative agreement with free energy surface calculations, and can be interpreted in terms of the vanishing of shell effects.

5. ACKNOWLEDGMENTS

This work was partially supported by the U.S. National Science Foundation under grant No. PHY-92-14992 and by the Department of Energy under grants No. DE-FG01-88ER40406 and DE-FG02-87ER40310. Oak Ridge National Laboratory is managed by Martin Marietta Energy Systems, Inc. under contract DE-AC05-84OR21400 with the U.S. Department of Energy.

6. REFERENCES

[1] K. A. Snover, Ann. Rev. Nucl. Part. Sci. 36, 545 (1986).
[2] J. J. Gaardhøje, Ann. Rev. Nucl. Part. Sci. 42, 483 (1992).
[3] M. Thoennessen, J. R. Beene, F. E. Bertrand, C. Baktash, M. L. Halbert, D. J. Horen, D. G. Sarantites, W. Spang, and D. W. Stracener, Phys. Rev. Lett. 70, 4055 (1993).
[4] P. Paul and M. Thoennessen, Ann. Rev. Nucl. Part. Sci. 44, in press (1994).
[5] A. Bracco, *et al.*, Phys. Rev. Lett. 62, 2080 (1989).
[6] J. Kasagi and K. Yoshida, Nucl. Phys. A 569, 195c (1994), T. Suomijärvi, *et al.* Nucl. Phys. A 569, 225c (1994), and references therein.
[7] D. W. Stracener, D. G. Sarantites, L. G. Sobotka, J. Elson, J. T. Hood, Z. Majka, V. Abenante, A. Chbihi, and D. C. Hensley, Nucl. Instr. and Meth. A 294, 485 (1990).
[8] M. T. Collins, C. C. Chang, S. L. Talbor, G. J. Wagner, and J. R. Wu, Phys. Rev. Lett. 42, 1440 (1979), M. T. Collins, C. C. Chang, and S. L. Talbor, Phys. Rev. C 24, 387 (1981).

[9] M. Thoennessen, *et al.*, Phys. Rev. C 43, R12 (1991).
[10] A. van der Woude, Nucl. Phys. A 482, 453c (1988).
[11] H. W. Ho and E. M. Henley, Nucl. Phys. A 225, 205 (1974).
[12] D. H. Youngblood, J. M. Moss, C. M. Rozsa, J. D. Bronson, A. D. Bacher, and D. R. Brown, Phys. Rev. C 13, 994 (1976), J. M. Moss, D. R. Brown, D. H. Youngblood, C. M. Rozsa, and J. D. Bronson, Phys. Rev. C 18, 741 (1978).
[13] F. E. Bertrand, G. R. Satchler, D. J. Horen, J. R. Wu, A. D. Bacher, G. T. Emery, W. P. Jones, D. W. Miller, and A. van der Woude, Phys. Rev. C 22, 1832 (1980).
[14] T. Chen, R. E. Segel, P. T. Debevec, J. Wiggins, P. P. Singh, and J. V. Maher, Phys. Lett. B 103, 192 (1981).
[15] G. Ciangaru, C. C. Chang, H. D. Holmgren A. Nadasen, P. G. Roos, A. A. Cowley, S. Mills, P. P. Singh, M. K. Saber, and J. R. Hall, Phys. Rev. C 27, 1360 (1983), G. Ciangaru, C. C. Chang, H. D. Holmgren A. Nadasen, and P. G. Roos, Phys. Rev. C 29, 1289 (1984).
[16] W. A. Richter, A. A. Cowley, R. Lindsay, J. J. Lawrie, S. V. Förtsch, J. V. Pilcher, R. Bonetti, and P. E. Hodgson, Phys. Rev. C 46, 1030 (1992).
[17] H. Feshbach, A. Kerman, and S. Koonin, Ann. Phys. 125, 129 (1980).
[18] R. Bonetti, M. B. Chadwick, P. E. Hodgson, B. V. Carlson, and M. S. Hussein, Phys. Rep. 202, 173 (1991),
[19] M. Hussein and M. Chadwick, private communication.
[20] D. R. Brown, I. Halpern, J. R. Calarco, P. A. Russo, D. L. Hendrie, and H. Homeyer, Phys. Rev. C 14, 896 (1976).
[21] A. Saha, R. Kamermans, J. van Driel, and H. P. Morsch, Phys. Lett. B 79, 363 (1978).
[22] S. Dietrich and B. Berman, At. Data Nucl. Data Tables, 38, 208 (1988).
[23] F. Pühlhofer, Nucl. Phys. A 260, 276 (1977).
[24] D. R. Chakrabarty, S. Sen, M. Thoennessen, N. Alamanos, P. Paul, R. Schicker, J. Stachel, and J. J. Gaardhøje, Phys. Rev. C 36, 1886 (1987).
[25] Y. Alhassid and B. Bush, Phys. Rev. Lett. 65, 2527 (1990).
[26] T. Werner, private communication.

PARTIAL PROTON ESCAPE WIDTHS OF GAMOW-TELLER RESONANCE

S.E.Muraviev and M.H.Urin

Moscow Engineering Physics Institute, 115409, Moscow, Russia

1.Introduction

The theoretical description of partial escape widths for the direct nucleon decay of giant resonances (GR) seems to be a serious test of nuclear structure models. The partial-hole basis is suitable for this description, because final states populated after the direct nucleon decay of GR can be simply described by using this basis. Therefore, the random phase approximation in the continuum (continuum-RPA) can be used to calculate partial nucleon escape widths $\Gamma_c^{\uparrow}$ of GR. Here, c is a set of quantum numbers of a decay channel. This set includes quantum numbers of a hole state of a product nucleus and a particle state in the continuum. A method for calculating the GR strength function within the continuum-RPA has long been formulated [1,2]. This method allows one to calculate the energy ε_d, total nucleon escape width $\Gamma_d^{\uparrow}$, and fraction of the relevant sume rule $(SR)_d$ for all particle-hole states (doorway states) carrying the GR quantum numbers. To evaluate the partial nucleon escape widths $\Gamma_{dc}^{\uparrow}$ of these states ($\Gamma_d^{\uparrow} = \sum_c \Gamma_{dc}^{\uparrow}$) within the continuum-RPA it is convinient to calculate the S-matrix of the nucleon scattering via GR virtual excitation. This method has been formulated recently [3,4]. A nuclear mean field and a particle-hole interaction are input quantities for the both methods. An alternative approach to the calculation of $\Gamma_{dc}^{\uparrow}$ has been also proposed recently [5,6].

The strength function calculations performed for a number of GR with the use of the realistic mean field and particle-hole interaction show that one or more narrow closely-spaced nonoverlapped doorway states exhaust the most part of the relevant sum rule (see, e.g. [1,2,4]). The energy dependence of nuclear reactions accompanied by GR excitation in medium and heavy nuclei exhibits a broad bump corresponding to GR. This bump is formed due to the coupling of the doorway state to many-particle configurations (they are complicated superpositions of 2 particle - 2 hole, 3 particle - 3 hole etc. configurations). Allowance for this coupling is beyond the RPA. However, this coupling can be taken into account by a simple phenomenological way under the assumption that the two following assertions are valid: (i) there are no common channels for the nucleon decay of the doorway and many-particle states; (ii) interaction between the different doorway states via the many-particle states vanishes after energy averaging reaction amplitudes (in other words, the coupling of each doorway state to the many-particle configurations occurs independently of other doorway states). As a result, the spreading (and the energy shift) of each resonance of the energy averaged S-matrix can be described in terms of a phenomenological spreading width $\Gamma_d^{\downarrow}$ (and an energy shift Δ_d) without changing the nucleon escape widths [4]. A direct approach for describing this coupling with the use of a limited basis of many-particle configurations has been proposed in refs. [6].

At the moment, the systematic comparison of experimental and theoretical partial nucleon escape widths of giant resonances seems to be important as a test of nuclear models. In the present work, we consider the partial proton escape widths of the Gamow-Teller resonance (GTR) in magic and near-magic nuclei (Pb and Zr) and in nuclei with the strong nucleon pairing (Sn isotopes). Recently, experimental values of $\Gamma_c^{\uparrow}$ for GTR in ^{208}Pb were obtained from an analysis of the cross-section of the $^{208}Pb(^3He,tp)^{207}Pb$ reaction [7]. We expect that analogous data for the $^{90,91}Zr$ parent nuclei will appear in near future.

The direct $(^3He,t)$ reaction was used for studying the fragmentation of the GT strength in the $^{117,120}Sn$ isotopes [8]. In particular, this study is interesting in connection with the effect of the GTR configurational splitting. This effect was predicted for nuclei in the vicinity of ^{118}Sn and ^{74}Ge in ref [9]. In the present work, this effect as well as its influence on the direct proton decay of the GTR are considered in detail for Sn isotopes. Experimental arguments in favour of this effect are given.

2. Partial proton widths of the GTR in ^{208}Pb and $^{90,91}Zr$

We calculated the partial proton escape widths of the GTR in ^{208}Pb and $^{90,91}Zr$ using the method given in detail in ref. [4]. A phenomenological (shell-model) mean field of the Woods-Saxon type and a Landau-Migdal particle-hole interaction were used in numerical calculations. The aim of the previous $\Gamma_c^{\uparrow}$ calculations performed in [4] only for ^{208}Pb was mainly to demonstrate possibilities of the proposed method. In the present work, we somewhat extend these calculations. The extension involves the two following points: (i) the use of experimental energies of the proton channels instead of calculated ones; (ii) the investigation of the $\Gamma_c^{\uparrow}$ dependence on small variations of the intensity $G' = g'350\ MeV fm^3$ of the spin-isospin part of the particle-hole interaction.

Because the calculated $\Gamma_c^{\uparrow}$ values are strongly dependent on the energy ε_c of the escaping proton ($\Gamma_c^{\uparrow}$ are proportional to the penetrability $p(\varepsilon_c)$ of the potential barrier), small uncertainties in the GTR energy and energies of final hole states can lead to large uncertainties in $\Gamma_c^{\uparrow}$. For this reason, we recalculated the $\Gamma_c^{\uparrow}$ values (obtained in ref.[4] within the continuum-RPA with the use of the $g' = 1.2$ value) using the experimental energies of the proton channels ε_c^{exp} according to equation:

$$\Gamma_c^{\uparrow}(\varepsilon_c^{exp}) = \Gamma_c^{\uparrow}(\varepsilon_c^{calc})p_c(\varepsilon_c^{exp})/p_c(\varepsilon_c^{calc}) \quad (1)$$

In so doing we used the expression for $p_c(\varepsilon)$ from ref. [11]. The calculation results ($\Gamma_c^{\uparrow}(\varepsilon_c^{calc})$ and $\Gamma_c^{\uparrow}(\varepsilon_c^{exp})$) for GTR in the ^{208}Pb parent nucleus are given in the Table 1 (the columns (a) and (b) respectively).

Experimental data on the $\Gamma_c^{\uparrow}$ are also given in Table 1. For comparison we give the calculated and experimental GTR energy obtained with the use of the above g' value: 18.9 MeV and 19.2±0.2 MeV [12]. The use of experimental energies of the proton channels allows us to improve the agreement between experimental and calculated $\Gamma_c^{\uparrow}$ values. To demonstrate the dependence of the $\Gamma_c^{\uparrow}$ values on the intensity g', we calculated $\Gamma_c^{\uparrow}$ using the $g' = 1.4$ value (the calculated GTR energy equals 19.7 MeV). The results are also given in Table 1 (the (c) column gives $\Gamma_c^{\uparrow}(\varepsilon_c^{calc})$, and the (d) column gives $\Gamma_c^{\uparrow}(\varepsilon_c^{exp})$). The dependence of the GTR escape widths reduced to the experimental energies of the proton channels on changes of intensity g' (the (b) and (d) columns) seems to be strong in some cases and would require an interpretation. We note that the values of $\Gamma_c^{\uparrow}$ calculated in ref.[5] within the complex-RPA are strongly different from our results. This difference is apparently to be explained by the fact that the GTR energy calculated in ref. [5] is strongly different from the experimental energy. An adjustment of these values to the experimental energies of the proton channels (for example, according to (1)) allows one to consist possibly these results with our results.

Table 1
Calculated and experimental partial proton escape widths of the GTR in ^{208}Pb parent nucleus.

Final state of ^{207}Pb	$\Gamma^{\uparrow}$ (keV)				
	experimental data [7]	theory			
		$g' = 1.2$		$g' = 1.4$	
		(a)	(b)	(c)	(d)
$(1/2)^-$	48.9±9.3	33	43.4	65	54.5
$(5/2)^-$	incl.in $3/2^-$	18	29.2	58	47.7
$(3/2)^-$	84.0±13.1	21	37.7	46	45.2
$(13/2)^+$	6.9±7.7	0.04	0.21	0.11	0.20
$(7/2)^-$	13.1±6.2	0.26	3.3	0.91	3.4
$(9/2)^-$		0.02	0.074	0.14	0.144
total	153.8±57.2	72	113.8	170	150.8

In connection with observation of separate low-energy GT states in the ^{208}Pb parent nucleus [7] we calculated the energies and strengths of these states. The results are given in Table 2 in comparison with experimental data [7]. (The bottom line of the Table 2 corresponds to GTR).

Having in mind future experimental investigations of the direct proton decay of the GTR in Zr isotopes, we calculated the proton escape widths of the GTR in the $^{90,91}Zr$ parent nuclei. The proton pairing was not taken into account in these calculations. We used the following value of the intensity of the spin-isospin part of the particle-hole interaction $g' = 1$. This value allows us to describe the experimental GTR energy in the ^{90}Zr very well (15.6±0.3 MeV [13] and 15.64 MeV in our calculations). The results are the following. Because the ground state of ^{89}Zr has a large moment $(9/2^+)$, and the energies of escaping protons in the case of decays into excited states are sufficiently small, the proton escape widths of the GTR in ^{90}Zr parent nucleus is very small (the total escape width $\Gamma^{\uparrow}$=0.021 keV). The single-neutron level $2d_{5/2}$ is partially filled in ^{91}Zr, and hence, the GTR proton decay into the ground state ^{90}Zr of is accompanied by escaping d protons. For this reason, the total escape width of the GTR in ^{91}Zr is essentially larger than one in ^{90}Zr and equals $\Gamma^{\uparrow}$=14 keV. Naturally, this width is mostly exhausted by the proton escape width for the decay into the ground state of ^{90}Zr.

Table 2
Energies and strengths of the 1^+ states of the Gamow-Teller type in the ^{208}Pb parent nucleus

Theory		Experimental data [7]
energy MeV	strength %	energy MeV
5.68	1.1	5.4
8.01	1.6	6.46
8.94	1.5	7.46
9.43	2.0	8.22
10.88	1.5	9.2
12.32	2.3	
13.38	5.8	
18.9	66	19.2

In connection with the results given above we note that the same method was successfully used recently to describe the partial proton widths of isobaric analog resonance in near-magic nuclei [16].

In conclusion of this Section we discuss a possible influence of the quenching effect on $\Gamma^{\uparrow}$. It is well-known that a part of the GTR strength is lost due to the GTR coupling to (Δ-isobar)-(neutron-hole) states (quenching effect). This effect is usually described in a phenemenological way in terms of a static effective charge $e_q \simeq 0.8$ (see, e. g., [14]). This raises a question whether the necessity exists to decrease the calculated $\Gamma^{\uparrow}$ values by a factor of e_q^2. The answer seems to be negative and can be supported by an analogy with the consideration of any static effective charge. It is well-known that low-energy particle-hole states can show the effective charge (induced by the coupling to the relevant GR) remarkably smaller than unity. Nevertheless, the escape widths of these states (or the widths for decay into any "noncollective" channels) are close to the corresponding single-particle values, because the admixture of the GR to the particle-hole state is small.

3. GTR configurational splitting and partial proton escape widths of the GTR in Sn isotopes

A special consideration of the GTR strength function and partial proton escape widths of the GTR in Sn isotopes is stimulated both by the experimental investigations [8,10] and by the prediction of the effect of the GTR configurational splitting for nuclei in the vicinity of the ^{118}Sn [9]. This effect consists in the splitting of the main maximum in the energy dependence of the GTR strength function into two components of comparable strengths. The splitting is a specific shell-model effect connected with the onset of the filling of the neutron $1h_{11/2}$ level when the strong neutron pairing takes place. In this case, the strength $(SR)_h$ of the particle-hole configuration $\{1h^p_{9/2}, (1h^n_{11/2})^{-1}\}_{1^+}$ is small, because of a small occupation number of the $1h_{11/2}$ level, and the energy E_h of this configuration is larger than energies of other particle-hole configurations approximately by $2(\varepsilon_{1h_{11/2}} - \mu)$, where $\varepsilon_{1h_{11/2}}$ is the shell-model energy of the level, μ is the neutron chemical potential. In the ^{118}Sn parent nucleus, the energy E_h is close to the energy $E_{G'}$ of the Gamow-Teller resonance built without this particle-hole state (GTR′). Therefore, it can be expected that this particle-hole state interacts with GTR′, but does not practically interact with other particle-hole configurations. Thus, we are led to a two-level eigen-problem, and the two-bump GTR (GTR_1 and GTR_2) is formed, when the interaction is taken into account.

To illustrate these statements we calculated the E_h, $E_{G'}$, E_{G_1}, E_{G_2} values and the corresponding fractions of the GT sum rule $(SR)_h$, $(SR)'$, $(SR)_1$, $(SR)_2$ for the $^{112-124}Sn$ parent nuclei. These data are given in Table 3.

To obtain these results we generalized the continuum-RPA approach used in the previous section to the case of the neutron pairing (the proton pairing in Sn isotopes is absent). A simplest version of the BCS model as well as standard parameters of this model [15] together with parameters used in the previous section were used. According to the data given in Table 3, nonmonotonic changes of the energy of the main GT component are expected in going from light Sn isotopes to heavy ones due to the configurational splitting effect. As for the observation of the GTR splitting in Sn isotopes, the experimental data from ref. [8] do not confirm this effect, but are compatible with the predictions, because the calculating splitting (about 3 MeV) is smaller than the observable total width of the GTR (about 5 MeV [8]). In such situation, the energy $\bar{E}_G$ obtained by averaging over the two main components (see Table 3) should be compared with the experimental GTR energy. It is seen from Table 3, that the $N - Z$ dependence of $\bar{E}_G$ is approximately linear, but the proportionality factor is different from ones for the two components.

The dependence of the energy of the main GT maximum on $N - Z$ leads to some pecularities of the dependence of the calculated GTR escape widths on $N - Z$. Because of the configurational splitting effect, the GTR energy is changed only slightly, and hence, the widths $\Gamma^{\uparrow}_c$ for main decay channels increase in going from light Sn isotopes to heavy ones [3]. For this reason, the experimental study of the N-dependence of GTR escape widths could give an additional information on the configurational splitting effect.

The existence of the configurational splitting effect is supported by results of work [10] in which the resonance $^{117}Sn(p,n)^{117}Sb$ reaction was experimentally studied. It was observed that the cross-section has two broad resonances which was related to GTR. These results can be explained [3] under the assumptions that (i) the Gamow-Teller resonance built on the $2d^n_{3/2} - [3s^n_{1/2}]^{-1}$ excited particle-hole state of ^{118}Sn (GTR*) is excited by means of this reaction together with GTR built on the ground state of ^{118}Sn; (ii) both GTR and GTR* are splitted. A satisfactory quantitative description of the experimental data was obtained within this interpretation [3]. This can be considered as some evidence for existense of the configurational splitting effect.

Table 3
Energies and strengths of the GT states in Sn isotopes

isotope	GTR'		$1h^p_{9/2}, (1h^n_{11/2})^{-1}$		GTR				
					GTR_1		GTR_2		Aver.
	$E_{G'}$ (MeV)	$(SR)_{G'}$ %	E_h (MeV)	$(SR)_h$ %	$(E_G)_1$ (MeV)	$(SR)_1$ %	$(E_G)_2$ (MeV)	$(SR)_2$ %	$\bar{E}_G$ (MeV)
^{112}Sn	16.9	75	20.3	3.2	16.8	71	20.5	11	17.3
^{114}Sn	16.2	73	18.6	4.1	16.0	59	19.0	19	16.7
^{116}Sn	15.4	69	16.9	6.2	15.0	43	17.8	35	16.2
^{118}Sn	14.7	66	15.6	9.2	14.1	30	17.2	48	16.0
^{120}Sn	13.9	61	14.4	11	12.8	18	16.3	58	15.5
^{122}Sn	13.1	53	13.4	14	11.8	15	16.1	58	15.5
^{124}Sn	12.4	56	12.7	23	10.9	13	15.8	66	15.0

5. Summary

The method for calculation of the GR partial escape widths which was previously formulated [3,4] has been applied to the calculation of the partial proton escape widths of the GTR in medium and heavy nuclei. A phenomenological mean field of the Saxon-Woods type and a Landau-Migdal interaction have been used. The satisfactory agreement between the calculated and experimental values [7] has been achieved with the use of experimental energies of the proton channels for the ^{208}Pb parent nuclei. The predictions for the $^{90,91}Zr$ parent nuclei have been also made.

The method has been generalized to the case of nuclei in which the strong neutron pairing takes place. It has been applied to the detailed analysis of the configurational splitting effect in Sn isotopes. The isotopic dependence of energies and strengths of two GT components have been analized. Theoretical and experimental arguments in favour of the configuration splitting effect have been given.

References

1. S.Shlomo, G.Bertsch, Nucl.Phys., A243 (1975) 507.
2. F.A.Gareev, e. a., Sov.J.Nucl.Rhys., 33 (1981) 337.
3. S.E.Muraviev, M.H.Urin, Nucl.Phys. A569 (1994) 267c.
4. S.E.Muraviev, M.H.Urin, Nucl.Phys. A572 (1994) No 2.
5. N.Van Giai, e. a., Phys.Lett., B233 (1989) 1.
6. G.Colo, e. a. Phys.Lett. B276 (1992) 279.
7. H.Akimune, e. a., Nucl. Phys., A569 (1994) 255c.
8. J.Janecke, e. a., Phys. Rev., C48 (1993) 2828.
9. V.G.Guba, M.A.Nikolaev, and M.H.Urin, Phys.Lett., B218 (1989) 283.
10. B.Ya.Gouzhovskii, B.M.Dzyuba, and V.N.Protopopov, JETP Lett., 40 (1984) 1322.
11. A.Bohr and B.Mottelson, Nuclear Structure,vol. 1(Benjamin,New York,1969).
12. D.Horen, e. a., Phys. Lett., B95 (1980) 27.
13. D.E.Bainum, e. a., Phys. Rev. Lett., 44 (1980) 1751.
14. A.B.Migdal, Theory of finite Fermi systems and applications to atomic nuclei, Wiley, New York, 1967.
15. V.G.Soloviev, Theory of complex nuclei, Pergamon, Oxford, 1976.
16. O.A.Rumyntsev, M.H.Urin, Phys. Rev., C49 (1994) 537.

DECAY OF THE PHOTONUCLEAR GIANT RESONANCE

B. S. Ishkhanov, I. M. Kapitonov
Institute of Nuclear Physics, Moscow State University, 119899 Moscow, Russia
A. M. Lapik, R. A. Eramzhyan
Institute for Nuclear Research, Russian Academy of Sciences, 117312 Moscow, Russia

Abstract

The formation and decay of the giant dipole resonance in 2s2d shell nuclei is discussed. New experimental data obtained in $(\gamma, x\gamma')$-experiments are utilized to extract some quantitative information about the configurational splitting of the GDR in this region of nuclei. Partial photoneutron spectra from the iron region is presented.

1. Excitation energies associated with the Giant Dipole Resonance (GDR) are sufficiently high to allow for decay by emission of nucleons. This makes it possible to study the properties of the GDR by experiments where decay by nucleon emission is registered. Branching ratios for decay into the various open channels convey much more detailed information on the structure of the GDR than the inclusive experiments alone. This circumstance makes such types of studies interesting and allows to test thoroughly various nuclear models elaborated to interpret the phenomenon of the GDR.

Particle decay can occur through various processes. The coupling of the coherent 1p1h-state to the continuum gives rise to semidirect decay into the hole states with a partial width $\Gamma^{\uparrow}$. This is an escape width. If this process is the only one, then the relative population of these states would reflect the microscopic structure of the GDR. The other decay component - the spreading width $\Gamma^{\downarrow}$ - arises from the mixing of 1p1h-states through the residual interaction with the numerous 2p2h-states in the vicinity of the resonance. These 2p2h-states couple again to 3p3h ones etc. At each intermediate level particle decay can occur. An understanding of the decay modes, and in particular of the systematic behavior of $\Gamma\uparrow$ and $\Gamma\downarrow$ is an essential ingredient for the completion of the description of the GDR.

Classification of the decay branches is often ambiguous because one has no experimental procedure for labeling a given nuclear decay as being due to a particular mechanism. Clearly a theory is needed which provides a unified description for all of these processes. In absence of such a unified theory one has to be satisfied with predictions of specific reaction models and compare them to the observed pattern.

2. Data on the partial photodisintegration channels are obtained in two types of experiment. One measures either the spectra of the emitted nucleons or the spectra of the γ-quanta from the deexcitation of levels in the daughter nucleus populated after emission of the nucleon. The simultaneous use of the results of measurements carried out by these two methods greatly advances the understanding the decay processes. Most of the deexcitation experiments were carried out for nuclei of the 2s2d-shell (A=16-40) - see Ref.1. That is why we will concentrate our attention on them.

Fig.1, taken from Ref.[2], demonstrates the photoproton decay channel in reaction $^{28}Si(\gamma,p_i)$. Here i corresponds to the ground (i=0), first excited (i=1) etc. levels of the daughter nucleus. Experimental data on $\sigma(\gamma,p_i)/\sigma(\gamma,abs)$ are shown by points. The results of calculation in the framework of Hauser-Feschbach procedure which singles out the statistical decay are given by solid line. Observed partial proton cross sections exceed significantly what is given by the statistical mechanism of decay. Observed partial proton cross sections show an intermediate structure. This structure depends upon the level of the residual nucleus.

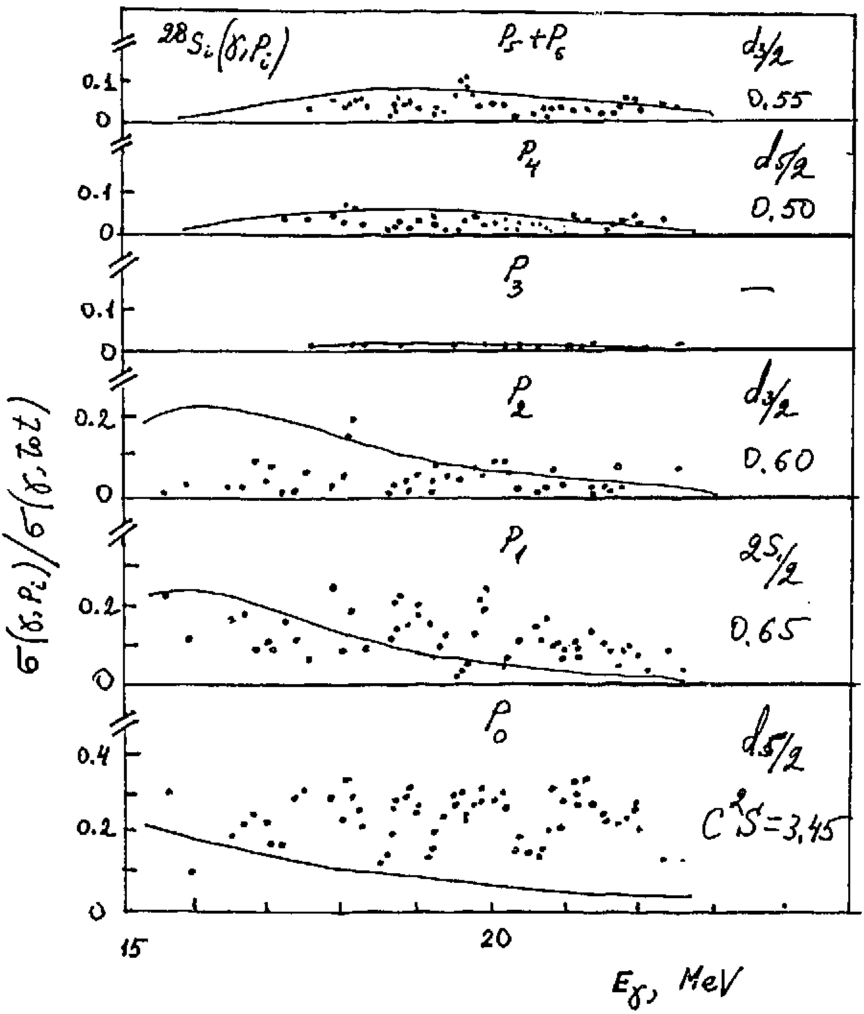
$^{28}Si(\gamma,P_i)$
P_5+P_6
$d_{3/2}$
0.55
P_4
$d_{5/2}$
0.50
P_3
—
P_2
$d_{3/2}$
0.60
P_1
$2S_{1/2}$
0.65
P_0
$d_{5/2}$
$C^2S=3.45$
$\sigma(\gamma,P_i)/\sigma(\gamma,tot)$
E_γ, MeV
15
20
0.1
0.2
0.4
0

Fig.1

Partial cross sections are correlated to the spectroscopic factors of proton pickup reaction - C^2S. They are given on the right hand side of Fig.1. All levels except the third one belong to the hole states of the target nucleus. In photonuclear reaction these holes are created as a result of the outer nucleons (2s2d) having absorbed the γ-quanta forming the dipole resonance with their subsequent emission to continuum. Such a correlation between the spectroscopic factors and the partial photonuclear cross sections is observed for all 2s2d-nuclei - see Ref.[3].

This preferential decay of the dipole resonance to particular one hole states in the residual nucleus is called semidirect. One can suggest that the decay of the GDR to the ground and low-lying states of the residual nucleus which have large spectroscopic factor is completely semidirect. As to the other states of the residual nucleus one can single out the semidirect part using the following prescription. Let $\sigma(\gamma,x_i)$ is the measured cross section when the level i in the residual nucleus is populating. Then the semidirect part $\sigma_{sd}(\gamma,x_i)$ of this cross section is equal to

$$\sigma_{sd}(\gamma,x_i)=\sigma(\gamma,x_i)*(C^2S_i/C^2S_0) ,$$

where in brackets stands the ratio between the spectroscopic factors of pickup reaction to the ground (0) and excited (i) state. To realize this procedure one needs to single out all levels in the residual nucleus.

Tab.1 taken from Ref.1 demonstrates how detailed became the information on the decay channels when the deexcitation photons have been detected. The role of the different hole states is elucidated and this allows to get the detailed decay pattern. After using this procedure one arrives to the decomposition of the photonuclear cross section in ^{24}Mg into the semidirect part (it is shown by the dashe line) and the rest as it is shown in Fig.2.

Not only the hole states which correspond to the outer shell nucleons but to the inner shell nucleons too are manifested in the photonuclear decay channels. The phenomenon of deep holes in 2s2d-

Tab.1. Partial cross sections in photoproton reactions on ^{24}Mg

Levels in ^{23}Na					Integral cross sections in MeV*mb	
n	E_f,MeV	J^{π}	nl_j	C^2S	$\gamma,p\gamma'$	γ,p
0	0	$3/2^+$	$1d_{3/2}$	0.26	-	11
1	0.44	$5/2^+$	$1d_{5/2}$	2.9	-	40
2	2.08	$7/2^+$			12.9±1.1	
3	2.39	$1/2^+$	$2s_{1/2}$	0.24	16.8±1.3	
4	2.64	$1/2^-$	$1p_{1/2}$	2.1	10.0±0.8	52
5	2.70	$9/2^+$			<1.8±1.0	
6	2.98	$3/2^+$	$1d_{3/2}$	0.16	6.3±1.3	
7	3.68	$3/2^-$	$1p_{3/2}$	0.7	5.2±1.2	
8	3.85	$5/2^-$			0	
9	3.91	$5/2^+$	$1d_{5/2}$	0.02	1.9±0.8	32
10	4.43	$1/2^+$	$2s_{1/2}$	0.1	6.1±0.6	
12	5.38	$5/2^+$	$1d_{5/2}$	0.49	3.8±1.5	18
18	5.97	$3/2^-$	$1p_{3/2}$	0.6	4.3±1.6	
	6.5-8.5		$1p_{3/2}$	0.9		18
	8.5-10.5		$1p_{3/2}$	2		9

shell nuclei touch the two adjacent upper shells - the filled 1p and valence (2s2d) shell and profoundly affects the structure of the GDR. It is precisely because of this phenomenon that transition from outer shell (type A) and inner shell (type B) in this nuclei are strongly separated in energy and a unified dipole

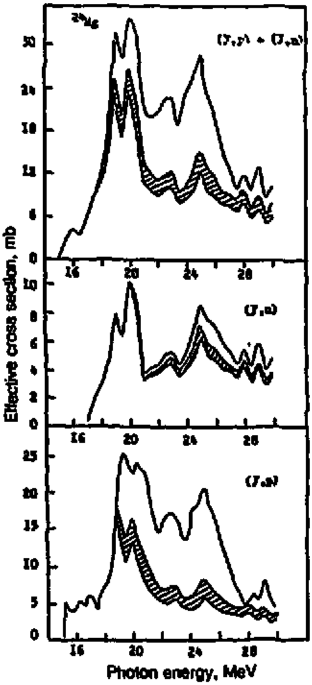

Fig.2

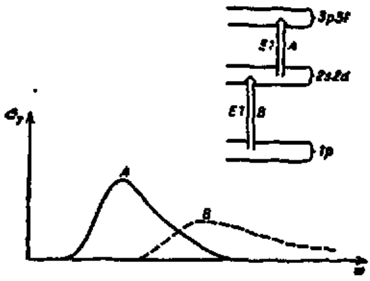

Fig.3

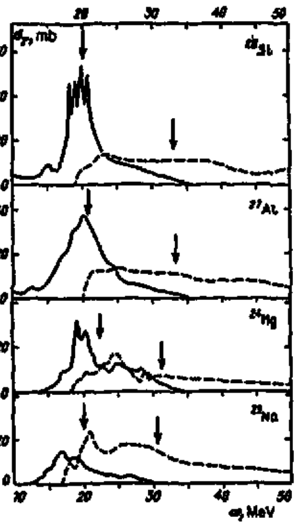

Fig.4

state is not formed. This situation was first pointed out in Ref. [4] and this phenomenon was called the configurational splitting of the GDR. The qualitative picture of the structure of the GDR in 2s2d-shell nuclei is given in Fig.3.

In Fig.4 the photoabsorption cross section of ^{28}Si, ^{27}Al, ^{24}Mg and ^{23}Na nuclei up to 50 MeV, divided into type A (solid curve) and type B (broken curve) transition is shown, demonstrating the dynamic of the configurational splitting of the GDR in 2s2d-shell nuclei.

At the same time it is clear that a comprehensive study of the GDR configurational splitting in the 2s2d shell nuclei requires that the experiments should be extended to the excitation energy region from 30 to 50 MeV, where enough large part of the photoabsorption cross section is located (Fig.5).

3. It is expected that in heavier nuclei the effect of the configurational splitting will become weak. However in region of 3p3f-nuclei one still expects this effect. Recently the energy spectra of neutrons with energy $\geq$ 3.7 MeV and the corresponding cross sections were measured in several 3p3f-nuclei - ^{51}V, ^{52}Cr, ^{54}Fe, ^{56}Fe, ^{58}Ni and ^{64}Zn- using a scintillation spectrometer [5]. It was observed that in contrast with total cross section [6,7] the measured ones show the resonant structure and almost have no smooth part (Fig.6). The measured cross section exhausts the total photoneutron cross section starting from about 22 Mev, where the resonance already have passed its maximum. In the measured neutron spectra in ^{51}V and ^{58}Ni no transitions have been observed from the high energy region of the giant resonance excitation to the ground and low-lying states of residual nucleus up to excitation energy of about 3 MeV. The nonstatistical part of the measured spectra is given in Fig.7.

One can speculate that this suppression of transitions to the low-lying states has the same origin as in 2s2d-shell nuclei, namely is due to the configurational splitting of the resonance.

It is interesting to mention that the width of the individual resonances as follows from the upper estimations turns out to be less than 80 keV (see Fig.6).

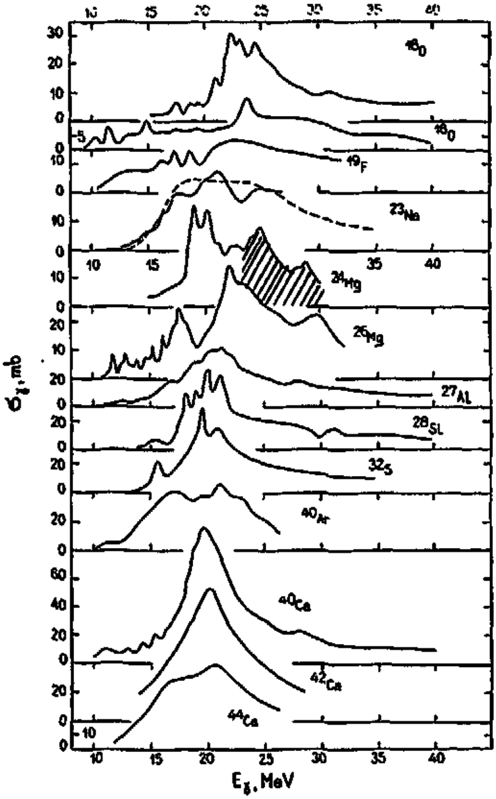

Fig.5

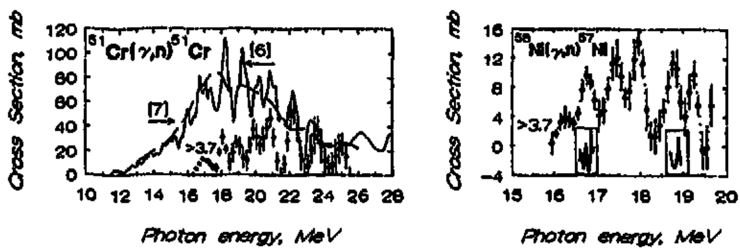

Fig.6

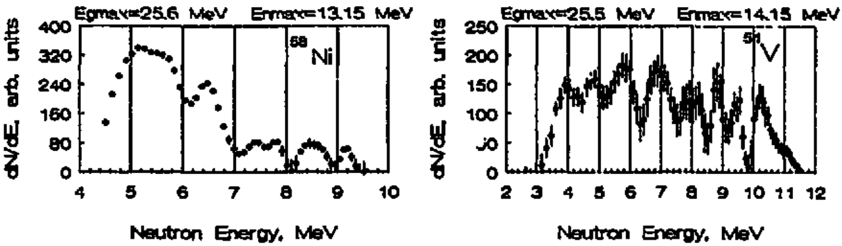

Fig.7

4.$(\gamma,x\gamma')$-reaction allowed to get the detailed information about population after the decay of the GDR of various levels in the residual nucleus. Hole state are preferentially populating when the GDR decays by the nucleon emission. Effect of configurational splitting is strongly pronounced in 2s2d-shell nuclei. It is interesting to continue to study the partial transitions in 3p3f-shell nuclei to learn more about the decay in this region of nuclei.

This work was partially supported by the Russian Fundamental Researcn Foundation.

References.

1. B.S.Ishkhanov, I.M.Kapitonov, R.A.Eramzhyan. Sov.J.Part.Nucl. 23(1992) 774
2. R.L.Gulbranson e.a., Phys. Rev. C27 (1983) 470
3. R.A.Eramzhyan e.a. Phys. Rep.136 (1986) 229
4. V.G.Neudachin, V.G.Shevchenko, N.P.Yudin. Phys.Lett.10(1964)180
5. I.M.Glatky, A.M.Lapik, B.S.Ratner, S.S.Verbitsky, A.V.Veselovsky. Nucl. Phys. A512(1990)167
6. B I.Goryachev et all. Izv. AN SSSR, ser. fiz. 33(1969)1736
7. J.Weize et all. Aust.J.Phys. 30(1977)401

Use and misuse of the "completeness" concept in nuclear spectroscopy

Jean Kern

Physics Department, University, CH-1700 Fribourg, Switzerland

1. Introduction

Completeness is a concept which was introduced following the development of the Average Resonance Capture (ARC) technique [1]. The (n,γ) reactions are non-selective but, because of the strong Porter-Thomas fluctuations, the primary transitions from a particular capture state do not populate all levels possibly fed (according to the angular momentum selection rules) with an intensity large enough to insure their observation. This problem is avoided when primary transitions issued from a large set of resonance capture levels are observed. The availability of "complete" level schemes has soon proved to be very useful [2,3] so that the concept has attracted much attention. It was claimed that other non-selective reactions, like fusion reactions [4] or inelastic neutrons scattering reactions [5], have also completeness properties. When a method becomes "fashionable" it can inevitably also be used in a more questionable or imprecise way. This will be the subject of this paper.

2. Domain of completeness in neutron capture reactions

By definition, a complete level scheme would be one where no level is missing. It is clear to anyone, however, that the level scheme of a heavy nucleus will (probably) never be known completely up to the neutron separation energy. To be precise, it is therefore necessary to specify the region in the spin *vs* excitation energy plane where the scheme is claimed to be complete. In ARC measurements, assuming s capture, the spin range of the final levels which can be populated by dipolar transitions is easily determined. Our first point is that the energy limit of completeness is not a sharp one. It is what we will call a *statistical* limit. It means that the *probability* of having a complete level scheme for some spin (or spin range) varies with energy, as shown in Fig. 1. There is no precise limit, but a gray zone (hatched in Fig. 1) which extends between a conservative E_1 and an optimistic E_2 limit. None of these limits is easily defined and an objective determination would require a detailed study based on the experimental energy resolution, intensity sensitivity and level density. Two consequences derive from this situation:

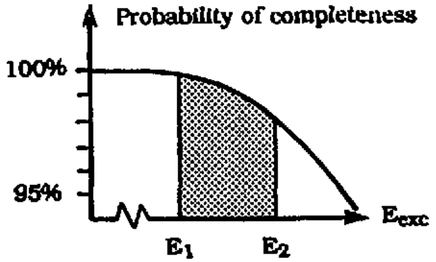

Fig. 1 :

Probability of completeness for a given spin as a function of the excitation energy.

First the authors of a study may not be consistent in the value of the completeness limit they themselves quote. Regarding the well known study of ^{168}Er by Davidson et al. [6], the authors claim in the abstract and in the introduction that the set of spin 2-5 levels below about 2.2 MeV is complete. Further in the text (sect. 2.7), the completeness limit is reduced to about 2000 keV and to about 1900 keV (sect. 3.3.2 and 4.4) for the positive parity levels. In another paper [7], some of the same authors state that a complete level scheme up to 2 MeV for ^{168}Er was constructed. This example shows that the completeness limit is somewhat fuzzy.

The second consequence is that there remains a small probability, close to the limit, that a level be missed. There are a few examples known, one regarding again ^{168}Er. A $I^{\pi} = 2^{+}$ level was discovered at 1893 keV by Kleppinger and Yates [8] which had been originally undetected [6]. This level has been confirmed in subsequent works [7,9]. The probability to miss a level close to the limit is small, but finite, whereas this will be quite unlikely well below the limit. The probability that a peak in the ARC spectrum be hidden by a more intense one increases with the excitation energy, since the level density then also increases. It is also important to note that to reach completeness it is not sufficient that a level be excited by a given process, some evidence of its population and/or depopulation must also be observed.

3. Physical consequences of completeness

The observation of a truly complete level scheme in some spin and energy range has very important consequences in the comparison of experimental results with model calculations, since a missed (or a spurious) level can lead to a serious bias and to wrong conclusions. The knowledge that a level scheme is complete can also have other useful applications and help, for instance, to unraveling the rotational structure of a deformed nucleus [3, 6]. The completeness argument, however, has sometimes been used beyond its range of validity or relevance. A first example regards ^{178}Hf. A detailed study of this isotope by (n,γ) spectroscopy, including ARC measurements, was performed by Hague et al. [10] who claimed completeness for spins 2 to 5 up to "about 1800 keV". They found a new 2^+ level at 1808 keV and proposed that it forms the head of a K = 2 rotational band including the known 3^+, 4^+ and 5^+ levels at 1862, 1953 and 2068 keV. The latter levels, however, are clearly identified [11] as members of the $K^\pi = 3^+$ {7/2⁻[514] - 1/2⁻[510]} two-quasineutron band. The assignment proposed in ref. [10] relies on an incorrect use of the completeness argument: the authors argued that, because no other 3^+ level had been observed, the one at 1862 keV had to be a member of the $K^\pi = 2^+$ rotational band. This argument is not valid, since the missing 3^+ level is expected at an energy *above* the completeness limit !

The second example deals with a challenging and controversial problem in ^{126}Te. In Fig. 2

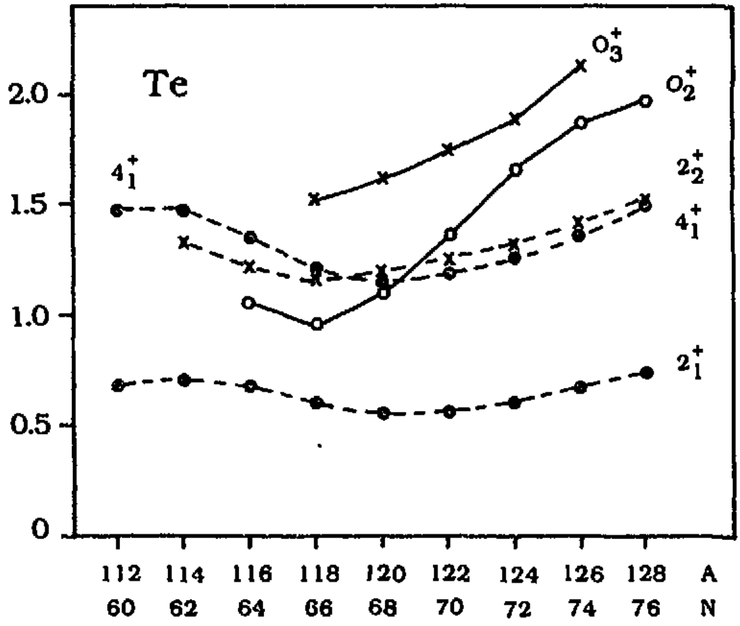

Fig. 2 : Systematics of selected experimental low-lying positive parity levels in $^{112-128}$Te.

are presented the partial level schemes, including the 0_1^+, 2_1^+, 4_1^+ 2_2^+, 0_2^+ and 0_3^+ levels, in a series of even Te nuclei. ARC measurements in ^{124}Te [12] and ^{126}Te [13] have shown that there is no other 0^+ level below 2.5 MeV as those reported in Fig. 2. The question which arises is to know if the 0_2^+ and 0_3^+ states are the expected 0^+ members of the 2-phonon triplet and 3-phonon quintuplet expected in the SU(5) limit, or, in the O(6) limit, one of the $(\sigma,\tau) = (N,3)$ or $(N-2,0)$ state and an intruder, for example. The authors of ref. [13] rejected the O(6) limit in ^{126}Te with the argument that it is not possible to reproduce simultaneously the $2_2^+/2_1^+$ energy ratio and the $2_2^+ - 4_1^+$ energy splitting, whereas there is no compelling argument against a (anharmonic) SU(5) description. The authors conclude that "there seems to be little need to invoke low-lying intruder states". This conclusion might be premature on the basis mainly of completeness arguments in view of the fact that

a) intruders have been observed in several nuclei in this region (e.g. Pd, Cd, Sn, Sb, I),
b) that the energy variation of the 0_2^+ levels is as expected for an intruder, and
c) the authors have considered the IBM-1 model in its simplest form and only in the limiting case of dynamical symmetries.

It is admitted that the subject is controversial. More detailed studies are needed and some are presently being performed, see e.g. ref. [14].

4. Completeness in fusion reactions

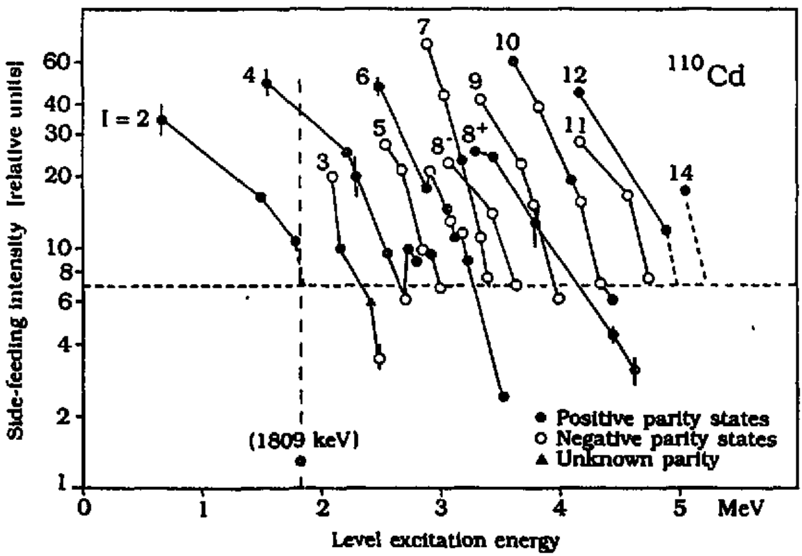

Fig. 3 : Side-feeding intensities for the ^{108}Pd(α,2nγ)^{110}Cd reaction [15] reported as a function of the level excitation energies. The bombarding energy was 27.1 MeV. The solid lines connect the data points corresponding to the same spin values. The dotted horizontal line indicates the lower limit of population needed to insure observation of the levels. The star indicates the experimental intensity of a transition of 1151.9 keV which was considered for the depopulation of a controversial 1809 keV level.

Charged-particle fusion reaction spectroscopy presents also completeness properties [4]. To prove the validity of this claim, it is necessary to show that all levels within a region of the spin *vs* excitation energy plane have a guaranteed minimum population, independent of their structure, and which is sufficient to ensure observation of their decay. In a recent study [15] of ^{110}Cd by the ^{108}Pd(α,2nγ) reaction, it has been shown that the side-feeding intensity (population from the continuum) follows some regular spin dependent pattern (Fig. 3).

This behaviour can be reproduced by Hauser-Feshbach calculations [16]. The example in Fig. 4 shows that the side-feeding intensity is independent of the particular structure of the

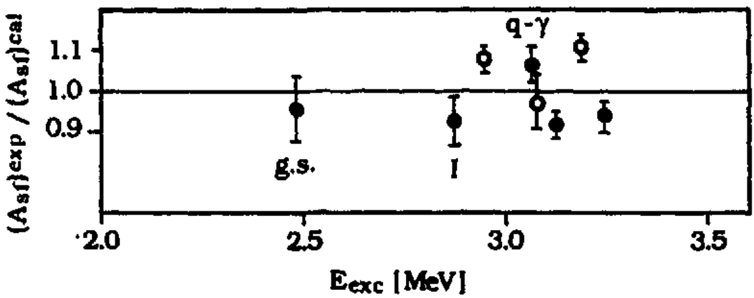

Fig. 4 : Ratios of the experimental [15] to the calculated [16] side-feeding intensities of the I = 6 levels for the ^{108}Pd(α,2nγ)^{110}Cd reaction. The dots (o) are for positive parity, the open circles (o) for negative parity final states; g.s stands for "ground state", I for "Intruder" and q-γ for "quasi-gamma". The errors bars represent the 1 σ statistical errors. It is apparent that the side-feeding intensity is independent of the parity, of the deformation and of any other level structure characteristic.

levels fed. Consequently, a minimum population (this can be increased by discrete transitions) is *guaranteed*, the value depending on the spin and on the excitation energy of the levels. It then becomes necessary to determine what intensity of population will insure observation of the levels. Considering [17] the maximum intensity of the transitions observed in the singles spectrum which could not be placed in the scheme, and with the hypothesis that it is very unlikely that a particular level decay by more than 2 transitions of about equal intensities, a minimum of 7 units (in a scale where the 2_1^+ to 0_1^+ transition has the intensity 1000 units) is required (Fig. 3). The intersection of the side-feeding intensity curves with the intensity limit provides for each spin an estimated upper limit of completeness. Specifying properly the region of completeness makes it possible to test, for example, the existence of levels with given spins observed in an experiment or expected on theoretical grounds to lie in some energy interval. It was thus possible to disprove [17] the existence of a controversial level at 1809 keV in ^{110}Cd having a possible spin 2, 3 or 4. As shown in Fig. 3, the side-feeding intensity would be 8, 20 or 37 units for these different spin values, respectively. These intensities lie above the minimum population of 7 units required to insure observation and are much higher than the intensity of 1.3 unit (star in Fig. 3) for a possible decay transition observed in the (α,2n) reaction [15]. Another example, pertaining to ^{112}Cd, is discussed in ref. [18]. As for ARC measurements, the limit of completeness is not sharp. The probability to miss a state decreases rapidly when its expected population rises above the minimum estimated feeding intensity necessary for its observation.

5. Concluding remarks and discussion

Other non-selective reactions have completeness properties. Yates et. al. [5,19] have claimed that the (n,n'γ) reaction excites all low-spin states up to about 100 keV below the incident neutron energy. Although a detailed justification is still needed, the claim seems quite sensible. Other authors invoked transfer reactions for establishing complete level schemes. As is well known, direct reactions are very selective and their main interest is to determine the structure of the observed levels. They have no completeness properties and can be used, in this respect, only as a complementary tool.

In view of the success and interest of completeness, many papers are entiteled "Complete spectroscopy of isotope xy". Frequently the region of completeness is not specified and it has to be understood simply that an extended level scheme is being proposed. Cautious authors write "complete" between quotation marks.

The title of this paper is a paraphrase of that of a talk by Prof. Lipas in a recent symposium. I hope he will not mind. The author thanks Prof. D.G. Burke for very helpful comments. The work was supported in part by the Swiss National Science Foundation.

References

1. L.M. Bollinger and G.E. Thomas, Phys. Rev. Lett. 18 (1967) 1143
2. R.E. Chrien, Trans. N.Y. Acad. Sci 44 (1980) 40
3. R.F. Casten, D.D. Warner, M.L. Stelts and W.F. Davidson, Phys. Rev. Lett. 45 (1980) 1077
4. P. von Brentano, A. Dewald, W. Lieberz, R. Reinhardt, K.O. Zell and W. Zipper, in Nuclear structure of the Zr region, edited by J. Eberth, R.A. Meyer and K. Sistemich (Springer, Berlin 1988) p. 157

5. A.J. Filo, S.W. Yates, D.F. Coope, J.L. Weil and M.T. McEllistrem, Phys. Rev. C 23 (1981) 1938
6. W.F. Davidson, D.D. Warner, R.F. Casten, K. Schreckenbach, H.G. Börner, J. Simic, M. Stojanovic, M. Bodganovic, S. Koicki, W. Gelletly, G.B. Orr and M.L. Stelts, J. Phys. G7 (1981) 455
7. W.F. Davidson, W.R. Dixon, D.G. Burke, J.A. Cizewski, Phys. Lett 130B (1983) 161
8. E.W. Kleppinger and S.W. Yates, Phys. Rev. C 28 (1983) 943
9. D.G. Burke, W.F. Davidson, J.A. Cizewski, R.E. Brown and J.W. Sunier, Nucl. Phys. A445 (1985) 70
10. A.M.I. Haguc, R.F. Casten, I. Förster, A. Gelberg, R. Rascher, P. Richter, P. von Brentano, G. Barreau, H.G. Börner, S.A. Kerr, K. Schreckenbach and D. D. Warner, Nucl. Phys. A455 (1986) 1
11. R.K. Sheline, D.G. Burke, M.M. Minor and P. Sood, Phys. Rev. C 48 (1993) 911; D.G. Burke, O. Straume, G. Løvøiden, T.F. Thorsteinsen and G. Graue, Proc. 8th Int. Symp. on Capt. Gamma-Ray Spectr., Fribourg 1993, edited by J. Kern (World Scientific, Singapore 1994) p. 207
12. R.F. Casten, J.-Y. Zhang and B.-C. Liao, Phys. Rev. C 44 (1991) 523
13. W.-T. Chou, R.F. Casten and N.V. Zamfir, Phys. Rev. C 46 (1992) 2283
14. R. Georgii et al., Proc. Int. Symp. on Capt. Gamma-Ray Spectr., Fribourg 1993, edited by J. Kern (World Scientific, Singapore 1994) p. 338
15. J. Kern, A. Bruder, S. Drissi, V.A. Ionescu and D. Kusnezov, Nucl. Phys. A512, (1990) 1
16. J. Kern, P. Cejnar and W. Zipper, Nucl. Phys. A554 (1993) 546; P. Cejnar and J. Kern, Nucl. Phys. A561 (1993) 317
17. J. Kern, Phys. Lett. 320B (1994) 7
18. J. Kern, Proc. 8th. Int. Symp. Capt. Gamma-Ray Spectr., Fribourg 1993, edited by J. Kern (World Scientific, Singapore 1994) 395
19. E.W. Kleppinger and S.W. Yates, Phys. Rev. C 27 (1983) 2608

THE EXPERIMENTAL INVESTIGATION OF THE STRUCTURE OF EXOTIC NUCLEI

Yu. E. Penionzhkevich

Flerov Laboratory of Nuclear Reactions, JINR, Dubna

In recent years, the use of sufficiently intensive (up to 10^{14} particle/sec) beams of heavy ions of intermediate energies allowed to extend considerably the investigation range of the nuclei in extreme states - extremely neutron - or proton-rich nuclei (large isospin) with high angular momentum and temperature. These investigations produced unexpected results allowing a new view of the nuclear matter properties. Primarily it concerns nuclei near the limits of nuclear stability. Such phenomena as the neutron and proton haloes, neutron "skin", new types of decay as well many others, were discussed in this field. Investigation of nuclei on the nuclear stability border is carried out in three basic directions: production and investigation of the structure of super neutron rich isotopes of the lightest elements, synthesis and study of nuclear decay properties near the shells, including deformed shells (of particular interest here are isotopes of ^{10}He, ^{28}O, ^{78}Ni, ^{100}Sn), experiments with beams of nuclei far from stability (radioactive beams).

The present work presents the results of similar research carried out at FLNR JINR and in collaboration with other scientific centers.

By the present time the maximum isospin value has been reached for the lightest nuclei. In this region have been found several nuclei in quasistationary state (^{4}H, ^{6}H, ^{9}He, ^{10}He, ^{10}Li, ^{13}Be), thus in the region of the nuclei of the lightest elements nuclides are already being synthesized beyond the nucleon stability border. Today, the only realistic direction for studying nuclear systems with the N/Z ratio > 2.5 lying beyond the nuclear stability border is investigation of the nuclei of the lightest elements. The structure of these nuclei may prove to be completely different. The most direct method for investigating the structure of weakly-bound nuclei is that of binary reactions [1]. Such reactions having two products in the exit channel allow one to determine the properties of one of the partners from the energy spectrum of the other. This becomes particularly important if the investigated nucleus has no bound states. This approach was successfully used for the first time in experiments measuring the masses of such nuclei as ^{4}H, ^{5}H, ^{6}H, ^{7}He, ^{8}He and ^{9}He in charge-exchange reactions with π-mesons [2], and recently in reactions with heavy ions [3]. For this purpose the so called rearrangement reactions are used, in which an exchange of several nucleons between the target nucleus and the projectile takes place. Information on the properties of superheavy isotopes of hydrogen, helium and lithium is presented in detail in ref. [1]. The present publication gives only the latest data obtained in collaboration between FLNR (Dubna), HMI (Berlin) and KSC (Moscow).

Data about excited states of ^{8}He are controversial: no excited state has been observed in the ^{9}Be(π^-,p) reaction [2], whereas an excited state at E_x=2.6 MeV has been reported for the ^{9}Be(^{7}Li, ^{8}B) ^{8}He-reaction [4], but the counting rate was very low (only a few counts per channel), and above the 1n- and 2n-thresholds of 2.58 MeV and 2.13 MeV, respectively, the few counts may be explained as fluctuations of the many-body background contributing in this region. Subsequent measurements performed in HMI with the Q 3D magnetic spectrograph at VICKSI have shown that in the reaction $^{9}Be(^{13}C, ^{14}O)^{8}He$ besides the ground-state peak of ^{8}He a weak peak of 0.11(5) μb/sr is observed at E_x=3.70(6) MeV with an intrinsic width of Γ=0.20(5) MeV (the experimental resolution is 0.37 MeV). From this width the most probable spin assignment $J^{\pi} = 2^{+}$ can be deduced using R-matrix theory. The lowest 2^{+} state of ^{8}He is predicted by Wolters *et al.* at 4.02 MeV [5].

An important step in investigating the stability of heavy helium isotopes was the experiment carried out in Los-Alamos by K. Seth [2] to determine the unstability of the ^{9}He nucleus in reactions with π-mesons. This experiment experimentally showed for the first time that though the binding energy of the neutron in ^{9}He is negative (B_n= - 1.14 MeV) it is 1-2.5 MeV higher than the binding energy predicted previously [6]. The most detailed measurements of the mass of the ^{9}He nucleus and investigations of its structure were carried out within the HMI-FLNR-RSCKI collaboration [7]. The ground state resonance has been calibrated with the $^{12}C(^{14}C,^{14}O)$- reaction, a mass excess of M.E.=40.94(10) MeV was obtained for ^{9}He. This value is slightly higher than the result of K.K. Seth *et al.* [2], but the errors are still overlapping. A one-neutron separation energy of S_n=-1.27 MeV is deduced. Further resonances are observed at 2.48 MeV, 4.31 MeV, 5.25 MeV (a broad structure appears also at 9.17 MeV) (fig.1).

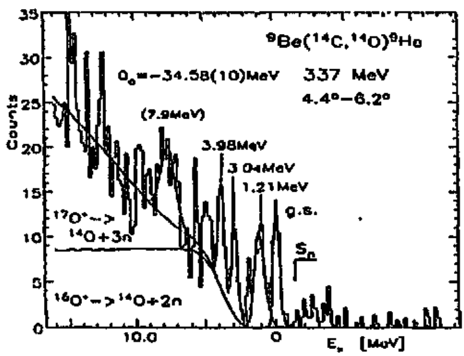

Fig.I

A many-body continuum is rising at about 3 MeV above the neutron threshold. It consists of two contributions: the decay of $^{16}O^{*}$ - > ^{14}O + 2n and $^{17}O^{*}$ - > ^{14}O + 3n, the continua extend down to the thresholds of these partitions. The contribution of the decay $^{15}O^{*}$ - > ^{14}O+ n is very small, because the population of ^{15}O-states requires a three-nucleon transfer, whereas the strong ^{16}O-channel is populated by the direct two-proton pick-up.

The observed resonances correspond to different neutron configurations, the protons are bound in the inert ^{4}He-core. Since two neutrons are added to the open shells, one can estimate the structure of the observed resonances as shown

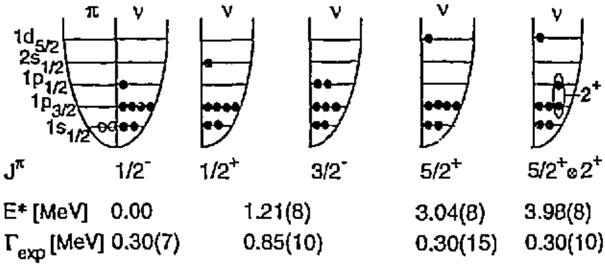

Fig.2

schematically in fig.2. An important information about the l-value of the resonance can be deduced from the observed total width, which is obtained by unfolding the line width with the experimental resolution. R-matrix calculations have been performed to deduce the most probable l-values for the measured resonances:
E_{res}=1.27 MeV: l=1 or 0; 4.31 MeV: l=2; 5.25 MeV: l=2.

The proposed configurations in fig. 2 are based on these l-assignments. The resonance at 2.48 MeV has probably l=1, because the matching conditions strongly suppress l=0 resonances in this transfer reaction.

After almost 20 years of efforts to synthesize the double magic ^{10}He nucleus, in 1993 were carried out two experiments to measure the mass and structure of this nucleus. HMI for this purpose used a reaction in which a

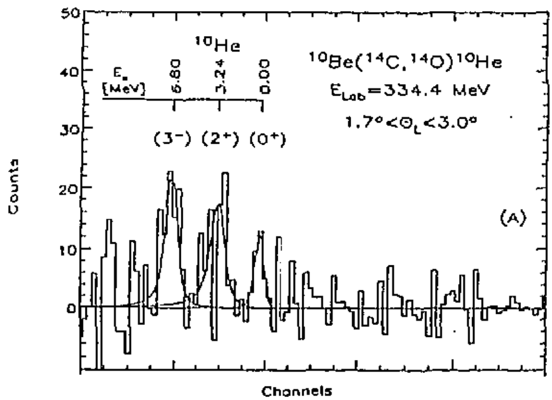

Fig.3

radioactive target ^{10}Be ($T_{1/2}$=1600 years) was irradiated by a radioactive beam ^{14}C

($T_{1/2}$=5730 years). In these experiments [8] the peak of the ^{10}He ground state resonance is observed at 1.07(7) MeV above the 2n-separation threshold with a statistical significance of 2.5σ. The Q-value is Q_0=41.19(7) MeV. The mass excess M.E.=48.81(7) MeV can be deduced. A second very prominent line is observed at a resonance energy of E_R=7.89(7) MeV (E_X=6.82(7) MeV), which is a good candidate for a 3^- resonance. The broad structure between these two lines at E_R=4.27(20) MeV (E_X=3.2(2) MeV) might be a 2^+ resonance, because it shows a similar angular dependence as the 0^+ (see fig. 3).

In another experiment at RIKEN in Japan the reaction CO_2(^{11}Li, 2n ^8He) was investigated with the help of a radioactive beam. For unambiguous identification of the reaction channel the coincidence of ^8He with neutrons (breakdown of the ^{10}He nucleus) was measured. In these experiments the peak observed in the spectra was identified as the ground state of the resonance in the ^{10}He nucleus with an energy of 1.2 ± 0,3 MeV and the width Γ≤1.2 MeV, which is in good agreement with the data of ref. [8]. The obtained results on the structure of super-heavy helium isotopes need theoretical interpretation. These nuclei are of particular interest as they belong to the group of nuclei having the so called neutron halo of the second type (the nucleus has a normal radius, but due to the compact configuration of the α-particle core, the core radius is very different from that of the neutron shell). Superheavy lithium isotopes (^{10}Li, ^{11}Li) belong to the nuclei having neutron halo of the first type (anomalous radius of the nucleus and correspondingly of the neutron shell).

The mass excess of ^{10}Li has been measured by Wilcox *et al.* [10] with the result M.E.=33.83(25) MeV; the quoted error of 250 keV is rather large. Another mass measurement has been reported by Amelin *et al.* [11], but the resulting mass excess value is 0.65±0.15 MeV lower than that of ref. [10]. The binding energy of ^{10}Li is of interest in calculations of the neutron-halo for ^{11}Li, and a more precise value is needed. In ref. [12] in reactions with ^{13}C and ^{14}C beams the mass of ^{10}Li and its excited states were studied. Since ^{10}Li is an odd-odd nucleus with Z=3, N=7, we expect a 1^+/ 2^+-doublet resulting from the coupling [π1p3/2 ⊗ υ1p1/2] and 1^-/ 2^--doublet from [π1p3/2 ⊗ υ2s1/2]. The level scheme of ^{10}Li is probably very similar to the one of ^{12}B (Z=5, N=7) at low excitation energies. The following result was obtained: ground state (1^+), M.E.=33.445(50) MeV, width Γ =0.15(7) MeV, S_n=-0.42(5) MeV; first excited state (2^+), E_x=0.38(8) MeV, width Γ=0.30(10) MeV. A second excited state is observed at E_x=4.05(10) MeV with a width Γ=0.7(2) MeV. The mass excess value of Wilcox *et al.* [10] corresponds to the 2^+-state and not to the ground state of ^{10}Li. Concerning higher excited states in ^{10}Li, we find a state at E_x=4.05±0.10 MeV. A preliminary spin assignment of 2^- is suggested by three observations: (i) the location and strength of this state corresponds to the cross section systematics for the population of the states with a v1d5/2-configuration in neighbouring nuclei, (ii) the width Γ=0.7±0.2 MeV is in agreement with an *l*=2 neutron decay, and (iii) in the structure-equivalent nucleus ^{12}B a spin-isospin-flip reaction populates the 2^--state with the largest strength among all states of the multiplet, coupled from the [π1p3/2 ⊗ υ1d5/2]-configuration. We assume a similar structure for ^{10}Li, in this case the observed state at 4.05 MeV would carry the main strength of the spin-dipole 2^- resonance in ^{10}Li.

Meanwhile, since experimental information on the nuclear structure with neutron halo is of utmost importance the experiments investigating the structure of the ^{10}Li nucleus should be continued and they are planned at different laboratories.

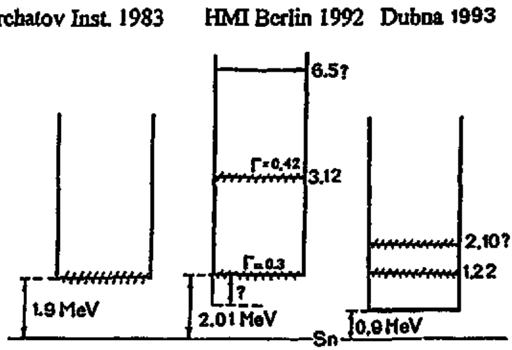

Fig.4

Our present knowledge of the ^{13}Be nucleus is shown in fig.4. In ref. [13] the mass and levels of the ^{13}Be nucleus were studied. The mass of ^{13}Be has been measured with the reaction ^{13}C(^{14}C,^{14}O)^{13}Be at E_{lab}=337 MeV. A Q-value of Q_0=-37.02(5) MeV was obtained and the mass excess is M.E.=35.16(5) MeV. If we assume that the observed line corresponds to the ground state, ^{13}Be is particle unstable with respect to the one-neutron emission by 2.01 MeV. The observed line width of 0.3(2)MeV supports an assignment of J^π=5/2$^+$ or 1/2$^-$, but excludes J^π =5/2$^+$. An excited state is seen at 3.12(7) MeV; there are indications of a second excited state at 6.5(2) MeV. The calculations predict a 1/2$^+$ ground state, unbound by ~0.9 MeV. However, it is not observed in the spectrum, probably because :1) of weak population of the 2s1/2 neutron-shell, and 2) an s-state has a large level width which is difficult to see at low statistics. This problem can be solved only with better statistics.

In ref. [14] the characteristics of the ^{13}Be nucleus were measured in the ^{14}C(^{11}B,^{12}N)^{13}Be reaction. As a result of these measurements the mass excess and, correspondingly, the binding energy of one neutron in the nucleus of ^{13}Be were obtained. This nucleus turned to be unstable with respect to the emission of one neutron by a value B_n=-0.78 MeV, which exceeds the earlier values of the neutron binding energy for this nucleus by 1.22 MeV. There have been also obtained the energy values of the first excited states (see fig.5). Thus, the first excited level in the ^{13}Be nucleus obviously lies at the energy of 1.22 MeV.

The nucleus ^{14}Be is particle stable in the ground state, but no other state is known. The lowest particle threshold is S_{2n}=1.34 MeV. A spectrum of the ^{14}C(^{14}C,^{14}O)^{14}Be-reaction was measured in [15]. A clear peak is seen with a significance of 3.5 σ at E_x=1.59 MeV, this is 0.25(6) MeV above the threshold. A $J^{\pi}=2^{+}$ assignment is most probable from the width and excitation energy.

An interesting result on the synthesis of exotic nuclei was recently obtained in a joint Dubna-GANIL-Warsaw experiment [16]. In this experiment in a quasi-fragmentation reaction of a ^{112}Sn beam for the first time were produced nuclei of the double magic isotope ^{100}Sn. Studies of N=Z and neighbouring nuclei, especially in the region of a double shell closure, are important for testing and further

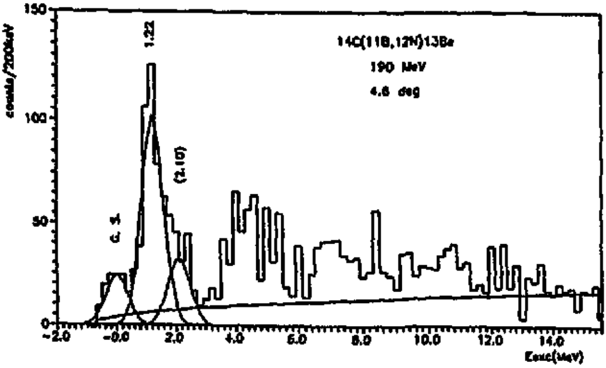

Fig.5

development of nuclear models. In particular, these studies provide information about the interaction between protons and neutrons occupying the same shell-model orbits. While N=Z nuclides of low mass are mostly stable, the heavier ones lie away from the line of beta stability. In the case of ^{100}Sn, the deficit of neutrons with respect to the mean atomic mass of the stable tin isotopes is about 18 and it is expected to be the heaviest N=Z nuclear system stable against ground-state proton decay. This stability is related to the doubly-magic character of ^{100}Sn. It may be noted that for heavier N=Z nuclei the condition of double shell closure is not sufficient to ensure stability: ^{164}Pb presumably lies well beyond the proton drip line. Mapping the proton-drip line in the neighbourhood of ^{100}Sn may also be of great importance in an astrophsical context as the properties of the proton-rich nuclei dictate the pathway of the rapid proton capture process in hot and dense stellar enviroments. Beta-decay in the ^{100}Sn region can be described in a very simple shell-model picture. It is strongly dominated by one channel, the $\pi g_{9/2} \rightarrow \nu g_{7/2}$ Gamow-Teller (GT) transition, and thus the observation of fast beta decays can lead to the unambiguous identification of the parent and daughter nuclear states. A meaningful verification of model predictions can be performed as, due to the high Q_{EC} values, the beta decay strength can be determined over a large energy range.

To produce and identify ^{100}Sn at GANIL a fragmentation-like reaction was employed in conjunction with the new SISSI device and the magnetic spectrometers Alpha and LISE3 which provided for the collection, separation and in-flight identification of the different reaction products. In order to enhance the production of neutron-deficient isotopes a beam of the lightest, stable tin isotope, ^{112}Sn, and a natural Ni target were used. It is then possible to calculate for a group of events, selected on the basis of the Z and A/Q, the masses of the individual ions from the measured TKE and TOF. The resulting mass distribution for $^{104}Sn^{+50}$,

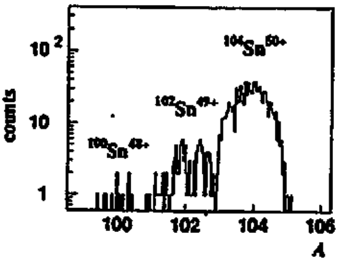

Fig.6

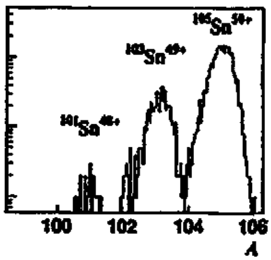

Fig.7

$^{102}Sn^{+49}$, $^{100}Sn^{+48}$ and $^{105}Sn^{+50}$, $^{103}Sn^{+49}$, $^{101}Sn^{+48}$ are given in Fig.6 and 7 respectively. Eleven events corresponding to $^{100}Sn^{+48}$ were observed.

Experiments in this field using extensive statistics for investigating the characteristics of ^{100}Sn decay and its lifetime are planned to be continued at GANIL and at the FLNR new accelerator.

REFERENCES

1. A.A. Oglobin, Yu.E. Penionzhkevich in Treatise on Heavy Ion Science. Plenum Press, edited by A. Browley, N.Y. (1989), p.261.
2. K.K. Seth and B. Parker. Phys. Rev. Lett. 66 (1991) 2448.
3. Yu. Penionzhkevich. Particles and Nuclei (in Russian), vol.25, (1994), p.930.
4. D.V. Alexandrov et al. Yad. Fizika 35 (1982) 277.
5. A.A. Wolters et al. Phys. Rev. C42 (1990) 2062.
6. H. Mann Proc. of Int. Conf. AMCO-6, Plenum Press, New York and London (1979),
p.51.

7. H.G. Bohlen et al. Proc. of Int. School-Seminar on Heavy Ion Physics, edited by

Yu.Ts. Oganessian, Yu.E. Penionzhkevich, R. Kalpakchieva, Dubna, 1993, vol.I, p.17.

8. A.N. Ostrowski et al. Annual Report, HMI, Berlin, 1993, HMI-B 520, (1994), p.44.

9. Tanihata I. - see ref.7, vol.I, p.3.

10. K.H. Wilcox et al. Phys. Lett. 59B, (1975), p.142.

11. A.I. Amelin et al. Yad. Fiz. 52, (1990), p.1231.

12. H.G. Bohlen et al. Z. Phys. A. A344 (1993), p.381.

13. A.N. Ostrowski et al. Z. Phys. A. A344 (1992), p.489.

14. A.V.Belozerov et al., Phys. Lett.B to be published.

15. H.G.Bohlen et al. Annual Report, HMI, Berlin, 1993, HMI-B 520(1994), p.42.

16. M. Lewitowicz et al. Phys. Lett. B332 (1994), p.20.

Particle decay of high angular momentum excited states

Nguyen Van Giai[a], Ch. Stoyanov[b] and V.V. Voronov[c]

[a])Division de Physique Theorique, Institut de Physique Nucleaire,
F-91406 Orsay Cedex, France

[b])Institute for Nuclear Research and Nuclear Energy,
boul. Tsarigradsko Chaussee 72, 1784 Sofia, Bulgaria

[c])Bogoliubov Laboratory of Theoretical Physics,
Joint Institute for Nuclear Research,
141980 Dubna, Moscow Region, Russia

A method for calculating non-statistical particle decay of excited states in odd nuclei is presented. Using the quasiparticle-phonon model, the partial cross sections and branching ratios for the neutron decay of the high angular momentum states in ^{209}Pb and ^{91}Zr excited by means of the $(\alpha,^3He)$ reaction have been evaluated.

1. INTRODUCTION

The nucleon transfer reactions induced by hadronic probes at intermediate energies have revealed giant resonance-like structures corresponding to the excitation of high angular momentum states [1]. These structures originate from the coupling of the initial single-particle mode with more complex states. The coupling of the single-particle state with surface vibrations is mainly responsible of the damping process of the single-particle mode [1,2].

The investigation of the decay of high-lying single-particle giant resonance states enables one to study the damping process through the determination of the relative contributions of the direct and statistical components. Recently, the neutron decay of high-lying states in ^{209}Pb excited by means of the $(\alpha,^3He)$ reaction has been studied at 122 MeV incident energy using a multidetector array [3]. The experimental data for ^{91}Zr and other nuclei will appeare in the nearest future.

In odd nuclei, the simplest excited states can be described as admixtures of single-particle states or quasiparticle states coupled to collective excitations (or phonons) of the even-even core. This weak coupling picture has been successfully applied to obtain the strength functions of a variety of odd nuclei [1,4]. A method for calculating particle escape widths in the framework of the quasiparticle-phonon model (QPM) has been suggested in ref. [2].

In this paper, the neutron decay of the high-lying states in ^{209}Pb into the ground state has been considered using the general procedure of refs. [5,6] where nucleon emission from giant resonances was calculated.

We present a method for calculating non-statistical particle decay of excited states in odd nuclei which enables one to consider a particle decay into the low-lying excited states. Using the quasiparticle-phonon model we calculate the partial cross sections and branching ratios for the neutron decay of the high angular momentum states in ^{209}Pb and ^{91}Zr excited by means of the $(\alpha,{}^3He)$ reaction and compare them with experimental data.

2. FORMALISM

Let us consider a nucleus of mass number (A+1) and assume for simplicity that the neighbouring A-nucleus is a doubly closed-shell core. It is not so difficult to generalize what follows to deal with quasiparticle instead of particle and hole states. The hamiltonian of the A+1 system can be written as

$$H = H_{sp} + H_{core} + H_{coupl} \tag{1}$$

where the three terms in eq. (1) are respectively the single-particle hamiltonian, the core hamiltonian and the particle-core coupling interaction. We use the QPM hamiltonian that includes an average field as the Woods-Saxon potential for protons and neutrons and the isoscalar and isovector residual interactions of a separable type (see ref.1 for details). Solving the Shroedinger equations for H_{sp} and H_{core} in large discrete spaces, one can find the eigen energies and wave functions for the single-particle and collective excitations. To study the particle decay of the eigenstates of the hamiltonian (1), one needs to take into account the continuum states too. Following [2], we divide the configuration space into two orthogonal subspaces, Q and P. The Q space is descrete whereas the P space is continuous and complementary to Q. The coupling of the Q states to the P space allows for particle emission.

Let us denote by α a discrete set of states obtained by diagonalizing H_{sp} on a harmonic oscillator basis [5,6], by ϵ_α and ϕ_α, respectively, the energies and wave functions, and by $a^\dagger_\alpha$ (a_α) the corresponding creation (annihilation) operators. Within the set α we can build a particle-hole configuration space corresponding to the core and find the RPA phonons by solving the RPA equations with H_{core}. We denote by E_n and $O^\dagger_n$ the energies and creation operators of these RPA states, respectively. To construct the Q space, we look for solutions of H of the type:

$$|\nu> = d^\dagger_\nu|0> = (\sum_\alpha C_\nu(\alpha)a^\dagger_\alpha + \sum_{\beta n} D_\nu(\beta,n)[a^\dagger_\beta \otimes O^\dagger_n])|0> \tag{2}$$

where $|0>$ is the RPA ground state of the core. The amplitudes C_ν and $D_\nu(\beta,n)$ and the energies ω_ν of $|\nu>$ are determined by diagonalizing H.

To build the P space one needs to calculate the scattering solutions of

$$[p(H_{sp})p - \varepsilon]\, u_\varepsilon^+ = 0 \tag{3}$$

where $p = 1 - \sum_\alpha |\phi_\alpha><\phi_\alpha|$. By construction, u_ε is orthogonal to all states ϕ_α. We denote by $c_\varepsilon^\dagger$ and c_ε the creation and annihilation operators of the state u_ε. Then, the P space consists of all states which are linear combinations of the following one particle- and one particle plus phonon-configurations where the particle is in a scattering state:

$$|\varepsilon> \equiv c_\varepsilon^\dagger |0>, \;\; |\varepsilon, n> \equiv [c_\varepsilon^\dagger \otimes O_n^\dagger]|0> \tag{4}$$

It is worth mentioning that in such an approach the particle decay from the phonons is not treated.

To solve H in the (P+Q)-space amounts to solve in the Q-space the effective hamiltonian:

$$\mathcal{H}(\mathcal{E}) \equiv QHQ + QHP\frac{1}{E^{(+)} - PHP}PHQ \equiv QHQ + W(E) \tag{5}$$

For each value of E, we look for a set of complex states which diagonalize $\mathcal{H}$:

$$|D_\mu> \equiv D_\mu^\dagger|0> = \sum_{\nu'} F_{\nu'}^{(\mu)} d_{\nu'}^\dagger|0> \tag{6}$$

The amplitudes $F_{\nu'}^{(\mu)}$ are solutions of

$$\sum_{\nu'}(E_{\nu'}\delta_{\nu\nu'} + <0|[d_\nu,[W(E),d_{\nu'}^\dagger]]|0>)F_{\nu'}^{(\mu)} = \Omega_\mu F_\nu^{(\mu)} \tag{7}$$

where

$$\Omega_\mu \equiv E_\mu - \frac{i}{2}\Gamma_\mu^\dagger \tag{8}$$

are the complex eigenenergies.

Neglecting H_{coupl} in the definition of W(E) one can rewrite the double commutator in (7) in terms of the inverse matrices of $K^{(0)} = (E^+ - H_{sp})^{-1}$ and $K^{(\nu)} = (E^{(+)} - E_\nu - H_{sp})^{-1}$ in the discrete single-particle space [2,7]. In this case, one can find the eigen energies η from the secular equation

$$\mathcal{F}(\eta) \equiv \epsilon_J - K_{JJ}^{(0)} - \eta - \sqrt{2}\sum_{\lambda ij}\Gamma(Jj\lambda i)D_j^{\lambda i} = 0 \tag{9}$$

To find D_j, we solve the linear set of equations

$$(\epsilon_j + \omega_{\lambda i} - \eta)D_j^{\lambda i} - \sum_{j'} K_{jj'}^{(\lambda i)} D_{j'}^{\lambda i} = \frac{1}{\sqrt{2}}\Gamma(Jj\lambda i) \tag{10}$$

All ingredients for the equations written above are given in [1,2].

At high excitation energies, when the level density becomes large, it is often more suitable to calculate the strength functions instead of solving exact equations. For example for the single particle components averaged over the energy interval Δ

$$C_j^2(\eta) = \frac{1}{\pi} Im \frac{1}{F(\eta + i\Delta/2)} \tag{11}$$

The transition amplitude in the DWBA describing the excitation of the complex doorway state (6) with the energy (8) and the following partial decay into a final state has the form:

$$T_{fi} = \sum_{lj}\sum_{\lambda} \sqrt{2\pi} \frac{< u_{lj}^-(E - E_n), n|H_{sp}|D_\lambda >< D_\lambda|V|i >}{E - \Omega_\lambda} \tag{12}$$

where $|i>$ is the wave function of the initial state and $< D_\lambda|V|i> \propto C_\lambda$. The partial escape amplitude has the form:

$$\gamma_{\lambda,n}(lj) \equiv < u_{lj}^-(E - E_n), n|H_{sp}|D_\lambda > \tag{13}$$

Doing a non-interference assumption, one can rewrite the cross section in the following form:

$$\frac{d\sigma_n}{dE_n} \propto \sum_{lj}\sum_{\lambda} \frac{|\gamma_{\lambda,n}(l,j)|^2 |C_\lambda|^2}{|E - \Omega_\lambda|^2}. \tag{14}$$

The branching ratio can be calculated by the following formula:

$$B_n = \frac{d\sigma_n/dE}{\sum_m d\sigma_m/dE} \tag{15}$$

3. SOME RESULTS

Recently, experimental data on the neutron decay of the high angular momentum states excited in the $(\alpha,{}^3He)^{208}Pb$ reaction have been published [3]. The branching ratios to low-lying levels in ^{208}Pb have been determined. According experimental data, the structure located between 8.5 and 12 MeV excitation energy in ^{209}Pb displays large departures from a pure statistical decay with significant direct feeding of the low-lying $3^-, 5^-$ collective states of ^{208}Pb. The observed neutron spectra can only be reproduced by assuming that high-spin states with $J = 17/2$ are predominant.

Using formulae presented above we have calculated the cross sections and the branching ratios for the direct neutron decay of the high-lying states with high angular momenta in ^{209}Pb and ^{91}Zr into the ground and low-lying states. We used the same set of parameters for the Woods-Saxon potential and the residual forces as in [8].

As the first example, we consider a decay of the $k_{17/2}$ state in ^{209}Pb to the first 2^+,3^-,4^+,5^-, 6^+, 7^-,8^+ states and to the ground state of ^{208}Pb. The relative cross sections for the excitation of the $k_{17/2}$ states in ^{209}Pb with the following neutron decay into the low-lying states mentioned above are shown in fig.1. The solid curve presents the sum of all 8 partial channels. The ground state and 3^-, 5^- channels are shown in fig.1 too. The contributions from the 7^-,8^+ channels are given in fig.2.

As one can see from fig.1 at the excitation energies below 7.5 MeV the ground state channel dominates and then the 5^- channel becomes the main contributor up to the energy 10 MeV. It is seen from fig.2 that the 7^-,8^+ channels contribute to the total cross section in the interval 9–11 MeV mainly. The last is valid for the 6^+ channel too. According to our calculations, a contribution of the neutron decay to the 2^+ state of ^{208}Pb is negligible. The most exciting feature of this calculation is the 5^- channel predominance in comparison with the 3^- channel. For the energy interval 8.5–10 MeV the calculated relative branching ratio R equals $B_{5^-}/B_{3^-} = 3.9$ that is in very good agreement with the experimental finding for the direct decay value for $R = 3.3$. An essential suppression of the ground state channel for these excitation energies is observed in experiment too [3]. It is worth mentioning that at the present time we can do a semi-quantitative comparison with experimental data because we calculated the relative cross sections for $k_{17/2}$ only. To perform a complete comparison, one needs to calculate the absolute values of the cross sections for the $j_{15/2}$ and $h_{11/2}$ states that can give some contribution at the same excitation energies too. Our calculation of the relative cross sections for the $j_{15/2}$ state shows that the 5^- channel dominates over the 3^- one in the energy interval 8–10 MeV, but for the $h_{11/2}$ state a contribution of the direct decay to the 3^- state exceeds a contribution from a decay to the 5^- state in the energy interval 6.6–8.6 MeV. As in the case of the $k_{17/2}$ state, at the excitation energies below 7.5 MeV the ground state channel dominates for the neutron decay of the $j_{15/2}$ and $h_{11/2}$ states. No quantitative estimation for a contribution of the direct decay of $j_{15/2}$ and $h_{11/2}$ states can be done from experimental data [3] at the present time.

The results of our calculations for the $i_{13/2}$ state in ^{91}Zr are shown in figs. 3,4. As one can see from these figs., a contribution of the ground state channel disappears at the excitation energy higher than 10 MeV. The most important channels are the 5^- channel (for the region 9.4–11 MeV) and the 6^+ one (for the region 11–13 MeV). Our predictions for the relative contributions of different channels to the integrated cross sections for the energy interval 9–13 MeV for the $i_{13/2}$ state are given in table 1. Besides the $i_{13/2}$ state, the $h_{9/2}$ state can contribute at the same excitation energies. The direct decay to the 5^- state dominates in the last case.

An analysis of data for ^{91}Zr and other nuclei is in progress now [3].

Table 1. Integrated cross sections $\int d\sigma_n$ (arbitrary units) for the excitation of the $i_{13/2}$ states in ^{91}Zr with the following neutron decay to the low-lying states of ^{90}Zr.

channel	g.s.	2^+	3^-	4^+	5^-	6^+
$\int d\sigma_n$	11	1	1	8	58	42

5. CONCLUSIONS

The microscopic approach has been applied to calculations of the direct neutron decay of the high angular momentum states excited in the one-nucleon transfer reaction. There is a semi-quantitative agreement with experimental data in ^{209}Pb. This is encouraging for the model, since one is looking at fine details of wave functions. Some predictions of the branching ratios for ^{91}Zr have been maden. To perform a complete quantitative comparison with experimental data, one needs to calculate the absolute values for the cross sections. To improve this approach it is necessary to perform such large calculations in a consistent framework using more realistic effective interactions like the Skyrme forces. To construct a separable parametrization for such an interaction is one of the possible ways to solve a problem of calculations in a large configuration space.

The research described in this publication was made possible in part by Grant $N^{\underline{o}}$N6N000 from the International Science Foundation. One of the authors (Ch.S.) has been supported by the Bulgarian Science Foundation (contract Ph.31).

REFERENCES

1. Ş. Gales, Ch. Stoyanov and A.I. Vdovin, Phys. Rep. 166 (1988) 127.
2. Nguyen Van Giai and Ch. Stoyanov, Phys. Lett. 272 (1991) 178.
3. D. Beaumel et al., Phys. Rev. C49 (1994) 2444.
4. Nguyen Van Giai, in: Highly excited states in nuclear reactions, eds. H. Ikegami and M. Muraoka (Osaka, 1980) p.682.
5. A. Bracco et al., Phys. Rev. Lett. 60 (1988) 2603.
6. Nguyen Van Giai and Ch. Stoyanov, Phys. Lett. 252 (1990) 9.
7. S. Yoshida and S. Adachi, Z. Phys. A325 (1986) 441.
8. V.Yu. Ponomarev et al., Nucl. Phys. A323 (1979) 446.

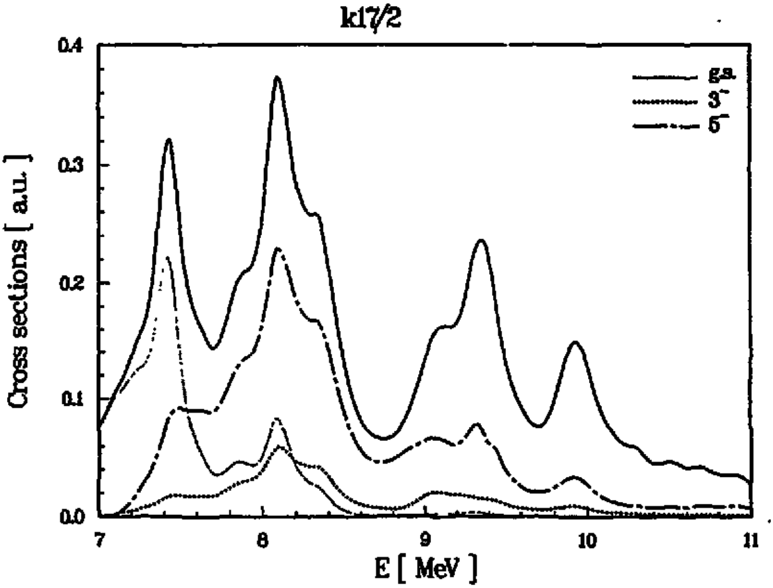
k17/2
g.s.
3⁻
5⁻
Cross sections [a.u.]
E [MeV]
0.0
0.1
0.2
0.3
0.4
7
8
9
10
11

Fig.1

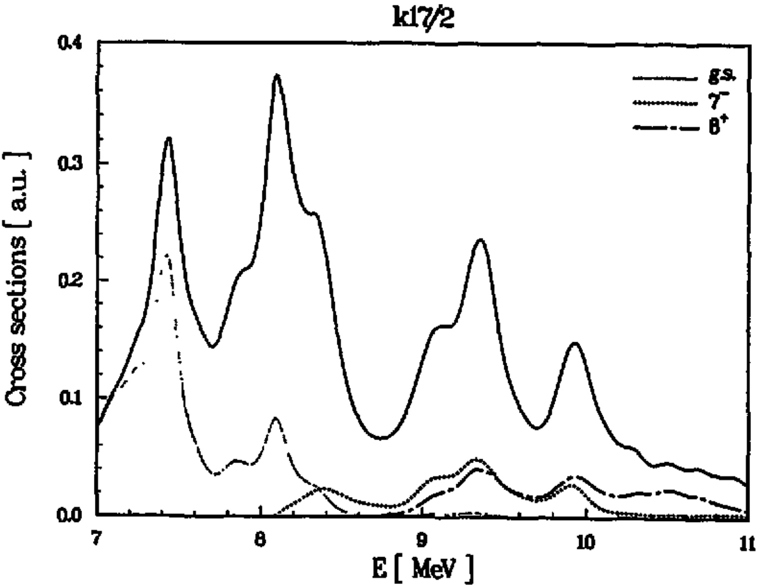
k17/2
g.s.
7⁻
8⁺
Cross sections [a.u.]
E [MeV]
0.0
0.1
0.2
0.3
0.4
7
8
9
10
11

Fig.2

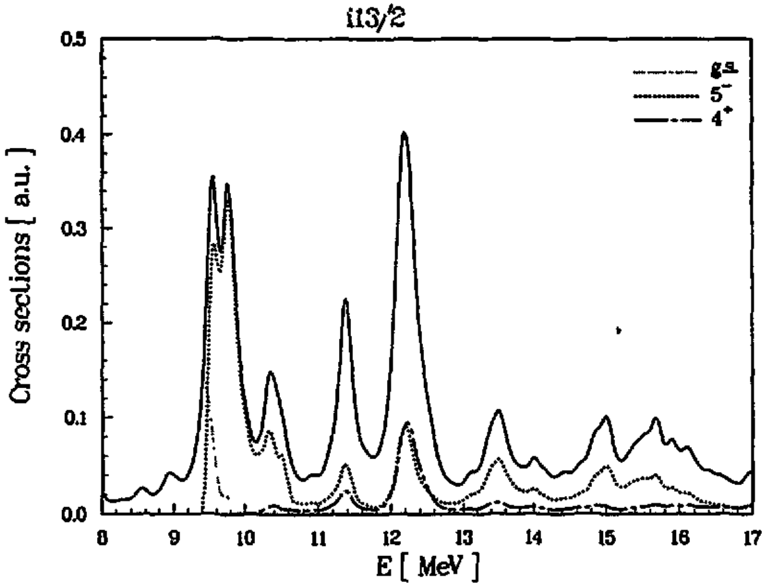
i13/2
g.s.
5⁻
4⁺
Cross sections [a.u.]
E [MeV]
0.0
0.1
0.2
0.3
0.4
0.5
8
9
10
11
12
13
14
15
16
17

Fig.3

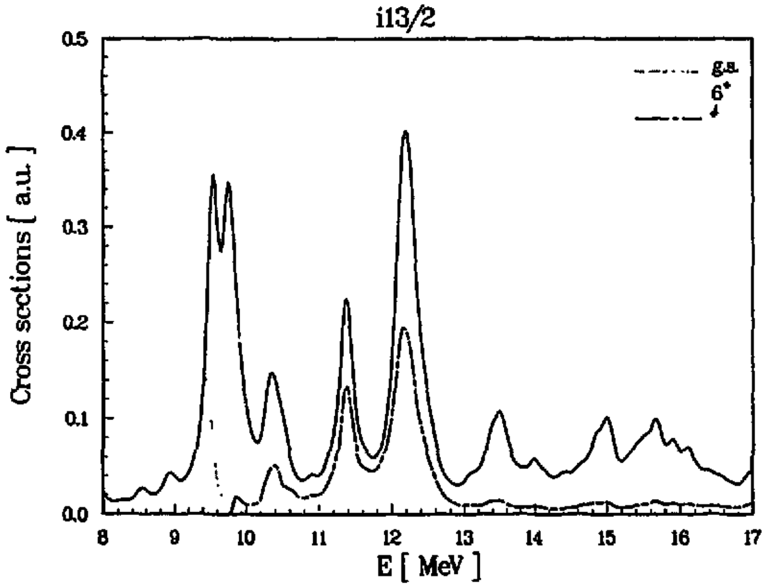
i13/2
g.s.
6⁺
4
Cross sections [a.u.]
E [MeV]
0.0
0.1
0.2
0.3
0.4
0.5
8
9
10
11
12
13
14
15
16
17

Fig.4

DECAY MODES OF HIGH-LYING SINGLE-PARTICLE STATES

S.Fortier
Institut de Physique Nucléaire,IN2P3-CNRS,91406 Orsay Cedex,France

Abstract

The neutron decay of high-lying single-particle states in ^{209}Pb and ^{91}Zr excited by means of the (α,^{3}He) reaction has been investigated using the multidetector array EDEN. The decay characteristics (neutron multiplicity, branching ratios, angular correlation data) confirm the high spin values of the high-lying structures observed at 13 MeV in Zr and 10 MeV in Pb, proposed to be due to the predominant excitation of single particle states in the external orbitals $1i_{13/2}$ and $1k_{17/2}$, respectively. The data are compared with the results of statistical model calculations in order to extract the direct branching ratios to the low-lying states of the target nucleus.

1. Introduction

Broad giant resonance-like structures have been observed in inclusive spectra of stripping reactions induced by various projectiles (α,^{7}Li, ^{20}Ne,^{40}Ar) on medium and heavy nuclei[1-4]. These structures have been shown to originate from the population of available outer high-spin orbitals, as for example the $1k_{17/2}$ subshell in ^{209}Pb[1]. In fact, stripping reactions at 20-50 A.MeV display a strong selectivity for exciting high-spin single-particle states due to the large mismatch between initial and final grazing angular momentum values. On the other hand, these high-lying structures are embedded in a continuum which may be due to fast three-body processes, such as the break-up of the projectile. The contribution of break-up processes to the experimental transfer spectra has to be properly evaluated in order to extract quantitative information about the properties of single-particle states in the continuum. It is hoped that exclusive experiments may reduce this background significantly as the angular correlation related to break-up should differ from those expected for the decay of the single-particle mode.

The damping of these "giant" states occurs through the mixing of the initial single-particle mode with the high density of underlying complex states. The investigation of the particle decay of these high-lying modes is an unique tool for studying the damping process, through the determination of the relative contributions of the "direct" and "statistical" decay modes, and for giving information about their microscopic structure. The total width Γ of the decaying state can be written as the sum of escape and spreading widths $\sum_b \Gamma_b^{\uparrow}$ and $\Gamma^{\downarrow}$. The partial escape widths $\Gamma_b^{\uparrow}$ are related to the direct decay process, e.g. a fast nucleon emission occuring either immediately after the primary excitation proress or during the first step of the damping process, usually described as the coupling to low-lying collective states of the target nucleus states [1]. In the following steps of the damping process, coupling to more complicated *mp-nh* particule-hole configurations may occur until complete thermalization of the mode. The spreading width $\Gamma^{\downarrow}$ is related to nucleon evaporation from a compound nucleus state with the same spin and parity at the same excitation energy, whose corresponding decay channels can be predicted by statistical model calculations.

Information about the wave function of the state can be obtained when the observed decay differs significantly from statistical model predictions. In this case, one can determine the degree of thermalization of the mode $\Gamma^{\downarrow}/\Gamma$, and the direct branching ratios $\Gamma_i^{\uparrow}/\Gamma$, which measure the coupling to the ground and low-lying excited states of the target nucleus. These direct branching ratios can be compared with the predictions of microscopic nuclear models.

The availability of the high efficiency neutron multidetector EDEN[5] has allowed to perform a detailed investigation of the neutron decay mode of high-lying single-particle states in several medium and heavy nuclei. Results on ^{209}Pb have recently been published[6]. The present paper will compare the decay properties of high-lying states in ^{91}Zr and ^{209}Pb, investigated through the $(\alpha,{}^3\mathrm{He}\ n)$ reaction, and discuss the information which may be obtained about their microscopic structure, through the evaluation of the statistical contribution to the neutron decay.

2. Experiment

The $(\alpha,{}^3$He-n)reaction has been investigated using an α-particle beam of 30A.MeV from the KVI AVF-cyclotron. The thicknesses of isotopically enriched targets of ^{208}Pb and ^{90}Zr were 6.8 and 5.0 mg/cm^2, respectively. The outgoing ^{3}He particles emitted in a solid angle of 10 msr around 0° were analyzed with the QMG/2 magnetic spectrograph. The focal plane detector consisted of a multiwire drift chamber, measuring the position of the particle and the trajectory angle and a plastic scintillator providing time of flight and energy loss informations for particle identification. Excitation energy ranges up to about 20 MeV above the neutron emission threshold could be investigated in a single setting of the magnetic field. The overall energy resolution was about 180 keV.

The neutrons in coincidence with ^{3}He particles were detected between 68° and 158° to the incoming beam direction using the neutron time-of flight multidetector EDEN[5], placed at 1.75 m of the target position. It consists of an array of 40 cylindrical cells, with respective diameter and thickness of 20 cm and 5 cm, filled with NE213 liquid scintillator, which ensures a good discrimination between neutrons and γ-rays. Details about the energy resolution and efficiency performances of this multidetector are given in ref.[5]. Multiparameter events corresponding to a coincidence between the focal plane plastic scintillator and the EDEN detectors were registered on magnetic tape, together with scaled-down singles events for absolute normalization of coincident data. Neutron energy spectra measured above a 0.5 MeV threshold have been corrected for efficiency effects and random events. These spectra are displayed as function of the residual energy

$E_{x_b} = E_{x_a} - E_n(c.m.) - S_n$, where E_{x_a} is the excitation energy of the emitting nucleus and S_n is the neutron emission threshold. It corresponds to the excitation energy of the final levels fed in the decay process in the case of one-nucleon emission.

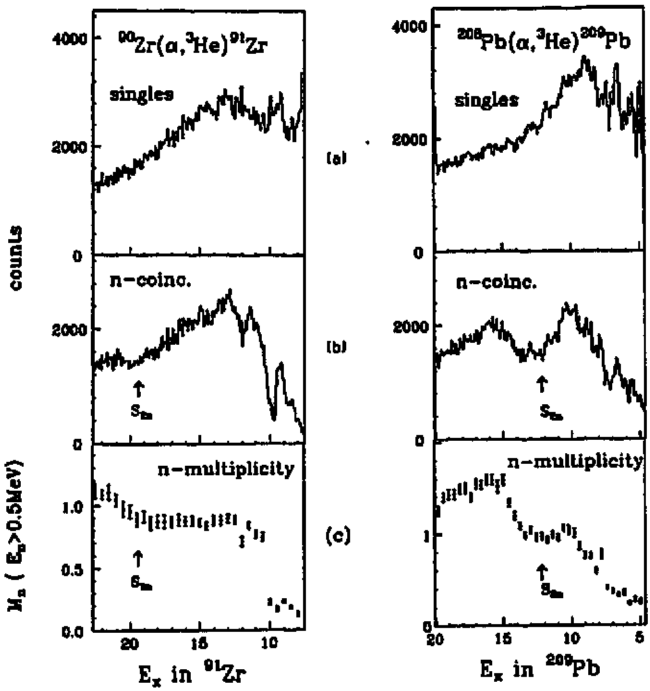

Figure 1: *a) Singles (α,^3He) spectra at E_α=30 A.MeV, $\theta_{^3He} = 0°$; b) spectra in coincidence with neutrons; c) neutron multiplicity deduced from the data analysis.*

Singles ^{3}He spectra corresponding to excitation energies in ^{91}Zr and ^{209}Pb above the neutron emission threshold are displayed in Fig.1a. As previously observed at 183 MeV incident energy[1], both spectra are dominated by a broad bump, located at abont 13 MeV in ^{91}Zr and 10 MeV in ^{209}Pb. The corresponding ^{3}He spectra in coincidence with neutrons detected by the EDEN array are shown in fig.1b. In both nuclei, one observes a sharp rise in the exclusive (α,^{3}He n) cross section between the threshold and the top of the bump, which therefore appears better defined than in the inclusive experiment. Moreover a second broad structure, very pronounced in the ^{209}Pb spectrum, appears a few MeV above the two-neutron emission threshold. In order to examine whether these additional structures could partly correspond to higher-lying single-particle excitations disantangled from the break-up background, one needs to perform a quantitative analysis of the angular correlation data and determine the neutron multiplicity.

3. Data analysis

3.1. Branching ratios

Neutron branching ratios B_b, corresponding to the decay from an energy bin E_{x_a} to some final target state with energy E_{x_b}, are deduced from the ratio of coincident events in each neutron detector $N_{a\to b}(\theta)$ over the number of singles events N_s according to the following expression:

$$N_{a\to b}(\theta) = N_s B_b \epsilon W(\theta) = \sum_k A_k P_k(cos\theta) . \quad (1)$$

where ϵ is the detector efficiency and $W(\theta)$ is the normalized angular correlation function. Due to the present cylindrical geometry provided by the detection of the ejectile around 0°, $W(\theta)$ can be expressed by a sum of Legendre polynomials. Here the branching ratios have been extracted by fitting the angular correlations with polynomials of even order k. The correlation of the neutron emitted in the decay process is in fact expected to be symmetric with respect to 90°(c.m.), provided that no interference occurs between states of different parities. One has to note that any significant deviation from this 90° symmetry could be due to neutrons produced in three-body processes such as break-up of the projectile.

The multiplicity of neutrons emitted from the E_{x_a} region, with energy above the 0.5 MeV threshold, is obtained by summing the B_b values over all neutron decay channels. The experimental multiplicity of neutrons emitted by ^{91}Zr and ^{209}Pb is plotted in fig.1c as function of excitation energy. Above 11 MeV and below the two-neutron emission threshold, the measured multiplicity in ^{91}Zr is consistent with 1, but small and fluctuating multiplicity values are observed at lower energies where the only open decay channels are the transition to the 0^+ ground state and γ-ray emission. Such an inhibition of the neutron decay can be explained considering the high spin values selected by the excitation process and the centrifugal barrier existing for emission of low-energy neutrons with large L values. In ^{209}Pb, the dependence of the multiplicity relative to excitation energy (fig.1c) displays the strong competition existing between neutron decay and γ-ray emission up to 10 MeV excitation energy, as well as the coexistence of the n and $2n$ decay channels up to 4 MeV above the two-neutron emission threshold. The shapes of the exclusive spectra shown in Fig.1b can be well reproduced by folding the singles spectra with the corresponding neutron multiplicity function of Fig.1c. In particular, it can be shown that the structure observed around 16 MeV in the exclusive ^{209}Pb excitation spectrum is clearly due to the slow rise of the multiplicity above the $2n$-threshold.

Partial branching ratios B_b to discrete low-lying states and groups of higher-lying levels in the target nucleus have been accurately determined as function of excitation energy in ^{91}Zr and ^{209}Pb. The values corresponding to the ground state decay from both nuclei are plotted in fig.2. Ground state branching ratios around 0.35 have been measured in the 5-7 MeV excitation energy range of ^{209}Pb, whereas the maximum value determined in ^{91}Zr is only 0.15. At higher excitation energy, where the neutron decay channels to excited states are open, one observes a sharp decrease of the ground state branching ratio. The ground state branching ratio is particularly small, but still measurable, in the region of the 10 MeV bump of ^{209}Pb. The average value obtained over a 3.5 MeV energy range without any background subtraction amounts to 0.4%. A significantly higher value of 1.4% is obtained for the ground state branching ratio of the 13 MeV structure in ^{91}Zr, by averaging B_{gs} over an energy bin between 11 and 15 MeV excitation energy. However it is important to note the variation of the ground state yield with excitation energy, as B_{gs} increases from a minimum value of 0.8% at 12 MeV up to about 4% at 20 MeV. It will be shown in the next section that the feeding of the ^{90}Zr ground state in the (α,^{3}He n) reaction at high excitation energy could be predominantly due to break-up processes.

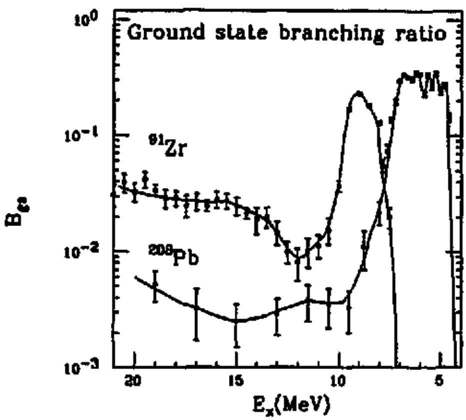

Figure 2: *Branching ratio B_{gs} for neutron decay to the ground state of the target nucleus, as function of excitation energy (the lines are to guide the eyes).*

3.2. Angular correlation analysis

Angular correlations measurements can provide information about spin values of the emitting state, by comparison with theoretical expectations. The general expression for the A_k coefficients in Eq.(1) may he found in Refs.[1,7]. For a transition to a final level with spin 0, the correlation only depends from the spin value of the emitting state and from its density matrix, averaged over the finite aperture of the spectrometer

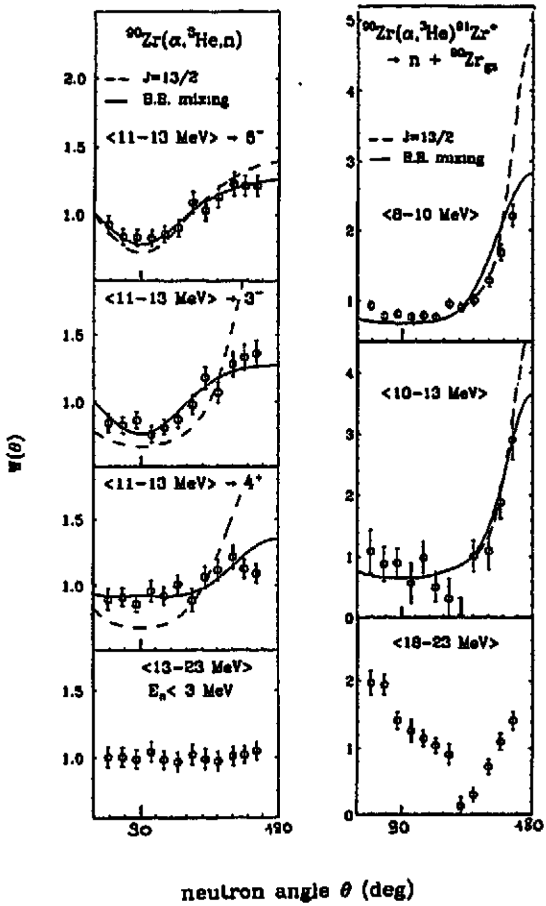

Figure 3: *Angular correlations for the neutron decay of energy bins in ^{91}Zr to the ground (right) and excited (left) states of ^{90}Zr. The correlations calculated for two different spin populations of the emitting states are also displayed for comparison: only J=13/2 (dashed line), and spin population mixing from ref.*[12] *(full line).*

around 0°. The theoretical correlations have been calculated using code Corely[8], with density matrices deduced from (α,^{3}He) transition amplitudes given by the DWBA code Dwuck4[9]. They are strongly peaked at 180° for high initial spin values, with a 180° − 90° anisotropy increasing from about 5 at $J_a = 9/2$ to 8 at $J_a = 17/2$.

In order to calculate angular correlations in the case of final states with spin different from 0, one has to make some additional assumptions about the relative contributions of various partial waves (l, j) participating to the decay. In the present case, it was assumed that there was no interference between the different partial waves, with amplitudes only depending on the transmission factors T_{lj}, calculated using the neutron optical potential from ref.[10].

Experimental angular correlations from the decay of various energy bins in ^{91}Zr and ^{209}Pb have been compared with the predictions using different assumptions for the spin values of the initial state. The conclusions deduced from this comparison in the case of ^{209}Pb are in good agreement with the results of previous inclusive measurements[1,11], which have in particular concluded to a predominant $1k_{17/2}$ single particle excitation in the region of the 10 MeV bump.

Angular correlations measured for the decay of some selected energy bins in ^{91}Zr to the ground state and low-lying levels of ^{90}Zr are presented in Fig.3. They have been compared with theoretical correlations calculated for various assumptions about the spin population of the emitting state. From the results of inclusive measurements, it has been proposed[1] that the bump observed around 13 MeV excitation energy mainly originates from the excitation of the $1i_{13/2}$ single-particle state. On the other hand, recent calculations[12] have been done in the frame of the Brink-Bonaccorso (BB) model[13] which describes stripping reactions to continuum states. The theoretical correlations displayed in Fig.3 correspond to the spin population assumptions of (i)J_a=13/2 alone (dashed line); (ii) BB predictions (full line) with about 60% of spin 13/2 in the 13MeV region. It can be seen that the results obtained using this last assumption are in rather good agreement with the angular correlations that are observed below 13 MeV.

At higher excitation energy, angular correlations observed for neutrons with energy below 3 MeV, which correspond to the largest part of the exclusive cross section, are nearly isotropic, (see fig.3-bottom left), as it can be expected from a statistical decay. On the other hand, the angular correlations corresponding to the feeding of the ground state of ^{90}Zr, measured for the same energy bin (fig.3-bottom right), display an asymmetry relative to 90°, with a sharp minimum at about 130°. Snch a correlation cannot he reproduced assuming neutron decay to the ground state.

It is therefore highly probable that the corresponding neutrons, which contribute to about 4% of the exclusive cross section in the angular range investigated here are produced in the elastic break-up of the projectile. Similar conclusions can be proposed about a predominant contribution of break-up processes to the very weak (about 0.5%) ground state transition observed at high excitation energy in the ^{208}Pb(α,^{3}He n) reaction[6].

3.3. Statistical calculations and extraction of direct branching ratios

The predictions of the statistical model for the decay of continuum states in ^{91}Zr and ^{209}Pb have been obtained using the code CASCADE[14]. A detailed investigation of the sensitivity of the calculated decay properties to the various input parameters (transmission coefficients, initial spin distributions and level densities in the final nuclei) has been done for both nuclei. The results of this investigation for the decay of ^{209}Pb have been reported in ref.[6]. Some adjustments of the density level parameters of the backshifted Fermi gas model have in fact to be made in order to better reproduce the low energy part of the neutron spectra. Below 5 MeV, known discrete levels have been included in the calculation.

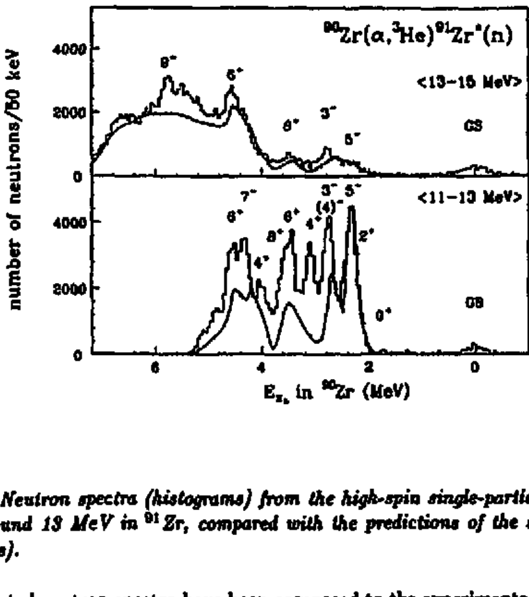

Figure 4: *Neutron spectra (histograms) from the high-spin single-particle structure observed around 13 MeV in ^{91}Zr, compared with the predictions of the statistical model (solid lines).*

Calculated neutron spectra have been compared to the experimental ones after suppression of energies below 0.5 MeV and folding with the energy-dependent line shapes. As an example, fig.4 displays neutron spectra from the decay of two energy bins in the region of the 13 MeV structure observed in ^{91}Zr. The normalisation of the calculated spectra to the data is done in such a way that the statistical contribution is assumed to be maximum, with the condition that the resulting statistical spectra never exceed the experimental ones. The same assumptions have been done in order to estimate the direct branching ratios $B_b^{\uparrow}$ corresponding to the neutron peaks observed above the normalized statistical spectra. In the expression $B_b^{\uparrow} = B_b^{exp} - B_b^{\downarrow}$, the statistical branching ratios $B_b^{\downarrow}$ have been taken equal to the product of the normalization factor by the values calculated by CASCADE for the corresponding neutron decay channels. However, it has to be stressed that this underlying assumption of a maximum statistical contribution to the decay may be questionable, and that this procedure can only determine a lower limit for the direct branching ratios.

Experimental spectra in fig.4 display several low-lying states in ^{90}Zr strongly populated in the neutron decay, in particular the lowest 5^-, 3^-, 4^+ states, and higher-lying groups of levels dominated by known 6^+, 7^-, 8^+ and 9^- states. Statistical spectra presented here have been calculated using as input data the spin distribution in ^{91}Zr from ref.[12], already used in the angular correlation analysis, and transmission coefficients deduced from ref.[15]. Other calculations assuming transmission coefficients from ref.[10] or a pure J=13/2 spin value for the emitting states led to only small modifications of the theoretical spectra. These calculations predict a strong excitation of the 5^- state in the lowest energy bin. According to the prescription chosen for the normalization, the decay to the 5^- appears therefore fully consistent with pure statistical emission. On the other hand, a sizeable amount of direct decay can be extracted for the transitions to other low lying states in ^{90}Zr.

Experimental branching ratios averaged over the 11-15 MeV energy bin in ^{91}Zr are given in Table 1 for the decay to well resolved low-lying ^{90}Zr states, together with those previously reported[6] for the 10 MeV bump in ^{209}Pb. One has to note that these branching ratios have been obtained without any background subtraction, therefore assuming that the contribution of three-body processes could be neglected in this energy region. However, it is not excluded that part of the neutrons feeding the ground state of ^{90}Zr could originate from the low-excitation-energy tail of the elastic break-up of the incoming α-particle, inducing an overestimation of the ground state branching ratio. On the other hand, the limits of the energy bin around the 13 MeV structure in ^{91}Zr are somewhat arbitrary, so that a 0.5 MeV shift may induce appreciable changes in the averaged branching ratios, due to the variation of the B_b values with energy.

The corresponding direct branching ratios $B_b^\uparrow$ extracted using the procedure explained above are reported in the last column of Table 1. These values may be compared with the results of recent microscopic calculations[16-18] reported in this conference, by calculating the theoretical branching ratio as the weighted sum of the predicted escape widths $(\Gamma_b^\uparrow)_J$ for the various single-particle states J lying in this energy range:

$$B_b^\uparrow = \sum_J \sigma_J (\Gamma_b^\uparrow/\Gamma)_J / \sum_J \sigma_J \tag{2}$$

The probabilities $\sigma_J(E_{x_a})$ for exciting the resonant state J at energy E_{x_a} can be evaluated using the energy and angular momentum dependence predicted by DWBA calculations, multiplied by the strength functions $S_J(E_{x_a})$ obtained from the microscopic calculations.

It may be noticed by looking at Fig.4 that a large part of the decay from ^{91}Zr proceeds through neutron emission to known high spin levels in the 3-6 MeV region. This fact cannot be accounted for by statistical calculations, giving evidence for significant direct escape widths for these decay channels. Large direct decay branches to 7^-,8^+,10^+ levels have also been observed in ^{209}Pb[6], provided that the actual high spin level density in ^{209}Pb be correctly reproduced in our statistical calculations. These non-collective levels could act as doorway states in the damping process and would have to be included in future microscopic calculations of the damping of the single-particle excitations in the continuum.

Table 1: *Comparison of experimental branching ratios with the values calculated for statistical decay, normalized according to the prescriptions given in the text. Direct branching ratios $B^{\uparrow}$ are obtained by assuming that the statistical contribution is maximum.*

Nucleus	E_x (MeV)		B_b^{exp} (%)	$B_b^{stat}(max)$ (%)	$B_b^{\uparrow}$ (%)
^{209}Pb	$< 8.5 - 12 >$	$\rightarrow$GS	0.43 ± 0.14	0.02	0.4
		$\rightarrow 3^-$	2.4 ± 0.3	0.6	1.8
		$\rightarrow 5^-$	6.6 ± 0.4	2.9	3.7
^{91}Zr	$< 11 - 15 >$	$\rightarrow$GS	1.4 ± 0.2	0.03	1.4
		$\rightarrow 5^-$	9.5 ± 0.2	9.5	0.
		$\rightarrow 3^-$	6.5 ± 0.2	4.1	2.4
		$\rightarrow 4^+$	8.8 ± 0.2	1.8	7.0

In the present analysis, no clear evidence could be found for direct decay of higher-lying single-particle states in both nuclei. Results obtained about the neutron decay of ^{209}Pb above 16 MeV are found to be consistent with the predictions of the statistical model, leading to the conclusion that there is an almost complete thermalization of the single-particle modes above this energy[6]. Similar conclusions can be drawn for ^{91}Zr above 18 MeV, as the main part of the decay may be accounted for by statistical calculations, whereas the angular correlation analysis show that the weak neutron line corresponding to the feeding of the ^{90}Zr ground state may be due to break-up processes.

4. Summary

The neutron decay of high-spin resonant states in ^{91}Zr and ^{209}Pb excited by the $(\alpha,^3\mathrm{He})$ reaction has been investigated in a wide range of excitation energy, using the multidetector EDEN. The large efficiency and the good energy resolution of this detector array has allowed the measurements of angular correlations, branching ratios and neutron multiplicity with high statistics. The large spin values of the high-lying structures observed in the transfer spectra, inferred from previous inclusive studies, are confirmed by the analysis of neutron angular correlations. This induces a strong competition between neutron and γ-decay several MeV above the neutron emission threshold.

The structures located around 13 MeV in ^{91}Zr and 10 MeV in ^{209}Pb predominantly decay to high-spin excited states of the target nucleus, and display only very weak ground state branching ratios. The results have been compared with the predictions of the statistical model. Whereas at higher excitation energy, the results are consistent with the assumption of an almost pure statistical decay, strong discrepancies may be observed in the region of the high-lying structures. From the comparison of experimental branching ratios with those predicted by statistical calculations, we have estimated the direct neutron branching ratios $B_b^{\dagger}$ to various low-lying states, directly related to the escape widths of the high spin resonant states present in this energy region. The comparison with the predictions of two microscopic calculations, performed in the framework of the quasi-particle-phonon model[17] and the coupled-channel-approach[18] is under way.

† *The experimental results reported here is the result of a collaboration between several laboratories. I wish to thank all the physicists which were involved in the EDEN project and participated to the different stages of the experiment: D.Beaumel, S.Gales, J.Guillot, H.Langevin-Joliot, H.Laurent, J.M.Maison, M.Renteria, J.Vernotte (IPN Orsay), J.Bordewick, S.Brandenburg, A.Krasznahorkay, S.Y.Van der Werf and A.Van der Woude(KVI), P.Massolo(Univ.La Plata) and G.Crawley(MSU).*

References

[1]S. Gales, Ch. Stoyanov and A. I. Vdovin, Phys. Reports 166,127(1988)

[2]G.H.Yoo et al., Phys.Rev.C31,94(1993)

[3]S.Fortier et al., Phys.Rev.C41,2689(1990)

[4]I.Lhenry,T.Suomijarvi,P.Chomaz and N.V.Giai, Nucl.Phys.A565,524(1993)

[5]H. Laurent et al., Nucl. Instr. Meth. A326, 517 (1993).

[6]D.Beaumel et al., Phys.Rev.C44,1559(1994).

[7]G.R.Satchler, Direct Nuclear Reactions,Oxford UP,New York(1983).

[8]J.Van de Wiele,private communication.

[9]P.D.Kunz, code Dwuck4, unpublished.

[10]J. Rappaport et al., Nucl.Phys.330,15(1979).

[11]P.Massolo et al., Phys.Rev.34,1256(1986)

[12]A.Bonaccorso, private communication.

[13]A.Bonaccorso and D. Brink, Phys. Rev.C44,1559(1991).

[14]F.Puhlofer,Nucl.Phys.A280,267(1970).

[15]D.Wilmore and P.E.Hodgson, Nucl.Phys.55,673(1963)

[16]Nguyen Van Giai and Ch. Stoyanov, Phys. Letters B272,178 (1991).

[17]Nguyen Van Giai,Ch.Stoyanov and V.Voronov,Invited talk to this Conference.

[18]G.A.Chekomazov and M.H.Urin, Contribution to this Conference, p31.

SCISSORS MODES: FROM SEMICLASSICAL TO MICROSCOPIC DESCRIPTIONS

N. LO IUDICE
Dipartimento di Scienze Fisiche, Università Federico II di Napoli
and
Istituto Nazionale di Fisica Nucleare, Sezione di Napoli
Mostra d'Oltremare Pad.19, Napoli, Italy

ABSTRACT

The semiclassical two-rotor model is shown to give a quantum mechanical definition of the M1 strength of the scissors mode which has general validity. Its consistency with the deformation properties of the mode as well as with some algebraic and microscopic descriptions is proved. The strength so defined, if properly computed, leads to the prediction of a new scissors like mode in the region of the isovector quadrupole giant resonance. The two modes may occur and be strongly collective in superdeformed nuclei. A RPA calculation carried out directly in the laboratory frame to describe the low-lying scissors mode is finally discussed.

1. Introduction

The $M1$ low-lying excitations, observed in all deformed nuclei, have been interpreted as scissors like oscillation modes since their first discovery in ^{156}Gd by Richter and coworkers[1,2], according to the picture provided by the semiclassical two-rotor model (TRM)[3].

These excitations have been object of extensive theoretical studies, carried out in a variety of different models, devoted to clarify their exact nature[2]. The conclusions of these investigation were not unique. Even their scissors nature has been questioned in some cases[4].

A conclusive support in favour of the scissors character of the mode has come from the recent discovery that in Sm isotopes the total $M1$ strength grows quadratically with the deformation parameter[5] and is closely correlated with the strength of the $E2$ transition to the lowest 2^+ state[6]. Such a deformation law has been confirmed in Nd isotopes[7].

Practically all models have been re-examined and found to be more or less consistent with these new deformation properties[8–19]. This long list includes also a phenomenological, largely model independent, analysis[16] based on the use of the M1 strength in the form borrowed from the two-rotor model (TRM)[3].

As we shall see, the TRM form of the M1 strength holds beyond the geometrical model and gives a definition of the scissors strength of general validity. Such a definition applies to most phenomenological model descriptions in their classical limit. We will discuss this aspect for the proton-neutron interacting boson model (IBM-2)[20] and the generalized coherent state model (GCSM)[21]. We will also show that the definition applies also to schematic RPA[22]. We can actually prove that the semiclassical approach is totally equivalent to schematic RPA and like this scheme, predicts a high energy scissor mode in the region of the isovector quadrupole giant resonance[23] as well as strongly collective scissors like excitations in super-deformed nuclei[24]. The semiclassical approach does not describe correctly the deformation properties of the mode. Realistic TDA[11] or RPA[9,18] calculations are needed to this purpose. These being carried out in the intrinsic frame, present some difficulties which can be circumvented by using rather involved techniques[25] unless a self consistent basis is adopted[26]. As a way of avoiding some of the intrinsic RPA problems, a RPA calculation carried out in the laboratory frame has been proposed recently to describe the mode[17]. This will be discussed briefly in the final part.

2. The scissors M1 strength

2.1 The two-rotor model and the scissors M1 strength

In the TRM protons and neutrons, described as two axially symmetric rotors with mass parameters $\Im_p$ and $\Im_n$ and angular momenta $\vec{J}_p$ and $\vec{J}_n$ respectively, perform rotational oscillations around a common axis orthogonal to their symmetry axes. The motion is determined by the Hamiltonian

$$H_{TRM} = \frac{1}{2\Im_p}\vec{J}_p^2 + \frac{1}{2\Im_n}\vec{J}_n^2 + V(\vartheta) , \tag{1}$$

where ϑ is half the angle between the symmetry axes of the two rotors.

Expressed in terms of the total and relative angular momenta

$$\vec{J} = \vec{J}_p + \vec{J}_n , \qquad \vec{S} = \vec{J}_p - \vec{J}_n , \tag{2}$$

the TRM Hamiltonian, apart from a Coriolis-like term which can be neglected, decouples into a rotational and an intrinsic part. This for small values of ϑ, has the form of a two dimensional harmonic oscillator Hamiltonian

$$H = \frac{1}{2\Im_{sc}}(S_1^2 + S_2^2) + \frac{1}{2}C\vartheta^2 , \qquad \Im_{sc} = \frac{4\Im_p\Im_n}{\Im_p + \Im_n} , \tag{3}$$

where C is the restoring force constant and $\Im_{sc}$ is the mass parameter, given by

$$\Im_{sc} = \frac{4\Im_p\Im_n}{\Im_p + \Im_n} . \tag{4}$$

In this Hamiltonian ϑ plays the role of radial variable ($\vartheta^2 = \vartheta_1^2 + \vartheta_2^2$) while $S_i = id/(d\vartheta_i)$ are the conjugate variables of ϑ_i.

The scissors mode is the first $K^\pi = 1^+$ state, with an excitation energy $\omega = \sqrt{C/\Im_{sc}}$. It is excited by the component of the magnetic dipole operator linear in S_μ with a strength ($g_r = g_p - g_n$)

$$B(M1)\uparrow = \frac{3}{16\pi}\sum_{\mu=\pm1} |< \mu|S_\mu|0 >|^2\, g_r^2\, \mu_N^2 \simeq \frac{3}{16\pi}\Im_{sc}\,\omega g_r^2\, \mu_N^2 . \tag{5}$$

The above expression follows from the harmonic relations

$$\Im_{sc} = \frac{1}{\omega} < 0|S^2|0 > = \frac{1}{\omega}\sum_{\mu=\pm1} |< \mu|S_\mu|0 >|^2 , \qquad C = \Im\omega^2 = \omega \sum_{\mu=\pm1} |< \mu|S_\mu|0 >|^2 . \tag{6}$$

These can be written in the form

$$\Im_{sc} = \sum_{\mu=\pm1} < 0|S_\mu^\dagger \frac{1}{H - E_0} S_\mu|0 > , \qquad C = \frac{1}{2}\sum_{\mu=\pm1} < 0|\left[S_\mu^\dagger,[H,S_\mu]\right]|0 > , \tag{7}$$

The above relations, first obtained in a sum rule approach[22], can be assumed as a general definition of the TRM physical parameters. They are valid for a Hamiltonian and an operator S_μ of general form. By using closure we obtain indeed

$$\Im_{sc} = \sum_{n\mu} \frac{1}{\omega_n} |< n\mu|S_\mu|0 >|^2 \quad , \qquad C = \sum_{n\mu} \omega_n |< n\mu|S_\mu|0 >|^2 , \tag{8}$$

By making use of the last two equations we obtain for the scissors energy weighted sum rule

$$\begin{aligned}\sum_n \omega_n B_n(M1)\uparrow &= \frac{3}{16\pi}\sum_{n,\mu}\omega_n \,|<n\mu|S_\mu|0>|^2\, g_r^2\,\mu_N^2 \\ &= \frac{3}{32\pi}\sum_{\mu=\pm1} <0|\left[S_\mu^\dagger,[H,S_\mu]\right]|0> \simeq \frac{3}{16\pi}\Im\omega^2 g_r^2\,\mu_N^2 \,. \end{aligned} \tag{9}$$

This sum rule is generally valid as long as the M1 transition is promoted by the operator S_μ. The scissors strength (eq.5) follows under the (experimentally supported) assumption of small fragmentation of the mode.

For a validity check we can consider the deformed mean field

$$H = \sum_i h_i \,, \qquad h = h_0 - \beta m\omega_0^2(Q_0^{(p)} + Q_0^{(n)}) \tag{10}$$

where h_0 is a spherical single particle harmonic oscillator Hamiltonian and β a deformation parameter. We easily get

$$\begin{aligned}\sum_n \omega_n B_n(M1)\uparrow &= \frac{3}{32\pi}\sum_{\mu=\pm1} <0|\left[S_\mu^\dagger,[H,S_\mu]\right]|0> \\ &= \frac{3}{16\pi}\frac{2}{3}\delta^2 m\omega_0^2 A <r^2> = \frac{3}{16\pi}\Im\omega \,, \end{aligned} \tag{11}$$

where we have put $\omega = \delta\omega_0$ and used the relation $\beta = \sqrt{(16\pi/45}\delta$ between the two deformation parameters.

2.2. Scissors M1 strength and nuclear deformation

The definition given above has been shown to be consistent with the observed deformation properties of the mode[16]. We started with the E2 classical energy weighted sum rule[28]

$$\omega_2 B(E2)\uparrow = (E_2 - E_0)B(E2, 0^+ \to 2^+) = \frac{2}{5}\frac{Z}{A}\chi_B S(E2) = \frac{5}{2\pi m}\chi_B\frac{Z^2}{A} <r^2> e^2 \tag{12}$$

where $\chi_B = B_{irr}/B_{rot} \simeq 1/5$ is the ratio between the irrotational and rotational mass parameters, m the nucleon mass, $<r^2> = 3/5\ R^2$ and $R = 1.2A^{1/3}\ fm$. We can derive from this equation an expression for the mass parameter using the relation $\Im \simeq 3/\omega_2$, which inserted into eq.5 yields the $M1 - E2$ relation

$$B(M1)\uparrow \simeq 0.0065\frac{A^{1/3}}{\chi_B Z^2}\omega B(E2)\uparrow \frac{\mu_N^2}{e^2 fm^4} g_r^2. \tag{13}$$

Making use of the standard expression of the E2 strength

$$B(E2)\uparrow = 5/(16\pi)\ Q_0^2 = 1/(5\pi)\ Z^2 R^4\delta^2 e^2 \,, \tag{14}$$

and substituting into the above equations, we obtain the δ^2 law

$$B_{sc}(M1)\uparrow \ \simeq\ 0.004\,\omega A^{5/3}\,\delta^2\, g_r^2\mu_N^2. \tag{15}$$

The procedure just outlined shows the strict link between the quadratic deformation law and the $M1 - E2$ relation in agreement with what suggested by the alike saturation properties observed for the two strengths[6].

Numerical calculations carried out by putting $g_n = 0$ and $g_r = g_p = 2g_R = (2Z)/A$ yield results in good agreement with experiments if we use for δ the values adopted in ref.5 ($B^{(\delta)}_{sc}(M1)$ in figure 1.). If the strength is computed using for the deformation parameter the value extracted directly from the experimental E2 strength through eq.13 ($B^{(Q)}_{sc}(M1)$) in figure 1.), the agreement with experiments is somewhat spoiled in the most deformed nuclei. The two strengths so determined differ by contributions coming from higher order terms in δ.

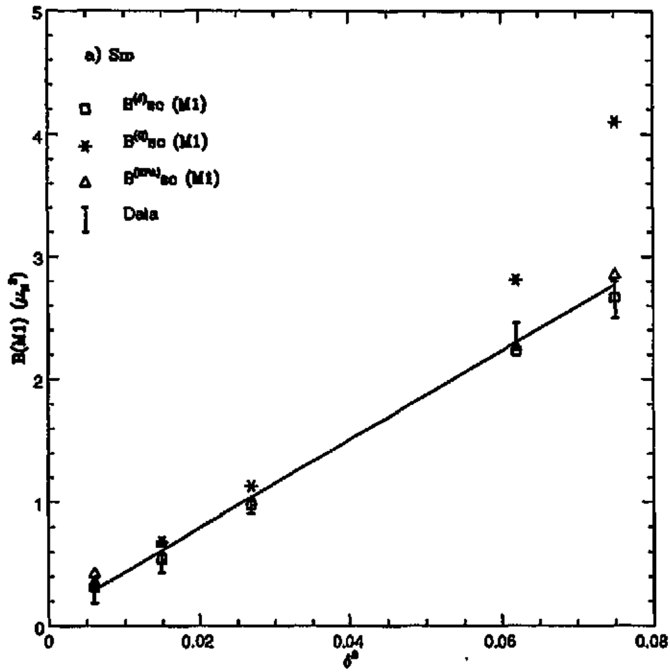

Figure 1. Summed M1 strength versus δ^2 in Sm isotopes. The line connects the experimental points. The data are taken from ref.5.

With the value used in ref. 5, the saturation properties are also well described[16]. This is shown in figure 2, where the M1 strength is plotted versus the fractional number of valence protons and neutrons $P = (N_pN_n)/(N_p+N_n)$, a quantity introduced by Casten[29]. The strength reaches rapidly a maximum value as P increases and remains constant for further increase of P, in agreement with experiments[6].

Such a good agreement is obtained by a largely model independent phenomenological procedure based on little more than assuming that the magnetic excitations are promoted by the scissors-like component of the $M1$ operator. This points strongly toward the scissors character of the observed low lying $M1$ excitations. Crucial to such a good agreement is the choice of a mass parameter close to the empirical moment of inertia. This suggests that protons and neutrons in promoting this mode behave roughly as superfluids, in agreement with the microscopic calculations where pairing correlations are shown to play a crucial role in enforcing the quadratic deformation law[9–11,14,18].

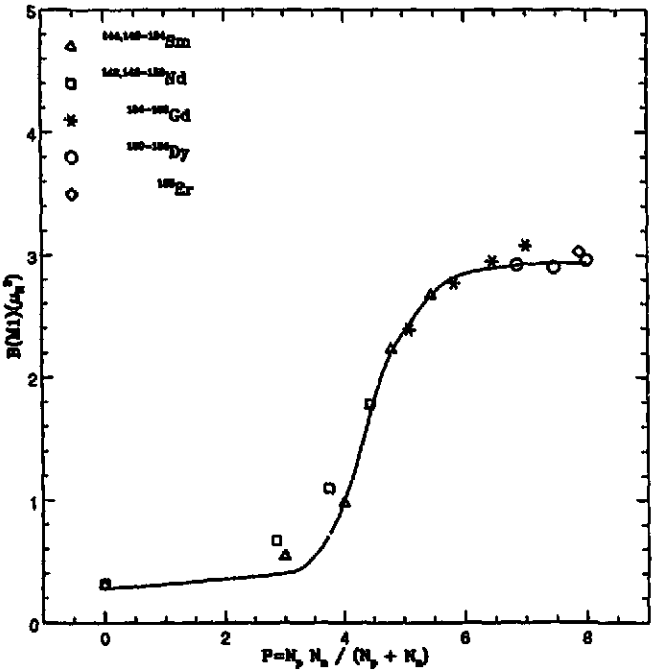

Figure 2. Summed M1 strength versus the fractional number $P = (N_pN_n)/(N_p + N_n)$ in Sm isotopes. The line is drawn just to guide the eyes.

3. Semiclassical versus algebraic approaches

The connection with other model descriptions is better shown once the TRM Hamiltonian is expressed in terms of the shape variables $\alpha_{2\mu}$ instead of θ. This is made possible by the relation

$$\alpha_{21} = \alpha_{2-1} = -i\sqrt{\frac{3}{2}}\beta\vartheta\,, \qquad \beta = \sqrt{\frac{16\pi}{45}}\delta \tag{16}$$

which inserted into eq.1 yields

$$H = \frac{1}{2}\Im_{sc}\dot{\vartheta}^2 + \frac{1}{2}C_\vartheta\vartheta^2 = \frac{1}{2}B\sum_{\mu=\pm1}|\dot{\alpha}_{2\mu}|^2 + \frac{1}{2}C_\alpha\sum_{\mu=\pm1}|\alpha_{2\mu}|^2, \tag{17}$$

where new and old parameters are mutually related by $\Im_{sc} = 3\beta^2 B$ and $C = 3\beta^2 C_\alpha$.

3.1 Relation to GCSM

In the GCSM[21] the mode is described by a state obtained by angular momentum projection from an intrinsic wave function of the form

$$\Phi_{sc} = (b_n^\dagger \otimes b_p)_{J=K=1}\Phi_0 \tag{18}$$

where $b_\tau^\dagger(b_\tau\ ), (\tau = p, n)$ are quadrupole boson creation (annihilation) operators acting on a coherent ground state of the form

$$\Phi_0 = exp[d\sum_\tau(b_{\tau 0}^\dagger - b_{\tau 0})]|0> . \tag{19}$$

Here d is a deformation parameter which can be related directly to the $E2$ strength. In the limit of strong deformation we have indeed $d \simeq (k_p\beta)/\sqrt{2}$, where the constant k_p in the harmonic limit becomes $k_p = (B_pC_p)^{1/4} \simeq (B_p\omega)^{1/2}$. In this limit the GCSM $M1$ strength can be written in the scissors form[15]

$$B(M1)\uparrow \simeq \frac{9}{4\pi}d^2g_r^2\mu_N^2 \simeq \frac{9}{8\pi}k_p^2\beta^2g_r^2\mu_N^2 \simeq \frac{3}{16\pi}\Im\omega g_r^2\mu_N^2 \tag{20}$$

having used $B_p \simeq B/2 \simeq \Im\beta^2/6$.

The numerical calculations[15] have been carried out once the model parameters have been fixed so as to reproduce some selected levels of the ground, β and γ bands and the E2 transition strength. The results of such a parameter free calculation are quite good. The $M1$ strength follows closely the observed quadratic law and saturates correctly with deformation.

3.2 Relation to IBA-2

If we put in eq.4 $\Im_p \simeq N_\pi/(N_\pi + N_\nu)\ \Im$ and $\Im_n \simeq N_\nu/(N_\pi + N_\nu)\ \Im$, where N_π and N_{nu} are valence proton and neutron pairs, we obtain

$$B(M1)\uparrow \simeq \frac{3}{16\pi}\Im_{sc}\ \omega g_r^2\ \mu_N^2\ , \qquad \Im_{sc} = \frac{4\Im_p\Im_n}{\Im} \simeq \frac{4N_\pi N_\nu}{(N_\pi + N_\nu)^2}\Im\ . \tag{21}$$

We show now by a heuristic procedure that this is the classical limit of the IBM2 $M1$ strength. Let us consider the general IBM M1 strength derived by Ginocchio[13]

$$B(M1)\uparrow = \frac{3}{16\pi} < 0|S^2|0 > g_r^2\mu_N^2 \simeq \frac{9}{8\pi}\frac{4N_\pi N_\nu}{(N_\pi + N_\nu)(N_\pi + N_\nu - 1)} < N_d > g_r^2\mu_N^2\ , \tag{22}$$

where $< N_d >$ is the ground state average of the quadrupole boson number operator $N_d = N_d^{(p)} + N_d^{(n)} = d_p^\dagger \cdot d_p + d_n^\dagger \cdot d_n$. Being this a scalar, we can compute its mean value in the intrinsic frame, where for axial symmetric systems only the $\mu = 0$ components contribute. Using as intrinsic ground state a coherent state of the form used in the GCSM (eq.19) so that $d_{\tau,0}\Phi_0 = d_\tau^\prime\Phi_0$ $(\tau = \pi,\nu)$ with $d_\tau^\prime$ pure numbers, we have

$$\beta_\tau =< \alpha_\tau >= 2\alpha_\tau^{(0)}d_\tau^\prime\ , \qquad \alpha_\tau^{(0)} = \sqrt{\frac{1}{2B_\tau\omega}}\ . \tag{23}$$

Assuming equal deformation for protons and neutrons ($\beta_p = \beta_n = \beta$) we get

$$3 < N_d >= \frac{3\beta^2}{4\alpha_0^2} = \frac{3}{2}B\beta^2\omega = \frac{1}{2}\Im\omega\ \ , \quad \Im = 3\beta^2(B_p + B_n) = 3\beta^2B \tag{24}$$

which inserted into eq.22 yields the TRM eqs.21 if we put $N_\pi + N_\nu - 1 \simeq N_\pi + N_\nu$, an approximation valid in the classical limit (large N).

4. Relation to RPA

The complete equivalence between the semiclassical approach and schematic RPA can be stated immediately. Once the TRM Hamiltonian in θ has been transformed into an equivalent Hamiltonian in the shape variable $\alpha_{2\mu}$, we just need to impose that the zero-point amplitude of $\alpha_{2\mu}$ is equal to that of the quadrupole field[29]. We can then obtain the schematic RPA results directly from the defining eqs.6 using an anisotropic harmonic oscillator basis with frequencies ω_1 and ω_2 obeying the volume conserving condition $\omega_1^2\omega_2 = \omega_0^3$ ($\omega_0 = 41A^{-1/3}$).

4.1. Low and a high energy scissors modes in deformed and superdeformed nuclei

For the low energy mode we may use the defining eqs.6 with $\omega = \omega_{sc}^{(0)} = 2E = \sqrt{(\delta\omega_0)^2 + (2\Delta)^2}$, where $E(\epsilon)$ is the quasi particle energy. This yields a superfluid mass parameter

$$\Im_{sc} \simeq \Im_{sf} \simeq (\frac{\delta\omega_0}{2E})^3\Im_{rig}\,, \qquad \Im_{rig} = \frac{2}{\delta\omega_0}\sum_{ph\in\delta\omega_0}|(S_1)_{ph}|^2 \simeq \frac{2}{5}mAR^2. \tag{25}$$

We decompose the restoring force constant into a kinetic and a potential part $C = C_0 + C_1$ and determine the unperturbed component again from eqs.6 obtaining $C_0 \simeq (2E)^2\Im_{sf}$. The potential component can be fixed from the ratio between the nuclear isovector and isoscalar potential strengths V_1 and V_0, which yields $C_1/C_0 = -V_1/(4V_0) \simeq 0.6$. The energy and strength result to be

$$\omega_- \simeq 1.26(2\Delta)\sqrt{1+x^2}, \qquad B_-(M1)\uparrow \simeq 0.001(2\Delta)A^{5/3}\frac{x^3}{1+x^2}g_r^2\mu_N^2 \tag{26}$$

where $x = \delta\omega_0/(2\Delta)$. The above equation shows that the strength goes like δ^3 for small deformations ($x \ll 1$) and becomes linear for very large deformations ($x \gg 1$). In the range of deformations observed in Sm and Nd isotopes the strength grows quadratically in δ but with a slope which produces a considerable overestimation of the experimental values in the most deformed isotopes. A quenching factor is needed. This can be effectively obtained only from realistic RPA calculations, like the one carried out in ref.9, which account for spin admixtures.

We may alternatively put in eqs.6 $\omega = \omega_{sc}^{(0)} = 2\omega_0$ obtaining an irrotational mass parameter $\Im_{sc} = \Im_{irr} = \delta^2\Im_{rig}$. The unperturbed restoring force constant follows from the relation $C_0 \simeq (2\omega_0)^2\Im_{irr}$ and the potential component from the symmetry energy mass formula yielding $C_1/C_0 \simeq 1.9$. Energy and strength are given in this case by

$$\omega_+ \simeq 139.4\,A^{-1/3}\,MeV, \qquad B(M1)_+\uparrow \simeq 0.12\,\delta^2\,A^{4/3}g_r^2\,\mu_N^2. \tag{27}$$

Though quadratic in δ the one given above is the $M1$ strength of the $K^\pi = 1^+$ component of the isovector quadrupole resonance. For ^{154}Sm we have indeed $\omega_+ \simeq 26\ MeV$ and $B(M1)_+\uparrow \simeq 4.7\ \mu_N^2$ having put $g_n = 0$ and $g_p = 2g_R = 2Z/A$.

The occurrence of a strongly collective low and high energy scissors excitation in superdeformed nuclei suggested recently in a RPA calculation[24], is naturally predicted in the semiclassical approach.

Let us assume that K is a good quantum number and that the transition goes from K to $K+1$. The $M1$ operator couples the state $|IMK>$ to the states $|I'M'K+1>$ with

$I' = I-1, I, I+1$. Using the standard expression for the transition matrix elements and the TRM intrinsic wave function[3], we obtain for $I \gg K$

$$\sum_{I'} B(M1, IK \to I'K+1) \simeq \frac{3}{16\pi}\, \Im_{sc}\, \omega \frac{1}{K+1} g_r^2\, \mu_N^2\,. \tag{28}$$

For $K=0$ we gain the standard scissors strength given by eq.5. We may assume that protons and neutrons behave as rigid rotors or as irrotational fluids according that we consider the low or the high energy mode. We can therefore use respectively eqs.26 (with vanishing pairing gap) or eqs.27. The analogy with RPA suggests to put $g_n = 0$ and $g_p = 1$ for the low and $g_p = 2g_R = 2Z/A$ for the high energy mode. We obtain for the superdeformed ^{152}Dy ($\delta \simeq 0.62$) in substantial agreement with the RPA results[24]

$$\omega_- \simeq 6.1 MeV, \quad B_-(M1)\uparrow \simeq 22.6\mu_N^2\,, \qquad \omega_+ \simeq 26 MeV, \quad B_+(M1)\uparrow \simeq 26.1\mu_N^2\,. \tag{29}$$

4.2 RPA in the Laboratory frame

For a study of the detailed properties of the mode realistic RPA calculations are required. These being carried out in the intrinsic frame, pose several problems. We remind here the occurrence of spurious rotational admixtures which can be eliminated by adopting special techniques[25] or by using a selfconsistent single particle basis[26]. Even free of spurious admixtures the intrinsic RPA states may need to be projected. What is the effect of such a projection is still an open question.

The above difficulties may be avoided by formulating the RPA directly in the laboratory frame. A calculation of this type has been carried out recently[27] by using a projected single particle basis which, though reproducing the Nilsson spectra to a good approximation, is composed of states of good angular momentum. The technique for constructing such a basis has been developed elsewhere[30,31]. The underlying ideas will be sketched below.

Let us consider the rotational invariant particle-core Hamiltonian:

$$\tilde{H} = h_{sph} + H_{core} - k_c \sum_\mu (b_{2\mu}^+ + b_{2-\mu}) Q_\mu^* \tag{30}$$

where $Q_\mu = r^2 Y_{2\mu}$. In the above equation h_{sph} stands for the spherical shell model one-body Hamiltonian, chosen to be an harmonic oscillator potential with spin orbit interaction and a l^2 term, H_{core} is an interacting quadrupole boson Hamiltonian describing a phenomenological core and the third component is a particle-core coupling term. We now use a coherent state of the form given by eq.19 to take the mean value

$$< \psi_g | h | \psi_g > = < \psi_g | (\tilde{H} - H_{core}) | \psi_g > = h_{sph} - 2k_c\, d\, Q_{20}. \tag{31}$$

This can be identified with the Nilsson Hamiltonian $h_{Nils}(\delta) = h_{sph} - m\omega_0^2 \beta Q_{20}$ if we put $2\, d\, k_c = m\omega_0^2\, \beta$.

Inspired by this property we consider particle-core angular momentum projected states of the form

$$\Phi_{\alpha IM}(d) = N_{\alpha I} P_{MI}^I [\varphi_{\alpha I} \psi_g] \tag{32}$$

where $\varphi_{\alpha I} = \varphi_{nljI}$ are spherical single particle states, $N_{\alpha I}$ is a normalization factor, P_{MI}^I a projection operator of standard form. We then considered these states as eigenstates of an effective Fermionic single particle Hamiltonian h_{eff} whose eigenvalues are assumed to be the mean values

$$\epsilon_{\alpha I} = \langle \Phi_{\alpha IM}(d) \mid h \mid \Phi_{\alpha IM}(d) \rangle\ . \tag{33}$$

These energies depend not only on (nlj) but also on I which plays here the same role as $|\Omega|$ in the Nilsson basis. The corresponding "eigenstates" are mutually orthogonal with respect to I and M. They are not exact eigenstates of the particle-core Hamiltonian (30) and therefore do no reproduce exactly the Nilsson spectrum. For a given deformation however, it is possible to obtain the Nilsson level scheme to a good approximation by a suitable choice of the strength k_c.

The correspondence with the Nilsson states is not one to one. Because of the degeneracy in M, $2I+1$ states of the present basis will correspond to a $|\Omega| = I$ Nilsson state. We can keep however all M-degenerate projected single particle states given by eq.32 as long as we normalize them to $2/(2I+1)$ rather than 1.

We adopted these projected basis to carry a QRPA calculation in the laboratory frame. To this purpose we used a rotational invariant many-body Hamiltonian composed of a one body term with single particle energies given by eq.33 and a two-body potential composed of proton (p) and neutron (n) monopole pairing treated in BCS and a p-p, n-n and p-n quadrupole and spin interactions.

The QRPA states obtained in this scheme are excited from the ground state by a M1 operator of the form

$$\mathcal{M}(M1,\mu) = \sqrt{\frac{3}{4\pi}} \sum_{i,\tau} [g_l^{eff}(\tau) l_\mu(i) + g_s^{eff}(\tau) s_\mu(i)] , \tag{34}$$

where $g_l^{eff} = g_l - g_c$ and $g_s^{eff} = g_s - g_c$. This is nothing but the standard M1 operator of the rotational model.

We applied the formalism to Sm isotopes. We found that practically all excitations of mainly orbital nature fall below 4 MeV while the spin levels are above. Figure 1 shows that the summed M1 strength of the orbital excitations below 4 MeV is linear in δ^2, in good agreement with the experimental data. As in the other microscopic approaches the deformation law is obtained only after pairing has been included. As shown in ref.27, the computed distribution of the orbital strength is in qualitative agreement with the experimental data. Also the $M1$ spin distribution with its characteristic double-hump structure observed recently[32] in ^{154}Sm is fairly well reproduced.

5. Concluding remarks

Inspired by the TRM we have obtained a quantum mechanical definition of the scissors M1 strength of general validity which is compatible with the observed deformation properties of the mode at least on phenomenological ground. The agreement is obtained for a mass parameter close to the empirical moment of inertia. The above facts indicate that the observed M1 excitations are promoted by a scissors-like motion between protons and neutrons behaving as superfluids.

The definition given here applies to phenomenological models like IBM-2 and GCSM as well as to schematic RPA. The reason why apparently unrelated models converge to the TRM is to be found in their common assumption that the M1 transition is dominantly if not totally promoted by the generator of the scissors mode, S_μ. In view of this fact, different model calculations may be viewed as effective ways of computing the same physical parameters entering into the scissors strength.

The detailed properties of the mode can be studied only by exploiting the full shell model structure as in realistic RPA. This, being formulated in the intrinsic system, present some limitations. We have proposed as a way of avoiding them, a RPA calculation carried out in the laboratory frame using a projected single particle basis. The results obtained are quite encouraging.

It is of great interest that according to the semiclassical and RPA analyses, there is room also for a high energy scissors mode and that strongly collective excitations of the same nature may occur in super-deformed nuclei. These semiclassical predictions should be sufficiently reliable since either in the case of the high energy mode or (and specially) in superdeformed nuclei, pairing and spin admixtures are expected to be strongly suppressed.

References

1. D. Bohle, A. Richter, W. Steffen, A.E.L. Dieperink, N. Lo Iudice, F. Palumbo and O. Scholten, *Phys. Lett.* **B137** (1984) 27.
2. For a review and references, A. Richter, *Nucl. Phys.* **A507** (1990) 99c; **A522** (1991) 139c and in "The building blocks of nuclear structure", A. Covello ed., (World Scientific, Singapore, 1992) p.135.
3. N. Lo Iudice and F. Palumbo, *Phys. Rev. Lett.* **41** (1978) 1532;
   G. De Franceschi, F. Palumbo and N. Lo Iudice, *Phys. Rev.* C29 (1984) 1496.
4. see for instance I. Hamamoto and S. Aberg, *Phys. Lett* **B145** (1984) 163; R. R. Hilton, *Z. Phys.* **A316** (1984) 121.
5. W. Ziegler, C. Rangacharyulu, A. Richter and C. Spieler, *Phys. Rev. Lett.* **65** (1990) 2515.
6. C. Rangacharyulu, A. Richter, H.J. Wörtche, W. Ziegler and R.F. Casten, *Phys. Rev.* **C43** (1991) R949.
7. J. Margraf et al., *Phys. Rev.* **C47**; F.R. Metzger, *ibid.* **C18** (1978) 1603.
8. S.G. Rohozinski and W. Greiner, *Z. Phys.* **A322** (1985) 271.
9. I. Hamamoto and C. Magnusson, *Phys. Lett.* **B260** (1991) 6.
10. E. Garrido, E. Moya de Guerra, P. Sarriguren and J.M. Udias, *Phys. Rev.* C44 (1991) R1250.
11. K. Heyde and C. De Coster, *Phys. Rev.* C44 (1991) R2262 ; K. Heyde, C. De Coster, A. Richter and H.-J. Wörtche *Nucl. Phys.* **A549** (1992) 103.
12. T. Mizusaki, T. Otsuka and M. Sugita, *Phys. Rev.* C44 (1991) R1277.
13. J.N. Ginocchio, *Phys. Lett.* **B265** (1995) 6.
14. L. Zamick and D.C. Zheng, *Phys. Rev.* C44 (1991) 2522; C46 (1992) 2106.
15. N. Lo Iudice, A.A. Raduta and D.S. Delion, *Phys. Lett.* **B300** (1993) 195; *Phys. Rev.* **C50** (1994) in press.
16. N. Lo Iudice and A. Richter, *Phys. Lett.* **B304** (1993) 193.
17. K. Heyde, C. De Coster, C. Ooms and A. Richter, *Phys. Lett* **B312** (1993) 267.
18. P. Sarriguren, E. Moya de Guerra, R. Nojarov and A. Faessler. *J. Phys: Nucl. Phys.* **G19** (1993) 291.
19. R.R Hilton, W. Höhenberger and H. J. Mang, *Phys. Rev.* C **47** (1993) 602
20. F. Iachello and A. Arima, *The interacting boson model* (Cambridge University Press, 1987).
21. A.A. Raduta, Amand Faessler and V. Ceausescu, *Phys. Rev.* **C36** (1987) 2111.
22. E. Lipparini and S. Stringari, *Phys. Lett.* **B130** (1983) 139.
23. N. Lo Iudice and A. Richter, *Phys. Lett* **B228** (1989) 291.
24. I. Hamamoto and W. Nazarewicz, *Phys. Lett.* **B297** (1992) 25.
25. R. Nojarov and A. Faessler, *Nucl. Phys.* **A484** (1988) 1.
26. K. Sugawara - Tanabe and A. Arima, *Phys. Lett.* **B206** (1988) 573.
27. A.A. Raduta, N. Lo Iudice and I.I. Ursu, *Nucl. Phys.* submitted to.
28. R.F. Casten, D. S. Brenner and P.E. Haustein, *Phys. Rev. Lett.* **58** (1987) 658.
29. A. Bohr and B.R. Mottelson, *Nuclear Structure* (Benjamin, N.Y. 1975), Vol. II, ch.6.
30. A. A. Raduta and N. Sandulescu, *Nucl. Phys.* **A591** (1991) 299.
31. A.A. Raduta, D.S. Delion and N. Lo Iudice, *Nucl. Phys.* **A551** (1993) 73.
32. D. Frekers *et al.*, *Phys. Lett.* **B244** (1990) 178; see also A. Richter, *Nucl. Phys.* **A553** (1993) 417c.

Low Energy Photon Scattering: Electric Dipole Strength Distributions in Heavy Nuclei [1]

Ulrich Kneissl

Institut für Strahlenphysik
Universität Stuttgart
D - 70569 Stuttgart, Germany

ABSTRACT

Systematic nuclear resonance fluorescence (NRF) experiments have been performed at the bremsstrahlung facility of the 4 MV Stuttgart Dynamitron to investigate the distributions of *magnetic* and *electric* dipole strengths in heavy nuclei. Precise excitation energies, transition strengths, spins and decay branching ratios were deduced for numerous low lying dipole excitations in heavy spherical and deformed nuclei. Measurements of the linear polarization of resonantly scattered photons using a Compton polarimeter enabled model independent parity assignments. In this report the results are summarized obtained for *electric* dipole excitations. The new data on the orbital *magnetic* dipole excitations (*"Scissors Mode"*) in even and odd deformed rare earth nuclei will be presented in the contribution by H.H. Pitz.

The experiments during the last years revealed the following new spectroscopic informations about E1 excitations in heavy nuclei:

- In the *spherical* even N=82 isotones strong $E1$ excitations are known which can be interpreted as transitions to the $J^\pi = 1^-$ members of $2^+ \otimes 3^-$ two phonon multiplets. Corresponding E1 excitations were observed for the first time in the semimagic (Z=50) Sn-isotopes ^{116,124}Sn. The coupling of an additional neutron to such two-phonon excitations has been studied in ^{143}Nd. In this nucleus recent experiments succeeded in the first identification of dipole excitations to a $2^+ \otimes 3^- \otimes$ particle multiplet.
- In all investigated even-even, *deformed* nuclei low lying *electric* $\Delta K = 0^-$ transitions of remarkable strengths have been observed near 1.5 MeV. These 1^- states are discussed in terms of a $K = 0$ rotational band based on an octupole vibration.
- Enhanced *electric* dipole excitations in *deformed* nuclei could be systematically observed at excitation energies near 2.5 MeV. As a common feature these states show systematically decay branching ratios which hint at a K-mixing. These strong $E1$ excitations can be interpreted as two phonon excitations due to the coupling of octupole ($J = 3^-, K = 1$) and quadrupole-γ-vibrations ($J = 2^+, K = 2$).

[1] *Supported by the Deutsche Forschungsgemeinschaft (Kn 154-21 and Br 799-33)*

1. INTRODUCTION AND MOTIVATION

Low-lying dipole excitations in heavy nuclei are of actual interest in modern nuclear structure physics. Low energy photon scattering off bound states, nuclear resonance fluorescence (NRF), represents a highly selective and sensitive tool to investigate low-lying dipole excitations in beavy nuclei. The discovery of a new class of enhanced *magnetic* excitations in heavy deformed nuclei in high resolution electron scattering experiments by Richter and coworkers [1] initiated numerous electron and photon scattering experiments [2,3,4,5] to study the fragmentation and systematics of this mode often referred to as *"Scissors Mode"*. On the other hand, these NRF-experiments also provided evidence for enhanced, low-lying *electric* dipole excitations in deformed nuclei [6,7,8,9]. The structure of the corresponding $J^\pi=1^-$ states are discussed in terms different collective excitation modes or two phonon excitations. For odd mass nuclei there are interestings topics like the search for the *"Scissors Mode"* [10] or the investigation of dipole excitations to two-phonon-particle multiplets in spherical nuclei near closed shells [11].

In this talk the results for strong low lying electric dipole excitations in heavy spherical and deformed nuclei are discussed in more detail. H.H.Pitz in his contribution to this conference summarizes the results on the systematics of the orbital M1 excitations (*"Scissors Mode"*) in deformed nuclei.

2. NUCLEAR RESONANCE FLUORESCENCE TECHNIQUE

Nuclear resonance fluorescence (NRF) experiments (photon scattering off bound states) represent an outstanding tool to investigate low-lying dipole excitations and to provide detailed spectroscopic informations. The low transfer of momentum q of real photons makes photon scattering highly selective in exciting low spin states. In particular, only $E1$, $M1$, and, to a much lesser extent, $E2$ transitions are induced. In addition, modern γ-spectroscopy offers highly efficient Ge-detectors with an excellent energy resolution, with which the NRF method can achieve a high sensitivity. This sensitivity is essential for detailed studies of the fragmentation of the strengths of specific collective modes. Furthermore, the use of continuous bremsstrahlung radiation enables all spin 1 states with sufficient ground state decay widths to be excited simultaneously.

The following quantities can he extracted in a completely model independent way [12]:

- the excitation energies
- the ratio Γ_0^2/Γ, (Γ_0 and Γ: ground state and total decay widths, respectively)
- the spins of the excited states
- the branching ratios for the decay to excited states
- the parities of the excited states

So far in most of the previous systematic photon scattering experiments parity assignments came from a comparison with electron scattering form factors [13] or by applying the Alaga rules [14]. Parities can be determined model independently in photon scattering experiments by measuring the linear polarization of the scattered photons using Compton polarimeters. The parity information is obtained from the measured azimuthal asymmetry ϵ :

$$\epsilon = \frac{N_\perp - N_\parallel}{N_\perp + N_\parallel} = P_\gamma \cdot Q \tag{1}$$

where $N_\perp$ and $N_\parallel$ represent the rates of Compton scattered events perpendicular and parallel to the NRF scattering plane defined by the directions of the photon beam and the scattered photons, respectively. The asymmetry ε is given by the product of the polarization sensitivity Q of the polarimeter and the degree of polarization P_γ of the scattered photons. At a scattering angle of $\Theta = 90^0$ to the beam axis the polarization P_γ amounts to -1 or $+1$ for pure $E1$ and $M1$ excitations, respectively (0-1-0 spin sequences). Therefore, obviously the sign of the asymmetry ε determines the parity. The characteristics of the fourfold sectored Ge(HP)-Compton polarimeter used in the Stuttgart experiments are given in ref.[15]. The polarization sensitivity of the device has been determined in the energy range up to 4.4 MeV studying $(p, p'\gamma)$-reactions on ^{12}C, ^{24}Mg, ^{28}Si and ^{56}Fe at the Cologne Tandem facility and the Stuttgart Dynamitron. The polarization sensitivity Q amounts to $\approx 20\%$ at 0.5 MeV and remains $\approx 9.5\%$ at 4.4 MeV [15]. The overall detection sensitivity of the polarimeter could be considerably increased recently by improving its response function using a BGO anti-Compton shield [16].

The experiments have been performed at the bremsstrahlung facility installed at the Stuttgart Dynamitron accelerator ($E_0 = 4.3$ MeV; $I^-_{typical} \approx 0.8\ mA\ (CW)$). The photon scattering technique, the experimental set-ups and procedure are described in detail in preceding papers [4,15,17] and by H.H. Pitz in his contribution to this conference.

3. RESULTS FOR SPHERICAL NUCLEI

3.1. $2^+ \otimes 3^-$ Two Phonon Excitations in N=82 Isotones

Collective excitations such as quadrupole or octupole vibrations are well known characteristic features in the low energy excitation schemes of spherical nuclei. Multiphonon excitations e.g. the coupling of two or more fundamental excitations were subjects of recent investigations. The coupling of two quadrupole 2^+ vibrations, forming a $0^+, 2^+, 4^+$ triplet represents a very extensively studied example [18]. Another case of two phonon excitations is known in the spherical N=82 isotones [19]. The 3^- octupole vibration couples with the 2^+ quadrupole vibration and creates a quintuplet of two phonon states with $J^\pi = 1^- \cdots 5^-$. The energy of the J^π member of this quintuplet should be close to the sum energy of the two single vibrations.

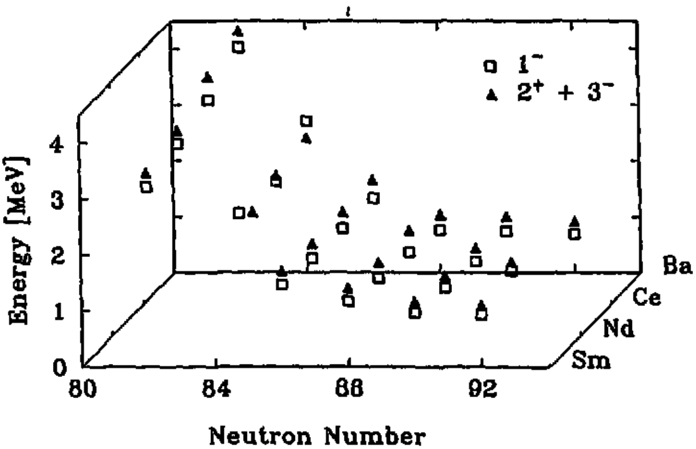

Fig.1: ($2^+ \otimes 3^-$) excitations in even-even nuclei around N=82. The excitation energies of the 1^- states (open symbols) agree nearly quantitatively with the sum of the energies of the quadrupole (2^+) and octupole (3^-) vibrational states (full symbols)[20].

Figure 1 shows the corresponding energies for even-even nuclei within the Sm, Nd, Ce ans Ba isotopic chains [20]. The strengths of the E1 decays of these $J^\pi=1^-$ states amount to about $20\cdot 10^{-3}\ e^2fm^2$ corresponding to some 10^{-3} Weisskopf units.

Figure 2 shows typical photon scattering spectra [20] for the spherical isotones (N=82) ^{138}Ba, ^{140}Ce, and ^{142}Nd, which are clearly dominated by the strong E1 transitions at 4.027, 3.643, and 3.425 MeV, respectively, as marked in the figure. Recently we studied the Ba isotopic chain [21] which represents a transition from a spherical nucleus (^{138}Ba; N=82) to more O(6) like nuclei (soft rotors). In fig.3 the spectra of photons scattered off the even Ba isotopes ^{138,136,134}Ba are depicted. As in the case for the well investigated transition from spherical to SU(3) like nuclei (deformed rotors) (Nd [22,23] and Sm [24] isotopic chains) the excitation energies of the $J^\pi=1^-$ are lowered when moving away from the magic neutron number N=82 (^{138}Ba). However, the 1^- excitation energies agree quite well with the sum of the 2^+ and 3^- excitations.

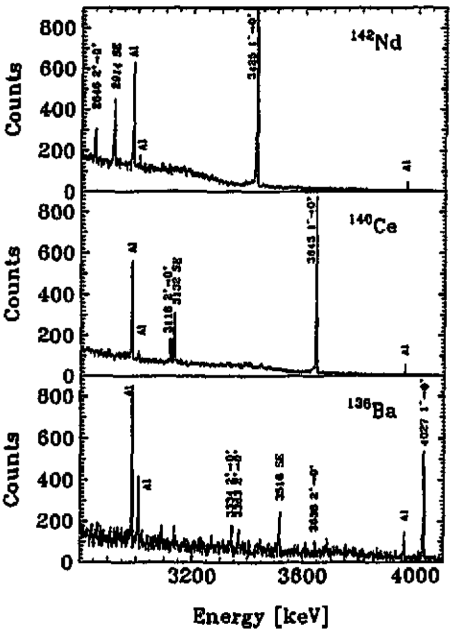

Fig.2: Energy spectra of photons scattered off the N=82 isotones ^{138}Ba, ^{140}Ce and ^{142}Nd [20].

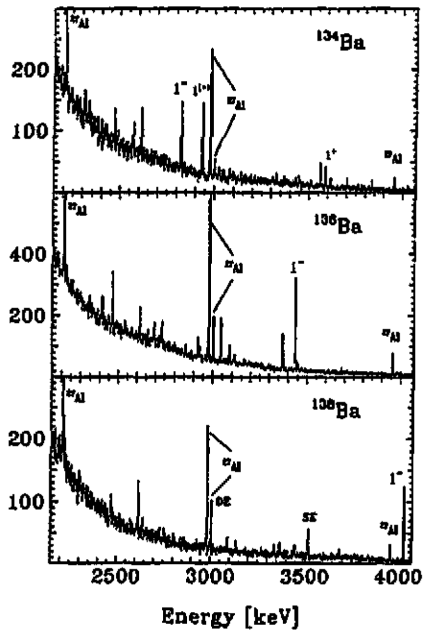

Fig.3: Energy spectra of photons scattered off the even Ba isotopes ^{138,136,134}Ba [21].

3.2. $2^+\otimes 3^-$ Two Phonon Excitations in Even-Even Sn Isotopes (Z=50)

These two phonon excitations $2^+\otimes 3^-$ should be a rather common feature in heavy spherical, semimagic nuclei. We therefore investigated even Sn isotopes (Z=50). The Sn isotopic chain is a very favourable case since there exist seven even-even stable isotopes, which all are known to be more or less of a spherical shape [25,26]. In a joint Stuttgart-Gent-Moscow collaboration [27] the low energy range of dipole excitations in ^{116}Sn and ^{124}Sn have been investigated at the Stuttgart Dynamitron facility. In addition the higher excitation energy range was studied at the Gent NRF set-up. In Gent a polarized bremsstrahlung beam was available allowing parity assignments [28]. The low energy part of the energy spectra of scattered photons is dominated in both isotopes by a single strong dipole transition at 3.334 in ^{116}Sn and 3.490 MeV in ^{124}Sn, respectively. The strengths measured in the Stuttgart experiments amounts to values of $B(E1)\uparrow = 6.55(65)$ and $6.08(66)\cdot 10^{-3}e^2fm^2$, respectively. These strengths are about 2 orders of magnitude higher than the usual E1 strength in this mass region [29]. The negative parity of 1^- state at 3.334 MeV in ^{116}Sn could be determined by the measurement of the azimuthal asymmetry of the scattered photons using the polarized bremsstrahlung beam of the Gent facility [28]. The excitation energies and transitions strengths could be explained by recent QRPA calculations [28] starting from a schematic model incorporating 1p-1h (one phonon) admixtures into the particular two phonon states ($2^+\otimes 3^-$) (see table 1).

	Excitation Energy (MeV)			Transition Probability ($e^2fm^2\cdot 10^{-3}$)	
Nucleus	$E_{Exp.}$	$E_{2^+}+E_{3^-}$	$E_{Theor.}$	$B(E1)\uparrow_{Exp.}$	$B(E1)\uparrow_{Theor.}$
^{116}Sn	3.334	3.560	3.15	6.55 ± 0.65	1.49
^{124}Sn	3.490	3.746	3.57	6.08 ± 0.66	4.39

Table 1.: Results for enhanced electric dipole excitations in the semimagic (Z=50) isotopes ^{116,124}Sn, which are interpreted as two phonon excitations ($2^+\otimes 3^-$) and comparison with recent QRPA calculations [27].

3.3. $2^+\otimes 3^-\otimes$ Particle Excitations in Odd Nuclei Near N=82

As discussed aboved the 1^- member of the $2^+\otimes 3^-$ multiplet has been found in various $N = 82$ isotones [19,30] in photon scattering experiments. In ^{142}Nd an isolated $E1$ transition from a 1^- state at 3425 keV was detected [22,30]. In a recent experiment [11] performed at the Stuttgart Dynamitron the coupling of an additional neutron to the $2^+\otimes 3^-$ multiplet has been investigated. In the case of ^{143}Nd the additional neutron occupies the $f_{7/2}$ subshell. Because of the coupling of the odd neutron the five levels of the $2^+\otimes 3^-$ multiplet in the core nucleus split into 31 levels in ^{143}Nd. Out of these, due to selection rules, in photon scattering experiments only states with spins 5/2, 7/2, and 9/2 can be excited from the groundstate (in total 15 levels).

The measured strength distribution exactly exhibits all these 15 excitations. The assumption of electric dipole character for these transitions is highly favourable from the known dipole excitations in the neighbouring nuclei. The total $B(E1)\downarrow$ strength observed in ^{143}Nd (deexcitation of J=5/2, 7/2, and 9/2 states) amounts to about three times the strength of the strong 3452 keV transition in the even core nucleus ^{142}Nd. The fact that the sum rule is fulfilled proofs the two-phonon $\otimes$ particle structure for the excitations in ^{143}Nd.

The experimental results could be explained by recent calculations. In these model calculations [11] first the prominent collective features of the core nucleus (energetic positions of the 2^- .... 5^- members of the multiplet) are described in the framework of the *sdf*-IBM. Then the coupling of the additional neutron is calculated using the code COUPLIN [31]. The calculated distribution is quite similar to the experimental one as shown in fig.4. The agreement between the experimental data and the core coupling calculations can be considered to be a strong argument in favour of the proposed $2^+\otimes 3^-\otimes$ particle structure of the observed states near 3 MeV.

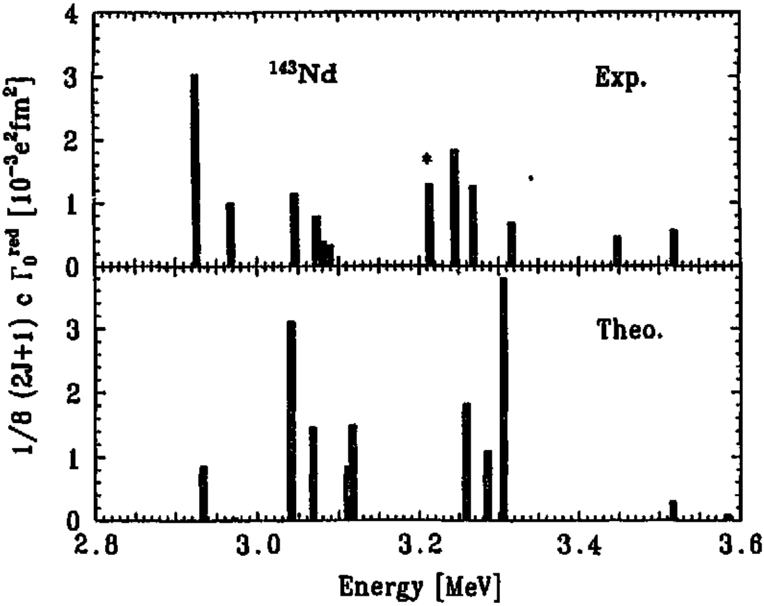

Fig.4: Experimental (upper part) and theoretical (lower part) dipole strength distribution in ^{143}Nd between 2.8 and 3.6 MeV [11]. If the transitions have an $E1$ character one finds for the plotted quantity $\frac{1}{8}(2J+1)\cdot c\cdot\Gamma_0^{red} = B(E1; J\rightarrow J_0)\downarrow$ (with $\Gamma_0^{red} = \Gamma(J\rightarrow J_0)\cdot E_\gamma^{-3}$ and $c = 0.9553\cdot 10^{-3}\ e^2fm^2\ \mathrm{MeV}^3/\mathrm{meV}$). The level marked by an asterisk shows a strong branching to the $3/2^-$ level at 742 keV and is not expected to be reproduced by the theoretical calculations [11].

4. RESULTS FOR DEFORMED NUCLEI

4.1. Low-Lying ΔK=0 Excitations in Even-Even Nuclei

The systematics of $K = 0$, $J^\pi = 1^-$ states in rare earth nuclei observed in our previous systematic photon scattering experiments [6] shows that the $K^\pi = 0^-$ strength is mainly concentrated in one or two transitions near 1.5 MeV with summed strengths of $\Sigma\ B(E1)\uparrow \approx 20\cdot 10^{-3}\ e^2fm^2$ (corresponding to a rather high value of $\approx 4\cdot 10^{-3}$ Weisskopf units), whereas the strength at higher energies is rather fragmented. These low lying 1^- states are discussed in terms of $K = 0$ rotational bands based on an octupole vibration as suggested by Donner and Greiner [32]. This explanation is supported by the observed linear correlation of the energies of the $K = 0$, $J = 1_1^-$ states with the energies of closely lying $J = 3^-$ states [6]. The strengths of these $K = 0$ $E1$ excitations could be explained by an admixture of the Giant Dipole Resonance (GDR) to these low lying 1^- states [33]. The same description already had been successfully applied for the interpretation of low lying 1^- states in ^{48}Ti, ^{164}Dy, ^{232}Th and ^{238}U observed in (e,e')-experiments [34]. Von Brentano et al. [35] explained on a quantitative scale both the transition widths Γ_0 and the decay branching ratios of these 1^--states using an improved $E1$ operator within the sdf-IBA-model. Recently Soloviev et al. [36] described these $\Delta K = 0$ E1 excitations and in addition weaker $\Delta K = 1$ transitions [37.)] microscopically within a quasiparticle-phonon model.

4.2. Two Phonon Excitations in Even-Even Deformed Nuclei

Our systematic polarization measurements in photon scattering off ^{150}Nd, ^{160}Gd, ^{162,164}Dy provided evidence for isolated enhanced *electric* dipole excitations at excitation energies of 2.414, 2.471, 2.520 MeV, and 2.670 MeV, respectively. The transition energies and the enhanced $B(E1)\uparrow$ strengths of 3 to $5\cdot 10^{-3}\ e^2 fm^2$ may suggest an interpretation in terms of the predicted new type of collective electric dipole excitations in deformed nuclei due to reflection asymmetric shapes like octupole deformations and/or cluster configurations [38.)]. Table 2 summarizes the results [38.)]. Both, the cluster and the octupole shape models are able to explain at least the right order of magnitude of the observed $E1$ strengths.

Nucleus	E_x (MeV)	Γ_0 (meV)	R_{exp}	$B(E1)\uparrow$ ($10^{-3}\ e^2 fm^2$)
^{150}Nd	2.414	14.9±2.0	0.86±0.09	3.0±0.4
^{160}Gd	2.471	16.4±2.6	1.56±0.21	3.1±0.5
^{162}Dy	2.520	30.2±4.0	1.31±0.08	5.0±0.4
^{164}Dy	2.670	27.0±4.7	1.14±0.24	4.1±0.7

Table 2.: Results for enhanced electric dipole excitation in deformed nuclei [38.)]: excitation energies E_x, ground state transition widths Γ_0, experimental decay branchings $R = B(1^- \to 0^+) / B(1^- \to 2^+)$ and reduced transition probabilities $B(E1)\uparrow$.

Another very tempting interpretation is to explain these states as two phonon excitations in strongly deformed nuclei caused by the coupling of octupole vibrations to the $K^\pi = 2^+$, γ-vibration. Such two phonon excitations were theoretically already explicitely treated by Donner and Greiner [32.)] within the Dynamic Collective Model in 1966, but up to now such states could not be detected experimentally. The resulting 1^- states can be excited by dipole transitions from the ground state as a result of the coupling of the giant electric dipole resonance to the octupole vibration [32.)].

In the following the 1^- states near 2.5 MeV are discussed as possible candidates for such two phonon excitations due to the coupling of quadrupole-γ-vibrations ($J = 2^+, K = 2$) and octupole vibrations ($J = 3^-, K = 1$). It is obviously impossible to generate states with J=1 by coupling the γ–vibration to octupole excitations with ($J = 3^-, K = 0$). Donner and Greiner [32.)]. showed that the energy of the two phonon excitation is simply given by the sum of the phonon energies in the examined case where K=1 and J_3=1 (J_3= third component of the octupole angular momentum):

$$E_{2Ph}^{K=1}(1^-) \;=\; E_{oct}^{K=1}(1^-) \;+\; E_{\gamma}^{K=2}(2^+). \tag{2}$$

The informations on the position of the octupole vibrational bandheads with K=1 are rather sparse. Therefore one has to assume in most cases that the first J^π=1$^-$ state following the K=0 octupole vibrational bandhead is a K=1 state. As possible candidates for the two phonon excitation besides the 1^- states in the four isotopes ^{150}Nd,^{160}Gd, and ^{162,164}Dy investigated so far by polarization measurements the lowest J=1 states above the octupole vibrational bandheads exhibiting an uncommon decay branching ratio have been taken. An excellent agreement between the excitation energies $E_{exp}^{K=1}(1^-)$ of the assumed two phonon excitations and the sum of the $K = 1$ octupole and the γ-vibrational excitations (according to eq. 2) can be stated. Figure 5 illustrates this fact in graphical form.

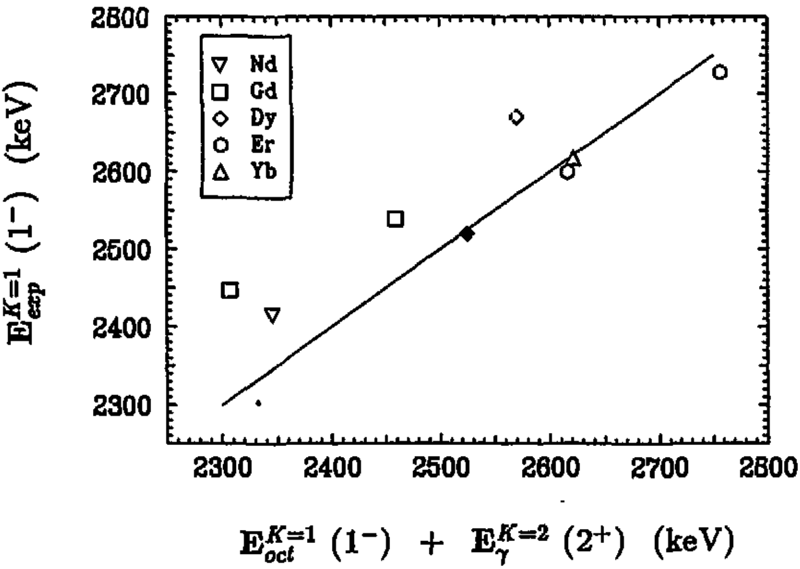

Fig.5: Experimental excitation energies $E^{K=1}_{exp}(1^-)$ of states attributed to a two phonon excitation versus the sum of the $K = 1$ octupole and the γ-vibrational excitations ($E^{K=1}_{oct}(1^-) + E^{K=2}_{\gamma}(2^+)$). The full line corresponds to the exact fulfilment of eq.2. In the case of ^{162}Dy (full symbol) all needed energies are experimentally known (from ref.[38.]).

In order to gain more information about the observed 1^- states calculations in the framework of the sdf-IBA model have been performed [38.], which support the interpretation as two phonon excitations. Therefore, the observed strong $E1$ excitations near 2.5 MeV in deformed nuclei exhibiting an uncommon decay branching may be attributed to a two phonon excitation caused by the coupling of the octupole and quadrupole-γ-vibrations. This conclusion is based on the nearly quantitative agreement of the experimental excitation energies with the sum of the $K = 1$ octupole and $K = 2$ γ-vibration as suggested by the collective model and on the results of sdf-IBA calculations which reproduce the experimental energies and the structure of the states. However, the sdf-IBA fails to account for the enhanced $B(E1)$ values. To obtain more information on the structure of these states it is important to get additional experimental data on the octupole vibrational bands as well as on higher-lying dipole excitations.

It should be emphasized that the $J^\pi = 1^-$ states corresponding to the enhanced $E1$ excitations near 2.5 MeV in the neighbouring nuclei ^{150}Nd, ^{160}Gd, ^{162}Dy, and ^{164}Dy as discussed above exhibit a decay branching ratio R_{exp} deviating from the expected values for pure $K = 0$ and $K = 1$ states and therefore hint to a possible K-mixing [40.].

Another indication for a direct relation to octupole vibrations delivers the observed correlation [41.] of the energies of these $J^\pi = 1^-$ states with the energies of the low lying $K = 0$, $J^\pi = 1^-$ states, which are interpreted in terms of $K = 0$ rotational bands based on an octupole vibration [6.]. Combing this linear correlation, not predicted within the Dynamic Collective Model [32.], with equ.2 a linear dependence should hold between the excitation energies of the J^π=1$^-$ band heads of the $K = 1$ and $K = 0$ octupole bands. This is shown in fig.6 for deformed nuclei in the Rare Earth and actinide region [42]. The linear correlation coefficient amounts to r=0.83. The two data points for Rare Earth nuclei strongly deviating from the systematics belong to ^{156}Gd and ^{172}Yb where the K-assignments are questionable due to a strong K mixing (see ref.[38]). Omitting these two data points in the analysis an increased correlation coefficient of r= 0.93 is obtained. To our knowledge such a correlation between these two octupole bands has not been discussed in the literature so far.

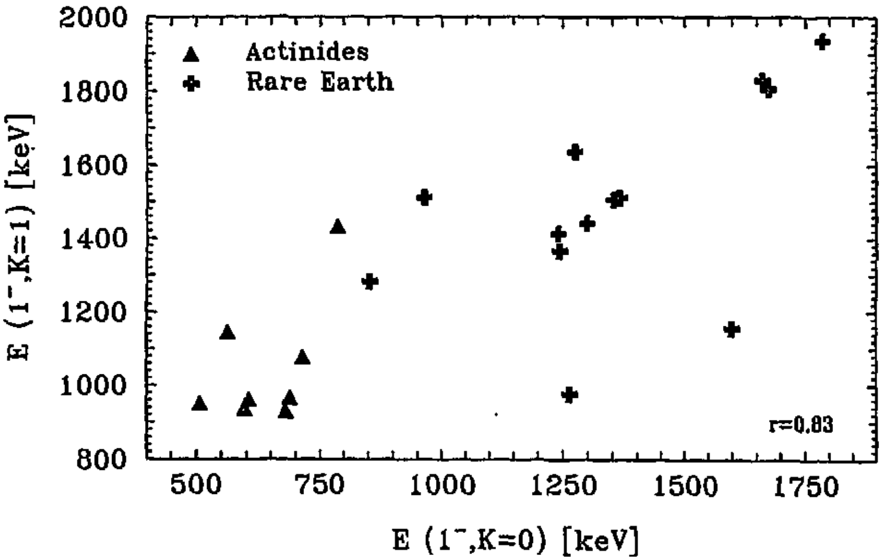

Fig. 6: Experimental excitation energies $E(1^-, K = 1)$ of the head of the $K = 1$ octupole vibrational band versus the energy of corresponding head of the $K = 0$ octupole vibrational band in Rare Earth and actinide nuclei [42].

5. ACKNOWLEDGEMENTS

The Stuttgart experiments have been performed in a long standing, pleasant collaboration with the group of Prof. von Brentano (Köln). The investigations of the Sn-isotopes are part of an international collaboration between IfS Stuttgart, University of Gent (Dr. E. Jacobs, K. Govaert) and the Kurchatov Institute Moscow (Dr. L. Govor). It is a pleasure to thank all colleagues for the very fruitful and stimulating collaboration. Special thanks are due to my longterm collaborators H.H. Pitz, J. Margraf, H. Maser (Stuttgart) and A. Zilges, R.-D. Herzberg, N. Pietralla (Köln) for their outstanding engagement and enthusiasm which enabled the realization of the various projects. The extensive financial support over many years by the Deutsche Forschungsgemeinschaft is gratefully acknowledged.

REFERENCES

1.) D. Bohle et al., Phys.Lett. 137B, 27 (1984).
2.) A. Richter, Nucl.Phys. A507, 99c (1990).
3.) A. Richter, Nucl.Phys. A522, 139c (1991).
4.) U. Kneissl, Prog.Part.Nucl.Phys. 24, 41 (1990).
5.) U. Kneissl, Prog.Part.Nucl.Phys. 28, 331 (1992).
6.) A. Zilges et al., Z.Phys. A 340, 155 (1991).
7.) H. Friedrichs et al., Phys.Rev. C45, R892 (1992).
8.) H. Friedrichs et al., Nucl.Phys. A553, 553c (1993).
9.) H. Friedrichs et al., Nucl.Phys. A567, 266 (1994).
10.) I. Bauske et al., Phys.Rev.Lett. 71, 975 (1993).
11.) A. Zilges et al., Phys.Rev.Lett. 70, 2880 (1993).
12.) U.E.P. Berg and U. Kneissl, Ann.Rev.Nucl.Part.Sci. 37, 33 (1987).
13.) D. Bohle et al., Nucl.Phys. A458, 205 (1986).
14.) G. Alaga et al., Dan.Mat.Fys.Medd. 29, no.9, 1 (1955).
15.) B. Schlitt et al., Nucl.Instr. a. Meth. in Phys.Res. A337, 416 (1994).
16.) H. Maser, Diploma Thesis, Stuttgart (1993), unpublished
17.) H.H. Pitz et al., Nucl.Phys. A492, 411 (1989).
18.) A. Bohr and B.R. Mottelson, Nuclear Structure, Vol. II, W.A. Benjamin Inc., New York, 477 (1975).
19.) F.R. Metzger, Phys.Rev. C18, 1603 (1978).
20.) R.-D. Herzberg et al., Proc. of the 8^{th} International Symposium on: *Capture γ-Ray Spectroscopy and Related Topics*, Fribourg, (1993) p. 185
21.) H. Maser, Ph.D. Thesis, Stuttgart, in preparation
22.) H.H. Pitz et al., Nucl.Phys. A509, 587 (1990).
23.) J. Margraf et al., Phys.Rev. C47, 1474 (1993).
24.) W. Ziegler et al., Phys.Rev.Lett. 65, 2515 (1990).
25.) S.C. Fultz et al., Phys.Rev. 186, 1255 (1969).
26.) A. Leprêtre et al., Nucl.Phys. A219, 39 (1974).
27.) K. Govaert et al., Phys.Lett. B, in press (1994).
28.) K. Govaert et al., Nucl.Instr. a. Meth. in Phys.Res. A337, 265 (1994).
29.) P.M. Endt, Atomic and Nuclear Data Tables 26, 47 (1981).
30.) F.R. Metzger, Phys.Rev. C18, 2138 (1978).
31.) F. Dönau and S. Frauendorf, Phys.Lett. 71B, 263 (1977) and F. Dönau, Z.Phys. A293, 31 (1979).
32.) W. Donner and W. Greiner, Z.Phys. 197, 440 (1966).
33.) A. Zilges et al., Z.Phys. A341, 489 (1992).
34.) Th. Guhr et al., Nucl.Phys. A501, 95 (1989).
35.) P. von Brentano et al., Phys.Lett. 278B, 221 (1992).
36.) V.G. Soloviev and A.V. Sushkov, Phys.Lett. 262B, 189 (1991).
37.) V.G. Soloviev, A.V. Sushkov, N.Yu. Shirikova, priv. comm. and to be published (1994)
38.) U. Kneissl et al., Phys.Rev.Lett. 71, 2180 (1993).
39.) F. Iachello, Phys.Lett. 160B, 1 (1985).
40.) A. Zilges et al., Phys.Rev. C42, 1945 (1990).
41.) I. Bauske et al., Proceedings of the XIII International Conference *"Particles and Nuclei"*, Perugia (Italy), 1993, Book of Abstracts Vol. 1, 413
42.) A. Zilges, priv. communication (1994).

THE ROLE OF DIPOLE TRANSITIONS IN DETERMINING THE COLLECTIVITY OF NUCLEAR EXCITATIONS

S. W. Yates, D. P. DiPrete, E. L. Johnson, E. M. Baum, C. A. McGrath, D. Wang, and M. F. Villani

Departments of Chemistry and Physics & Astronomy
University of Kentucky, Lexington, KY 40506-0055, USA

and

T. Belgya, B. Fazekas, and G. Molnár

Institute of Isotopes, Hungarian Academy of Sciences
Budapest H-1525, Hungary

Abstract

Doppler-shift attenuation method (DSAM) measurements following the inelastic neutron scattering (INS) reaction have been employed to measure the lifetimes of states that decay by dipole transitions and, from the transition rates, the degree of nuclear collectivity of these states can be assessed. The electromagnetic decay properties of the known M1 scissors mode states in ^{162}Dy and ^{164}Dy have been examined, and the DSAM-INS has been used to measure directly the lifetimes of these excitations. The M1 strengths determined are in general agreement with those measured previously in nuclear resonance fluorescence experiments; however, a significant discrepancy is found for three states near 3.1 MeV in ^{164}Dy. A number of fast E1 transitions have been identified in light rare earth nuclei, and candidates for two-phonon octupole and quadrupole-octupole vibrational multiplets have been suggested. In a detailed study of the transitional nucleus ^{146}Nd, a viable candidate for the lowest mixed-symmetry 2^+ state has been identified from measured M1 transition rates.

1. Introduction

While the degree of nuclear collectivity is frequently assessed by examining the quadrupole characteristics of nuclei, the use of dipole transitions in determining collectivity is considerably more ambiguous. However, a wealth of new information about E1 and M1 transition rates has become available in recent years, and with these data has come new information about collective structures. At the University of Kentucky, we have employed the INS or $(n,n'\gamma)$ reaction with accelerator-produced monoenergetic neutrons, coupled with the DSAM, to measure a large number of lifetimes of states that decay by M1 or E1 transitions. We have studied several even-even rare earth nuclei having significantly differing deformations and report our conclusions about the existence of collective excitations in these nuclei from measurements of dipole transition rates.

2. Experimental Procedures and Analysis

Nuclear structure studies have been conducted for many years with the inelastic neutron scattering reaction at the University of Kentucky 7.0 MV Van de Graaff accelerator and associated neutron scattering facilities. The experimental apparatus and methods have been reported on many occasions, and the latest developments in our laboratories, including the Doppler-shift attenuation (DSA) lifetime methodology, have recently been described [1]. The non-selective nature of the INS reaction and the high level densities in the regions of interest frequently lead to complex γ-ray spectra, but careful selection of the incident neutron energy can often alleviate many of these complications.

DSAM has been used in a variety of nuclear reactions to obtain lifetimes of various excited states in the fs to ps range, and the reliability of DSAM-INS has been demonstrated [2]. In DSAM-INS lifetime determinations, a decay γ-ray from a recoiling excited nucleus produced by the INS reaction is subject to a Doppler-shift whose magnitude depends upon the instantaneous velocity and the relative direction of emission. If the slowing process induced by interactions with the bulk target material can be accurately described, the lifetime of the decaying state can be determined from the observed Doppler shift. The equation for the energy of the emitted γ-ray is [3]

$$E_\gamma(\theta) = E_0 \, [1 + F(\tau) \, \beta \cos \theta]$$

where θ is the angle between the recoil and emission directions, $E_\gamma(\theta)$ represents the observed γ-ray energy at angle θ, E_0 is the unshifted γ-ray energy, $F(\tau)$ is the velocity attenuation factor, and $\beta = v/c$ gives the initial recoil velocity. A typical experimental plot of $E_\gamma(\theta)$ versus cos θ is shown in Fig. 1. An experimental $F_{exp}(\tau)$ value can be extracted from a linear fit of these data. Lifetimes can then be obtained from a comparison of $F_{exp}(\tau)$ with a theoretically generated $F_{th}(\tau)$ versus τ curve based on stopping theory. The method of Winterbon [4] was used to obtain $F_{th}(\tau)$ versus τ values for these analyses.

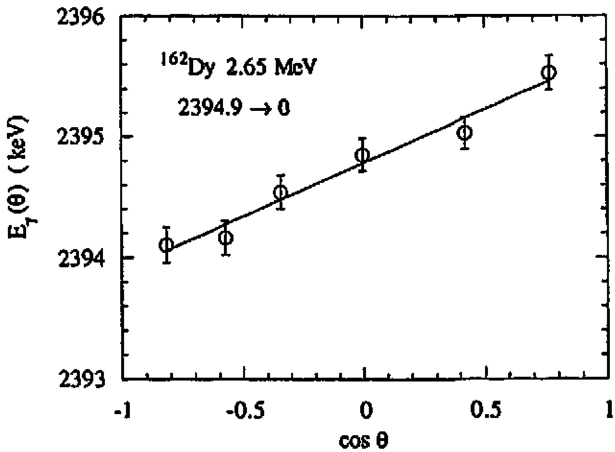

Fig. 1. Plot of γ-ray energy versus cos θ used to determine the experimental attenuation factor $F_{exp}(\tau)$ of the 2395 keV γ-ray of ^{162}Dy.

In all measurements, multigram enriched oxide powders of the isotope of interest packed into thin-walled cylindrical polyethylene vials were used as scattering samples. The resulting γ-rays from the $(n,n'\gamma)$ reaction were detected using a BGO Compton suppressed n-type HPGe detector having a relative efficiency of 52% and an energy resolution of 2.0 keV at 1.33 MeV. The entire detector assembly was mounted on a carriage which permitted measurements to be performed at various angles. Time-of-flight suppression was also used to reduce extraneous background events, and γ-ray thresholds and placements were determined from excitation function measurements. Spin limitations can also be inferred from the shapes of the excitation functions and the magnitude of the inelastic scattering cross sections. Information on the spins and lifetimes of states, as well as the multipolarities of transitions, can be extracted from the angular distribution data.

3. Electric Dipole Transitions

The interesting behavior of electric dipole transition rates observed in the N = 82 nuclei has been reported by Gatenby et al. [1,5] who observed a large number of fast E1 transitions and suggested candidates for two-phonon octupole and quadrupole-octupole vibrational multiplets. One explanation of these large E1 strengths is that they are a consequence of the N = 82 shell closure [6,7]. If this interpretation is correct, the effect should decrease in nuclei removed from the closed shell. We have, therefore, chosen to study $^{146}Nd_{86}$ where shell effects should be less crucial but large quadrupole deformation is not prominent.

The decay properties of the low-spin excited states of ^{146}Nd at energies below 4.0 MeV were investigated with the $(n,n'\gamma)$ reaction [8]. From γ-ray excitation functions and angular distributions, many new levels have been established, and spin-parity assignments and multipole mixing ratios were been determined. A total of 161 levels were observed in these measurements; 70 of these were previously unknown. Level lifetimes were obtained for 135 levels and limits were established for many others.

The measured reduced transition probabilities for all transitions of known E1 multipolarity are shown in Fig. 2. (Similar data are also available for M1 and E2 transitions [8].) The E1 strengths appear to decrease with excitation energy, but this trend is consistent with the behavior expected for collective excitations. If B(E1) values greater than 10^{-3} W.u. are taken as indicative of "fast" E1 transitions, it is clear that a number of such transitions are observed. For comparison, the E1 strengths observed in the N = 82 isotones ^{144}Nd and ^{144}Sm are given in Fig. 3, as is the distribution of E1 strength for nuclei in the region A = 91-150 obtained from the compilation by Endt [9]. The E1 distributions for these three nuclei are clearly shifted to larger B(E1) values than that of the Endt compilation. It should be noted, however, that the lower E1 strengths in the Endt distribution can generally be attributed to nuclei in the low mass portion of this region, and sparse data were available for the higher mass nuclei. Moreover, a comparison of the distributions for the three nuclei indicates that fast E1 transitions may be regarded as a general characteristic of this mass region.

As noted previously, fast E1 transitions may be taken as evidence for octupole excitations and have been used as evidence for octupole-octupole and quadrupole-octupole two-phonon excitations [5]. Some evidence of the fast E1 signatures of the octupole-octupole or quadrupole-octupole multiplets was found in ^{146}Nd. Likely candidates for members of the $2^+ \otimes 3^-$ quintet are states which decay primarily to the 2_1^+ state (quadrupole phonon) by fast E1 transitions or the 3_1^- state (octupole phonon) through enhanced E2 transitions. The 1^- state at 1377.0 keV, with a 66% branch to the 2_1^+ state and a B(E1) of 2.4×10^{-3} W.u., stands out as a likely candidate for the lowest-spin member of the quintet. Additional candidates for members of the multiplet and their decay properties are shown in Fig. 4, where evidence of large anharmonicities is apparent.

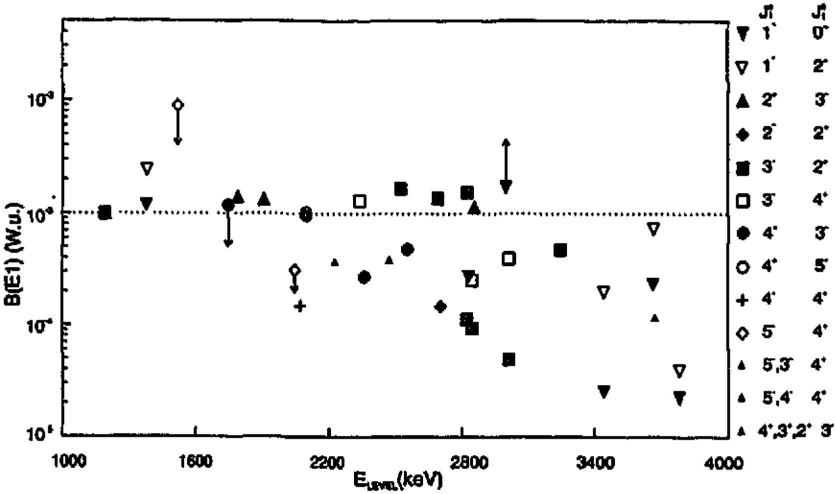

Fig. 2. The E1 transition strength distribution in ^{146}Nd. Transitions for which only upper or lower limits of the transition strength could be determined are noted with an arrow. The horizontal dotted line represents 10^{-3} W.u.

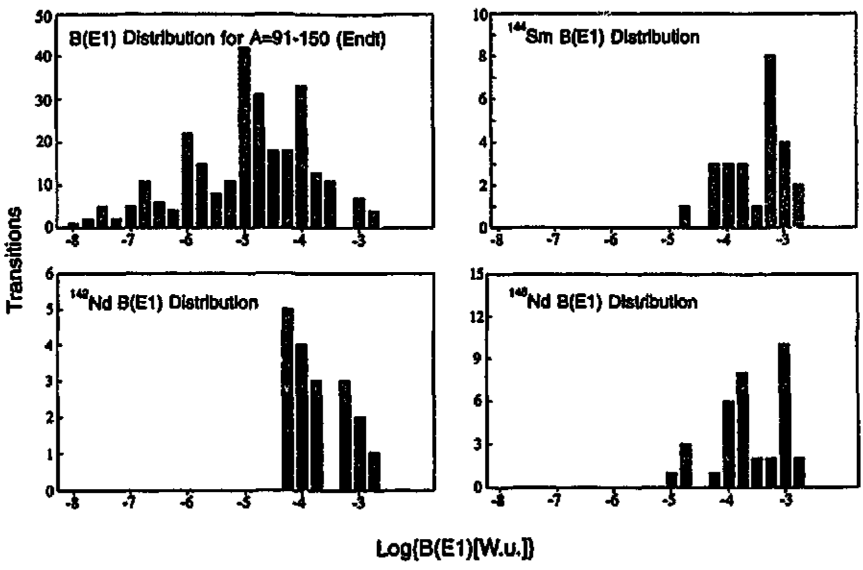

Fig. 3. Comparison of E1 strengths of transitions in ^{146}Nd to those of ^{142}Nd [5] and ^{144}Sm [1,5], as well as the E1 strengths for the A = 91-150 region [9].

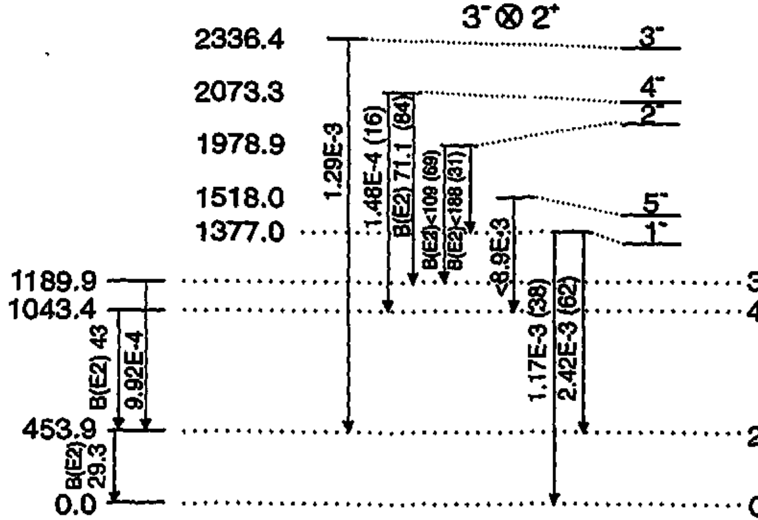

Fig. 4. Possible members of the quadrupole-octupole multiplets in ^{146}Nd. Reduced transition probabilities are given in W.u., and branching intensities are provided in parentheses.

The 2^+ and 4^+ members of the $3^-\otimes3^-$ two-phonon octupole quartet might be expected to decay to the 3^- octupole phonon by fast E1 transitions. While the 2^+ state at 2855.4 keV decays primarily with a B(E1) of 1.1×10^{-3} W.u., there are no outstanding candidates for the 4^+ member among the three known 4^+ states between 2.0 and 3.0 MeV. The 4^+ state at 2553.2 keV decays primarily to the first 3^- state with a B(E1) of 4.8×10^{-4} W.u. An overview of the possible two-phonon octupole states is given in Fig. 5.

4. Magnetic Dipole Transitions

4.1 Scissors Mode States in ^{162,164}Dy

Since their discovery [10] in 1984, weakly collective M1 scissors mode states, so-called because of the their interpretation as arising from scissorslike oscillations of the proton and neutron distributions, have been observed in nuclei from ^{46}Ti to ^{238}U [11]. In numerous studies, the low-energy magnetic dipole strength distribution in deformed even-even rare earth nuclei has been determined and has been shown to be concentrated (summed M1 strength of $\sim$ 2-3 μ_N^2) in at most only a few 1^+ states near 3 MeV. in excitation [11,12]. Theoretical approaches [13-20] have included various collective models as well as a variety of microscopic calculations, and it is now generally agreed that, in any successful description of these states, protons and neutrons must be treated as distinguishable and that this is predominantly an orbital mode. Measurements of related excitations in transitional nuclei have also been performed.

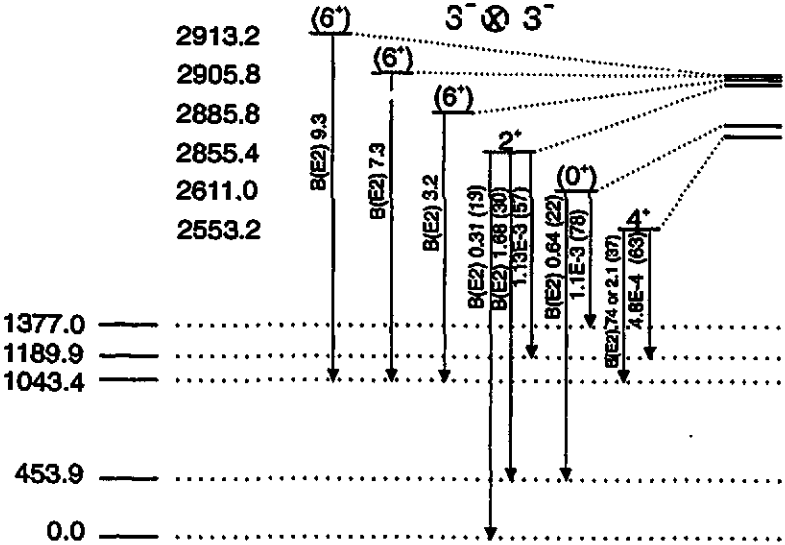

Fig. 5. Possible members of the two-phonon octupole multiplet in ^{146}Nd. Reduced transition probabilities are given in W.u., and branching intensities are provided in parentheses.

Two dysprosium nuclei, ^{162}Dy and ^{164}Dy, have been shown to display particularly interesting characteristics [21]. A 1^+ state at 2900 keV in ^{162}Dy has the largest measured B(M1) of any known scissors mode state. Significant fragmentation of M1 strength exists in ^{164}Dy as 7 levels with $J^\pi = 1^+$ have been identified below 3.2 MeV [21], and the summed B(M1) strength for these levels is anomalously large when compared to the systematics of neighboring nuclei [22]. Moreover, in a ^{165}Ho(t,α) reaction study, it was found that the 2539 keV state observed previously in elastic electron and photon scattering with a large M1 strength is dominated by a two-quasiproton configuration, an observation clearly inconsistent with a collective interpretation for the structure of this state [23]. In addition, intermediate energy proton scattering at small angles has been used to confirm that spin contributions are small in scissors mode states, except possibly in ^{164}Dy [24]. No satisfactory explanations have yet emerged for the puzzling results in ^{164}Dy.

A large amount of data on scissors mode excitations has been collected for nuclei in the rare earth region, primarily through electron scattering and nuclear resonance fluorescence (NRF) measurements, and it has been shown that the determination of accurate M1 strengths is important for understanding the structure of these excitations [12]. The present inelastic neutron scattering (INS) studies were initiated to determine directly the lifetimes of the scissors mode states of the heaviest stable even-A Dy isotopes, to identify branches to lower-lying excitations such as the γ band, to assess the degree of fragmentation of the scissors mode M1 strength, and to search for rotational excitations built on the scissors mode states.

The specific information provided by our INS measurements of scissors modes excitations is complementary to that obtained from electron scattering and NRF, the two methods most often used to examine these states. While the electron and photon scattering reactions are much more selective in exciting these states than INS, they are also limited in the information that can be obtained. Electron scattering is limited in the resolution attainable and provides no information about the decays of these states, while NRF suffers from a high bremsstrahlung background at lower energies that makes it difficult to observe the decay branches to states other than the ground state. Both methods, however, provide information that can be related to the M1 transition strengths. On the other hand, the INS reaction, combined with the Doppler-shift attenuation method (DSAM), provides a means for determining the B(M1)'s directly from the measured lifetimes, if the parities of the states can be confirmed with independent methods.

Results of lifetime measurements for the 1^+ states in ^{162}Dy and ^{164}Dy are summarized in Tables 1 and 2, respectively. The reduced transition probabilities given are based on previous positive-parity assignments for these states [21,25]. Comparisons of B(M1)↑ values from NRF [21] and our INS measurements are shown in Fig. 6. The INS results are in good agreement with those obtained from NRF for ^{162}Dy and for the four states near 2.6 MeV in ^{164}Dy. However, we find significantly lower strengths for the grouping of states near 3.1 MeV in ^{164}Dy. Reasons for these differences are not obvious.

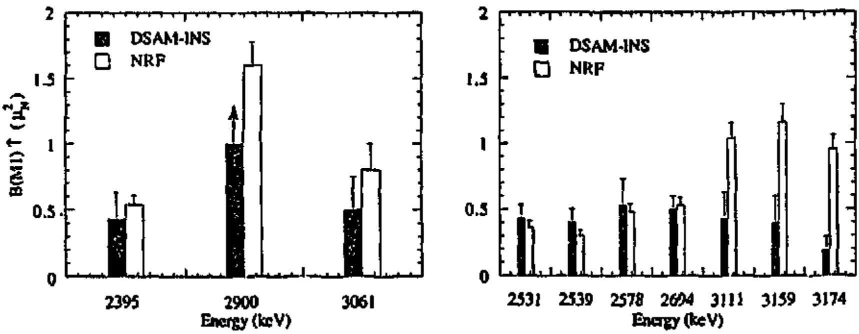

Fig. 6. Comparison of B(M1)↑ values of scissors modes states in ^{162}Dy and ^{164}Dy determined from INS (this work) and NRF [21] experiments. The arrow for the 2900 keV state indicates that only a lower limit was determined.

It should also be noted that, while the parities of these states could not be determined from our data alone, all of the γ-rays listed in Tables 1 and 2 displayed angular distributions consistent with dipole transitions. Moreover, the branching ratios obtained are in good agreement with those given by Wesselborg et al. [21] and are consistent with those expected for K = 1 states.

In addition to determining the properties of the known scissors mode states in these nuclei, we have searched for additional decay branches from these states. With the possible exception of a 2337 keV γ-ray from the 3099 keV 1^+ state to the 2^+ γ vibration in ^{164}Dy [26], no other transitions from scissors mode states to levels not in the ground state band could be positively identified in this study.

Table 1. Decay properties of $J^\pi = 1^+$ states in ^{162}Dy.

E_x(keV)	E_γ(keV)	E_f(keV)	J^π_f	Branching Ratio (%)	τ(fs)	B(M1)↑ (μ_N^2)
2394.9(3)	2394.9(2)	0.0	0^+	66(3)	12(5)	0.43(20)
	2314.1(2)	80.7	2^+	34(3)		
2900.3(5)	2900.3(4)	0.0	0^+	74(4)	<5	>1
	2819.0(4)	80.7	2^+	26(4)		
3061.2(5)	3061.4(4)	0.0	0^+	71(4)	8(4)	0.50(25)
	2980.3(4)	80.7	2^+	29(4)		

Table 2. Decay properties of $J^\pi = 1^+$ states in ^{164}Dy.

E_x(keV)	E_γ(keV)	E_f(keV)	J^π_f	Branching Ratio (%)	τ(fs)	B(M1)↑ (μ_N^2)
2530.8(3)	2530.7(2)	0.0	0^+	69(4)	17(4)	0.43(10)
	2457.5(2)	73.4	2^+	31(4)		
2539.1(3)	2539.1(2)	0.0	0^+	73(4)	18(4)	0.40(10)
	2465.7(2)	73.4	2^+	27(4)		
2577.9(3)	2577.9(2)	0.0	0^+	69(4)	13(5)	0.53(20)
	2504.5(2)	73.4	2^+	31(4)		
2694.0(5)	2694.1(4)	0.0	0^+	72(4)	11(3)	0.50(10)
	2620.5(4)	73.4	2^+	28(4)		
3111.1(5)	3111.0(4)	0.0	0^+	73(5)	10(4)	0.43(20)
	3037.8(4)	73.4	2^+	27(5)		
3159.1(5)	3159.4(4)	0.0	0^+	64(5)	9(4)	0.40(20)
	3085.3(4)	73.4	2^+	36(5)		
3173.6(5)	3173.6(4)	0.0	0^+	64(5)	20(6)	0.19(7)
	3100.1(4)	73.4	2^+	36(5)		

If the scissors mode states are, as believed, the bandheads of $K^\pi = 1^+$ bands, higher-lying rotational states would be anticipated. We have searched for additional band members. Some candidates for 2^+ members of a scissors mode rotational band have been identified. Unfortunately, the data are generally insufficient to characterize with certainty even the spins of these states, so these assignments remain tentative.

The vast majority of experimental evidence relating to scissors mode excitations has been obtained by techniques utilizing the electromagnetic interaction; we have demonstrated that these states can also be populated with fast neutron scattering. However, the non-selective nature of INS reaction, coupled with high level densities in deformed nuclei, results in very dense γ-ray spectra, and the difficulty with accurately deconvoluting multiplets in these spectra places practical limits on this technique.

4.2 Mixed-Symmetry States in ^{146}Nd

While the E1 transition strengths (see section 3) were a primary motivation for our INS study of ^{146}Nd, we have been able to address related nuclear structure questions about this nucleus. For example, we have been able to search for mixed-symmetry states in this nucleus. Little was known previously about these excitations in N = 86 nuclei. Since ^{146}Nd is positioned between nearly spherical ^{142}Nd and moderately deformed ^{150}Nd, we searched for evidence of both the 2^+ mixed-symmetry states characteristic of spherical nuclei and the fragmented 1^+ mixed-symmetry states characteristic of deformed nuclei.

The primary signature used to identify mixed-symmetry states in ^{146}Nd is evidence of fast M1 transitions. Typically, in nearly spherical nuclei, low-lying mixed-symmetry states with J^π = 2^+ are expected to decay predominantly to the "symmetric" 2^+ counterpart with an enhanced M1 and with a small multipole mixing ratio [27]. We found seven states to which we could unambiguously assign a J^π of 2^+ up to 3.5 MeV. The branching ratios of the transitions to the first 2^+ state, as well as the multipole mixing ratios and reduced transition probabilities of these states were determined. The 1977.9 keV state, with a pure M1 transition to the first 2^+ state and a B(M1) of 0.1 W.u., appears to display the requisite features to be considered a viable candidate for the lowest mixed-symmetry 2^+ state. Additional 2^+ states at 1787.5 and 1905.9 keV also display some mixed-symmetry character with substantial M1 strengths of 0.051 and 0.027 W.u., respectively.

In nuclei with one neutron boson and one proton boson above a closed shell, the symmetric 2_1^+ state and the 2^+ state of mixed-symmetry are predicted to couple and give rise to mixed-symmetry 1^+ and 3^+ states which decay primarily to the 2_1^+ state by enhanced M1 transitions. With the addition of more bosons above a closed shell, as is the case in ^{146}Nd, the number of mixed-symmetry states increases considerably. A 1^+ mixed-symmetry state would be expected to have a fast M1 transition to the ground state, with a resulting B(M1) of the order of 1 μ_N^2; however, due to fragmentation this strength could be spread over a number of states. There were eleven spin-1 states observed in this experiment up to 3.5 MeV, in addition to the low-lying 1^- state at 1377.0 keV. Except for the information provided by Margraf et al. [28], the parities are unknown for all but three of these. While we have observed several candidates for these additional mixed-symmetry states, compelling identifications cannot be made for any of them.

5. Acknowledgements

We wish to thank U. Kneissl, J. Margraf, H. H. Pitz, C. Wesselborg, and A. Zilges for valuable discussions and for communicating their results prior to publication. This work was supported by the U. S. National Science Foundation under Grants Nos. PHY-9001465, PHY-9300077, and No. INT-901770 and by the OTKA subprogram of the Hungarian Academy of Sciences.

6. References

[1] R. A. Gatenby, E. L. Johnson, E. M. Baum, S. W. Yates, D. W. Wang, J. R. Vanhoy, M. T. McEllistrem, T. Belgya, B. Fazekas and G. Molnár, Nucl. Phys. A560 (1993) 633

[2] E. K. Warburton, D. E. Alburger and D. H. Wilkinson, Phys. Rev. 129 (1963) 2180

[3] T. Belgya, B. Fazekas, G. Molnár, R. A. Gatenby, E. L. Johnson, E. M. Baum, D. Wang, D. P. DiPrete and S. W. Yates, Proc. 8th Int. Symposium on Capture Gamma-Ray Spectroscopy and Related Topics, ed. J. Kern (World Scientific, Singapore, 1994) p. 878

[4] K. B. Winterbon, Can. J. Phys. 50 (1972) 3147; Nucl. Phys. A246 (1975) 293

[5] R. A. Gatenby, J. R. Vanhoy, E. M. Baum, E. L. Johnson, S. W. Yates, T. Belgya, B. Fazekas and G. Molnár, Phys. Rev. C41 (1990) R414

[6] G. A. Leander, W. Nazarewicz, G. F. Bertsch and J. Dudek, Nucl. Phys. A453 (1986) 58

[7] P. A. Butler and W. Nazarewicz, Nucl. Phys. A533 (1991) 249

[8] D. P. DiPrete, E. M. Baum, E. L. Johnson, C. A. McGrath, S. W. Yates, D. Wang, M. F. Villani, T. Belgya, B. Fazekas and G. Molnár, to be published

[9] P. M. Endt, At. Data Nucl. Data Tables 26 (1981) 47

[10] D. Bohle, G. Küchler, A. Richter and W. Stefen, Phys. Lett. 148B (1984) 260

[11] A. Richter, Proc. Int. Conf. on Contemporary Topics in Nuclear Structure Physics, ed. R. F. Casten, A. Frank, M. Moshinsky and S. Pittel (World Scientific, Singapore, 1988) p. 127; Nucl. Phys. A522, (1991) 139c

[12] U. Kneissl, Prog. Part. Nucl. Phys. 28 (1992) 331

[13] N. Lo Iudice and F. Palumbo, Phys. Rev. Lett. 41 (1978) 1532

[14] F. Iachello, Phys. Rev. Lett. 53 (1984) 1427

[15] R. R. Hilton, Z. Phys. A316 (1984) 121

[16] I. Hamamoto and S. Åberg, Phys. Lett. B145 (1984) 163

[17] K. Sugawara-Tanabe and A. Arima, Phys. Lett. B206 (1988) 573

[18] A. Faessler, R. Nojarov and F. G. Scholtz, Nucl. Phys. A515 (1990) 237

[19] C. DeCoster and K. Heyde, Nucl. Phys. A524 (1991) 441

[20] D. Zawischa and J. Speth, Z. Phys. A339 (1991) 97

[21] C. Wesselborg, P. von Brentano, K. O. Zell, R. D. Heil, H. H. Pitz, U. E. P. Berg, U. Kneissl, S. Lindenstruth, U. Seemann and R. Stock, Phys. Lett. B207 (1988) 22

[22] C. Rangacharyulu, A. Richter, H. J. Wörtche, W. Ziegler and R. F. Casten, Phys. Rev. C43 (1991) R949

[23] S. J. Freeman, R. Chapman, J. L. Durell, M. A. C. Hotchkis, F. Khazaie, J. C. Lisle, J. N. Mo, A. M. Bruce, R. A. Cunningham, P. V. Drumm, D. D. Warner and J. D. Garrett, Phys. Lett. B222 (1989) 347; Nucl. Phys. A554 (1993) 333

[24] D. Frekers, D. Bohle, A. Richter, R. Abegg, R. E. Azuma, A. Celler, C. Chan, T. E. Drake, K. P. Jackson, J. D. King, C. A. Miller, R. Schubank, J. Watson and S. Yen, Phys. Lett. B218 (1989) 439

[25] J. Margraf, private communication, 1993

[26] C. Wesselborg, dissertation, University of Cologne, 1988

[27] P. O. Lipas, P. von Brentano and A. Gelberg, Rep. Prog. Phys. 53 (1990) 1355

[28] J. Margraf, R. D. Heil, U. Kneissl, U. Maier, H. H. Pitz, H. Friedrichs, S. Lindenstruth, B. Schlitt, C. Wesselborg, P. von Brentano, R.-D. Herzberg and A. Zilges, Phys. Rev. C47 (1993) 1474

NUCLEAR AND CLASSICAL CHAOS

V.E.Bunakov
Petersburg Nuclear Physics Institute
188350, Gatchina, Russia

Abstract: A new conception is suggested: instead of the blind search for quantum "reflections" of classical chaos to look for a *purely quantum* criterion of chaoticity, which transfers in the classical limit into the standard classical criteria of Lyapunov exponent (λ) or the stability parameter χ of the monodromy matrix. This criterion should be the same irrespective of the number of degrees of freedom in the system. Analysis of our experience in compound-nucleus physics plus the use of Heller's Gaussian wave-packets allows to prove that all these conditions are satisfied by the well-known parameters of nuclear strength function - its spreading width $\Gamma_s/\hbar$ and the ratio of Γ_s to single-particle level spacing D_0. It is also demonstrated that the generic source of chaoticity both in quantum and classical mechanics is the lack of symmetries for the Hamiltonian of the system.

I. Introduction

The problems of regularity and chaos were attracting growing interest of the physical community in recent decade, because it realized at last that chaotic behaviour is not a specific property of a complicated system with many degrees of freedom, when we are unable or unwilling to follow the motion in details. To our amazement, it turned out that very simple systems, like two-dimensional classical billiards, might behave in a chaotic way. Contrary to our previous notions of "statistical" chaos, this behaviour was named "deterministic" or "dynamical" chaos. Moreover, now we realize that a typical system in classical mechanics is chaotic rather than regular. Intensive investigations in classical mechanics demonstrate that a generic feature of a chaotic system is its nonintegrabilty, i.e. lack of constants of motion associated with specific symmetries of the system. The main criterion of chaoticity is the exponential instability of the trajectory to small variations of the initial conditions: the distance between two nearby trajectories in a chaotic system grows with time as $\exp(\lambda t)$. The Lyapunov exponent λ in this expression serves a numerical measure of chaoticity (it is also closely connected with mixing and K-entropy). A very popular way to see whether the classical motion is regular or chaotic is to map its phase portrait (Poincare surfaces of section). The existence of constants of motion for a regular system creates the invariant tori in phase space, which in turn produce smooth curves on Poincare surface. If the system is chaotic, the invariant tori become smeared out and disappear, thus building up a random collection of points on a phase portrait.

However, this understanding of dynamical chaos, based on a century of investigations in mathematics and mechanics refers only to classical macroscopic systems. The problem of chaoticity in quantum mechanics, especially in the case of discrete spectrum, is still unresolved. Since the notion of a phase space trajectory looses its meaning, so does the notion of instability to the initial conditions and of Lyapunov exponent. The bound-state quantum dynamics is also characterized by quasiperiodicity of recurrences after time lapse which is roughly inversely proportional to a typical level spacing. All these facts cause the doubts of whether "dynamical" chaos can be exhibited by quantum systems at all. Therefore the majority of specialists share the opinion of M.Berry [1] that "the inaccurate phrase 'quantum chaos' is simply shorthand, denoting quantum phenomena characteristic of classically chaotic systems, quantal 'reflections' or 'parallels' of chaos". This opinion precisely characterizes the main direction in present investigations of quantum chaos: we start with classically chaotic system and then study more or less blindly the properties of its quantum analogue, hoping to find possible traces of classical chaos in quantum mechanics. The main drawback in such an approach is that its only sound foundation lies in the classical definition of chaos. Since quantum mechanics is a general approach, which involves the classical one only as its particular limit, it is impossible in principle to find a definition of quantum chaos in a consistent way, starting with the classical limit. Therefore the majority of systematic studies on these lines do not go further than quasiclassical approximations: while discussing quantum systems, we still stick to their phase portraits as main criteria of their chaoticity, and there is a popular opinion that chaotic regime of motion might exist only as long as the quasiclassical conditions are satisfied.

A decisive step, indicating that there are purely quantum characteristics of chaos, was done by Bohigas et al [2, 3] who demonstrated that quantum analogues of classically chaotic systems have energy spectra with statistical properties described by Gaussian orthogonal ensembles (GOE) of random matrices. These features of the spectra were first encountered in the theoretical analysis of neutron resonances (see below). However the universality of this characteristics is still open to doubts (see par. 16.7 of ref.[4]).

To our opinion, in a consistent approach to the problem of quantum chaos one should start from quantum mechanics, i.e. look for a purely quantum definition and criterion of chaoticity. This criterion should satisfy the following conditions: (A) After performing the (well defined) transition from quantum mechanica to its classical limit this criterion should coincide with the classical criterion of chaoticity, namely with Lyapunov exponent λ and other quantities, connected to λ. (B) Since the notion of Lyapunov stability in classical mechanics does not depend on the number of degrees of freedom in the system, there is a good chance to believe that quantum criterion of chaoticity should not be different for "statistical" and "dynamical" chaos.

II. Compound-Nucleus Experience

At the first glance such a trivial suggestion still opens infinite number of ways in guessing the desired quantum criterion. However condition (B) immediately narrows the choice, if we use the vast experience, accumulated during last 4-5 decades in nuclear physics, especially in the theory of compound-nucleus states and neutron resonances. It was in nuclear physics that we first faced experimentally a purely quantum chaotic system of compound nucleus and had to develop theoretical ways of its investigation. The conception of chaotic compound nucleus which does not 'remember' the way of its formation (or "black absorber" in scattering) was introduced by Niels Bohr and Weisscopf already in late 30-ies. A more refined mathematical technique of nuclear Hamiltonian random matrices was developed in 50-ies. This allowed to reproduce the experimentally observed statistical properties of neutron resonances–Wigner distribution law for resonance spacing, Porter-Thomas law for neutron width distribution and corresponding laws for the distribution of γ-widths. The main physical idea underlying these approaches was that nucleon-nucleon interactions are so complicated (we shall try to clarify this somewhat vague definition below) and strong that the nuclear Hamiltonian matrix consists of random numbers, distributed according to the Gaussian law with zero mean. This assumption immediately led to Wigner repulsion of neighbouring eigenstates. The corresponding eigenvectors are then linear superpositions of a very large number N of components with random coefficients c_i subjected only to normalization condition. Since neutron and γ-widths are proportional to square moduli of those coefficients, we get the corresponding distribution laws for them in agreement with experiments. In short words, that was a purely stochastic approach based on the assumption of "statistical" chaos in nuclei, arising *from nucleon-nucleon interactions* that strongly couple the single-particle motion to many degrees of freedom in the target system.

However a bit later we realized that Pauli principle reduces the strength of nucleon-nucleon interaction considerably, thus making the nucleus rather semi-transparent for neutrons than black. This gave rise to the optical model and to better understanding of neutron strength-function phenomenon. It turned out that neutron strength function $S_n(E_i)$, which is defined as an average probability $|c_s^i(E_i)|^2$ to find single-particle component ϕ_s in the wave-function ψ_i of compound-nucleus state, weighted by the compound-state density D^{-1}, behaves in a Lorenzian way (see e.g. [5]):

$$S(E_i) \sim \frac{|c_s^i|^2}{D} \approx \frac{1}{2\pi} \frac{\Gamma_s}{(E_i - E_s)^2 + \Gamma_s^2/4} \tag{1}$$

Here E_s is a position of the single-particle state ϕ_s, i.e. the eigenvalue of the 'unperturbed' shell-model Hamiltonian H_0:

$$H_0 \phi_s = E_s \phi_s \tag{2}$$

The spreading width Γ_s characterizes the coupling of this single-particle state to other degrees of freedom involved in the compound-nucleus excitation (3 quasiparticles, quasiparticle-phonon, etc.). The fact of major importance for nuclear physics is that Γ_s is smaller than the characteristic spacing D_0 of single-particle states in eq.(2):

$$\neq_s = \frac{\Gamma_s}{D_0} < 1 \tag{3}$$

It is the smallness of $\neq$ which makes the nucleus semi-transparent for an incident nucleon. It also shows that there are still observable traces of single-particle *regular* motion in the seemingly chaotic system of compound-nucleus. Indeed, suppose that at time $t = 0$ we created a wave-packet ϕ_s in our compound nucleus:

$$\phi_s(t = 0) = \sum_i c_s^i \psi_i(t = 0) \tag{4}$$

If we wish to define the probability amplitude $A(t)$ for this packet to survive after time t, then:

$$\begin{aligned} A(t) &= (\phi_s(0)|\phi_s(t)) = \sum_i |c_s^i(E_i)|^2 \exp(-\frac{iE_i t}{h}) \\ &\approx \int \frac{dE}{2\pi D} \frac{\Gamma_s}{(E - E_s)^2 + \Gamma_s^2/4} \exp(-\frac{iEt}{h}) = \exp(-\frac{\Gamma_s}{2h}t - i\frac{E_s t}{h}) \end{aligned} \tag{5}$$

while the corresponding probability is:

$$P(t) = \exp(-\frac{\Gamma_s}{h}t) \tag{6}$$

Thus Γ_s/h is the damping rate for the single-particle mode of motion in compound nucleus. Now, the single-particle Hamiltonian is very close to harmonic oscillator. Then $D_0 = h\omega_0$, where $\omega_0 = \frac{2\pi}{T}$ is the oscillator frequency and T is the corresponding period. Therefore (3) means that after one period of oscillation our wave-packet ϕ_s will be damped only slightly.

There is still another meaning of eq. (3) which is usually not clearly understood – only its validity allows us to do various calculations by diagonalizing the nuclear Hamiltonian H in the shell-model basis of H_0. Indeed, one can expand the eigenfunctions ψ_i of H using *any* complete set of basic states, but the number of terms N in this expansion should in general be infinite, which makes the problem of H numerical diagonalization impossible in principle. Practically, we always need to cut off the series for ψ_i (the rank of the Hamiltonian matrix) at some finite number N hoping for some kind of convergence. Looking at the expansion coefficients in (1) we see that only the smallness of $\neq$ really guarantees us this convergence at $N \sim \Gamma_s/D$ (to be more exact, it allows to work with strap-diagonal Hamiltonian matrices). We emphasize this fact because the use of matrix diagonalization instead of perturbation theory often creates the impression that there is no need for a small parameter in the theory. The above arguments show that this is not true and that $\neq$ is the basic (and perhaps the only) small parameter in nuclear theory, which allows us to do various shell-model calculations, placing the independent shell-model basis in a 'privileged' position with respect to any other complete basic sets.

Suppose that Nature would make $\neq \gg 1$ in nucleus. Then the independent shell-model basis of ϕ_s would loose its "privileges" with respect to all the other (infinite) possible choices of basic states. We will not be able to find any traces of single-particle motion in compound-nucleus states and will be forced to return back to the original idea of the chaotic "black" nucleus.

Taking this into account, we can see better the physics behind the technique of GOE matrices which were first used to describe the statistical properties of neutron resonances. Formally, those ensembles can be obtained (see [6, 7]) on demanding that the distribution of matrix elements should be invariant with respect to arbitrary unitary transformation of basis states, in other words, they should remain the same irrespective of our choice of the basis. This statement means that there is no way to define a 'privileged' basis like a shell-model one, i.e. whatever basis we shall choose, the quantity $\neq$ for it would always be much larger than 1. In this connection one should also point that the value of $\neq$ for a system with Hamiltonian H obviously depends on the choice of the "regular" Hamiltonian H_0. Thus the system with H might show considerable stability (small $\neq$) with respect to eigenstates of one regular H_0 and complete chaoticity (large $\neq$) with respect to other choices of H_0. Moreover, the value of $\neq$ might vary for different eigenstates of the same H_0. For instance, neutron resonances show stability with respect to single-particle modes, while hot discussion still goes on (see e.g. [8]) about the "non-statistical" effects observed for other "regular" components of compound nucleus wave functions. Another well-known example of marked "non-statistical" structure in the wave functions of highly-excited nuclear states is the strength function of γ-absorption which demonstrates a Lorenzian peak of giant dipole vibration mode in nucleus (the corresponding $\neq$ lies in the range 0.3–0.4).

III. From Order to Chaos in Quantum System

Let us sum up our experience with regularity and "statistical" chaoticity in compound nucleus in order to generalize it.

Regular (integrable) quantum systems likewise the integrable classical ones are characterized by high degree of symmetry, i.e. the number of constants of motion caused by the symmetry of the Hamiltonian (the number of good quantum numbers) equals (or exceeds) the number of degrees of freedom. In our nuclear case an example of such a system is the single-particle one (or A noninteracting particles in mean field) governed by the Hamiltonian H_0. This high symmetry also causes a high degree of degeneracy of its eigenstates. When we switch on the nucleon-nucleon interactions, which in principle have no symmetry with respect to H_0 variables, we remove those degeneracies and destroy the majority of good quantum numbers. The system becomes nonintegrable, its only constants of motion (quantum numbers) being its energy E, spin J and parity. This is already a chaotic system. The natural way to study the properties of this system is to diagonalize its Hamiltonian matrix using the basis of the regular Hamiltonian H_0 and investigate the "fragmentation" of regular states ϕ among the eigenstates ψ_i of H or, in other words, the strength functions for regular states ϕ. If the strength of symmetry-breaking two-body interactions is sufficiently small, this leads to small values of the corresponding spreading widths, since Γ_s can be expressed (see e.g. [5]) in terms of average squares of matrix elements v of this interaction and average level spacing D:

$$\Gamma_s = 2\pi \frac{\overline{v^2}}{D} \tag{7}$$

Therefore the traces of regular states ϕ_s in the strength function of such a system are very strong ($\neq \ll 1$). This intermediate situation seems to be a *quantum analogue* of ***soft chaos*** (see e.g. [4]). With increasing strength of two-body interactions those traces of regular states gradually dissolve into the background of the strength function and for $\neq_s \gg 1$ the regular basis of H_0 completely loses its "privileged" position. This situation, which we used to call "black nucleus" is the quantum equivalent of *hard chaos*.

From this analysis we see that a natural criterion of quantum chaoticity is given by a parameter $\neq$. Naturally, with increasing strength of two-body interactions destroying the symmetry of H_0, we can also trace the evolution of the energy spectrum statistics from Poissonian to that of GOE–this evolution, apart from removing the degeneracies of H_0, was traced several times (see e.g. [9, 10]). This would lead us to the above quantum chaoticity criterion of Bohigas et al. However, our experience with neutron resonances shows that $\neq$ is a much more sensitive measure of chaoticity than level statistics–while the experimental spectra of compound nucleus states perfectly follow GOE laws (see [11]), the experimental neutron strength function still shows strong peaking characterized by $\neq = 0.3 - 0.4$. Moreover, it is hardly possible to find any simple connection between the statistical properties of spectra in quantum system and the Lyapunov exponent in its classical analogue (see our condition (A) in Introduction).

IV. Classical Limit of the Quantum Chaoticity Criteria

It remains now to show that this connection with classical stability exponent really exists for the above parameters $\neq$ and Γ_s.

The major part of this task was already performed by Heller (see e.g. [12, 13] and references therein), who used the Gaussian wave packets for the analysis of the so called "scars" in the wave functions of classically chaotic systems. The use of the Gaussian wave packets $|G\rangle$ (often called the coherent states) allows to localize a quantum system in a small volume of phase space at time $t = 0$ and then to follow its evolution in time. The packet is launched along the periodic orbit (those orbits exist in any chaotic system although with zero measure compared to typical ones). Heller demonstrated that such a packet returns to the initial position after the period $T = 2\pi/\omega$ in such a way that its center still lies on the periodic orbit while its spread in the quasiclassical limit is defined by the classical dynamics of trajectories in the vicinity of this orbit, i.e. by the so called monodromy (or stability) matrix M. It is exactly via this matrix (or its eigenvalues) that the Lyapunov exponent was introduced in classical mechanics. Heller analyzed the overlap of his Gaussian packets:

$$A(t) = \langle G(t = 0)|G(t)\rangle \tag{8}$$

and proved that $A(t)$ in the quasiclassical limit consists of periodic peaks with period T corresponding to wave-packet recurrences, but the amplitude of these peaks is modulated by the factor $\exp\left(-\frac{\lambda T}{2}\right)$, where λ is the classical Lyapunov exponent. The meaning is obvious – λ characterizes the spread of the packet over the nearby unstable orbits. The decrease of probability $P(t) = |A(t)|^2$ for two successive overlaps is

$$e^{-\lambda T} = e^{-\chi} \tag{9}$$

where $\chi = \lambda T$ is called the stability parameter (or geometric exponent) in classical mechanics.

Following Heller, we can add up our regular states ϕ_n of eqs.(2),(4) in order to construct a Gaussian wave packet:

$$|G\rangle = \sum_n A_n \phi_n \tag{10}$$

Consider for simplicity that the potential in H_0 is harmonic oscillator. Then:

$$A_n = \frac{\xi_0^n e^{-\xi_0^2/4}}{2^n n!} \tag{11}$$

where

$$\xi_0 = a\sqrt{\frac{m\omega}{\hbar}}$$

and a is the initial displacement of the packet. Inserting (11),(10) into (8) and using (5) we get:

$$P_G(t) = e^{\xi_0(\cos\omega t - 1)} \cdot e^{-\Gamma t/\hbar} \tag{12}$$

The first factor here reflects the periodic recurrences of the packet, while the second gives the modulation due to the instability of the periodic trajectory. Comparing this with Heller's results, we see that in the classical limit:

$$\frac{\Gamma}{\hbar} = \lambda \tag{13}$$

and

$$\frac{\Gamma}{D_0} = \neq = 2\pi\chi \tag{14}$$

Thus we proved that purely quantum criteria of chaoticity $\Gamma_s/\hbar$ and $\neq$ satisfy our condition (A) of Introduction.

V. Compound-Nucleus Complexity - Degrees of Freedom or Symmetry Breaking?

Originally it seemed to nuclear physicists that success of "statistical approach" to neutron resonances was caused by many degrees of freedom involved in compound nucleus motion and leading to the complexity of compound nucleus states. However a closer analysis of the problem shows that this is not exactly so.

First of all, the actual number of quasiparticles n_q participating in neutron resonance excitation is not very large. One can estimate it [5] as:

$$n_q \simeq \left(\frac{6}{\pi^2} g_0 E\right)^{1/2} \ln 4 \simeq \left(\frac{3AE}{2E_F}\right)^{1/2} \tag{15}$$

where E is the excitation energy of a nucleus A, g_0 is the single-particle level density and E_F is the Fermi energy. For neutron resonances $E \approx 8Mev$ and therefore $n_q \sim (0.3A)^{1/2}$, i.e. $n_q \approx 5-6$ for $A \approx 100$.

The real complexity of compound resonances comes from the fact that nucleon-nucleon interactions V remove all the degeneracies of the noninteracting system, thus increasing the average level density roughly by a degeneracy factor

$$N_d \sim \exp(2n_q) \tag{16}$$

This factor arises (see [5]) from counting all the combinatorial possibilities to obtain the same total excitation energy E by "reshuffling" the n_q quasiparticles in the unoccupied single-particle levels.

The number N of "regular" components in the compound-resonance wave *function*, which defines the complexity of our system, is:

$$N \approx \frac{\Gamma_s}{D} = \neq N_d \sim \frac{\overline{v^2}}{D^2} \tag{17}$$

Thus we come to a general conclusion: The major difference between regular and chaotic quantum systems is defined by their symmetry properties (N) rather than by the number of their degrees of freedom (n_q). Each regular system in quantum as well as in classical mechanics is so symmetric, that the number of corresponding constants of motion in involution (or corresponding operators which commute with each other and with the Hamiltonian H_0) is not smaller than the number of its degrees of freedom. In the majority of cases the symmetry is even higher, which leads to a high degree of degeneracy in the system.

Quantum chaoticity appears, when we add to such a regular Hamiltonian H_0 additional perturbation V, which *destroys the original symmetries* of H_0 (and removes its degeneracies). The degree of chaoticity might be characterized by the complexity N of the eigenfunctions of the Hamiltonian $H = H_0 + V$ (see eq(17)). It is defined by the interaction strength $V_0 \simeq \sqrt{\overline{v^2}}$ (see eq.(7)) and by the degeneracy factor N_d. In the simplest case of $N_d = 1$ this complexity is given just by parameter $\neq = \Gamma_s/D_0$, which transforms in the classical limit into the stability parameter χ of the monodromy matrix, while Γ_s/h becomes the Lyapunov exponent of the classical mechanics. The case $\neq < 1$ corresponds to soft chaos, when we can still see traces of regular Hamiltonian H_0 in the eigenfunctions of H as peaks in the strength function (the classical analogue of this are traces of invariant tori). The case $\neq > 1$ corresponds to hard chaos when all these traces are completely smeared out– GOE for Hamiltonian matrix in quantum mechanics, or completely destroyed invariant tori in classical one.

Since the number of degrees of freedom was not essential in the above considerations, those criteria are valid both for "statistical" and "dynamical" chaos. In quantum mechanics this is even more evident because there we have a perfectly natural equivalent of numerical integration for the equations of motion in a chaotic system, namely the diagonalization of the Hamiltonian matrix on a suitable basis of H_0 eigenfunctions, which is applied *irrespective* of the number of degrees of freedom in the system.

VI. Other Possibilities

We have already mentioned the level statistics as possible criterion of quantum chaoticity and stressed that this was the first indication that chaos can be defined in a purely quantum system. We also mentioned, however, that this criterion in neutron resonances turns out to be less sensitive to the traces of regularity in the system than the strength function one. Its other drawback is that, contrary to $\neq$, it has no classical analogue. Therefore its connection with the classical stability parameters can be traced only via the above approach of strength functions.

Another criterion, suggested in [14] was the stability of the overlap of two coherent wave packets

$$| < G(q,t)|G(q + \delta q, t > |^2 \tag{18}$$

to the small variations of a "control" parameter q in the Hamiltonian of the system. In case of chaotic system this overlap shows a rapid decay with time even for small δq, while for regular system it shows regular oscillations with time. A claim was even made (see [10]) that the time decay of (18) is governed by $\exp(-\frac{\Gamma_s t}{\hbar})$. On this grounds the authors of [10] even called $\Gamma_s/\hbar$ a quantum analogue of classical Lyapunov exponent. However, the proof of these claims in [10] was rather obscure. Moreover, it was shown numerically in [14] that the actual value of λ in their case was *much larger* than the rate of decay for overlap (18). We can add to this, that while the exponential decay $\exp(-\lambda t)$ of eq.(6) is a direct consequence of the strength function peaking (5) even for *equidistant* level spacing D, the decay in time of (18) results only from *randomness* in eigenvalue shifts, produced by the Hamiltonian variation δq. Therefore this latter decay is closely connected to the complexity of the eigenfunctions, but its rate is governed by δq and *becomes exactly zero* for $\delta q \to 0$. However, in spite of all these inconsistencies, we see that the idea of associating Γ_s with Lyapunov exponent, mentioned in [10], is basically sound.

VII. Open Problems and Perspectives

In the above analysis of the complexity of compound-nucleus state, we have seen that it is defined rather by $N = \neq N_d$ than simply by $\neq$. It is quite tempting therefore to suggest the quantity N as a more general candidate for the quantum chaoticity criterion. Then, however, a question arises of the meaning of purely quantum degeneracy factor N_d in the classical limit.

Another problem is that Γ_s and $\neq$ obviously depend on the choice of the regular H_0 whose eigenfunctions are used as a basis in diagonalizing the H matrix. This problem seems to be of the same origin as the problem of proper choice of canonical transformation in classical regular systems - there exist no well-defined rules for this procedure and much depends on physical intuition and experience. We also mentioned that quantal chaoticity criterion might vary even for different eigenfunctions ϕ_s of the same regular Hamiltonian. Analogous situation occurs in classically chaotic systems, where we have different degrees of smearing of invariant tori in different regions of the phase space (different islands of regularity and regions of ergodicity on a phase portrait). Therefore the above difficulties are recognized and accepted in classical chaos, and one can not reject our general idea on this grounds. We should just accept that speaking about chaoticity one needs to specify with respect to which symmetry it is defined. However, one should point that in principle the quantal chaoticity criterions based on level statistics or on eq.(18) have advantages, since they are independent of the choice of H_0 basis.

If the suggested conception of quantum chaos and its higher rank with respect to classical chaos is accepted by the physical community, this opens numerous possibilities of general studies of chaos with the aid of huge experience, accumulated in nuclear physics during half a century of its development - compound nucleus is a purely quantal chaotic system created by nature. Presently I can only briefly mention some of these possibilities. The trace formula of Selberg-Gutzwiller, which is up to now considered as the only bridge between classical and quantal regimes of chaos, relies heavily on "semiclassical" Van Vleck propagators, characterized by Gutzwiller [4] as a "*mixture* of classical and quantal ideas". It might be interesting instead to start deriving this formula with purely quantum Green's functions whose properties are well studied in nuclear physics. In going to classical limit we might face again the above mentioned interesting problem of classical reflections of quantal degeneracies. A close-lying problem in going from quantal to classical regimes might be that of classical "reflections" of symmetry with respect to discrete transformations.

Up to now we were considering for simplicity in our paper only the bound state systems, ignoring their decay widths via different physical channels (particles or γ-emission). It seems to be a natural next step to generalize the above results by taking into account those (purely quantal) decay widths.

VIII. Conclusion

Thus a systematic analysis of ideas, underlying the statistical approach in nuclear physics, allows to suggest a purely quantum definition of regular and chaotic systems, which is based on the symmetry properties of their respective Hamiltonians. A regular system is highly symmetric, so that the number of its constants of motion (good quantum numbers) equals or exceeds the number of its degrees of freedom. These symmetries are destroyed in the chaotic system, so that its eigenstates can be characterized only by energy, total momentum J and parity. Among several possible numerical criteria of quantum chaoticity we prefer to choose the parameters of strength function $\Gamma_s/\hbar$ and $\neq = \Gamma/D_0$ which define how strong are the traces of regular Hamiltonian H_0 eigenstates in the expansion of eigenstates *of our chaotic system*. The case $\neq < 1$ corresponds to *soft* chaos when these traces of regularity are still considerable. The case $\neq \gg 1$ corresponds *to hard chaos*.

We have shown with the use of the Gaussian wave packets that those purely quantum criteria transform in the classical limit into the classical stability criteria: $\Gamma/\hbar \Rightarrow \lambda$ (Lyapunov exponent) and $\neq \Rightarrow 2\pi\chi$ (stability parameter of the monodromy matrix, or geometrical exponent). We have also demonstrated that, like in classical mechanics, those criteria are valid irrespective of the number of degrees of freedom, i.e. both for "statistical" and "dynamical" chaos. We stress that the complexity of the eigenstates N for the chaotic system is defined mainly by the properties of symmetry-breaking interactions in it (see Eq.(17)).

We have not mentioned the well-known (and already trivial) fact of recurrences in quantum system after time t_{rec}, thus simplifying our estimate (5). In order to take this fact into account, we should not substitute the sum in (5) by the integral. Then the exponential decay of (5) will last only until the value of $P(t)$ reaches $1/N \sim D/\Gamma$, and starts irregular oscillations around it (see e.g. [10]). It was also demonstrated in ref.[10] that for chaotic system $t_{rec}\lambda \gg 1$.

References

[1] M.Berry, in "Quantum Chaos. Adriatico Research Conf., Trieste,1990", H.A.Cerdeira, R.Ramaswamy, M.Gutzwiller, G.Casati (editors), World Scientific, 1991, p.VII

[2] O.Bohigas, M.Giannoni, C.Schmit, Phys.Rev.Lett. **52**(1984)1

[3] O.Bohigas, M.Giannoni, C.Schmit, J.Physique Lett. **45**(1984)L1015

[4] M.Gutzwiller, Chaos in Classical and Quantum Mechanics, Springer Verlag,1990

[5] O.Bohr, B.Mottelson, Nuclear Structure, v.I, Benjamin, N-Y, 1969

[6] C.Porter, N.Rosenzweig, Ann. Acad. Sci. Finland. **A6**(1960)N44

[7] M.Mehta, Random Matrices, N-Y, 1967

[8] V.G.Soloviev, Nucl.Phys. **A554**(1993)77

[9] M.Zirnbauer, J.Verbaarschot and H.Weidenmueller, Nucl.Phys. **A411**(1983)161

[10] B.Milek, W.Noerenberg, Nucl.Phys. **A545**(1992)185c

[11] O.Bohigas, R.Haq and A.Pandey, in "Nuclear Data in Science and Technology", K.Boeckhoff(ed.), Dordrecht, 1983, p.809

[12] E.Heller, Phys.Rev. **A35**(1987)1360

[13] E.Heller, in "Chaos and Quantum Physics, Les Houches, Ses.LII, 1989", Elsevier, 1991, p.548

[14] A.Peres, in "Quantum Chaos. Adriatico Research Conf., Trieste, 1990", H.A.Cerdeira, R.Ramaswamy, M.Gutzwiller, G.Casati (editors), World Scientific, 1991, p.48

Study of M1 Excitations in Deformed Even-Even and Odd-A Rare Earth Nuclei [1]

Heinz-Hermann Pitz

Institut für Strahlenphysik
Universität Stuttgart
D - 70569 Stuttgart, Germany

ABSTRACT

Systematic Nuclear Resonance Fluorescence (NRF) experiments have been performed throughout the last years to investigate dipole excitations below 4 MeV. Using high intensity bremsstrahlung as photon source enabled the measurement of detailed strength distributions. With the sectored Compton polarimeter unambiguous parity assignments for the excited states were possible. This paper reports on the results for the M1 excitations of the socalled Scissors mode in spherical and deformed Rare Earth nuclei. The deformation dependence and the saturation near mid shell are discussed. Data for the odd-A nuclei ^{163,161}Dy are presented, where for the first time a concentration of dipole strength in the energy region of 3 MeV was observed. A comparison with theoretical calculations supports the interpretation that here the Scissors mode has been observed in odd-A nuclei.

1. INTRODUCTION AND MOTIVATION

Low-lying collective excitations of heavy deformed nuclei, like rotations and vibrations are known since a long time. The prediction of a new class of orbital M1 excitations[1] and the discovery of the socalled Scissors Mode in the deformed nucleus ^{156}Gd in inelastic electron scattering[2] by the Darmstadt Group of A.Richter in 1983 caused a wealth of theoretical and experimental work (see e.g. refs. [3,4,5,6]). Today these M1 excitations are a phenomenon which has been observed in all regions of deformed nuclei from the fp-shell[3,4,7] to the actinides[8,9].

The Nuclear Resonance Fluorescence (NRF) method is a technique well suited for the study of these excitations. Because of the small momentum transfer of real photons the method is highly selective to dipole excitations and by measuring polarization observables an unambiguous parity assignment can be achieved. This is crucial for the interpretation of the data, because in this energy region between 2 and 4 MeV excitation energy also enhanced E1 excitations are expected (for a discussion of the E1 excitations see the contribution of U.Kneissl). This report will summarize the NRF measurements performed at the bremsstrahlung facility of the Stuttgart Dynamitron accelerator on deformed Rare Earth nuclei, both even-even and odd-A, to investigate the systematics of these excitations.

[1] *Supported by the Deutsche Forschungsgemeinschaft (Kn 154-21 and Br 799-33)*

2. NUCLEAR RESONANCE FLUORESCENCE TECHNIQUE

Nuclear Resonance Fluorescence is the resonant absorption of real photons exciting a nuclear level and its decay by reemission of a photon. Due to the small momentum of real photons only dipole and with much smaller probability E2 transitions are induced. This spin selectivity enables to investigate dipole excitations in energy regions, where the level density is already very high. The sensitivity of the excitation to the ground state decay width enables the determination of the transition strength. The use of a continuous photon source, such as bremsstrahlung, allows to measure simultaneously in detail the strength distribution of dipole excitations in the energy interval covered by the photon source.

The cross section integrated over one level I_s for the scattering of a photon off a nuclear level into a final state f is given by:

$$I_s = \frac{2J+1}{2J_0+1} \cdot (\pi\lambda)^2 \cdot \Gamma_0 \frac{\Gamma_f}{\Gamma} \tag{1}$$

J and J_0 are the spins of the excited and ground state, respectively, λ is the reduced wavelength of the incident photon. Γ_0, Γ_f, and Γ are the decay widths to the ground state, the final level and the total decay width. The peak areas measured in the experiment are proportional to the integrated scattering cross section for the level:

$$A = N_{at} \cdot N_\gamma \cdot \varepsilon \cdot d\Omega \cdot \frac{W(\theta)}{4\pi} \cdot I_s \tag{2}$$

with N_{at} the number of scattering nuclei, N_γ the number of photons at resonance energy, ε, $d\Omega$ the efficiency and solid angle of the detector and W the angular distribution.

In well deformed nuclei the decay branching ratio for the excited state contains information about the K quantum number, that is the projection of the angular momentum on the symmetry axis of the deformed nucleus. It is defined as the ratio of the reduced transition probabilities to the first excited state of the rotational band and the ground state. For even-even nuclei it is:

$$R_{exp} = \frac{B(\pi 1 \to 2^+)}{B(\pi 1 \to 0^+)} = \frac{\Gamma_1/E_{\gamma 1}^3}{\Gamma_0/E_{\gamma 0}^3} \tag{3}$$

This ratio is according to the Alaga rules[11] 0.5 for the excitation of a K=1 level and 2.0 for a K=0 state. The K value of the excited state contains information on the parity of the excited state. While in the case of a ΔK=1 excitation both parities are possible, in the case of a ΔK=0 transition from the ground state only 1^- states can be excited.

The spins of the excited states can be extracted in NRF experiments from the angular distribution of the scattered photons. In the case of even-even nuclei, the spin cascades for dipole and quadrupole excitations (spin sequences 0→1,2→0) lead to very different angular distributions. Thus the measurement of the intensity ratio for only two different angles, namely 90° and 127°, is sufficient for an unambiguous spin assignment. In the case of odd-A nuclei the angular distributions are, due to the half-integer spins involved, nearly isotropic. Therefore, it is difficult to extract information about the spin of the excited level and can be achieved in the present set-up only in a few favourable cases.

Parities of excited states can be measured in photon scattering experiments by measuring polarization observables. In the region below 4 MeV excitation energy the favourable technique is the measurement of the linear polarization of the photons scattered by the NRF process. For the excitation of a spin 1 level from the ground state and a decay back to it (spin sequences

0→1→0), the scattered photons detected at 90° with respect to the incident beam are completely linearly polarized. The electrical field vector $\vec{E}$ lies in the NRF scattering plane for M1 and is perpendicular to it for E1 excitations. Thus the measurement of the direction of $\vec{E}$ of the scattered photons e.g. by a Compton polarimeter allows model independent parity assignments.

3. EXPERIMENTAL SET-UP

The NRF measurements reported on have been performed at the bremsstrahlung facility of the Stuttgart Dynamitron accelerator[12]. The set-up is shown schematically in Fig.1. The high current CW electron beam with a maximum energy of 4.3 MeV is bent by 120° and focused on the bremsstrahlung radiator target consisting of a water cooled gold plate thick enough to completely stop the electron beam. The resulting bremsstrahlung beam is formed by a lead collimator with a hole of 10 mm diameter and 98 cm length. The radiation production is well separated from the experimental set-ups by 2 m of concrete, resulting in a low level of background radiation. The photon beam is guided by a vacuum tube to the NRF set-ups. The excellent beam quality and the very high flux of typically 10^9 photons per MeV and second for 3 MeV photons enables to run NRF experiments at two different set-ups simultaneously.

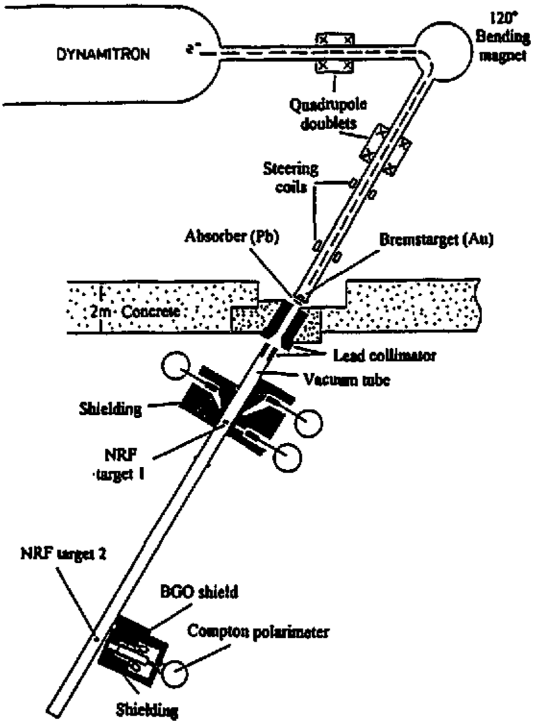

Fig.1: The bremsstrahlung facility at the Stuttgart Dynamitron accelerator. The excellent quality of the well collimated bremsstrahlung beam allows to run two NRF experiments simultaneously. At the first set-up the angular correlation and cross section measurements take place, while at the second set-up the polarization measurements are performed.

The first NRF site consists of three carefully shielded Ge(HP) detectors placed at scattering angles of 90°, 127°, and 150° with respect to the incident beam. At the second site the sectored Ge(HP) Compton polarimeter is installed at slightly backward angles of 97° with respect to the photon beam for background reasons. This detector measures the polarization of the resonantly scattered photons utilizing the Compton effect. The outer electrode of this true coxial germanium crystal is carved into four electrically insulated surfaces, dividing the crystal into four detectors. This enables the measurement of the direction of the Compton scattering in the detector and thus the polarization of the photons. The device is described in detail in ref.[13)].

The sensitivity of the Compton polarimeter is now improved by our new BGO shield consisting of eight optical insulated trapezoidal BGO crystals, each equipped with a photomultiplier. It runs in anticoincidence mode with the Compton polarimeter and gives a considerable reduction of the background. For a radioactive ^{56}Co source the background suppression factor varies from 4 at lower energies to 9 at about 3.5 MeV photon energy. For experiments with bremsstrahlung as photon source the reduction factor is 2 over the entire energy range. The remaining background is due to the unavoidable nonresonant scattering of the incident bremsstrahlung in the target. This is of particular importance for the parity measurements, because in the data evaluation the background enters twice. Therefore, the use of the BGO shield together with the Compton polarimeter considerably increases the sensitivity of our polarization measurements.

For both set-ups the NRF targets consist of pills of isotopically enriched material sandwiched between aluminum disks of the same diameter. Typically 1–2 g of enriched isotopes are needed for set-up 1 and 5 g for the polarization measurements. The nucleus ^{27}Al has three well known excitations[14)] between 2 an 4 MeV, which serve several calibration purposes in these experiments. Due to the half integer spins, the photons from the 2982 keV excitation are emitted nearly isotropically and are nearly unpolarized . They serve as an online calibration for the angular distribution and the polarization. The well known decay widths and decay branching ratios of the levels at 2212, 2982, and 3957 keV are used for the photon flux calibration. The results are in very good agreement with Monte Carlo calculations of the bremsstrahlung shape[15)] and experimental determinations. In addition, the measurement of the NRF cross section relative to the excitations in ^{27}Al eliminates all effects due to changes in beam energy and intensity. The accuracy of the measured cross sections is only limited by the error of the aluminum standard. Therefore, we performed a NRF self absorption experiment on these levels[16)]. The results are in excellent agreement with the literature[14)] and we succeeded in cutting the error for the width of the most important level at 2982 keV to 2.4%.

4. M1 EXCITATIONS IN RARE EARTH NUCLEI

Since the discovery of a strong orbital M1 excitation at an energy of 3.07 MeV in ^{156}Gd in (e,e') experiments[2)], these excitations have been studied systematically in the Rare Earth nuclei by various probes (see ref.[4.,17.)] and references therein). The photon scattering experiments allow, due to the excellent energy resolution of the Ge-detectors, a detailed study of the strength distribution and the fragmentation of the orbital M1 mode. The model independent strength determination and the model independent parity determination using Compton polarimeters have made a valuable contribution to the investigation of these M1 excitations.

4.1. Systematics of M1 Excitations in Even-Even Rare Earth Nuclei

Fig.2 shows an example for the information obtained from photon scattering experiments. The upper part shows the spectrum of scattered photons for the detector at 90° with respect to the bremsstrahlung beam. The peaks marked Al belong to transitions in the photon flux standard

^{27}Al. Peaks marked by an asterisk belong to ground state transitions in ^{164}Dy. They are connected with the peaks of the inelastic transitions to the 2_1^+ level by brackets. The intensity ratio of these two decay modes contains the information on the K quantum number. It can be seen in the second part, where the experimentally observed branching ratio R_{exp} is plotted that the three very strong excitations around 3.1 MeV have a branching ratio R_{exp}=0.5, which means K=1 for the respective levels.

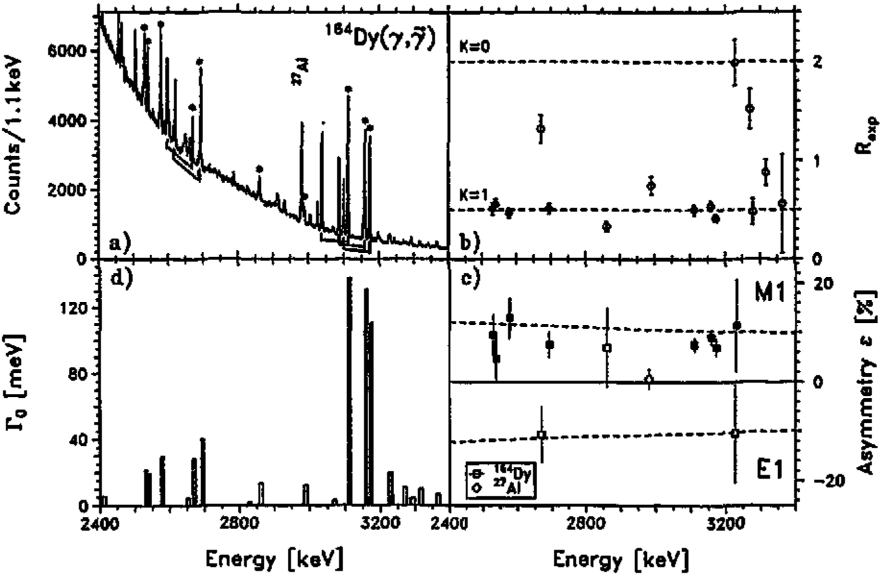

Fig.2: Results of the (γ,γ') experiment on ^{164}Dy.

a) Spectrum of scattered photons detected at 90°. Peaks marked by Al belong to the photon flux standard, peaks marked by an asterisk belong to ground state transitions in ^{164}Dy. They are connected with the respective transition to the 2_1^+ level by brackets.

b) Experimentally observed decay branching ratio for the decay to the first excited state and the ground state. The lines marked with K=0 and K=1 give the values from the Alaga rules[11.)].

c) Azimuthal asymmetry of the scattered photons measured with the Compton polarimeter. The dashed lines give the expectation values for completely linearly polarized photons. Positive asymmetries correspond to M1 transitions, negative asymmetries to E1.

d) Ground state decay widths extracted from the experiment. Full bars belong to M1 transitions, shaded bars to E1 transitions. Open bars indicate that no parity could be extracted for the respective levels.

The third part shows the experimental asymmetry ϵ measured with the Compton polarimeter. Positive values correspond to M1 character of the transition and therefore positive parity of the excited level, negative values to E1 character and negative parity. There are two groups of M1 excitations around 2.5 and 3.1 MeV, the upper group attributed to the Scissors mode. The extracted strength distribution is shown in the lower part of Fig.2. The group of M1 excitations around 2.5 MeV is not included in the systematics of the Scissors mode, because a ^{165}Ho(t,α) experiment[17.)] identified a nearly pure 2qp M1 excitation in this energy region.

Therefore, in the picture for the systematics of M1 strength in the Rare Earth nuclei[18.] the strength in the energy region 2.6–4.0 MeV is summed, leaving out the lower energy group. The data are taken from the systematic studies on the different Nd, Gd, Dy, Er, Yb, and W isotopes[19.,20.,12.,21.,22.,23.,24.,25.] of the Stuttgart-Giessen-Cologne collaboration and the Sm data of the Darmstadt group[26.,27.]. Since parity information is available only in few cases, we have summed up the strength for all states in this energy region with a K quantum number K=1. Thus we cannot exclude systematic errors stemming from the counting of K=1 states with negative parity, but the polarisation measurements show that the assumption of M1 excitations for ΔK=1 is justified. It turns out, that all strong transitions with ΔK=1 have M1 character in this energy region and only in the case of ^{160}Gd[21.] a weak ΔK=1 excitation with E1 character was observed.

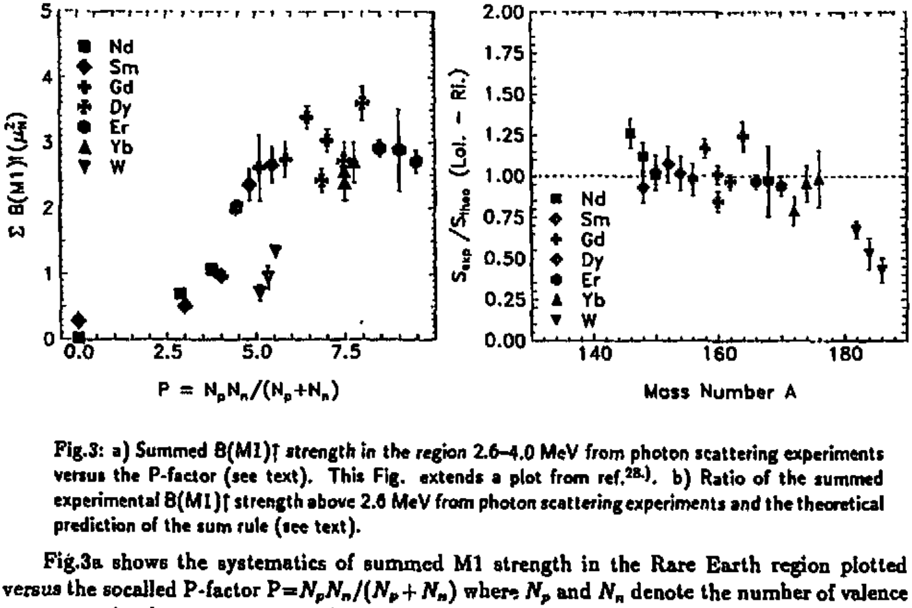

Fig.3: a) Summed B(M1)↑ strength in the region 2.6–4.0 MeV from photon scattering experiments versus the P-factor (see text). This Fig. extends a plot from ref.[28.]. b) Ratio of the summed experimental B(M1)↑ strength above 2.6 MeV from photon scattering experiments and the theoretical prediction of the sum rule (see text).

Fig.3a shows the systematics of summed M1 strength in the Rare Earth region plotted versus the socalled P-factor $P=N_pN_n/(N_p+N_n)$ where N_p and N_n denote the number of valence protons and valence neutrons. This P-factor is proportional to the strength of the proton-neutron interaction. It is obvious that the M1 strength rises with increasing P and reaches a saturation value around mid-shell. The small strength for the W isotopes is partly due to the decrease in P approaching the shell closure and a possible hexadecupole deformation. But another contribution might be caused by experimental reasons, namely strength missed in the experiment. In these nuclei a very pronounced fragmentation was observed, which can cause a considerable number of excitations with strengths below the experimental detection limit and too small experimental values of summed M1 strength.

The saturation value for the B(M1)↑ strength near mid-shell is $\simeq 3\mu_N^2$. The qualitative behaviour of saturation is the same as observed for the systematics of B(E2) values in this mass region[28.] and has also been observed in the other region of strongly deformed nuclei, the Actinides[10.]. The rise of the summed M1 strength from spherical to well deformed nuclear shape has been studied in detail in the Sm[28] and Nd[29] isotopic chains. It turned out that the summed M1 strength scales with the square of the nuclear deformation ("δ^2 law"). This behaviour can be explained by different theoretical approaches[30,31,32,33] and is one of the most exciting findings in the last years.

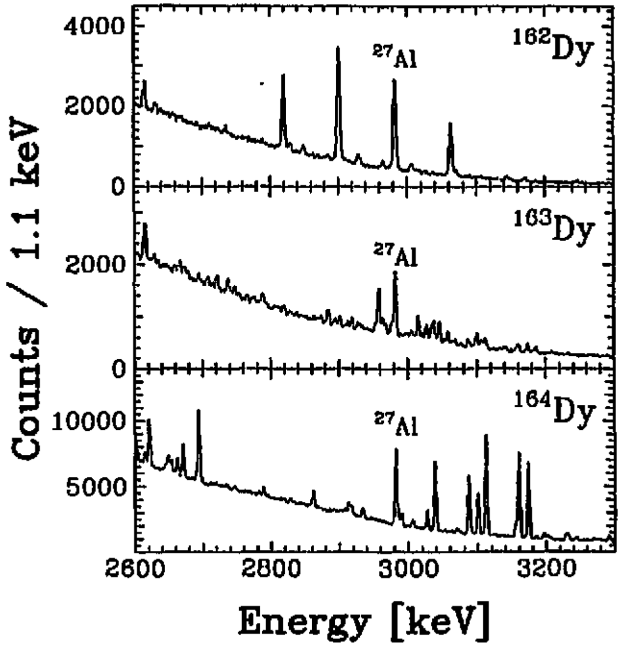

Fig.4: Photon scattering spectra off ^{162,163,164}Dy in the energy region of the Scissors mode.

Recently, LoIudice and Richter[34] derived a simple sum rule for the M1 strength, starting from the sum rule of Lipparini and Stringari[35]. They finally arrived at the following expression for the sum rule of the Scissors mode:

$$B(M1)\uparrow \approx 0.0042\frac{4NZ}{A^2}\cdot \omega_{Sc}\cdot A^{5/3}(g_p-g_n)^2\cdot \delta^2[\mu_N^2] \tag{4}$$

with ω_{Sc} the energy of the Scissors mode, δ the nuclear deformation and the g-factors g_n=0 and g_p=2Z/A. This formula contains no free parameters and predicts the absolute strength for the Scissors mode. Fig.3b shows the success of this sum rule in the Rare Earth region. Plotted is the ratio of experimentally observed summed M1 strength (see Fig.3a) and the prediction by the sum rule versus mass number. There is an excellent agreement with the experimental data, ranging from the hardly deformed Nd and Sm nuclei to the well deformed Gd and Dy isotopes and even the Yb nuclei are well reproduced, where one observes the onset of a strong fragmentation of the Scissors mode. Again only the W data deviate. The exhaustion of the sum rule by the experimentally observed strength points to the fact, that in the photon scattering experiments nearly all orbital M1 excitations in these nuclei have been observed.

4.2. The Scissors Mode in Odd-A Rare Earth Nuclei

Up to now, the studies dealt with the Scissors mode in even-even nuclei. But what happens, if an unpaired nucleon is coupled to the even-even core, as is the case in the odd-A Rare Earth isotopes? This problem has been studied theoretically by Van Isacker and Frank[36,37] in the framework of the IBFM and in the particle-core coupling model by Raduta et al.[38]. The theoretical works predict a fragmentation of the orbital M1 strength due to different couplings of the unpaired nucleon to each of the M1 excitations in the even-even core and due to the mixing with single particle levels.

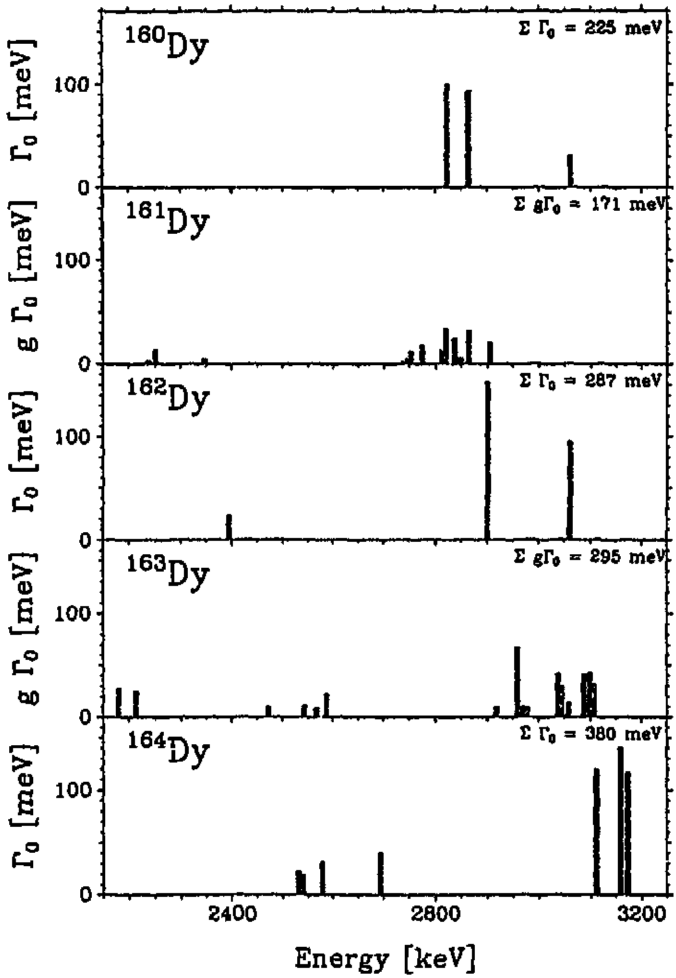

Fig.5: Dipole strength distributions for the $\Delta K=1$ transitions in all five investigated even and odd Dy isotopes. In the case of the odd nuclei because of the unknown spin of the excited state the product of the ground state decay width Γ_0 and the spin factor g is plotted.

A first photon scattering experiment on the proton-odd nucleus ^{165}Ho by the Darmstadt group[39.)] showed no strong excitations in the region around 3 MeV. Theoretically, the orbital M1 strength should be separated more clearly from the single particle excitations in nuclei with odd neutron number. Therefore we measured ^{163}Dy[40.)], which has the additional advantage that in both neighbouring even-even nuclei the strength is concentrated in 2 or 3 very strong excitations. Fig.4 shows the (γ,γ') spectrum for the odd nucleus together with the spectra for the neighbouring even-even nuclei. There is a clear concentration of dipole strength in the region around 3.1 MeV, where the excitations of the Scissors mode are expected. Due to the half integer spins of the levels involved in the odd-A nuclei and the resulting nearly isotropic angular distributions it is in this photon scattering experiment not possible to determine the spin of the excited levels. Therefore, for the odd-A nuclei the product of the ground state decay width Γ_0 times the spin factor $g = (2J+1)/(2J_0+1)$ is given in the strength distribution.

Fig.5 shows the strength distribution for all five investigated Dy isotopes. In the case of the even-even nuclei parities are known for ^{162,164}Dy. One can see that for ^{163}Dy the energetic position as well as the magnitude of summed strength fit quite well in the systematics in the neighbouring even-even nuclei. The comparison with theoretical IBFM calculations[40.)] is given in Tab. 1. Inspection of the second column shows, that for different spins of the excited state different decay branching ratios are expected. If the experimental data are classified according to this scheme, the respective number of states and their summed strengths can be calculated. There is obviously a good agreement between experiment and theory, so that a first observation of the Scissors mode in a deformed odd-A nucleus can be stated.

$J_i \rightarrow J_f$		Decay Branching R_{theo}	$B(M1)\uparrow^{theo}_{ns}$ $[\mu_N^2]$	$B(M1)\uparrow^{exp}_{>2.6MeV}$ $[\mu_N^2]$	States
$5/2_1$	$3/2_{ns}$	0.00	0.41	0.24±0.04	5
$5/2_1$	$5/2_{ns}$	2.20	0.20	0.20±0.07	2
$5/2_1$	$7/2_{ns}$	0.36	0.62	0.47±0.10	3
$5/2_1$	$(J_f)_{ns}$		1.23	0.91±0.21	10

Table 1.: Comparison of the experimental results for M1 excitations in ^{163}Dy with recent IBFM calculations[40.)]. The nonsymmetric Scissors mode states are denote by ns.

This interpretation is supported by the new measurements on ^{161}Dy. These complete the experiments on the Dy isotopic chain. The strength in ^{161}Dy is more fragmented and the centroid is shifted to lower energies. But both, strength and energy, fit well into the systematics. This is true not only for the excitations at 3 MeV but also for the group around 2.5 MeV.

The situation is dramatically different for the third odd-n nucleus we investigated in (γ,γ') experiments, namely ^{157}Gd. Here the preliminary data show no concentration of dipole strength, but an extreme fragmentation. We observe about 40 excitations spread equally over the energy range 2.1–3.3 MeV, which all have a typical ground state decay width of 10 meV. This is totally different from the behaviour in the odd Dy isotopes, where we observed a concentration of strength in the region of the Scissors mode. Up to now, the reason for this is not clear. Theoretical calculations and more experimental data are needed to gain a deeper insight in the structure of these excitations.

5. ACKNOWLEDGEMENTS

The experiments have been performed in a long standing, pleasant collaboration with the group of Prof. von Brentano (Köln) and the NRF group from Giessen. It is a pleasure to thank Prof. Kneissl and all colleagues for the very fruitful and stimulating collaboration. Special thanks are due to my colleagues R.-D. Heil, J. Margraf, H. Maser (Stuttgart), A. Zilges, R.-D. Herzberg, N. Pietralla (Köln) and C. Wesselborg, H. Friedrichs, S. Lindenstruth (Giessen) for their outstanding engagement which enabled the realization of the various projects. The extensive financial support by the Deutsche Forschungsgemeinschaft is gratefully acknowledged.

REFERENCES

1.) N. LoIudice and F. Palumbo, Nucl.Phys. A326, 193 (1979).
2.) D. Bohle et al., Phys.Lett. 137B, 27 (1984).
3.) A. Richter, Nucl.Phys. A507, 99c (1990).
4.) A. Richter, Nucl.Phys. A522, 139c (1991).
5.) U. Kneissl, Prog.Part.Nucl.Phys. 24, 41 (1990).
6.) U. Kneissl, Prog.Part.Nucl.Phys. 28, 331 (1992).
7.) A. Degener et al., Nucl.Phys. A513, 29 (1990).
8.) R.D. Heil et al., Nucl.Phys. A476, 39 (1988).
9.) J. Margraf et al., Phys.Rev. C42, 771 (1990).
10.) J. Margraf et al., Phys.Rev. C45, R521 (1992).
11.) G. Alaga et al., Dan.Mat.Fys.Medd. 29, no.9, 1 (1955).
12.) H.H. Pitz et al., Nucl.Phys. A492, 411 (1989).
13.) B. Schlitt et al., Nucl.Instr. a. Meth. in Phys.Res. A337, 416 (1994).
14.) P.M. Endt and C. van der Leun, Nucl.Phys. A310,1 (1978).
15.) S. Lindenstruth et al., Nucl.Instr. a. Meth. in Phys.Res. A300, 293 (1991).
16.) N. Pietralla et al., to be published
17.) S.J. Freeman et al., Phys.Lett. 222B, 347 (1989).
18.) P. von Brentano et al., Nucl.Phys., in press.
19.) H.H. Pitz et al., Nucl.Phys. A509, 587 (1990).
20.) R.D. Heil et al., Nucl.Phys. A506, 223 (1990)
21.) H. Friedrichs et al., Nucl.Phys. A567, 266 (1994).
22.) C. Wesselborg et al., Phys.Lett. 207B, 22 (1988).
23.) S. Lindenstruth, PhD Thesis, Giessen (1994)
24.) A. Zilges et al., Nucl.Phys. A507, 399 (1990).
25.) R.-D. Herzberg et al., Nucl.Phys. A563, 445 (1993).
26.) W. Ziegler et al., Phys.Rev.Lett. 65, 2515 (1990).
27.) W. Ziegler et al., Nucl.Phys. A564, 356 (1993).
28.) C. Rangacharyulu et al., Phys.Rev. C43, R949 (1991).
29.) J. Margraf et al., Phys.Rev. C47, 1474 (1993).
30.) S.G. Rohoziński and W. Greiner, Z.Phys. A322, 271 (1985).
31.) R. Nojarov et al., Z.Phys. A324, 289 (1986).
32.) I. Hamamoto et al., Phys.Lett. 260B, 6 (1991).
33.) E. Garrido et al., Phys.Rev. C44, R1250 (1991).
34.) N. LoIudice and A. Richter, Phys.Lett. 304B, 193 (1993).
35.) E. Lipparini and S. Stringari, Phys.Lett. 130B, 139 (1983).
36.) P. Van Isacker and A. Frank, Phys.Lett. 225B, 1 (1989).
37.) A. Frank et al., Nucl.Phys. A531, 125 (1991).
38.) A.A. Raduta and D.S. Delion, Nucl.Phys. A513, 11 (1990).
39.) N. Huxel et al., Nucl.Phys. A539, 478 (1992).
40.) I. Bauske et al., Phys.Rev.Lett. 71, 975 (1993).

FROM "THE ORDER" OF THE LOW-LYING LEVELS TO "THE CHAOS" OF NEUTRON RESONANCES:(EXPERIMENT)

A.M. Sukhovoj

Joint Institute for Nuclear Research, Frank Laboratory of Neutron Physics, Dubna, Russia 141980

1. Introduction

Neutron capture experiments allow one to either determine the peculiarities of the structure of low-lying states ($E_{ex} \leq 2$ MeV) via measurements of level energies, spins and parities, and γ-ray branching ratios, or to investigate the properties of the primary γ-ray spectra from the decay of capture states. In fact, little is known about the properties of high excited states in heavy nuclei, for instance, for excitation energies, E_{ex}, from 2-3 MeV up to the neutron binding energy B_n. So, it is necessary to extend our experimental knowledge to the region $E_{ex} \simeq B_n$ in order to develop nuclear models able to describe the properties of nuclei at intermediate excitation energies between the simple structure of low-lying states and the extremely complicated structure of compound states.

Nowadays, it is possible to measure and analyse in detail two-step γ-decay cascades between the compound state (neutron resonance) and a given group of low-lying states [1]. The advantage of this experiments is its ability to extract useful information even in cases where the spaces between decaying states are smaller than the γ-ray detector resolution.

A comprehensive idea about nuclear level properties in heavy nuclei ($A > 100$) below the neutron binding energy B_n, and their γ-decay modes, can be achieved if the following are known:

- the dependence of level density for a given spin on nuclear excitations;
- the dependence of excitation and decay probabilities (via a given channel) of a certain nuclear level upon its structure; and
- if there are, or are not, any other processes affecting the γ-decay modes, *e.g.* phase transitions.

Such information could be easily obtained if a set of high efficiency Ge-detectors were used to measure the γ-decay cascades after thermal or resonance neutron capture in heavy nuclei.

In the present work the main information about, and properties of, high-lying states in some heavy nuclei in the mass region ($114 \leq A \leq 196$) are discussed. The experimental data of: nuclear level densities at excitation energies above 2 MeV; the peculiarities of the structure of the intermediate levels of two-step cascades; the distribution of level spacings between the most intense cascades; the dependence of average intensities on the energy of the primary transitions; and the experimental possibilities to observe phase transitions and their influence on γ-decay modes, for these heavy nuclei are presented and discussed in some detail. The data of these measurements are compared with the analogous ones predicted by different theoretical models.

2. Level density

The validity of any nuclear model may be tested only when its predictions are compared with experimental results. Evidently, discrepancies between experimental and calculated values from different theoretical models may occur and adjustments of these models are necessary to fit the experimental data.

Typical examples of experimental data concerning the number of excited states at an energy $E_{ex} > 1$ MeV for some even-even nuclei, ^{114}Cd, ^{156}Gd, and ^{196}Pt, are shown in figures 1-3. The number of levels which were measured that lie in the energy interval $\Delta E_{ex} = 100$ keV is compared with that predicted by two quite different nuclear models, namely:

- the Fermi-gas model with a back-shift [2];
- the Ignatyuk model [3], which makes use of the Strutinsky shell corrections approach and shell inhomogeneities for a single-particle scheme.

The common feature which can be obtained from all the studied nuclei is: that although these two models predict the same level density at the excitation energy B_n, they yield different predictions for other ranges of excitation energies. The first model, ref.[2], gives values close to the upper limits and the second model, ref.[3], determines the most likely lower limits of the nuclear level densities, see figures 1-3, for excitation energies up to $\simeq 3$ MeV. The figures clearly show that all nuclear states excited by primary dipole transitions could be observed up to excitation energies of 3-4 MeV, or higher, for cases where the peaks in the two-step cascade γ-ray spectrum were still well resolved. Our experience suggests that the Ignatyuk model describes the density of few-quasiparticle nuclear states rather than the total level density. The best level density description for levels excited by intense primary dipole transitions can be attained by a model in which the energy dependence of level density at low excitation energies is less strong than that actually considered in these two models. This conclusion will be confirmed again in the next section when comparison between the experimental and the calculated cascade intensity distributions for ^{156}Gd, figure 4, is made. Analogous dependences were observed for other deformed nuclei.

Systematic measurements of the two-step cascade intensities for some heavy nuclei in the mass region ($114 \leq A \leq 196$) were carried out in the excitation energy range $0 \leq E_{ex} \leq B_n$. Table 1 shows a comparison between the number of intermediate cascade levels observed in these measurements in the energy range $2 \leq E_{ex} \leq 3$ MeV and the corresponding numbers predicted from the models mentioned in ref [2,3]. This comparison shows the differences and indicates the necessity for more experimental investigations of nuclear level density at excitation energies above 2 MeV, in particular for the mass region ($150 \leq A \leq 190$). Additional information about two-step cascades for many neutron resonances would create more convenient conditions for determining the density of nuclear levels excited by primary dipole transitions, especially in such cases where the partial radiative width fluctuation is at a minimum.

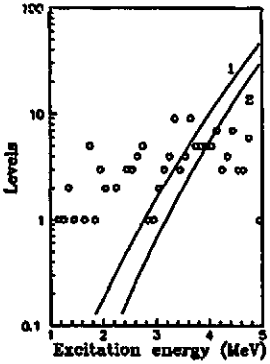

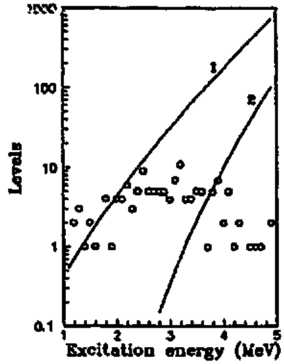

Fig.1. Number of observed levels with $J = 0, 1$ and 2 in ^{114}Cd for an excitation energy interval of 100 keV (points). Curves 1 and 2 represent the BSFG (ref.[2]) and the Ignatyuk thermodynamical model (ref.[3]) predictions for negative parity.

Fig.2. The same as in Fig.1 for levels with $J = 1$, 2 and 3 in ^{156}Gd and the model predictions for positive parity.

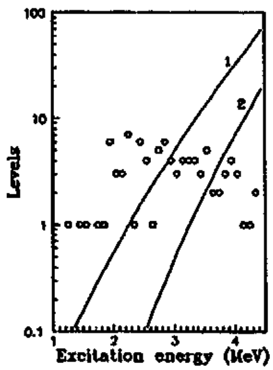

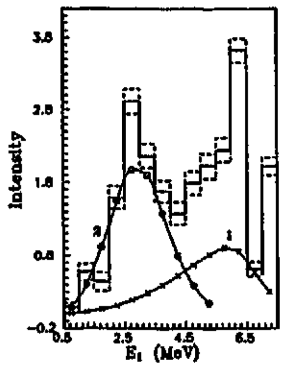

Fig.3. The same as in Fig.1 for levels with $J = 0$, 1 and 2 in ^{196}Pt and the model predictions for positive parity.

Fig.4. Sum intensity of cascades for the three low-lying levels in ^{156}Gd (% per decay) as a function of primary transition energy. Histograms represent the experimental data with ordinary statistical errors; curves 1 and 2 correspond to predictions according to models mentioned in ref.[2,3] respectively.

Table 1. Experimental intensities of two-step cascades (% per decay) $I_{\gamma\gamma}$ to the low-lying levels. n_i^{exp} and n_i^{cal} are the experimental and the predicted theoretical numbers of intermediate levels in the excitation energy interval $2 \leq E_{ex} \leq 3$ MeV in accordance with the models mentioned in ref.[1] and [2] respectively.

Nucleus	$I_{\gamma\gamma}$	n_i^{exp}	$n_i^{cal}[1]$	$n_i^{cal}[2]$	Nucleus	$I_{\gamma\gamma}$	n_i^{exp}	$n_i^{cal}[1]$	$n_i^{cal}[2]$
^{114}Cd	12(1)	22	6	2	^{164}Dy	46(2)	47	211	11
^{124}Te	14(1)	12	8	0.1	^{165}Dy	55(7)	57	164	58
^{137}Ba	76(25	10	15	13	^{168}Er	27(2)	34	126	15
^{138}Ba	26(1)	9	3	1	^{174}Yb	22(1)	44	73	23
^{139}Ba	102(4	10	14	15	^{175}Yb	69(9)	48	120	58
^{143}Nd	30(2)	17	13	25	^{178}Hf	17(1)	44	160	16
^{144}Nd	55(4)	13	5	2	^{179}Hf	67(4)	57	187	81
^{146}Nd	34(1)	41	12	4	^{180}Hf	10(1)	49	103	16
^{150}Sm	20(1)	54	82	1	^{181}Hf	52(4)	61	222	94
^{156}Gd	26(1)	51	136	1	^{183}W	36(3)	50	202	71
^{158}Gd	17(1)	44	102	6	^{187}W	43(2)	45	264	129
^{163}Dy	28(2)	57	214	68	^{196}Pt	32(2)	40	22	2

Remarks: a) The intensities of high-energy primary transitions exciting final levels n_f are not included in the table.

b) Parities of intermediate levels n_i^{exp} are unknown.

c) The model predicted values n_i^{cal} [1] are given for one parity only.

3. Intensity of two-step cascades and the structure of intermediate levels

For all practical purposes, there are not enough data relevant to the structure of excited states, for instance, for even-even deformed nuclei above an excitation energy of $\simeq$2 MeV. However, an indirect conclusion about their nature can be obtained from an analysis of integral characteristics, such as the total intensity of two-step cascades between levels of known structure. For example, the intensities of two-step cascades exciting the final levels of a single-particle nature in ^{143}Nd, ^{163}Dy, and ^{183}W nuclei are compatible with theoretically predicted values [4]. Analogous intensities exceed, by at least a factor of 1.5, the values obtained from the statistical model calculations for nuclei such as ^{165}Dy, ^{175}Yb, $^{179,181}Hf$, and ^{187}W. Such divergence is due to different values of the reduced neutron width Γ_n^0 (or to different structures of the neutron resonances). In the first case Γ_n^0 is about 10-20% of the average $< \Gamma_n^0 >$; in the second case it is either equal to or greater than $< \Gamma_n^0 >$.

Experiments show that cascades with large Γ_n^0 mainly *excite few*-quasiparticle low-lying final states. Those of small Γ_n^0 excite many-quasiparticle (collective) high-lying final states of rather complex structure. This result leads to a qualitative explanation [4] of cascade enhancements between compound-states with large Γ_n^0 and states of a pure single-quasiparticle nature. Such an explanation assumes a system of intermediate levels with reasonable few-quasiparticle components in their wave functions to be excited in the case of a compound-state with a relatively large single-particle component in its wave function (in the case of a sufficiently large Γ_n^0). It also assumes a system of a collective nature to be excited in cases of small single-particle components in the structure of the compound-state. A test of the validity of this assumption requires more investigations of two-step cascades for different neutron resonances in the same nucleus.

Figure 4 shows the dependence of cascade intensities on the energy of E_1 primary transitions for ^{156}Gd nucleus. It is clear that enhanced cascades for these transitions are observed in the region of $2 < E_1 < 3$ MeV. Analogous dependences were obtained for ^{150}Sm, ^{158}Gd and ^{164}Dy. This enhancement can be attributed to the influence of single-particle primary transitions $4s \rightarrow 3p$, or to the increase of widths of secondary transitions due to the influence of the Giant Magnetic Dipole Resonances (GMDR).

Cascade intensities predicted from different model calculations depend mainly on the nuclear level density of high-lying states and the widths of γ-transitions which populate and depopulate the excited states of the nucleus. Consequently, discrepancies between such predictions may occur. Figure 4 demonstrates examples of such discrepancies. Neither the Fermi-gas model nor the Ignatyuk model describe the experimental results of two-step cascades intensities very well. The first model fails to describe the low energy part of cascade primary transitions while the second model is not able to describe the higher part. This can be explained qualitatively by assuming that different collective structure states are more weakly excited than those states of few-quasiparticle ones, at least for the region of the $4s$-maximum of the neutron strength function. Again, as mentioned before, better agreement with experimental data could be achieved by a model which can predict the values for level density that lie between the estimated values from models mentioned in ref.[2,3].

The cascade intensity, $I_{\gamma\gamma} = (\Gamma_{\lambda i}/\Gamma_\lambda))(\Gamma_{if}/\Gamma_i)$, depends on the partial widths of the primary $\lambda \rightarrow i$ and the secondary $i \rightarrow f$ transitions. That is why the intensities summed over all the final states for cascades exciting the same intermediate level, $\sum_f I_{\gamma\gamma} = \Gamma_{\lambda i}/\Gamma_\lambda$, permit the experimental determination of the sum over a given interval of values, $\Gamma_{\lambda i}$, irrespective of the excitation energy of level i. The values of $I_{\gamma\gamma}$ and $\sum_f I_{\gamma\gamma}$ for a large enough set of final levels f, *e.g.*, $n_f \simeq 10 - 50$ (depending on the investigated nucleus) determine the ratio of the secondary transition partial width to the total radiative width of the decaying level, Γ_{if}/Γ_i, averaged over a given excitation energy interval. A direct and similar conclusion about the nature of the observed enhancement may be obtained when the γ-decay cascades of many neutron resonances in the same target nucleus are studied. Such investigations will allow a better understanding of different observed γ-decay structure effects.

The role of collective excitations in γ-decay of neutron resonance ("tails" of Giant Electric Dipole Resonance (GEDR) and GMDR can be determined from an analysis of the ratios between the primary (or secondary) transition radiative widths to the total radiative widths of decaying levels. The GEDR "tail" determines the radiative strength function (RSF) of primary transitions. It may be noted here that the experimental data [5] can be described more precisely by the GEDR model [6], assuming that at low energy γ-transitions the GEDR width depends on the temperature of the nucleus and on the γ-quantum energy. Precisely, the experimental RSF data, obtained over all regions of the primary transition energies $E_1 > 0.5$ MeV, contain

information about:
- shell effects,
- the general influences of the GEDR and GMDR "tails",
- the temperature of the excited nucleus, and
- the presence (or the absence) of phase transitions which may influence γ-decay processes.

Shell effects appear as local and sufficiently narrow maxima in the background corresponding to the smooth dependence of the RSF upon the γ- quantum energy. Such maxima were observed in the RSF data of $^{137,139}Ba$, and ^{181}Hf nuclei [4,7]. These shell effects are explained qualitatively by single-particle transitions between the $4s$ and $3p$ neutron subshells.

The influence of GEDR "tails" on RSF is, in general, clearly observed at high excitation energies in the investigated nuclei. But, little is known about the effect of GMDR states on neutron resonance γ-decay cascades at low excitation energies. The influence of GMDR can only be observed for compound states which populate the levels over which the strength of the GMDR is fragmented. It is impossible to differentiate the influence of either GEDR or GMDR on two-step cascade intensity without additional information. The nuclear resonance fluorescence (NRF) is one of the most efficient methods, up to now, for experimental investigations of GMDR in deformed nuclei [8]. This method observes the GMDR states which have a pure fixed quantum number K and have no interference with any other excited states with the same J^π. These states are referred as "Scissor modes".

Known GMDR states can, in principle, be excited by two-step cascades connecting the compound states of ($J^\pi = 0^- + 2^-$) to the ground state of either even-even nuclei such as $^{156,158}Gd$, ^{164}Dy, ^{174}Yb, and ^{196}Pt, or even-odd nuclei such as ^{143}Nd and ^{163}Dy. A comparison of the measured [9-13] intensities, in the mentioned list of nuclei, for the cascades populating the ground-state and the first excited levels with the data corresponding to NRF, ref.[8] for the even-even nuclei, and ref.[14,15] for ^{143}Nd and ^{163}Dy, shows that known states of GMDR, or multi-phonon-particle states, are usually not excited by primary E1-transitions. One can assume in such a case that the experimentally observed cascades [9-13] mainly excite intermediate levels of the few-quasiparticle structure and not the levels of vibrational states. Also, neutron radiative capture is selective for, at least, the excitation processes of Scissor modes in even-even deformed nuclei. It is fair to note here that this conclusion was obtained from a small set of compound states in the investigated nuclei for which Γ_n^0 is greater than $< \Gamma_n^0 >$.

4. Nuclear temperature and phase transitions

One of the major domains of nuclear research is the behaviour of nuclei as excitation energy is increased, and the possibility that these nuclei reveal information on the nuclear properties.

The experimental data analysis [16] of level density in heavy nuclei at excitation energies $E_{ex} \simeq 4 - 5$ MeV shows that the energy dependence of level density changes in shape at a certain energy, E_s. Below this energy is the region where many nuclear properties can find their explanation in the superfluid-nucleus and the constant temperature models. Above this energy, the existence of transitions between the superfluid-liquid and the usual Fermi-gas states (referred to phase transitions) can be assumed [17]. Phase transitions determine the features of the nucleus and may manifest themselves not only as a change of the shape of the excitation energy dependence on level density, but also as a change of the partial widths of primary transitions, which excite levels whose energies lie arround E_s.

Radiative strength function deduced from measurements of two-step cascades in $^{137,139}Ba$ shows that these nuclei could have temperatures less than those estimated from the thermodynamical representation $T = \sqrt{u/a}$, which relates the nucleus temperature to the single-particle state density, a, near the Fermi-surface, and the effective excitation energy u of the nucleus. To improve the comparison between predicted theoretical values and experimental results a matching parameter, M has been introduced, and the previous relation can be rewritten in the form $T = M\sqrt{u/a}$, where $0 < M < 1$.

Figure 5 shows a comparison between the experimental and the theoretical RSF values predicted by the model mentioned in ref. [7] for the cases where $M^2 = 1$, $M^2 = 0.5$, $M^2 = 0.25$, and $M^2 = 0.1$, respectively. It is clear that better agreement between the experimental estimates and the theoretical predictions is obtained as the nuclear temperature decreases. Also, the figure shows that, the slope of the energy dependence for the ^{137}Ba nucleus (and for the ^{139}Ba nucleus, too) are changed, relative to that of model calculations, when the energy of the primary transitions is at $E_1 \simeq 2$, and 1 MeV, respectively. These energies correspond to excitation energies of about 5, and 4 MeV in these nuclei. At such excitation energies the dependence of nuclear level density, for this range of mass, turns from constant temperature to Fermi-gas status. This is one of the main reasons that the two-step γ-decay cascades of compound states in heavy nuclei would allow, in principle, the study of possible phase transitions in heavy nuclei.

5. Equidistance in the positions of the intermediate level groups of intense cascades

As is shown in ref. [18] the intermediate levels of the most intense cascades may with high probability be presented as the groups with the practically constant difference in the excitation energy of single levels (or their multiplets). Moreover, one can unambiguously identify at least 1-3 triples of such states or of their multiplets. The equidistance period in same type nuclei (i.e. having same neutron number parity, transitions multipolarity or compound-state Γ_n^o values) varies more or less monotonously as a function of A (figure 6).

From here it follows that all nuclei exhibit harmonic excitations of the vibrational type, which, for some reasons, almost do not interact with inner nuclear excitations or, at least, with some of them.

From the above data on:

(a) the density of the states excited in the (n,γ) reaction;

(b) the presence of a colder than theoretically predicted nucleus;

(c) the equidistance of excitation energies of the most intense cascades one can assume that at the excitation energy below 3-4 MeV in the (n,γ) reaction only part of nuclear levels, i.e. those with the structure different from that of the majority of levels, can be excited. Moreover, all these effects are of common nature.

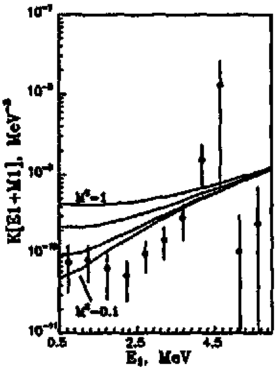

Fig.5. Experimental RSF (o) estimates for the primary γ-transition energies $E_1 \geq 0.52$ MeV in ^{137}Ba. Curves represent the recently developed GEDR model (ref. [6]) using different chosen values for the parameter M . The curves correspond to $M^2 = 0.1, 0.25, 0.5, 1$, respectively.

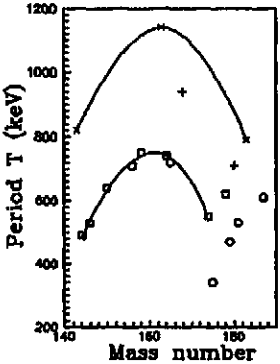

Fig.6. The dependence of the most probable equidistance period T on the mass number of the studied nuclei. □ - even-even nuclei, cascades of E1+M1-transitions; o - even-odd nuclei with $\Gamma_n^o / < \Gamma_n^o > > 1$; ×- even-odd nuclei with $\Gamma_n^o / < \Gamma_n^o > < 1$; + - nuclei ^{168}Er and ^{180}Hf, cascades of E1+E1-transitions. The maximum and minimum values are connected by lines separately.

CONCLUSIONS

The comparison between the observed number of intermediate cascade levels over the 24 investigated compound states (in complex heavy nuclei in the mass region ($114 \leq A \leq 196$, Table 1) and that predicted by two different theoretical models illustrates the necessity of additional experimental investigations on the nuclear level densities excited by primary dipole transitions at energies above 2 MeV. Such experiments are now feasible. A survey of available experimental data on level density and intensity of two-step cascades demonstrates the lack of information about the γ-decay cascades of many neutron resonances. The experimental analysis of cascade intensities of compound states for some heavy nuclei in this region clearly shows that it is impossible to describe the widths of primary and secondary transitions for heavy nuclei, in particular, in the region of the 4s-maximum strength function, without taking into account the influence of level structures below the neutron binding energy. Experimental results show a low nuclear temperature relative to the thermodynamical estimates for, at least, two spherical nuclei and illustrate that phase transitions are possible, and could be measured, at excitation energies $\simeq 5$ MeV for mass $A \simeq 130$ nuclei. The non-observation of known 1^+ states in the Scissor mode for even-even deformed nuclei may indicate that the neutron radiative capture reaction is a selective one.

REFERENCES

1. Boneva S.T., Vasilieva E.V., Popov Yu.P., Sukhovoj A.M., Khitrov V.A.// Sov. J. Part. Nucl., 1991, 22(2), 232
2. Dilg W., Schantl W., Vonach H., Uhl M.// Nucl. Phys., 1973, A217, 269
3. Ignatyuk A.V., Smirenkin G.N., Tishin A.S.// Yad. Fiz., 1975, 21, 485
4. Boneva S.T. et al.// Sov. J. Part. Nucl., 1991, 22(6), 698
5. Boneva S.T. et al.// Z. Phys., 1993, A346, 35
6. Kadmensky S.T., Markushev V.P., Furman V.I.// Yad. Fiz., 1983, 37, 165
7. Bondarenko V.A. et al.// Yad. Fiz., 1991, 54, 901
8. Pitz H.H., Berg U.E.D., Heil R.D., Kneissl U., Stock R., Wesselborg C., Brentano P.von// Nucl. Phys., 1984, A492, 411
   Wesselborg C. et al.// Phys. Lett., 1988, 207B, 22
   Zilges A. et al.// Nucl.Phys., 1990, A507, 399
9. Vasilieva E.V. et al.// JINR preprint, P3-93-3, Dubna, 1993
10. Ali M.A. et al.// JINR preprint, E3-91-428, Dubna, 1991
11. Vasilieva E.V. et al.// JINR preprint, P3-93-4, Dubna, 1993
12. Bondarenko V.A. et al.// Izv. RAN Ser. Fiz., 1993, 57, 56
13. Boneva S.T., Vasilieva E.V., Popov Yu.P., Sukhovoj A.M., Khitrov V.A., Yazvitsky Yu.S.// Izv. Akad. Nauk. SSSR, Ser. Fiz., 1986, 50, 1832
14. Zigles A. et al.// Proceedings of the 6^{th} International Conference on Nuclei Far From Stability, Kiev, July 1992
15. Bauske I. et al.// Phys. Rev. Lett., 1993, 71, 975
16. Reffo G.// Nuclear Theory for Application, 1980, IAEA-SMR-43 p.205, Triesta
17. Ignatyuk A.V.// Statistical Properties of Excited Nuclei (in Russian), Energoatomizdat, Moscow, 1983
18. Vasilieva E.V. et al.// Izv. RAN Ser. Fiz., 1993, 57, 118

SCATTERING AND DIRECT NUCLEAR REACTIONS IN THE HIGH-ENERGY APPROXIMATION

Lukyanov V.K.

Bogoliubov Lab. of Theor. *Physics, JINR, Dubna,* 141980 Moscow Region, Russia

Abstract

The three-dimensional distorted waves obtained in the high-energy approximation (HEA) for the case of a nuclear complex potential with the Coulomb forces included, are (applyed) used for calculating the cross sections of elastic, inelastic scattering and one-nucleon transfer reactions with heavy ions. The resulting expressions are in an analytical form, ~~and have the clear physical meaning. The corresponding applications at the intermediate energies show~~ a good agreement with experimental data.

1 Introduction

The direct processes are usually considered using the distorted wave Born approximation where the basic ingradient of the theory is the distorted waves introduced in *in-* and *out-*channels. For the heavy ions at intermediate energies two important simplifications can be done. The first one is the quasi-elastic consideration which comes true if the energy loss in a reaction occurs very small as compared with kinetic energies of colliding nuclei, e.g. $\Delta E \ll E$. The second is the quasi-classical (QC) calculation of distorted waves since the condition $kR \gg 1$ is usually working well. However, the traditional methods utilize the QC-distorted waves, expanding them in sets of partial waves and calculating every partial phase, so in the case of heavy ions one needs to take into account hundreds of partial waves. Here we apply the HEA-method which uses the three-dimensional quasi-classical waves as the whole to perform calculations of the corresponding matrix elements [1,2]. The method can be applied when $kR \gg 1$, $E \gg V$ and $\theta > \theta_c \simeq |V|/E$, where θ_c is the limited classical angle of a deflection. As the result we obtain in the framework of the DWBA, analytic expressions for qualitative physical estimations and for a quantitaive comparison with experimental data.

2 The High-Energy Approximation Method

Starting with the wave equation with the complex potential $\tilde{V} = V + iW$ the QC-solution is constructed in the form

$$\Psi = ue^{iS}, \qquad S = S_1 + iS_2, \tag{2.1}$$

where the real and imaginary parts of the action function obey a set of the coupled equations (see ref.[2]). They can be solved if one assumes the imaginary part of a potential being small as compared with its real part $|W| \ll |V|$. Then,

$$(\vec{\nabla} S_1)^2 = k^2 - \frac{2m}{\hbar^2} V_c, \quad \vec{\nabla} S_1 \vec{\nabla} S_2 = -\frac{m}{\hbar^2} W, \quad \vec{\nabla} \vec{j} = u^2 \frac{2m}{\hbar^2} e^{-2S_2}. \tag{2.2}$$

In HEA the action function S is expended in small V_c/E:

$$S_1 = \vec{k}\vec{r} - \frac{1}{\hbar v} \int_{\vec{r}_0}^{\vec{r}} V_c(\vec{r} - \hat{k}s) ds, \quad S_2 \simeq -\frac{1}{\hbar v} \int_{\vec{r}_0}^{\vec{r}} W(\vec{r} - \hat{k}s) ds, \tag{2.3}$$

where integration runs along the trajectory of motion. Here an effective real potential V_e is induced by the imaginary part of the initial potential. By the way, this fact has no serious meaning, if V_e is calculated from the scattering data in the framework of quasi-classics. Then, these effective potentials will also be appropriate in calculating other processes, if one uses the corresponding QC-distorted waves.

From the law of changing the current it was obtained the amplitude u [2]:

$$u = 1 - \frac{V_e}{4E} z, \quad z = 1 + \frac{\rho}{V_e} \frac{dV_e}{d\rho}. \tag{2.4}$$

In the case of the heavy-ion collisions it is important to introduce the limited classical angle of scattering $\theta_c = \max(|V(\Re)|/E)$, which characterizes a deflection of the local momentum $\vec{k}_\Re$ with respect to $\vec{k}$ in the asymptotics:

$$\vec{k}_\Re = \vec{k} - \vec{q}_c/2, \quad q_c/2 \simeq k \sin(\theta_c/2). \tag{2.5}$$

Now one can write the corresponding *in*- and *out*-distorted waves [2]:

$$\Psi^{(+)}_{\vec{k}_i} = \exp\{i(\vec{k}_i - \frac{\vec{q}_{ci}}{2})\vec{r}_i - \frac{i}{\hbar v_i} \int_{-\infty}^{z_i} V(\sqrt{\rho_i^2 + \lambda^2}) d\lambda + \frac{1}{\hbar v_i} \int_{-\infty}^{z_i} W(\sqrt{\rho_i^2 + \lambda^2}) d\lambda\}, \tag{2.6}$$

$$\Psi^{(-)*}_{\vec{k}_f} = \exp\{-i(\vec{k}_f + \frac{\vec{q}_{cf}}{2})\vec{r}_f - \frac{i}{\hbar v_f} \int_{z_f}^{\infty} V(\sqrt{\rho_f^2 + \lambda^2}) d\lambda + \frac{1}{\hbar v_f} \int_{z_f}^{\infty} W(\sqrt{\rho_f^2 + \lambda^2}) d\lambda\}. \tag{2.7}$$

Integrations run along the straight lines parallel to the momentum $\vec{k}(\|o\vec{z})$, and $\vec{r} = \vec{\rho} + \vec{z}$, $s + z = \lambda$, $\vec{\rho} \perp \vec{z}$. One should remind that if necessary, here the small flux factor $(1 - V/4E)$ can be included.

Based on the QC-distorted waves (2.6),(2.7) it is possible to calculate matrix elements of the direct processes having the typical form:

$$t = \int d\vec{r}\, \Psi^{(-)*}_{\vec{k}_f} \hat{O}(\vec{r}) \Psi^{(+)}_{\vec{k}_i} = \int d\vec{r}\, \hat{O}(\vec{r}) \exp\{i\tilde{\Phi}(\vec{r})\}, \tag{2.8}$$

where the transition operator

$$\hat{O}(\vec{r}) = P(r) f^{(l)}(r) Y_{L0}(\hat{r}) \tag{2.9}$$

includes the typical Fermi-like functions usually used in many practical calculations:

$$f(r) = (1 + \exp\frac{r - R}{a})^{-1}, \quad f^{(l)}(r) = \frac{d^l f}{dR^l}, \quad l = 1, 2, 3 \ldots. \tag{2.10}$$

R and a correspond to the radius and the "surface thickness" of an interaction. For example, in the case of elastic scattering we have [3,4,5] $L = 0$, $l = 0$, $P(r) = 1$; for inelastic scattering with the collective state excitations there are various combinations of $L = 0, 2, 3, 4$, $l = 1, 2$, $P(r) = 1, 1/r$ [6,7]; for direct one nucleon transfer reactions one may use $L \geq 1$, $l = 1$, $P(r) = 1/r$ [6,8,9].

The whole phase $\tilde{\Phi}$ was calculated in [2] for the complex nuclear Woods-Saxon and the Coulomb potentials and has the form:

$$\tilde{\Phi} = 2a_0 + \tilde{\beta}\mu + n_1\mu^2 + c_1\mu^3 + n_2(1-\mu^2)\cos^2\tilde{\varphi} + c_2\mu(1-\mu^2)\cos^2\tilde{\varphi} \qquad (2.11)$$

where $\mu = \cos\tilde{\theta}$, and $\tilde{\theta}$, $\tilde{\varphi}$ are the angles of $\vec{r}$ in a spherical coordinate system and

$$\tilde{\beta} = \tilde{q}r = q_{ef}r + 2k_6\alpha r, \quad k_6 = -[B^V + B^C(3 - \frac{r^2}{R_C^2})], \quad a_0 = -B^V R_V + \frac{B^V r^2}{2dR_V},$$

$$n_1 = -\frac{B^V}{dR_V}(\alpha r)^2, \qquad n_2 = -\frac{B^V}{dR_V}(1-\alpha^2)r^2, \qquad (2.12)$$

$$c_1 = -\frac{4B^C}{3R_C^2}(\alpha r)^3, \qquad c_2 = -\frac{4B^C}{R_C^2}(1-\alpha^2)\alpha r^3.$$

Here $\alpha = \sin(\theta/2)$, $B^V = V_0/\hbar v$, $B^C = V_B/\hbar v$, with V_0 being the strength of a nuclear potential and $V_B = Z_1Z_2e^2/R_C$. The fitted parameter d is useful in calculations of nuclear phases.

The integration in (2.8) over angular variables was performed in [2,6] in the following analytic form:

$$t = \int_0^\infty dr P(r) f^{(l)}(r) \left\{ F^{(+)}(r) - (-1)^L F^{(-)}(r) \right\} Y_{L0}(1), \qquad (2.13)$$

where

$$F^{(\pm)}(r) = \frac{r}{\tilde{q}L(\pm)} e^{i(2a_0+n_1)} e^{\pm i(\tilde{\beta}+c_1)}, \qquad L(\pm) = \frac{i}{\tilde{\beta}}\sqrt{\Delta_{(\pm)}(\Delta_{(\pm)} \mp \delta_{(\pm)})}, \qquad (2.14)$$

$$\Delta_{(\pm)} = \tilde{\beta} + 3c_1 \pm 2n_1, \quad \delta_{(\pm)} = 2(n_2 \pm c_2).$$

In calculating these typical integrals "the pole method" was developed which uses the properties of the functions $f^{(l)}(r)$ on the complex r-plane, where they have poles near the radius of nuclear interaction at $r_n^{\pm} = R \pm ix_n$ with $x_n = \pi a(2n+1)$ and $n = 0, 1, 2 \ldots$. Then, the result for such integrals is expressed through a sum of the corresponding residues. For example, in the case of elastic scattering one can use some approximations and sum up the simple poles to obtain:

$$t \simeq -\frac{i\pi aR}{\tilde{q}} Y_{00}(1)(1 + i\frac{\pi a}{R}) e^{i\phi(R)} \left\{ \frac{e^{i(\tilde{q}R + y(R))}}{\sinh[\pi a(\tilde{q} + y'_R + \phi'_R)]} + \xi \frac{e^{-i(\tilde{q}R + y(R))}}{\sinh[\pi a(\tilde{q} + y'_R - \phi'_R)]} \right\}. \qquad (2.15)$$

The functions ϕ, y, their derivatives and ξ are done in [2]. In a qualitative consideration one can put $\pi a/R \ll 1$ which carries to $\xi \ll 1$ and $(\phi'/\pi a) \ll 1$. So, we get at large $\pi a q_{ef}$:

$$t \sim e^{-\pi a k(\alpha - \alpha_c)} \cos(\tilde{q}R + y'_R), \qquad (2.16)$$

where $\alpha = \sin(\theta/2)$. It is seen that the elastic amplitude t is decreasing with the angle of scattering as an exponential function [1,5] with a slope determined by the thickness parameter a of a surface of an interaction. Simultaneously it oscillates with a frequency depending mainly on the radius parameter R. This is a typical behaviour for the so-called Fraunhofer diffraction scattering on nuclei. However, for large $(\phi'/\pi a)$ only one term of (2.15) gives contribution, and in this case no oscillations will appear:

$$|t|^2 \sim e^{-2\pi a k(\alpha-\alpha_e)}. \tag{2.17}$$

Under some conditions this kind behaviour is observed in the heavy ion elastic scattering at angles θ larger than θ_c, the limited deflection angle.

In other cases, when $f^{(l)}(r)$ takes place in the integrand, the pole method can also be applied to obtain simple analytical expressions for the corresponding matrix elements.

3 DWBA-amplitudes for the HI-collision Processes

Heavy ion elastic scattering at energies larger than several dozen Mev per nucleon is considered using the amplitude obtained in [3,4] for large angles $\theta > (1/kR)$ and $\theta > \theta_c \simeq (|V|/E)$ covering in practice a wide region of scattering angles

$$T^{el} = -\frac{m}{2\pi\hbar^2}\int d\vec{r}\,\Psi^{(-)*}_{\vec{k}_f} V \Psi^{(+)}_{\vec{k}_i} = -\frac{m}{2\pi\hbar^2}\int d\vec{r}\,(V_N + V_C)\exp\{i\bar{\Phi}(\vec{r})\}. \tag{3.1}$$

Here we have [2]

$$\bar{\Phi} = i\vec{q_{ef}}\vec{r} + \Phi, \quad \Phi = \Phi^{(+)}_i + \Phi^{(-)}_f, \quad \Phi^{(\pm)} = -\frac{1}{\hbar v}\int\limits_{\mp z}^{\infty}[V_N(\sqrt{\rho^2+\lambda^2}) + V_C(\sqrt{\rho^2+\lambda^2})]d\lambda,$$

$$V_N = V + iW = V_0 f_V(r) + iW_0 f_W(r), \quad V_C = \frac{Z_1Z_2e^2}{R_C}\int\frac{\rho_c(x)d\vec{x}}{|\vec{r}-\vec{x}|} \tag{3.2}$$

with the charge density distribution $\rho_c = \rho_0 f_c(r)$ and the effective momentum transfer $\vec{q_{ef}} = \vec{q} - \vec{q_c}$, where $\vec{q}\|\vec{q_c}$, $q_{ef} = 2k(\alpha - \alpha_c)$, $\alpha = \sin(\theta/2)$, and $\alpha_c \simeq [V(R_t) + V_C(R_t) + iW(R_t)]/2E$, taken at the radius R_t of the external limited trajectory of motion. All the distribution functions are taken in the form of the Fermi-function

$$f_p(r) = \frac{1}{1+\exp\frac{r-R_p}{a_p}}. \tag{3.3}$$

Thus, the scattering amplitude consists of three terms:

$$T^{el} = T^{el}_V + iT^{el}_W + T^{el}_C \tag{3.4}$$

It was shown in [2] that the 6-dimensional integral T^{el}_C can be transformed to the 3-dimensional one:

$$T^{el}_C = -\frac{m}{2\pi\hbar^2}\int d\vec{r}\,v_c(r)\exp\{i\bar{\Phi}(\vec{r})\}, \qquad v_c(r) = \frac{Z_1Z_2e^2\rho_0}{q_e^2 R_C}f_c(r), \tag{3.5}$$

where $q_e \simeq q_{ef}$, and $v_c(r)$ plays the role of a quasi-potential of scattering on a spread nuclear charge. Thus, consisting with (2.8) and (2.13) each term of the scattering amplitude (3.4) has the same form:

$$T^{el}_p = \frac{im}{\hbar^2}Y_p\int\limits_0^{\infty} f_p(r)\left\{F^{(+)}_p(r) - F^{(-)}_p(r)\right\}dr. \tag{3.6}$$

In practice, for the typical nuclear parameters it is enough to take into account only a couple of poles $r_0^{\pm} = R \pm ix_0$ of the Fermi-function nearest to the real axis ("two-pole approximation"), because every next pair contributes approximately an order smaller than the previous one. Then, we have [7]

$$T_p^{el} = -\frac{im}{\hbar^2} Y_p 2\pi ia[F^{(+)}(r_0^+) + F^{(-)}(r_0^-)]. \tag{3.7}$$

Substituting into this expression the corresponding poles one can easily find that the amplitude behaves as an exponential function, depending on the exponent $-2\pi ak\sin\theta/2$ and oscillating with a frequency as a function of the radius R.

For calculating the inelastic scattering of light and heavy ions with excitation of the collective nuclear states we have used DWBA with QC-wave functions whose phases are calculated as it is shown here. The energy change in the *out*-channel is neglected since usually $E_{ex} \ll E$. The transition interaction is taken in the form of derivatives in small quadrupole and octupole additions $\delta R = R\sum \alpha_{LM} Y_{LM}^*(\hat{r})$ to the radius of a potential in the elastic channel. The result for the amplitude is the same as if one uses the sudden approximation [6,7]:

$$T^{in} = (J_f M_F|\hat{T}_V^{el} + i\hat{T}_W^{el} + \hat{T}_C^{el}|J_i M_i), \tag{3.8}$$

where

$$\hat{T}_p^{el} = -\frac{m}{2\pi\hbar^2}\int d\vec{r} Y_p f_p(r, R + \delta R)\Psi^{(-)*}\Psi^{(+)} \tag{3.9}$$

is the operator, depending on the internal nuclear coordinates α_{LM}. Then, in the first order in small δR we get

$$T_p^{in} = \sum_{LM}(J_f M_f|\alpha_{LM}|J_i M_i)\,\hat{T}_{LM}^{in}, \tag{3.10}$$

where

$$\hat{T}_{LM}^{in} = -\frac{m}{2\pi\hbar^2} Y_p R \int d\vec{r}\Psi^{(-)*}\Psi^{(+)}\frac{df}{dR} Y_{LM}^*. \tag{3.11}$$

Transforming the structure matrix element in (3.10) through the reduced one and using the definition of $B\downarrow(EL)$-transition, one can write the inelastic cross section:

$$\frac{d\sigma}{d\Omega} = \frac{(2J_f+1)}{(2J_i+1)}\frac{1}{(2L+1)}\sum_{LM}\frac{B\downarrow(EL)}{D_L^2}|\hat{T}_{LM}^{in}|^2 \tag{3.12}$$

with

$$D_L = Z_2 e\rho_0 R_C J_L^c, \quad J_L^c = \int \frac{df_c}{dR_C} r^{L+2} dr \simeq R_C^{L+2}, \tag{3.13}$$

$$\hat{T}_p^{in} = \frac{im}{\hbar^2} Y_p Y_{L0}(1) R\tilde{q}\int_0^\infty dr f_p\left(\frac{dF_p^{(+)}(r)}{dr} - (-1)^L\frac{dF_p^{(-)}(r)}{dr}\right). \tag{3.14}$$

Subsequent calculations are the same as in the case of elastic scattering, using the two-pole approximation [7].

As to the one-nucleon transfer reaction $a + A \to b + B$ where $a = x + b, B = A + x$ and the transferred particle x is proposed to be spinless, the corresponding amplitude in the zero-range approximation is as follows:

$$\tilde{T}_l^{tr} = -D_0 \int d\vec{r} \Psi_\beta^{(-)*}(\vec{r}) \Psi_\alpha^{(+)}(\vec{r}) \Re_l(r) Y_{l0}^*(\hat{r}), \tag{3.15}$$

where $D_0 = 8\pi\sqrt{(m_a\hbar^2/2m_x m_b)^3 \epsilon_{xb}}$ with ϵ_{xb}, the seperation energy of a nucleon x in the incident particle a. Here $\Re_l(r)$ is the radial wave function of the x-particle in the final nucleus B. This function has the asymptotic behaviour $\exp(-\kappa_l r)/r$ and goes to the constant as $r \to 0$. Its slope is determined by $\kappa_l = \sqrt{2m_x \epsilon_l/\hbar^2}$, depending on the seperation energy ϵ_l of x in B. We have emphasized that the main effect in heavy-ion reactions comes from the region near the interaction radius. This means that the behaviour of the function $\Re_l$ at $r < R$ is of no importance, and one can select it in the form [8,9]

$$\Re_l(r) = N_l \frac{1}{r} \frac{df_s(r, R, a_l)}{dr}, \tag{3.16}$$

where

$$f_s = \frac{\sinh(R/a_l)}{\cosh(R/a_l) + \cosh(r/a_l)} \tag{3.17}$$

is the symmetrized Fermi-function having the asymptotics $\exp(-a_l r)/r$ and being a constant at $r = 0$. The "thickness" parameter of the transition region is to be taken $a_l = \kappa_l^{-1}$. The constant N_l can be calculated by chaging variables $x = 1 + \cosh(r/a_l)/\cosh(R/a_l)$ in the normalisation condition:

$$\int_0^\infty \Re_l^2(r) r^2 dr = N_l^2 \int_0^\infty \left(\frac{df_s}{dr}\right)^2 dr = \frac{N_l^2}{a_l} \frac{\sinh^2(R/a_l)}{\cosh^2(R/a_l)} \int_0^\infty \frac{\sinh^2(r/a_l)}{\cosh^2(R/a_l)} \frac{1}{x^4} dr = 1. \tag{3.18}$$

Neglecting here the terms $\cosh^{-1}(R/a_l)$ as compared with 1, we reduce the latter integral to the table one:

$$\int_1^\infty \frac{x-1}{x^4} dx = \frac{1}{6}. \tag{3.19}$$

So,we get $N_l = \sqrt{6a_l} = \sqrt{6/\kappa_l}$.

Using the usual procedure of the HEA-method, we get the amplitude for the one-nucleon transfer reaction in the typical form [8,9]:

$$\tilde{T}_l^{tr} = \frac{m_b}{2\pi\hbar^2} D_0 \sqrt{6a_l} Y_{l0}(1) 2\pi i \int_0^\infty dr \frac{1}{r} \frac{df_s}{dr} \left\{ F^{(+)}(r) - (-)^l F^{(-)}(r) \right\}. \tag{3.20}$$

It is easy to show that the main contribution here is coming from two poles closest to the real r-axis and (3.19) is reduced to two the second order residues. As in the previous case here we also have the general exponential decrease at angles $\theta > \theta_c$, depending on the acting thickness a_l in the region of the surface of transition. Its magnitude depends on the slope of a "tail" of a bound state function in the final nucleus B.

4 Conclusion

Here we have shown how the three-dimensional quasi-classics can be adopted for constructing nuclear distorted waves using the high-energy approximation. The pole method is appropriate for calculations of the amplitudes for typical direct processes in analytic form. This gives a possibility both for the qualitative analysis of main physical features of processes and the quantitative fit to experimental data.

Calculations of differential cross sections for elastic and inelastic scattering within the two-pole approximation were performed in [7]. As an example, Fig.1 shows the calculations for scattering $^{17}O + ^{60}Ni$ at $E = 1435MeV$ in comparison with the experimental data from [10]. It is easy to see from (3.14) that because of the presence the factor $(-1)^L$ the oscillating part of the amplitude as a function of the scattering angle is the *cos*- or *sin*-function depending an *L*-even or odd, respectively. In this case the cross section will have visible oscillations which coincide for excitations of the even collective states in their phases with the elastic scattering oscillations. The depths of potential wells are in limits of $V_0 = 60 - 70MeV$ and $W_0 = 5 - 6MeV$, the $B(EL)$-transitions obtained are approximately twice those cited in [10]. As a general result one can mention a rather good agreement with experimental data in the range of scattering angles $\theta > \theta_c \simeq 2^\circ$ in coincidence with the initial assumptions of the HEA-method.

In Fig.2,3 the results are presented of calculations [8,9] of the one-nucleon transfer reactions, the proton stripping from ^{12}C to the ground state of ^{209}Bi and ^{28}Si and also stripping from ^{16}O to the ground state of ^{29}Si as well as for the pick-up reaction of one neutron from the ground state of ^{208}Pb to the hole state $(2f_{7/2})$ of ^{207}Pb. Solid lines show the differential cross sections in comparison with experimental data from [11-13]. The parameters of calculations are presented in [8,9]. One can mention that for explanation experimental data at various bombarding energies from $50MeV$ to $600MeV$ the main effect comes from changing the depth of the imaginary part of the potential W_0 from $3MeV$ to $38MeV$ and thickness parameter a_I changing in the limits of $0.5 \div 0.6 fm$. At higher energies, the reaction is characterized by a simple exponential slope with the angle decrease. At the energy decrease the diffraction-like picture in angular distribution appears.

One can summarise that the DWBA calculations with the quasi-classical distorted waves in the framework of HEA give good agreement with experimental data at energies begining from $10MeV$ per nucleon and higher.

Thus, investigations of heavy ion-collisions in the quantum region of scattering angles $\theta > \theta_c$, outside the limited trajectories of motion, are very sensitive to the precise structure of a nucleus-nucleus interaction. For instance, the slope of curves with θ feels the "thickness" of the acting region in the channel. It may be used also for searching the "halo" distributions of nuclei in the radioactive beams which now become available.

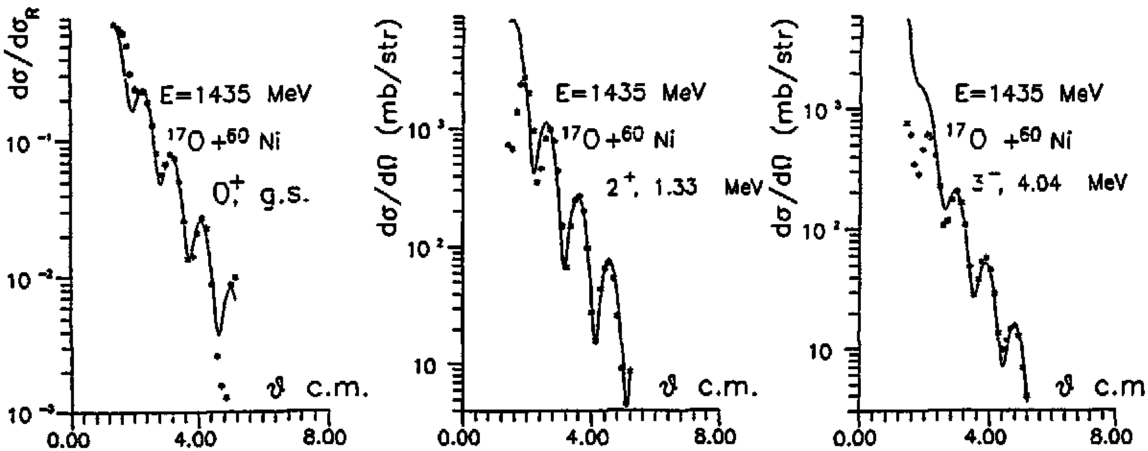

Fig.1 The heavy ion elastic and inelastic cross sections $^{17}O + ^{60}Ni$; $E_{lab} = 1435MeV$; exp. data from [10]; solid lines– theory.

Fig.2 Angular distributions for the stripping reactions (a) $^{12}C+^{208}Pb \Rightarrow {}^{11}B+^{209}Bi$, $E = 50MeV/n$; (b) $^{12}C+^{27}Al \Rightarrow {}^{11}B+^{28}Si$, $E = 50MeV/n$. Solid lines are the theoretical calculations, squared points are the experimental data from [11].

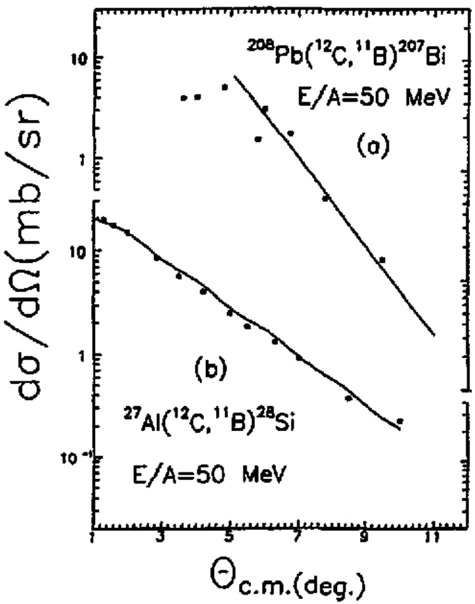

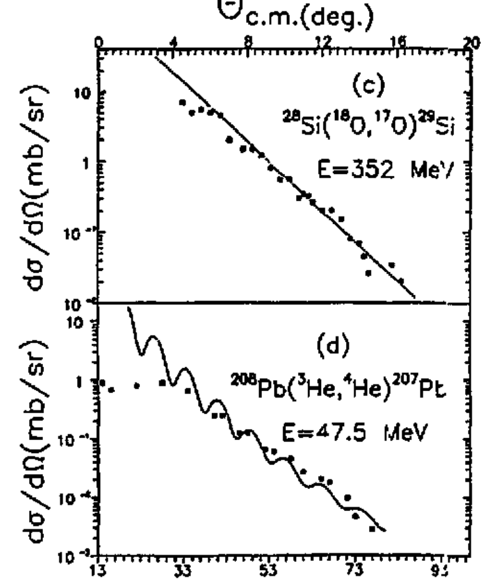

Fig.3 Angular distributions for the proton stripping in (c) $^{18}O+^{28}Si \Rightarrow {}^{17}O+^{29}Si$, $E = 352MeV$; and for the neutron pick up reaction (d) $^{3}He+^{208}Pb \Rightarrow {}^{4}He+^{207}Pb$, $E = 47.5MeV$. Solid lines are the theoretical calculation, squared points are the experimental data from [12,13].

References

1. Lukyanov V.K. // Proc.Int.School-Seminar on HI Phys.(Dubna) 1993. E7-93-274. V.2. P.129.
2. Lukyanov V.K. // Preprint JINR. Dubna. 1994. E4-94-314.
3. Schiff L.I. // Phys.Rev. 1956. V.103. P.443.
4. Lukyanov V.K. // Bull.of Russ.Acad.of Sc., Physics. 1994. V.58. P.6. (*in russian* Izv. RAN, ser.fiz. 1994. V.58. P.8.)
5. Lukyanov V.K., Gridnev K.A., Embulaev A.V. //Bull.of Russ.Acad.of Sc., Physica. 1994. V.58. P.19. (*in russian* Izv. RAN, ser.fiz. 1994. V.58. P.23.)
6. Lukyanov V.K. // Preprint JINR. Dubna. 1994. E4-95-308.
7. Lukyanov V.K., Embulaev A.V., Permyakov V.P. // JINR Rapid Comm. Dubna. 1994. 4[67]-94.
8. Fedotov S.I., Lukyanov V.K. // JINR Rapid Comm. Dubna. 4[67]-94.
9. Fedotov S.I., Gridnev K.A., Lukyanov V.K. // Preprint JINR. Dubna. 1994. E4-94-354.
10. Liguori Neto R. et al. // Nucl.Phys. 1993. V.A560. P.733.
11. Winfield J.S. et al. // Phys.Rev. 1989. V.C39. P.1395.
12. Fernandes M.A.G. et al. // Phys.Rev. 1986. V.C33. P.1971.
13. Satchler G.R. et al. // Phys.Rev. 1969. V.187. P.1491.

SEMICLASSICAL APPROACH TO THE DYNAMICS OF HOT NUCLEI

João da Providência Jr.

Departamento de Física, Universidade de Coimbra, P–3000 Coimbra, Portugal

Abstract

A semiclassical formalism which is based on an energy functional and generalizes the fluid dynamical model (first sound) of Eckart ~~et al~~ has recently been developed and extended to a finite temperature. The model accounts for important transverse components in the current of low-lying modes with $\ell > 1$. It is shown that new eigenmodes appear when the temperature does not vanish. In the limit of $T \to 0$ the strength of the new eigenmodes goes to 0 proportionally to T^2 and the currents and transition densities are proportional to T. The inclusion of tensor fields in the action integral lead to important changes as compared with the results of the simpler model based on first sound dynamics.

1. Introduction

We are interested in the description of the average features of nuclear structure which remain when shell effects are neglected. Semiclassical methods deal with quantities like distribution functions, densities and currents. These methods are therefore adequate to our aim.

The description of collective modes, in nuclei at finite temperature, requires the knowledge of the equilibrium state. We assume a sharp density profile for the equilibrium density. The equilibrium distribution function is the product of a step function in coordinate space by a Fermi-Dirac distribution function in momentum space,

$$f_0 = \frac{\Theta(R_0 - r)}{1 + \exp[(\frac{p^2}{2m} - \varsigma_0)/T]}, \tag{1}$$

where $\varsigma_0 = U_0 - \mu$. Here U_0 is the equilibrium selfconsistent potential, R_0 is the radius and μ is the chemical potential.

The equilibrium distribution fuuction is a step function in coordinate space, because the expression we adopt for the energy functional does not contain terms with derivatives. The two body interaction we consider is of the form $v_{12} = \delta(\mathbf{x}_1 - \mathbf{x}_2)(a + b\rho^{1/6})$, where a and b are constants and ρ is the nuclear density. The energy is a functional of the distribution function

$$E = \int d\Gamma f \frac{p^2}{2m} + \frac{1}{2} \int d\Gamma_1 d\Gamma_2 v_{12} f(1) f(2) \tag{2}$$

where $d\Gamma = gd^3xd^3p/(2\pi\hbar)^3$ is the volume element in phase space and g is the spin-isospin multiplicity. The energy may be written

$$E = \int d^3x \left(\tau + \sum_\nu a_\nu \rho^\nu\right) + \sigma\Sigma \tag{3}$$

where we have added the term $\sigma\Sigma$ in order to account for the surface energy. The constants a_ν are connected with the δ interaction. The surface tension is σ and Σ stands for the area of the nuclear surface. The density ρ and the kinetic energy density τ are computed from the distribution function f.

We are considering independent particle mixed states. The single particle wave functions are solutions of the eigenvalue problem $h_0\psi_i = \epsilon_i\psi_i$ where ϵ_i is the single particle energy, $h_0 = \frac{p^2}{2m} + U_0$ is the single particle hamiltonian.

The entropy is given by $S = -(\partial\Omega/\partial T)_{V,\varsigma}$ where Ω is the grand potential, $\Omega = -T\int d\Gamma \ln\left[1+\exp(\varsigma - \frac{p^2}{2m})\right]$.

The chemical potential μ and the equilibrium nuclear radius R_0 are obtained by minimizing the free energy $F = E - TS$ with the subsidiary condition that the particle number A remains constant,

$$\delta\left\{\int d^3x \left(\tau + \sum_\nu a_\nu\rho^\nu - Ts - \mu A\right) + \sigma\Sigma\right\} = 0. \tag{4}$$

Here s stands for the entropy density. The variation with respect to ς and the radius R [1], leads to the equations

$$\left[\frac{\partial\tau}{\partial\zeta} + \frac{\partial\rho}{\partial\zeta}\left(\sum_\nu a_\nu \nu\rho^{\nu-1} - \mu\right) - T\frac{\partial s}{\partial\zeta}\right]_{\zeta=\zeta_0} = 0, \tag{5}$$

$$\left(\tau + \sum_\nu a_\nu\rho^\nu + \frac{2\sigma}{R} - \mu\rho - Ts\right)_{\zeta=\zeta_0} = 0. \tag{6}$$

It should be borne in mind that the model is classical in nature except that the Pauli principle is taken into account. Since shell effects are neglected, the predictions of the model apply only to the average behaviour at which one arrives after shell fluctuations have been smoothed out or for temperatures above 3 MeV.

2. Small amplitude oscillations

An exact semiclassical description of the mean field dynamics would require solving the Vlasov equation. As an alternative we consider a variational formalism which leads to the Liouville-von Neumann equation of statistical mechanics.

We start from the classical limit of a variational formulation [2] of the Liouville-von Neumann equation of statistical mechanics in order to obtain a mean field approximation appropriate to mixed states. The lagrangian

$$L = i\hbar \ tr(\dot{U} D_0 U^\dagger) - tr(U D_0 U^\dagger H), \tag{7}$$

determines the time-evolution of the density matrix $D = U D_0 U^\dagger$, where D_0 stands for the density matrix describing a state of equilibrium and U is a unitary operator. If we write

$$U = \exp\left(\frac{i}{\hbar}\hat{\mathcal{G}}\right), \tag{8}$$

the lagrangian L reduces, for small amplitude oscillations, to the following harmonic lagrangian

$$L^{(2)} = tr\left(D_0\left(\frac{i}{2\hbar}[\hat{\mathcal{G}},\dot{\hat{\mathcal{G}}}] - \frac{1}{2\hbar^2}[\hat{\mathcal{G}},[\hat{H},\hat{\mathcal{G}}]]\right)\right). \tag{9}$$

We will consider the classical limit of the lagrangian (9), retaining only the leading order terms in a Wigner-Kirkwood expansion in powers of $\hbar$.

We start by determining the equilibrium state. Suppose now that the system deviates from the equilibrium state. The system oscillates. From the lagrangian (9) we will calculate the eigenmodes. If we do not allow for a completely general variation of the generator $\mathcal{G}$ then the dynamics of the system will be affected by the restrictive parametrization we impose on the generator $\mathcal{G}$. There are many choices possible for parametrization of the distribution function. Each one implicitly assumes a choice of relevant and irrelevant degrees of freedom. Therefore the parametrization we impose on $\mathcal{G}$ is a way of selecting the relevant collective variables for the dynamics.

In the classical limit we have

$$\hat{\mathcal{G}} = \sum_{i=1}^{A} \mathcal{G}(\mathbf{x}_i, \mathbf{p}_i, t), \tag{10}$$

where the generator $\mathcal{G}(\mathbf{x},\mathbf{p},t)$ may be decomposed into a time-even term Q and a time-odd term P ($\mathcal{G} = Q + P$). A parametrization by means of a scalar field $\psi(\mathbf{x},t)$ and a tensor field $\phi_{\alpha\beta}(\mathbf{x},t)$ is chosen for the generator Q

$$Q = \psi(\mathbf{x},t) + \frac{1}{2}p_\alpha p_\beta \phi_{\alpha\beta}(\mathbf{x},t). \tag{11}$$

The time-even generator Q is responsable for the existence of time-odd components in the distribution function. In particular the divergence of the tensor $\phi_{\alpha\beta}(\mathbf{x},t)$ will introduce transverse components in the current.

In the derivation of the equilibrium distribution function a spherical symmetrical distribution function in momentum space was assumed. Such a restriction should not be imposed on the dynamical formulation. Therefore, we will assume that the generator is such that by means of a canonical transformation of f_0 we obtain a time-even distribution which is distorted in momentum space. We assume P is the generator of a canonical transformation such that the following equation is approximately satisfied

$$f_0 + \{f_0, P\} + \frac{1}{2}\{\{f_0, P\}, P\} + ... = \frac{\Theta(R_0 + R_1(\theta,\phi,t) - r)}{1 + \exp\left[\left(\frac{p^2}{2m} - \varsigma_0 - \varsigma_1(\mathbf{x},t) + \frac{p_\alpha p_\beta}{2m}\chi_{\alpha\beta}(\mathbf{x},t)\right)/T\right]}. \tag{12}$$

This equation generalizes to a finite temperature the generator P given in refs. [3,4]. We remark that R_1 describes the surface displacements. It is clear that at a finite temperature no generator P exists such that eq. (12) holds exactly. This means that, at a finite temperature, R_1, ς_1 and $\chi_{\alpha\beta}$ are not an adequate parametrization since these quantities can not be generated by a canonical transformation. However the errors involved in the deviation from canonicity will be minimized if we require that the fields R_1, ς_1 and $\chi_{\alpha\beta}$ are such that the entropy remains constant.

From the distribution function f,

$$f = f_0 + \{f_0, \mathcal{G}\} + \frac{1}{2}\{\{f_0, \mathcal{G}\}, \mathcal{G}\} + ..., \tag{13}$$

we derive the physical quantities, such as the density, the current and the energy. Up to first order in the variational fields we have the following expressions for the density

$$\rho \equiv g\int \frac{d^3p}{(2\pi\hbar)^3} f = \rho_0 + A_1\varsigma_1 - \frac{\rho_0}{2}\chi_{\alpha\alpha}, \tag{14}$$

and for the current

$$j_\alpha \equiv g \int \frac{d^3p}{(2\pi\hbar)^3} f \frac{p_\alpha}{m} = \frac{\rho_0}{m}\partial_\alpha \psi + \frac{2\tau_0}{3}\left(\frac{1}{2}\partial_\alpha \phi_{\mu\mu} + \partial_\beta \phi_{\alpha\beta}\right). \tag{15}$$

In order to arrive at the expression (15) we have imposed the following boundary condition [5]

$$n_\alpha \phi_{\alpha\beta}|_{r=R_0} = 0, \tag{16}$$

where $n_\beta = x_\beta / r$ and which ensures that the current is not singular at the surface.

We ensure that the boundary condition (16) is fulfilled and that the entropy S and the particle number A are conserved on the average by means of the Lagrange multipliers ξ_β, T and μ. From the classical limit of the lagrangian (9), with the choices for the generators Q and P implied by eqs. (11) and (12) and taking into account the subsidiary conditions which ensure the boundary condition (16), the conservation of the entropy S and of the particle number A, the following effective lagrangian is obtained

$$\mathcal{L}^{(2)} = (L + \mu A + TS)^{(2)} + \oint_{\Sigma_0} d\Sigma \xi_\beta n_\alpha \phi_{\alpha\beta}. \tag{17}$$

For the chosen parametrization, the lagrangian is given by

$$\begin{aligned} \mathcal{L}^{(2)} = &- \int_{D_0} d^3x \left\{ \dot{\psi}\left(\rho_0 + A_1\varsigma_1 - \frac{\rho_0}{2}\chi_{\mu\mu}\right) \right. \\ &\left. + m\dot{\phi}_{\alpha\beta}\left[\delta_{\alpha\beta}\left(\frac{\tau_0}{3} + \frac{\rho_0}{2}\varsigma_1\right) - \frac{\tau_0}{3}\left(\chi_{\alpha\beta} + \delta_{\alpha\beta}\frac{1}{2}\chi_{\mu\mu}\right)\right]\right\} \\ &+ \oint_{\Sigma_0} d\Sigma \xi_\alpha n_\beta \phi_{\alpha\beta} - \oint_{\Sigma_0} d\Sigma R_1 \left(\rho_0 \dot{\psi} + \frac{m\tau_0}{3}\dot{\phi}_{\mu\mu}\right) - \mathcal{T}^{(2)}[\psi, \phi_{\alpha\beta}] - \mathcal{E}^{(2)}[\varsigma_1, \chi_{\alpha\beta}, R_1], \end{aligned} \tag{18}$$

where

$$\begin{aligned} \mathcal{T}^{(2)}[\psi, \phi_{\alpha\beta}] = \int_{D_0} d^3x &\left\{ \frac{\rho_0}{2m}(\nabla\psi)\cdot(\nabla\psi) + \frac{2\tau_0}{3}(\partial_\alpha\psi)\left(\frac{1}{2}\partial_\alpha\phi_{\mu\mu} + \partial_\beta\phi_{\alpha\beta}\right) \right. \\ &\left. + \frac{2mG}{15}\left[\left(\frac{1}{2}\partial_\alpha\phi_{\mu\mu} + \partial_\beta\phi_{\alpha\beta}\right)^2 + \frac{1}{6}(\partial_\alpha\phi_{\beta\gamma} + \partial_\beta\phi_{\gamma\alpha} + \partial_\gamma\phi_{\alpha\beta})^2\right]\right\}, \end{aligned} \tag{19}$$

$$\begin{aligned} \mathcal{E}^{(2)}[\varsigma_1, R_1, \chi_{\alpha\beta}] = \int_{D_0} d^3x &\left[\frac{1}{2}A_1\varsigma_1^2 + \frac{\tau_0}{6}\left(\chi_{\alpha\beta}\chi_{\alpha\beta} + \frac{1}{2}\chi_{\mu\mu}\chi_{\nu\nu}\right) - \frac{\rho_0}{2}\chi_{\nu\nu}\varsigma_1 \right. \\ &\left. + \frac{1}{2}\sum_\nu a_\nu \nu(\nu-1)\rho_0^{\nu-2}\left(A_1\varsigma_1 - \frac{1}{2}\rho_0\chi_{\nu\nu}\right)^2\right] + \frac{\sigma}{2R_0^2}\oint_{\Sigma_0} d\Sigma R_1^2[\ell(\ell+1) - 2]. \end{aligned} \tag{20}$$

$$G = g \int \frac{d^3p}{(2\pi\hbar)^3} f_0 \left(\frac{p^2}{2m}\right)^2. \tag{21}$$

The dots over the variational fields stand for time-derivative. By requiring that the action integral is stationary for arbitrary variations of the fields ψ, $\phi_{\alpha\beta}$, ς_1, $\chi_{\alpha\beta}$ and R_1, the equations of motion and boundary conditions are obtained.

We obtain two transverse sound velocities which in the limit $T \to 0$ are identical to the ones derived in refs. [3,4]. While at zero temperature this model leads to two longitudinal sound velocities which were previously obtained at zero temperature in refs. [3,4,6], at a finite temperature an additional longitudinal sound velocity is obtained, so that an additional degree of freedom arises. This is a remarkable result! This happens due to the fact that at finite temperature the profile of the Fermi surface in an infinite medium acquires a finite width. We remark that information concerning the profile of the Fermi surface is contained in the moments of f_0, namely, ρ_0, τ_0 and G, which appear in the effective lagrangian. Therefore, taking into account the fields ψ, ς_1, $\chi_{\alpha\beta}$ and $\phi_{\alpha\beta}$, leads to the appearence of 4 (T=0) or 5 ($T > 0$) sound velocities. As we will see the appearence of a larger number of sound velocities implies also a larger number of eigenmodes.

It may be shown that the eigenmodes fulfill an orthogonality relation. It may also be proved that for electric modes the energy weighted (m_1), the cubic energy weighted and the inverse energy weighted sum rules are fulfilled.

We note that the fluid dynamical model (first sound) considered at zero temperature by Eckart *et al* [7], may be obtained from the present effective lagrangian if we constrain the tensor fields $\phi_{\alpha\beta}$ and $\chi_{\alpha\beta}$ to remain zero. Therefore in this simpler formulation [1] the time-even distribution function (see eq. 12) is constrained to remain spherical in momentum space. In this case the dynamical variables are only R_1, ς_1 and ψ, and only one dispersion relation is obtained. In order to obtain the surface modes it is crucial to allow for the displacement of the surface by means of the variable R_1. Also in such a simple model surface modes are obtained which are proportional to the surface tension and to $A^{-1/2}$.

3. Numerical results

We have considered a potential energy density of the form $u = a_2\rho^2 + a_{2+1/6}\rho^{2+1/6}$, where $a_2 = -\frac{3}{8} \times 3075.8$ MeV fm^3, and $a_{2+1/6} = \frac{1}{16} \times 20216.4$ MeV fm$^{3+\frac{1}{2}}$. We have additionally considered a temperature dependent surface tension. Since the surface of the nucleus becomes more diffuse when the temperature increases, we have assumed that the surface tension σ decreases with temperature according to $\sigma(T) = \sigma(0)(1 - xT^2)$ (see ref. [8], where $\sigma(0) = 1.0$ MeV fm^{-2} and $x = 6 \times 10^{-3}$ MeV^{-2}.

Table 1

T [MeV]	0	1	2	3	4	5
ρ_0 [fm^{-3}]	0.1479	0.1476	0.1465	0.1447	0.1422	0.1389
τ_0 [MeV fm^{-3}]	3.104	3.102	3.096	3.086	3.068	3.041
ς_0 [MeV]	34.97	34.89	34.66	34.25	33.67	32.90
μ [MeV]	-11.76	-11.85	-12.10	-12.52	-13.11	-13.87
$E^{(0)}/A$ [MeV]	-10.79	-10.74	-10.58	-10.31	-9.926	-9.424
$4\pi R_0^2\sigma$ [MeV]	607.0	604.3	596.2	582.6	563.3	538.1
S	0	29.37	58.88	88.66	118.8	149.6

We note that we evaluate quantities involving integrals of the Fermi distribution function in momentum space, such as ρ_0, τ_0 and s_0, using an expansion in powers of T and considering the terms up to T^4. In the present paper we are mainly interested in extending the results of refs. [3,4] to a finite temperature taking into account the effect of the surface tension. We arbitrarily consider a nucleus with A=208. In table 1, we give, for different values of the temperature, the equilibrium values of ρ_0, τ_0, ς_0, μ, $E^{(0)}/A$, of the surface energy and of the entropy for the system with A=208.

For the electric modes we consider the operators

$$D(\mathbf{x}) = r^2 \text{ for } \ell = 0, \quad D(\mathbf{x}) = (r - r^3/R_0^2)Y_{10} \text{ for } \ell = 1, \text{ and } D(\mathbf{x}) = r^\ell Y_{\ell 0} \text{ for } \ell > 1. \tag{22}$$

The results presented in table 2 were obtained using this set of parameters and give us the energies (in MeV) and the percentages of the sum rule m_1 (energy weighted sum rule) corresponding to different electric eigenmodes for a nucleus with A=208.

For $\ell = 0$ and T=0 we observe that 95.15% of the m_1 sum is concentrated 15.87 MeV, while in the simpler model of ref. [1] we obtain 92.00% of the m_1 sum located at 14.03 MeV. At a finite temperature we see that new eigenmodes appear, 0_1^+, 0_4^+, 0_5^+... The new vibrational mode 0_1^+ at T=5 MeV absorves 23.13% of m_1.

For $\ell^\pi = 2^+$, we note that most of the m_1 sum is concentrated in the state 2_2^+, which corresponds to the giant quadrupole resonance, and in the low-lying mode 2_1^+. The low-lying mode 2_1^+ is a surface mode, since $\delta\rho$ is rather close to zero in the interior of the nucleus, and we also note that, from the behaviour of $\nabla \times \mathbf{j}$, it is clear that it has strong transverse components.

Table 2

For $\ell^\pi = 3^-$, the m_1 sum is basically distributed through several modes, but still the two states exhausting a larger fraction of m_1, at T=0 MeV, are 3_1^- which is the low-lying mode, and exhausts 34.10% of m_1 at T=0 MeV, and 3_3^- which exhausts 43.44% of the m_1 sum at T=0 MeV and corresponds to the giant octupole resonance (GOR). It is however very interesting to note that at T=5 MeV this picture has changed considerably.

For $\ell^\pi = 4^+$ and $\ell^\pi = 5^-$ we see that the strength is distributed in a larger number of states being the low-lying mode the one which exhausts a larger fraction of the m_1 sum rule.

	T=0 MeV		T=1 MeV		T=3 MeV		T=5 MeV	
ℓ^π	$\hbar\omega_i$	m_1 [%]	$\hbar\omega_i$	m_1 [%]	$\hbar\omega_i$	m_1 [%]	$\hbar\omega_i$	m_1 [%]
0_1^+	—	—	14.00	1.223	13.62	9.752	12.90	23.13
0_2^+	15.87	95.15	15.85	93.78	15.65	84.05	15.25	68.07
0_3^+	18.95	2.256	18.93	2.396	18.75	3.566	18.16	6.261
0_4^+	--	—	27.75	2.248×10^{-1}	26.62	4.789×10^{-1}	25.13	6.550×10^{-1}
0_5^+	28.14	2.838×10^{-1}	28.38	9.275×10^{-2}	28.46	4.940×10^{-2}	27.87	5.977×10^{-2}
0_6^+	36.83	3.428×10^{-1}	36.79	3.328×10^{-1}	36.39	2.801×10^{-1}	35.02	2.496×10^{-1}
0_7^+	41.29	1.458	41.31	1.427	40.69	1.347×10^{-2}	38.90	1.060×10^{-3}
0_8^+	--	—	41.99	1.857×10^{-2}	41.45	1.334	41.49	1.154
2_1^+	3.473	30.90	3.496	31.43	3.641	35.23	3.810	40.73
2_2^+	11.70	64.19	11.73	63.63	11.99	59.55	12.33	53.00
2_3^+	17.45	2.165	17.43	2.196	17.28	2.525	16.80	3.680
2_4^+	20.54	1.094	20.55	1.114	20.53	1.209	20.40	1.213
2_5^+	21.12	1.002	21.15	9.750×10^{-1}	21.36	8.183×10^{-1}	21.70	6.560×10^{-1}
2_6^+	—	—	25.65	5.393×10^{-4}	24.75	9.638×10^{-5}	23.49	6.407×10^{-3}
2_7^+	27.30	5.717×10^{-2}	27.33	5.717×10^{-2}	27.33	6.421×10^{-2}	26.76	9.119×10^{-2}
3_1^-	2.923	34.10	2.929	34.50	2.960	37.24	2.931	40.95
3_2^-	8.428	2.879×10^{-1}	8.465	2.283×10^{-1}	8.724	6.333×10^{-3}	9.084	2.035×10^{-1}
3_3^-	18.53	43.44	18.55	42 85	18.72	38.08	18.73	27.93
3_4^-	22.80	10.88	22.79	11.15	22.68	13.58	22.37	20.00
3_5^-	25.15	3.847	25.18	3.794	25.43	3.428	25.81	2.916
3_6^-	26.87	5.178	26.89	5.195	26.99	5.300	27.02	5.185
3_7^-	—	—	30.88	2.322×10^{-1}	29.65	1.958×10^{-1}	28.03	3.874×10^{-1}
4_1^+	4.505	33.85	4.518	34.31	4.581	37.45	4.557	41.78
4_2^+	12.26	2.046	12.31	1.894	12.62	1.008	13.07	2.428×10^{-1}
4_3^+	23.36	22.39	23.36	21.90	23.35	18.16	22.96	11.97
4_4^+	27.64	8.859	27.66	9.186	27.78	11.82	27.89	16.63
4_5^+	29.67	17.10	29.70	16.90	29.90	15.22	30.21	11.96
4_6^+	33.45	8.450	33.48	8.281	33.49	4.588	32.13	2.033×10^{-3}
4_7^+	35.38	4.184	35.27	4.224	34.43	7.182	34.10	10.27
4_8^+	—	—	36.56	1.928×10^{-1}	36.21	1.434	35.46	3.949

The states 3_1^-, 4_1^+ and 5_1^- have energies which are approximately proportional to $A^{-1/2}$ as is also the case in the simpler model of ref. [1], but now have lower energies and strong transverse components in the current. However for $\ell^\pi = 2^+$ we were not able to find an analogous state, since the state 2_1^+, as well as the other states, have an energy which is approximately proportional to $A^{-1/3}$.

Au interesting feature of this model is that new states appear at a finite temperature. As the temperature decreases, these states exhaust a smaller fraction of the energy wheighted sum rule. Examples of the new states at finite temperature are 0_1^+, 0_4^+, 0_8^+, 1_8^-, 1_{11}^-, 2_8^+, 3_7^-, 4_8^+ and 5_8^-. At low temperatures, the fractions of the m_1 sum corresponding to these modes, are proportional to T^2. As a consequence, the amplitude of the transition density and of the transition current are proportional to the temperature T. The energies of these states are stable when we consider the limit $T \rightarrow 0$.

4. Conclusions

The present model predicts an appreciable redistribution of transition strength with temperature. This effect agrees, in tendency,with recent experimental findings [9,10], but is admittedly much less dramatic. At T=3 MeV the redistribution of the strength in the calculations, compared with T=0, is sizeable but not very impressive, while in the experiments the redistribution is much larger. This is not surprising because of the artificial discretization of the excitation spectrum due to the constraints imposed on the tryal functions, may tend to hide the redestribution of strength. It is natural to expect that the collision terms, which are not taken into account in the present calculation and in RPA contribute significantly to the actual width.

One of the interesting features of the model we have investigated is that at a finite temperature it provides an additional dispersion relation which leads to a larger fragmentation of the strength. The effect of the appearence of new vibrational modes is also present in RPA microscopic calculations due to the fact the two particle and two hole transitions are now accessible, due to the smooth profile of the Fermi surface at finite temperature, which is not the case at zero temperature, when f_0 is a step function in momentum space. Therefore at a finite temperature T the configuration space in a microscopic calculation is much larger.

The fact that some of these states only exist at finite temperature means they originate at the Fermi surface, being in this case crucial the profile of the Fermi surface with a finite width. The information concerning the profile in momentum space of the equilibrium distribution function f_0 is given by its moments ρ_0, τ_0 and G which are used in the dynamical calculations.

With the present parametrization we are able to desintangle the low-lying modes from the giant resonances.

This work benefitted from computation facilities offered by the Instituto Nacional de Investigação Científica, Lisboa and by the Fundação Calouste Gulbenkian.

References

[1] J. da Providência Jr., Nucl. Phys. A523 (1991) 247.

[2] J. da Providência and C. Fiolhais, Nucl. Phys. A435 (1985) 190.

[3] L. Brito and C. da Providência, Phys. Rev. C32 (1985) 2049; L. Brito, Phys. Lett. 177B (1986) 251; L. Brito, Ph. D. Thesis, Coimbra 1986.

[4] J. da Providência, L. Brito and C. Providência, Nuovo Cimento 87 (1985) 248.

[5] J. P. da Providência and G. Holzwarth, Nucl. Phys. A39? (1983) 59; J.P. da Providência, J. Phys. G13 (1987) 783.

[6] J.P. da Providência, Journal de Physique (1984) C6-333; J.P. da Providência and G. Holzwarth , Nucl. Phys. A439 (1985) 477.

[7] G. Eckart, G. Holzwarth and J.P. da Providência, Nucl. Phys. A364 (1981) 1; J.P. da Providência, J. of Phys. G13 (1987) 481.

[8] C. Guet, Strumberger and M. Brack, Phys. Lett. B205 (1988) 427.

[9] J. J. Gardhoj et al., Phys. Rev. Lett. 56 (1986) 1783.

[10] D. R. Chakrabarty et al., Phys. Rev. C36 (1987) 1886.

On the Gauge Structure of the Time-Dependent Hartree-Fock Manifold

Fumihiko Sakata and Kazuo Iwasawa
Institute for Nuclear Study, University of Tokyo, Tanashi, Tokyo 188, Japan

ABSTRACT

To understand shape coexistence phenomena, an importance of elucidating the constrained Hartree-Fock theory is pointed out. A relation between the adiabatic and diabatic single-particle states, and between their corresponding potential energy surface is discussed within the time-dependent Hartree-Fock manifold. In order to discuss large-amplitude collective motion that involves more than two local minima, a necessity of exploring the gauge degrees of freedom is discussed.

1. Introduction

In this talk, a necessity of exploring the gauge structure of the time-dependent Hartree-Fock (TDHF) manifold is discussed. According to the recent development of the nuclear structure physics, it has been clarified that there often coexist many stationary mean-fields with different geometrical shapes in one nucleus [1]. As an example, the level scheme of ^{152}Dy taken from Ref. [2] is shown in Fig. 1. There are a prolate normal deformed stable mean-field, a prolate super deformed mean-field and an oblate mean-field. When one is only interested in *local* property well explained by an appropriate stationary mean-field, one may independently introduce various mean-fields into one nucleus, without paying any attention to the other mean-fields. When one wants to study *global* property influenced by many stable mean-fields, one has to pay careful attention to mutual relation among many local minima of the potential energy surface (PES). In this case, one is inevitably involved into the following basic theoretical issues; a) Dynamical role of adiabatic and diabatic PES. b) Physical meaning of real- and avoided-crossings of the single-particle orbits. c) Role of the topological (Berry) phase and the gauge degrees of freedom. d) Microscopic meaning of the PES with and without configuration constrained. These problems are specific for the nuclear physics because the stationary mean-fields characterizing different phases are not necessarily orthogonal with one another, unlike the case in the infinite system.

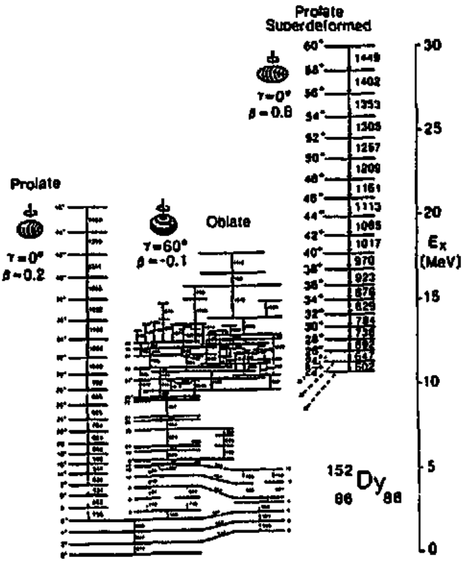

Figure 1. Level scheme of ^{152}Dy taken from Ref. [2]

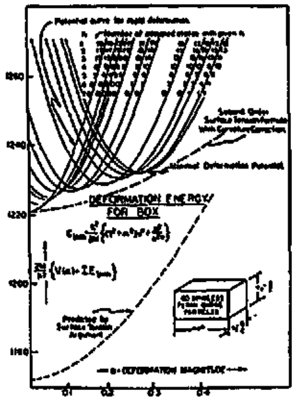

Figure 2 Diabatic and. adiabatic potentials. Taken from Ref.[3].

In §2, we briefly discuss how the adiabatic and diabatic PES are introduced on the basis of the microscopic theory. In §3, the CHF theory is elucidated within the TDHF-coordinate space, which can uniquely specify the PES. It is shown that the CHF equation gives a set of differentiable lines in this space, and every HF state rests on one of these lines. By using the differentiable property of the CHF solutions in the TDHF-coordinate space, one may thus establish a general method to obtain many HF points not accessible by the usual numerical method of the CHF equation. For each HF point, one may introduce a TDHF *local coordinate system* whose origin is located at the corresponding HF point. In §4, it is discussed that these local coordinate systems are related with each other by the singular gauge transformation.

2. Adiabatic and Diabatic Collective Potentials

To understand the structure of the TDHF-manifold that has more than two local minima, one is involved into one of the important problems in the nuclear physics for more than forty years dated back to the early fifties. According to Hill-Wheeler's speculation [3] shown in Fig. 2, the collective motion feels a diabatic potential when its speed is rapid enough. When its speed is sufficiently slow, it feels an adiabatic potential which is an envelop of the diabatic potentials. Thus we start with discussing how to get the adiabatic and diabatic potentials microscopically.

The microscopic derivation of the adiabatic PES is given by the constrained (C-) HF theory or its approximation through the Nilsson-Strutinsky method. The basic equations of the CHF theory is given by

$$\delta < \phi|\hat{H} - \lambda\hat{Q}|\phi >= 0, \quad < \phi|\hat{Q}|\phi >= q \,. \tag{1}$$

Here $|\phi>$ denotes the most general single-Slater determinant. In numerically solving the CHF equation by either using the nonlinear eigenvalue equation or the gradient method, one has been only interested in the most energetically favorable solution (adiabatic requirement) for a given constraining condition $< \phi|\hat{Q}|\phi >= q$. It provides us with the adiabatic PES as well as the adiabatic single-particle states satisfying the non-crossing rule. These treatment is essentially based on the Born-Oppenheimer approximation introduced in the molecular physics. However, an applicability of this approximation to the nuclear system is by no means trivial.

On the other hand, there have been proposed many practical methods called "diabatic recipe," which intend to phenomenologically introduce the diabatic single-particle states satisfying the real-crossing, so as to explain the experimental data. After Hamamoto's suggestion [4] on an inadequacy of the cranking model near the level crossing region in the high spin physics, the diabatic base introduced by keeping the single-particle configuration of intruder orbit unchanged is widely accepted. This base is constructed by using a fairly general method which eliminates a so-called "virtual interaction" appearing near the single-particle level crossing region [5]. In the heavy ion deep inelastic collision, Nörenberg [6] has developed the dissipative diabatic dynamics by introducing the diabatic base, which is defined in such a way that the nodal structure of the single-particle wave functions are kept unchanged during the collision process.

The basic idea of employing the diabatic base is related with an existence of various *intrinsic* states, which may associate with different type of collective motion. Since the different intrinsic states are characterized by different single-particle configurations within the independent particle approximation, and the intrinsic state is supposed to be unchanged within the same band structure of collective excited states, one gets the diabatic base by regarding the single-particle configuration as an approximate good quantum numbers.

Recently, Bengtsson-Nazarewicz [7] pointed out the superiority of diabatic potential over the adiabatic one. When they apply the usual adiabatic Nilsson-Strutinsky method to the collective potential near the ground state in the neutron deficient Pb-isotopes, they get the adiabatic potential which has small shoulder in the oblate region. When they apply the diabatic recipe developed in the high spin physics to this particular case, they obtain three diabatic potentials; the lowest spherical potential, the next lowest oblate potential and occasionally the third lowest prolate potential. As is shown in Fig. 3, they found that the local minimum of the oblate diabatic potential well reproduce the systematic behavior of the

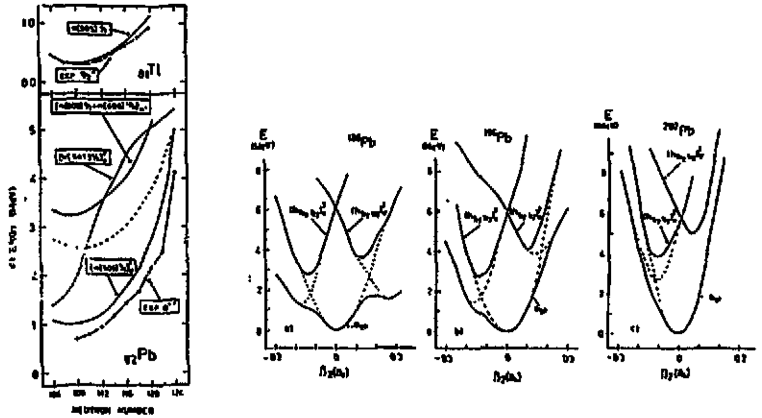

Figure 3. Adiabatic and diabatic collective potentials in the neutron deficient Pb-isotopes. Taken from Ref.[7]

excited 0^+ state in the neutron deficient Pb-isotopes. They clarified that the ACHF solution does not always give a sufficient information on the nuclear excited states, and a particle number of the intruder orbits may play a role of an approximate good quantum number in characterizing the excited states.

3. CHF Solution within the TDHF-Coordinate Space

To study the microscopic meaning of the adiabatic and diabatic PES [8], and to find many stable HF-points without using the diabatic recipe, it is desirable to explore the CHF theory within the TDHF-coordinate space $\{x_{\mu i}\}$, rather than the constraining coordinate space $\{q\}$ where the CHF equation is usually expressed. Here the TDHF-coordinate space is defined as follows. Suppose there is a certain HF state $|\phi_0\rangle$. Then the general time-dependent single-Slater determinant is expressed as

$$|\phi\rangle = \exp(\hat{F})|\phi_0\rangle, \qquad \hat{F} = \sum_{\mu i}(f_{\mu i}\hat{a}^\dagger_\mu \hat{b}^\dagger_i - \text{h.c.}), \tag{2}$$

where $\hat{a}^\dagger_\mu$ and $\hat{b}^\dagger_i$ stand for the particle- and hole-creation operators with respect to $|\phi_0\rangle$, and $\hat{F}$ a general anti-Hermitian one-body operator. Introducing a variable transformation through

$$C_{\mu i} = (f\frac{\sin\sqrt{f^{\dagger}f}}{\sqrt{f^{\dagger}f}})_{\mu i} \ , \tag{3}$$

one gets the TDHF symplectic manifold $\{C_{\mu i}, C^*_{\mu i}\}$. Since the PES is defined within the coordinate space, the TDHF-coordinate space $\{x_{\mu i}\}$ is obtained by means of the coordinate-momentum representation of the TDHF-manifold through

$$x_{\mu i} = \frac{1}{\sqrt{2}}(C_{\mu i} + C^*_{\mu i}), \quad p_{\mu i} = \frac{i}{\sqrt{2}}(C_{\mu i} - C^*_{\mu i}) \ . \tag{4}$$

Here, the dimension of the TDHF-coordinate space is equivalent to a number of the particle-hole pairs, giving a complete set of the coordinates.

By means of the second equation in Eq. (1), on the other hand, the constraining coordinate space $\{q\}$ is given by the expectation values of the constrained operators $\hat{Q}$ put in by hand. Since $|\phi\rangle$ under consideration is expressed by $x_{\mu i}$ alone, the constrain condition is expressed as

$$< \phi|\hat{Q}|\phi >= Q(x_{\mu i}, X^*_{\mu i}) = q \ . \tag{5}$$

The dimension of $\{q\}$ is just a number of constrain operators. Here it should be noticed that $\{x_{\mu i}\}$ uniquely specifies the system, whereas $\{q\}$ does not. Consequently, it is preferable to study the CHF theory within the TDHF-coordinate space.

In the following discussion, we will show that the CHF equation gives *continuous* and *differentiable* lines within $\{x_{\mu i}\}$. For this aim, let us take the simple three-level SU(3) Hamiltonian given by

$$\hat{H} = \hat{H}_0 + \hat{H}_V + \hat{H}_Y, \qquad \hat{H}_0 = \varepsilon_0\hat{K}_{00} + \varepsilon_1\hat{K}_{11} + \varepsilon_2\hat{K}_{22} \ ,$$

$$\hat{H}_V = \frac{V_1}{2}(\hat{K}_{10}\hat{K}_{10} + \text{h.c.}) + \frac{V_2}{2}(\hat{K}_{20}\hat{K}_{20} + \text{h.c.}) \ ,$$

$$\hat{H}_Y = V_3\{\hat{K}_{10}(\hat{K}_{11} + \hat{K}_{22}) + \text{h.c.}\} + V_4\{\hat{K}_{10}(\hat{K}_{12} + \hat{K}_{21}) + \text{h.c.}\}$$

$$+ V_5\{\hat{K}_{20}(\hat{K}_{11} + \hat{K}_{22}) + \text{h.c.}\} + V_6\{\hat{K}_{20}(\hat{K}_{12} + \hat{K}_{21}) + \text{h.c.}\}, \tag{6}$$

$$\text{where} \quad \hat{K}_{ij} \equiv \sum_{m=1}^{N}\hat{c}^{\dagger}_{im}\hat{c}_{jm} \ . \tag{7}$$

There are three N-fold degenerate levels with $\varepsilon_0 < \varepsilon_1 < \varepsilon_2$. We hereafter consider an even N-particle system where the lowest orbit is completely occupied. As a constraining operator $\hat{Q}$, we consider the most general Hermitian one-body operator given by

$$\hat{Q} = Q_{1x}(\hat{K}_{10} + \mathrm{h.c}) + Q_{1y}(\hat{K}_{20} + \mathrm{h.c}) + Q_{2x}\hat{K}_{11} + Q_{2y}\hat{K}_{22} + Q_3\hat{K}_{00} + Q_4(\hat{K}_{21} + \mathrm{h.c}). \tag{8}$$

In the present case, the general single Slater determinant $|\phi\rangle$ is expressed as

$$|\phi\rangle = e^{\hat{F}}|\phi_0\rangle;\ \hat{F} = \sum_{i=1}^{2}(f_i\hat{K}_{i0} - \mathrm{h.c.}),$$

$$|\phi_0\rangle = \prod_{m=1}^{N}\hat{c}_{0m}^{\dagger}|0\rangle,\ (\hat{c}_{im}|0\rangle = 0,\ i = 0,1 \text{ and } 2), \tag{9}$$

and the complete set of canonical variables is given through

$$C_i = \sqrt{N}\frac{\sin\sqrt{\sum_j f_j f_j^*}}{\sqrt{\sum_j f_j f_j^*}} f_i \quad \text{and c.c. ;} \quad (i = 1 \text{ and } 2),$$

$$x_i = \frac{1}{\sqrt{2}}(C_i + C_i^*),\ p_{x_i} = \frac{i}{\sqrt{2}}(C_i - C_i^*);\quad i = 1 \text{ and } 2. \tag{10}$$

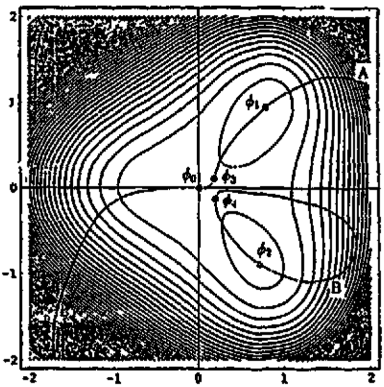

Figure 4. Contour map of $V(x_1, x_2)$

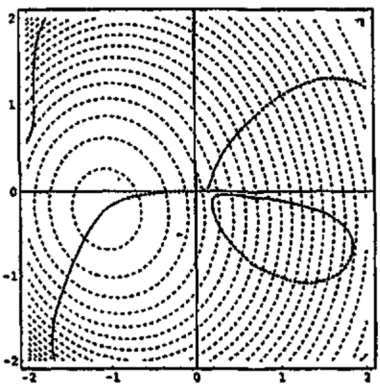

Figure 5. Contour map of $Q(x_1, x_2)$

By applying the CHF theory to the Hamiltonian in Eq. (6) with the constraining operator in Eq. (8), we get the PES $V(x_1, x_2)$ and the constraining operator surface $Q(x_1, x_2)$ in the two dimensional TDHF-coordinate space, which are shown in Figs. 4 and 5. A set of parameters used in our numerical calculation is: $N = 4$, $\varepsilon_0 = 0$, $\varepsilon_1 = 16.4$, $\varepsilon_2 = 18$, $V_1 = V_2 = -16/3$, $V_3 = -4/15$, $V_4 = -2/15$, $V_5 = 0$, $V_6 = -8/3$, $Q_{1x} = 1$, $Q_{1y} = 1/5$, $Q_{2x} = Q_{2y} = 2$ and $Q_3 = Q_4 = 0$. The parameters in the Hamiltonian are chosen in such a way that the system has more than two local minima besides the trivial HF-point $|\phi_0\rangle$, and there exist neighboring two saddle points. Within the region shown in Fig. 4, there are three stable HF-points (denoted by $|\phi_0\rangle$, $|\phi_1\rangle$ and $|\phi_2\rangle$) and two unstable HF-points (saddle points denoted by $|\phi_3\rangle$ and $|\phi_4\rangle$). In a region near to $x^2+y^2=2N$ that is not included in Fig. 4, there are three other unstable HF-points (one saddle and two maxima) which are irrelevant to the following discussion.

In the TDHF-coordinate space, the first CHF equation in Eq. (1) is expressed as

$$\frac{\partial V}{\partial x_1} = \lambda \frac{\partial Q}{\partial x_1}, \quad \frac{\partial V}{\partial x_2} = \lambda \frac{\partial Q}{\partial x_2}. \tag{11}$$

By eliminating the Lagrange multiplier λ from Eq. (11), one obtains

$$0 = \frac{\partial V}{\partial y}\frac{\partial Q}{\partial x} - \frac{\partial V}{\partial x}\frac{\partial Q}{\partial y}, \tag{12}$$

which defines differentiable lines in $\{x_1, x_2\}$. The parameters in the constraining operator are determined in such a way that the solution of Eq. (12) has more than two continuous lines. There are two different differentiable lines, which are denoted by A and B in Fig. 4. Here it should be noticed that the every HF stationary point rests on one of these lines, irrespective to whether it is the local stable point or local unstable saddle point. Equation (11) is then used to get a concrete value of the Lagrange multiplier at each point on the resultant lines.

On the other hand, the second CHF equation given by $Q(x_1, x_2)=q$ gives a many-to-one transformation $\{x_1, x_2\}\rightarrow\{q\}$, i.e., from $\{x_1, x_2\}$ to the constraining coordinate space $\{q\}$. By using the mapping $\{x_1, x_2\}\rightarrow\{q\}$, the potential energies on A and B are transformed into those in the constraining coordinate space shown in Fig. 6. As is seen from Figs. 4 and 6, there are some region where the CHF equation has more than two solutions for one given value of q. To avoid this many-valuedness, one usually picks up the most energetically favorable states by applying the adiabatic requirement so as to obtain an adiabatic PES

Figure 6. Potential energy curves along the branch A and B of Fig. 4 versus $\langle \hat{Q} \rangle$.

$\mathcal{V}_{adia.}(q)$ in $\{q\}$. However, there are no dynamical reason to connect a set of the most energetically favorable states by a single line, because they do not always belong to a single continuous line in Fig. 4. When one do so in Fig. 6, one can only find a small shoulder in $\mathcal{V}_{adia.}(q)$ without knowing a well developed second stable HF-point $|\phi_2\rangle$.

In Fig. 7, the CHF solution for ^{82}Sr with Skyrme interaction is shown [9]. Since we have exploit differentiable property of the CHF solution in the TDHF-coordinate space, we get many local minimum points. It also turned out that the diabatic recipe of eliminating the virtual interaction gives a practical method to jump over from one continuous line to the other near the saddle point of the PES in the TDHF-coordinate space.

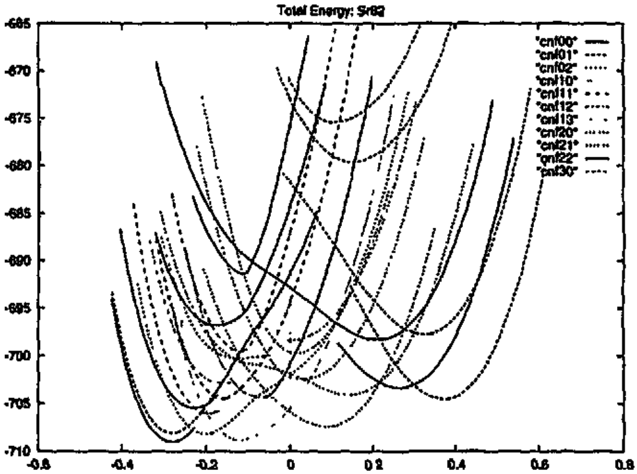

Figure 7. CHF solution for ^{82}Sr with Skyrme interaction.

4. Gauge Structure of the TDHF-Manifold

According to the previous section, one may introduce many stationary HF-points $\{|\phi_i\rangle; i = 0, 1, 2, ...\}$ into the single nucleus. Referring to the HF state $|\phi_0\rangle$, one may introduce a *coordinate neighborhood* denoted by $\{U_{\phi_0}; x, x^*\}$ into the TDHF-manifold. Here U_{ϕ_0} denotes an open set enclosing $|\phi_0\rangle$, and (x, x^*) means a local coordinate system defined in Eq. (4) whose origin is located at $|\phi_0\rangle$. By using another HF state $|\phi_1\rangle$, one may introduce another coordinate neighborhood $\{U_{\phi_1}; z, z^*\}$. When one wants to numerically solve the Hamilton equations of motion so as to get the TDHF-trajectory for a given initial condition, or to get the Poincaré section map, it does not matter what type of local coordinate system one may choose.

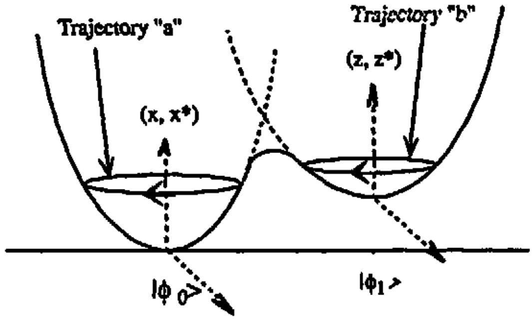

Figure 8. Coordinate neighborhood in the TDHF-manifold.

In order to get analytical information of the adiabatic invariant characterizing each trajectory, according to the nonlinear dynamics, one has to use the *most natural coordinate system*. When one wants to get an analytic information of the adiabatic invariant specific for the trajectory "b" in Fig. 8, it is decisive to use the local coordinate system (z, z^*) rather than (x, x^*). Unlike the classical phase space where the local coordinate systems are related with each other through the simple Galilei transformation, the local coordinate systems (x, x^*) and (z, z^*) in the TDHF-manifold are related with each other through the *singular gauge transformation* [10]. This singularity is coming from a finite degeneracy of the single-particle level, which is specific for the nuclear system. In understanding the structure of the TDHF-manifold, therefore, one has to bear in mind this specific feature of the TDHF-manifold. If one express the TDHF theory by means of the usual single Slater determinant (8), this gauge degrees of freedom appears as a phase factor that has been discussed in connection with the topological phase [11] and with the const.-$\langle\phi|\dot{\phi}\rangle$ method [12].

References

1. J.L. Wood, K. Heyde, W. Nasarewicz, M. Huyse and P. Van Duppen, Phys. Rev. 215 (1992) 101
   S. Åberg, H. Flocard and W. Nasarewicz, Annu. Rev. Nucl. Part. Sci. 40 (1990) 439
2. J.F. Sharpey-Schafer, Prog. Part. Nucl. Phys. 28 (1992) 187
3. D.L. Hill and J.A. Wheeler, Phys. Rev. 89 (1953) 1102
4. I. Hamamoto, Nucl. Phys. A271 (1976) 15
5. R. Bengtsson and S. Frauendorf, Nucl. Phys. A327 (1979) 139
   T. Bengtsson and I. Ragnarsson, Nucl. Phys. A436 (1985) 14
   T. Bengtsson, Nucl. Phys. A496 (1989) 56
6. W. Nörenberg, Phys. Lett. 104B (1981) 107

7. R. Bengtsson and W. Nazarewicz, Z. Phys. A 334 (1989) 269
8. K. Iwasawa, F. Sakata, W. Nazarewicz, T. Marumori and J. Terasaki, INS-Rep.-1036 (June, 1994)
9. K. Iwasawa, F. Sakata and J. Terasaki, In preparation
10. F. Sakata, to appear
11. P. Ring, in Proc. Workshop on Microscopic Models in Nuclear Structure Physics, Oak Ridge (World Scientific, 1988) 298
    A. Bulgac, Phys. Rev. C41 (1990) 2333
12. K.K. Kan, J.J. Griffin, P.C. Lichter and M. Dworzecka, Nucl. Phys. A332 (1979) 109

Transition probabilities in superdeformed bands

A. Dewald[†], R. Krücken[†], P. Sala[†], J. Altmann[†], D. Weil[†], K.O. Zell[†],
P. von Brentano[†], D. Bazzacco[‡], C. Rossi-Alvarez[‡],
R. Menegazzo[‡], G. De Angelis[§], M. de Poli[§]
† Institut für Kernphysik der Universität zu Köln, Köln, Germany
‡ Dipartimento di Fisica dell' Università and INFN Sezione Padova, Padova, Italy
§ INFN, Laboratori Nazionali di Legnaro, Legnaro, Italy

July 1, 1994

Abstract

Intrinsic quadrupole moments Q_0 of the two SD bands in ^{146}Gd could be measured in a DSAM experiment using the GASP spectrometer at Legnaro. It was found that the deformation of the excited SD band is almost identical to that of the first SD band. In two coincidence plunger experiments two and three lifetimes of low lying SD states in ^{192}Hg and ^{194}Pb, respectively could be measured. The determined transitional quadrupole moments Q_t are found to be constant also for the low lying SD states where the decay out of the SD bands already starts. Squared mixing amplitudes of normal deformed states were determined for the spin 10 and spin 12 state in ^{194}Pb and ^{192}Hg respectively.

1. Introduction

Superdeformation is still one of the most interesting subjects in nuclear structure physics. Much experimental and theoretical effort was devoted to it up to now and many superdeformed (SD) bands were found in the A=130, 150 and 190 mass regions. Lifetime information mainly obtained from mean Doppler shift data proved that one deals with deformations of $\beta = 0.35$, $\beta = 0.5$ and $\beta = 0.57$ for the A=130, A=150 and A=190 mass regions, respectively. One still open question in this field is addressed to the sudden decay out of the SD bands. Lifetimes of the lowest SD states where this decay takes place are well suited to learn more about the decay mechanism involved.

The existence of excited SD bands in several nuclei is a prove that the potential minimum which can be attributed to the superdeformation is well developed. Experimental values of quadrupole moments of excited SD bands are known only in a few cases because the excited SD bands are populated much weaker than the first SD bands. Therefore lifetime measurements are important also for these bands in order to determine the deformation and to obtain the experimental data needed for a more profound interpretation of the underlying nuclear structure.

In this paper we want to report on a Doppler shift attenuation (DSA) measurement for the first and the excited SD band in ^{146}Gd and in addition on two recoil distance Doppler shift (RDDS) measurements for ^{192}Hg and ^{194}Pb.

2. DSAM measurement in ^{146}Gd

In ^{146}Gd two superdeformed bands were found first by Hebbinghaus et al. [1] and later by the Chalk-River/Strasbourg-Collaboration [2]. For the first time a bandcrossing in a SD band was discovered by Hebbinghaus et al. [1] in the first SD band. Up to now in the A=150 mass region about 20 SD bands have been found which could be described in a consistent way by Ragnarsson [3] in the framework of standard Nilsson-Strutinsky cranking model calculations neglecting pairing. In his interpretation the bandcrossing in the first SD-band of ^{146}Gd is due to the crossing of the s.p. orbitals $[642, \alpha = -5/2]$ and $[651, \alpha = -1/2]$. In his calculations Ragnarsson obtained also values for the intrinsic quadrupole moments Q_0 which agree quite well with the experimentally deduced ones except for that of the second SD band in ^{146}Gd.

In order to investigate this problem further, we performed a thick target experiment [4] at the GASP spectrometer [5] with the aim to measure the E2 strengths in the two SD bands. The results obtained so far for these quantities are characterized by quite large experimental errors [1, 6].

The experiment was performed at an early stage of the GASP spectrometer with 32 Compton suppressed Ge detectors and with the 80 BGO detectors of the inner ball. Excited states in ^{146}Gd were populated in the $^{122}Sn(^{29}Si, 5n)$ reaction at beam-energies of 155 MeV and 158 MeV. Events were collected if at least 3 BGO detectors and 2 Ge detectors fired. The target consisted of a 0.49 mg/cm^2 ^{122}Sn layer evaporated onto a 8.3 mg/cm^2 Ta backing. In total $1.45 \cdot 10^9$ events were stored on tape. The data was sorted into 49 different matrices, corresponding to the possible combinations of detectors which are grouped into rings in which the detectors are positioned at about the same angle with respect to the beam axis ($32° - 36°, 58° - 60°, 72°, 90°, 108°, 120° - 122°, 144° - 148°$). To separate the 5n channel gates were set on the BGO-sum energy and on a multiplicity ≥ 16. The resulting matrices contained $230 \cdot 10^6$ $\gamma\gamma$-coincidences in the range of 512 to 1536 keV. A second set ($10 \cdot 10^6$ coincidences) was sorted from triple events with an additional gate on the discrete transitions below the 958 keV transition ($29^+ \rightarrow 27^+$) which is the highest known transition coincident with both SD bands. Very pure matrices were sorted from triple events with gates on the transitions of the SD bands.

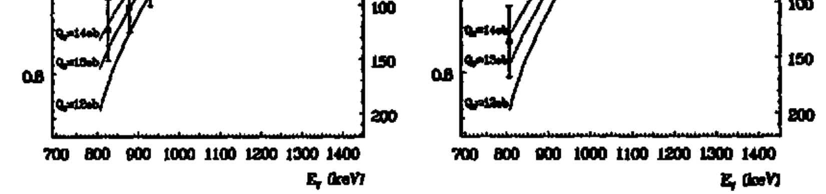

Figure 1: The measured (squares) and calculated F-factors(solid line) of the two SD bands in ^{146}Gd

Table 1: Comparison of quadrupole moments Q_0 of the SD bands in ^{146}Gd.

SD-band	Q_0 from our experiment	calc. Q_0 from [3]	exp. Q_0 from [1, 6])
1.	13.0 ± 1.0 eb	14.7 eb	12 ± 2 eb
2.	13.3 ± 1.5 eb	14.7 eb	8 ± 2 eb

It was possible to determine the quadrupole moments for both SD bands (figure 1), by comparing the measured with the calculated F-factors (fractional Doppler-shift) for several Q_0's. The calculated F-factors were determined from theoretical line shapes calculated with the computer code DSAM [7]. The stopping process was calculated with the program DESASTOP [8] where the electronic stopping is treated according to Ziegler [9] and the nuclear stopping is calculated with the Monte Carlo method assuming nuclear scattering by a screened Thomas-Fermi potential.

Table 1 summarizes the determined quadrupole moments Q_0 from our measurement and those from refs. [1, 3, 6].

For the first SD band our value of Q_0 agrees within the errors with that determined in ref. [6] but it was possible to reduce the experimental error by a factor of two. The value of $Q_0 = 8 \pm 2$ eb for the second SD band given in ref. [6] is in contradiction with the result of this work. The result obtained in the present work agrees quite well with the expected values from the calculations [3].

The obtained Q_0 values correspond to deformations of $\beta = 0.58 \pm 0.03$ and $\beta = 0.59 \pm 0.06$ for the first and second SD band, respectively. For the calculation of the deformation β the relation

$$Q_0 = \frac{3}{\sqrt{5\pi}} Z R_0^2 (\beta + 0.16\beta^2 + 0.2\beta^3) \quad ; R_0 = 1.2 A^{\frac{1}{3}} fm \tag{1}$$

was used.

3. RDDS lifetime measurements

Superdeformed states in ^{192}Hg were simultaneously observed by groups in Berkeley [10] and Argonne [11] and studied later by Lauritsen et al. [12]. DSAM lifetime measurements were performed by Moore et al. [23] In ^{194}Pb the SD band was observed by groups in Bonn [13] and Rutgers [14] and studied later with the NORDBALL and EUROGAM spectrometers [15, 16]. Lifetimes of SD states in ^{194}Pb were measured by Willsau et al. [17] using the DSAM technique.

In the A=190 mass region the SD bands are thought to feed the normal-deformed states at a spin of about 10 $\hbar$ which is relatively low in comparison to the A=150 region, where the SD bands decay into normal deformed states at about 30 $\hbar$. The transition energies are also much lower than those in the A=150 region. Therefore the A=190 superdeformed region offers the possibility to apply the plunger technique to measure individual lifetimes of the lowest states of the SD bands and to overcome the uncertainties of the Doppler shift attenuation method (DSAM).

We performed two RDDS measurements in γ-γ coincidence mode for ^{192}Hg [18] and ^{194}Pb [19] using the GASP spectrometer at the LNL Legnaro. In both experiments the Cologne plunger [20] was used which was especially constructed for γ-γ coincidence measurements. For both measurements all the 40 large volume Compton suppressed Ge detectors of the GASP spectrometer were used. In order to mount the plunger apparatus into the GASP frame it was necessary to dismount six BGO detectors of the inner ball which are positioned closest to the beam line at the beam entrance. An overview of the experimental details is given in table 2.

Table 2: Experimental details for the RDDS experiments on ^{192}Hg and ^{194}Pb.

	^{192}Hg	^{194}Pb
Target:	$0.5 \frac{mg}{cm^2}$ ^{160}Dy	$1.0 \frac{mg}{cm^2}$ ^{162}Dy
	on	on
	$1.3 \frac{mg}{cm^2}$ ^{181}Ta	$1.4 \frac{mg}{cm^2}$ ^{181}Ta
Stopper:	$10 \frac{mg}{cm^2}$ ^{197}Au	$10 \frac{mg}{cm^2}$ ^{197}Au
Reaction:	^{160}Gd(^{36}S, 4n)	^{162}Dy(^{36}S, 4n)
Beam energy:	168 MeV	168 MeV
Recoil velocity:	1.55(4)% c	1.65(5)% c
Used distances:	21, 46 μm	15, 22, 31, 54, 97 μm
Beam current:	6 pnA	6.8 pnA
Recorded events:	$160 \cdot 10^6$/distance	$635 \cdot 10^6$/distance

4. Data analysis

The most important detectors for a RDDS experiment are those furthest away from 90° where shifted and unshifted components of the γ transitions can be separated. For the GASP spectrometer these

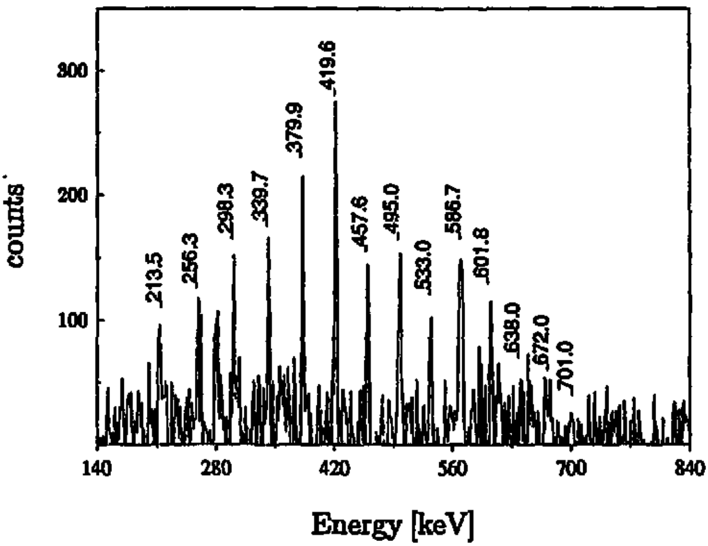

Figure 2: Double gated sum spectrum of the SD band in ^{194}Pb obtained by gating on all combinations of SD transitions. The SD transitions are labeled with their energies.

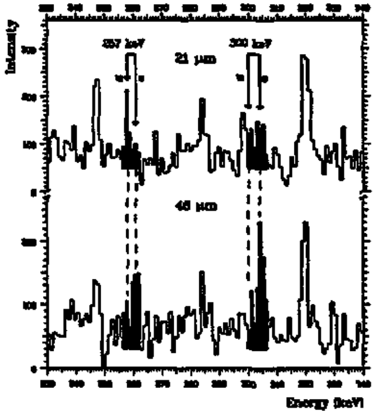

Figure 3: Doppler shifted (s) and unshifted (u) peaks in the coincidence spectra of the SD band in ^{192}Hg gated with the shifted component of all higher SD transitions for both target-to-stopper distances.

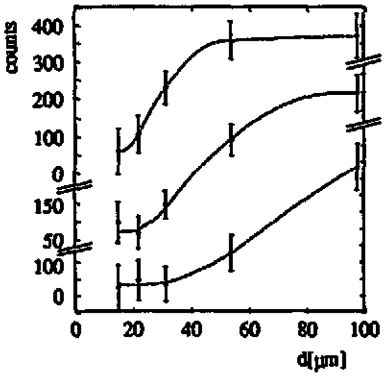

Figure 4: Curves of the shifted components versus target-to-stopper distance for the lowest three transitions in the SD-band in ^{194}Pb (298 keV(top), 256 keV(middle), 213 keV(bottom)). The smooth lines are only supposed to guide the eye.

are 24 detectors positioned at (31.7°, 36.0°), (58.3°, 60.0°), (120.0°, 121.7°) and (144.0°, 143.8°) with respect to the beam axis.

These detectors were grouped into four rings with 6 detectors per ring where the detectors belonging to the same ring are positioned at almost the same angle with respect to the beam. For the analysis the data were sorted into 8 (14) different matrices for ^{192}Hg (^{194}Pb) for each target to stopper distance. The matrices created were combinations of the different rings. In case of ^{194}Pb an additional group of detectors was used which contains all detectors positioned at 72°, 90° and 108°. These detectors could be used only for gating.

Fig. 2 shows the SD band in ^{194}Pb obtained from triples data where double gates of all combinations of the transitions belonging to the SD band were used.

The lifetimes were determined by using the differential decay curve method (DDCM)[21, 22]. According to this method lifetimes can be calculated from RDDS coincidence data by the relation [20]:

$$\tau = \frac{I_{su}^{BA}(x) - \alpha I_{su}^{CA}(x)}{I_{ss}^{BA}(x+\Delta x) - I_{ss}^{BA}(x-\Delta x)} \frac{2\Delta x}{v} \tag{2}$$

where

$$\alpha = \frac{I^{CA}}{I^{CB}} = \frac{I_{su}^{CA} + I_{ss}^{CA}}{I_{su}^{CB} + I_{ss}^{CB}}$$

v is the recoil velocity and x is the target-to-stopper distance. The intensities I_{su}^{BA}, I_{ss}^{BA} are the number of events where the shifted (s) component of a direct feeding transition B is coincident with the shifted (s) or unshifted (u) component of a depopulating transition A of the level of interest. The intensities for indirect feeding I_{su}^{CA}, I_{ss}^{CA} are defined analogously. In the case of ^{192}Hg where data were taken only at two target-to-stopper distances $x_1 = x - \Delta x$ and $x_2 = x + \Delta x$, the intensity $I(x)$ was obtained by averaging: $I(x) = \frac{1}{2}(I(x+\Delta x) + I(x-\Delta x))$.

If only direct feeding transitions are used, equation 2 simplifies to [20]:

$$\tau = \frac{I_{su}^{BA}(x)}{I_{ss}^{BA}(x+\Delta x) - I_{ss}^{BA}(x-\Delta x)} \frac{2\Delta x}{v} \tag{3}$$

Examples of gated spectra which were used to determine the quantities I_{su}^{CA}, I_{ss}^{CA}, I_{su}^{CB} and I_{ss}^{CB} are shown in fig. 3. The shifted components of the γ-transitions depopulating SD states in ^{194}Pb deduced from gated spectra with gates set on the shifted components of transitions above the levels of interest are shown in fig. 4.

Due to the fact that only gated spectra with gates on feeding transitions were used in the analysis all problems concerning sidefeeding are excluded.

5. Results and discussion

5.1. ^{192}Hg

In ^{192}Hg it was possible to determine the lifetimes of two SD states which are depopulated by the 300 keV and the 258 keV transitions, respectively [18]. The values are given in table 3 as well as the B(E2) values and the transitional quadrupole moments Q_t for which the intensities and spin assumptions from Becker et al. [10] were used. For comparison the Q_t values for the higher transitions given by Moore et al. [23] are presented as well as those measured by Willsau et al. [24] in an EUROGAM experiment. Within the error bars the lifetimes determined in the different experiments agree quite well. The data from Moore et al. and Willsau et al. give constant Q_t values in the upper part of

Table 3: Obtained Lifetimes, B(E2) values and transition quadrupole moments Q_t for ^{192}Hg. For comparison the Q_t values by Moore et al. [23] and Willsau et al. [24] are presented.

E_γ (keV)	τ (ps)	B(E2) (W.u.)	Q_t (eb) this work	Q_t (eb) Moore et al. [23]	Q_t (eb) Willsau et al. [24]
258.2	4.4 (1.5)	1950 ($^{+1010}_{-406}$)	19.3 ($^{+5.0}_{-2.5}$)		19.9 ($^{+1.6}_{-1.8}$)
300.4	3.0 (1.7)	1540 ($^{+2010}_{-565}$)	17.2 ($^{+11.2}_{-3.7}$)		19.6 ($^{+1.1}_{-1.1}$)
341.7					20.4 ($^{+2.9}_{-2.2}$)
382.0					20.3 ($^{+5.6}_{-0.9}$)
421.2					
459.5				22.0 ($^{+4.8}_{-2.9}$)	21.1 ($^{+3.1}_{-2.8}$)
496.8				20.6 ($^{+2.7}_{-1.9}$)	19.6 ($^{+1.7}_{-1.1}$)
532.8				20.6 ($^{+4.9}_{-2.9}$)	19.9 ($^{+1.6}_{-1.9}$)
568.0				21.8 ($^{+4.1}_{-2.6}$)	19.8 ($^{+1.9}_{-1.3}$)
602.5				19.1 ($^{+3.0}_{-2.0}$)	17.8 ($^{+1.2}_{-1.2}$)
636.1				19.3 ($^{+4.6}_{-3.0}$)	17.5 ($^{+4.4}_{-1.5}$)
669.0				18.7 ($^{+3.1}_{-2.1}$)	19.5 ($^{+2.9}_{-2.3}$)
700.9				17.2 ($^{+6.7}_{-2.8}$)	17.0 ($^{+1.8}_{-2.0}$)

Table 4: Obtained lifetimes, B(E2) values and transition quadrupole moments Q_t in SD transitions in ^{192}Hg and ^{194}Pb.

E_γ (keV)	I ($\hbar$)	τ (ps)	B(E2) (10^3 W.u.)	Q_t (eb)
213	(10)	8.6 ($^{+3.2}_{-3.2}$)	2.0 ($^{+1.5}_{-0.4}$)	19.7 ($^{+7.5}_{-2.0}$)
256	(12)	3.5 ($^{+2.0}_{-1.5}$)	2.9 ($^{+1.7}_{-1.2}$)	23.6 ($^{+7.3}_{-5.0}$)
298	(14)	2.6 ($^{+1.5}_{-1.0}$)	2.0 ($^{+1.1}_{-0.8}$)	19.6 ($^{+5.7}_{-3.9}$)

the SD band. In the lower part of the SD band where the decay out of the band already starts the measured Q_t values are almost the same as in the upper part. This constancy of Q_t throughout the complete SD band clearly proves that the band has a dominant SD configuration down to the levels where the decay out takes place. From a mean quadrupole moment Q_o=19.6(20) we determine a deformation of β=0.56(6)

5.2. ^{194}Pb

In ^{194}Pb it was possible to determine the lifetimes of three low lying SD states. The results are given in table 4 in addition with the corresponding reduced E2 transition probabilities and the transitional quadrupole moments Q_t. For comparison the Q_t values for the higher lying SD levels given by Willsau et al. [17] are also presented. As in the case of ^{192}Hg the Q_t values are constant within their statistical errors and we can determine a mean quadrupole moment of Q_0=20.0±1.3 eb which corresponds to a deformation of β = 0.57(4). Experimental intensities and spin assumptions used in the calculations were taken from ref. [15].

6. Study of the decay out of the SD bands

The sudden decay out of the SD bands is one of the still not fully understood problems of the phenomenon of superdeformation. In ^{192}Hg the decay out starts at a spin 12 state with an intensity of

Table 5: Lifetimes τ, transition quadrupole moments Q_t, intensities N_{out} and obtained probability for the decay out of the SD bands in ^{194}Hg and ^{194}Pb. * - constant Q_t was assumed

Nucl.	J [$\hbar$]	τ [ps]	Q_t [eb]	N_{out}	λ_{out} [ps^{-1}]
^{194}Pb	10	8.6 (3.2)	19.7($^{7.5}_{2.0}$)	0.22	0.025 ($^{11}_{11}$)
	8			0.57	0.035 ($^{8}_{8}$)*
^{192}Hg	12	4.4 (1.5)	19.3($^{5.0}_{2.5}$)	0.16	0.05 ($^{2}_{2}$)
	10			0.95	1.5($^{2.6}_{0.6}$)*

Table 6: Examples of squared mixing amplitudes for the spin 10 and 12 SD states in ^{194}Pb and ^{192}Hg, respectively. The corresponding λ_n^{E1}-values are also given.

Nucl.	E [MeV]	λ_n^{E1} [ps^{-1}]	a_n^2
^{194}Pb	2.5	3.8	0.007
	4.5	40	0.0006
^{192}Hg	2.5	2.2	0.023
	4.5	32	0.0016

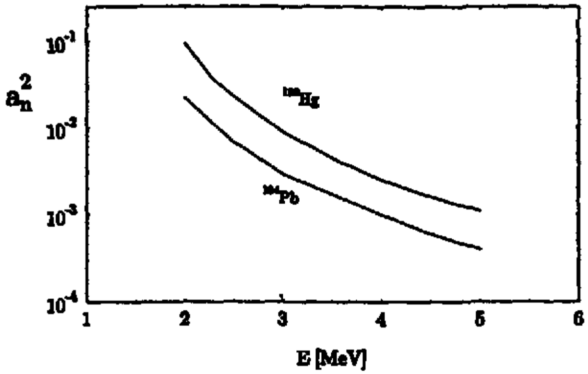

Figure 5: Squared mixing amplitudes a_n^2 of the spin 10 SD state in ^{194}Pb (dashed line) and the spin SD 12 state in ^{192}Hg (solid line) as a function of excitation energy above yrast.

16% of the total SD band intensity and already at the spin 10 state it has reached 95%. In ^{194}Pb the situation is quite similar as can be seen in table 5. As already mentioned above from the measured lifetimes of the spin 12 state in ^{192}Hg and for the spin 10 state in ^{194}Pb the same deformation can be deduced as for states in the upper parts of the corresponding SD bands. Unfortunately up to now there is no lifetime information on the lowest observed levels in these SD bands where the decay out is the dominant part of the level depopulation. The constancy of the deformation in the whole SD bands indicates that there is no strong change in the underlying nuclear structure which supports the model proposed by Vigezzi et al. [28] for the decay out of the SD bands. In this model it is assumed that the decay is caused by the mixing of the SD states with normal deformed (ND) states. Because of the high excitation energy of the SD states at which the decay out occurs the mixing with ND states is considered to be very complex and a statistical treatment of it is justified. An other consequence of the relatively high excitation energy of the admixed ND states is that their decay is dominated by E1 transitions. E2, M1 or higher multipole transitions can be neglected. The pure SD states are assumed to decay via strong collective E2 transitions because the level density in the potential minimum which can be attribuced to the superdeformation is too small for a significant statistical decay. For the following discussion it is useful to decompose the wave function of a real SD state into two parts: a superdeformed one (S) with an amplitude a_S and a normal deformed part (N) with an amplitude $a_N = \sqrt{1-a_S^2}$. The decay out probability λ_{out} is equal to the transition probability $\lambda_{(N\rightarrow norm)}$ from the normal deformed component (N) of the wave function to pure normal deformed states ($norm$), and can be described as:

$$\lambda_{out} = \lambda_{(N\rightarrow norm)} \simeq (1-a_S^2)\cdot\lambda_n^{E1} \tag{4}$$

where λ_n^{E1} is the statistical E1 transition probability.

From the observed branching ratios and the level lifetimes one can determine the maximum ND admixtures of $a_n^2(12) \leq 0.23$ for ^{192}Hg and $a_n^2(10) \leq 0.18$ for ^{194}Pb without any further assumption of the decay mechanism involved. From the experimental values λ_{out} which are given for ^{192}Hg and ^{194}Pb in table 5 it is possible to determine directly the mixing amplitudes a_n by using equation 4 if the corresponding statistical E1 transition probabilities λ_n^{E1} are known. We calculated the quantities λ_n^{E1} within a statistical model according to:

$$\lambda_n^{E1} = \xi_{E1} \cdot \int_{E_{yr}}^{U} \frac{\rho(U - E_\gamma)}{\rho(U)} \cdot f_{GDR}(E_\gamma) \cdot E_\gamma^3 \quad dE_\gamma.$$

For the level density $\rho(U)$ the Fermi-gas approximation from ref. [25](see eq.(4)in this ref.) was applied. A pairing gap at the spin 10 state of $2\Delta_{10} = 1$MeV and a level density parameter of $a = 22.4 MeV^{-1}$ were used. ξ_{E1} is the E1 strength fitted to neutron resonance data [26], E_{yr} is the energy of the yrast state, U is the excitation energy of the decaying state. f_{GDR} is the strength function of the Giant Dipole Resonance (GDR) for which the parameters were taken from ref. [27]. The E1 transition probabilities λ_n^{E1} for ^{192}Hg and ^{194}Pb were calculated in the energy range of 2.5–4.5 MeV above the yrast energy. The results for the limiting energies are presented in table 6 as well as the corresponding squares of the mixing amplitudes a_n^2. Fig.6 shows the calculated ND mixing components a_n^2 as a function of the excitation energies above yrast of the mixing ND levels.

If one assumes constant transitional quadrupole moments Q_t for the ($8 \rightarrow 6$) and ($10 \rightarrow 8$) transitions in ^{194}Pb and ^{192}Hg, respectively, it is possible to determine the corresponding decay out intensities if the E1 transition probabilities λ_n^{E1} are known. Using our calculated λ_n^{E1} values it is possible to obtain the experimental decay out intensities for the corresponding states if we assume the SD ground state of ^{194}Pb (^{192}Hg) to be at an excitation energy of 6.0 MeV (6.2 MeV).

7. Summary and conclusion

In a DSAM measurement for ^{146}Gd it was possible to determine intrinsic quadrupole moments Q_0 for the first as well as for the excited SD band. The result for the first SD band is in agreement with a previously published result. Here the experimental error could be reduced by a factor two. For the excited SD band we measured 13.3(15) eb which is in contradiction with the value of 8(2) eb given in ref.[6]. The experimental values obtained in the present work are in agreement with those calculated by Ragnarsson [3].

In two coincidence plunger experiments we could determine two and three lifetimes of low lying SD states in ^{192}Hg and ^{194}Pb, respectively. The lifetimes show that the deformation does not change even at states where one observes already a decay out of the SD bands. Following a model for the decay out of the SD bands [28] we determined squares of mixing amplitudes a_n^2 of admixed ND states in the lowest observed SD states. If E1 transition probabilities λ_n^{E1} are used which were calculated applying a statistical model we obtained mixing components $0.0006 \leq a_n^2 \leq 0.006$ and $0.0016 \leq a_n^2 \leq 0.023$ for the spin 10 state in ^{194}Pb and for the spin 12 state in ^{192}Hg, respectively. It is also possible to describe in both nuclei the observed SD decay out intensities in a consistent way if the SD ground states are assumed to lie at an excitation energies of 6.2 MeV in ^{194}Pb and 6.0 MeV in ^{192}Hg.

Acknowledgements

The members of the Cologne group particularly want to thank INFN for the kind hospitality and the possibility to use the GASP spectrometer and the Legnaro XTU. This work has been funded by the German Federal Minister for Research and Technology (BMFT) under contract number 06OK602 I and by the Istituto Nazionale di Fisica Nucleare (INFN).

References

[1] G. Hebbinghaus et al., Phys. Lett. B240 (1990) 311

[2] V.P. Janzen et al., Proceedings of the International Conference of High-Spin Physics and Gamma-Soft Nuclei, World Scientific (1991) 225

[3] I. Ragnarsson, Nucl. Phys. A557 (1993) 167c

[4] J. Altmann, A. Dewlad, D. Weil, P. Sala, M. Luig, S. Albers, M. Eschenauer, K.O. Zell, P. von Brentano, W. Gast, R.M. Lieder, D. Bazzacco, C. Rossi-Alvarez, M. de Poli, G. Maron, J. Rico, G. Vedovato, N. Blasi, G. lo Bianco, to be published

[5] D. Bazzacco, in: Proc. Intern. Conf. on Nuclear structure at high angular momentum, (Ottawa, 1992), Vol.2, Proceedings AECL 10613

[6] K. Strähle et al., Proc. Int. Conf. on Nuclear Structure at High Angular Momentum, Ottawa, 1992, Volume I, contributions, AECL 10613, p. 15

[7] P. Petkov, Program DSAM, unpublished

[8] G. Winter, Program DESASTOP, unpublished

[9] J.F. Ziegler, J.P. Biersack, U. Littmark, *The stopping and range of ions in solids.* Vol. 1, Pergamon Press (1985)

[10] J.A. Becker et al., Phys. Rev. C41 (1990) R9

[11] D. Ye et al., Phys. Rev. C41 (1990) R13

[12] T. Lauritsen et al., Phys. Lett. B279 (1992) 239

[13] K. Theine et al., Z Phys A336 (1990) 11

[14] M.J. Brinkmannet al, Z. Phys. A336 (1990) 115

[15] W. Korten et al., Z. Phys A344 (1993) 344

[16] F. Hannachi et al., Nucl. Phys. A557 (1993) 75c

[17] P. Willsau et al., Z. Phys. A344(1993) 351

[18] A. Dewald, R. Krücken, P. Sala, J. Altmann, O. Stuch, P. von Brentano, D. Bazzacco, C. Rossi-Alvarez, G. de Angelis, J. Rico, G. Vedovato, G. lo Bianco, J. Phys. G 19 (1993) L177

[19] R. Krücken, A. Dewlad, P. Sala, C. Meier, H. Tiesler, J. Altmann, K.O. Zell, P. von Brentano, D. Bazzacco, C. Rossi-Alvarez, R. Burch, R. Menegazzo, G. de Angelis, G. Maron, M. de Poli, submitted to Phys. Rev. Lett.

[20] A. Dewald et al., Nucl. Phys. A545 (1992) 822

[21] A. Dewald, S. Harrisopulos, P. von Brentano, Z. Phys. A334 (1989) 163

[22] G. Böhm, A. Dewald, P. Petkov, P. von Brentano, Nucl. Instr. Meth. A329 (1993) 248

[23] E.F. Moore et al., Phys. Rev. C64 (1990) 3127

[24] P. Willsau et al. , submitted to Nucl. Phys. A

[25] A. Mengoni and Y. Nakajima, Jour. Nucl. Sience and Techn. 31 (1994) 151, and priv. comm.

[26] S.F. Mughabghab, *Neutron Cross Sections* vol 1b, Academic P ress Inc., Orlando (1984)

[27] S.S. Dietrich and B.L. Berman, At. Dat. Nucl. Dat. Tab. 38 (1988) 199

[28] E. Vigezzi, R.A. Broglia, T. Døssing , Nucl. Phys. A520 (1990) 179c

MICROSCOPIC STRUCTURE OF HIGH-SPIN SPECTRA OF NUCLEI IN THE $Z\sim 42\div 45$ AND $N\sim 46\div 49$ REGION

A.V.Afanasjev[1,2], I.Ragnarsson[1]

[1]*Department of Mathematical Physics, Lund Institute of Technology Box 118, S-22100, Lund, Sweden*
[2]*Nuclear Research Center, Latvian Academy of Sciences LV-2169, Salaspils, Miera str.31, Latvia*

ABSTRACT

The non-collective and collective high-spin configurations in selected $A\sim 90$ ($Z=42\div 45$, $N=46\div 49$) nuclei are analysed within the configuration-dependent shell-correction approach using the cranked Nilsson potential. With this method, various high-spin features of nuclei, such as shape coexistence, shape changes, band termination and superdeformation are studied along the yrast line. We concentrate on the $^{89}_{43}Tc_{46}$ nucleus as a representative example, while other nuclei are treated in a more schematic way.

1. INTRODUCTION

During last few years a lot of experimental data at medium-high spin ($I\leq 20\hbar$) of nuclei with $Z\sim 42+45$ and $N\sim 46+49$ have been obtained [1-10]. These nuclei belong to region in which superdeformed shapes were predicted at high-spin $I\sim 40\hbar$ [11]. Considering the fast development of experimental devices, a detailed theoretical investigation of the high-spin spectra of nuclei in this region has been performed within the configuration-dependent shell-correction approach [12] using the cranked Nilsson potential.

In the region under study, spherical single-particle states at low spin should coexist with deformed rotational states at high spin. These features can be seen, for example, in the chain of zirconium isotopes ($Z=40$) [13,14,15], where for $N\leq 44$ and $N\geq 56$ collectivity is ubiquitous with clear band structures of enhanced E2 transitions at low spin values. For $46\leq N\leq 54$ on the other hand, there is almost no band structure and the quadrupole matrix elements show little or no enhancement over the single-particle values, since the spherical neutron ($N=50$) shell closure dominates and collectivity dissapears entirely. However, with increasing spin values deformation driving orbitals become occupied and thus, collective rotational bands are formed in the yrast region. A more striking example is the tin isotopes. It is now well known that the even nuclei ^{106}Sn,^{108}Sn [16,17] close to the doubly magic $^{100}_{50}Sn_{50}$ possess rotational states at high spin. In tin isotopes these rotational bands result from two-particle-two-hole (2p-2h) excitations across the proton closed shell at $Z=50$.

The microscopic structure of the nuclei in the $A\sim 90$ mass region is primarily determined by the $1g_{9/2}$, $2p_{1/2}$, $1f_{5/2}$, $2d_{5/2}$ and $1g_{7/2}$ orbitals. In this region the Nilsson diagrams (see, for example, figs.2 and 3 in ref.[12]) show that the main quadrupole-driving orbitals are the strongly down-sloping ones emerging from $d_{5/2}$, $g_{7/2}$ and $h_{11/2}$ subshells and the upsloping ones emerging from the $p_{1/2}$ and $f_{5/2}$ subshells.

The single-particle level density in the $A\sim 90$ nuclei is noticeably lower than that in e.g. the $A\sim 100$ mass region. Indeed, with the number of single-particle states per unit energy about a factor of two smaller, the single-particle gaps and, more generally, the shell-structure effects manifest themselves in the A$\sim$90 nuclei in a comparatively dramatic way. In particular, they give rise to a strong shape variation as a function of both particle number and spin and lead to pronounced shape-coexistence effects.

Fig.1. The nuclei of A$\sim$90 region studied in the present article.

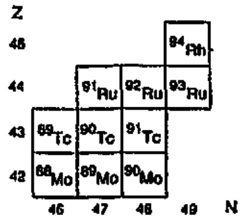

In this article we have investigated in detail the shape transitions and shape coexistence, together with the related band-termination effects in selected A$\sim$90 nuclei (see fig.1) within the configuration-dependent shell-correction method. This method of calculating high-spin states of nuclei within the Nilsson-Strutinsky framework is presented and discussed in detail in ref.[12]. A short description and some specific features of this method used in our calculations is presented in section 2. We concentrate mainly on the $^{89}_{43}Tc_{46}$ nucleus as a representative example. That is done in section 3. In fact, because of similarities between the proton and neutron single-particle spectra some of the results of this study can also be used for a qualitative discussion of several other neutron-deficient nuclei of region under study. For this nucleus, we discuss in detail all the configurations which appear near the yrast line. Special attention is given to the single-particle structure in different spin regions. The other nuclei are treated in a more schematic way (sect.4). The total tendency of development of collectivity along the yrast line as a function of Z and N in the nuclei of interest is also discussed in section 4.

2. THE CONFIGURATION-DEPENDENT SHELL-CORRECTION APPROACH AT HIGH-SPINS

Since the configuration-dependent shell-correction approach was discussed in detail in refs.[12,16], we only outline in brief this approach and the special features used in our calculations. In this approach, the virtual crossings between the single-particle orbitals are removed, and, as a result the total single-particle energy and spin for protons and neutrons within a band can be treated as smooth functions of ω. The total energy of a rotating nucleus is expressed by a sum

$$E_{tot} = E_{LD} + \delta E_{shell} \tag{1}$$

where the first term denotes the deformation dependent parts of the liquid-drop model energy,

$$E_{LD} = E_{surf} + E_{Coul} + E_{rot} \tag{2}$$

while the quantal (shell) correction is given by δE_{shell} and calculated according to the Strutinsky method. The last term in eq.(2) is usually assumed to have the form

$$E_{rot} = \frac{\hbar^2}{2J_{rig}} I^2 \tag{3}$$

where the rigid-body moment of inertia J_{rig} is calculated with a sharp nuclear surface and a radius parameter $r_0 = 1.2$ fm.

When calculating the shell correction term, one starts by diagonalizing the single-particle cranking Hamiltonian

$$H^\omega \psi_\nu^\omega = e_\nu^\omega \psi_\nu^\omega; \quad H^\omega = H - \omega j_x \tag{4}$$

where the eigenvalues e_ν^ω are referred to as the single-particle energies in the rotating system (or the routhians). In the present work, we have used the cranked Nilsson hamiltonian with standard values [12] for the parameters κ, μ. The shell energy is then calculated as

$$\delta E_{shell} = \delta E_{shell}(\{\psi_\nu^\omega\}) = \sum_{\nu \in conf} e_\nu - \sum_{\nu = 1} e_\nu n_\nu^\omega \tag{5}$$

where e_ν are the energies in the laboratory system $e_\nu = \langle \psi_\nu^\omega \mid H \mid \psi_\nu^\omega \rangle$ and n_ν^ω are the Strutinsky occupation coefficients. The shell energy is defined for a specific configuration and for a fixed spin I in the one-dimensional cranking approximation, $I = I_x$, where

$$I_x = \sum_{\nu \in conf} \langle j_x \rangle_\nu \tag{6}$$

In the cranking model hamiltonian, parity π and signature α are good quantum numbers for reflection symmetric nuclear system. Different high-spin states and rotational bands are formed by filling different orbitals of the rotating potential. Many-particle configurations can then be specified by the total parity π_{tot} and total signature α_{tot} as

$$\pi_{tot} = \prod_{occ} \pi_i, \quad \alpha_{tot} = \sum_{occ} \alpha_i \ mod\ 2 \tag{7}$$

Keeping track of π_{tot} and α_{tot} means that we separate the total yrast line of the nucleus into four yrast lines, characterized by their parity and signature. In our formalism, the diagonalisation is carried out with the eigenstates of the rotating oscillator as basis states. We then make the approximation to neglect matrix elements (mainly from the ε_4 -deformation) between different N-shells (N_{rot} -shells). This has the great advantage that we can easily keep track of the number of particles in each N-shell. In the present application, we have furthermore identified the high-j orbitals after the diagonalisation. Thus, for example in the N=4 shell, we can distinguish between the particles of (approximate) $g_{9/2}$ character and the particles belonging to other subshells. This is necessary when specifying the number of particles excited across the N=50 (or Z=50) shell.

Because pairing correlations are neglected, it is not meaningful to make any detailed comparison between theory and experiment for very low spins. It is still not well understood for which spins the pairing energies are more or less unimportant. However, it is clear that only in special cases the yrast deformations are essentially affected by pairing [19].The calculations of high-spin spectra of neighbouring Sr-Kr region [18] show that above I=20$\hbar$ the results obtained with and without pairing are in general similar. Calculations carried out for nuclei of other regions show that the high-spin spectra calculated without inclusion of pairing can be considered as realistic for spin above 20$\hbar$. For the nuclei under study, one particle-one hole excitations become yrast typically for spins I~15+20$\hbar$ so we consider all yrast configurations from I~13-14$\hbar$. The highest spin considered in these calculations come close to 60$\hbar$ that corresponds to the spin values of the rotating liquid drop model at which the fission barrier is not smaller than 8 MeV [20].

We have used wave functions without any additional symmetrization. However, in case of an odd-odd nucleus, a more realistic basis function would be a product of the type $\Psi_p \Psi_n$ so that symmetric and antisymmetric combinations of these functions could be considered. Other limitation is the exclusion of n-p interaction. For these reasons, in case of the odd-odd nuclei, we will focus only on the competition between aligned and collective configurations and look at overall trends within the yrast bands.

3. HIGH-SPIN YRAST CONFIGURATIONS IN $^{89}_{43}Tc_{46}$

In the yrast configurations of $^{89}_{43}Tc_{46}$ there is generally competition between two main coupling schemes: a non-collective rotation around the oblate (γ=60°) or prolate (γ=-120°) symmetry axis and a collective rotation both for triaxial ($\gamma \sim 30°$) and for prolate or near-prolate ($\gamma \sim 0°$) shapes. The configurations which contribute to yrast line are displayed in figs. 2 and 3 as the functions of total energy minus average liquid-drop contribution. The assignments of these configurations relatively to a spherical "core" $^{90}_{40}Zr_{50}$ are presented in fig.4 and in table 1.

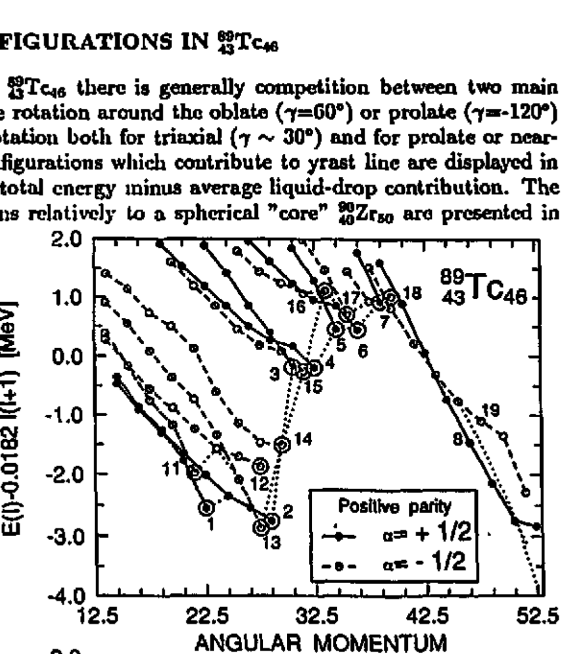

Fig.2. Calculated configurations of positive parity in the yrast region of $^{89}_{43}Tc_{46}$. The energies are given relative to a smooth liquid-drop expression $\frac{\hbar^2}{2J_{rig}} I(I+1)$, where the moment of inertia parameter $\frac{\hbar^2}{2J_{rig}}$=0.0182 MeV. The bands with labels 1÷9 (solid line, filled circles) correspond to the α=+1/2 signature, while the bands with labels 11÷19 (dashed line, open circles) - to the α=-1/2 signature. The configuration assignments are given relative to a $^{90}_{40}Zr_{50}$ core in fig.4 and in table 1. The aligned states (band terminations) are encircled. The dotted lines are used for keeping track of yrast lines of different signature.

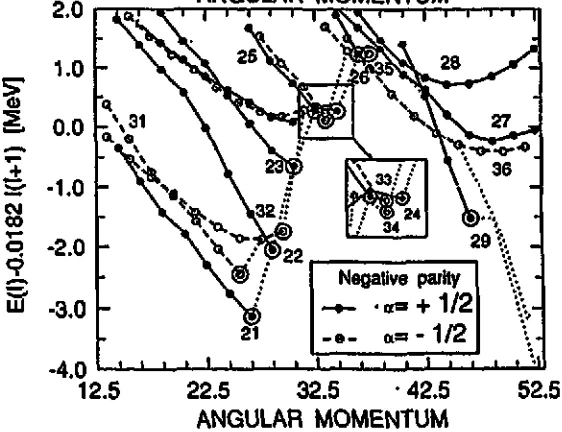

Fig.3. Similar to fig.2, but for negative parity configurations. The following notations are used: the labels 21÷29 for α=+1/2 configurations, while the labels 31÷36 for α=-1/2 configurations.

	$\nu1$	$\nu2$	$\nu3$	$\nu4$	$\nu5$	$\nu6$	$\nu7$	$\nu8$	$\nu9$
$\pi1$	$\boxed{11}$	$\boxed{1}$							
$\pi2$	31	21		$\boxed{23}$					
$\pi3$		13	$\boxed{3}$		24		17	22	
$\pi4$	12	2	$\boxed{15}$	$\boxed{4}$	33	25	6	32	
$\pi5$		$\boxed{34}$		$\boxed{35}$					$\boxed{18}$
$\pi6$		$\boxed{5}$							
$\pi7$					16			14	
$\pi8$				$\boxed{26}$					$\boxed{7}$

	$\nu10$	$\nu11$	$\nu12$	$\nu13$
$\pi9$	$\boxed{29}$			
$\pi10$		8		
$\pi11$		19		
$\pi12$		36		
$\pi13$			27	28

Fig.4. The configuration assignments of the bands contributing to yrast line are given (see also table 1). The aligned configurations terminating at spherical and near-spherical deformations (ϵ_2 ≤ 0.1) are shown on left side, while the strongly deformed configurations (ϵ_2 ≥ 0.25) are presented on right side. The aligned configurations which terminate on the oblate ($\gamma = 60^\circ$) axis are squared. Other aligned configurations shown on left side terminate on the prolate ($\gamma = -120^\circ$) axis.

Table 1. The notation of proton $\pi1 \div \pi13$ and neutron $\nu1 \div \nu13$ configurations assigned relatively to a $^{90}_{40}Zr_{50}$ core

Proton configurations
$\pi1 = \pi(g_{9/2})^{3}_{10.5}$
$\pi2 = \pi[(g_{9/2})^{4}_{12}(f_{5/2})^{-1}_{2.5}]_{14.5}$
$\pi3 = \pi[(g_{9/2})^{5}_{12.5}\ (p_{1/2}f_{5/2})^{-2}_{3}]_{15.5}$
$\pi4 = \pi[(g_{9/2})^{5}_{12.5}(f_{5/2})^{-2}_{4}]_{16.5}$
$\pi5 = \pi[(g_{9/2})^{4}_{12}(f_{5/2})^{-2}_{4}(h_{11/2})^{1}_{5.5}]_{21.5}$
$\pi6 = \pi[(g_{9/2})^{5}_{12.5}(p_{1/2}f_{5/2})^{-3}_{4.5}(h_{11/2})^{1}_{5.5}]_{22.5}$
$\pi7 = \pi[(g_{9/2})^{6}_{12}(p_{1/2}f_{5/2})^{-3}_{4.5}]_{16.5}$
$\pi8 = \pi[(g_{9/2})^{4}_{12}(p_{1/2}f_{5/2})^{-2}_{3}(h_{11/2})^{1}_{5.5}]_{20.5}$
$\pi9 = \pi[(g_{9/2})^{4}_{12}\ (g_{7/2})^{1}_{3.5}\ (p_{1/2})^{-2}_{0}\ (f_{5/2})^{-1}_{1.5}\ (h_{11/2})^{1}_{5.5}]_{22.5}$
$\pi10 = \pi(g_{9/2})^{5}\ (d_{5/2}g_{7/2})^{2}\ (p_{1/2}p_{3/2}f_{5/2})^{-6}\ (h_{11/2})^{2}$
$\pi11 = \pi(g_{9/2})^{6}\ (d_{5/2}g_{7/2})^{1}\ (p_{1/2}p_{3/2}f_{5/2})^{-6}\ (h_{11/2})^{2}$
$\pi12 = \pi(g_{9/2})^{6}\ (d_{5/2}g_{7/2})^{2}\ (p_{1/2}p_{3/2}f_{5/2})^{-6}\ (h_{11/2})^{1}$
$\pi13 = \pi[3]^{-4}\,[4]^{6}\,[5]^{1}$
Neutron configurations
$\nu1 = \nu(g_{9/2})^{-4}_{11}$
$\nu2 = \nu(g_{9/2})^{-4}_{12}$
$\nu3 = \nu[(g_{9/2})^{-5}_{12.5}(d_{5/2})^{1}_{2.5}]_{15}$
$\nu4 = \nu[(g_{9/2})^{-5}_{12.5}\ (g_{7/2})^{1}_{3.5}]_{16}$
$\nu5 = \nu[(g_{9/2})^{-4}_{12}(d_{5/2})^{1}_{2.5}(f_{5/2})^{-1}_{2.5}]_{17}$
$\nu6 = \nu[(g_{9/2})^{-4}_{12}(g_{7/2})^{1}_{3.5}(f_{5/2})^{-1}_{2.5}]_{18}$
$\nu7 = \nu[(g_{9/2})^{-4}_{12}(f_{5/2})^{-1}_{2.5}(h_{11/2})^{1}_{5.5}]_{20}$
$\nu8 = \nu[(g_{9/2})^{-3}_{10.5}(f_{5/2})^{-1}_{2.5}]_{13}$
$\nu9 = \nu[(g_{9/2})^{-5}_{12.5}(h_{11/2})^{1}_{5.5}]_{18}$
$\nu10 = \nu[(g_{9/2})^{-5}_{12.5}\ (g_{7/2})^{2}_{6}\ (p_{1/2})^{-2}_{0}\ (h_{11/2})^{1}_{5.5}]_{24}$
$\nu11 = \nu(g_{9/2})^{-4}\ (d_{5/2}g_{7/2})^{2}\ (p_{1/2}f_{5/2})^{-4}\ (h_{11/2})^{2}$
$\nu12 = \nu[3]^{-3}\,[4]^{-2}\,[5]^{1}$
$\nu13 = \nu[3]^{-4}\,[4]^{-2}\,[5]^{2}$

The states contributing in the yrast line can be conveniently divided into three groups, each one corresponding to a particular spin region and a well defined location in the deformation plane. These groups are discussed separately in the next three subsections.

3.1. Aligned or near-aligned spherical or near-spherical states with $I \leq 39.5\hbar$. This group contain practically all bands excluding the bands 8,19,27,28,29 and 36. Only states 1 and 11 have vacuum structure. Other these states have particle-hole structure, mainly, π:2p-2h$\otimes\nu$:$\bar{0}$, π:2p-2h$\otimes\nu$:1p-1h, π:3p-3h$\otimes\nu$:$\bar{0}$, π:3p-3h$\otimes\nu$:1p-1h type for positive parity configurations and π:1p-1h$\otimes\nu$:$\bar{0}$, π:2p-2h$\otimes\nu$:1p-1h, π:1p-1h$\otimes\nu$:1p-1h and π:2p-2h$\otimes\nu$:$\bar{0}$ type for negative parity configurations, where vacuum state in corresponding subsystem (proton or neutron) is denoted by $\bar{0}$.

The structure of states corresponding to ph excitations for prolate (γ=-120°) and oblate (γ=60°) shapes can be easily identified from the e_i versus m_i plots. Fig.5 allow to define the structure of states which terminate at very small deformation $\varepsilon_2 \leq 0.025$ (see fig.6). For example, the 30.5^- state (configuration 23) is built from the optimal 14.5^- proton configuration (π2) indicated in the figure and a 16^+ neutron configuration (ν4) (not indicated). The latter is obtained as a particle-hole excitation, $[(g_{9/2})^{-1}(g_{7/2})^1]$, relatively to the 12^+ optimal states (ν2) shown in fig.5. The energy price for such excitation is high and equals $\sim$ 3 MeV (see fig.3).

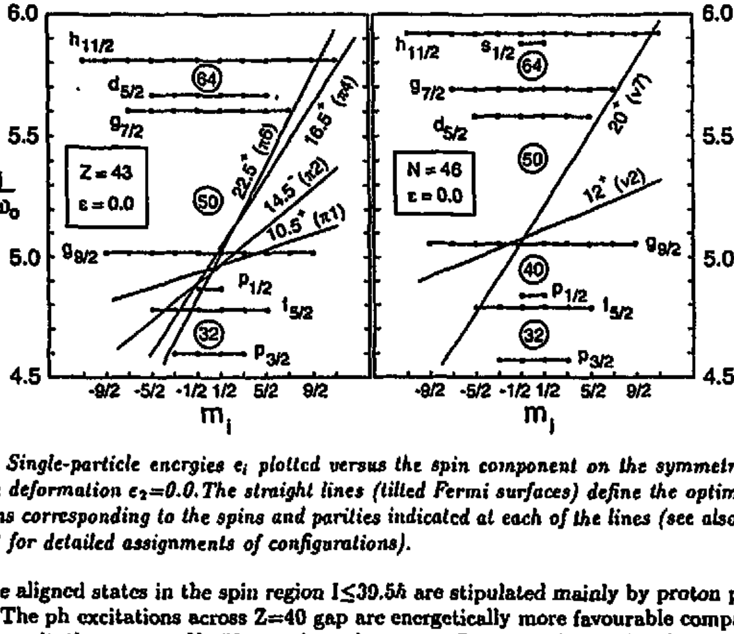

Fig.5. Single-particle energies e_i plotted versus the spin component on the symmetry axis m_i for the deformation ε_2=0.0. The straight lines (tilted Fermi surfaces) define the optimal configurations corresponding to the spins and parities indicated at each of the lines (see also fig.4 and table 1 for detailed assignments of configurations).

The aligned states in the spin region $I \leq 39.5\hbar$ are stipulated mainly by proton ph excitations. The ph excitations across Z=40 gap are energetically more favourable compared with the ph excitations across N=50 gap since the proton Z=40 gap is smaller than the neutron N=50 gap at the deformations close to zero.

The termination on the γ=60° axis or on the γ=-120° axis depends mainly from the shell effects[21,22] due to small deformation of states at spin close to band termination. That is a reason why the group of bands terminating on the prolate (γ=-120°) axis contains approximately one half of total number of yrast configurations in this spin region. Such situation is typical for termination at near spherical shapes, while the termination on the oblate (γ=60°) axis is more energetically favourable for strongly deformed configurations [21].

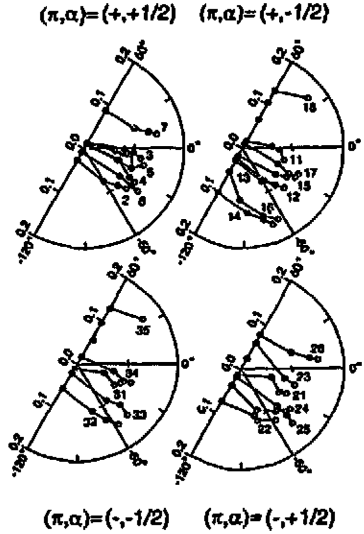

Fig.6. Shape trajectories in the (ϵ_2,γ) plane for configurations terminated below I=40ħ. The deformation points are given in steps of 2ħ within the bands only for the last four spin values before band termination. The bands are labelled according to the notation of fig.4.

3.2.Transitional region in which triaxial rotational bands (0.35< ϵ_2 <0.5,γ ~30°) as well as terminating bands with large quadrupole deformation (0.25< ϵ_2 <0.4) at band termination contribute. All yrast states in spin region 37.0ħ $\leq$ I $\leq$ 48.5 ħ belong to this group. An illustrative example of the shape trajectories in the (ϵ_2,γ) plane for the negative parity and positive signature rotational bands which are yrast or near-yrast in this spin region are shown in fig.7. Using this figure, we will discuss the common features of yrast bands of this group.

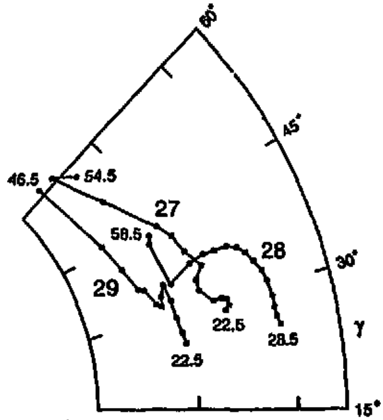

Fig.7. Shape trajectories in the (ϵ_2,γ) plane for configurations of negative parity and $\alpha = +1/2$ signature which became yrast in the transitional region. The deformation points are given in steps of 2ħ. The highest spin values shown in figure correspond to band termination in case of configurations 27 and 29 and highest spin under study in case of configuration 28. The lowest spin values are chosen arbitrarily.

1. Aligned or near-aligned spherical and near-spherical states.

2. Triaxial superdeformed rotational bands as well as terminating bands with large quadrupole deformation at band termination (transitional region).

3. Near-prolate superdeformed rotational bands.

The shape trajectories in the (ϵ_2,γ) plane for transitional and superdeformed regions along the yrast lines of different parity and signature are shown in fig.8 for two nuclei which are on the border of mass region of interest, namely, $^{93}_{44}$Ru$_{49}$ and $^{88}_{42}$Mo$_{46}$. Only few rotational bands with deformation typical for the 2:1 elongated shapes ($\epsilon_2 \sim 0.6$ [23)]) are yrast at spin $\sim 50\hbar$. The rotational bands having larger deformation become yrast with increasing spin, and at spin above $55\hbar$ all yrast bands in the nuclei under study have quadrupole deformation larger than 0.65.

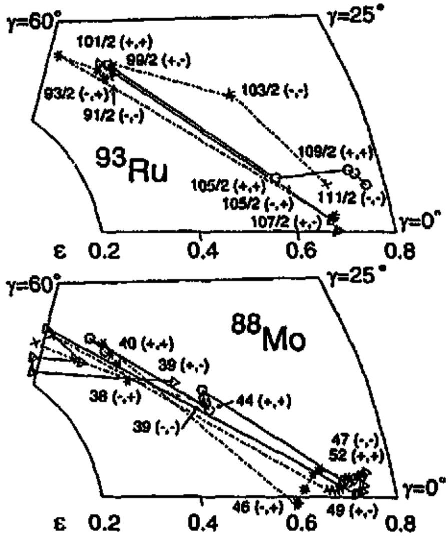

Fig.8. Shape changes along the yrast lines of different parity and signature in transitional and near-prolate superdeformed regions of the $^{88}_{42}Mo_{46}$ and $^{93}_{44}Ru_{49}$ nuclei. The deformation points are given in steps of $2\hbar$. Since the signature depends on the type of nucleus (even or odd), we use the following notation for simplicity: $(\alpha=+)\equiv(\alpha_{tot}=+1/2(odd))\equiv(\alpha_{tot}=0(even))$; $(\alpha=-)\equiv(\alpha_{tot}=-1/2(odd))\equiv(\alpha_{tot}=+1(even))$. The following marks are used: the circles for $(\pi=+,\alpha=+)$, the triangles for $(\pi=+,\alpha=-)$, the stars for $(\pi=-,\alpha=+)$ and the crosses for $(\pi=-,\alpha=-)$ yrast states. The positive parity yrast lines are shown by solid lines, while negative parity ones by dashed lines. The values of spin at which sharp shape changes occur, are displayed with indication of parity and signature.

In order to have a look on total tendencies of development of collectivity along the yrast line we will use the mean spin values, averaged on parity and signature, at which transition from one group to other occurs, because ones strongly depend from parity and signature. These mean spin values are shown as the functions of Z and N for the nuclei of interest both for transition from the region of mainly non-collective rotation to the transitional region in fig.9a and for the transition from the transitional region to region of near-prolate superdeformed rotation in fig.9b. With increasing both Z and N (coming nearer to the doubly magic ^{100}Sn), the region, in which the non-collective regime of rotation is more energetically favoured than collective one, increases at higher spins due to the domination of the spherical proton (Z=50) and neutron (N=50) closures. The same tendency is observed also for the transition from the transitional region to the region of near-prolate superdeformed rotation. The transitional region decreases from $\sim 11\div 12\hbar$ units for Mo (Z=42) and Tc (Z=43) nuclei up to $\sim 7\hbar$ units for Ru (Z=44) and Rh (Z=45) nuclei (see figs.9a and 9b).

Two terminating bands 27 and 29 are displayed in this figure. The band 29 represents an example of "favoured" band termination since the terminating state is yrast. This band with π:3p-3h$\otimes\nu$:3p-3h structure contains one aligned $h_{11/2}$ proton and one aligned $h_{11/2}$ neutron. The band 27 which is yrast at spin I$\sim$40$\hbar$ is an example of so-called "unfavoured" band termination since the terminating at I=54.5$^-$ state lies $\sim$ 6 MeV above yrast line. As a result, the observation of this band termination is very difficult, if, in general, it is possible, even in future experiments. The above mentioned band terminations are "soft" ones since the gradual shape changes take place over many transitions with γ increasing and ϵ_2 decreasing. The calculations show that the minima for terminating states 27 and 29 are slightly away from γ=60°. The origin of that is the relative errors caused by interpolations between the mesh points in the deformation plane which might easily be a few hundred keV in cases of large shape changes [22]. However, that does not destroy the main physical conclusions presented above.

The other feature inherent to this region is the presence of triaxial collective states with large quadrupole deformation ($0.35 < \epsilon_2 < 0.5$), the deformation of which changes smoothly with increasing spin, and which do not reach the band termination at highest spin under study ($\sim$60$\hbar$). The near-yrast band 28 is a typical example. The yrast bands 8,19 and 36 belonging to this subgroup have a large deformation ($\epsilon_2 \sim$0.48, $\gamma \sim$24°) and become yrast even at I=36.5÷38.5$\hbar$. The configurations of these bands contain one (28,36) or two (8,19) $h_{11/2}$ aligned protons and two aligned $h_{11/2}$ neutrons. The filling of the $h_{11/2}$ subshell by two neutrons leads to more collective behaviour of the nucleus in this spin region.

3.3. *Superdeformed* (ϵ_2 >0.5) *near-prolate states with* I$\geq$48.5$\hbar$. At the highest spins all yrast or near-yrast bands correspond to strongly elongated shapes. These bands are not shown in figs.2 and 3 since new reference related to large quadrupole deformation should be introduced. For example, the lowest superdeformed near-prolate rotational bands ($\epsilon_2 \sim$ 0.57, $0.8° \leq \gamma \leq 6.5°$) with $\alpha = +1/2$ signature which become yrast have the following configurations. $\pi[3]^{-7}[4]^{8}[5]^{2}\otimes\nu[3]^{-6}[4]^{-2}[5]^{3}[6]^{1}$ for positive parity and $\pi[3]^{-6}[4]^{7}[5]^{2}\otimes\nu[3]^{-6}[4]^{-1}[5]^{3}$ for negative parity, containing two aligned $h_{11/2}$ protons and, at least, three aligned $h_{11/2}$ neutrons. Moreover, the ($\pi = +, \alpha = +1/2$) band have neutron configuration which contain also one aligned $i_{13/2}$ neutron. The presence of several strongly aligned high-j particles is typical for the superdeformed bands. The rotational bands having larger deformation become yrast with increasing spin and subsequent alignment of high-j particles. All yrast bands at spin above $\sim$ 52$\hbar$ have quadrupole deformation larger than 0.73.

4. HIGH-SPIN SPECTRA OF NUCLEI IN THE A$\sim$90 MASS REGION

Although a lot of experimental data on high-spin spectra of nuclei in the A$\sim$90 region have been obtained during the last few years [1-10] the yrast spectra were only known up to spins of about 20$\hbar$. In this spin region the quantative comparison of our calculations with experiment is not reliable since the pairing correlations are neglected in our approach. The lack of experimental high-spin data results partly from the experimental difficulties associated with this mass region, in which nuclei excited in HI reactions may decay via a variety of channels with emission of charged particles. Taking into account above-mentioned we have focused our attention in this section on total tendencies of development of high-spin spectra along the yrast line as a function of Z and N for the nuclei shown in fig.1 and for which we have made extensive calculations of the high-spin properties.

The high-spin spectra of the nuclei under study show the same features as one of $^{89}_{43}Tc_{46}$. That means that all yrast states can conveniently be divided into three groups, each one corresponding to a particular spin region and a well defined location in deformation plane:

Fig.9. The mean spin values at which the transitions from the region of mainly non-collective rotation to transitional region (a) and from transitional region to region of near-prolate superdeformed rotation (b) occur.

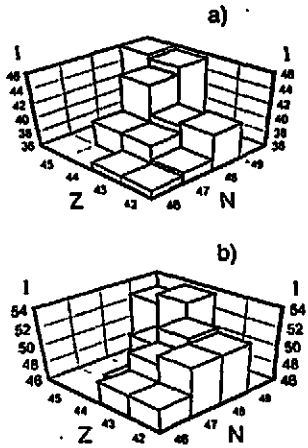

The next spin yrast state with $I_{ph}=I_{f.a.}+2$ above the first fully aligned state at $I_{f.a.}$ is usually observed relatively higher in energy than state at $I_{f.a.}$. That is connected with the necessity of additional ph excitation for generation of state at I_{ph}. The magnitude of such energy gap in experimental spectra depends from energy price for particle-hole excitation. In the case when the energy gap is larger than 1.5 MeV, the definition of first fully aligned state is enough reliable in the spin region $\sim 15\hbar \div 25\hbar$. This feature can be used for comparison of results of our calculation with experiment, since the last give us some examples of such energy gaps in experimental spectra. However, this comparison have only illustrative character because the pairing correlations which can play significant role at spin below $20\hbar$ are neglected in our calculations. While our calculations satisfactorily reproduce the maximal spin of first fully aligned state for positive parity yrast states, the situation for negative parity yrast states is quite different. For all experimentally observed energy gaps between the states of negative parity, our calculation give values of maximal spin of first fully aligned states which are larger on $2\hbar$ than the same in the experiment. Such result can be connected not only with the neglection of pairing correlations but also with the correctness of description of the $f_{5/2}$ and $p_{1/2}$ subshells position relatively to $g_{9/2}$ subshell in Nilsson potential. The calculations with accounting of pairing correlations at spin $I \leq 20\hbar$ is necessary in order to clarify this problem.

5. SUMMARY AND CONCLUSIONS

We have applied the configuration-dependent shell-correction method with cranked Nilsson potential to a number of nuclei in the $A\sim 90$ ($Z=42\div 45$, $N=46\div 49$) region with the goal to study along the yrast line of various high-spin features such as shape coexistence, shape changes, band termination and superdeformation. Pairing correlations are neglested in our calculations which means that it is not reasonable to make any quantitative comparison to existing nowadays experimental data ($I\leq 20\hbar$).

The most important results which emerge are the following:

1) In the nuclei of interest the region of non-collective regime of rotation is expanded up to $I\sim 36\div 46\hbar$ depending from the nuclei. The most of the aligned or near-aligned states

which contribute in the yrast line in this spin region are with only few exclusions spherical or near-spherical ($\epsilon_2 \leq 0.1$). With coming nearer to the doubly magic ^{100}Sn this region reveals at higher spins.

2) The full or partial alignment of one or two $h_{11/2}$ neutrons and one or two $h_{11/2}$ protons leads to terminating bands with large quadrupole deformation ($\epsilon_2 > 0.3$) at band termination as well as to triaxial superdeformed rotational bands in the yrast region. Both types of bands are yrast is spin region $36\hbar \leq I \leq 54\hbar$ in dependence of nuclei.

3) With increasing of spin up to $\sim 47\hbar \div 54\hbar$ the near-prolate superdeformed rotational bands become yrast. The presence of several strongly aligned high-j particles is typical for superdeformed bands. The transition to the region of near-prolate superdeformed rotation occurs at higher spin values coming nearer to the doubly magic ^{100}Sn.

One should note, however, that each specific combination of N and Z leads to specific properties, e.g. well defined maximum spins within the valence space or with one particle excited etc. It is also evident that the collectivity at low spins increases when going away from the N=50 closed shell.

6. ACKNOWLEDGEMENTS

The authors are grateful for financial support from the Swedish Natural Science Research Council and from the Crafoord foundation.

7. REFERENCES

1. M.Weiszflog et al, Z.Phys.A342 (1992) 257
2. M.Weiszflog et al, Z.Phys.A344 (1993) 395
3. S.E.Arnell et al, Phys.Scr. 46 (1992) 389
4. M.K.Kabadiyski et al, Z.Phys.A343 (1992) 165
5. D.Rudolph et al, Z.Phys.A342 (1992) 121
6. D.Rudolph et al, Phys.Rev.C47 (1993) 2574
7. S.E.Arnell et al, Phys.Scr.47 (1993) 142
8. S.E.Arnell et al, Phys.Scr.47 (1993) 355
9. S.E.Arnell et al, Z.Phys.A346 (1993) 111
10. S.E.Arnell et al, Phys.Rev.C49 (1994) 51
11. S.Aberg, Nucl.Phys.A520 (1990) 35c
12. T.Bengtsson and I.Ragnarsson, Nucl.Phys.A436 (1985) 14
13. R.K.Sheline, I.Ragnarsson and S.G.Nilsson, Phys.Lett.41B (1972) 115
14. C.J.Lister et al, Phys.Rev.Lett. 59 (1987) 1270
15. M.A.C.Hotchkis et al, Phys.Rev.Lett. 64 (1990) 3123
16. R.Wadsworth et al, to be publ. in Phys.Rev.C
17. R.Wadsworth et al, Nucl.Phys.A559 (1993) 461
18. W.Nazarewicz et al, Nucl.Phys.A435 (1985) 397
19. M.Brack et al, Rev.Mod.Phys. 44 (1972) 320
20. S.Cohen, F.Plasil and W.J.Swiatecki, Ann.Phys. 82 (1974) 557
21. M.J.A. de Voigt, J.Dudek and Z.Szymanski, Rev.Mod.Phys. 55 (1983) 949
22. I.Ragnarsson, Z.Xing, T.Bengtsson and M.A.Riley, Phys.Scr. 34 (1986) 651
23. I.Ragnarsson, S.G.Nilsson and R.K.Sheline, Phys.Rep. 45 (1978) 1

PRE-EQUILIBRIUM GIANT DIPOLE RESONANCES: A PROBE OF THE REACTION MECHANISM

V.Baran[1,2], *M.Colonna*[3], *M.Di Toro*[1], *A.Guarnera*[3], *A.Smerzi*[1] *and Zhong Jiquan*[1,4] *

[1]*)Laboratorio Nazionale del Sud, INFN*
44, Via S.Sofia, 95125 Catania, Italy
and
Dipartimento di Fisica dell' Universitá di Catania,

[2]*)IFA Bucharest, Romania*

[3]*)GANIL, Caen, France*

[4]*)Institute of Modern Physics, Lanzhou, China*

ABSTRACT

Some new features of nuclear giant resonances are discussed, which can be direclty related to the reaction dynamics:

1) The use of giant dipole γ-decays from long-living intermediate nuclear systems to get a direct insight into the dynamics of fusion and deep inelastic collisions;

2) The observation of pre-equilibrium giant dipole photons in relatively fast fusion reactions induced by charge asymmetric entrance channels.

An attempt to make predictions useful for planning future experiments for a detection of the effect is always present.

1. Introduction

Nuclear Giant Resonances, and in particular the Giant Dipole Resonance (GDR), represent universal collective excitation modes involving all the nucleons, very well established in all nuclei. They have always been precious sources of information for nuclear structure as well as for the dynamics. Aim of our report is to show how to extract information on the fusion dynamics from a direct observation of pre-equilibrium Giant Dipole emissions. We will consider two energy ranges, just above the coulomb barrier and around the upper limit of the complete fusion mechanism.

At lower beam energy the times involved in the dynamics of fusion in some cases are long enough to allow the formation of long living intermediate very deformed compound nuclei, close to di-nuclear systems. The effect seems to be ruled by the entrance channel mass-symmetry. This is discussed in Sect.2, where we also evaluate the very characteristic features of a GDR γ-decay from such exotic systems.

In fusion reactions at relatively high energy (between 15 and $30 MeV/u$ beam energy), we have looked at the possibility of a pre-equilibrium collective dipole γ- emission due to the fact that the charge can be not fully equilibrated when a fused nucleus is formed. This is shown in Sect.3. The results are quite appealing. The effect seems to be noticeable for N/Z asymmetric entrance channels.

Finally some conclusions and perspectives are presented in section 4.

---

* *Report presented by M.Di Toro*

2. Collective Dipole emission from a very deformed di-nuclear system in the fusion dynamics.

It is well know that properties of the GDR give direct information on the structure of the nuclear system on top of which the resonance is built [1]. So the possibility of observing some GDR photon emission from intermediate dinuclear states in fusion, fusion-fission and deep inelastic collisions looks extremely stimulating in order to gain a direct insight into the dynamics of the process. We will focus our analysis on the fusion path.

We are addressing our attention to a γ-emission in relatively slow processes, where a long living di-nuclear system can be formed. The charge degree of freedom will equilibrate but not the shape [2] and there is a chance of observing a statistical emission of GDR-photons from a very deformed *compound* nucleus. Now the dynamics of the reaction is playing a major role and important entrance channel effects will be related to the mass asymmetry and corresponding shape equilibration times [2].

The most evident feature of a Giant Dipole γ-emission from a very deformed system will be a clear splitting of the resonance: i.e. for a quadrupole leading shape we expect to see two main peaks in the γ-yield with a separation proportional to the amount of deformation [1]. There are some first experimental evidences of this effect in fusion reactions [3,4]. In ref.[3] such two-bump γ-emission is needed to account for the measured spectrum when the fused system, ^{164}Yb at $E_x \simeq 50MeV$ is formed in a more mass-symmetric entrance channel, where one expects longer times for the fusion dynamics [5]. In ref. [4] coincidence α-particles are used as a clock for the emission times. When the γ-spectrum is measured, in the $^{nat}Sn +^{20}Ne$ reaction at $164MeV$ beam energy, in coincidence with forward emitted α's (short living source), the two bumps are neatly seen. They disappear in spectra with α-backward coincidences.

Evidences of GDR-photon emission from very deformed systems have been observed also in exit fission channels, either in fusion-fission reactions [6] or in spontaneous fission decays [7]. A quite complete recent review can be find in [8]. Similar effects in most dissipative deep inelastic collisions have been recently seen [9].

Our aim is to follow a microscopic description of the fusion dynamics to clearly show the presence of long living intermediate states and the properties of their giant dipole decays. We have followed a fully mean field picture of the dynamics based on the solution of the Vlasov kinetic equation [10,11]. Since we are considering fusion processes above the coulomb barrier we are confident that our semiclassical approach retains a good validity. We have solved the equation using the test particle method introduced by Ch.Gregoire et al.[12], where the time evolution of gaussian phase space wave packets is considered [13]. Fifty test particles per nucleon are used, which represents a reasonably good phase space mapping to have a fermionic dynamics. The mean field is built from simplified Skyrme forces corresponding to a soft equation of state. Surface effects are accounted for through the gaussian widths.

We are considered just the systems studied in the ref.[3], i.e. the formation of a compound nucleus ^{164}Yb at $E_x \simeq 50MeV$ in two different entrance channels, the mass-asymmetric $^{16}O +^{148} Sm$ at $83MeV$ beam energy, and the mass-symmetric $^{64}Ni +^{100} Mo$ at $237MeV$ beam energy. In order to have the same angular momentum in the compoud system we will compare the dynamics of the impact parameter $b = 5fm$ for the $O - Sm$ reaction with the $b = 3fm$ collision of the $Ni - Mo$ case. In fig.1 we show the density plots on the reaction plane for the two reactions, at $t = 100fm/c$ time intervals, up to $1000fm/c$. The compound nucleus formation times are clearly different. In the mass symmetric case the system has a still elongated shape at $1000fm/c$.

The effect is quite evident from the analysis of the mass quadrupole moment shown in fig.2.

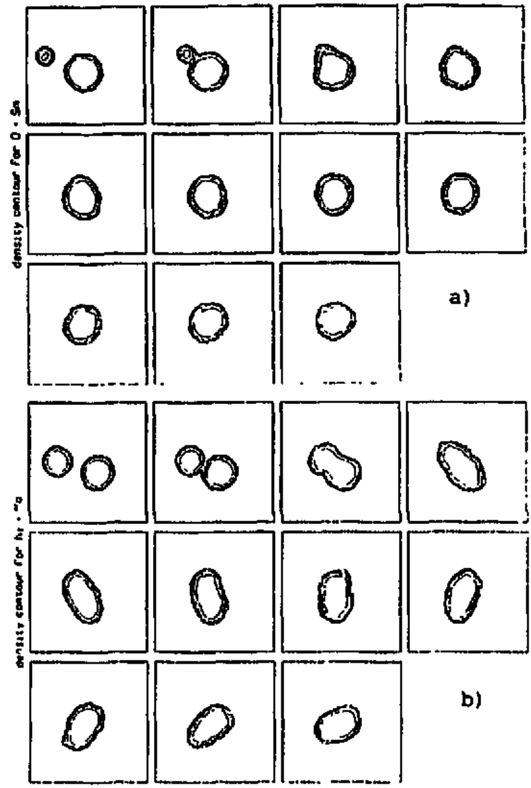

Fig. 1. Time evolution of the density plots on the reaction plane for the collision: (a) $O - Sm$ at $83MeV$ beam energy, $b = 5fm$; (b) $Ni - Mo$ at $237MeV$, $b = 3fm$.

The asymmetric case shows a shape equilibration already at about $300fm/c$. We remark the interesting oscillations in the symmetric case. This means that the elongation of the intermediate dinuclear system is slowly oscillating and we should see the effect on the corresponding dipole emission in a adiabatic picture. We have computed the isovector dipole moment in coordinate space at each time step, choosing the $z-$direction along the rotating maximum elongation axis and the $x-$direction on the reaction plane:

$$D_z(t) = \frac{N\ Z}{A}\ [< z >_{proton}\ -\ < z >_{neutron}] \tag{1}$$

where

$$< z >_{proton} = \Sigma_{i \in p} z_i/Z\ \ ,\ \ < z >_{neutron} = \Sigma_{i \in n} z_i/N \tag{2}$$

and the same for the $x-$ and $y-$ components. It is instructive to see the time evolution of the absolute values of the $z-$ component $|D_z(t)|$ and of the orthogonal part $|D_{orth}(t)| = (D_x(t)^2 + D_y(t)^2)^{1/2}$ shown in figs. 3 and 4 for the asymmetric and symmetric case respectively.

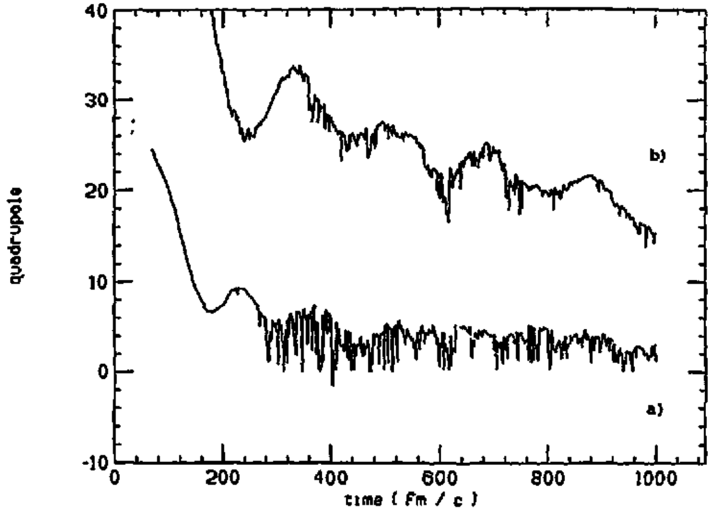

Fig. 2. Time evolution of the mass quadrupole moment for the collision: (a) $O - Sm$ at $83MeV$ beam energy, $b = 5fm$; (b) $Ni - Mo$ at $237MeV$, $b = 3fm$.

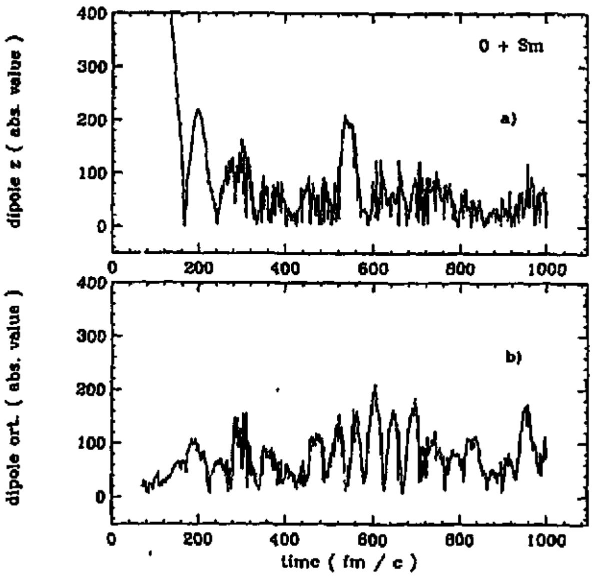

Fig. 3. Time evolution of the absolute value of the dipole moment for the collision $O - Sm$ at $83MeV$ beam energy, $b = 5fm$: a) component parallel to the elongation axis; b) component orthogonal to it.

We clearly see two different frequencies in the mass-symmetric case, with the smaller one for the parallel component, as expected for a deformed system.

This effect is particularly evident from the Fourier transforms, defined as

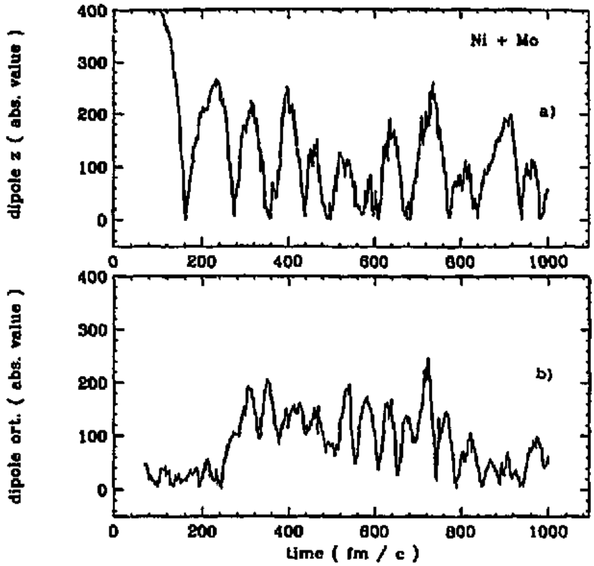

Fig. 4. Time evolution of the absolute value of the dipole moment for the collision $Ni - Mo$ at $237MeV$ beam energy, $b = 3fm$: a) component parallel to the elongation axis; b) component orthogonal to it.

$$S(\omega) = |F(\omega)|^2$$

with

$$F(\omega) = \int_{t_{min}}^{t_{max}} dt\, e^{i\omega t} D(t) \tag{3}$$

In all our calculations we have chosen $300 - 1000 fm/c$ for the $t_{min} - t_{max}$ interval, following the interpretation of fig.2.

In fig.s 5, 6 we have the results of the mass-asymmetric case $O - Sm$ and of the more symmetric $Ni - Mo$ respectively, for the three components of the dipole.

As expected, in the mass-asymmetric case, where a compound nucleus is already formed at $300fm/c$, we do not see any appreciable variation in the strength distribution of the three components.

In the more symmetric case we have quite remarkable differences in energy distribution as well as in the absolute values. The z−component strength is concentrated at smaller energies, between $6 - 10MeV$, with a relatively broad distribution which seems to reflect the oscillations of the deformation amplitude (see fig.2). The orthogonal component x, on the reaction plane, has a very nice peak at $\simeq 14MeV$ (although the scale in fig.6b is different), while the y−component, orthogonal to the reaction plane, shows also a peak about at the same energy but with a much smaller value. This seems to be also an entrance channel effect due to momentum conservation on the reaction plane which reduces the y− oscillation orthogonal to it until the equilibration is reached.

Since the largest strength oscillations are both along axes which lie on the reaction plane, which is also the plane orthogonal to the direction of the collective spin of the intermediate system, we should be able to see a definite angular distribution of the emitted two main frequency giant phonons with respect to the spin axis. In particular since the dipole

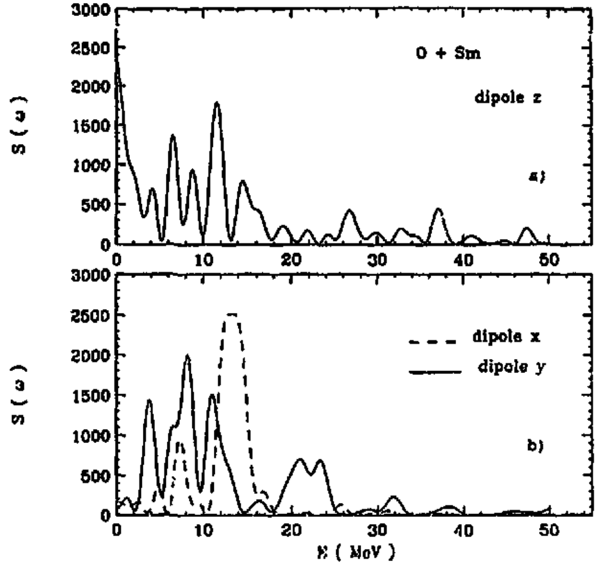

Fig. 5. Fourier transform of the dipole moment for the collision $O - Sm$ at $83 MeV$ beam energy, $b = 5fm$: a) $z-$component parallel to the maximum elongation axis; b) $x-$component on the reaction plane (dashed line) and $y-$component (solid).

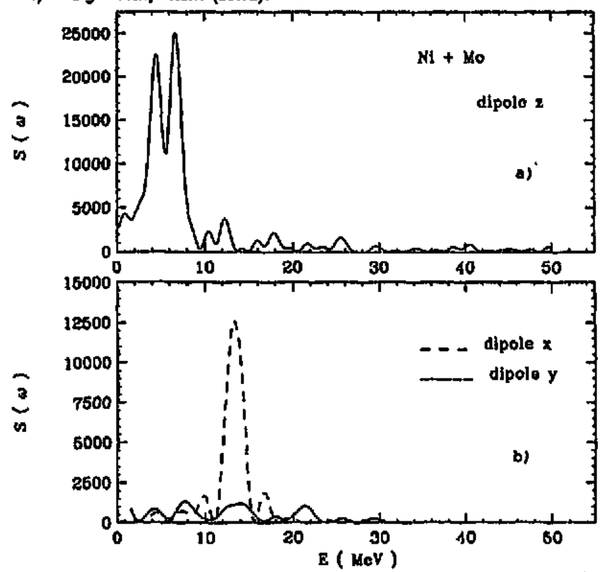

Fig. 6. Fourier transform of the dipole moment for the collision $Ni - Mo$ at $237 MeV$ beam energy, $b = 3fm$: a) $z-$component parallel to the maximum elongation axis; b) $x-$component on the reaction plane (dashed line) and $y-$component (solid). Remark the different scale with respect to the a) curve.

photons are emitted preferentially orthogonal to the oscillation axis we should observe two bumps, around 8 and $14MeV$, for the $\gamma-$ energy dependence of the anisotropy ratio $W(0^0, E_\gamma)/W(90^0, E_\gamma)$ between the number of dipole photons emitted parallel ($\theta = 0^0$) and orthogonal ($\theta = 90^0$) to the spin axis, and similarly with respect to the beam axis.

Our conclusion is that there is a chance to observe directly the GDR γ-emission from very deformed intermediate di-nuclear systems in fusion processes just above the barrier, using some very peculiar features, particularly for the angular distribution. In any case this can represent an important pre-equilibrium cooling mechanism before the compound nucleus is formed. Similar results were shown in a preliminary way for deep inelastic collisions in ref.[14].

We are now performing a systematical study in order to evaluate the corresponding cross sections and to select the best systems to look at. This method could give also valuable information on the best entrance channel choices for the population of very deformed bands in highly rotating compound nuclei.

3. Pre-equilibrium GDR strength.

We will discuss now another interesting source of pre-equilibrium giant dipole photon emission to be seen in fusion reactions at higher energies (between 15 and 30 MeV/u beam energy) where we expect to have a fast fusion process with the possibility of having the charge *not* fully equilibrated when the fused system is formed. This will lead to a direct dipole mode for charge asymmetric entrance channels with different N/Z ratios for the two colliding ions. A thorough analysis has been performed in refs [15,16] particularly in connection with the properties of the GDR in the formed very hot compound nucleus. We will stress here the main points more related to a possible direct observation of this effect.

The γ-emission probability, integrated over the Giant Dipole region, will be much dependent on the GDR strength present in the fused system before a complete equilibration:

$$P_\gamma = P_\gamma^{eq} \frac{\mu}{\mu + \gamma_{ev}} [1 + n_0 \frac{\gamma_{ev}}{\lambda}] = P_\gamma^{eq} + (n_0 - \lambda/\mu) \frac{\gamma_\gamma}{\mu + \gamma_{ev}} \quad (4)$$

where μ and λ are the phonon decay and excitation rates, γ_{ev} is the particle evaporation rate and n_0 is the mean number of GDR phonons present at the time of compound nucleus formation.

$$P_\gamma^{eq} = \frac{\gamma_\gamma}{\gamma_{ev}} \frac{\lambda}{\mu} \quad (5)$$

is the statistical equilibrium prediction, γ_γ being the partial width for photon emission.

In general eq.(4) says that if $n_0 > \lambda/\mu$ (equilibrium value of the number of GDR phonons) we should expect to actually see an enhancement of Giant Dipole photon emissions. This seems indeed to be a quite likely case since, from level density considerations,

$$\frac{\lambda}{\mu} = \frac{\rho(E_x - E_{GDR})}{\rho(E_x)} << 1. \quad (6)$$

and particularly for N/Z asymmetric entrance channels [15]. However if the spreading width in the hot compound system becomes large this entrance channel effect will be less evident since the mean number of GDR phonons is quickly reaching the equilibrium value. This can be seen from fig.7 where the GDR-integrated γ-emission probability is plotted as a function of the excitation energy for various values of n_0 $(0, 1/2\lambda/\mu, \lambda/\mu, 3/2\lambda/\mu, 3\lambda/\mu$, bottom to top): fig.7a for an increasing spreading width , fig.7b for a saturating one.

Our point is that these entrance channel effects could give some independent experimental information on the behaviour of hot GDR's. Moreover there is a good chance of a direct

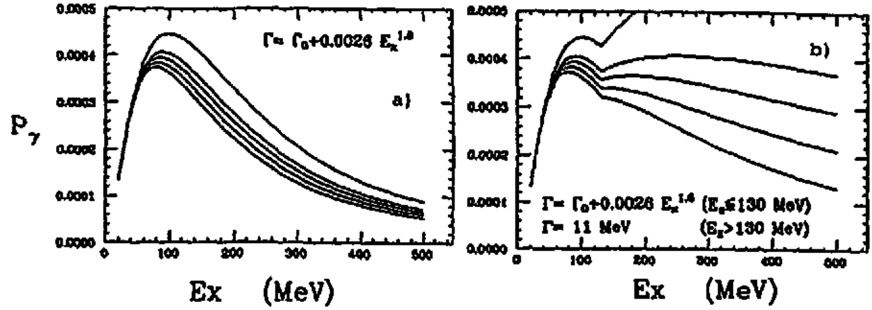

Fig. 7. E_x-dependence of the GDR-integrated γ-emission probability for Sn isotopes: a) increasing spreading width; b) saturating spreading width.

observation of pre-equilibrium collective dipole photons. More experimental work is certainly needed in this medium energy region, possibly also with radioactive beams in order to enhance the range of N/Z asymmetries.

In order to check this point we have performed a fully microscopic dynamical calculation [13,17] for a central collision, leading to a fused system in the Sn region, at 26 MeV/n beam energy in different entrance channels ^{36}Ar $(N/Z = 1.0)$ + ^{96}Zr $(N/Z = 1.4)$, asymmetric, and ^{40}Ar $(N/Z = 1.22)$ + ^{90}Zr $(N/Z = 1.25)$, symmetric.

In fig.8 we report the time evolution of the isovector dipole moment in momentum space for the composite system

$$D(t) = \frac{N\,Z}{A}\ [< P_z >_{proton} \ - \ < P_z >_{neutron}] \tag{7}$$

where

$$< P_z >_{proton} = \Sigma_{i=p} p_{zi}/Z \ \ , \ \ < P_z >_{neutron} = \Sigma_{i=n} p_{zi}/N \tag{8}$$

in the N/Z asymmetric fig(8a) and N/Z symmetric (fig.8b) case. The difference seems quite evident. In the same figure we show the corresponding isoscalar quadrupole moment, which gives a measure of the overall equilibration of the fused nucleus. We see that at $t \simeq 140 fm/c$ the fused system is equilibrated for both entrance channels. At the same time in the N/Z asymmetric entrance channel we still see quite clear dipole oscillations.

This effect is particularly evident from the Fourier transforms, shown in Fig.9, defined as in eq.(3). Now we have chosen the time interval $0 - 300 fm/c$ in order to avoid the contribution from the compound nucleus. For the asymmetric case (fig.9a) we clearly see a nice peak around 16 MeV, which roughly corresponds to the GDR energy for the compound system. It is interesting to notice a peak in the same position, but with a much reduced strength (the scale is different) also for the symmetric entrance channel (fig.8b): this could be interpreted as due to N/Z fluctuations present in incomplete fusion events.

We can conclude that studying different reactions with or without entrance channel asymmetry in the N/Z ratio one should be able to observe the presence of a pre-equilibrium collective dipole γ-emission [18].

To check the interpretation of these quite exciting results obtained at intermediate energies we have also looked at the entrance channel N/Z asymmetry effect at lower energies, where

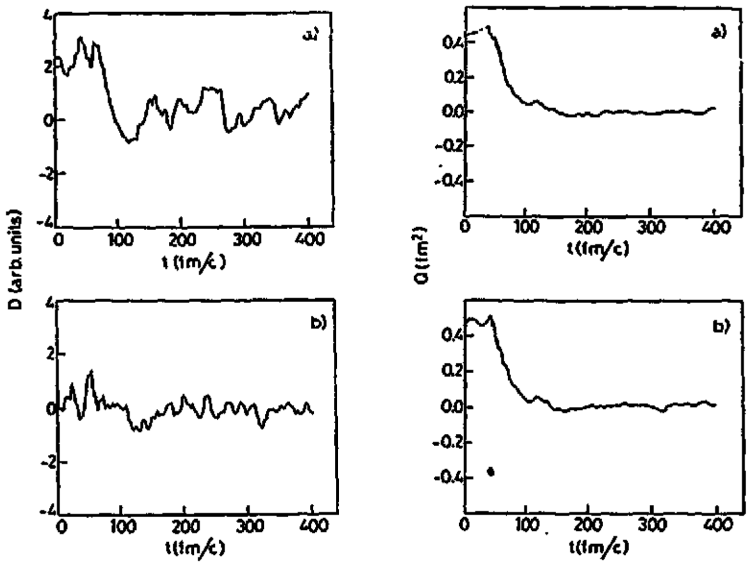

Fig. 8. Time evolution of isovector dipole (left) and isoscalar quadrupole (right) moments for central collisions of charge asymmetric (a) and symmetric (b) $Ar + Zr$ entrance channels.

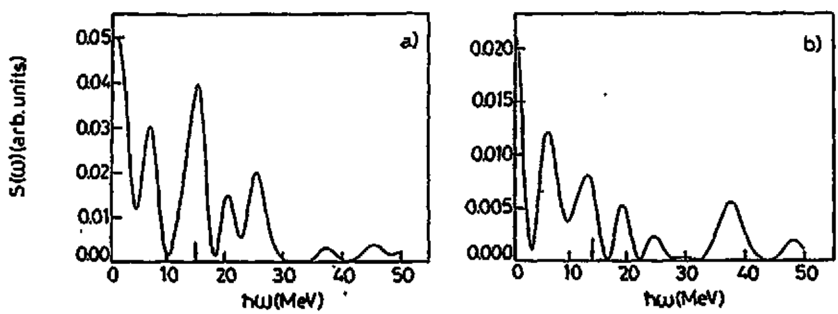

Fig. 9. Fourier transforms of the dipole oscillations of fig.8 for a) the asymmetric case and b) symmetric.

actually more data are available. When we decrease the beam energy the initial amplitude of the dipole oscillation in the asymmetric case will decrease due to a smaller shift of the neutron and proton Fermi spheres. In fact what we finally observe is a clear disappearance of the asymmetry effect with decreasing beam energy [16]. Moreover the time involved to form a fused system is longer and therefore charge asymmetry effects in the entrance channel cannot be seen since there is enough time for charge equilibration.

At higher energies, where the incomplete fusion mechanism is dominating, this pre-equilibrium GDR strength will be again reduced due to the large charge fluctuations. In conclusion we predict a definite energy interval, between 15 and 30 MeV/u beam energy, to detect this enhanced Giant Dipole emission in fusion reactions from charge asymmetric entrance channels.

4. Conclusions

We have shown the possibility of detecting *GDR* γ-decays from long living intermediate very deformed nuclear systems in fusion reactions just above the barrier. The strength and angular distribution of such exotic photon emission will present very peculiar features which should favour a direct observation. This would represent a nice picture of the fusion and *DIC* dynamics, particularly interesting for the study of fusion paths leading to hyperdeformed bands.

Pre-equilibrium emission is a well known mechanism in nuclear collisions. Pre-equilibrium light particles and incoherent photons have been well detected. We stress here the possibility of observing pre-equilibrium emissions of collective dipole photons in *fast* fusion processes. Charge asymmetry in the entrance channel is playing an essential role and consequently these experiments are very appropriate for the new available radioactive beams.

We warmly thank Ph.Chomaz for agreable and stimulating discussions.

8. References

1) K.A.Snover, Ann.Rev.Nucl.Part.Sci. 36 (1986) 545
2) Ch.Gregoire, "Winter College on Fundamental Nuclear Physics" , Ed.s K.Dietrich, M.Di Toro and H.J.Mang, World Sci. 1984, Vol I p.501
3) M.Thoennessen et al., Phys.Rev.Lett. 70 (1993) 4055
4) V.V.Kamanin et al., Z.f.Physik A337 (1990) 111
5) H.Feldmeier, Rep.Progr.Phys. 50 (1987) 915
6) J.J.Gaardhoje, Ann.Rev.Nucl.Part.Sci. 42 (1992) 483 and ref.s therein
7) H.Van der Ploeg et al., Phys.Rev.Lett. 68(1992) 3145 and 69 (1992) 1148 (errata)
8) P.Paul and M.Thoennessen, "Fission time scales from Giant Dipole Resonances", Preprint MSUCL-936 June 94, Ann.Rev.Part.Nucl.Sci. 1994 in press
9) TRASMA Exp., Collab. LNS Catania-Napoli-LNL Legnaro-Saclay 1993 and L.Campajola et al. "Dynamic excitation of giant dipole modes in dissipative heavy ion collisions", subm. Phys.Rev.Lett.
10) G.F. Bertsch, Z.f.Physik A289 (1978) 103
11) M.DiToro, Ref.2) Vol.I, p.451
12) Ch.Gregoire et al., Nucl.Phys. A465 (1987) 315
13) A.Bonasera et al. Phys.Lett. B221 (1989) 233; B259 (1991) 399
14) Cai Yanhuang, M.DiToro, M.Papa, A.Smerzi and Zhong Jiquan, "Nuclear Giant Resonances: a never ending story", Proc. "Dynamical Features of Nuclei and Finite Fermi Systems", Ed.s X.Vinas et al., World Sci. 1994 in press
15) Ph. Chomaz, M. Di Toro and A. Smerzi, Nucl.Phys. A563 (1993) 509
16) Ph.Chomaz, Zhong Jiquan, A.Smerzi and M. Di Toro "New pieces into the Hot Giant Dipole Resonance puzzle" Int.Winter Meeting on Nuclear Physics, Bormio 1993, Ed.I.Iori, p.427-450
17) A.Smerzi, Ph.D.Thesis, Catania 1993
18) R.Alba et al., OUVERTURE Proposal with the first test *Ni* beams of the *LNS* Superconducting Cyclotron, Catania 1994.

A SEMICLASSICAL APPROACH OF LARGE AMPLITUDE COLLECTIVE MOTION, THE CASE OF RAPIDLY ROTATING NUCLEI

P. QUENTIN /1,2/ and I.N. MIKHAILOV /2,3/

/1/ CENBG (IN2P3-CNRS and Université Bordeaux-1), Gradignan, France
/2/ Bogolyubov Lab. Theor. Phys. (JINR), Dubna, Russia
/3/ CSNSM (IN2P3-CNRS), Orsay, France

ABSTRACT: *We provide here a semiquantal generalization of the usual routhian or cranking approach used for global rotations, to allow the study of a variety of collective modes. For that purpose, we have used a formal analogy between canonical (local) point transformations in Classical Mechanics and specific unitary transformations in Quantum Mechanics. Even though the formalism presented below is capable of describing a large class of collective modes, we have merely illustrated here the approach by studying the coupling of a global rotation with a uniform intrinsic vortical motion in the aligned case, analogous to the flow motion in classical S-type Riemann ellipsoids. In a simple quadratic energy limit, it is demonstrated that the quantal results may yield a staggering in rotational bands similar to what has been recently found experimentally in* ^{159}*Dy and* ^{194}*Hg.*

To keep the hamiltonian formalism under a local point transformation in Classical Mechanics, it is well known that one must add to the hamiltonian a generating function of the type $\alpha.p$, where p is the moment and α a vector field depending only on the position [1]. Particular realizations of these transformations correspond to definite shape and orientation changes of a *reference surface*, roughly representing the nuclear shape, as assumed in many approaches of the nuclear collective dynamics [2]. In such cases, the corresponding velocity field u is exactly $-\alpha$, as it has been demonstrated in ref. 3. In the same paper, it has also been shown that the unitary Thouless transformations of one-body density matrices where the time-dependence is factorized out and which are linear in p, can be considered as quantal analogs of such local point transformations [4]. These unitary transformations yield an extra hamiltonian term in the semiquantal TDHF equation of motion which is precisely of the above $\alpha.p$ type. The corresponding stationary problem is therefore cast into a variational form :

$$\delta\left(h(\rho)+\alpha.p\right)=0 \qquad (1)$$

where $h(\rho)$ is the Hartree-Fock field depending on the density matrix ρ of its solution. This particular analytical form of the semiquantal generating function entails interesting consequences for the corresponding semiclassical solutions, where semiclassical is to be understood in the Wigner sense [5], i.e. as the first terms of an expansion in powers of $\hbar$. Indeed, one can reproduce in the general case, most of the analytical calculations performed in ref. 6 for the particular routhian case within the Hartreee-Fock approximation and using the most general Skyrme force. As a result it is found, that the Thomas Fermi order yields exactly the classical result, generalizing thus the finding of ref. 6 of a rigid body rotation at that order in that specific case. Therefore, in particular, considering $-\alpha$ as the quantal analog of the collective velocity associated to the considered motion is fostered by the fact that in the Thomas-Fermi limit the current associated with the solution of eq. (1) may be written as

$$j(r)=-\frac{\hbar}{m}\rho(r)\alpha(r) \qquad (2)$$

As in ref. 6, one can obtain rather simple analytical expresions at the next order in $\hbar$, for various densities and mass parameters in terms of local one-body densities. It is worth noting that whereas the currents are found to be linear in the α field, the mass parameters are quadratic, yielding thus an interesting additivity property for the currents in the case of a combination of collective transformations together with a straightforward framework to compute diagonal mass terms as well as coupling terms.

Now, we assume that the collective flow is a combination of a global rotation of angular velocity Ω with a uniform intrinsic vortical motion defined by a "vortical angular velocity" ω, aligned with Ω, e.g. along the z-axis. The associated coordinate transformation is sketched on Fig.1. The components on the principal axis of the field $u = -\alpha$ in the inertial frame, are:

$$u_x = -(\Omega + \omega q)y, \quad u_y = \left(\Omega + \frac{\omega}{q}\right)x, \quad u_z = 0 \tag{3}$$

where q is the ratio of the characteristic lengthes a_x, a_y in the x and y directions respectively. This field encompasses a wide variety of flow motions, as it is illustrated in Fig. 2, which displays the current density lines. The ansatz given by eq. (3) constitutes a particular solution of the well known classical Dirichlet problem defined by the most general linear field bounded by an ellipsoidal surface as studied by Riemann and later by Chandrasekhar [7] and currently applied for the study of the equilibrium shapes of celestial objects [8]. Using such a linear velocity field in Nuclear Physics had been already discussed by many authors, as by Cusson [9], Rowe and Rosensteel [10], Rosensteel [11,12] as well as by one of the authors [13,14]. It has been extensively analysed for the classical case in refs 11 and 12, within the limit where the shape parameters are fixed.

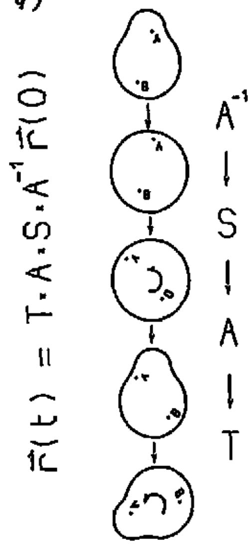

Figure 1

Schematic representation of the studied coordinate transformation $r(0) \rightarrow r(t)$.

Upon solving the generalized cranking problem of eq. (1), one gets the total laboratory energy E as a function of Ω and ω. Even though the study of the most general case is possible and has been sketched in ref. 3, we will only illustrate here the dynamical motion under study, in the particular case where E is a quadratic function of Ω and ω :

$$E(\Omega, \omega) = \frac{1}{2} A \omega^2 + B \omega \Omega + \frac{1}{2} C \Omega^2 \tag{4}$$

where the inertia parameters A, B and C are determined from the solutions of the variational calculation of eq. (1).

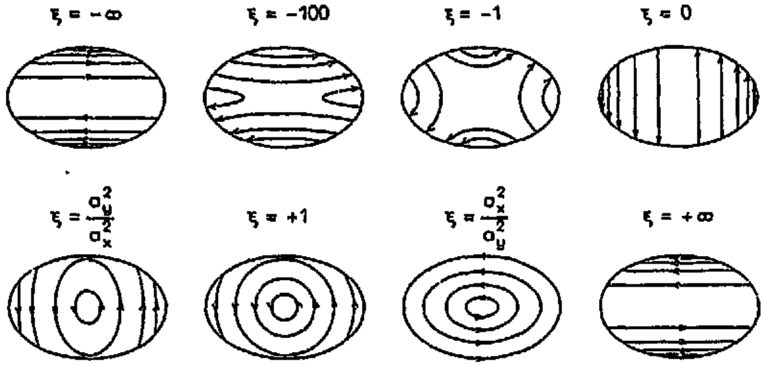

Figure 2

Current density lines as functions of the dimensionless parameter ξ, defined by $\xi = \left(1+q\left(\omega/\Omega\right)\right)/\left(1+q^{-1}\left(\omega/\Omega\right)\right)$ and where $a_x > a_y \geq a_z$.

Defining two functions I and J of Ω and ω, and their inverses, such that

$$\frac{\partial E}{\partial I} = \Omega, \quad \frac{\partial E}{\partial J} = \omega \tag{5}$$

one then gets

$$I = B\omega + C\Omega, \quad J = A\omega + B\Omega \tag{6}$$

$$E(I,J) = \frac{1}{AC - B^2}\left(\frac{A}{2}I^2 - B\,IJ + \frac{C}{2}J^2\right) \tag{7}$$

One may now define the yrast line by imposing

$$\left.\frac{\partial E}{\partial J}\right|_I = 0 \tag{8}$$

which leads readily to

$$J_{yrast} = \frac{B}{C}I, \quad E_{yrast} = \frac{I^2}{2C} \tag{9}$$

Thus, E_{yrast} assumes exactly the pure rotor value, since C is the dynamical moment of inertia associated to the global rotation, as seen in eq. (4), as well as the corresponding kinetic moment of inertia for a vanishing value of ω, as seen in eq. (6). Was it therefore necessary to introduce a new degree of freedom to describe the yrast line? It is crucial at this point to introduce the quantification of this classical model, in particular the quantification of J, suggested from intuitive arguments in ref. 13, and substantiated by a group-theoretical analysis in refs. 10 and 14. Indeed, J is found to commute with H and to satisfy :

$$[J,\Theta]=0,\quad [J,\theta]=\frac{\hbar}{i} \tag{10}$$

where Θ and θ are the angles associated with the rotations of which Ω and ω respectively, are the angular velocities. Equations (10) leed to the following form for the operator associated to J :

$$J=\frac{\hbar}{i}\frac{\partial}{\partial\theta} \tag{11}$$

The quantization of J results, as in the case of the angular momentum I, from the matching of the corresponding wavefunction at the end points of the definition domain[1] for the angle θ. If a left-right reflection symmetry (C_2) is present, J will be quantified by two units of $\hbar$. As a consequence, J_{yrast} is now given by

$$J_{yrast}=2\hbar\left[\frac{B}{C}\frac{I}{2\hbar}\right] \tag{12}$$

where [x] stands for the integer part of x. The plot of the energy E(I) as a function of I, is a collection of points located on displaced identical parabolas, each corresponding to a given value of J :

$$E(I,J)=\frac{J^2}{2A}+\frac{1}{2}\frac{A}{AC-B^2}\left(I-\frac{B}{A}J\right)^2 \tag{13}$$

and similarly

$$E(I,J)=\frac{I^2}{2C}+\frac{1}{2}\frac{C}{AC-B^2}\left(J-\frac{B}{C}I\right)^2 \tag{14}$$

The yrast energy parabola given by eq. (9) is the envelope of these parabolas. The true quantal yrast line is made of pieces of parabolas each corresponding

[1]Intuitively and whatever the exact relation between the collective variable θ and the particle coordinates should be, it is clear that the nuclear evolution as a function of this variable must be periodical, hence the variation domain of θ should have boundaries.

to a given value of J, see Fig. 3. Neglecting the residual interactions beyond the model colective hamiltonian of eq. (7), it then appears that this yrast line presents kinks at each parabola crossing. These kinks will result *in irregularities in* the yrast line transition energies. The periodicity in I of the contact of each J-parabola with the envelope is given by $\Delta I = (2C)/B$. Now, if $(B/C) = 1/2$, one gets for the yrast line energy

$$E_{yrast} = \frac{I^2}{2C} + \frac{2}{4A-C}\left(2\left[\frac{I}{4}\right] - \frac{I}{2}\right)^2 \qquad (15)$$

which does exhibit a $\Delta I = 4$ structure, i.e. a staggering of the energies whose evidence has been recently reported from experimental transition energies within rotational bands in some super deformed nuclei [15,16]. For these structures, one has proposed some alternative explanations. They involve the Y_{44} deformation mode [15,17,18]. Now, a stringent test of these speculations merely based so far on energies, is clearly provided by the assessment of electromagnetic properties. In our case, does the fragmentation of the yrast line into several parabolic cusps prevent such a set of states to constitute a band whose members are linked by strong E2 transitions ?

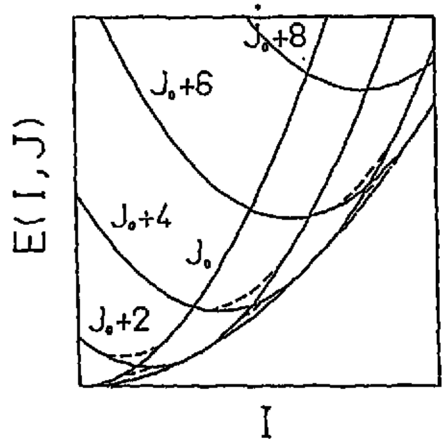

Figure 3

Schematic representation of the band pattern E(I,J). The parabolas are labelled by the corresponding J numbers. The parabola enveloping the various energy curves is the classical yrast band. Note that here J_0 is equal to 0.

Let us answer this question in the idealized case of a $\Delta I = 4$ energy structure as given by eq.(15). It is likely that the residual interaction will mix for a given value of I, the unperturbed yrast state and its closest neighbour, as for instance

$$|I\rangle_{yrast} = \alpha|I, J_0\rangle + \sqrt{1-\alpha^2}\,|I, J_0+2\rangle \qquad (16)$$

$$|I-2\rangle_{yrast} = \beta|I-2, J_0\rangle + \sqrt{1-\beta^2}\,|I-2, J_0+2\rangle \qquad (17)$$

with obvious notation. It may be proven [3] that the Poisson bracket of J with an E2 perturbative electromagnetic field is vanishing. Therefore in the quantal case, the J value is not affected by this supplementary field [7], so that between two yrast states with spins I and I-2, the E2 transition probability will write

$$\langle I|O(E2)|I-2\rangle = \left(\alpha\beta+\sqrt{(1-\alpha^2)(1-\beta^2)}\right)X \tag{18}$$

where X is some matrix element involving the intrinsic state common to both states. If one assumes I to be a spin where parabola crossing occurs and that the mixing is maximum there (i.e. $\alpha^2 = 0.5$) and if one also estimates the mixing for the other spin to be reasonably weak (for instance $\beta^2 = 0.9$), one gets a quenching factor for the relevant matrix element of ~ 0.9, which is within the experimental error bars from lifetime measurements in superdeformed states [19]. As a conclusion for this point, our hypothesis for the staggering is not contradicted by the present status of electromagnetic properties measurements.

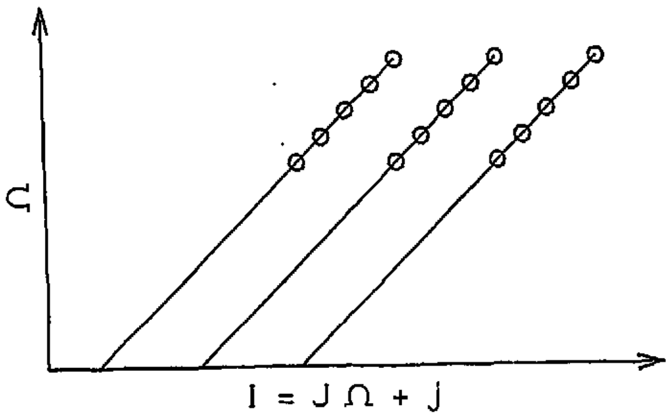

Figure 4

Alignment properties of bands having the same value of the quantum number J. The intersection with the $\Omega = 0$ axis represents the amount $j = (B/A)\,J$ of quantized, yet not necessarily integer or half integer, collective alignment due to the intrinsic vortical motion. Here J is the moment of inertia $(AC-B^2)/A$.

Let us also mention that from eq. (6), one may find for a set of given J states, a collective alignment given by (B/A) J, as it is illustrated on Fig. 4, since

$$I = \left(C - \frac{B^2}{A}\right)\Omega + \frac{B}{A}J \tag{19}$$

We have provided here a rather natural extension of the routhian approach, in a direction which has been found classically important [7,11,13]. There are obvious limitations to the present approach. We have only studied the quadratic case, excluding all "Harris formula" effects due to contributions to the energy of the angular velociti~s at powers higher than two. Nevertheless, the intrinsic vortical motion seems to generate in our case, a potentially interesting new set of collective degrees of freedom whose quantification yields amusing consequences as an alternative description of the staggering in rapidly rotating nuclei or a quantified, not integer or half-integer necessarily though, collective alignment independent of size. For the staggering, it should be noted however that the validity of our conclusions requires only a quadratic form of the energy in terms of two quantized quantities. The first one (I) being obviously unescapable, our description of the second (J), relies only on some classical analogies as well as on a qualitative assessment of the range of the relevant hamiltonian parameters. Ultimately, as in all collective model modelisations, it would be crucial to check whether or not the intrinsic vorticity mode is rather pure, i.e. not strongly coupled with many other degrees of freedom.

Acknowledgments: *This work has benefitted from a collaboration agreement between the JINR Dubna and IN2P3 which is gratefully acknowledged. The authors wish to express their thanks to the Bogolyubov Laboratory for Theoretical Physics, as well as to the CSNSM, for the warm hospitality extended to them during frequent fruitful visits.*

References:

[1] see e.g. H. Goldstein, "Classical Mechanics" (Wesley, Reading, 1950).
[2] starting with the pioneering works of N. Bohr and J.A. Wheeler, Phys. Rev. 56 (1939) 426 ; Å. Bohr, Mat. Fys. Medd. Dan. Vid. Selsk., 26 (1952) n° 14.
[3] I.N. Mikhailov and P. Quentin, preprint CSNSM Orsay # 25-94 (August 1994), submitted. for publication.
[4] generalizing thus the so-called "scaling" transformations of e.g. M. Brack, Phys. Lett. B123 (1983) 143.
[5] E.P. Wigner, Phys. Rev. 40 (1932) 749.
[6] K. Bencheikh, P. Quentin and J. Bartel, Nucl. Phys. A571 (1994) 518.
[7] S. Chandrasekhar, "Ellipsoidal Figures of Equilibrium" (Yale Univ. Press, New Haven, 1969).
[8] see e.g. N.R. Lebovitz, Annu. Rev. Astr. Astrophys. 5 (1967) 465.
[9] R.Y. Cusson, Nucl. Phys. A114 (1968) 289.
[10] G. Rosensteel and D.J. Rowe, Phys. Rev. Lett. 46 (1981) 1119.
[11] G. Rosensteel, Ann. of Phys. 186 (1988) 230.
[12] G. Rosensteel, Phys. Rev. C46 (1992) 1818.
[13] E.B. Balbutsev, I.N. Mikhailov and Z. Vaishvila, Nucl. Phys. A457 (1986) 222.
[14] M. Cerkaski and I.N. Mikhailov, Ann. of Phys. 223 (1993) 151.
[15] S. Flibotte et al., Phys. Rev. Lett. 71 (1993) 4299.
[16] B. Cederwall et al., Phys. Rev. Lett. 72 (1994) 3150.
[17] I. Hamamoto and B. Mottelson, preprint Lund MPh-94/05 (May 1994); B. Mottelson, Proc. Int. Conf. on Phys. from Large γ-Ray Detectors, Berkeley (1994).
[18] I.M. Pavlichenkov and S. Flibotte, Proc. Int. Conf. on Phys. from Large γ-Ray Detectors, Berkeley (1994) ; I.M. Pavlichenkov, Phys. Rep. 226 (1993) 173.
[19] see e.g. E.F. Moore et al., Phys. Rev. Lett. 64 (1990) 3127.

Coulomb Excitation of ${}^{180m}_{73}\mathrm{Ta}_{107}$

J. de Boer, A. Levon[1], M. Loewe, H.J. Maier, M. Würkner, H.J. Wollersheim[2]
Sektion Physik, Universität München,
Am Coulombwall 1, D-85748 Garching, Germany

Ch. Schlegel, P. von Neumann-Cosel, A. Richter
Institut für Kernphysik, TH Darmstadt,
Schlossgartenstr. 9, D-64289 Darmstadt, Germany

J. Bielčik
Dept. of Physics, Charles University,
V Holešovičkách 2, 180 00 Praha 8,
Czech Republic

ABSTRACT

The extremely rare odd-odd nucleus ^{180m}Ta, surviving in nature in its 9^- isomeric state with an isotopic abundance of 0.01 %, has been Coulomb excited using 130 MeV ^{32}S projectiles impinging on a 0.1 mg target enriched to 5.6%. Three gamma ~~rays~~, with energies of 203, 226 and 429 keV, are assigned to the $10^- \rightarrow 9^-$, $11^- \rightarrow 10^-$ and $11^- \rightarrow 9^-$ transitions, respectively, which belong to the first two rotational states that are built on the $K=9^-$ isomer.

[1] Volkswagen Foundation Professor. Permanent address: Institute for Nuclear Research, Kiev, Ukraine

[2] On leave from GSI, D-64220 Darmstadt, Germany

Invited talk presented at the IV International Conference on Selected Topics in Nuclear Structure, Dubna, Russia, July 5 - 9, 1994

1 Introduction

Tantalum is the element with the smallest abundance in the solar system and the isotope ^{180}Ta has one of the smallest relative abundancies (0.01%) on the nuclear chart. ^{180}Ta survives in nature in its 9^- isomeric state while the 1^+ ground state decays to Hf and W with a half-life of 8 h. The production as well as the survival of the high-spin isomer in the astrophysical environment pose so far unresolved puzzles [1,2]

2 Previous experiments

2.1 Light-ion reactions

Numerous excited states have been found in ^{181}Ta(p,t)^{180}Ta, ^{179}Hf(^{3}He,d)^{180}Ta, and ^{179}Hf(^{4}He,t)^{180}Ta reactions [3]. They are interpreted in terms of Nilsson orbitals, occupied by the two odd nucleons, including the following:

1^+ ground state:	$\frac{7}{2}^+[404\downarrow]_p \otimes \frac{9}{2}^+[624\uparrow]_n$,	$E^* = 0$
9^- isomer:	$\frac{9}{2}^+[624\uparrow]_n \otimes \frac{9}{2}^-[514\uparrow]_p$,	$E^* = 73$ keV
10^- rotational state built on 9^- isomer		$E^* = 285$ keV

2.2 Photon excitation

Natural tantalum sheets were exposed to photon beams. After photon irradiation the ground-state radioactivity was measured. From these measurements [4] it was concluded that an intermediate state with excitation energy $E^* = 2.8$ MeV must be excited that has a prompt decay chain feeding the 8 h ground state. The reduced width obtained, $\sigma\Gamma = 1.2(-25)$ cm^2 keV is the largest known below neutron threshold.

2.3 Coulomb Excitation using natural Ta

Ta disks werde bombarded with ^{36}S and ^{32}S projectiles with energies around the Coulomb barrier. The decay of the ground-state was observed out-of beam after ~ 4 h irradiation periods. A comparison of the yields for the two projectiles and for a range of bombarding energies gave the following results [5]

$$0 < E^* \leq 1 MeV$$
$$B(E2, 9^- \rightarrow E^*) \simeq (0.02 - 0.25) W.U.$$

3 Present experiment

3.1 Target

$^{180}Ta_2O_5$ powder with an isotopic enrichment of 5.0% was purchased from ORNL. A quantity of 0.1 mg of this powder was deposited on a carbon backing of 16 mg cm^{-2} thickness which had a dimple of 1.5 mm diameter in its center. A layer of 500 μg cm^{-2} of colloidal graphite was used to glue the Ta_2O_5 powder to the backing.

3.2 Counters

Five Compton-suppressed Ge (35%) counters of the NORDBALL type, arranged in a plane, recorded the gamma rays in coincidence with each one of an array of 24 PIN diodes of 1 cm^2 each. The beam intensity ($\sim$ 30 nA) was limited by the counting rate ($\sim$ 20 kHz) in the gamma counters, stemming mainly from reactions in the C backing.

3.3 Projectiles

The Munich MP Tandem accelerator supplied a beam of 130 MeV ^{32}S ions corresponding to 90% of the barrier energies. The relatively high bombarding energy was chosen to improve counting statistics. It is planned to measure excitation functions.

3.4 Coincidence spectra

Two gamma-ray spectra, recorded in coincidence with backscattered ^{32}S ions, are depicted in figure 1. The lines at 203 and 226 keV are interpreted as the M1+E2 cascade transitions $10^- - 9^-$ and $11^- - 10^-$, respectively, in ^{180}Ta. The line at 429 keV corresponds to the E2 $11^- - 9^-$ crossover. For comparison a spectrum taken with a ^{181}Ta target under the same conditions, is shown on the lower part of the figure.

4 Results

4.1 Gamma-ray energies

The transition energies give an inertial parameter, defined by $E_I = E_0 + A(I+1)I$, of $A = 10.16$ keV for $10^- - 9^-$, and $A = 10.25$ keV for $11^- - 10^-$.

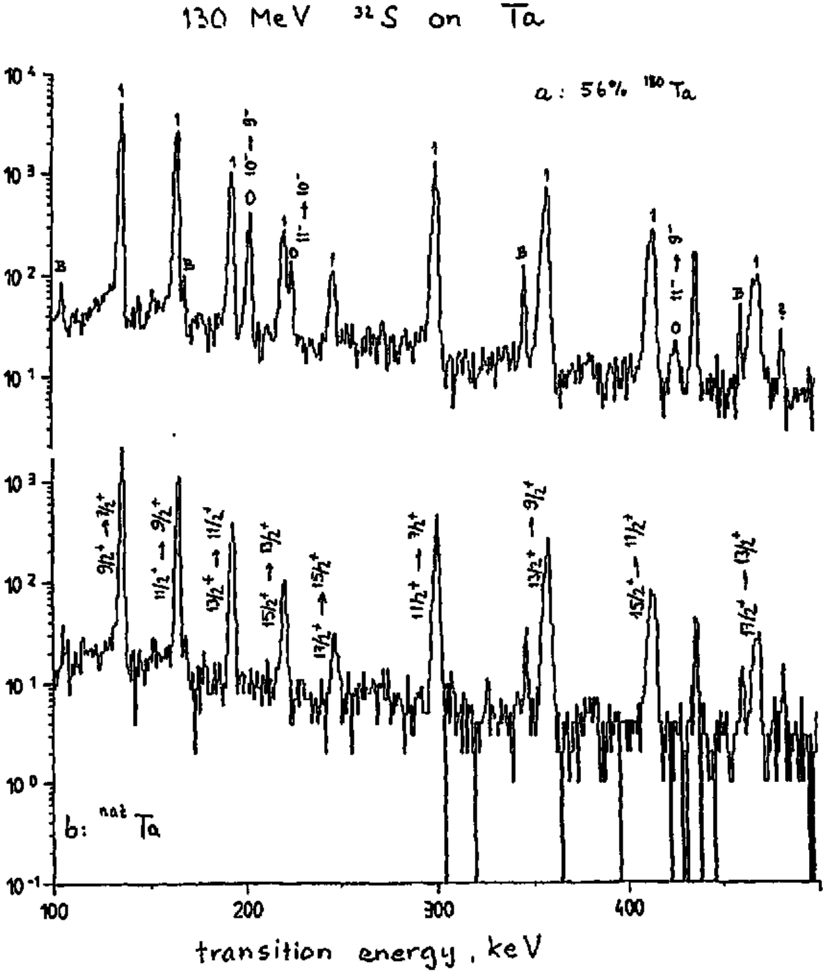

1. Gamma rays, recorded in coincidence with the 130 MeV ^{32}S projectiles, backscattered into an array of 24 PIN diodes.

a) 5.6% enriched ^{180}Ta target

b) ^{nat}Ta target.

The peaks belonging to ^{181}Ta are labelled by 1 in figure 1a, and their assignment is given in figure 1b. The peaks belonging to ^{181}Ta are labelled by 0 and their assignment is given in figure 1a. Known background lines are labelled by B.

4.2 Gamma intensities

Their interpretation must await a careful evaluation of the present data and of bombardments at lower projectile energies. The ratios of the intensities to those observed for ^{181}Ta indicate similar values for the intrinsic quadrupole moments in the two isotopes. An effort will be made to evaluate the cascade-to-crossover ratios so that M1 and E2 matrix elements can be determined separately.

5 Outlook

It is planned to produce a (weak) beam of ^{180}Ta at GSI's UNILAC to study the Coulomb excitation of ^{180}Ta impinging on ^{208}Pb. Since it is expected that the beam will be too weak to be measured electrically, the counting rate of the characteristic gamma line found here may serve to optimize the accelerator parameters.

In this pilot experiment, no evidence of transitions to the ground state has been found.

References

1. Zs. Nemeth, F. Käppeler and C. Reffo; The Astrophysical Journal **392** (1992) 277
2. H. Beer and R.A. Ward; Nature **291** (1981) 308
3. E. Warde et al.; Phys. Rev. **C27** (1983) 98
4. C.B. Collins et al.; Phys. Rev. **C42** (1990) R1813
5. C. Schlegel et al.; submitted to Phys. Rev. **C** (1994)
6. P. von Neumann-Cosel et al.; Verhandl. DPG (VI) **29** (1994) 1954
7. M. Loewe et al.; Verhandl. DPG (VI) **29** (1994) 1954, and Diplomarbeit, University of Munich, 1994, unpublished.

Редактор Э.В.Ивашкевич. Макет Р.Д.Фоминой

Подписано в печать 9.11.94
Формат 60×90/16. Офсетная печать. Уч.-изд.листов 30,08
Тираж 250. Заказ 47704. Цена 5400 р.

Издательский отдел *Объединенного института ядерных исследований*
Дубна Московской области